TUDelft

Delft University of Technology

Design of pattern-placed Revetments

Peters, Dirk Jan

Important note
To cite this publication, please use the final published version (if applicable).
Please check the document version above.

Design of Pattern-placed Revetments

Proefschrift

ter verkrijging van de graad van doctor
aan de Technische Universiteit Delft,
op gezag van de Rector Magnificus Prof. Ir. K.Ch.A.M. Luyben,
voorzitter van het College voor Promoties,
in het openbaar te verdedigen op
27 juni 2017 om 15:00 uur

door

Dirk Johannes PETERS,
Civiel Ingenieur, geboren te Gouda, Nederland

This dissertation has been approved by:

Promotor: Prof. Ir. J.K. Vrijling and
Copromotor: Ir. H.J. Verhagen

Composition of the doctoral committee:

Prof. Ir. K.Ch.A.M. Luyben	Rector Magnificus
Prof. Ir. J.K. Vrijling	Promotor
Ir. H.J. Verhagen	Copromotor

Independent members:

Prof. Dr. Ir. S.N. Jonkman,	TU Delft
Prof. Dr.-Ing. H. Schüttrumpf,	Aachen University
Prof. Dr. Ir. A. Bezuijen,	Ghent University
Prof. W. Allsop,	Southampton University
Dr. Ir. M.R.A. van Gent,	Deltares
Prof. Dr. Ir. D.A. Hordijk,	TU Delft (reservelid)

Cover design: Renate van Beynum

The following trademarks are mentioned in this thesis: Basalton®, C-star®, Haringman®, Hillblock®, Hydroblock®, Rona®ton+ , Verkalit®.

Printed by: www.proefschriftmaken.nl.

Summary

Es gibt nichts Praktischeres als eine gute Theorie.
Emanuel Kant (1724 – 1804)

Dikes and dunes protect low-lying land against flooding. High tides and surges create conditions under which dikes and dunes are actually in service. Waves from the sea tend to erode beaches and dunes. Sandy material is taken away and disposed elsewhere on the coast, where it contributes to accretion of dunes again. For man-made dikes this survival mechanism is not an option. They have too little volume and are designed to maintain their shape. Although made of sand, they are covered with impermeable clay which is, when overgrown with grass, to some extent resistant to erosion caused by waves. This resistance however falls short in the tidal zones, where grass has no chance to survive and at high tides the waves can become too high for grass-and-clay dikes. In such circumstances dikes are therefore covered with armour layers in the appearance of stones, rock or concrete elements.

In order to understand the development of the system a historic perspective is useful. The present-day typical revetment system is a result of developments through the last 200 years. As in many fields of engineering, revetment systems could be developed because of an increase in knowledge as well as improved economical means.

Amongst the variety of available systems the pitched Basalt-type column revetment on an open granular filter layer became dominant since 1870. They have become an icon of the Dutch hydraulic engineering structures, and are even valued as monumental elements of the coastal scenery in Zeeland and elsewhere.

During the 20th century a number of experimental concrete protection systems were developed and tested in practice. After the big flood of 1953, in the beginning of the dike upgrade under the Delta Act, concrete blocks on clay were popular but rejected later. More recent concrete revetments are again of the column type, with an open granular filter layer, more or less inspired by the Basalt slopes. Studying the history of revetments it can be noticed that some technical improvements did not meet the expectations. Although empirical knowledge was dominant, important principles and valuable experiences were not always valued and incorporated in more recent developments.

Non-technical influences play a role as well. Maintenance, periodical upgrade and replacement of the revetment structures have always been costly activities. An interesting coincidence with the economic and regional societal background of the protected polders can be observed. Remarkable recent arguments for the persistent preference for gentle slopes and smooth pitched revetments are their accessibility and esthetical appearance.

The design of the revetment system is influenced by the wave conditions, the foreland geometry, the slope angle and slope length and consequently interacts with the complete dike design. Many authors provide supporting data obtained in field observations. The phenomena of wave loads on slopes are explored through literature, data on flume tests and field observations. In this thesis recent findings with respect to these subjects are collected from international literature. The findings are described in detail, discussed and where possible improved.

The principle of placing the stones or elements in a regular pattern is vital to the functioning of the armour.

Firstly, pattern-placing is creating a pretty much closed slab, the so-called top-layer, which controls the water flows during the cyclic wave loading. When the holes and joints of the slab are adequately designed and the permeability properties are balanced with the gravel and rubble layers underneath they determine and control the build-up of water pressure under the top-layer, and therewith play an essential role in the stability of the system under wave loads.

It seems likely to believe that the pattern-placing as such also makes the structure stronger. The elements cannot be lifted out by just exerting them with forces that balance their weight. This aspect of the pattern-placing has not been researched nor extensively verified and has been the focus of the research conducted for and described in this thesis.

A definition of how pattern-placed revetment and the associated element-to-element interaction works relies on gravity forces.

The elements encounter frictional forces which cause them to respond like interlocking elements, and not as single elements. This is called frictional interlocking and the forces that compress the elements and joints are called in-plane forces, or normal forces.

As such, available knowledge of structural mechanics can be applied to the unknown behaviour of the revetments by considering the revetment as a coherent structural system. Various authors have suggested solutions in this direction. This study provides a comprehensive introduction of state-of-art structural modelling dedicated to modelling revetments as elements with joints, beams, slabs, dynamic systems, etcetera. This way of modelling of the revetment structure creates a possibility of a better evaluation of test data collected by different authors.

Theoretical evaluation of the stability of pattern-placed revetments has begun with testing. Pull tests have been designed and executed by various authors. This started in the 1970s and 80s and ultimately resulted in a very large test campaign in the 1990s with over 10,000 single element field tests.

In this study the evaluation of these tests was revisited and interpreted based on a newly developed structural slab model. From the experimental results, evidence was derived for the latent presence of normal force of a certain level. The experiments however fall short in really testing the wave-resisting capabilities of the revetments.

An important original element in this thesis is the design of new tests. Tests that simulate wave action in a measurable and comprehensible way were not executed before. The existing single stone pull tests do not represent wave loads on the revetment. Tests in wave flumes may entangle the unknowns in the hydraulic and the mechanical performance of the system. Therefore the results of the real wave tests could not be correctly nor reliably interpreted and could not be translated to design rules up to now. The newly designed tests fill the gap between the existing test methods. New pull tests focus on the mechanical behaviour and were performed using a load pattern that represents real wave loads.

A first new experimental verification has been obtained with a full scale load tests in the laboratory.

From those tests evidence was found for the principle of the revetment acting as a beam or slab forming a coherent structure consisting of loose elements. Moreover the exact behaviour could be measured. Model predictions could be verified and further interpretation and refinement became possible.

Partly similar new field tests were executed on real structures. Those experiments were useful to investigate real properties, parameter values as well as for correlating them with initial conditions of in-plane stress states in the slopes. The well-known finding that pull-out strengths are location dependent was confirmed. They are stronger at lower positions on the slope because a larger portion of the slope, with a larger weight, is providing interlock forces. Weak spots were however found close to the toe structure at the bottom edge of the revetment slab. Additionally, an undesirable influence of the ambient temperature was found for some types of revetments. It was also found that old revetment slopes are more resistant than young slopes. This was already common knowledge through past experiences. Maiden revetment slopes are much more vulnerable to waves. Cases of revetments that showed damage and even large failures in their first year are well-known.

In order to find out what series of waves do to this in-plane stress state on the slope, extra data were extracted from large-scale flume tests using additional instrumentation. It was found that during the exposure to waves the revetment slope tends to build-up normal force and hence becomes stronger over time.

The undervalued effect of the structure at the toe of the dike slope as an important stiff boundary and important condition for effective development of interlocking action is included in the models and verified by means of field tests.

A dominant observation in many tested structures was the substantial uncertainty in the experimental results. The principle of frictional interlocking has – in the dry condition – a large inherent uncertainty caused by the undetermined equilibrium of the element of the slope. In theory, the elements do not need the toe and their downstairs neighbours to withstand gravity. Concrete elements positioned on an e.g. 1:4 rubble slope can find equilibrium based on friction forces between the top-layer and the bedding. The elements can remain in position without any in-plane force. In practise the in-plane force was not zero, but has low values now and then. Wave action needs to shake up the elements, re-arrange their positions and with that their in-plane stress state. That mechanism develops easier at steeper slopes. Steeper slopes are therefore considered more reliable for their dependency on frictional interlocking.

Full scale testing of instrumented revetment slopes in wave flumes has been performed by various researchers. The experiments results were now used to calibrate model formulas of wave heights, breaker heights on the slope, differential water heads over the top-layer and ultimately in the achieved stability numbers. The ultimate experiment results in terms of revetment failures were used as a calibration of the total model approach.

A design philosophy for pattern-placed revetments that is based on present day structural design methods is now available, rather than a design method solely based on empirical methods and the results of arbitrarily interpreted tests. This results in a calibrated design model that helps to understand the real behaviour and resistance of revetments under wave attack. The model more clearly distinguishes between safe and unsafe structures. Based on the model better and more economic structures can be designed.

The findings and implications are in summary:

- A strong and stiff toe structure capable of supporting the component of the weight of the full revetment slope length is a key factor for the development of the potential of resistance of the pattern-placed revetment.
- The tallness of the individual elements (or a high height over width ratio) is more important than their individual weight.
- It is beneficial if a revetment type generates in-plane forces in both directions. Plunging breakers form the highest load on the revetment. They create high pressures with a short peak and a limited footprint in both the transverse and the long direction of the dike. Frictional interlocking in both directions is hence contributing to the resistance of the system.
- Recent innovations of revetment types have concentrated on wave run-up reduction. A next step might be possible in improving the reliability by optimising the shape and the mechanical and permeability properties of the joints.
- Steep slopes experience a larger contribution from frictional interlocking forces and are hence stronger than gentle slopes. Combined with the effect that a gentle slope is longer, gentle slopes require significantly more revetment material. Steep slopes however have a higher risk of instability of the impermeable cover layers and have an impact on the required dike height in order to prevent overtopping. In order to avoid both drawbacks, dikes with steep top and bottom slopes and wide berms might be an economic solution.

This study forms a part of a wider research effort which has led to an integrated approach of flood defence safety evaluation that was implemented and used during the recurring national dike ring evaluations of 2007 and 2012 in the Netherlands.

Samenvatting

Dijken en duinen beschermen laaggelegen land tegen overstromingen. Het risico van overstromingen doet zich voor bij hoge getijde waterstanden en stormvloeden. Dan ontstaan er condities waaronder de waterkeringen hun functie daadwerkelijk moeten vervullen. De windgolven die zich onder deze omstandigheden voordoen hebben de neiging om de kust en de waterkeringen te eroderen. Het zandige materiaal van het strand en de duinen verdwijnt in het water en belandt elders aan de kust, waar het bijdraagt tot aanwas van duinen. Bij dijken is het mechanisme van het toelaten van erosie geen optie. Dijken hebben te weinig volume. Het zijn door de mens ontworpen objecten die hun vorm moeten behouden. De kern van de dijken is in sommige gevallen - evenals de duinen - van zand gemaakt, maar is afgedekt met klei. Deze klei is, indien met gras begroeid, in een bepaalde mate bestand tegen erosie door golven. De weerstand tegen erosie schiet echter tekort in de getijde zones, waar het gras heeft geen kans heeft om te overleven. Bij hoog water kunnen de golven te hoog worden voor gras-en-klei dijken, waardoor er eveneens een erosie-risico ontstaat. Dijken worden daarom bekleed met beschermende lagen in de vorm van stenen, rotsblokken of betonnen elementen.

Een historisch perspectief is nuttig voor het begrip van de ontwikkeling van dit beschermingssysteem. De huidige typerende bekleding van de Nederlandse dijken is een resultaat van 200 jaar ontwikkeling. De bekledingssystemen konden steeds worden verbeterd door toename van kennis en ervaring en door gunstiger economische omstandigheden.

Van de verschillende beschikbare systemen werd na circa 1870 de bekleding van gezette basaltzuilen op een laag van doorlatend granulair materiaal het meest toegepast. Deze bekleding is het icoon van de Nederlandse waterbouwkundige constructies geworden en wordt nu zelfs gewaardeerd als monumentaal element van het kustlandschap in Zeeland en elders.

Gedurende de 20ste eeuw zijn een aantal experimentele betonnen bekledingssystemen ontwikkeld en getest in de praktijk. Na de grote watersnoodramp van 1953, bij de dijkverbeteringsprojecten onder de Deltawet, was het toepassen van rechthoekige betonnen blokken op klei korte tijd populair. Later werd dit type onvoldoende betrouwbaar bevonden. Recente betonnen bekledingen zijn weer van het zuilen type met een open granulaire filterlaag, min of meer geïnspireerd door de basalt hellingen. Bij het bestuderen van de geschiedenis van de dijkbekledingen kan worden opgemerkt dat technische verbeteringen niet altijd voldeden aan de verwachtingen. En hoewel er voornamelijk empirische kennis voorhanden was, bleven belangrijke principes en waardevolle ervaringen niet altijd behouden en werden ze niet altijd toegepast in latere ontwikkelingen.

Niet-technische invloeden spelen eveneens een rol. Onderhoud, periodieke opwaardering en vervanging van de bekledingsconstructies zijn altijd kostbare activiteiten geweest. Een interessante samenloop met de economische en regionale maatschappelijke achtergrond van de beschermde polders kan worden waargenomen. Opmerkelijke recente argumenten voor de blijvende voorkeur voor flauw hellende, gladde dijkbekledingen zijn hun toegankelijkheid en esthetische uitstraling.

Het ontwerp van het bekledingssysteem wordt beïnvloed door de golfomstandigheden, door de geometrie van het voorland, de hellingshoek en de lengte van de hellingen en hangt dus

samen met het gehele dijkontwerp. Vele auteurs hebben bijdragen geleverd aan het onderzoeken van golfbelastingen op hellingen. De beschikbare literatuur bevat theoretisch onderzoek, laboratorium experimenten en veldwaarnemingen. In dit proefschrift zijn recente bevindingen met betrekking tot deze onderwerpen verzameld uit de internationale literatuur. De bevindingen zijn in detail besproken en evaluaties zijn mogelijk verbeterd.

Het principe van het plaatsen van de stenen of betonnen elementen in een regelmatig patroon is van cruciaal belang voor het kunnen weerstaan van de golven.

Het aanbrengen van de bekledingselementen in een patroon heeft tot doel een vrijwel gesloten plaat te creëren, de zogenaamde toplaag, waar water door in- en uitstroomt tijdens de cyclische golfbelasting. De gaten en voegen in de toplaag zijn adequaat ontworpen indien de doorlatendheidseigenschappen ervan in balans zijn met die van het grind en puin van de onderlagen. Tezamen bepalen en controleren deze eigenschappen de opbouw van waterdruk onder de toplaag, en daarmee spelen ze een essentiële rol voor de stabiliteit van het systeem onder golfbelastingen.

Het plaatsen van de elementen in een regelmatig patroon maakt de constructie als zodanig ook sterker. De afzonderlijke elementen kunnen niet meer worden opgetild met een kracht die gelijk is aan hun gewicht. Dit aspect van de weerstand van de bekleding is in het verleden niet systematisch en uitputtend onderzocht, noch verifieerd in de praktijk. Het verschijnsel van de toegevoegde stabiliteit − die kan worden toegeschreven aan het feit dat de bekledingselementen onderdeel zijn van een groter geheel − is het onderwerp van dit proefschrift en het onderliggende onderzoek.

De werking van de zwaartekracht is bepalend voor de sterkte van gezette steenbekledingen en de daarbij belangrijke interactie tussen de elementen. De elementen zijn daardoor tevens onderhevig aan wrijvingskrachten die ervoor zorgen dat de groep van elementen reageert als waren zij elementen met onderlinge haakweerstand, en niet als een verzameling afzonderlijke elementen. Dit wordt *frictional interlocking* genoemd: haakweerstand door wrijving. De krachten die de elementen en verbindingen tegen elkaar aan drukken worden normaal-krachten of krachten-in-het-vlak genoemd.

Beschikbare kennis uit de constructiemechanica kan worden toegepast op het onbekende gedrag van de bekledingselementen door deze te beschouwen als een samenhangende constructie. Verschillende auteurs hebben oplossingen in deze richting voorgesteld. Dit proefschrift geeft een uitgebreid overzicht van hoe constructie modellen kunnen worden toepast op steenbekledingen, bijvoorbeeld door ze te modelleren als losse elementen met voegen, als balken, platen of dynamische systemen, etc. Deze manier van modellering van de bekledingsconstructie creëert de mogelijkheid van een betere evaluatie van beschikbare gegevens uit experimenten van verschillende auteurs.

Theoretische evaluatie van de stabiliteit van de steenzettingen is begonnen met het testen ervan in de praktijk. Verschillende auteurs hebben trekproeven op steenhellingen uitgedacht en uitgevoerd. Dit begon in de jaren 1970 en '80 en uiteindelijk resulteerde dit in een zeer grote testcampagne in de jaren '90 met meer dan 10.000 trekproeven.

In deze studie is de evaluatie van deze proeven herzien en opnieuw geïnterpreteerd op basis van een nieuw ontwikkeld plaatmodel. Uit de experimentele resultaten kan bewijs worden verkregen van de aanwezigheid van normaalkracht van een bepaald niveau. De experimenten

schieten echter tekort om de weerstand van de bekledingen tegen golfbelastingen betrouwbaar te voorspellen.

Een belangrijke originele bijdrage van dit proefschrift betreft het ontwerpen en uitvoeren van nieuwe experimenten. Trekproeven die de golfbelasting simuleren en waarbij de weerstand op begrijpelijke wijze wordt gesimuleerd en gemeten waren niet eerder uitgevoerd. De bestaande veldproeven waarbij één enkele steen wordt belast vormen geen goede representatie van de golfbelasting. Bij de golfproeven op steenhellingen in golfgoten spelen de onbekenden in de hydraulische en mechanische prestaties van het gehele systeem een rol, waardoor het eenduidig vaststellen van belasting en weerstand niet goed mogelijk is. Dat is de reden waarom resultaten van golfgoot experimenten tot nu toe moeilijk eenduidig konden worden geïnterpreteerd of vertaald naar ontwerpregels. De nieuw ontworpen experimenten vullen het gat tussen de bestaande testmethoden. De nieuwe trekproeven zijn gericht op het mechanische gedrag en zijn uitgevoerd met een belastingpatroon dat echte golfbelastingen representeert.

Een eerste nieuwe experimentele verificatie werd verkregen met een experiment waarbij het mechanisme van *frictional interlocking* is getest op werkelijke schaal in het Stevin II laboratorium van de TU Delft.

Uit deze onderzoeken werd bewijs gevonden voor het principe dat de bekleding werkt als een balk of plaat met samenhang van de losse elementen. Bovendien is het precieze gedrag gemeten. Modelvoorspellingen konden worden geverifieerd en verdere verfijning van de theorie bleek mogelijk.

Deels vergelijkbare nieuwe praktijkproeven zijn uitgevoerd op echte constructies. Deze experimenten waren nuttig om de werkelijke eigenschappen en parameter waarden te bepalen. De bedoeling was om in de praktijk de in de steenhellingen aanwezige normaalkracht te onderzoeken. De reeds bekende constatering dat de uittreksterkte van de bekledingselementen positie-afhankelijk is werd bevestigd. De bekleding is sterker op de lagere posities in de helling omdat daar een groter gedeelte van de helling, met een groter gewicht, bijdraagt aan de normaalkracht en de *interlock*-krachten. In tegenstelling met deze bevinding werden er echter zwakke plekken gevonden nabij de teenconstructie aan de onderrand van de bekleding. Bovendien werd een opmerkelijke en ongewenste invloed van de omgevingstemperatuur gevonden voor bepaalde soorten bekledingen. Sommige bekledingen zijn 's winters minder strek dan 's zomers. Ook werd geconstateerd dat oude steenhellingen zijn beter bestand zijn tegen trekproeven dan jonge hellingen. Ook dat was al bekend uit ervaringen in het verleden. Net aangelegde bekledingen zijn veel kwetsbaarder golven. Bekend zijn diverse schade gevallen of zelfs het falen van grote delen van bekledingen in hun eerste jaar.

Om uit te zoeken wat de invloed is van een reeks golven op de spanningstoestand in het vlak van de steenhelling, werden meetresultaten verkregen middels het aanvullend instrumenteren van grootschalige golfgoot experimenten. Het bleek dat tijdens de blootstelling aan golven de bekledingshelling de neiging heeft om geleidelijk normaalkracht op te bouwen en dus inderdaad na verloop van tijd sterker wordt.

De teenconstructie aan de voet van de helling is een solide en onvervormbare begrenzing van de steenbekleding. De functie van de teenconstructie als een belangrijke voorwaarde voor de effectieve ontwikkeling van coherentie wordt in het algemeen onderschat. In dit proefschrift is aangetoond wat het effect is van een sterke en vrijwel onvervormbare

teenconstructie, in tegenstelling tot een te zwakke of slappe teenconstructie. De eigenschappen van de teenconstructie zijn vastgesteld met veldmetingen.

Een overheersende bevinding in de vele geteste constructies is de aanzienlijke spreiding in de experimentele resultaten. Het principe van *frictional interlocking* is in droge toestand reeds onderhevig aan een grote inherente onzekerheid als gevolg van het onbepaalde evenwicht van een element op een flauwe helling. In theorie hebben de elementen de teenconstructie en/of de benedenburen niet nodig om de zwaartekracht te weerstaan. Betonelementen geplaatst op een grind helling van 1:4 kunnen evenwicht vinden op basis van wrijvingskrachten tussen de toplaag en de onderlaag. De elementen kunnen in positie blijven zonder enige aanvullende kracht in het vlak. De grootte van in de praktijk vastgestelde normaalkrachten is niet gelijk aan nul, maar er werden af en toe wel zeer lage waarden gevonden. Hellingen met een lage normaalkracht zijn nog niet belast door voldoende grote golven. Golfslag beweegt en herschikt de bekledingselementen en bouwt daarmee de spanningstoestand in-het-vlak op. Dit mechanisme ontwikkelt zich gemakkelijker op steilere hellingen. Steilere hellingen worden daarom beschouwd als meer betrouwbaar voor wat betreft hun afhankelijkheid van wrijvingskrachten.

Verschillende onderzoekers hebben de stabiliteit van steenbekledingen getest in golfgoot-experimenten op grote schaal. Daarbij werd in sommige gevallen ook gemeten aan de deel-processen. De resultaten van die experimenten zijn in deze studie gebruikt om modelformules van de golfhoogte, de brekerhoogte op de helling te verifiëren, stijghoogte verschillen over de toplaag te meten en uiteindelijk om stabiliteit van de bekledingsdikte ten opzichte van de golfhoogte te bepalen. De experimentele resultaten van het falen van de bekledingen zijn gebruikt als een kalibratie van het totaal van de modellen in dit proefschrift.

Daarmee is een ontwerpfilosofie voor gezette steenbekledingen beschikbaar gekomen die gebaseerd is op de werkwijze die momenteel gebruikelijk is bij het ontwerp van constructies, in plaats van een ontwerpmethode die uitsluitend was gebaseerd op empirische methoden en een niet op modellen gebaseerde interpretatie van proeven. Dit heeft geresulteerd in een gekalibreerd model dat helpt om het werkelijke gedrag en weerstand van bekledingen onder golfaanval te begrijpen. Het model maakt duidelijker onderscheid tussen veilige en onveilige constructies. Op basis van het model kunnen betere constructies worden ontworpen.

De bevindingen, implicaties en aanbevelingen zijn in het kort:

- Pas een sterke en stijve teenconstructie toe die als ondersteuning dient voor de component van het gewicht van de bekleding over de volledige lengte van de helling.
- De slankheid (of een grote hoogte/breedte verhouding) van de afzonderlijke elementen is belangrijker dan het individuele gewicht.
- Gebruik een type bekleding waarbij optimale normaalkracht omstandigheden in beide richtingen ontstaan. Omdat werd vastgesteld dat overstortende brekers een concentratie van waterdruk op het talud veroorzaken met een relatief beperkt oppervlak in zowel de dwars- als de langsrichting van de dijk ontstaan balkwerking in beide richtingen. Een bijdrage van *frictional interlocking* in beide richtingen is daarom belangrijk.
- De recente innovaties in bekledingstypen hebben zich gericht op reductie van golfoploop. Het vergroten van de betrouwbaarheid van de bekleding door het optimaliseren van de vorm en de mechanische en de doorlatendheidseigenschappen van de voegen kan een mogelijke volgende stap zijn.

- Steile hellingen zijn duidelijk sterker dan flauwe hellingen. In combinatie met het effect dat een flauwe helling langer is, vereisen flauwere hellingen aanzienlijk meer bekledingsmateriaal. Steile hellingen hebben echter een negatieve invloed op de vereiste dijkhoogte ter voorkoming van overslag. Om de genoemde nadelen beide te vermijden, zouden dijken met relatief steile onder- en boventafels en brede bermen een goede oplossing zijn.

Dit onderzoek maakt deel uit van een omvangrijker onderzoeksprogramma dat heeft geleid tot een geïntegreerde aanpak van de evaluatie van de veiligheid van waterkeringen die is uitgevoerd en gebruikt tijdens de periodieke nationale dijkring evaluaties van 2007 en 2012 in Nederland.

List of symbols and abbreviations

Logic

$e_1 \not< e_2$	e_1 not smaller than e_2, or max(e_1, e_2)
$e_3 \not> e_4$	e_3 not larger than e_4, or min(e_3, e_4)
$e^{(\cdots)}$	Exponential function exp(…)
Eq.	Labelled equation or mathematical expression
×	Multiplication

Latin

a		Contant in equation
a		Damage category for start of damage, defined in Table 3-8
A	[m]	Amplitude of dynamic motion
A	[m²]	Cross sectional area of beam
ANAMOS		Computer programme with analytic model of revetment strength based on single element weight
b		Constant in equation
b		Damage category with minor damage, defined in Table 3-8
B	[m]	Footprint (1-dimensional) of concentrated load
B_{imp}	[m]	Width of wave impact pressure
B_{trough}	[m]	Width of wave trough between wave front and impact of plunging breaker
B_x	[m]	Element width in x-direction
B_y	[m]	Element width in y-direction
c		Damage category with moderate damage, defined in Table 3-8
c	[Pa]	Cohesion (in soil mechanics)
c	[Ns/m]	Damping parameter in SDOF model
c_c	[Ns/m]	Critical damping
c_k, c_F		Elastic constants axial beam model
c_M	[Nm/rad]	Rotational spring stiffness
c_{zL}		Correction factor for effect of revetment length on in-plane force
c_w	[N/m]	Water surface tension
c1		Damage category with moderate single element failure
C		Compression constant of soils
C_c		Compression index
C_i		Coefficient in equation
C_R		Reflection coefficient
CB		Concrete blocks
CC		Concrete columns
CI		Confidence interval
d		Damage category with group failure, defined in Table 3-8
d1		Damage category with complete single element failure
d	[m]	Effective top layer thickness for axial load transfer (D minus chamfered edges)
d	[m]	Water depth

d_f	[m]	Filter layer thickness
D	[m]	Top layer thickness, revetment element height
D_{f15}	[m]	Characteristic filter material diameter
D_{n50}	[m]	Nominal average diameter of armour units
DAF		Dynamic amplification factor
e		Void ratio
e	[m]	Eccentricity of axial force in cross section, or internal lever arm
E	[Pa]	Young's modulus
E_{bed}	[Pa]	Young's modulus of bedding material
E_a	[Pa]	Axial Young's modulus
E_f	[Pa]	Fictitious flexural Young's modulus
$E(f)$		Wave energy in spectrum
f_n		Natural frequency
f_{fr}		Friction factor, or friction coefficient
F	[N]	Force
F_{yx}	[N]	(Friction) force acting on y-surface, in x-direction
FALSE		Pull tests that fails under 900 kg load
g	[m/s²]	Gravitational acceleration, 9.8 [m/s²]
G	[Pa]	Elastic shearing modulus
G	[N]	Single element weight
G_i	[N]	Gross weight of beam portions
h	[m]	Hydraulic head
H	[m]	Wave height
H_b	[m]	Breaker height, wave height at which a wave breaks
H_{rms}	[m]	Root mean square of wave heights
H_s	[m]	Significant wave height
H_{m0}	[m]	Significant wave height defined as spectral period
$H_{p\%}$	[m]	Wave height with exceedance percentage
L_{op}	[m]	Wave length on deep water
k		Weibull parameter
k	[m/s]	Filter permeability
k'	[m/s]	Top-layer permeability
k	[N/m]	Spring stiffness in SDOF model
k_{toe}	[N/m²]	Elastic spring stiffness of toe, line force [N/m]
k_x	[N/m³]	Bedding stiffness in x-direction, frictional/shearing stiffness
k_z	[N/m³]	Bedding stiffness in z-direction, compression stiffness
K	[Pa]	Compression modulus (continuum mechanics)
K	[Pa]	Flexural plate modulus, E corrected for plain strain in cross direction
K_a, K_p		Active and passive soil pressure coefficients
K_{ah}		Horizontal active soil pressure coefficient
K_D		Empirical stability coefficient in Hudson formula
K_L		Load factor (dynamic)
K_M		Mass factor (dynamic)
K_s		Shoaling coefficient

|		
l	[m]	Length of revetment beam
L	[m]	Length of up-lift load, along the slope, $L = L_a + L_b$
L_a	[m]	Part of length L between peak and wave
L_b	[m]	Part of length L between peak and 'air'
L_x , L_y	[m]	Length of deformed shape in x- resp. y-direction (in 2-dimensional pull tests)
L_0	[m]	Beam length between zero displacements points (= up-lift portion of beam)
L_o	[m]	Deep-water wave length = $g\,T_p^2/2\pi$
M	[Nm/m]	Plate moment (M / beam or plate width)
m		Bottom slope of foreshore
m_0, m_{-1}		Moments of wave spectrum
M	[Pa]	Constraint modulus (continuum mechanics)
M	[Nm]	Bending moment in beam
M	[kg]	Mass
M_{ext}	[Nm]	Extreme value of bending moment after re-distribution due to non-linear rotational deformation in a continuous revetment beam
n_{LF}		Load factor in pull tests in terms of weight of a single revetment element
N		Number of waves in flume experiment
N	[N]	Normal force, in-plane force or axial force
N_{cr}	[N]	Critical normal force (buckling)
N_x	[N]	Normal force, in-plane force or axial force in transverse direction
N_y	[N]	Normal force, in-plane force or axial force in longitudinal direction
NB		Natural blocks
NC		Natural columns
p	[Pa]	Water pressure
p		Probability
P	[N]	Concentrated load, point load
p_{max}	[Pa]	Maximum value of wave impact pressure $p(x,y,t)$ above the slope
p_{dip}	[Pa]	Pseudo-static peak value of water pressure in filter, directly after wave impact
q or q_s	[N/m]	Revetment weight = $\rho_s g\, DB_y$, or $(\rho_s - \rho)g\, DB_y$,
q_x	[N/m]	Transverse revetment weight component = $q \sin(\alpha)$
q_z	[N/m]	Perpendicular revetment weight component = $q \cos(\alpha)$
q_s	[Pa]	Effective revetment weight = $\rho g\Delta D$
q_w	[Pa]	Pressure that corresponds to the peak water head difference = $\rho g\, \phi_{\text{dip}}$
q_w / q_s		Load factor, indicating the ratio between the peak load and element weight
Q_w	[N]	Total load = $\int q_w\, dx$
r	[m]	Radius of circular footprint of concentrated load
R	[m]	Outer radius of circular plate
R_d	[m]	Vertical position of wave run-down relative to SWL
R_{toe}	[N]	Reaction force at the toe
R_u	[m]	Vertical position of wave run-up relative to SWL
Ref		Reference datum, e.g. Chart Datum, or in the Netherlands: NAP (Nieuw Amsterdams Peil)
s_o		Wave steepness = H_s/L_o with L_o based on T_p

s_{m-10}		Wave steepness $= 2\pi\, H_s / (g\, T_{m-10}{}^2)$, with wave length based on T_{m-10}
S		Damage factor for slope with armour units = damaged area in cross section $/ D^2$
SDOF		Single Degree of Freedom model for dynamic load, with mass, spring and damping properties
SLS		Serviceability Limit State
STEENTOETS		MS Excel based computer programme for checking of all failure mechanisms of pattern-placed revetments against established methods
SWL		Still water line
t_d	[s]	Duration of peak load
t_r	[s]	Rise time of dynamic load (duration of gradient from ambient value to peak value)
T	[s]	Wave period
T	[s]	Natural period of SDOF system
T_p	[s]	Spectral wave period at peak of spectrum energy
T_{m-10}	[s]	Spectral wave period
T	[°]	Temperature
T_0	[°]	Reference or ambient temperature
TRUE		Pull test with capacity above 900 kg (not failed)
u	[m]	Displacement, deformation or deflection, u_x = axial, u_z = perpendicular
u_{part}	[m]	Particular solution for u
u_c	[m]	Displacement in the centre of a group of elements in pull tests
$\dot{u}$	[m/s]	Velocity du/dt
$\ddot{u}$	[m/s^2]	Acceleration du/dt
u_{150}, u_{300}	[m]	Displacement at 150 resp. 300 kg load in pull test
ULS		Ultimate Limit State
V	[N]	Shear force in beam
V_{ext}	[N]	Extreme value of shear force in revetment beam after redistribution due to non-linear rotational deformation
W	[N]	Gross weight, or total water force
x	[m]	Horizontal ordinate perpendicular to the dike, of in longitudinal direction of the flume (see figure on page xvii)
x	[m]	Rotated ordinate parallel to the slope, in transverse direction, perpendicular to the dike (see figure on page xvii)
x'	[m]	Horizontal ordinate perpendicular to the dike in case x is used for the rotated ordinate (see figure on page xvii, used in chapter 5.3)
x_0	[m]	Position of toe, boundary of the revetment beam
x_0	[m]	Half of the length of uplift portion of beam ($2x_0$ = length of confined beam)
x_i		General variable, e.g. in multiple regression analysis
x_2	[m]	Distance between positive and negative extremes of water head difference over top-layer
x_{top}	[m]	Position of top boundary of the revetment beam
x–joint		Joint perpendicular to the x–axis
y	[m]	Horizontal ordinate in longitudinal direction of the dike
y–joint		Joint perpendicular to the y–axis
z	[m]	Vertical ordinate (see Figure 1-5)
z	[m]	Ordinate perpendicular to the revetment plan in case of rotated x-axis (see Figure 1-5)
z_c	[m]	Cross-sectional dimension of stress area (part of beam depth in compression)

z_{imp}	[m]	Vertical position of wave impact relative to SWL
z_L	[m]	Vertical projection of the length of the revetment
z_{SWL}	[m]	Vertical position of SWL in Reference system, e.g. + 4 m Ref
z_{top}	[m]	Vertical position of top of revetment in Reference system, e.g. + 5 m Ref
ZSTEEN		Computer program based on flow model for calculation of filter pressures based on measured pressures on the slope

Greek

α		Slope angle with horizontal line
α		Geometric factor for stress area in cross section of beam
β	[m^{-1}]	Bedding parameter $= \sqrt[4]{k_z/(4EI)}$
β		Geometrical factor for centroid of stress area in cross section of beam
$1/\beta$	[m]	Inverse of characteristic length of beam on elastic foundation
δ	[m]	Mid-span deflection of beam
δ_0	[m]	Spatial correlation distance, with δ = distance and $\rho(\delta)$ = correlation function
Δ		Buoyant revetment element weight / water weight $= (\rho_s - \rho)/\rho$
ε		Material strain
ϕ	[m]	Water head difference
ϕ_b	[m]	Water head at top of breaker
ϕ_{min}	[m]	Water head at wave trough
ϕ_{dip}	[m]	Peak value of head difference $\phi(x) - \phi'(x)$ over top-layer
$\phi_{inertia}$	[m]	Effect of inertia of motion of a single element, expressed as reduction of static load, in [m] water head
$\phi_{suction}$	[m]	Effect of suction or restrained inflow of water under single element in motion
ϕ		Angle, beam rotation
ϕ		Soil critical friction angle
$\Phi(x)$		Shape function
γ	[N/m^3]	Soil weight
γ'	[N/m^3]	Effective soil weight (under water)
γ_{sat}	[N/m^3]	Saturated soil weight
γ_b		Breaker coefficient $= H_b/d_b$
$\Gamma_{friction}$		Magnification factor on single element weight counting on element-to-element friction (old theory)
κ	[m^{-1}]	Beam curvature
λ		Weibull parameter
λ_k	[m]	Characteristic length of elastically supported axial beam $= \sqrt{E_a D/k_x}$
Λ	[m]	Leakage length $= \sqrt{(b\,D\,k/k')}$
Λ/D		Leakage factor = leakage length / top layer thickness
η_{min}, η_{max}	[m]	Wave depression, wave set-up
ν		Poisson coefficient (material mechanics)

θ		Phase angle
θ_f		Gradient of water head $d\phi/dx$, expressed as angle
ρ		Correlation coefficient
ρ or ρ_w	[kg/m³]	Specific water weight = 1000 .. 1025 kg/m³
ρ_s	[kg/m³]	Specific revetment element weight = 2300 .. 2900 kg/m³
σ	[MPa]	Material stress
σ_u	[Mpa]	Ultimate value of material stress, material strength of joint material
σ_w	[N/m]	Surface tension of water
ω_h		Radial natural frequency
ξ		Breaker parameter, or Iribarren number = $\tan\alpha / \sqrt{s}$
ξ_{op}		Breaker parameter based on wave period T_p
ξ_{m-10}		Breaker parameter based on wave period T_{m-10}
ψ		Angle of dilatancy (soil mechanics)
ζ		Damping coefficient
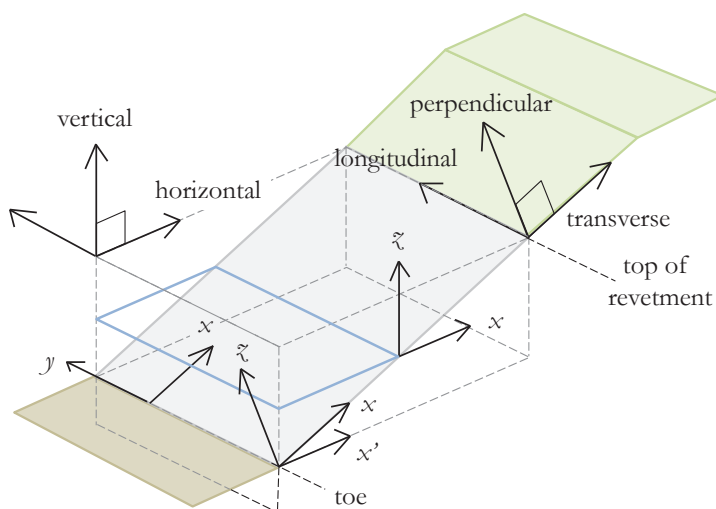
Conventions of directions and ordinates related to the revetment slope and to the water level in this thesis

TABLE OF CONTENTS

Preface

This thesis presents a summary of my research into the subject of the stability of pattern-placed revetments. The habit or art of placing revetment elements in a pattern, thus creating a smooth cover of the seaward slope of dikes is practised since a few centuries. Like arches these structures never sleep. They are regularly tested by the forces of nature. The subject of the stability of those revetments has hence been studied by many authors before.

This thesis would therefore not tell a complete story if it was limited to my original contributions to the subject. The heart of my research work is summarised in the chapters 1, 3.1, 6 and 7 and in the Annexes A, B and E to H. This thesis contains a critical review and description of relevant work by others, written including my own interpretation and contributions, in the chapters 2, 3, 4 and 5.2 and in the Annexes D and J.

Parts of my work have been published between 2003 and 2009 in the form of Dutch-language research reports. Writing this thesis is an attempt to integrate the relevant material into a comprehensive piece of work. It presents a methodology and justification for the design of present-day and possibly for future pattern-placed revetment systems.

Dirk Jan Peters, May 2017

1   INTRODUCTION

1.1   Dutch dike revetments

Large areas of the coastal provinces of the Netherlands are prone to flooding by the sea. Over the centuries many storm surges have led to damage to the dikes and occasionally to inundation. Historically, the main threats to dikes are simple overflowing, overtopping by waves, erosion of the outside slope due to waves, and erosion of the foreland which leads to flow slides and sudden geotechnical collapse of the dike. For centuries the dike crest height was defined by the height of the penultimate storm surge plus a safety margin. Due to settlement of the dike, due to human intervention in the geometry of the estuaries, due to sea level rise, and climate changes, there happened to appear higher floods all the time. The 20th century development of knowledge of hydraulics and geotechnical engineering has provoked a more theoretical and scientific approach of the design and evaluation of the resistance of dikes. After the storm surge of 1953 it became practice to base dike design on a statistical extrapolation[1] of historical storm surge conditions.

Figure 1-1   Traditional Basalt column revetment construction at Afsluitdijk, 1931

For the protection of the outside dike slopes a similar story can be told. In the past, the protection of the wave exposed slopes was labour intensive and costly. The slope protection systems evolved from clay, grass and wicker, via irregular stone revetments[2] to pitchings or pattern-placed revetments.[3] As for dike designs slope protection systems were improved after the occurrence of damaging storms. For the revetments the 1953-flood did not really

---

[1] The methods were available, see P.J. Wemelsfelder, "Wetmatigheden in het optreden van stormvloeden," *Ing.* 54:9 (1939): 31–35

[2] A dike revetment is an engineered protection of the dike slope against erosion by waves, presently consisting of stones, rock, concrete elements of various shapes or rigid structures.

[3] Pattern placed revetments is used as a general term for what is internationally known as pitched revetments or block revetments. The term block revetment is rejected as a general term because the revetment elements are distinguished in blocks and columns.

change this practice. Since there was not much damage to the revetments during that disaster[4], the revetment designs were not changed as dramatically as the dike designs.

Pitching stones of regular shapes and sizes instead of placing them randomly has become a common practice in the 19th century. Pitched or pattern-placed revetments consist of a top layer of selected natural stone blocks or columns of similar size. The natural stone – e.g. Basalt – columns are carefully selected and placed in a regular pattern perpendicular to the slope. The regular pattern creates a coherent structure which provides additional resistance. This is the reason to create pitched slopes in the first place. The increased resistance has been empirical knowledge for quite some time, and has not been extensively researched up to recent years.

Figure 1-2   **Modern column revetment construction Noord Beveland, 2008**

For dike systems in the Netherlands designed under the Delta Act (1958) failure due to too low crests or too steep inner slopes has become less probable. As a result the revetment systems became the weak factor. The hydraulic engineering community has been aware of this problem since the mid-1980s[5]. It became apparent that several new types of revetments that were used after 1953 tended to fail under conditions[6] they were supposed to withstand. Also older types of revetments failed below design conditions. Systematic research into the stability of revetments was initiated. The research activities ranged from simple pull tests to

---

[4] Reported damage of revetments during the 1953 flood is limited to: (1) the Brielse Maas dam, constructed in 1949, with a 0.25 to 0.30 m pitched natural stone revetments and a 0.6 m clay cover over a sand core. 540 m length of revetment was heavily damaged and the clay cover was eroded. The dam did not breach due to emergency repairs just after the fall of the first storm tide. (2) 'heavy damage' (over 1100 m length) to the Basalt revetment of the Westkapelse Zeedijk, without consequences. (3) a dike stretch of 100 m at the North side of the former island Wieringen, (4) many cases of minor damage. Source: Rijkswaterstaat and KNMI, eds., *Verslag over de Stormvloed van 1953* ('s Gravenhage: Staatsdrukkerij- en uitgeverijbedrijf, 1961).
(Van der Veen, 1954) gives a similar damage description of the Brielse Maasdam and confirms that this case was one of the few cases where outside slope erosion was the only cause of an imminent breach. The damaged section was constructed with Maaszetsteen. Sections Basalt column sections survived.
J. van der Veen, "De schade en de herstelwerkzaamheden in de Provincie Zuid-Holland," *Polytech. Tijdschr.* 9:31–34 (1954): 573–580
[5] The Technische Adviescommissie Waterkeringen (TAW) has commissioned systematic research around 1980, resulting in design manuals dated 1984 and 1992
[6] Conditions with return periods of 2 or 5 years.

full scale modelling in the Delta flume. Various authors[7] supported this work with theoretical modelling.

The river flood threats in 1993 and 1995 accelerated the formal introduction of a mandatory assessment of flood defence systems. Every five years all dike rings need assessment against formalised requirements. The first safety assessment round was executed in 2002. Adequate and reliable assessment methods were needed for all failure mechanisms including revetment failure.

The generally felt urgency that revetments were underperforming has led to large replacement and improvement projects of revetment systems in the Netherlands since 1997. Old natural stone and concrete block revetments were replaced by new revetments consisting of concrete columns. In some cases the revetment weight was doubled. This was clearly an improvement, but to some extent the behaviour and stability performance of the revetments was still unknown.

1.2 Service criteria and safety philosophy of the revetment

1.2.1 *Failure mechanisms of dikes*

Wave attacked dikes may be subject to a number of identified failure mechanisms. The dominant mechanisms of sea dikes in tidal areas are: overflow, wave overtopping, foreland erosion and outer slope instability. Piping can be a dominant mechanism in river and lake dikes.

Wave erosion can be a threatening failure mechanism when high water levels occur together with waves. Strong wind fields can cause surges and high waves. To some extent waves can be resisted by well-maintained grass-overgrown clay layers, but in many cases the outer slope of the dike is protected against wave erosion by the revetment layer.

Revetment failure as such is therefore not instantly causing dike failure but further exposure to waves is needed before erosion of the unprotected clay cover and erosion of the dike body results in dike failure.

The revetment system on the outside slope consists of the top-layer, granular sub-layers and a clay layer. This (sub-) system has a parallel arrangement. All components have to fail before the system fails. The sub-system is part of a series arrangement with (1) other failure mechanisms and with (2) other cross sections of a dike protecting one area. The occurrence of one failure mechanism or the failure of one cross section is sufficient for failure of the system. Failure mechanisms of flood defences are defined and categorised. Ultimately all initiated failure paths end up in the undesired top-event of dike failure, defined as a breach with inundation.

---

[7] Teams of WL|Delft Hydraulics and GeoDelft, successor Deltares, staff and students of Delft University and consulting engineers. See chapter 4.1, and see the list of references.
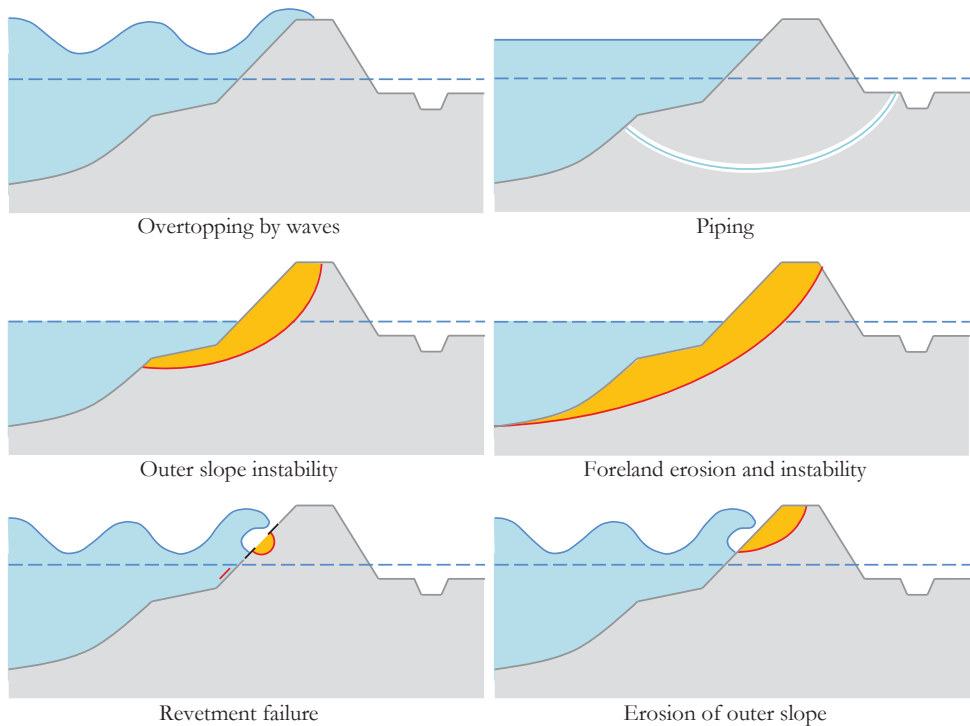
Figure 1-3   Dike failure mechanisms (not exhaustive)

The probability of failure of all failure paths together needs to be below the permissible value. Normally this is achieved by defining one dominant failure path as leading in the design. This path is allowed to have a probability equal to the permissible value. By making all other mechanisms considerably less probable to occur, the design shall be safe. In TAW,
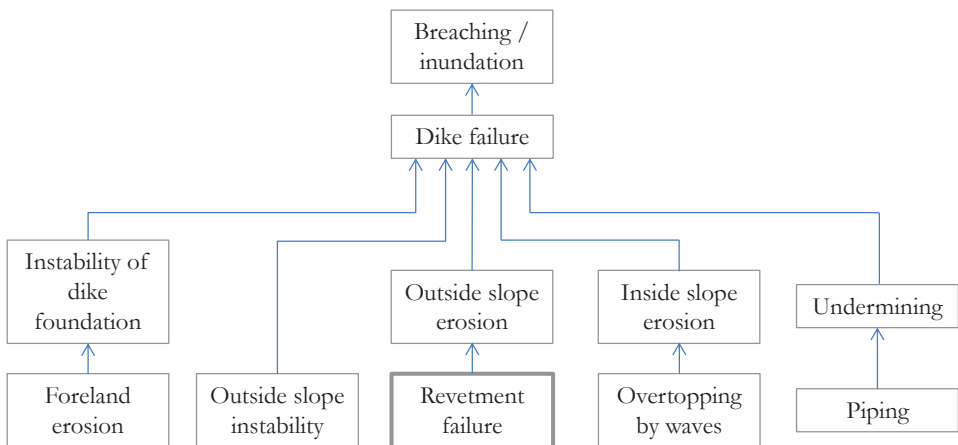
Figure 1-4   Summary of dike failure events

1999[8] overtopping is said to be treated as: failure due to a probable discharge should be lower than the norm probability of flooding. As a safe approximation all other failure mechanisms should be 10 times safer. In case the probability contribution of 'outside slope erosion' is limited under certain design conditions, the revetment itself shall not fail and requires overdesign.

Since the revetment is an expensive component of the dike system it might be favourable to make revetment failure the dominant mechanism and to make the other mechanisms safer. This idea is studied by Voortman[9] and will be further discussed in Chapter 7 of this thesis.

Failure of a dike is an unacceptable event. Designers try and focus on a defined comprehensible limit state just before failure where the structure is still stable and safe. This is called the ultimate limit state (ULS) of the system. Based on models and experimental verifications or based on empirical knowledge the system in the ultimate limit state has the ability to withstand extreme, rare conditions with a sufficiently low probability of failure. Damage to the system, deformations and any beginning of failures that later stabilise are normally permitted, since they do not lead to total system failure. However, at less severe, more frequent conditions these damages might be undesirable, since they are associated with maintenance cost and may affect serviceability over time. Those defined limit states are called serviceability limit states (SLS).

1.2.2 Functional requirements and criteria

The requirements for dike revetments have developed over the years.

A revetment system on a wave attacked dike currently has to meet the following general criteria:

- resistant in the sense of ability to withstand wave attack and ability to resist high water tables inside the dike, combined with low tides,
- prevention of erosion of subsoil,
- flexibility in following settlement of subsoil,
- ease of construction and suitable for straight and curved sections,
- run-up reducing properties,
- redundant in case of overgrowth and siltation,
- ease of repair[10],
- possibilities for re-use,
- ecological effects and accessibility for the general public[11]
- aesthetics and vandal-proof[12]

---

[8] W. van der Kleij, ed., "Leidraad toetsen op veiligheid" (TAW report L5, 1999)

[9] H.G. Voortman, "Risk-based design of large-scale flood defence systems" (PhD thesis TU Delft, 2003)

[10] The wish for ease of repair is, according to A. Glerum and G.M. Wolsink, *Achtergronden bij de leidraad cementbetonnen dijkbekledingen* (CUR-VB COW-report, 1984), to mitigate damage that was explicitly accepted as 'always possible', reportedly due to poor knowledge on the stone revetments.

[11] Added in M.C.J. Bosters, *Handleiding toetsing en ontwerp, Technische werkwijze projectbureau zeeweringen*, 2012.

[12] Aesthetics and vandal-proof are new late 20th century additions.

The main function of pitched revetments is to prevent erosion of the dike. Erosion of the outside slope of the dike is a known failure mechanism that finally results in loss of the performance of the dike. The revetments form a protective structure that may be sacrificial if the dike with a clay layer and without a revetment can withstand the conditions during (the remainder of) a design event.

The views on the importance and necessity of a revetment that can survive the design conditions safely have developed over the decades. A number of considerations are important.

– As described in chapter 2, the technical and economical means to withstand the natural conditions changed gradually. The way of looking to revetment systems has changed. Storm damage that was historically accepted as 'maintenance' was later interpreted as a sign that the revetments were possibly sub-standard. At present there is no willingness to accept and accommodate the risk of maintenance or remedial measures under or shortly after storm conditions.

– The revetment types have improved. Local failure and maintenance due to overloading under design conditions does not happen too often anymore.

– In past years inspections and regular maintenance were crucial for the judgement whether a slope was in good condition and safe enough. The present guidelines require maintenance-free, theoretically verified dike designs that evidently suffice the rules.

– The hydraulic conditions became more severe over the years. Existing revetments were replaced by stronger structures, without changing the underlying dike geometry and materials. This changed the relative contribution of residual strength. The new revetment must meet higher loads and must have a higher survival probability given the loads. In some cases those higher loads might go beyond known limits for clay erosion. The endurance properties of clay layers to survive an extreme storm are deemed doubtful.[13] Especially in a case where revetment has failed already and revetment elements moving back and forth may contribute to wear and erosion of the clay.

– Designers tend to stretch the design rules and range of economic applicability of pattern-placed revetments for the reason that those revetments simply are the preferred system. They do not step to another type of revetment. The design loads under ultimate conditions fall beyond the range of verified stability of the pattern-placed revetment.

There is a tendency to consider the revetment armour layer as the main defence line for the failure mechanism of erosion of the outside slope.

It is important to realise that pattern-placed revetments are brittle structures, especially when the design capacity of the armour layer is upgraded without improvement of the residual strength. Rock slopes are to some extent self-healing under overloading. Revetments fail in

---

[13] M.M. de Visser, *A clay layer as a revetment for sea dikes – The behaviour of clay under wave loading* (MSc thesis TU Delft, 2007)

case a limited number of elements are removed. It is just a matter of time during a serious storm and the structure's integrity is vanished. This is an undesirable situation for reasons of robustness of design, design economy, possible future requirements of extension of service life and possibly increase of design loads over time.

The brittleness is also a feature that is determined by the dike geometry as a whole. Residual strength is easier obtained with gentle slopes, e.g. 1:6 or 1:8.[14] Gentle slopes however are less ideal for revetment stability make the revetment more expensive. These opposite effects will – for cost reasons – lead to steeper slopes, e.g. 1:4 or 1:5, which have a more stable revetment, but less residual strength. Steeper slopes might have implications for other failure mechanisms of the dike system, as geotechnical stability and overtopping tend to become more critical.

We observe that the hydraulic engineering community tended to give arguments for two design philosophies.

1. The pitched revetment layer is a 'lining'. Since the revetment is only a first layer, and there is a solid clay layer underneath, what is the problem of a failing element in the system? Not the revetment but the total system provides the required redundancy. The clay-layer is the main defence line, and the revetment is only there to minimise maintenance of the system. This philosophy has the best arguments from the historical development of the position of the revetment in dike construction and also has the easiest task in proving a safe and redundant flood protection system. The required revetment thicknesses will stay in the range of empirical knowledge and proven strength. An important consequence of this philosophy is that the second line of defence must be able to perform under conditions belonging to the level of failure of the first line of defence.

2. The revetment system is an always vital, preferably maintenance-free system able to withstand extreme[15] design load conditions.[16] Failure of the revetment system could be a first event in a chain of events inevitably leading to failure of the dike. When waves are high enough to cause failure of a safely designed revetment, these waves will surely be able to erode the second defence layer and possibly the complete dike structure. A problem related to adopting the philosophy that the revetment must be resistant to extreme conditions is that it poses a design requirement that goes beyond the empirically tested range of the systems. It also might stretch the design requirements of the revetment system in such a way that a pattern-placed revetment is no longer the best choice. A related question concerns the impact of a failure of a single element within the pitched revetment system. Traditionally, one failing element is not considered a problem. If, for reasons that will be explained later, single element failure is no longer acceptable: what will be the implication for the design philosophy?

---

[14] The Maasvlakte damage case (see section 4.3.3) is interesting, since there was no significant damage to the sub layers, possibly due to the 1:8 slope and due to the fact that the revetment elements where transferred higher on the slope creating a slight S-shaped profile, which was evidently stable: actually a very high residual strength. Also damage cases of clay and grass dikes tell how a dike will behave after damage of the revetment.

[15] Extreme load conditions with e return period of 1/4000 years

[16] This functional definition is identical to the armour layer of a breakwater structure, which normally is subjected to 1/100 year design conditions.

The design requirements for pattern-placed revetment structures need clear definition based on a straight forward design philosophy. The question on the armour or lining function may be answered as follows. In many historical cases the revetment was sacrificial. In many existing cases the revetment has become the slope armour. Accepting this and improving the level of reliability of the structure is the best option. Redundancy and robustness should be optimised compared to the existing practise, since the systems are vulnerable to overload.

1.3 Aim of the thesis

This thesis is about the performance and wave-resistance of pattern-placed revetments. The physical resistance obtained by the pattern-placing has been undetermined for many years. Empirical knowledge about the overall stability is available. Its interpretation can be improved. The central question in this thesis is:

> How can the resistance of pattern-placed revetments be understood,
> predicted and optimised?

The aim of the thesis is in answering this question from the perspective of how the revetment structure ideally works and what design philosophy should be adopted for revetment design as a part of economical dike design.

The central question touches a number of issues. In slope protection and breakwater design the overall performance and the ability of the elements to remain in position or to meet movement tolerances is expressed as *stability*. The element is stable when its equilibrium of destabilizing and stabilizing forces equals zero. In case some motion of single elements does not lead to loss of function of the whole system, the system can still be characterised as stable. Evaluation of the pitched revetment slope does not focus on the performance of the individual elements, but on the performance of the coherent structural system. Destabilizing forces are actions or loads, and – in terms of structural systems – the stabilizing forces can be captured under *resistance*. Resistance may apply to a structural element, or to a structural system.[17]

In hydraulic engineering the term stability includes the effects of both loads and resistance. In pattern-placed revetments the effects of loads and resistance tend to interfere. The destabilizing loads are water head differences over the top-layer of the revetment. The magnitude of the head difference is controlled by the proportion of the permeability properties of the top-layer and the filter layers underneath. The resistance of the pattern-placed elements depends on their self-weight and to friction forces (in the joints) between the elements. This means that the joints and the element interaction to some extent control the load as well as the resistance. Loads and resistance cannot easily be unravelled.

Due to research by various authors[18] insight into the hydraulic performance of the system has been considerably improved. In these studies the performance of the revetment to withstand waves is consequently expressed as stability. The main contribution of this study is in improving insight and in model verification on the aspect of resistance. Integrated in the work of the mentioned earlier authors this leads to improved knowledge of the total system.

---

[17] The word *strength* is reserved to material strength in recent structural definitions, e.g. concrete compressive strength.
[18] See literature references in Glerum and Wolsink, *Achtergronden bij de leidraad cementbetonnen dijkbekledingen*

The subject and limitations of this study can be further explained by looking into the various types of revetments. A general international term for the type of structure is *block revetments*. For the Dutch situation the term block seems to refer to only a part of the element shapes, since these can be subdivided in blocks and columns. Block revetment as a general term does not cover the stone column (Basalt) revetments, and its concrete remakes. Therefore, the term *pitched revetments* or *pattern-placed revetments* is preferred in this study. The study is about single layer regularly placed revetment elements on a permeable granular sub-layer which functions as a filter layer and as a foundation layer. The revetment materials that are covered in this study include natural stone and concrete. Single stones or concrete columns or blocks are referred to as 'elements'.

The scope of the revetment research in this thesis is limited to single layer pattern-placed revetment linings which were always assumed and constructed as structures with some level of coherence between the elements.

The theory is applicable to blocks and columns and is best verified for column revetments with open joints on a permeable filter layer.

1.4 Methodology

The methodology of the investigations of this thesis follows a stepwise approach. The research is part of a cycle that leads to better understanding and is as such instrumental to designing and constructing better flood protection systems.

The cycle[19] consists of a problem, a hypothesis, a predictive model and experiments to test the hypothesis. The aim is to come to a reliable, consistent and non-arbitrary understanding of the relevant phenomena and processes.

Considering that scientific research on revetment has been performed for many years already by a large community, we have specifically extended the cycle for this research task as indicated in Figure 1-5.

The 'real system' to be understood and if possible improved is a pattern-placed revetment slope. This system has had many appearances and has developed over time. This is described in chapter 2.

Prior to formulating a hypothesis of how this system works and responds to loads, the performance of the existing system can be observed. Other researchers have defined test methods and carried out experiments that give insight that contribute to a formulation of a theory.

The hypothesis and basic model description is formulated in chapter 3.1, 3.2 and 3.5. Scattered contributions in literature and description of existing experimental verifications of the stability of revetments are described in chapter 4.

The revetment system has many aspects. Like for other types of structures load and resistance tends to be modelled separately, although the system has a level of complexity that makes this not always possible. Components and properties of the system control and reduce the loads on other components of the system. The models for wave loads are described in chapter 5.

---

[19] Many sources, e.g. E. Bright Wilson, *An Introduction to Scientific Research* (New York: Mc Graw Hill, 1952)
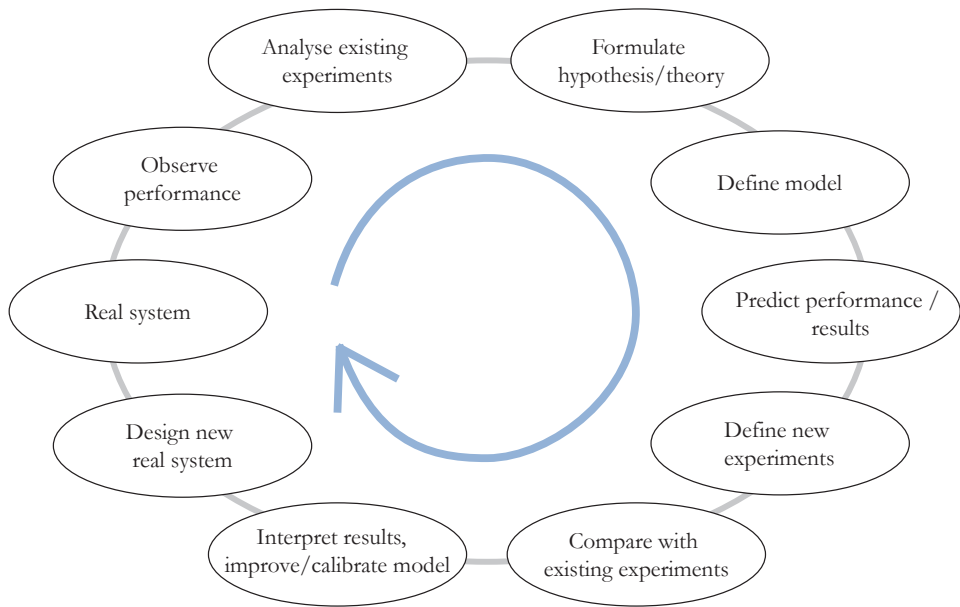
Figure 1-5   Cycle with methodology of this thesis

Detailed model descriptions of the resistance is given in Annex A and B. Existing experiments are described in Annex C, whilst those existing experiments are re-analysed with and compared with new model predictions in Annex D.

The model predictions are verified with newly designed experiments. Those experiments focus on aspects of the model, and/or components of the system, such as the friction tests in Annex E and the trivial model verifications by means of a re-make of a axially pre-loaded top-layer in the laboratory in Annex F.

New field tests were designed also. We have design pull tests on real revetment slopes in order to verify predictions of the resistance in the field. Also the important silent enabler of the revetment slope, the toe structure was tested in the field. Those experiments are presented in Annex G and annex H respectively.

Since around 1980 the revetment research community has executed a huge number of large scale flume tests. They are listed in Annex I. Although the flume tests are certainly not identical to the 'real system' those experiments can somehow be seen as an adequate synthesis of the various aspects that need experimental verification. Quite a number of flume experiments have been intensively instrumented which facilitates the understanding of sub-processes and the behaviour of sub-systems and components. A stand-alone analysis of those experiments (captured as 'analysis of existing experiments') can be found in Annex J. A comparison of those tests with the model predictions is presented in chapter 6.

A conclusive chapter 7 closes the cycle and describes how all findings feed into a better understanding of the revetment slopes and where potential for improvement of the designs of pattern-placed revetments can be found.

2 A HISTORY OF SLOPE REVETMENTS

Chapter introduction

A historical perspective is in many cases relevant for understanding present-day technology. Flood defence technology and – as a part of that – the protection of the outside dike slopes against erosion by wave attack has gone through a technical development process, with influences of economic and societal aspects at different scales. When exploring the historical development of revetment systems the relevance and means for reliable outside slope protection has not been a constant factor. Emerging from a variety of trials and improvements pitched revetments of natural stone columns became a dominant system in the tidal estuaries in the Netherlands in the second half of the 19th century.

New materials such as reinforced concrete and plastics initiated further developments of the revetment systems in the 20th century. The 1953-flood changed insights in the dike designs, but did not result in revetment developments. New revetment types were developed though, based on different hydraulic, geotechnical and structural concepts. Some of them were rejected later. The most successful types are concrete re-makes of the traditional pitched Basalt slopes. It took until 1997 before the increased safety levels required in the Delta Act were implemented in the revetment designs. After this year large upgrade and replacement projects were executed. The research activities have been intensified and have cumulated in verification methods with probabilistic background.

2.1 Dike construction and slope protection

2.1.1 Dikes

People in flood prone areas tend to protect themselves with the means and knowledge they have. Sufficient means for adequate prevention were not always available and knowledge of the threats fell short. History shows repetitive examples of improvements after events with an unacceptable loss. In the Delta areas of Holland and Zeeland dike building started after the year 1000. On the island Schouwen[20] original higher grounds were first supplemented with artificial refuge terps, subsequently smaller areas were diked in and after a flood in the 12th century a ring dike was built around the entire island. By then the ground level was approx +2 m sea level.[21] The dikes were simple man-made raised embankments, consisting of clay, constructed on locations with high foreland. Use of sand became an issue only after the dikes needed to be built higher and the required volumes exceeded the availability of good quality clay.

---

[20] The protection of the island of Schouwen, presently part of Schouwen-Duiveland, is a typical case for illustrating the economic conditions and technical progress in flood protection with dikes and revetments. (Kool-Blokland, 2003) provides a comprehensive description of the complete history of the flood calamities and the water management of the island. The hydraulic engineering innovators A. Caland and Jhr. R.R.L. de Muralt have worked on the island.

[21] A lowland system with a dike ring necessarily develops into a system with managed dewatering of rain water, and consequently with settling of the peat and soft clay grounds, which increases the water level differences and causes salty seepage water. The present ground level of Schouwen is between −0.5 and −1.5 m sea level.

Present-day research and design methods are based on a systematic analysis of the possible failure mechanisms. The historical developments are described from this viewpoint.

2.1.2   Dike shape and crest height

Historic flood levels were very important for the dike designs. The dike crest height of severely attacked dikes was and still is governed by limitation of run-up and overtopping of waves. The Zeeland estuaries dikes used to have outside slopes of 1:3[22]. Although it became known that gentler sloped dikes require less slope protection and a lower crest, the 1:3 slope angle has remained common practice in Zeeland for centuries[23]. Wave run-up was resisted by the introduction of a shoulder or berm. The outside slope is in that case split in a lower slope of 1:3 or 1:3.5, an almost horizontal 5 to 10 m wide berm at the level of the highest known flood level, and an upper slope of 1:3. It is important that the flood water level does not exceed the berm level, because in that case the steep upper slope was not able to limit run-up and overtopping. In case the flood level has a significant deviation from historic levels, the dike design becomes less effective and may fail. This happened in 1953 when the flood levels exceeded the known levels by 0.6 to 0.8 m. Most failures were caused by inside slope erosion, but also many incidents with outside slope erosion above the top of revetment were observed.[24]
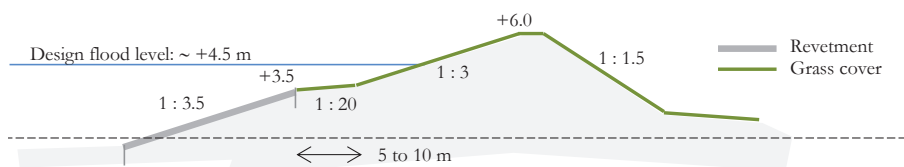
Figure 2-1   Typical profile of Zeeland estuary dike (Huitema, 1947)

Figure 2-2 shows typical sea dike profiles potentially subject to heavy wave attack. They differ regarding the position and height of the berm. The differences between the Hondsbossche and Pettemer sea defences are interesting since they have almost the same orientation and exposure. Kuiper[25] and Jansma[26] report on their performance during the 1953 flood. Both profiles experienced serious overtopping, but were not threateningly damaged. Parts of the clinker lining of the Pettemer dike were damaged. It should be noted that the foreland conditions of the Hondbossche sea defence were more favourable. There is a noticeable difference in the amount and costs of revetments.

The angle of the outside slope is an important design parameter for the revetment. Huitema, 1947[27] states that the effect of wave impact depends on the wave height and on the sine of the slope angle. Steep slopes are more heavily attached than gentle slopes. He also observes that run-up and the speed of the run-down of waves increase with increasing slope angle.

---

[22] The Zuiderzee estuary dikes have slopes of 1:2.5, Wadden Sea dikes have 1:4 to 1:6. North Sea dikes have 1:8 or steeper.

[23] The introduction of stone protected slopes did not change this, because of less steep slopes would require more square metres of revetment.

[24] Rijkswaterstaat and KNMI, *Verslag over de Stormvloed van 1953*

[25] J.H. Kuiper, "Commentary Golfoploop tegen zeedijken en middelen daartegen," *OTAR* 39:8 (1955): 199–201

[26] K. Jansma, "Commentary golfoploop," *OTAR* 40:2 (1955): 33–35

[27] T. Huitema, *Dijken* (Antwerpen: Kosmos, 1947)

The effect of the waves also increases with larger water depth. It was assumed that the power of the waves is proportional to the square of the water depth in front of the dike. Huitema therefore especially raises concerns for dikes along shallow waters, where the wave attack during high storm surges can be significantly more severe than with normal high tide.
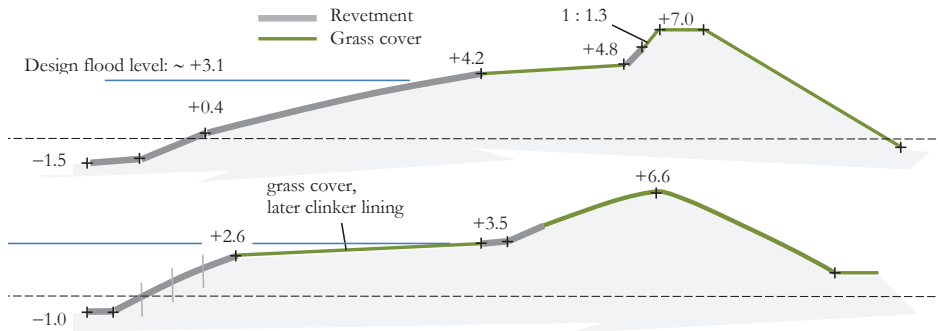
Figure 2-2   Typical profiles (with exaggerated vertical scale) of Hondsbossche (top) and Pettemer (bottom) sea defenses, design approx 1880 (Kuiper, 1955)

Reasoning from the water depth dependency he comes up with an ideal inverted S-shape for the outside slope (see Figure 2-3), where a uniform revetment has sufficient strength at all attacked locations. Apparently he assumes that the more horizontal, the stronger the revetment is.[28] He observes that due to the high outside shoulders or berms many Zeeland dikes have this shape, but for a different reason: to minimise overtopping.
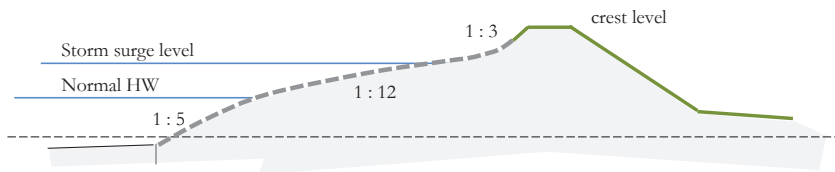
Figure 2-3   Idealised profile of sea side slope according to Caland and Huitema (Huitema, 1947)

The linear sections of the cross section are normally constructed in a slightly cylindrical shape, with a camber of 1/40 of the width.

2.1.3 Foreland protection

Foreland protection and prevention of sudden dike subsidence is vital to dike stability. Stone was used for the protection of the foreland well before it was used for the protection of the outer slopes. Foreland protection with dumped stone was first reported in 1480. Protection of eroded and instable foreland with osier and stone became common practice in 15th and 16th century. [29] The consumption of 'sink stone' gradually increased over the years. Stone

---

[28] A. Caland did the same.

[29] The central government of the Zeeland islands in Brussels provided necessary means for foreland protection, and did not contribute to solving the foreland erosion issue by abandoning land and construction of inland dikes. Also on other issues, such as gentler dike slopes, the construction of a shoulder and scour protection, the central government forced improvements in the dike construction and management. Source: Kool-Blokland, 2003.

from Belgian quarries, and also foreign types of stone (ballast of merchant ships, e.g. Granite from Norway) were procured and used in big quantities. The investments in stone protection in front of the dike remained high. Later, in the 17th and 18th century, the scour was resisted by fascine mattresses, constructed of bundles of osier, sunk down and held in position with 'accurately' dumped stone or heavy clay lumps. Only in the 19th century the foreshore defence was organised on a much bigger scale, more effective, and cheaper in the end. Protection of the steep underwater slopes with dumped stone on fascine and geotextile mattresses is still common practice.
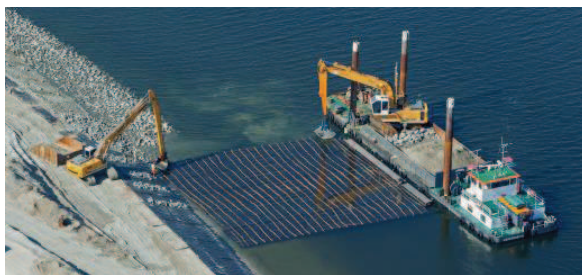
Figure 2-4   **Construction of stone ballasted fascine mattresses, Rotterdam area 2012, source: www.grienthouthandel.nl**

2.1.4   Slope protection

Early dikes were constructed on positions with a sufficient area of high grass-covered foreland in front of the dike. Consequently only rare high floods actually reached and attacked the dike. For the regular high waters no erosion protection was needed. Over the years the foreland either disappeared or grew as alluvial land. The latter was considered as valuable land and was diked in. As a result dikes became more vulnerable to wave attack.

For the protection of the seaward slope grass sods were used above water level and bundles of wicker or reed under water level. These bundles were connected to the dike body with straw brackets/stirrups, driven into the clay. Every winter and every summer new straw was applied. This method required a considerable volume of straw. Dike slopes which suffered from wave attack had additional protection by means mattresses of wicker, woven osier or other types of brushwood. The wicker was processed on site on the dike slope and was connected to stakes anchored into the slope. On severely attacked locations the wicker mattresses were strengthened with fascines, pine trunks, connected to small oak piles, driven into the dike slope. If necessary the wicker mattresses were also weighted with stones. The stones were dumped in between the brushwood structure. These practices were laborious and the required quantities of wicker material became problematic.

2.1.5   Slope protection with stone layers

During the 18th and 19th century the mattresses were gradually replaced by permanent stone layers. First the stones were laid over the wicker. Later the stones were placed side by side in close, regular order. There is no clear decade or even century to mention for the invention of stone-protected slopes[30].

---

[30] Vierlingh (1507-1579), one of the first authors of a hydraulic engineering textbook, has mentioned and drawn a Vilvoord stone slope already. His design may have been not successful, or certainly became not common in is

Figure 2-5   **Photograph of wicker mattresses as slope protection, source: (Kool-Blokland, 2003), pp 122**

The construction of stone revetments started with relatively small slope lengths, initially between 2 and 3 m.[31] Construction of full stone layers were big investments. Maintenance was potentially cheaper, although in many of the first stone dikes there was a continuous amount of work in strengthening, renewal and extension of the stone lining. With present knowledge it can be understood that – given the tide and surge level differences – this practice created very vulnerable structures.

Heavily attacked slopes as the North coast of Schouwen and the Westkapelle dike at the island Walcheren were also protected with what we would now call low palisades[32]. A number of vertical pile rows sticking out 1 metre, connected with walings were constructed in order to break the waves, just before they attacked the slope. On the Westkapelle dike this system was combined with a compartment system of pile rows[33].

---

time. In the 2nd half of the 17th century the placing of stones was reported for Schouwen. Source: J.L. Kool-Blokland, *De rand van 't land - Waterschapsgeschiedenis van Schouwen en Duiveland* (Middelburg: Koninklijk Zeeuws Genootschap van wetenschappen, 2003) Placing of Nordic stone was first reported in 1738. According to Caland, 1833, the stone layers were invented (in the 18th century) by Brunings. Source: W. Barendsen, "De zeedijk van zijn ontstaan tot het jaar 1730," *OTAR*:45: 9 and 46: 1 (1961)

[31] The stone slopes became longer also: first started with 2 to 3 m, in the 19th century the width of the revetment zone increased with 1 to 1.5 m. In the annual report of Schouwen of 1903 a quantity of 434,323 m² revetment above low water was mentioned, which complies with 5.5 to 6.0 m width, assuming a total sea dike length by then of 75 km.

[32] Around 1730 piles and timber structures suddenly were threatened by exotic worms that appeared to be able to eat so much timber mass, that the piles completely lost their strength. Over a number of decades this was a serious threat to the safety of the sea defenses. The replacement of structures with timber piles by structures with stone became necessary in the years after 1730. In later ages new structures were adequately protected against worms and beetles.

[33] See section 2.2.4

Table 2-1   Historic slope protection systems, source: Bolier, 1916

Type	Remarks	Service life
Reed and straw mattresses	summer and winter types	One season
Woven osier[34] revetment		4 years maximum
Nailed osier revetment weighted with stone		7 years maximum
Vilvoord*) or Lessin stone layer	irregular and round shapes	in order of increasing potential service life
Doornik stone layer	more regular shapes	
Basalt layer	column shapes	

*) Stone types were named after the quarry locations, see Table 2-2

In the 19th century the work of A. Caland (1789-1869) was of major importance to the dike protection in Zeeland. Caland intensified the replacement of osier revetments by stone revetments. He improved the existing transversal pile rows for protection of the foreland against longitudinal currents by lowering them. He also performed series of tests on stone linings. There seem to be attempts of increasing stability by the mass of the single elements, but also tendencies of increasing stability by working on slope angles, element shape and element interaction. In his days still mostly used was round Vilvoord stone, named after the quarry location in Belgium, but according to his recommendation preferably in selected batches of stone with straight faces. The first application of this stone type in a closed, pitched, revetment structure at Schouwen was in 1827. The main cause of the popularity of Vilvoord stone was its price. The large scale replacements with stone protection were a threat to contractors who cultivated and supplied the osier.

Figure 2-6   Photograph of a natural stone slope, patch work of block stone, Vilvoord stone and Basalt columns

Vilvoord stone revetments appeared to be not strong enough in heavy storms. A change towards an increasing use of basalt stone started. Basalt was expensive, but considered to be the best available stone. The intensified quarrying of stone and the better means of transport

---

[34] Osier is the flexible twig of the willow tree.

(railways) made basalt cheaper and affordable for the dike management.[35] Basalt became the common revetment stone after approximately 1860, but Vilvoord stone also persisted[36]. After 1875 all new stone linings were constructed with basalt and after 1892 the replacement of Vilvoord slopes with basalt slopes started.

In history the polder districts were in a permanent process of balancing the interest in flood safety and the potential for bearing the costs of this. As a basic law, the inhabitants bear the costs of the water defence of their area. However for any substantial damage repair and upgrading works sources outside the economic system of the polders were needed. Districts that had to appeal for this support very often, were given the status 'calamitous'. This created a complicated mutual dependency of the polder districts and the higher governments. It limited innovation and preventive maintenance. For the island of Schouwen the decision to become a 'free' and no longer a 'calamitous' polder district was taken in 1872. This decision was based on an own risk assessment. This moment more or less coincides with the introduction of basalt as the common revetment type. This emphasises the positive impact of the more reliable stone revetments on the economy of the polder. In Figure 2-7 the strong increase in Basalt pitchings starting from 1872 can be noticed.
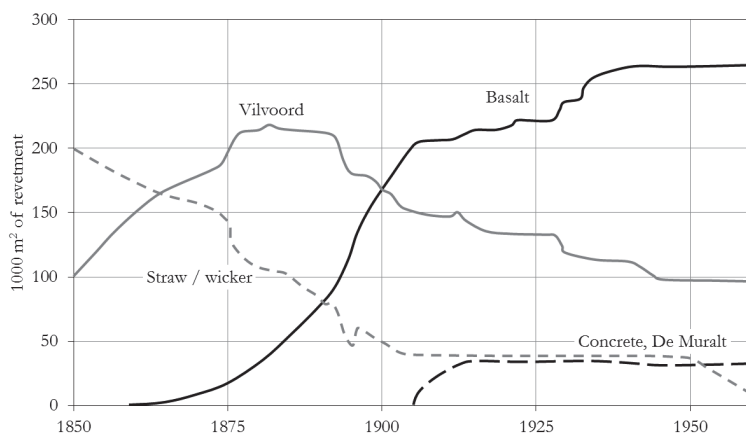
Figure 2-7   Dike protection systems of island Schouwen from 1850 to 1960 (source: Wilderom II)

2.1.6   Clay and grass covers

The clay cover on the dikes prevents saturating and as a consequence weakening of the soil mass of the dike body. This clay cover needs to be impermeable, cohesive and viscous or tough.

In Plasschaert, 1902[37] it is argued that osier revetments as well as stone revetments need to be based on a clay layer. The heavier the wave climate, and the bigger the chance that storms can last longer, the thicker the clay layer has to be. The clay layer is to be designed for a

---

[35] In order to minimise risks in the big investments in stone protection works the polder management of Schouwen acquired shares in German basalt quarries after 1872.

[36] A description of the development of the Westkapelle sea defence gives roughly the same information. Source: Q.M. van der Linde, "De Westkapelse zeewering" *OTAR.* (1955).

[37] L.R. Plasschaert, *Oever-, strand-, duin- en dijksverdediging* (Amsterdam: C.A.J. van Dishoeck, 1902)

scenario where the revetment fails and cannot be repaired during the storm. For the locations of the heaviest wave attacks (e.g. Westkapelle) a 1 m thick clay layer is mentioned.

Huitema, 1947 still describes the grass cover of the outer slope as a first choice for resistance against erosion. He suggests that people tend to make newly designed stone revetments broader/higher than needed only for the reason of being not aware or uncertain about the strength of the grass covers. Grassy clay layers are able to withstand wave attack if the slope is not too steep, and if the clay is protected against drying out. Boulder clay cannot be overgrown, so the first layer under a grass-cover needs to be of normal, granular clay. Grass covers with the ability to withstand waves can be considered above 0.5 to 1.0 m above average high tide. The slope needs to be 1:8, which as a side effect causes less wave run-up and better possibilities to raise the dike in the future. A stone slope reduces the clay consumption and the footprint of the dike. Huitema nevertheless calculates[38] that in a case with a toe at +0.50 m a grass dike is cheaper.

In a publication in 1959 Huitema[39] points out the historical development of grass dikes on high grounds, towards dikes with the toe under mean high water. Slope protection started with osier revetments, pile rows, timber sheet piles, even brick walls and dumped stone. When the pitched stone revetments became successful, the costs of installation of slope protection increased significantly. In many but not in all cases this also led to a spectacular decrease of maintenance costs and to an increase of safety. In his view there was an overinvestment in many places where a grass slope would have been sufficient. He even suggests that the high costs of slope protection put pressure on necessary investments in raising the crest level and maintenance of the inner slopes. Tendencies to also cover the inside slope with asphalt are also a signal of underestimation and lack of attention to the performance of a well-conditioned crass cover.

Clay covers, or clay with grass covers as a revetment are studied in (De Visser, 2007). All available experiments of wave resistance of clay are up to a maximum wave height H_s of 1.5 m. Most of the tested slopes are 1:4 or steeper. Average clay layers (0.8 to 1 m) can resist these condition 3 to 7 hours dependent on the clay quality. Older clays perform worse. Structured clay, due to vegetation and shrinkage and cracks also perform worse. In the models the horizontal erosion path seems decisive for the survival time, which suggests that gentle slopes with a similar cover thickness perform better. German studies[40] recommend constructing thicker clay covers on higher dikes for the reason of increased water head in the cracks, namely $d_c = 0.6 + 0.125\ h_{SWL}$, not dependent on the slope angle.

Along the German and Danish coasts in the German bight and along the Baltic Sea grass dikes are still quite common, mostly with outside slopes of 1:6 or 1:8 or less. The grass cover is seen as a structural element that needs verification under design conditions. In 2009 large scale tests[41] were performed on a 1:4 slope with a 0.8 m clay-grass cover. The wave height

---

[38] The rates used are: ƒ10 for a m² stone revetment (all in) and ƒ1.25 for a m³ earthwork.

[39] T. Huitema, "De grasmat op waterkerende dijken," *OTAR* 43:10 (1959): 191

[40] W. Pohl, "Die Bemessung der Kleiabdeckung von Deichausenboschungen. Ein Konzept zum Entwurf gleichermassen sicherer wie wirtschaftlicher Seedeiche," *Tagungsband zum HTG Kongress* (Bremen, 2005), 129–138

[41] T. Piontkowitz, "Erograss - large-scale investigations of grass cover faillures at sea dikes," *Hydralab III Jt. user Meet.* (Hannover, 2010) Ibid. T. Piontkowitz and K. Christensen, *Erograss - Failure of grass cover layers at seaward and shoreward dike slopes - performance, results and conclusions* (Lemvig, Denmark, 2012) At $H_s = 0.9$ m, the wave period T_{m-10} was around 4.3 s. the water level at the toe was 3.3 m, the foreshore slope 1:40.

was varied and increased during the tests up to a value of H_s of 0.9 m. The accumulated duration of testing was 11 hours. The clay layer was significantly damaged. Local wash out of soil and formation of clay lumps were observed. The clay layer was not fully eroded.

Grass covered clay layers can be a reliable slope protection in cases with $H_s < 1$ m. This criterion can also be used to define the required top of the revetment.
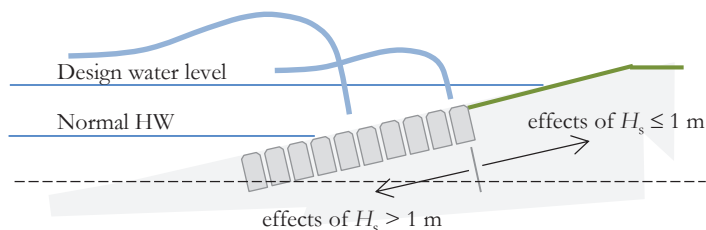
Figure 2-8   **Definition figure for range of applicability of grass slopes**

2.1.7 *Alternative to stone slopes: closed concrete and asphaltic revetments*

Pattern-placed revetments cover many kilometres of man-made coastal structures in the Netherlands. Elsewhere block revetments do exist also, but there is more completion from randomly placed rock slopes, rock slopes partly bonded with concrete and with in-situ slab systems in general[42]. Slabs include closed concrete slabs, concrete mattresses with drainage openings and hydraulically closed asphaltic slabs.

Protective asphaltic[43] revetments became more popular in the Netherlands after 1953. The advantages are that large surface areas could be covered relatively fast and cheap. Another advantage is that a watertight top layer could be applied on and over the crest, which allowed more overtopping and a lower crest height. The toe of the closed asphalt slab should be not lower than normal high tide, in order to create sufficient drainage under the asphalt layer. Like open revetments asphalt has the ability to follow settlements with a certain flexibility.

The main threats for failure of an asphalt revetment are (1) quasi static overpressure under the lining, (2) wave impact, which is high on a hydraulically closed surface and (3) deterioration of the material due to adverse effects of the environment. Edelman et al, 1961[44] presented a comprehensive guideline which reflects the status of knowledge shortly after 1953. Over the years knowledge of asphalt revetments has increased[45] and also has contributed to insight in open revetments.

---

[42] K. McConnell and W. Allsop, *Revetment systems against wave attack – A design manual* (Thomas Telford, 1998); Bundesanstalt für Wasserbau, *Empfehlungen G 2002 - Seedeiche und Tidestromdeiche* (Die Küste, 65 EAK (2002 korrigierte Ausgabe 2007))

[43] Asphalt was used as replacement of clinker road surfaces from late 19th century.

[44] T. Edelman, *Stabiliteit van dijkbelopen*, 1958

[45] P.A. Van de Velde, E.H. Ebbens, and J.A. Van Herpen, *The use of asphalt in hydraulic engineering* (TAW/COW report TR1, 1985) and E. Schonian, *The Shell bitumen hydraulic engineering handbook* (London: ICE Publishing, 1999)

2.2 Early guidelines for stone slopes

2.2.1 Aspects of functional design

In his text book on dike construction[46] Huitema defines the primary function of stone revetments as to prevent the dike soil to be eroded, to move or disintegrate. The revetment itself must stay in place under wave action. Also wash out of soil through the revetment top layer must be prevented. If this happens, the revetment will be undermined and will either collapse or settle unacceptably. He recommends that, because of these risks, the underlying soil/clay cover should be dimensioned as if the revetment was not there.

This is perfectly in line with the *Schouwse Voorwaarden*[47], 19th century specifications of traditional dike works, as they start with the instruction that the outer slope of the sea wall should first be raised with the best available clayey soil from the salt marches. Then they require a 1½ cm layer of wheat or rye straw or a 2 cm layer of reed to be installed on top of the clay. A sub-layer of average thickness of 20 cm was constructed of broken brick stones or rubble with the size of a quarter of a brick. The revetment stones were placed on top. Huitema also describes the practise of building up a system with an interface layer of wicker and a sub-layer of rubble[48] underneath a soil-tight top layer. This structure is a good predecessor of the modern top layer and filter layer, sometimes supplemented with geotextiles, although insight in the function of the permeability or the top layer was lacking in those days.

2.2.2 Solid pitching

The execution of the pattern-placed revetment themselves was bound to a number of general technical instructions. All stone layers must form a strong structure with a flat, level top surface. A stable, immoveable grid structure amongst the stones must be achieved. To that purpose the structure should not be relying on the joint filling. Several authors[49] emphasise the principle of execution of the stones in a close pattern. Thus the self-weight of the stones, as well as the interaction will resist movement.

The instructions include guidance for working with several types of stones, and it is implicitly clear that with some of the stone types the target of a strong interconnecting layer is hard to achieve. For Vilvoord and Lessin stone the use of rubble and stone spalls is necessary, which makes them of course vulnerable to movements. The difficulties in constructing well placed, immovable slopes is according to Huitema most striking with the *Drentse* and Nordic stones, which have flat top surfaces, but round sides. The stones touch each other only at a small portion of the height, and tend to rotate easily in wave action.

Several remarks of Huitema seem to reflect proper understanding of the conditions for adequate beam action of the revetment layer:

---

[46] Huitema, *Dijken*

[47] *Schouwsche Voorwaarden – behorende bij de bestekken voor de uitvoering van werken ten laste van het Waterschap Schouwen* (Zierikzee: De Mooij & Mommaas, 1891)

[48] Minimum and maximum values of the rubble layer were given, supplemented with the recommendation that if during construction the thickness tends to become less than 15 or more than 25 cm the soil profile needs to be adopted.

[49] M.B.N. Bolderman and A.W.C. Dwars, *Waterbouwkunde*, 2nd ed. (Amsterdam: L.J. Veen, 1919)

- Best placed slopes are with stones of a top surface smaller than the square of the height and with the sides perpendicular to the top surface.
- Variations in stone height need to be prevented. The strength of the slope in terms of stone height is determined by the smallest stone rather than the average.
- It is observed that of stones types with equal thickness, the type with bigger top surface show damage in less severe conditions. The uplift pressure on the bottom surface of a bigger stone is not easily balanced by the grip of the neighbouring stones.
- The weight of the smallest single unit is often defining the strength of the slope. Contrary Huitema observes that slopes that consist of big heavy units and small intermediate contact area (e.g. Nordic stone) often perform worse than slopes constructed with small units with maximum contact area to adjacent units.
- Huitema also states that a high specific gravity of the elements contributes to the strength, but is less important than good stone shape conditions. The specific gravity varies from 2000 to 3000 kg/m^3 for bricks and basalt respectively.
- Economical design requires adapting the strength of the applied revetment according to the position on the slope. The highest strength is required between high tide and the highest flood level. Above and below this zone a less strong slope can be applied. For the transition between the stone revetment and the grass slopes high up, bricks (clinkers) can be applied, first a section with bricks top-down, and then a section of bricks on their side (see Figure 2-9). This transition is usually applied in the Zuiderzee projects after 1916, including the *Afsluitdijk*. On Zeeland dikes this transition coincides with the shoulder.

With regard to the top-layer Huitema seems to be focussed on tightness rather than on certain permeability. The filling of joints with stone spalls improves the tightness of the slope. As ideal material to obtain a tight slope he suggests concrete can be used, although he mentions that a concreted slope would become too stiff to follow any settlement or erosion, which can result in hollow spaces under the revetment.

The various available stone types are named after the location of the quarries, primarily in Belgium and Germany.

Table 2-2   Details on stone types, source: *Schouwse Voorwaarden*, 1891 and Huitema, 1947

Stone type	Origin, dimensions, shape	Stone weight
Vilvoord stone	Rectangular or trapezoidal shape Minimum 25 × 22 × 8 cm Maximum 60 × 40 × 20 cm Stones places on their longest side Average stone layer thickness 25 cm	min 8 kg
Doornik stone	Stones applied below high tide because of risk of chipping of the surfaces above water. Sorted stone (block stone) Square shape	50 – 200 kg
Lessin stone	Sorted stone with sufficiently flat surfaces Square shape Stone layer thickness 20 cm	25 – 40 kg

Stone type	Origin, dimensions, shape	Stone weight
Block stone	Either Vilvoord, Lessin or Doornik stones Regular rectangular shape of 25, 35 or 45 cm thickness, length 30 to 65 cm and width 20 to 55 cm. Applications in the Zuiderzee projects. Applied flat, at least 25 cm thick. Sometimes applied in flat and standing rows by turn.	Min 40 kg
Nordic or *Drentse* stone	Stone type granite Stone with rounded sides, big stones were cleft, providing flat surfaces Nordic stones arrived as ship ballast. *Drentse* stone was collected as boulders. First applied as dumped stone along dikes in the northern provinces. After 1800 also applied in pitched slopes. Mostly > 50 kg	
Basalt	Regular pentagonal or hexagonal prismatic column shapes Quarries along the Rhine river in Germany Column width between 12 and 35 cm Available column heights in 20 to 45 cm (step 5 cm) Stone batches of a certain height are bound to +/− 5 cm, where 2/3 might be longer and 1/3 might be shorter than the nominal column length.	Min 20 kg

2.2.3   Toe structure

Stone slopes need a solid support at the bottom edge. At steep slopes the stone weight tends to be supported by forces at the bottom edge rather than the friction on the underlying layers. Huitema also notices that under severe wave action the compression at the toe becomes 'quite important'. If the toe deforms to the seaside the stones will loose their coherent placing and can move.

The specifications in the *Schouwse voorwaarden* require the revetment structure to end in a trench, providing a proper transition between the stone slope and the foreland. In the trench a row of oak piles was installed: 1.6 m long, for circular sections: periphery 30 cm, for split sections: 75 cm² cross sectional area, 45 new or 50 old piles for every 10 m.

Huitema, 1947 mentions among the common ways of construction of toes a timber sheet pile wall (1.8 m long)[50]. The use of a (small) sheet pile wall enables to start the slope somewhat below low tide, because of the water retaining capacity. Huitema judges the practice of a starting the slope against the toe with a small horizontal berm of 0.5 to 1.0 m as better than just starting the slope against the pile row. In case the slope starts in a bank protection of rock a row of heavy toe stones is applied as a transition.

Plasschaert, 1902 also recommends a toe structure of heavy Doornik stone. Any local ditch in the foreland will weaken the resistance of the toe and will cause loose stones on the slope.

2.2.4   Limiting damage propagation by making compartments

In case a number of stones are swept away from the slope, the remainder of the slope in the close vicinity will lack coherence, and damage may propagate quite fast. For that reason in Zeeland slopes were divided in compartments separated with pile rows. Bolderman and Dwars (1913) describe this common practise of strengthening the basalt slopes. The system

---

[50] Huitema requires at least a timber plank to prevent erosion through the open pile row of the toe.

consists of longitudinal rows of 1.6 m oak piles, sticking out 0.4 m[51], spacing 2.5 m, with intermediate 1.2 m oak piles, without (or with 5 cm) protrusion, hammered in the revetment creating compartments as a potential damage limitation. For the same reason pile cross rows were applied every 10 to 20 m in longitudinal direction. A row consists of 4 or 5 piles per m[1]. In early times those piles were combined with run-up and wave attack resisting palisade works (see Figure 2-10).

2.2.5   Brick stone

Brick stones and later concrete were alternatives to natural stone. Brickstone is not affected by the sea water. Also wear and frost resistance can easily be obtained for the more solid material grades. In this respect bricks are potentially even better than natural stone types because natural stone types have initial faults, and may sooner or later crack, spall or crush. Bricks are not applied widely. Huitema, 1947 suggests that this is due to reluctance of the dike management to apply small units. Bricks are however not only available in small units. Caland constructed slopes with specially produced bricks of 100 × 100 × 50 cm and also with bricks of 100 × 75 × 50 cm applied on their side. In 1825 and 1828 the use of these heavy bricks was recommended by the governor of Zeeland. Slightly smaller bricks were more common, such as the 40 × 40 × 20 cm bricks from the *Corman* factory near Nijmegen[52]. Huitema, 1947 reports a first trial (1808) with these brick blocks (61 kg) at several locations. At one location in Zeeland this slope type still lasts more than 100 years without damage and without maintenance. Huitema also notices the existence of 40 × 30 × 20 cm blocks. They allow application in three different slope thicknesses. Despite these good experiences the brick blocks are not used often. The brick blocks were expensive in production.

Smaller units are applied widely in the form of clinkers on their side or in top-down position (see Figure 2-9), mostly in the upper parts of the slopes, but occasionally also in lower parts, where they perform well. The clinkers are placed on the bare soil and washed in with silt.

Figure 2-9   **Rectangular stone, block or brick types applied in flat position, 'on their side' and 'top-down'**

2.2.6   Yes or no granular base layers

In a paper dating from 1958 Huitema[53] discusses the granular base layers. Most stone revetment types first have a levelled base layer and a rubble layer that was used to adjust the vertical positions of the uneven stones, creating a flat top surface. The layers do not seem to have an intended filter function. Huitema suggests that omitting the granular layers would

---

[51] These protruding piles are considered disadvantageous by Huitema, being an obstacle during the construction of a tight and strong stone slope.
[52] M.H. Wilderom, *Tussen afsluitdammen en deltadijken – deel II – Noord-Zeeland* (Middelburg: Littooij & Olthoff, 1964)
[53] T. Huitema, "Glooiing van zuilenbasalt," *OTAR* 43:4 (1958): 59

improve the revetments, with the argument that using basalt columns of unequal length this will result in a rough top surface, which decreases the run-up. Washing the revetment with clay and silt would create a strong revetment. He states that brick revetments on clay, require 1.5 times less thick top layer thickness compared to a traditional basalt structure on a granular base layer.

2.2.7   Maintenance and damage repairs

In his textbook[54] Huitema also pays attention to maintenance of sea dikes. He emphasises the need for immediate repair of stone revetments after storm damage in the winter season. Holes must be closed. The upper edge of a hole can be supported with steel pins. Repair works under the line of high water must be finished within one tide. If – due to the limited time – repair of underlying clay layers, osier (if any) and rubble layers is not possible, simply closing with rubble and re-pitching is a second option. A last option is dumping rubble and stones in the hole and adding fixation with osier. Repair of settlement of the slope can be delayed to the spring.

The use of the word 'crust' that can be found in 19th and 20th century textbooks for the stone lining, is an expression of the brittle, non-ductile behaviour of the structure. The brittle nature of the protection of the outer slope with stones is also illustrated in his recommendations for emergency repairs and averting the wave attack on the unprotected slopes. The use of sailcloth ballasted with sandbags, the use of straw bales and bundles of osier against (further) erosion of the edges of a breach in the outer slope is recommended. These materials had to be permanently available on regular, short distances along the dikes.

2.3   Developments in revetment and dike design in the 20th century

2.3.1   De Muralt

Jhr. R.R.L. de Muralt (1871-1936) was engineer of the district water board of Schouwen from 1903 to 1913. When he started in this position the island of Schouwen had 41,000 m² of osier revetments, 6,000 m² rubble slopes, 155,000 m² Vilvoord stone and 200,000 m² basalt stone revetments.[55] The change from osier to stone revetments was a still ongoing (see Figure 2-7) and very costly project. De Muralt therefore started to use innovative and cheap concrete solutions. Before De Muralt a number of tests and pilot projects were performed with concrete sea defence structures. De Muralt introduced the *trapglooiing* (stair slope), which consists of reinforced concrete T-shaped beams on slope and small horizontal concrete slabs in between. He also created revetments on low dams consisting of bigger concrete slabs, in overlapping positions.

During a big storm in 1906 numerous kilometres of dikes proved to be too low. The floodwaters overran the dikes and threatened the stability of the inside slope. De Muralts solution was an L-shaped reinforced concrete wall on top of the dike crest, meant to resist overtopping. The solution with flood walls was a cheap and fast provision for extra dike height avoiding a larger footprint. Increasing the width of the dikes was problematic. Widening to the seaside would mean destruction of capital because of the expensive stone

---

[54] Huitema, *Dijken*
[55] Source: Kool-Blokland

and foreland protections. Widening to the landside would consume valuable land. De Muralt's floodwall solution spared trouble and was applied widely over Zeeland. Between 1906 and 1925 25% of all main sea defences in Zeeland were equipped with floodwalls. The walls were also applied in Belgium and France, and more recently in the South American colonies and in Bangladesh. The floodwalls in Zeeland performed well, but were unable to resist the flood of February 1953. Most of the floodwalls were buried in the dike reinforcements after 1953.

The cast-in-situ concrete applications suffer from harmful effects of seawater on the fresh concrete, as (Huitema, 1947) states. At first this was anticipated using watertight formwork. As this is very laborious and expensive, the De Muralt structures at a later stage were only applied a little above high tide. Precast concrete elements have the advantage of not exposing the immature concrete to the sea water. The De Muralt *trapglooiing* indeed exists in partly pre-cast versions.

For the upper dike slopes De Muralt designed a light weight concrete lining solution, the *spijkerglooiing* (nailed slope). The De Muralt revetments survived many heavy storms, and performed very well compared to traditional stone revetments. The slopes however proved to be vulnerable to undermining and needed regular inspection and replacement in case of undermining or settlement.
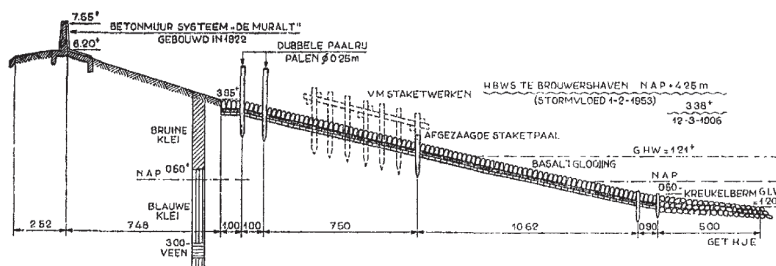
fig. 189. Dijksverdediging aan de Langendijk, noordkust Schouwen langs het Brouwers-havensche Gat. De laatste staketwerken zijn in 1958 opgeruimd.

Figure 2-10 **Cross section of dike at the North coast of Schouwen (Wilderom, 1964), pp 218**

2.3.2 *Closure of the Zuiderzee*

The Zuiderzee projects were put forward after the flood of January 1916. According to (Huitema, 1947) most, if not all of the dike failures were due to overtopping or overflow and erosion of the steep inside slopes of the dikes. The habit of making the seaside slope gentler by dumping rubble in front of the dike increases the seepage since a bigger portion of the cross-section of the dike has a very high permeability. This appeared a cause of damage in 1916.

A series of large scale polder projects was undertaken. The Wieringermeer polder project was the first. In 1932 the 32 km long Afsluitdijk was completed. This closure dam project changed the tidal, salinity, and surge risk conditions of the IJsselmeer area completely. The dam itself functions as a storm surge barrier. Since there was a lot more freedom in design than with slope replacement projects, the Afsluitdijk can be considered as having an – at the time – ideal revetment design. The design flood level was +3.5 m N.A.P. The outside slope is 1:4. The design shows an approach with distinct solutions per zone. In the zone between +2.0 and +4.0 m a heavier revetment stone was applied than below and above. Below a
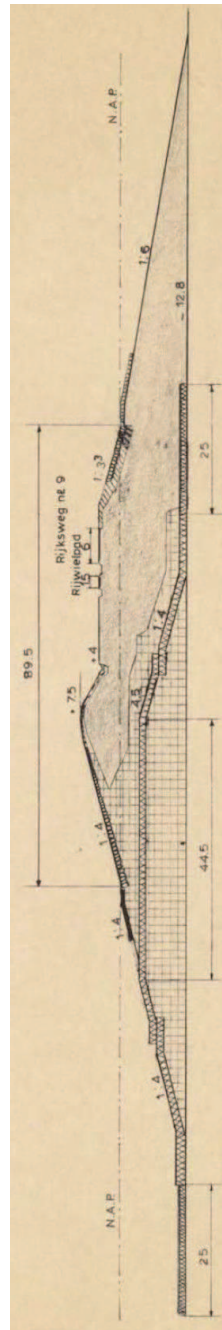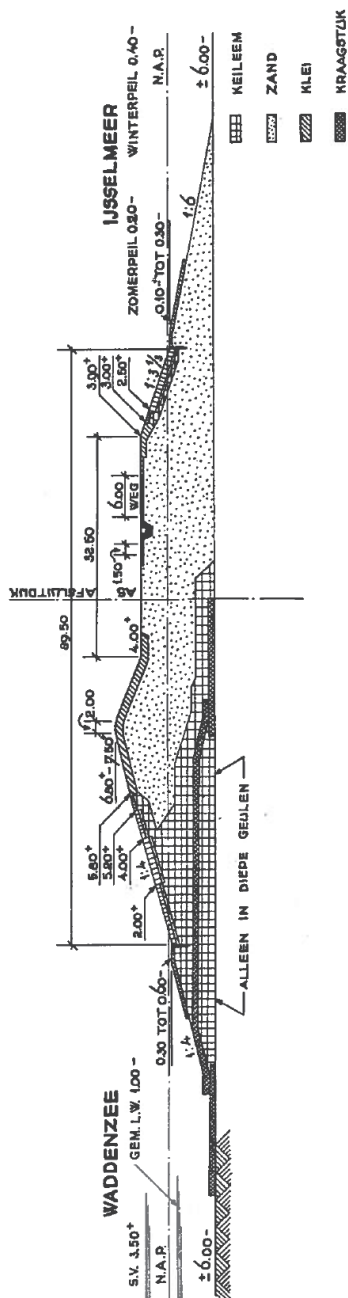
Figure 2-11 **Cross sections of Afsluitdijk, left the original cross section, source:** *Gedenkboek twee eeuwen waterstaatswerken* (Amstelveen: Kramer, 1959) **and right the 'improved' cross section, source:** C. van der Burgt, *Literatuurstudie blokken bekledingen*, 1969

Design of pattern-placed Revetments

similar basalt structure but of lesser thickness (smaller column height) was applied. Above +4.0 m a clinker slope was applied. It was reported that these design sufficed for years. Following the experiences during the storms of February 1953, with HW 3.70 – 3.73, and December 1954, with HW 3.55 – 3.86, the basalt stone on the weakest spots were replaced by 0.4 to 0.5 m high columns. Also the top edge line of the clinker slope was extended from +5.8 to +6.25 m. The load conditions on the dam vary from place to place due to the varying water depths in front of the dam. During both storms overtopping occurred, but the dam performed well. There is a complete 1 m thick clay cover over the crest. Up to the design flood water level of +3.5 m there is a clay core.

During later replacement works of the revetment it was decided to improve[56] the design and as a result the largest stone height was applied just above MSL and decreasing stone heights are applied higher on the slope (see Figure 2-11). It can be seriously questioned whether this really is an improvement (see section 3.1.5 and 3.3).

2.3.3 *Dike strengthening after 1953-flood*

Like earlier storm surges the historic storm surge of 1953 made apparent that many dikes were too low; this time with devastating consequences. Almost all reported dike failures[57] were caused by overflow and overtopping, causing damage to the inside slope, which initiated a breach. The inside slopes were very steep and any significant erosion led to geotechnical instability of the complete dike body.

In 1958 the Delta Act was accepted. This meant that dike designs were to be based on a safety level defined for a probability of inundation, rather than on water level records. Also it was decided to construct closure dams between the isles of the delta area. Still many dikes had to be raised and strengthened. Due to the required speed and due to shortage of clay, the dike strengthening was often performed with an additional sand mass behind and over the old clay dike. The sand core was covered with a clay layer. In many cases the crest of the old dike became a shoulder in the cross section of the new dike. Using this method the existing revetment was maintained. In quite a number of cases stone revetments were only projected in the area of the normal tide, in many other cases the revetment was extended in width, also covering a part of the new, longer slope. For the newly constructed revetments predominantly 20 or 25 cm thick flat concrete blocks were applied directly on the clay. Also asphalt was introduced as a revetment type. Other hydraulically closed revetment slopes were sometimes constructed by filling the voids between old Vilvoord stone slopes with concrete.
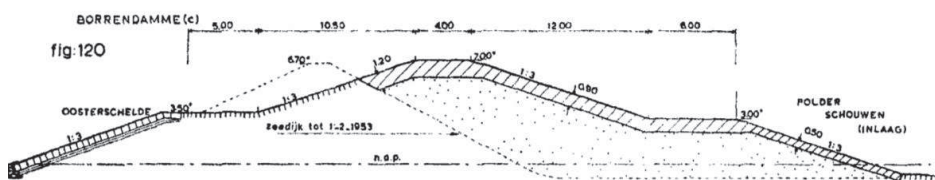
Figure 2-12 **Typical cross section, source: Wilderom, 1964, pp 273**

---

56 J. Th. Thijsse, *Een halve eeuw zuiderzeewerken 1920 - 1970* (Groningen: Tjeenk Willink, 1972)
57 Rijkswaterstaat and KNMI, *Verslag over de Stormvloed van 1953* J.A. Exalto, "Algemene beschouwingen omtrent dijkbouw waartoe de ramp aanleiding heeft gegeven," *Polytech. Tijdschr.* 9:31–34 (1954): 691–694

The Delta commission produced an extensive report in 1960. The dike construction guidelines[58] in the report of the Delta commission can be summarised as follows:

- Dike crest heights must follow the probabilistic flood level (nationally defined), plus an excess height determined by local meteorological conditions, wave run-up, expected subsidence, subsidence and settlement of the dike body. There is no prescribed crest height, there is freedom of slope design.
- Stability of the dike body should be determined addressing pore pressures in the sand core and their effect on the stability of the clay cover.
- Slope protection of grass is still recognised as adequate. The many failures were deemed due to the low crests and the steep inside slope, not due to performance of grass covers as such.
- For asphalt linings investigations and gaining experience is recommended.
- An undamaged and not ruptured condition and water tightness of the clay cover is required
- Measures to decrease the wave run-up on the outer slope must be taken
- On the vertical position of the berm. In case the berm is well below the design flood level, the berm could better be omitted
- In case of a stone or concrete element revetment, these need to be the heaviest between the design flood level and half the wave height below
- The revetment weight near the toe and the properties of the toe structure need to be suitable to accommodate water overpressure under the lining
- Inside slopes not steeper than 1:3
- Even sufficiently high, theoretically non-overtopping dikes need to be designed as were the conditions worse, e.g. with a sufficiently wide crest and a well-conditioned inside slope

Although there were a few near-misses[59] the 1953-flood did not cause dike breaches initiated by revetment damage, and has maybe thereby not boosted improvements in revetment design. Dike design, revetment design and revetment construction were also not questioned or further developed during the years of implementing the Deltaplan[60]. Thus – with hindsight – it can be stated that the decision to design for a less frequent and more serious storm surge was not implemented in the revetment designs.

2.3.4 New concepts of revetments

Filter rules were formulated by Terzhagi in the 1930's and have led to innovations in the revetment structures only after approximately 1950[61]. Between 1950 and 1980 dozens of

---

[58] T. Huitema, "Voorstellen van de Deltacommissie, richtlijnen voor dijkontwerp," *OTAR* (1962)

[59] See footnote 4 on page 2.

[60] The periodical Deltawerken, published during 25 years, does not pay any attention to stone or concrete revetments. Exceptional weather conditions are reported and are used for validation of models and assumptions. Various storm seasons are discussed (1965, 1972, 1973). Dune erosion is reported and analysed, but there is no report on damage to dike revetments.

[61] E.g. Huitema, 1947 is very comprehensive on the structures, but does not mention them.

variations in concrete revetment types are developed[62]. The types differ with respect to many properties. The important differences are in: closed or open systems, block or column shapes, interlocking of joints, smooth or rough run-up properties and methods of placing.

Apart from new types with hydraulically open top layer a number of 'new' layered structure concepts were invented and applied. In one of the structures (#2 in Table 2-3) open top layer systems are combined with a gradually less open, but still permeable, layered system, where the sand body of the dike is the least permeable. In that structure there is no clay layer or clay core. This structure is not suitable of resisting permanent water level differences. In most of the new concepts the thickness of the intermediate granular layer seems to have decreased compared to traditional structures.

Clay layers have the function of preventing soil to be washed out through the open revetment (filter function), providing extra safety in case of failure of the revetment, making the dike watertight and thus limiting pore pressures during high tide.[63] Clay layers also have advantages in the temporary stages of construction of the dike. Traditionally a granular fill layer is applied in between the clay and the blocks. Alternatively, the blocks are now applied directly on the clay or on bituminous sand. In practice this concept (#5) appeared to be problematic, since the clay surface was nowhere flat. Voids could occur> They can eroded quickly and threatened the stability of the blocks.

Table 2-3   Selection of layered revetment structure concepts (after: Glerum and Wolsink, 1984)

#	1	2	3	4	5	6
Top layer	Open joints 0.2-0.5 m columns		Continuous with small joints 0.15-0.25 m concrete blocks			closed grass over-grown open blocks
Bedding layer	permeable 0.1 m granular filter *					
Cover layer on core	impermeable 0.8-1.0 m clay	permeable 0.5-1.0 m mine stone *	impermeable 0.8-1.0 m clay	permeable 0.5-0.8 m mine stone *	impermeable 0.8-1.0 m clay	
Core material	sand		sand or clay		sand	

* with filter cloth / geotextile at interface

2.3.5   Function of under-layers of an open top-layer

The experiments with the build-up of layered systems as described in the previous section should not give rise to underestimating the importance of the role of the sub- or under layers. The clay core or clay cover of a dike blocks the water from seeping and draining trough the dike. The top-layer or cover layer protects against wave attack and erosion by waves. The top-layer is commonly designed as to maintain it shape. The individual elements of the top-layer must be stable under wave attack. The sub-layer directly below the top-layer

---

[62] A 1984 manual and especially the comprehensive background document provide a summary of available types of concrete revetment. The studies are performed in the framework of CUR-VB, a cooperation of the research committees on water defences and the Dutch concrete society. Glerum and Wolsink, *Achtergronden bij de leidraad cementbetonnen dijkbekledingen* J.F. Agema et al., *Betonnen bekledingen op dijken en langs kanalen*, ed. J.F. et. al. Agema (VNC, 1986)

[63] Glerum & Wolsink pay quite some attention to the required viscous, plastic and shrinkage properties of clay.

has a filter function avoiding migration of overlain fine material to move out, and also has a function in drainage of the wave run-up and equalizing the hydraulic heads of the wave action above the hydraulically open slope. This function is crucial to the concept of load-reduction on the top-layer as explained in sections 3.1.1 and 3.4. The sub-layer also levels the unevenness of deeper layers and provides a flat surface for easy mechanised construction of the top-layer system.

Failing functionality of the sub-layers potentially leads to increase of exposure of the top-layers and loss of stability. A wrong design of the thickness and permeability properties of sub-layers may leads to build up of pore pressures and to sliding of the revetment structure and/or to geotechnical instability. The distinguished layers usually increase in permeability properties from inside to outside.

2.3.6 Reported damage cases

Damage to pitched revetments has been reported in various sources. A brief summary[64] of numbers of historic dike failures gives 373 reported dike failure events out of an estimated total of 1735 dike failures. 6% of the reported failure events are labelled as caused by erosion of the revetment or erosion of the outside slope.

Revetment damages without consequential dike failure have occurred in bigger numbers. The Westkapelle sea defence e.g. has been heavily damaged by war activities in 1944. The closure works of 1945 are well known, but also many temporary revetment repairs and subsequent storm induced revetment damages are reported[65]. There was shortage of basalt columns, and the original paling works were missing and not re-installed. Damage area's caused by February 1946 storms amounted to 70,000 m^2 of revetment, combined with 60,000 m^3 of eroded soil.

source: http://rens.vanadrighem.com/

source: http://www.voornewiki.nl

Figure 2-13   Photographs of damage Brielse dam, February 1953

In 1953 a limited number of pretty serious revetment damages have been observed.[66] The cases did not lead to dike breach thanks to intervention with emergency repairs during the

---

[64] S. van Baars and I.M. van Kempen, "The causes and mechanisms of historical dike failures in the Netherlands," *E-WAter* 2009:6 (2009) reporting between AD 1134 and 2006.
[65] Linde, "De Westkapelse zeewering"
[66] Rijkswaterstaat and KNMI, *Verslag over de Stormvloed van 1953*

storm. The cases got understandably less attention compared to the numerous cases that actually led to breaches and inundation.

The Brielse dam and the Afsluitdijk were both relative young designs, dating from 1950 and 1932 respectively. The crest level was apparently high enough to avoid damage at the inside slope.

source: http://www.archiefhvw.nl (Historische Vereniging Wieringen)

Figure 2-14   **Photograph of damage to the dike and the emergency repairs at the North side of Wieringen, near Hypolytushoef, February 1953**

http://data.collectienederland.nl/page/aggregation/nimh/2109-P102-C42-027

Figure 2-15   **Aerial photographs of serious damage to the outside slope without breaching or inundation, location unknown, February 1953**

source: http://www.archiefhvw.nl (Historische Vereniging Wieringen)

Figure 2-16   Photographs of damage to stretches of the Afsluitdijk near Wieringen, February 1953

After 1953 a number of moderate storm surge conditions have occurred. Damage came about specifically at transitions, below a restraint, and also concrete blocks on bare clay performed worse than expected. In the clay small grooves were formed due to erosion of seepage water. Little channel systems were created that transferred uplift pressures and pushed the blocks out. This failure mechanism occurred at relatively mild storm conditions.

Between 1975 and 1991 a total of 725 cases of damage to revetment was reported[67]. 85 of the cases concerned concrete top layer elements, of which 71 block revetment and 14 column revetment slopes. Small damages are often reported near transition structures, where the element interaction is discontinued.

Table 2-4   Size of damage cases

Damage area [m²]	No of reported cases
0-10	59
10-100	20
100-1000	4
1000-10000	2 *)

*) a 1300 m² damage to a blocks on clay revetment due to erosion of the clay (1978) and a 10,000 m² damage to the new Basalton column slope of the Maasvlakte (1988), see section 4.3.3.

The issues of rarity of the load conditions, uncertainties about the permeability properties, uncertainties related with construction of traditional revetments and the unknowns in the newer developed types returned in these damage cases. Exactly these issues were the subject of research after 1980.

2.3.7   Concrete revetment element types

A number of concrete element types that were developed and are at the moment no longer used are listed below.

–   The precast De Muralt *spijkerglooiing* was not recommended for sea defences. It consists of concrete tiles 40 × 40 × 6 or 8 cm with rebate sides, alternately fitted with a small concrete spike, with 8 × 8 × 40 or 50 cm dimensions, pinned into the soil.

–   In 1936 M. Leendertse improved the stair slope of De Muralt. He used 50 × 50 cm concrete tiles, placed in overlap pattern with a rebate. The system was easier to install, had a better flexibility for settlement and a better resistance against wave run-up.

–   J. Streefkerk developed the *diaboolglooiing* (1941), concrete blocks with a swallowtail interlocking.

–   In 1954 C. Pieters developed the *Pit*-system, hexagonal blocks with an elevated top surface against wave run-up.

–   Haringman-blocks, a 50 × 50 × 25 cm concrete block with a dented top surface, became very popular after 1953. After 1997 they were re-used on their side.

---

[67] M. Klein Breteler, *Handboek voor dimensionering van gezette taludbekledingen* (CUR / TAW report 155, 1992)

Between 1997 and 2010 almost all new slopes are fitted with Basalton or Hydroblocks.

- Basalton was developed in early 1980s by J.A. Kant and is – as the name suggests – a concrete imitation of basalt columns. Basalton consists of an irregular pattern, which is in effect created with only three different pentagonal or hexagonal prismatic elements.

- The Hydroblock is developed around 1995. Hydroblock slopes consist of a one size, fish shaped element. It is oriented in rows.
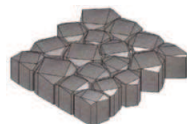
Both systems are available in various heights and densities of concrete. Both systems are hydraulically relatively open and leave a 12 – 15% open area. Installation can be mechanised. Both systems are also suitable for application in bends.

The Ronaton and Hillblock systems are among the developments after 2005.

- The Ronaton block of H. Pannekoek is a hexagonal block that is not a prismatic shape over its full length. It has special features for interlocking and for containing the broken stone joint filler. The slope forms a honeycomb pattern.

- The Hillblock consists of a cube with a mushroom shaped element on top. A constructed slope creates numerous small voids under the top surface that slows down the wave run-up and dampens the development of dynamic water pressure in the joints.
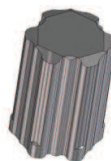
Many other types exist[68], based on variations in shape (like C-star) or with respect to physical interlocking (like the German Verkalit system). Concrete block revetments have a very wide application in the Netherlands. Similar structures are also found in Germany, Denmark, Surinam, Guyana, Vietnam, and in protective structures for lake, reservoir and river shore lines in the UK, US and Canada. Examples of interlocking blocks range from very subtle rebate to board puzzle-like connectors.[69] In the US there is a much wider use of block mattresses with cable ties and interlocking blocks. Mattresses combine easy mechanised placing and interlocking of the individual blocks.

For the transition between stone revetments and grass slopes, very open systems are available that allow overgrowth of grass.

---

[68] Agema et al., *Betonnen bekledingen op dijken en langs kanalen* K.W. Pilarczyk, "Design of Revetments" (Book section)

[69] McConnell and Allsop, *Revetment systems against wave attack – A design manual*

2.4 Reviews and recent developments

2.4.1 *Awareness of underperformance of revetments*

In 1996 a safety standard with an acceptable probability of exceedance was confirmed for each dike ring system.[70] The tasks of the different government bodies to prove and maintain this safety level and to finance maintenance, remedial and upgrading works was defined also. A recurrent 5-year cycle of inspection and update of the load conditions and safety calculations of all dike stretches became mandatory, to be reported to the national government.[71]

At the start of the first test round the authorities were informed about the new insight that a there was an overall lack of safety of the revetment layers. A major investment in upgrading works had to be made. In a letter dated March 1997[72] the chairman of the TAW[73] and consulted specialists explain this situation to the government. They conclude there has been a 'collective blindness' for a lack of sufficient safety of the revetments. Research has merely been focussed on the big closure projects. Over the years since 1953, damage of revetments under frequent (once in 5 to 10 year) storm conditions has been accepted as normal, not realising that since the Delta Act the structures have to withstand significantly more severe conditions. These conditions go beyond the experiences. Structures based on empirical design rules can therefore not be considered as sufficiently reliable. Special concerns were raised for the relatively light concrete blocks directly on clay, which were applied in considerable quantities after 1953. These structures appear not safe because they fail to protect and maintain the quality and water tightness of the clay layer. This insight was gained during and after years of service of these structures.

As a result of research in 1970s and 80s the importance of the permeability properties has become obvious. There were still unknown factors that troubled the question how to value the pattern-placed revetments. Van der Kleij, Maas & Paape position the pattern-placed revetments in between rock slopes, with the single stone weight as governing factor, and asphalt as a continuous structure. The pattern-placed revetments consist of elements that jointly resist the loads. This joint action is assessed as 'very complicated'.[74]

Also ageing, the variation of properties in time is considered as complicating. Hydraulic and structural properties of joints and vents tend to change due to material transport and sedimentation.

---

[70] In 1993 and 1995 exceptionally high river discharges created a threat of flooding of the Rhine and Meuse river areas. Large scale preventive evacuations took place. This was the immediate cause for the new national Water Defence Act (1996) to come into force. Draft versions of this Act were discussed since 1988.

[71] The results of these water defence safety inventories were published in 2001, 2006 and 2011/12.

[72] W. van der Kleij, P. van Maas, and A. Paape, *Het probleem van de stabiliteit van steenzettingen* (Note DWW, attached to letter to RWS Director, 3 maart 1997, 1997)

[73] The Technical Advisory Committee for Flood Defence (TAW) was inaugurated by the national government in 1965 to give advice on flood risk matters and to coordinate research. The TAW also has been commissioner of many studies on stability revetments. The research activities were carried out by the hydraulic engineering department of the Ministry of Transport, Public works and Water Management and by contract parties as Delft Hydraulics. In 2005 the TAW was discontinued, and has been partly replaced by the ENW, the Expertise Network on Water defences.

[74] Also Van der Meer (2000) judges pull test evaluations and theoretical research on lock-in phenomena promising but not convincing due to complexity.

2.4.2   Reinforcement works Zeeweringen

For the coordination of the major upgrading works in Zeeland the project organisation *Zeeweringen* (sea defences) was formed, a joint venture of the water boards and the national Ministry of civil works. From 1997 an execution program was started of reinforcement and in many places complete replacement of revetments and toe structures. Also research activities were intensified, with the purpose to get a more clear picture of the physical failure processes and as a result the actual safety level.

In 2006 after a first phase of substantial upgrading works and research activities the results[75] of the safety assessment of the revetment were as shown in Table 2-5.[76]

Table 2-5   **Quantities of revetment reconstruction works after 1997**

[km]	Dike length	of which with stone revetment	Not safe 2006	Not known 2006
Western Scheldt*	135	125	30	55
Eastern Scheldt	201	152	121	27
Wadden Sea	277	210	21	91

* Between 1997 and 2003 the Western Scheldt dikes were reconstructed.

The typical overhaul of the revetments was a replacement of the lower slope, sometimes on top of the old one. The new revetment is placed with mechanical means, mostly of the type Basalton or Hydroblocks. Also old material was re-used: initially applied flat 0.25 × 0.50 × 0.50 Haringman blocks were placed on their side and Basalt columns were sorted and re-used as dumped quarry stone on the low berm in front of the toe structure. The possibilities to evaluate ideal slope angles, berm positions et cetera in relation to the revetment design were very limited. The revetment upgrading works were significant. In some places the revetment weight was more than doubled.

The works were completed in 2015. The estimated total expenses are 900 million Euro[77] for 325 km dike. This makes the project one of the bigger national infrastructure projects.

2.4.3   Review studies

The reinforcement works were discussed by several researchers in the field. They criticise the insufficient knowledge level on basis of which structures are rejected and re-designed, but they do not all use the same arguments or come to the same conclusions.

Den Heyer[78] promotes a design method that includes joint probability of the water level and wave parameters, and a stability formula calibrated on Delta flume results and applies this to a slope, reconstructed in 1998, with 0.35 m thick *Pit-polygoon* concrete columns. Neglecting the effects of other failure mechanisms, he finds a single revetment element failure probability (P_f) of 1/200 yr for the applied revetment. A P_f of 1/4000 yr is obtained only with an element thickness of 0.50 m.

---

[75] C.J. Dorst, "Blokje eraf en blokje erop voor de veiligheid," *Cement*:7 (2003): 28–31

[76] The results of the 2011/12 evaluations typically show hardly any dike stretches with non-safe revetments. That does not mean that the dikes are safe. Piping is now considered to be the most dominant threat. M.J.J. Boon, *Veiligheid Nederland in kaart 2 - Overstromingsrisico dijkringgebeid 26: Schouwen-Duiveland*, 2012

[77] Source: Jaarbericht Rijkswaterstaat 2011

[78] F. den Heijer, *Veiligheid huidige ontwerpmethodiek steenzettingen*, 1998.

Van der Meer[79] compares measured and calculated figures and points at the large uncertainty margin. Old structures of which we do not know if they are safe are not all unsafe. He recommends not condemning old revetment types on the bases of too much unknowns. Investments in research on those types should precede a final judgement on their stability. New structures designed around 1997 are in his view (very) safe[80], which is not a problem since the money spend in a certain margin of overdesign is well spent.

2.5   Discussion and conclusions

The general image that arises from the summary of the development of stone revetments is a fight against the threats of nature that could step by step develop from a responsive into a proactive attitude. Technical developments and economic means were vital ingredients in changing the scene in this fight.

From the technical perspective the history shows that the understanding of how systems work, sometimes only becomes clear when people start experiments which sometimes appear not to be improvements.

Particular signs of insight in how the structure of interacting revetment elements works are present in 19th and 20th century textbooks, but seem to be not included in later developments.

– There was a clear picture of the function of the toe as horizontal support for the slope.
– The strength of the slope is not defined by the weight of the smallest element but by its ability to transfer forces to the neighbouring blocks.
– The element faces need to be straight with as much contact area as possible.
– Column shaped elements perform better than block shaped elements of the same thickness. Application of blocks 'on their side' was known since early 19th century.
– Filter laws were unknown, although the thickness of the granular sub layer was deliberately chosen between 15 and 25 cm.

The damages to revetments that occurred during the flood in 1953 did not attract much attention because those cases did not lead to dike breach. The cases Brielse Maasdam, Westkapelle and Wieringen showed serious revetment damage. In certain cross sections the revetment failed and was eroded completely. Thanks to delay in erosion of the clay layers and thanks to emergency repairs a breach was prevented. The many breaches that actually occurred at other locations were due to overtopping and overflow. Those dikes were too low, and also the revetments on those dikes were not really exposed to waves because of a too low position. They were submerged.

The dike strengthening projects of the Delta Law period have increased safety against overtopping, but the related higher design surge levels and associated wave attack, have decreased the safety of revetments. Existing revetments were not replaced. New revetments were mostly of the innovative type of concrete blocks on clay, which later appeared not safe.

---

[79] J.W. van der Meer, *Veiligheid in rekentechnieken van steenzettingen*, 2000.
[80] Reference is made to section 4.1.3 which describes the design methods around 1997.

Gradually pattern-placed revetment with permeable top-layers have increased in thickness and slope coverage and have become the first choice slope protection system for the Dutch sea and estuary dikes. Grass covers and asphalt covers tended to become less favoured.

Between 1997 and 2015 the revetments on most of the dikes in Zeeland were subjected to large upgrading projects. Extensive research programmes have been carried out since the 1980s. Knowledge has extended step by step. Knowledge of the revetment as a coherent structural system has been developed and has been implemented in the design methods since 2007.

3   DESIGN PRINCIPLES OF PATTERN-PLACED REVETMENTS

Chapter introduction

The development process of revetments over time has produced a diversity of revetment types (see Chapter 2). Up to quite recent years the knowledge of their stability was predominantly empirical and lacked a theoretical basis.

The revetments are purposely pattern-placed. As a consequence they are optimised with respect to permeability properties and they generate in-plane forces and frictional interlocking. Those are the main causes that make the revetment a coherent structure rather than a collection of loose cubes or columns. In this chapter these subjects are treated as ingredients of the design philosophy of the revetment.

- A design philosophy is introduced in section 3.1 and further substantiated throughout this thesis. In the cross-section of the dike (the transverse direction) the revetment can be modelled as a beam, supported by a proper toe structure. The resistance of the beam is provided by the self-weight and by frictional interlocking through in-plane forces.
- Provided that the hydraulic load is concentrated, the longitudinal direction can be considered as well. The structure can be modelled as a plate with two-way beam action.
- Verifications of the resistance of the revetment against known loads, other than wave loads are available in the form of pull tests and friction tests. Available tests are collected and re-analysed in Annex C and D. New tests are designed and presented in annex E, F and G.
- A reliable definition of revetment stability has a multi-disciplinary nature, in which aspects of wave theory, wave shoaling and breaking, hydraulics and permeability, soil properties, and aspects of structural mechanics play a role. Processes and uncertainties in loads and resistance are therefore investigated and addressed separately. Wave load effects are discussed in chapter 5.
- Older literature on revetment research includes aspects of the design philosophy already. It tends though to provide overall insights based on integral models and empirical verifications, in which load and resistance are not systematically split. A separate chapter 4 is devoted to discussion of models in literature.
- The pattern-placing and the created joints control the effects of the wave loads (section 3.2). The wave load is reduced by flow-heads under the elements. This principle differs from randomly placed armour and cubes of which stability formulas are discussed in section 4.2.
- A systematic approach of explaining revetment failure mechanisms is presented in section 3.3.
- Prototype stability verifications are hardly available. The best available proof of model evaluations is large scale testing. The available test results are presented in section 4.3.

3.1 Design philosophy

3.1.1 *How do pattern-placed revetments work?*

In its basic appearance a present-day pattern-placed revetment consists of a top-layer of column type elements with relatively open joints, a course granular sub-base layer functioning as a filter. Under this layer the dike has an impermeable, erosion resistant clay cover.[81]

The revetment protects the dike against erosion by waves. Waves run through a cyclic process that consists of run-up filling of the filter layer and joints with water, run-down to a deep point with a steep wave front, and subsequent development of a breaker, that may eventually cause a sudden, short and high dynamic impact load on the slope.

Traditional pattern-placed revetments create a relatively smooth outer surface of the dike slope. This surface does not obstruct wave run-up or wave run down. Roughness of the outer slope would diminish run-up of waves, which requires a less elevated crest level and also the wave run down will be less deep. Smooth, but hydraulically very open revetments also limit wave run-up.

(a) Permeable core and impermeable top-layer

(b) Permeable core and permeable top-layer

(c) Permeable core, filter layer and impermeable dike body
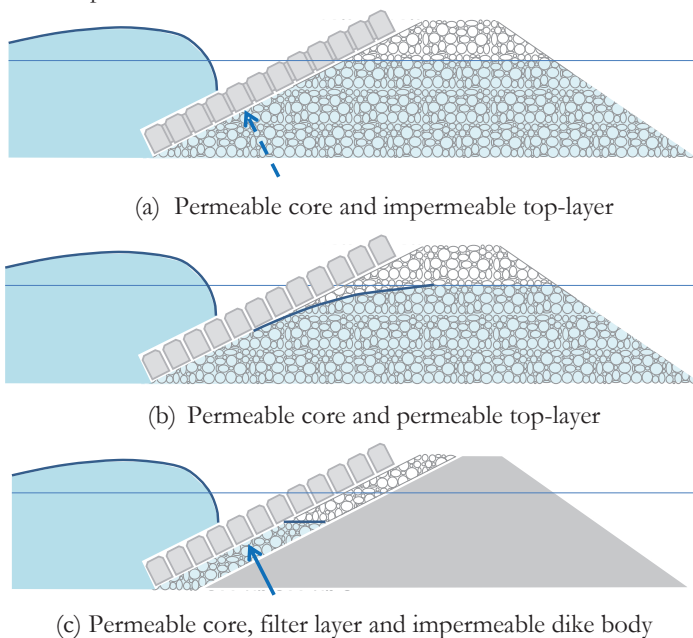
Figure 3-1   Principle of controlling the load by top-layer permeability

Pattern-placed revetments differ from randomly placed revetments by the mechanism of controlling the load by the top-layer permeability.[82] This can be understood by assuming no effect of the top-layer permeability on the run-up and run-down and assessing the response

---

[81] Modern designs with alternative layer configurations with geotextiles follow the same principle. Refer to section 2.3.4.
[82] The stability of random-placed and regular placed cubes is discussed in section 4.2.

of the hydraulic head under the top-layer. For almost impermeable top-layers and (very) permeable cores a run-down situation leads to a static uplift pressure caused by the water in the dike body and filter layers that does not respond to the changed water pressures on the outside of the slope. The water head inside the core and the filter keeps its constant value and thus a water head difference occurs. In Figure 3-1 (a) this is indicated for a permeable core with a water table at mean sea level. If the permeability of the top-layer has a finite value (b), the water pressure at the inside will drop. For traditional dikes and most of the revetment systems the permeable material is limited to a relatively thin filter layer on top of a clay layer (c). The combined effect of the top-layer permeability, the filter layer permeability and the filter layer thickness is expressed in the so-called leakage factor (see section 3.3).
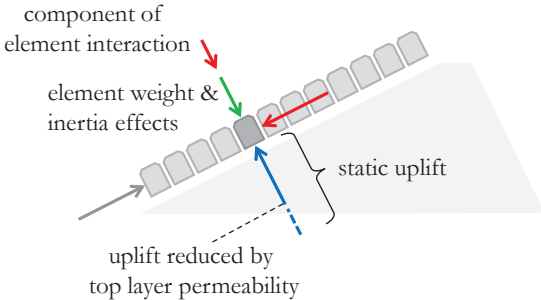
Figure 3-2   **Principle of reducing and resisting the load**

Optimised permeability properties are favourable and reduce the magnitude of water head difference over the top-layer.
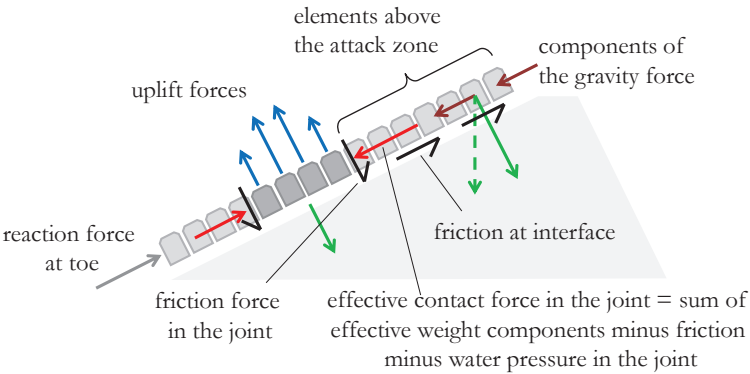
Figure 3-3   **Principle resisting the load on multiple elements with help of frictional interlocking**

The resulting uplift load is resisted by element weight and inertia, since the load is a dynamic load with a short duration in time. Additionally there is a component of element-interaction through friction. The ordinary blocks and columns are closely placed and are assumed to

transfer forces[83] and to interact on friction. The joint fill consists of broken stone, sometimes with asphalt. The function and influence of the joint fill is discussed in section 3.1.5.

3.1.2   Beam action

The very basic understanding is of the load-structure interaction of pattern-placed revetments is that the wave action causes perpendicular loads. The initial in-plane stress state and in-plane load effects determine the resistance against these perpendicular loads through beam action.

In order to benefit from beam action the load must be non-uniform. Typical points of time of potential revetment instability are the run-down of the wave front and the wave impact. At both points of time large head differences are generated between the water in the filter and the water (or air) above the top-layer. The lifted areas of the revetment are limited in size. Only a few elements may be loaded and experience uplift forces, and neighbouring elements are less heavily loaded (see Figure 3-3).

The ability of revetment elements to withstand concentrated high loads is being determined by its possibilities to transfer forces to the adjacent less-loaded elements. The required interaction within the structure can consist of physical interlocking and/or physical connections, but can also exist due to in-plane forces present in the revetment plane. Compressive in-plane forces occur due to gravity, due to friction forces at the interface of the top-layer and the bedding layer and e.g. due to temperature effects. The steepness of the slope plays an important role here.

The compressive forces between the elements are called normal forces, since they work in the direction of the normal vector of an imaginary cross section of the row of revetment elements, i.e. the x-axis in Figure 3–4. The normal force (or in-plane force) in the revetment elements enables the series of elements to act as a beam. The beam has axial and flexural flexibility and resistance against bending moments and shear loads. The in-plane forces occur in transverse (x) and in longitudinal (y) direction.
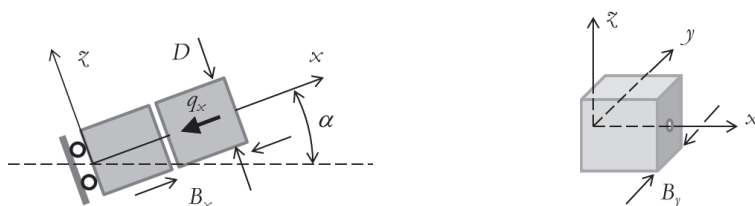
Figure 3–4   Definition diagram top-layer elements

The contribution of the element interaction is basically described using an axially pre-loaded beam model. Due to gravity forces revetment elements on a slope are pressed against elements at a lower position. It should be kept in mind that friction forces between the

---

[83] (Klein Breteler, 1992) makes the assumed interaction more explicit and defines (for all types) that when an element moves 5 to 10% of its height, the (frictional) interlock, the mattress or neighbouring elements must react with a force at least equal to the element weight. The structure types concerned are: geometrically interlocking blocks, block mattresses, and ordinary blocks and columns.

elements and the bedding layer also resist the gravity force and as a result the normal forces between the elements are statically undetermined.

The presence of in-plane force is a crucial principle in the revetment's coherence and resistance to concentrated loads. Due to short crestedness of the waves their impact loads are limited in <u>longitudinal direction</u> of the dike also. This means that normal forces in longitudinal direction could potentially also contribute to the resistance of the revetment, provided that existence of normal force in that direction is predictable. This is further discussed in section 3.1.8.

3.1.3 Axial beam model

Axial beam models describe the in-plane stress state of the structure. A simple model is a beam on a sliding foundation with a stiff end-support provided by the toe structure (see Figure 3–5).
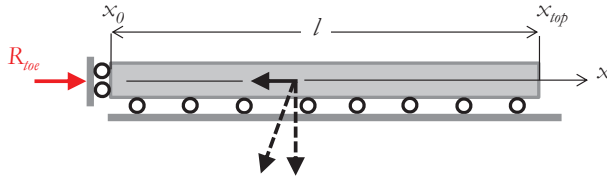
Figure 3–5   **Axially loaded beam on sliding foundation**

The outcome of this model is here – arbitrarily – defined as the neutral normal force N_{neutral}. In reality and as an outcome of more sophisticated models the normal force can become lower as well as higher than in this neutral, non-friction case.

$$N_{\text{neutral}} = \rho_s g D B_y (x - x_{\text{top}}) \sin(\alpha) \quad \text{or} \quad \rho_s g D B_y (z - z_{\text{top}}) \qquad \textbf{Eq. 3.1}$$

$$R_{\text{toe}} = \rho_s g D B_y (z_0 - z_{\text{top}})$$

A more complicated and more realistic model is a beam model with axial springs, with limited capacity in shear, as shown in Figure 3–6. The model outcomes of the friction beam are lower (see Annex A.1). A low toe stiffness will cause that the elements will be experience support forces of the bedding springs. It was found that settlement of the dike may cause the opposite and may cause increased axial pre-loading of the beam.

The model seems rather adequate in defining the initial stress state, although the large uncertainty of bedding friction will make the stress state in reality undetermined.
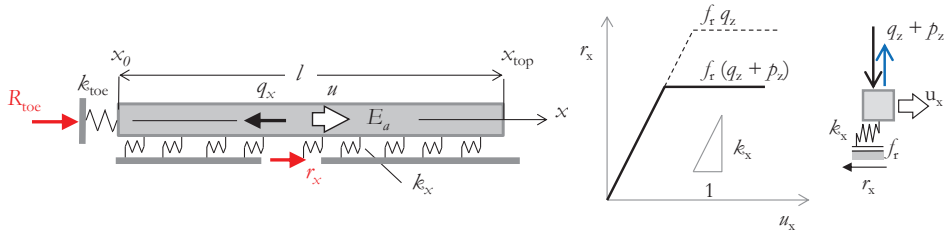
Figure 3–6   **Axial beam model with axial spring supports and friction cut-off**

Since the wave action also influences the in-plane stress state the simple beam models needs to include this effect. The waves shake the system and lift the elements for a very short moment of time. The revetment elements are as a result re-positioned on the bedding and the friction force is re-set to zero.

This process of how wave loads affect the axial force is – as a part of this study – demonstrated and measured in the Delta flume.[84] Measurements in the Delta flume have shown that waves of critical magnitude actually cause an increase in normal force that goes all the way down to the toe. The measured normal force increased almost up to the level of the neutral normal force, defined as the outcome of a model with a fully sliding bedding layer.
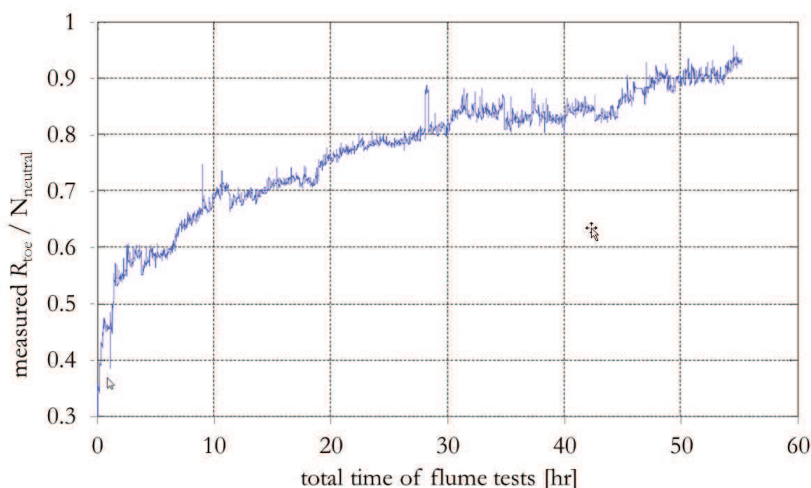
Figure 3–7 **Measured development of the in-plane force in the Deltaflume (source: Wolters & Klein Breteler., 2007)**

The Delta flume test was meant to find out what happened to the in-plane force during wave loading.

Various models have been used in the past to calculate the revetment load against the toe caused by waves on the revetment. In the CUR 155 manual (Klein Breteler, 1992) it is assumed that the portion of revetment between SWL and a vertical distance of H_s downward is assumed to have no bedding contact, and hence will slide, and rest against the lower portion. The lower portion has some spare capacity in case the slope angle α is smaller than the friction angle, $(f_{fr} - \sin\alpha) > 0$.[85] If the friction force of this lower part is less than the force required for equilibrium, the remainder of the in-plane force capacity will be provided by the toe.

---

[84] G. Wolters and M. Klein Breteler, *Normaalkracht in steenzetting met blokken op hun kant*, 2007. The tested slope was a 10.15 m long slope of 0.5 m thick blocks. 85% of the slope was under water. $N_{neutral}$ is here defined taking into account the partial submergence.

[85] Refer to K.J. Bakker and P. Meijers, "Stability against sliding of flexible revetments," *Int Symp Model. Soil Water Struct. Interact.* (Delft, 1988); K.J. Bakker, "Soil retaining structures - ch. 5: Block Revetments" (PhD-thesis TU Delft, 1998)

The sliding equilibrium and the role of the toe is also recently evaluated by 't Hart[86]. In this study a sliding part with a length of two times the leakage length is recommended as the part of the revetment that has no bedding contact. This approach introduces an effect of the permeability of the top-layer. The more permeable the top-layer is, the less vulnerable it is for uplift and loss of sliding equilibrium.

The Deltaflume test reported by Wolters (2007) shows that the neutral value of the in-plane force is reached shortly after starting the flume tests. The values $H_s / \Delta D$ are not very high and hence the revetment was stable. The increase in normal force was hence due to pressure build up in the joints and due to the mechanical response of the dynamic downward loads. The plunging waves cause a sudden pressure of the revetment on the bedding followed by a sudden pressure loss, which relaxes and/or resets the bedding contact and the friction force between the bedding and the revetment beam.

The pressures in x-direction in the joints between the elements can also be quite high and can cause sliding of the portion of the revetment between the point of wave attack and the toe.

A series of subsequent wave attacks will cause a rapid development of the normal force against the toe. It must be noticed that the stiffness and resistance of the 'toe' in the Delta-flume is relatively high. It the stiffness of a real toe structure is similarly high, the tendency of the development of in-plane forces will be the same. But in reality the toe may deform when the load increases, and thus limit the build-up of normal forces. If so, the lowest part of the revetment may experience some relaxation and this part may utilise friction forces to transfer the force to the bedding.

As a model for the normal force calculation we follow the recommendation of splitting the normal force in three parts:

1. A 'dry' in-plane force developed through settlement and lack of friction. The level of this force build up over time is dependent on geometrical and mechanical properties as the slope length, the shear stiffness of the bedding and the stiffness and resistance of the toe.

2. A component of buoyancy below the still water level. This contribution has few uncertainties. It varies with the still water level.

3. A component caused by the wave attack. The existence of this part is subject to uncertainty with respect to things being logically sequential or not. The waves threaten the stability, but the waves also increase the stability. When there is a gradual build-up of water level and waves, the in-plane force can also build-up and provide resistance against high waves coming later.

3.1.4 *Flexural beam model*

The revetment beam under perpendicular loading is best modelled as a beam on an elastic no-tension foundation.[87] This model (Figure 3–8) can be used to calculate the flexural response to concentrated wave impact. The results for bending moments and shear in the

---

[86] R. 't Hart, *Afschuiving steenzettingen en stabiliteit teenconstructie in relatie tot klemming toplaag*

[87] This model is used for various other civil engineering applications with interaction of continuous structures and continuous supports, like embedded piles, flexural retaining walls and train rails.

revetment top-layer are easily obtainable (see Annex A.2). The model formulas show that shear might dominate the response, which coincides with flume test observations which show shear failures in the impact zone.
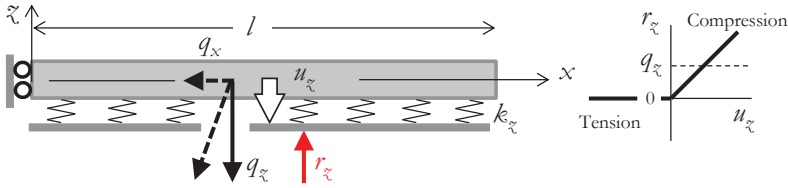
Figure 3–8   Perpendicular loaded beam on elastic foundation with no-tension springs

Uplift loads cause a more complicated case with an unsupported beam portion in between two elastically supported portions (see middle picture in Figure 3–9). The downward load cases associated with plunging wave loads have a dynamic nature, which implies the need of a dynamic response calculation, with mass-spring systems (see A.2.2).
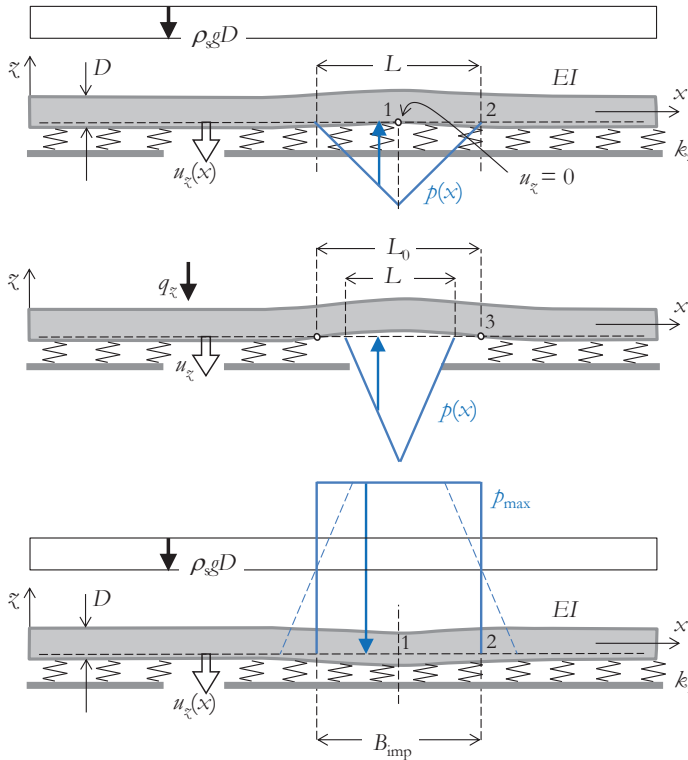
Figure 3–9   Beam on elastic no-tension foundation with uplift loads and with concentrated downward loads

For evaluation of the resistance in the critical case it appears that a simplification in the form of an isolated confined beam model is adequate for calculation of the response to uplift load. This is an important conclusion since this simplifies the calculation of the response

considerably. Uplift loads can be considered as a quasi-static load and the response can be treated as static.

The concept of this model (Figure 3–10) is that the beam boundaries do not transfer shear. Hence the beam weight balances the load. Mathematically the zero-shear points coincide with the extreme bending moments. The isolated part of the beam includes the critical section. For various load shapes and load magnitudes the length of the confined beam can be calculated, as well as the extreme values of the bending moments and shear forces. Refer to Annex A.3.

effect of elasticity of the revetment on elastic bedding on $M(x)$

effect of excess rotation at maximum M on $M(x)$
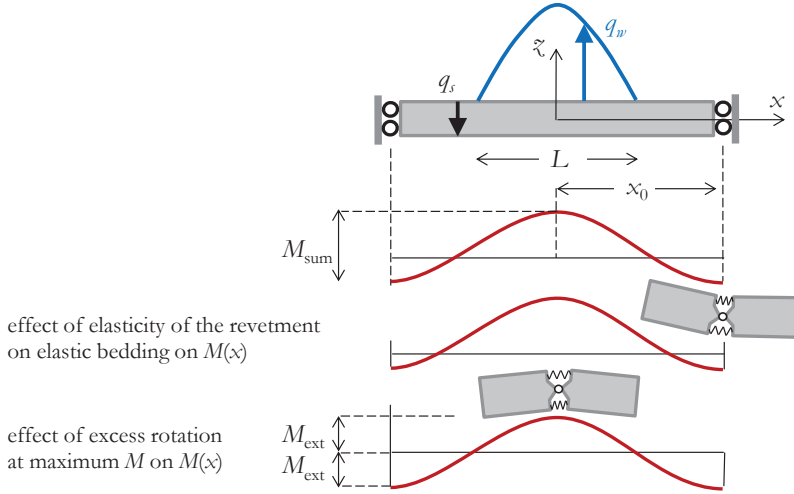
Figure 3–10 **Model of the beam portion subject to uplift load q_w balanced by the beam weight q_s (confined beam model)**

The equilibrium of the isolated beam, given the presence of the normal force N, is shown in Figure 3–11. It can be understood that the beam deformation δ reduces the flexural capacity $M = N \times e$. This is a geometrical non-linear effect.
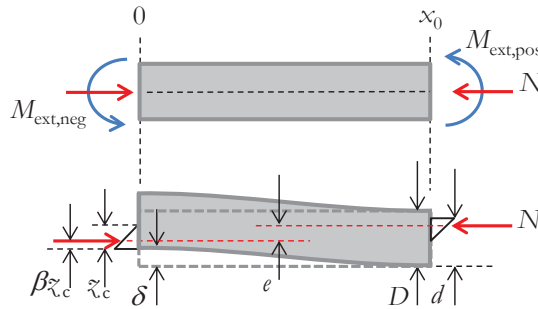
Figure 3–11 **Equilibrium of beam portion in deformed state**

This model is verified by a series of experiments in the Stevin II laboratory in Delft in 2004. During this series of experiments details of the behaviour of the joints were studied which resulted in model refinements. The experiments are presented in Annex E.

3.1.5 Parameters of the revetment beam model

The slope angle α influences the breaker parameter ξ and therewith the magnitude and location of the wave loads on the slope.

The slope angle also influences development of the in-plane forces. Steep slopes have higher in-plane forces. The positive effect of the in-plane force on revetment resistance introduces a new variable in the question of the ideal slope angle. The effect of element weight decreases and the contribution of normal force increases with steepness of the slope. For a 1:2.5 slope and a 1:5 slope the differences are shown in Figure 3-12 and Table 3-1. The case is with irregular waves with average steepness $s_o = 0.02$. The uplift forces are assumed equal in both cases due to a small leakage length and due to a similar wave front angle.
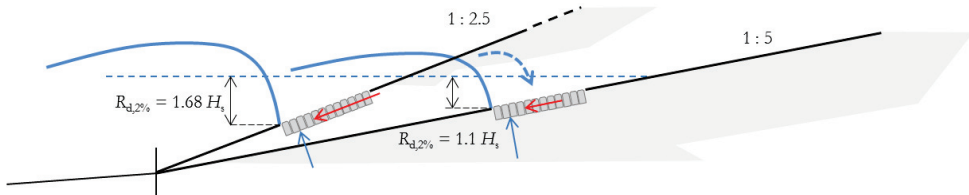
Figure 3-12 **Load situation for two slope angles, run-down for irregular waves with $s_o = 0.02$**

Table 3-1 **Effects of normal force for two slope angles**

Slope angle	1 : 5	1 : 2.5
Run down point $R_{d;2\%}$ below SWL, refer to Eq. 5.31	1.1 H_s	1.68 H_s
Element self-weight perpendicular: $\Delta D \cos\alpha$	0.98ΔD	0.93ΔD
Indicative system resistance (assuming an effective normal force based on double lengths of the attack zone, friction-less bedding), see chapter 6.1	1.16ΔD	1.37ΔD
Wave impact	yes	no
Revetment thickness relative to the 1:5 case	100%	84%
Revetment length relative to the 1:5 case	100%	50%
Extra length needed to protect against wave run-up	no	yes

Theoretically the magnitude of the normal force is highly undetermined due to the possible occurrence of friction forces on the interface between the top-layer and the bedding layer. The direction of the friction forces can either be in positive or negative x-direction. The extent of the influence of the slope angle on the normal force development is shown in Figure 3-13.

From this figure it can be concluded that on a slope with friction which is more gentle than 1 : 1.67 the elements do not need support from neighbouring elements or from the toe in order to find static equilibrium of the self-weight. On these gentle slopes the bedding needs to move downward, or the elements need to vibrated and/or lifted in order to break the friction and to achieve a neutral in-plane stress state that is similar to the equilibrium state on a friction-less slope. In practise effects of settlement of the dike and/or wave action are needed to achieve this state.

The slope length also influences the build-up of normal force. The elastic parameters of very long slopes are such that the build-up of normal force is low. Gentle slopes normally are long, which has a double negative effect on the magnitude of the normal force.

The effective element weight is $\Delta D B_x B_y$ (see Figure 3–4) in which Δ is the effective buoyant weight $\Delta = (\rho_{s} - \rho_{w})/ \rho_{w}$. Because the uplift load F_w equals $\phi_{dip} B_x B_y$, Δ and D are the relevant parameters of the resistance by element weight. Larger element width dimensions B_x and B_y tend to dampen spatial peaks of $\phi_{dip}(x, y)$. See section 5.3.2.

The plot shows Normal force N / weight $\Sigma \rho_s g D$ on the vertical axis (0.0 to 1.4) versus slope angle [cot α] on the horizontal axis (0 to 6). Curves: $\sin \alpha + f_{fr} \cos \alpha$ (with friction, sliding upward), $\sin \alpha$ (friction less), $\sin \alpha - f_{fr} \cos \alpha$ (with friction, sliding downward).
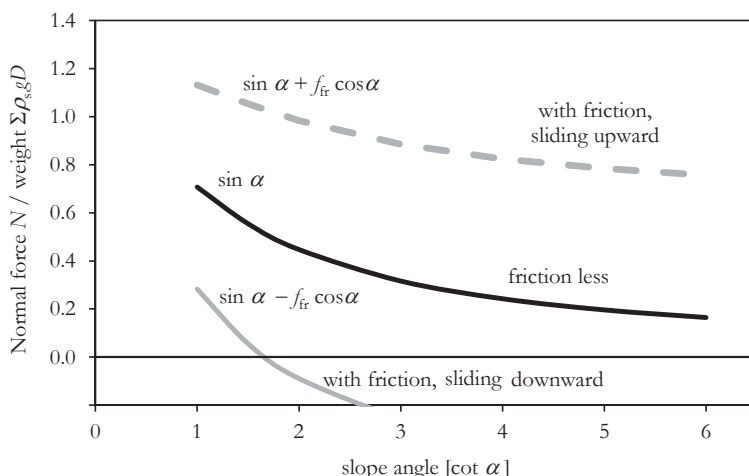
Figure 3-13   Theoretical range of dependency of normal force on slope angle, with f_{fr} = 0.6

The Element height D is the main determining factor for stability. As soon as transfer of forces to neighbouring elements in the interaction model through bending moments plays a role, a stronger dependency on D might be expected. In a coherent top-layer system single element weight is not a governing parameter. Given a certain D, elements can increase in weight due to specific weight $\rho_s g$ and/or due to larger dimensions B. Increase by means of a larger width does not necessary improve the stability since this means that the D/B ratio will decrease. For avoidance of single element failure a larger specific element weight is advantageous.

The height-width ratio, D/B has an effect on the stability of the single element on a slope. Tall inclined columns tend to lean against the neighbours, which is beneficial for the element interaction. Block-like elements need larger rotations before perpendicular element movement is blocked in the joints.

Element regularity has a two-fold effect. Regular columns with vertical sides have a lot a contact area, but also tend to make the piston mechanism possible (see section 3.5). Vertical sides are the result of the production process of the elements. Not all elements are perfectly prismatic. Basalton is very slightly tapered. Ronaton has notches at the corners. The natural stone columns show much more irregularity. Placing of the natural stone columns in a close pattern is therefore a human activity. If this is done well, the irregularity is an advantage. The individual elements can not move out. Slightly spherical shapes are a disadvantage. They

occur due to broken edges and corners or due to early removal of the elements from the mould and settling of the concrete.

Table 3-2   Columns versus blocks

	Blocks, $\dfrac{D}{\sqrt{B_x B_y}} \leq 1$	Columns, $\dfrac{D}{\sqrt{B_x B_y}} > 1$	Irregular
Concrete	Concrete blocks, e.g. Haringman blocks, Clinkers	System Pit-Polygon, Basalton, Hydroblocks, Ronaton	
Natural stone	Granite blocks Doornik stone	Basalt columns 'Petit granite'	Vilvoord stone Lessin stone
Rest products	Copperslagblocks		

Friction forces play a role on various places in the system.

- Between top-layer and bedding, in x-direction, thus influencing the build-up of normal force. Refer to Figure 3-13. The causes and the effects of this friction are investigated in Annex A1 and Annex E.

- The capacity to allow shear forces in the joints also relies on friction in z direction. The contact pressure caused by the normal force enables friction forces to occur in the joints. For the behaviour and mechanisms in the joint analogy can be found in joints filled with granular (preferably angular) material in block pavement subjected to concentrated wheel loads.[88]

- Friction between the elements in x-y direction plays a role in the distribution of N_x and N_y, the in-plane forces in x- and y-direction.

Rock or rubble mound breakwaters have a permeable core. These structures very rarely have pitched revetments. A relatively closed top-layer is disadvantageous for the concept and for the revetment cost. Dikes normally have a clay core or a sand core covered with clay layers to fulfil the water retaining function of the dike. In breakwaters with a sand core and a geotextile the water retaining function cannot be assigned to one layer. The drainage properties gradually diminish and the geotextile prevents wash-out of fine material. The response to wave loads of structures with thick graded filter layers differs from revetments with an open top-layer and a thin filter layer and an impermeable layer directly underneath.

The granular sub-layer has a double function. The permeability and pore volume determines the response to the wave loads. Reasoning from this function the layer is called filter layer. The granular sub-layer also forms an elastic foundation of the top-layer. Applied perpendicular loads acting on the top-layer will generate reaction forces in the sub layer, which is associated with (usually elastic) deformations. Reasoning from this function the granular sub-layer is called bedding layer. The bedding stiffness k influences the bending moments and shear forces in the top-layer. See chapter 5. For continuous structures like asphaltic revetments the influence of this phenomenon is large. Measurements of stiffness properties can be extracted from tests on asphalt slopes. Recently pitched revetments were

---

[88] M. Huurman, "Permanent deformation in concrete block pavements" (PhD thesis TU Delft, 1997)

also subjected to dynamic impact testing[89], normally typically used to test road surface structures and asphaltic revetments.

The <u>joints</u> have a multiple function. The joints control the top-layer permeability and the mechanical properties of the revetments, such as friction coefficient and stiffness. Joints between structural elements can have different appearances. Bricks often have cemented joints. But in early construction practise stones were cut and the shape was adapted to fit in their position and to create flattened load-bearing surfaces. In recent years this is achieved in concrete block work construction for quay walls and e.g. in the ClickBrick® system. Forces on the interfaces between elements can be taken by friction or geometrical interlocking.

http://www.arscives.com/approx./seeing_art.htm

http://www.daasbaksteen.nl
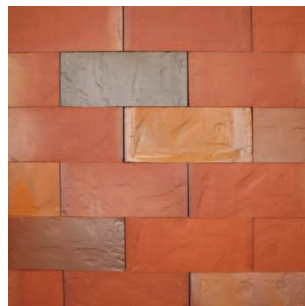
Figure 3–14   Examples of compressed not-bonded joints

Together with the granular sub layer the jointed revetment is part of a layered filter system that prevents migration and erosion of soil particles. The joints enable the revetment layers to flexure and follow settlements of the dike. They determine the elasticity and flexural rigidity of the revetment. The joints will lock the elements in, enabling transfer of (eccentric) normal forces and shear forces between the elements and thus preventing the piston mechanism to occur. The joint fill provides flexural deformation capacity, but a structure with gravel joints is potentially less able to transfer lateral forces and eccentric loads (see Figure 3–15). It would e.g. be difficult to imagine the arch structure of Figure 3–14 constructed with the gravel joints of Figure 3–15.

The position of the <u>upper boundary</u> of the revetment, where it changes into grass cover, differs per location and is generally chosen based on historical information on frequency of loading and damage. As a rule of thumb a position halfway the design water level and the crest is recommended[90], assuming a continuous slope. This recommended position is (well) above most historical observations. A more rigorous analysis into the position where grass covered clay can withstand the erosive forces of wave run-up is preferred. This is beyond the scope of this study.

<u>Transitions</u> in the revetment should be avoided. In many cases in practise revetments are constructed or re-constructed in partitions and as a result horizontal transitions occur. Sometimes these transitions are hydraulically tight, which is unfavourable for development

---

[89] R. 't Hart, *Klemming in steenzettingen bepalen met VGD-metingen*, 2012 R. 't Hart, *Vaststellen van klemming in dijkbekledingen van gezette steen met valgewichtdeflectie- metingen*, 2013
[90] M. Klein Breteler, *Handboek voor dimensionering van gezette taludbekledingen* (CUR / TAW report 155, 1992)

of locally high filter pressures. When transition beams or piles are applied that disturb the ability of sliding of the elements, sudden drops in the in-plane force distribution may occur, which may cause a locally lower stability.

Failures at horizontal transition structure are quite frequent (refer to 4.3.2). It is advised to avoid horizontal transitions that introduce discontinuities in permeability and/or mechanical properties between the design SWL and $2 \times H_s$ below.

| Stable arrangement of blocks with flat contact surfaces | Stable, but more flexible arrangement with gravel or broken stone filled joints | Joint fill adapts to deformation, element settlement and rotation |
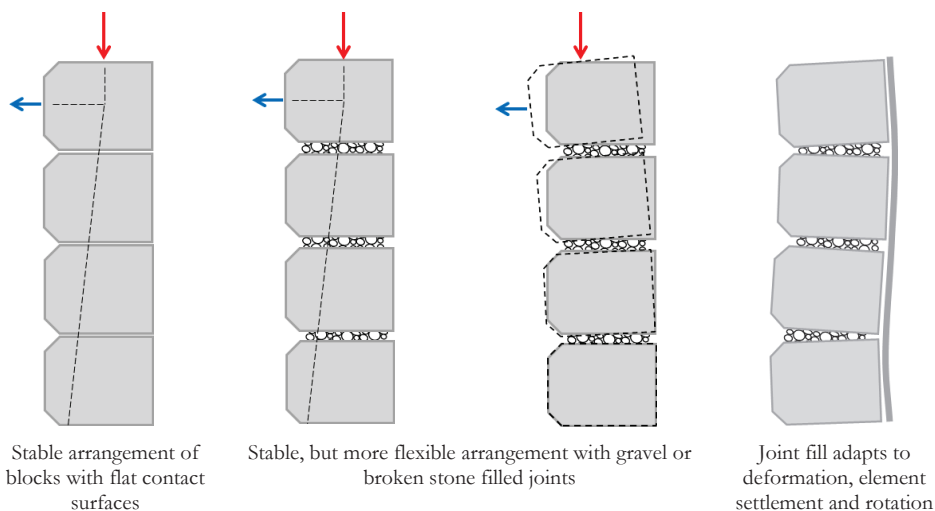
Figure 3–15   Imaginary columns of revetment elements

3.1.6   *Prediction of normal forces*

The normal force in the transverse direction is generated by the gravity force acting on the elements. The elements higher on the slope lean against the lower elements that rest against the toe to balance the normal force. The normal force can also act in longitudinal direction.

The normal force depends on a few of the parameters described in the section above. Although the normal force might not always seem a reliable design parameter it cannot be missed in explaining how revetments work as they do. Due to the presence of normal force, the revetment beam has the capacity to transfer shear forces and bending moments.

In addition to the element thickness, the in-plane stress state just before wave loading actually determines the stability of the revetment. It is therefore important to find out what the actual in-plane force level is in real structures. Looking from the perspective of the designer it should be researched how the in-plane stress state can be made more predictable and reliable.

In the past pull tests were executed in order to translate pull-out strength into resistance against waves. Those test results are collected and presented in Annex C. Although this is not a straightforward translation, in Annex D is tried to hindcast normal force levels from the measured pull-out force values (refer to Figure 3–16) and from the measured displacements.
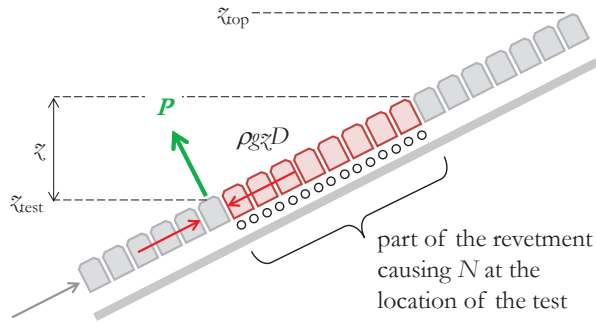
Figure 3–16 **One-dimensional definition diagram finding the normal force by analysis of pull tests**

The resistance against concentrated loads like pull-out forces is best modelled with plate models instead of beam models. Concentrated loads occur in reality in the form of wave impacts and short-crested sea states. Unintended local voids in the sub-layers can also lead to concentrated loads. Two-directional models (x, y) are therefore needed to extract parameters from the real structures that can successively be used in beam models for design purposes.
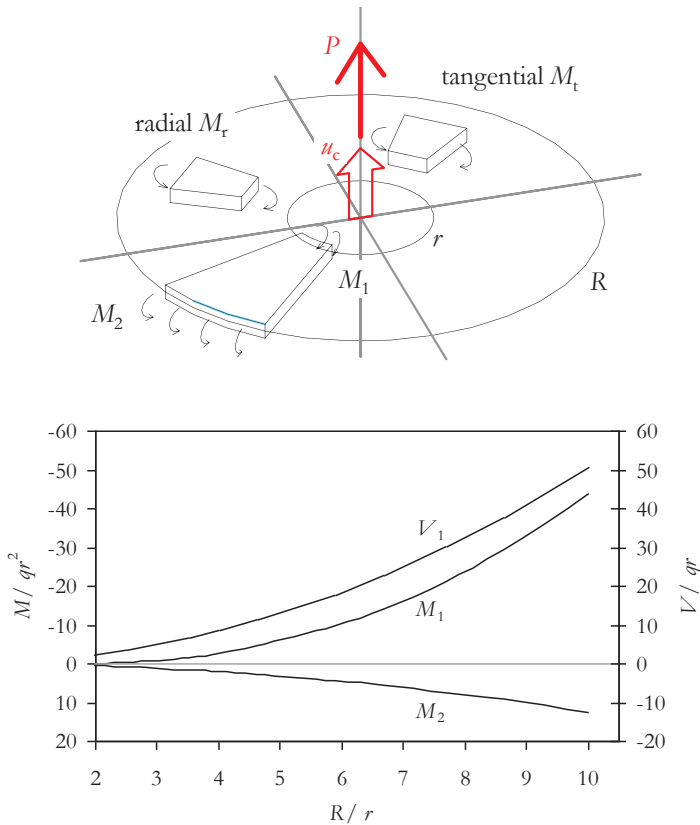
Figure 3–17 **Definition diagram and results of continuous circular plate model**

The plate model (Annex B.1) is relevant of the understanding explanation of the sometimes very high resistance against concentrated loads.[91] While progressively loading a circular plate in the middle with a force that equals the weight of the total plate, $P = \pi\, q\, R^2$, with $q = \rho_s\, g\, D$, the circle expands and the bending moment at the outer edge M_2 increases, as well as the bending moment M_1 and shear force V_1 in the centre. The in/plane loading of the inner edge causes a geometrical effect that disturbs the uniform in/plane stress state N_0, and eliminates the tangential part, thus creating a concentration of the undisturbed normal force N_0 at the edge to a much higher value N_r around the pulled element.
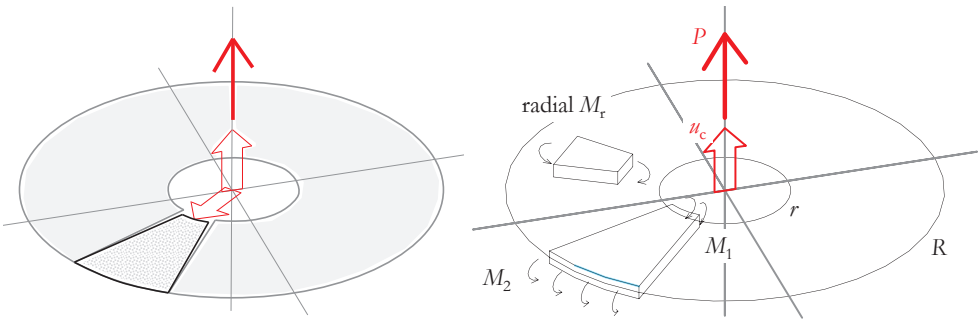
Figure 3–18   Definition diagram for segmented model with only radial bending moments

The model of Figure 3–18 is introduced as the segmented model (see Annex B.1.2) and was used for interpretation of the pull-tests and for derivation of normal force level and stiffness parameters from those tests. Stiffness parameters can be extracted by comparing the pull-out values (in terms of the load factor $n_{LF} = P/G$, representing the number of pulled elements) and the measured centre displacement u_c. The displacement is best measured on the element adjacent to the pulled element, because the pulled element sometimes experiences some slip before more resistance is build-up.
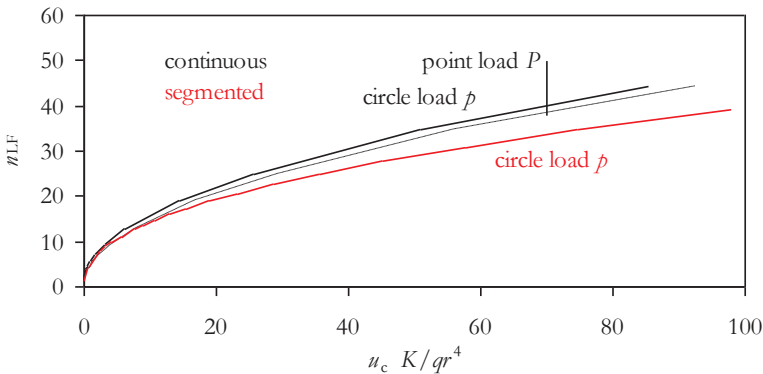
Figure 3–19   Elastic displacement results for plate model calculations

---

[91] In the past high pull-test results have been a reason for assuming high revetment strength against waves also. This is not right and potentially unsafe.

The plate models are too complex and less relevant for assessment of the effects of wave loads. Two-way beam models (as in Figure 3–20) seem more adequate. They are not accurate with respect to shear and bending in the centre of the model, but provide reliable results for the equilibrium and the magnitudes of the loads.

This model is also suitable to derive directional differences in the normal forces. This is presented in Annex B.2 and G.2.1. The longest direction of the deformed shape is associated with the highest normal force.

3.1.7 Findings on in-situ normal forces

The models for normal force prediction were used to hindcast normal forces from in situ tests. We have analysed the numerous 'small' pull-out tests available in literature. Those tests were truncated at 9 kN pull force. This is presented in Annex D. Also we have design new tests with loads up to 100 kN. Refer to Annex G.
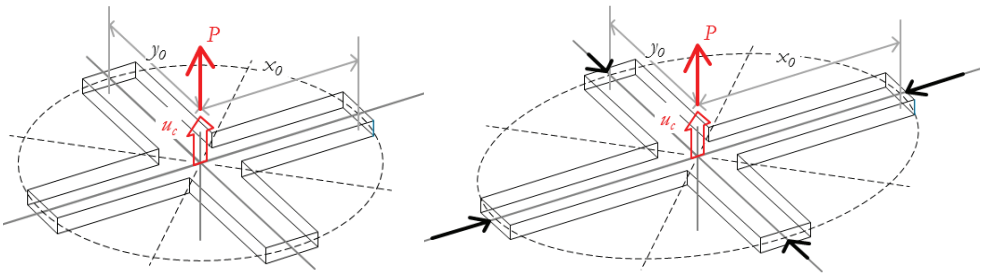
Figure 3–20   **Two-beam models for single element loads**
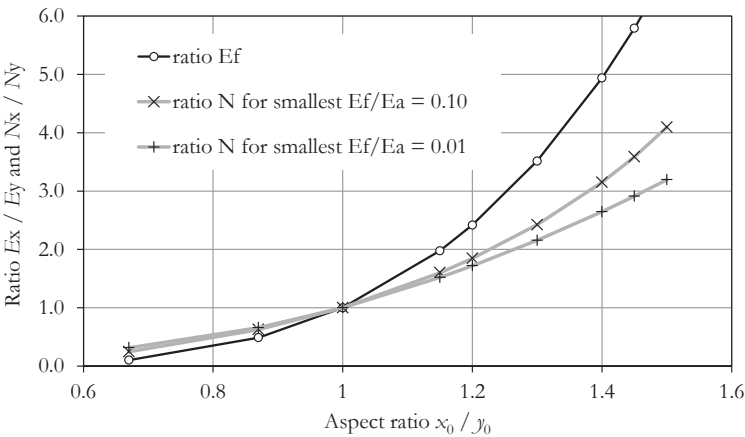
Figure 3–21   **Directional flexural stiffness and normal force ratios for unequal dimensions of the deformed shape**

A number of conclusions can be drawn based on the in-situ normal forces:

In line with conclusions of (Plooster, 1995) and (Coeveld & Klein Breteler, 2003) it was found that temperature influences the pull out strength. Revetment types that are highly susceptible to build up of temperature forces tend to become looser when the temperature

drops. Column revetments have less temperature influence: due to a larger joint area is the axial stiffness lower, and joint material can move to wider parts of the joints. Column revetments also have the possibility of re-arrangement. Individual elements can move a little bit outside the row, towards an upward or downward position. On the scale of the whole structure it can be stated that temperature expansion in column revetments leads to re-arrangement without built up of high stresses in longitudinal direction. Reversely a temperature drop will loosen the in-plane pre-load of the elements, but to a lesser extend than with row-oriented revetment types.

Besides temperature dependency, we find dependency on the age of the top-layer as an important variable. It is widely known that revetments need to settle and be subjected to a 'maiden' storm before they are strong enough. It is important that this first wave load is below the design strength. Small damage of young revetments used to be common. The Maasvlakte damage[92] case is an example of a substantial damage as a result of a first wave load (which was also beyond the design load).

The pull tests results also reflect this phenomenon The dependency could be treated as a boolean variable for being in the first year or not, but this does not really cover the effect, since also the settlement is believed to contribute to the increase of strength. Settlement of the dike body is logarithmic in time. In quite a number of the investigated test slopes, the dikes were raised and new stone revetments were placed. In that case a settlement process occurs with significant effects after say 5 to 8 years. Given the average lifetime of the structure of 25 years and the change of e.g. 1/10 year that a serious load occurs, modeling the effect of age as a linear process over the lifetime is not unrealistic.

The position dependency of the pull tests was already observed since the pull tests were first carried out.[93] It forms extra evidence that the pull-out strength is related to the normal force in the revetment. For longer slopes a linear relation of the normal force N and the position z is likely not true. The results of the very long slope of the Afsluitdijk (over 25 m) deviate from the results at other locations.

The observed in-situ normal force that is responsible for the resistance against concentrated pull loads is somehow based on a normal force present in two directions. Relating the observed or 'measured' normal force to the normal force in the transverse direction the basic formula is $N_{neutral} = \rho g D z$. Based on the findings obtained in the field experiments presented in Annex D the following adoptions are considered.

- The longitudinal normal force is believed to be susceptible to temperature. We assume a neutral 'pressure' coefficient of 0.5 at 10 °C, which relates the longitudinal normal force as 0.5 times the transverse normal force. This coefficient changes linearly and doubles when the temperature change is 30 degrees. The unidirectional share of the normal force is the average of the transverse and longitudinal normal force.

- The age dependency is difficult to quantify. We recommend an age dependency factor following the empirical formula $0.75 + age/40$ [yr], which means that the slope is at full strength after 10 years. Reference is made to Annexes D.4.3 and G.4.3. This

[92] J.A. Hernandez, J.C.P. Johanson, and J.C. van der Burg, *Zuidwal – analyse schade en ontwerp taludbekleding* (DWW report WBA-N 88.053, 1988)

[93] H.J. Verhagen, *Trekproeven op glooiingsconstructies in de Oosterschelde* (RWS report Adviesdienst Vlissingen WWKZ-84.V002, 1984)

formula is meant to count for a reduced strength of young slopes, with age below 10 years. Counting for further increase of resistance of slopes older slopes is not recommendable.

- We also find a factor which corrects the normal force on very long slopes. This factor depends on the length of the slope and the position of the slope and is given with Eq. D.1.

- Evidence was found that for slopes where the test force was sufficiently high an average in-plane force of 3 $\rho_s\, g\, D^2$ is present, which increases with lower position on the slope. The scatter of the measurements is high, and typically follows a lognormal distribution, which gives a 5%-lower bound of approx. 2 $\rho_s\, g\, D^2$. These values however are believed to be biased by the limitation of the small pull-force in the tests. The results are reliable as a lower bound but not as a realistic indicator of the real average normal force.

The new experiment set-up with multiple pull tests using higher loads (Annex G) and measuring deformation has proven to be very useful and has provided insight in the in-plane stress state of the revetment when it is in rest. It was found that in-plane forces are present in two directions, but in the same time a large scatter was found. Based the insights gained by the new tests we tend to conclude the following.

- On older slopes of moderate slope angle ($\cot\alpha = 3.8$ in the tests), with a traditional toe structure, that have experienced wave loading and maybe also have experienced some dike settlement an average in-plane force in transverse direction of approximately 0.7 $N_{neutral}$ is present. There is a large scatter in results.

Some other conclusions are:

- A drop of normal force for revetment on a 1:4 slope, close to the toe structure was observed. The deformation of the toe-structure is likely reducing the horizontal support of the revetment slab.

- A temperature dependence of the longitudinal normal force was observed. This is in line with the conclusions based on the small pull tests

- The calculated effective axial plate stiffness E_a including the flexibility of the joints is in the order of 300 MPa. The calculated flexural stiffness E_f is in case the normal forces are quite high around 200 MPa, and in case they are low around 75 to 150 MPa.

3.1.8 Two-directional normal forces

Normal forces appear to be present in two directions, and with that both directions can potentially contribute to resistance provided that the wave loads are concentrated. The contribution is only of practical value if (a) the load is non-uniform, and (b) if the presence of the normal force is reliable.

Uniformity of the load

Real waves always have a finite crest length. Wave fronts run down relatively slowly. Perpendicular waves tend to load a larger stretch of revetment in the same time. The short-crestedness of the waves due to directional spreading in random wind wave field will limit this length. Coastal refraction in practise significantly reduces the directional spreading and

increases the crest length. A typical maximum load length is easily 10 or 20 times the wave height or ¼ to ½ the wave length, which is more than enough to model the revetment response as cross-sectional problem. Oblique waves occur when dikes are not straight and/or not parallel to the coastline. Oblique waves will cause a shorter load length.

Plunging breakers cause high and sudden impact forces. The typical duration of the peak load (0.2 s) is so small compared the wave period (typically 5 to 7 s or more) that very slight effects of directional spreading and obliqueness of the waves cause a phase shift in the peak load. As discussed in chapter 5, measurements of a dimension in longitudinal direction of the dike are not available. The y-dimension of the simultaneously loaded area is assumed to be two times the x-dimension.[94]

This means that the revetment response to wave impact can be considered as a 3-dimensional problem, which is a beneficial effect, subject to the presence and reliability of normal force in the longitudinal direction.
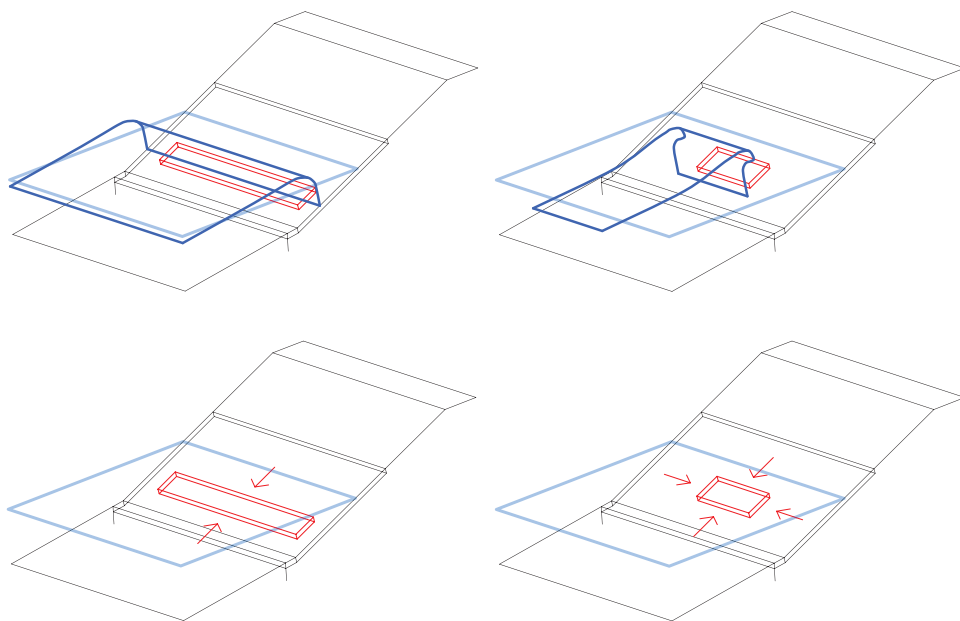
Figure 3-22   **Load type, attack zone and relevant in-plane force components**

Reliability of normal force in longitudinal direction

As discussed in 3.1.7 normal forces appear to be present in two directions. The presence in the transverse x-direction on the slope is a direct consequence of the gravity force, but is made a bit undetermined by the friction action between top-layer and bedding. In the longitudinal y-direction there is no gravity component. The presence of normal force might

---

[94] Small scale test results and ZSteen model outcomes support this assumption. $B_{impact, x} = 0.75$ H$_s$ (see chapter 5.2), based on the assumed aspect ratio of 2: $B_{impact, y} = 1.5$ H$_s$

physically be arbitrary, although the experiments provide evidence that the *y*-direction has resistance in the same order of magnitude as the *x*-direction.

In many field pull tests on Haringman blocks, for instance, the elements experienced more lock-in in longitudinal *y*-direction than in transverse *x*-direction. Rectangular blocks applied in horizontal rows have no dependency of N_y on N_x. For other element shapes this dependency can be explained and might be a phenomenon to rely upon. In an ideal packing of circular cylindrical columns the horizontal stress state depends on the 'vertical' stress, like in soil. For frictionless circles the horizontal stress is 0.5 times the vertical stress. Assuming a friction coefficient between the circular shapes of e.g. 0.4 this factor can decrease to 0.15 in case the elements are not, or weakly supported, or can increase to 0.85 in case the friction direction swaps. In case pressure is imposed at the vertical edges the horizontal stress can increase further due to direct horizontal stress paths.

In soil mechanics the indeterminate horizontal stress state of soils is characterised with coefficients *K*. The formula[95] for the neutral value K_n for granular material is $1 - \sin \varphi$, with φ = angle of repose or critical friction angle. For uniform sands, or more in general uniform angular granular material the critical friction is 35 to 40°. Coulomb[96] developed formulas for coefficients of active and passive earth pressure against walls. The active earth pressure occurs when the wall deforms and the soil stress state relaxes to a minimum. Using these formulas with wall friction equal to the soil friction, the horizontal stress state K_{ah} is given in Eq. 3.2. For $\varphi = 40°$, we find $K_n = 0.36$ and $K_{ah} = 0.16$.

$$K_{ah} = K_a \cos\delta = \frac{\cos^2 \varphi}{\left(1 + \sqrt{\dfrac{\sin(\varphi+\delta)\sin\varphi}{\cos\delta}}\right)^2}$$

Eq. 3.2

with

φ = critical friction angle of granular material,

δ = interface friction angle

According to this theory a development of normal force in transverse direction, due to dike settlement and due to shaking by wave action, will be accompanied by development of normal force in longitudinal direction. A neutral state leads to $N_y/N_x = 0.36$. In case the initial packing in y-direction is loose, a lower stress state could remain, with 0.16 as a minimum. A question to be answered is how predictable and reliable N_x and N_y are.

A normal force in *y*-direction is not necessarily developed in all revetment types. For the rectangular types the development of any normal force N_y is not likely to be correlated with N_x (case (a) of Figure 3-23). Hydroblocks also belong to this category. A force N_y can however occur and exist independent of N_x. For those types settlement and adhesion of the joint material, expansion caused by raised temperatures and also geometrical second-order effects can lead to normal forces. Those causes are not reliable.

Opportunities for manipulating the ratio N_y/N_x with revetment designs are discussed in section 7.1.

---

[95] Jaky, 1948
[96] Coulomb, 1776, extended by Maniel, 1908, introducing wall friction
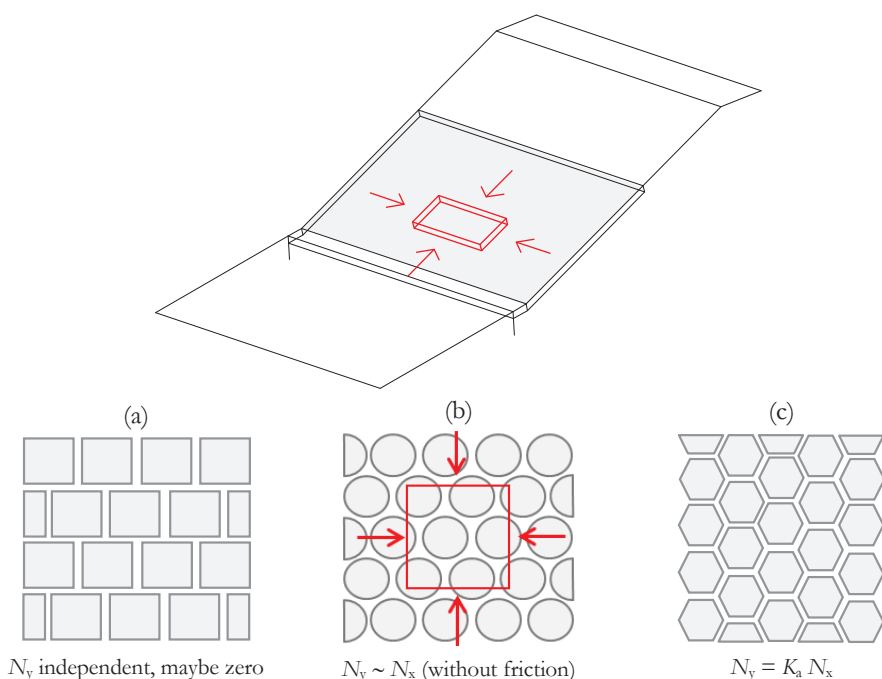
Figure 3-23   Dependency and independency of N_y and N_x for various revetment shapes.

Longitudinal normal force in flume experiments

An interesting question is how this phenomenon influences the stability in flume tests. When flume testing just started the revetments were placed against the concrete wall of the flume, which resulted in build-up of normal force in longitudinal direction, and consequently in a restraint for vertical movement. The revetment elements are able to transfer vertical loads to the flume wall and could in extreme cases form a span from wall to wall. Later rubber was applied between revetment and wall. Also steel angles were used to avoid the elements directly adjacent to the wall to move up. The flexible material apparently avoids build-up of normal force, although build-up of N_x with $N_y = 0$ is for the circular element types theoretically not possible.

It is therefore believed that early tests may have led to a large normal force in y-direction and hence an overestimated stability. The practise which the rubber strips has let to low values of N_y, developed through friction between the top-layer and the bedding layer. The encountered resistance in the flume experiments is hence based on a lower bound of the contribution of N_y, which might be conservative.

3.2 Toe structure

The function of the toe structure is to avoid migration of soil and filter material, but also to provide support for the revetment. Revetment layers on steep slopes tend to move downwards under gravity and wave attack and the toe structure provides support. The toe

does not allow, or at least minimises movements and is important for the equilibrium of the top-layer structure. Ideally toe structures of revetment armour consist of unmovable heavy blocks or rocks or caissons. Sheet pile rows or single pile rows occur also.

3.2.1 Types of toe structures

Traditional Dutch toe structures of pattern-placed revetments consist of timber pile rows supported by rock. This is irrespective the weight, angle and length of the revetment. The question is whether this is an adequate solution for providing stiff support to the revetment.

Figure 3–24   Photographs of construction of toe structure type (b) at Schouwen-Duiveland in 2008

In most cases the structures have empirical designs and consist of a timber pile row or a continuous timber sheet pile row of e.g. 1.5 to 2 m length. Sometimes the toe is supported by extended horizontal parts of the revetment, or by rock (see Figure 3–24). Although the depth and weight of revetment slabs have increased since 1997, the toe structure dimensions are in rough lines similar to older structures.

The toe structure forms the transition between the pattern placed revetment slope and the foreland or the berm. The foreland mostly consists of clay or sand deposits, or in some cases overlain with random placed rock that protects the soil against scour and provides extra weight to support to toe. The toe structure is at the bottom of a slope and will in the hypothetical case without any slope armour also experience horizontal load due to the equilibrium state of a soil on a slope, and horizontal deformations due to settlement of the dike body (see Figure 3–26).

The typical toe structures in this overview are for slope in tidal area's where the toe structure is constructed at low tide, almost at the surface level of the foreshore, with no wave loads during construction. Wave loads will only occur when the water level is higher, and those waves will not directly touch the toe structures.[97]

Reasoning from this load condition, the toe at sea dikes is normally a hydraulically open structure of oak piles at spacing of the double or triple pile thickness, with a timber or concrete plank, which provides a straight line for support of the revetment blocks. The risk of wash out of soil and filter material is avoided by filters or a geotextile. In case the toe structure forms a step-up from the foreland, the risk of scour becomes apparent. In case a berm supports the toe, it should be noticed that the run-down can cause pulling forces on the material and the toe, which worsen the load condition of the toe. The toe piling structure should be sufficiently deep to overcome loss of stability due to scour and due to weak soil properties.

---

[97] For wave attacked lake dikes (at constant water level) toes are not submerged and tend to be loaded by the wave action.

(a) toe block

(b) wooden piles and small rock (Dutch: kreukelberm)

(c) horizontal part

(d) pile row

(e) embedded
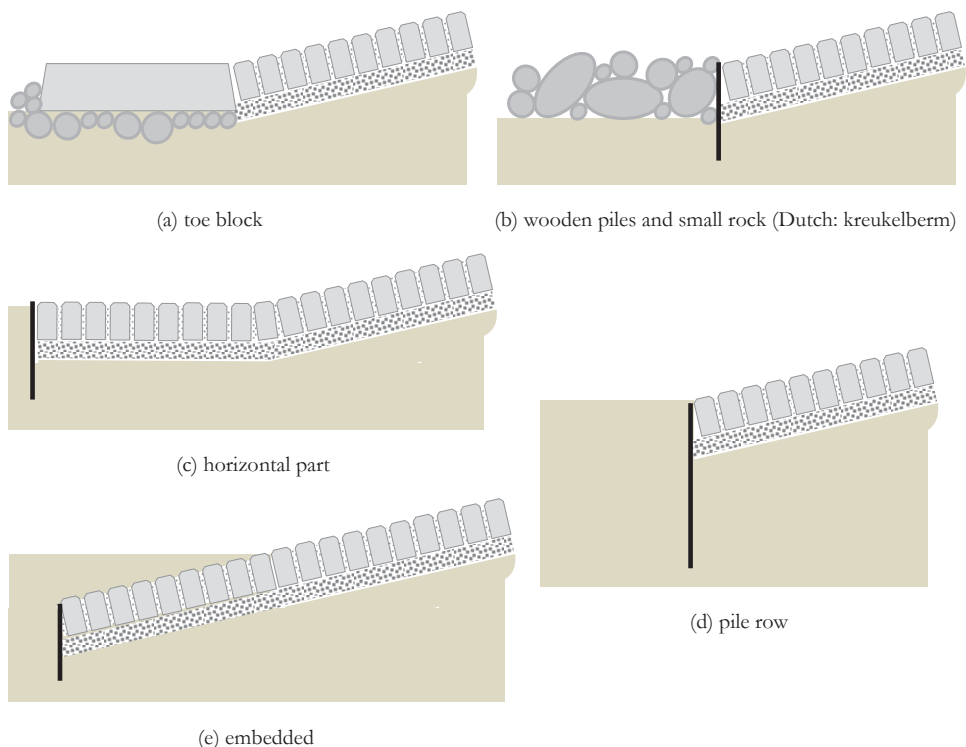
Figure 3–25   Types of toe structures

The toe structure prevents the elements on the slope above to slide downwards.[98] The lateral load capacity and the rigidity of the toe obviously vary per type. The rigidity of the toe structure is important since it determines the built up of normal force against the toe. The effect of toe stiffness is investigated in models and is measured also (refer to Annex A1 and H).

In practise there are not much problems with toe structures. Reported failures under wave attack are very rare.[99] During super-storm conditions they are likely to be sufficiently deep under water. The fact that toe structures did not show much trouble so far could also be caused by the hold off of serious storms. The structures may never been exposed to the design loads. Full development of the loading on the toe only occurs when high water levels and large waves are present.

---

[98] W. van der Kleij, ed., "Leidraad Zee- en Meerdijken" (TAW report L3, 1999)
[99] In the Maasvlakte damage case (see section 4.3.3) the toe structure was also destroyed.

(a) Reference case: no revetment, no toe

(b) Revetment experiencing friction forces, partially resting against the toe

friction interface

(c) Sliding revetment, resting against the toe

sliding interface
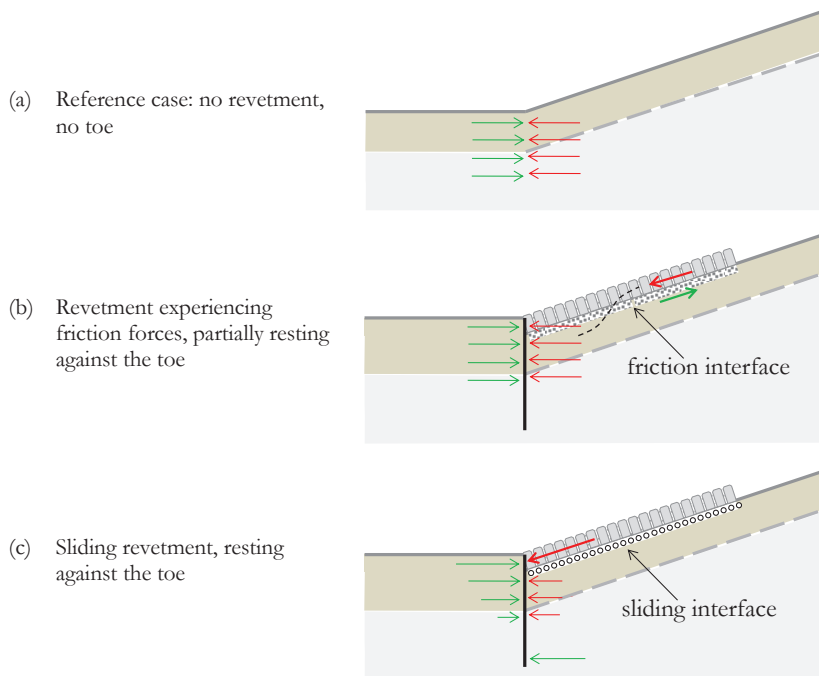
Figure 3–26   **Effect sliding revetment on location of loading of the toe structure**

3.2.2 *Loading of the toe*

A small toe structure would not increase the stability of the slope itself. For slope stability considerations refer to section 4.1.7. If the slope is armoured with a relatively light revetment that is stiffer but not much heavier than the specific weight of the soil (2500 versus 1800 kg/m^3), and if the revetment has a friction interface underneath and is stable in slip, the stress state at the toe for verification of the stability is in rough lines the same as without a revetment. The hydraulic heads during waves loading might change this.

If the revetment rests on a sliding interface (case (c) in Figure 3–26), the revetment weight is accumulated into a concentrated force at the low end of the slope. This force needs to find equilibrium and is to be considered as a load on the toe structure.

The sliding equilibrium for the revetment top-layer itself has also been considered with a static model. The revetment is assumed impermeable and experiences upward friction forces R_{fr}. If the friction force is too small, the remaining force required for equilibrium is the force that forms the load of toe structure. An impermeable revetment experiences relative large uplift force W_2 and would hence have the tendency to slide downward, resulting in a larger force R_{toe}. In this model a very permeable revetment will be more stable and conditions for which the revetment does not need support from the toe at all can be calculated
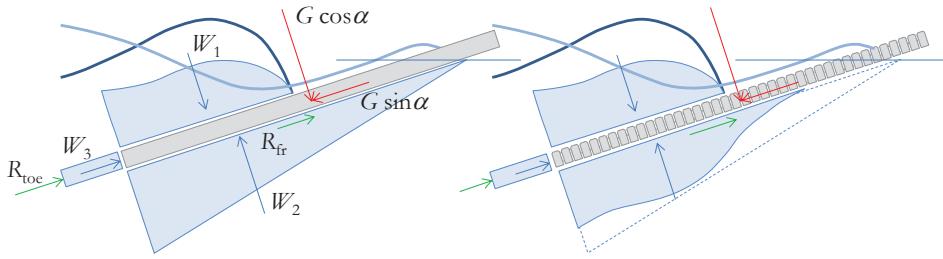
Figure 3–27 Sliding revetment beam with water pressures, left impermeable, right permeable

$$G = \rho_s g D L_x$$
$$W_i = \int \rho g(\phi - z)\,\mathrm{d}x$$
$$R_{fr} = f_{fr}(G\cos\alpha + W_1 - W_2)$$
$$R_{toe} = G\sin\alpha - R_{fr} - W_3$$

Eq. 3.3

Waves on the slope do not only cause forces perpendicular to the revetment, but also change the pressures in the joints. Considering these pressures as 'internal' pressures and neglecting them assuming that they do not affect the equilibrium of the total beam is not realistic. The joint pressures can be very high and could hence push the top part of the revetment upward (potentially causing the friction force to change its direction), and the lower part of the revetment downward. The lower part can as a result loose its sliding equilibrium, and consequently start resting against the toe much earlier than assumed in the static model.

Also individual elements may be lifted from the bedding, which resets the friction force between element and bedding to zero. The revetment element rests against its lower neighbour. This process also causes that for the total revetment beam the support by the toe will increase and support by friction forces on the interface of revetment elements and bedding layer will decrease.

3.3 Shallow foreshore

Depth limitation of the wave height is an important phenomenon especially relevant for pattern-placed revetments that are a favoured revetment type in tidal areas with shallow foreshores. As such the foreshore condition is considered an inseparable component of the dike design and the revetment slope design.

The effect of water depth on the characteristic and the maximum wave heights is discussed in detail in section 5.1.

Determination the location and magnitude of the load should also include the effect of limited water depth. The design conditions for wave height and period are normally associated with a surge level. During a serious storm the water level may vary due a process of increasing wind set-up or due to astronomical tide. Also the design wind speeds and development of a design wave field is not always associated with a high water levels, this only holds for certain wind directions.

Therefore, the design wave attack for a certain slope should be combined with a range of water levels below the anticipated maximum level. Given a certain deep-water wave period and -height, the waves will start to be affected by depth below a certain water level. A

portion of the waves will then break before the slope and not on the slope. Also the breaker type will change, since the waves will respond to the foreland bottom slope angle rather than the dike slope angle, or to a combination of both. The depth limitation causes a decrease of H_s compared to the undisturbed H_{so} and will change the wave height distribution. The high (2%) waves within the spectrum will be lower. Associated with that the run-down is less deep and the revetment load is smaller (see Figure 3-28).

For the water level range between the depth limit and the design level the wave effects are constant. At the design level the full wave spectrum is acting, meaning that the run-down and wave impact of less extreme waves have load effects higher on the slope. This leads to a load envelope as indicated with required revetment thickness in Figure 3-28. Refer to Figure 2-11 also.
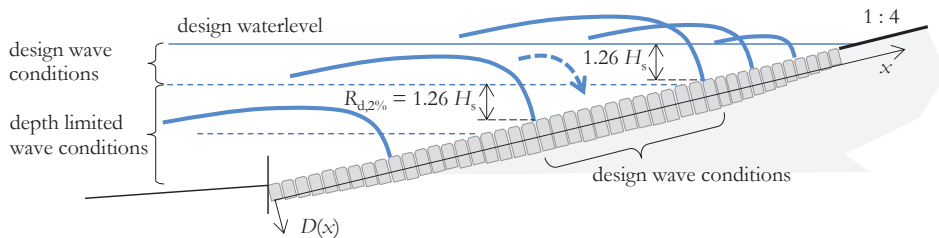
Figure 3-28 **Load envelopes for various water levels, run-down for irregular waves with $s_o = 0.02$**

The phenomena of depth limitation and slope angle can be utilised as favourable effects while designing a robust revetment system. This could either lead to differentiation of revetment thickness[100], or to designs with variable slope angles. For the revetment design at low water levels it can also be considered to adopt a more relaxed damage-acceptance, since the smaller waves will not threaten the clay layer and the water levels will not cause flooding.[101]

3.4 Permeability properties

The permeability properties of classic and modern pattern-placed revetments are an integral component. The effect of the waves in terms of loading of the top-layer is besides the wave height and wave period, determined by the permeability properties of the system.

3.4.1 *Theory and typical parameter values*

After 1980 systematic research on the stability of revetments was started as part of the design activities for the Oesterdam[102]. The focus was on 'modern' structures, like blocks applied directly on clay, which were later considered as unfortunate. Other types were investigated also, amongst them concrete column elements on permeable sub layers, which show similarity to traditional, proven structures.

---

[100] Like the original Afsluitdijk design.
[101] Damage at low positions will propagate upwards since the lower elements do not support the normal force-state in the higher elements anymore.
[102] Although failure mechanisms of blocks on clay were known during the construction of the Oesterdam in 1985, it was decided for economic reasons to apply blocks on clay. This system was applied between NAP +0.8 en + 4.0 m, in the wave attack zone and failed later in a moderate storm.

The two concepts considered, on clay or on permeable sub layer, differ with respect to the permeability properties which were understood to be very important parameters for the stability. In the research publications of the 1980s the drainage or leakage factor Λ/D was introduced. The drainage factor determines the filter pressures that occur simultaneously with wave loads on the slope, or with a little phase shift. The water pressures in the filter and corresponding uplift forces are the main cause of instability of the top-layer elements. The open revetments can therefore looked upon as a structure that controls the design load by its own permeability properties. An open top-layer is favourable. A thin filter layer also, but a thin filter layer gives high flow rates, which may be critical for sand layers under the filter. A courser filter prevents washing through an open top-layer, but is more permeable, which is sub-optimal from stability point of view. The calculation of filter and top-layer permeability makes use of turbulent flow formulas.

The chosen ratio of permeabilities of top and filter layer k'/k should not decrease in time, which is the problem with blocks on clay. In Klein Breteler (1992) the stability formulas of the revetment are based on the theory of hydraulic filter action and resulting water head differences, using the drainage length Λ, which is a length along the slope[103], and usually is between 0.5 and 3 m.
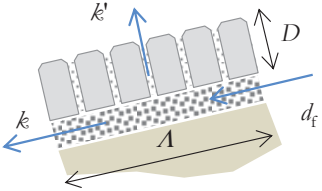
Figure 3-29   Definition diagram flow balance and leakage factor

$$\Lambda = \sqrt{d_f D \frac{k}{k'}} \text{ [m] or } \frac{\Lambda}{D} = \sqrt{\frac{d_f}{D} \frac{k}{k'}} \text{ [-]}$$ **Eq. 3.4**

with
k = filter permeability [m/s], in case of more than one filter layer: $d_f k = d_{f1}k_1 + d_{f2}k_2$
k' = top-layer permeability [m/s]
d_f = filter thickness [m]
D = top-layer thickness [m]

The applicability of the theory is limited to the cases for which $k' << k$, and $k > 0.001$ m/s.

Table 3-3   Top-layer permeability

Top-layer type	Top-layer permeability	k' [10^{-3} m/s]
Open spaces	Very large	60 -100
Columns with washed in joints / broken stone	Large	5 – 20
Large blocks with cracks, without holes	Small	3 – 10
Cracks silted up	Very small	< 1

---

[103] In older literature sometimes a vertically projected length factor is used: $\lambda = \Lambda \sin\alpha$.

The smaller the top-layer permeability, the larger the indicated bandwidth of k', and as a result the larger the inherent uncertainty of the system is. Typical values of the filter permeability are indicated below.

Table 3-4   Filter layer permeability determining parameters

Material		D_{f15}	Porosity n
Broken natural stone, chippings, gravel a/b		0.8 – 1.3 a	0.3 – 0.4
Mine stone *) 0/70		1 – 5 mm	0.2 – 0.35
10/125		5 – 15 mm	0.25 – 0.35
Silex **) 5/25		4 – 7 mm	0.3 – 0.4
25/70		18 – 35 mm	
Slag ***) 8/25		6 – 12 mm	0.3 – 0.4
Slag 5/70		4 – 8 mm	0.25 – 0.35

*) by-product from coal mining
**) rest product from cement industry
***) rest product from metal mills

Internal stability of the filter material must be checked also.

3.4.2   Calibration with field tests

Model values and measured values on slopes used in full scale flume tests were compared as part of a calibration study[104].

Field measurements of the permeability of top-layers have been performed as a part of field testing campaigns (see references in Table E-2). The field measurements did not produce reliable results but the general conclusion is that the measured top-layer permeability k' is in many cases much higher than predicted by theory, up to 10 m/s for Basalton-like revetments. For block type revetments with small joints, a dependency on the position on the slope could be observed. At low positions the permeability is around the theoretical value and at high positions the value is much higher. A high top-layer permeability is positive for the stability. The high values might be caused by empty joints, which is not good for element interaction.

For too high top-layer permeability, and associated theoretically very low value of the leakage length Λ, the design loads may become low and very localised. Since a high top-layer permeability might be difficult to sustain in practise, a minimum value for the factor Λ/D has been recommended, leading to a maximum stability number (see 3.4).

3.4.3   Siltation risk

Sand collection in the filter layer significantly reduces the filter permeability, and through that compromises the stability of revetments which were designed with an open filter.[105] For those revetments collection of sand can thus induce failure. For revetments with a relatively closed top-layer and insecure interlocking contributions filter siltation is potentially

---

[104] D.J. Peters, "Veiligheidsbeschouwing SteenToets, bepaling partiële factoren", annex C in: M. Klein Breteler, *Validatie Steentoets2008* (WL|Delft Hydraulics report H4846, 2008)
[105] T.P. Stoutjesdijk, *Stabiliteit steenzetting te Breskens* (GeoDelft report, 1995)

beneficial. Stoutjesdijk & Bezuijen[106] have developed a model that can predict the propagation of siltation over time. The siltation starts at the toe and goes up to the normal high tide level. Dependent on occurrence of waves the slope can be filled with sand in 2 to 10 years. Siltation of revetments has been simulated with large scale flume tests on revetments with simulated siltation.[107] Measured beginning of damage (element movement) was observed at load levels compared to new, clean revetments. Serious damage was measured at equal or higher load levels. Higher head differences were measured, which means that (contrary to the leakage theory) siltation has a negative effect on the load, but apparently a (larger) positive effect on the resistance.
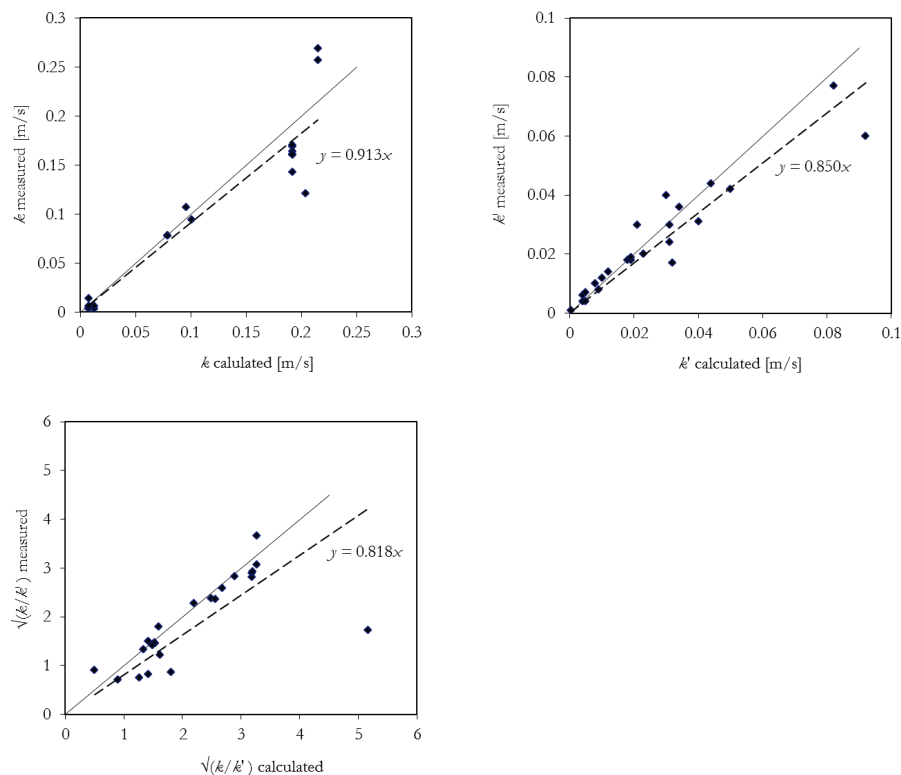
Figure 3-30   Measured permeability parameters compared

[106] T.P. Stoutjesdijk, A. Bezuijen, and P. Lubking, *Taludbekledingen van gezette steen - Verouderen van steenzettingen* (Grondmechanica Delft report CO-316860/3, 1991) T.P. Stoutjesdijk and A. Bezuijen, *Modelleren van verouderen van steenzettingen* (GeoDelft report CO-353150/15, 1995)

[107] M. Klein Breteler, K.W. Pilarczyk, and R. 't Hart, "Influence of ageing and wide wave spectra on stability of placed block revetments," *ICCE* (Sidney, 2000)

3.5 Revetment failure mechanisms

3.5.1 Failure definitions

The function of the revetment is to protect the dike from erosion by waves.

- <u>Revetment failure</u> is therefore defined as loss of ability to prevent erosion of the sub layers.
- Revetment failure is hence not the top failure-event, but is followed by slope erosion before <u>dike failure</u> occurs. This contribution is called residual resistance.

A revetment is allowed to fail under conditions that go beyond the defined design conditions, but is not allowed to fail when exposed to those defined design conditions, amongst those an enduring exposure. The state of non-failure is defined as an ultimate limit state[108] (ULS) and this criterion must be met with an appropriate level of reliability. If the structure does not fail it is acceptable if it deforms or is weakened. It is however undesirable that this happens too frequently. The structure must, as a principle, maintain its serviceability during environmental conditions that have a high probability of occurrence during the service life. Conditions with return periods equal or shorter than the service life may not violate possible so-called serviceability limit states (SLS), such as a limit state of deformation, or a limit state of vibration. Serviceability limit states can be distinguished in reversible and irreversible states. Those conditions are normally much lower than the design load condition.

A number of processes may affect the properties of the revetment system during service life, such as dike settlement, change in water depth or foreland height, toe deformation, sand and sediment in the joints, joints material wash-out, movement of a group of elements, etcetera. These events should be avoided in the design when evaluated against SLS conditions. Proper maintenance should keep the structure in good condition. These events can create unfavourable pre-conditions that might decrease the revetment stability in ULS conditions.

The failure state which is unacceptable in ULS is a loss of position in the pattern of two or more top-layer elements (see (a) in Figure 3-32). This is caused by two types of failure of the revetment beam action: shear failure (b) and bending failure (c).

The other deviations from the initial state, like one lost element of uneven settlement are not ULS failure state as such. In those damaged states the revetment still protects the dike slope against erosion. Those states might lead to failure if the load persists. This is indicated in the fault tree of Figure 3-31 where the failure states leads to pre-conditions that worsen the stability and might lead to failure in a later stage.

The analysis of the failure mechanisms presented below is supported by a failure patterns in (scale) model tests and by observations in literature and available descriptions of real failure events.

---

[108] Eurocode EN 1990 definition: A limit state is the state beyond which the structure no longer fulfils the relevant design criteria. Or in A.C.W.M. Vrouwenvelder and P. Schiessl, "Durablity aspects of probabilistic ultimate limit state design," Heron 44:1 (1999): 19–29: A limit state is the border that separates the acceptable state from the adverse state.
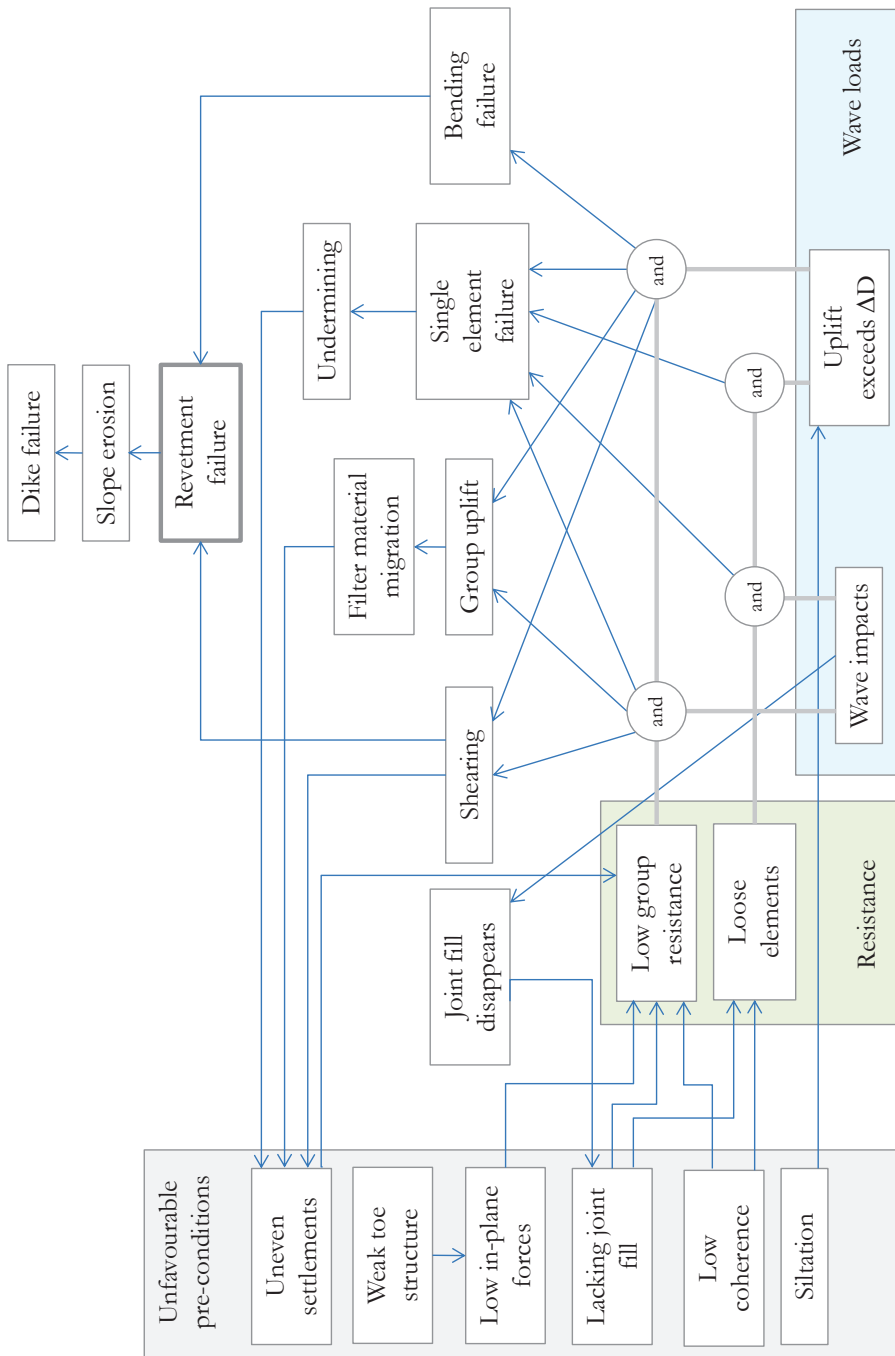
Figure 3-31   Failure relation diagram with revetment failure events

Top-layer with joint fill (not failed) (a) Revetment failure

Group uplift Uneven settlement

Single element failure Undermining

(b) Shear failure (c) Bending failure

Deformed toe with loss of in-plane force Deformed toe with rotated and sheared elements
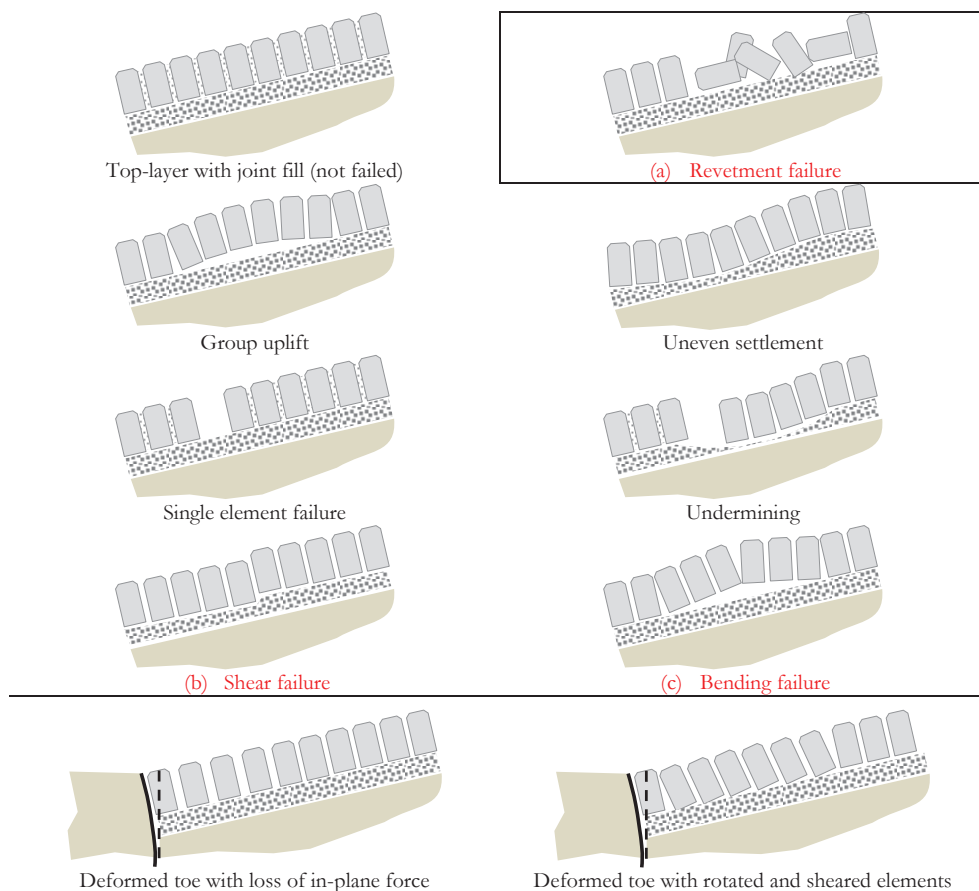
Figure 3-32   Revetment failure mechanisms

3.5.2   *Failure initiation*

Failure might be initiated by several smaller events or phenomena, which cause a chain of events resulting in 'revetment failure'.

Failure may be initiated by:

- Unstable uplift of a group of elements due to overloading
- Stable uplift of a group of elements due to overloading, combined with too much deformation and sub-layer disturbance
- Single element failure or the piston mechanism. If one revetment element fails and sub layer material will be washed out, the top-layer will experience local undermining and a larger amount of elements may fail successively.
- Shear failure and/or shear deformation at the interface between revetment elements
- Lack of sufficient stabilizing in-plane forces
- Permanent deformation of the toe
- Too low position of the top edge of the revetment

- Siltation of the top-layer
- Siltation of the filter layers
- Wear and tear of the revetment elements, creating decreasing straightness and round edges and spherical sides
- Erosion of filer layer material through the top-layer
- Subsidence and settlement of the dike body combined with poor ability of the revetment system to adapt to that deformation may case undermining.

The causal relations of all these factors are indicated in the scheme in Figure 3-31. The scheme contains the different failure mechanisms and the successive events, as well as how these events, if they do not lead to immediate failure, influence the pre-conditions of the structure, making it more vulnerable for a new event with design conditions.

3.5.3 *Discussion on failure and reliability levels*

In literature the failure definition, the failure mechanism and its initiation, the ability to really define the beginning of failure, and the probability of the conditions leading to beginning of failure and the probability complete loss of revetment function are sometimes mixed up.

The analytical model ANAMOS (refer to section 4.1) designs for single element motion. Single element failure is defined as beginning of failure. The failure definition within this approach was also discussed by Den Heijer[109]. It was suggested that there is a large margin between single element motion and complete revetment failure. It differs per revetment type whether this is true or not. When the revetment structure becomes unstable under wave loads it will be subject to motions and rearrangements. Elements become loose, are lifted up, can lock-in, may become loose again, etcetera, and can finally be moved out completely.

Stroeve[110] also distinguishes between the nature of failure of the different revetment types. Regular shaped, rectangular blocks tend to lift up completely shortly after they become unstable. Irregularly shaped columns tend to lock-in again after a minor uplift deformation. Also a proper joint fill helps to stabilise potentially unstable single elements. Stroeve introduces a brittle and more ductile nature of failure.

In the proposed scheme of Figure 3-31 a 'sudden/brittle' single element failure (through the piston mechanism) is not considered as equivalent to revetment failure but will create a risk of undermining and might worsen the ability of the revetment to withstand new and higher loads.

The proposed limit state design approach for a revetment structure can be outlined as follows:

A ULS design requirement can be defined in line with national regulations for reliability[111]: to survive a storm event with a probability of failure of the order of 10^{-4} or 10^{-5}.

---

[109] F. den Heijer, *Veiligheid huidige ontwerpmethodiek steenzettingen* (WL|Delft Hydraulics report H3437, 1998)

[110] J.M. Stroeve, *Veiligheidsanalyse steenzettingen - voor enkele dijkvakken langs de Westerschelde* (Bouwdienst RWS report, 2000)

[111] *Leidraad Kunstwerken* (TAW report L15, 2003); B. van Bree et al., *Leidraad Waterkerende kunstwerken in regionale Waterkeringen* (STOWA 2011-15, 2011); J.J. Flikweert, *Technisch rapport Steenzettingen* (TR25, TAW report by Royal Haskoning, 2003)

- The toe structure must be strong and stiff at all times, ensuring that normal force has been built up prior to the design event
- The type of top-layer elements must be able to keep the joint fill in place and maintain the drainage properties at a constant level during the event
- Bending and shear failure are not allowed at the level of the 0.1% wave, being the highest waves in a series of 1000 waves. Given the variability of the resistance the reliability level of the design value of the resistance must be in the order of 10^{-2}. In practice this requirement might be expressed and related to the 2% wave with a certain partial factor, expressing the uncertainty of the exceedance of the wave load.
- Group uplift and single element failure are not allowed at the level of the 5% wave. The consequence of this requirement is that the revetment is allowed to move and to settle and might loose single elements under the conditions of the highest 5% of the waves. This number of waves is considered small enough to avoid the development of an undesired damaged condition during the design event. This condition requires maintenance and/or repair afterwards.

Service-ability is guaranteed by defining load levels below which the revetment is maintenance-free. SLS design requirement: a storm with return frequency of the order of 1/10 or 1/50 year.

- Bending and shear failure are not allowed at the level of the 0.1% wave. The reliability must be in the order of 10^{-1}. In practice this requirement might be expressed and related to the 2% wave with a certain partial factor.
- Group uplift and single element failure are not allowed at the level of the 0.1% wave.

4 DISCUSSION OF DESIGN METHODS AND RESEARCH IN LITERATURE

The behaviour of pattern-placed revetments is systematically researched since the 1980s. This had led to test programs and to reports with theoretical background and model descriptions. Parts of this work have been a basis for the definition of a design philosophy as presented in chapter 3. The development of the theories and design ideas is outlined below.

Further the source and nature of failure data from experiments and from real cases is discussed.

4.1 Stability formulas of pattern-placed revetments in literature

4.1.1 Single element failure

The single element weight has for a long time been seen as the determining factor for the stability of pattern-placed revetments. This has similarities with the empirical design for random placed armour (see section 4.2).

The recommended failure criteria in Klein Breteler, 1992 for the failure mechanism 'instability of the top-layer' are based on single element failure. It is stated that, despite stability contributions based on element interaction, a single element failure always can occur. It must be said that this statement is probably related to the flat concrete block revetments which were very common in the 1980s. The probability of single element failure also proved to be a risk in practise. A couple of actual damage cases show failure of single, obviously loose elements.

The single element failure mechanism was evaluated by considering effect of wave heights from the irregular wave height distribution. More specific, it is stated that waves with significant height H_s must not destabilise revetment elements, and waves between H_s and $H_{2\%}$ must not cause element motion larger than 10% of the element height. The difference in resistance belonging to the first and second criterion is in the resistance provided by inertia and restraint inflow of water in the volume under the element in motion (suction forces).

Pulling tests on single elements were performed as a part of the investigations into the stability of the pattern-placed revetments. Pulling tests were performed in model tests as well as on dike slopes in realty. After a couple of singular studies in the 1970s and 80s a systematic pulling test campaign was started in the 1990s. The pull tests covered two objectives: proving that the revetment structure was stronger than the single element weight, and counting numbers of loose elements. On basis of good results of in-situ pulling tests recommendations were formulated for stability numbers larger than the one based on single element failure. The pulling tests were not systematically reviewed on bases of a theoretical model (see Annex C).

As a result of the research activities design rules were developed. The design methods are verified for 1:3 and 1:4 slopes only. The general application range is between 1:2.5 and 1:6.

The design manual CUR 155 (Klein Breteler, 1992) extensively reports on design rules based on the filter law equations. These rules were incorporated in the computer program ANAMOS, which is based on analytical formulas and is meant for open top-layers on thin filter layers. Soon after these rules were applied, it was realised that these rules stimulated

designers to apply very small leakage factors making the structure vulnerable for wave impacts, which compromised a quest for redundant designs. To overcome this, structures with a courser, more permeable filter became common. The design rules were changed, introducing the 6ξ-rule (see Figure 4-1).

4.1.2 Simplified analytical design formulas

A simple run-down formula for smooth slopes can be given as.[112]

$$\frac{R_d}{H_s} = 0.33\xi_{op} \not> 1.5$$

Eq. 4.1

For an impermeable top-layer, and no drainage of the core of filter material, the absence of water pressure above the top-layer causes an uplift pressure p_w, or an uplifting hydraulic head $\phi_{dip} = \rho g\, p_w$.

$$p_w = \rho g R_d = 0.33\rho g\, H_s\, \xi_{op}$$

Eq. 4.2

The resisting uniformly distributed stone weight is:

$$p_s = (\rho_s - \rho)gD\cos\alpha$$

Eq. 4.3

Requiring equality of Eq. 4.2 and Eq. 4.3 this leads to:

$$\frac{H_s}{\Delta D} = 3\frac{\cos\alpha}{\xi_{op}}$$

Eq. 4.4

with

Δ = the relative buoyant density: $\Delta = \dfrac{\rho_s - \rho}{\rho}$

ρ_s = density of top-layer material
ρ = density of water

When applied to revetments with permeable properties the factor 3 in Eq. 4.4 leads to conservative results. The formula has however been used in a number of studies as the basis for a 'high level' assessment of revetment stability.

For the effect of permeability and drainage of the system refer to sections 3.4. and 5.3. The combined unknown effects on the stability and the reliability of the system results in a quite large area between the empirical line above which the revetments are unsafe, and the theoretical line below which the revetments are safe (see Figure 4-1).

4.1.3 Black box formulas

As a general empirical formula for the stability of permeable revetment the following expression is used since the early 1990s[113].

$$\frac{H_s}{\Delta D} = F\frac{\cos\alpha}{\xi_{op}^{\,b}}$$

Eq. 4.5

---

[112] See section 5.2.2 for considerations on the run-down-point.
[113] K.W. Pilarczyk, M. Klein Breteler, and A. Bezuijen, "Wave forces and structure response of placed block revetments on inclined structures," *Int. conf. Coast. Eng.*, 1995

F is taken as 6, b as 0.67 and $\cos\alpha$ as 1, resulting in:

$$\frac{H_s}{\Delta D} = 6\,\xi_{op}^{-\frac{2}{3}} \text{ for cot } \alpha \geq 2 \qquad\qquad\qquad \textbf{Eq. 4.6}$$

This dependency $\xi^{2/3}$ was a theoretical fit confirmed by regular wave tests. After irregular wave test became more common, there were initially no tests beyond the range $\xi = 1.1 - 2.2$. Later tests confirmed that the stability in the range $\xi > 2.5$ was much larger. Hence a correction was introduced[114], resulting in an increase of the stability number with 1.5 over the range $2 < \xi_{op} < 5$. Also the coefficient b was changed into a value of 0.33.
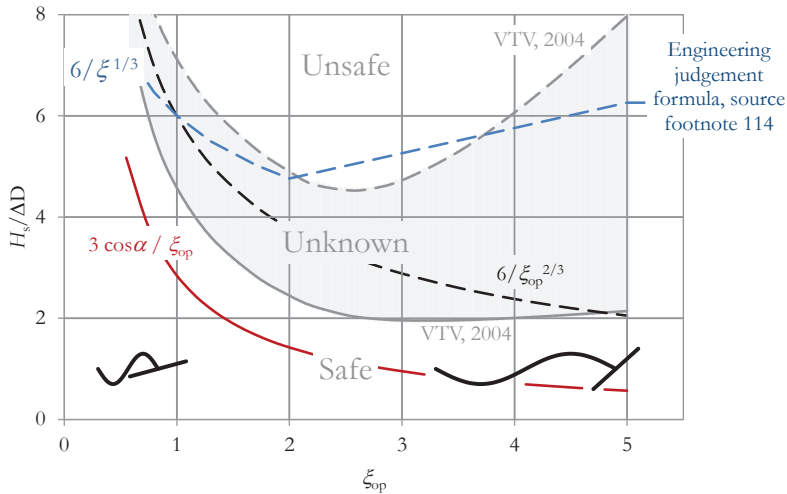
Figure 4-1   Design formulas plotted in chart with stability number against breaker parameter

4.1.4   *Further development of design rules*

After Delta flume model testing in the 1990s and the evaluation reports of 2000, the design rules became more subtle and more complicated, which led to the computer program SteenToets. SteenToets allows for an automated verification of designs and of existing slopes subjected to new hydraulic load conditions, and evaluated according to the newest insights. Also simplified design charts were developed and published[115]. One of these is shown in Figure 4-1.

In the evaluation methods of around 2001, the first start of the work on this thesis, the effect of element interaction was not fully integrated in the design methods. Researchers were aware of the contribution of lock in forces to stability but were reluctant to explicitly take profit of these effects.

---

[114] M. Klein Breteler, G.C. Mourik, and M.C.J. Bosters, *Stabiliteit van steenzettingen bij golfaanval, Samenvatting onderzoeksresultaten 2003 – 2013* (Deltares report 1208045-016 for RWS-WVL, 2014)

[115] *Veiligheid van de primaire waterkeringen in Nederland, Voorschriften Toetsen op veiligheid voor de tweede toetsronde* (DWW report VTV, 2004)

The reasons for this included the following considerations:
- the risk of loose elements. This risk differs per revetment type.
- the complicated nature of the lock-in phenomena
- the necessity to also investigate a number of possible other negative effects on stability

During 2001-2007 the effects of mechanical element interaction were studied and published[116]. These studies were commission by Rijkswaterstaat, DWW and subsidised by Delft Cluster. In the SteenToets versions after 2008 a number of design rules have improved. Amongst them the contribution of element interaction to stability, but also the hydraulic loads during wave breaking, the effect of the number of waves and the effect of variable water levels during a storm. All this has led to more accurate but not necessarily more favourable design rules.

4.1.5 Model Bezuijen

In 1990 Bezuijen[117] presented a model to control element movement by friction interlocking of the adjacent elements. He refers to earlier contributions of Sellmeyer and Wolsink who described bending action by eccentric normal forces[118]. In the model consists of a string of elements was loaded with head differences f. The deformation and equilibrium of the element was formulated using a spring constant C as characteristic of the element-element interaction. The bending moment $M_i = (\theta_{i-1} - \theta_i)\,C$. The element equilibrium is given by:

$$V_i - V_{i-1} + G\cos\alpha - \tfrac{1}{2}(f_i + f_{i+1})B = 0$$
$$M_i - M_{i-1} + V_{i+1}B + \tfrac{1}{2}G\cos\alpha\,B - \tfrac{1}{6}f_i B^2 - \tfrac{1}{3}f_{i+1}B^2 = 0$$

Eq. 4.7

Substituting rotations θ for the bending moments M and adding an equation requiring that the sum of the angular deviations of all considered elements is zero, results in a set of 2n+1 equations for n unknown element rotations and n+1 unknown shear forces. This formulation provides a correct and adequate equilibrium criterion for single elements and element groups, based on friction interaction, forming a beam. The design formulas developed after 1990 however were generally focussed on loose elements.
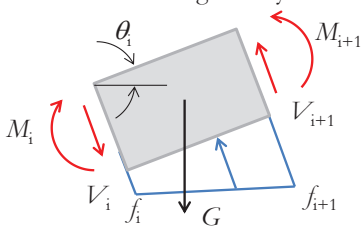
Figure 4-2   **Friction forces experienced by block pulled out by perpendicular force**

[116] D.J. Peters, *Placed revetments under wave attack - Study of structural mechanics* (Delft Cluster report DC1-325-1, prepared by Royal Haskoning, 2003) J.A.H. Blom, L. van Nieuwenhuijzen, and D.J. Peters, *Test result and analysis report on prototype tests on clamped revetments in Zeeland*, 2007

[117] H den Adel and A. Bezuijen, *Mechanische sterkte toplaag*, 1994; A. Bezuijen, A.M. Burger, and M. Klein Breteler, *Taludbekledingen van gezette steen - Samenvatting onderzoeksresultaten 1980- 1988* (WL / GD / DWW report H1795/H195 deel XXIV, 1990)

[118] Chapter *Beweging van blokken* by A. Bezuijen in: M. Klein Breteler, *Taludbekledingen van gezette steen - stabiliteit van de toplaag* (WL Delft Hydraulics report M1795 part XX, vol. B / GeoDelft report CO 285453/7, 1992)

Single element failure is dominating the stability formulas. The fact that the blocks are closely placed and interact is assumed not to provide a reliable contribution to the stability, apart from a small effect of friction of a single block against the neighboring block at a lower position.

The stability formula[119] is as follows, where the left-hand terms represent the loads and the right-hand terms the 'resistance'.

$$\phi_{dip} - \phi_{suction} = \Gamma_{friction} \Delta D \cos \alpha + \phi_{inertia} \qquad \text{Eq. 4.8}$$

The main load component is the water head difference ϕ_{dip} which is calculated with the formulas presented in section 5.3. A term $\phi_{suction}$ represents a local effect of restraint flow of water into the cavity that a moving element leaves behind. Sudden motion is assumed to generate suction forces.

$$\phi_{suction} = \frac{1}{1.5\pi} \frac{\varepsilon\, D^2 \sqrt{B_x B_y}}{k' \Lambda t_0} \left(0.56 + 0.18 \ln(\frac{\sqrt{B_x B_y}}{\Lambda}) \right) \qquad \text{Eq. 4.9}$$

The suction effect is later criticised by Bakker.[120] When single elements move individually but one after another, in cascade, they will not experience effects of restrained inflow through the filter, but will transfer the required air volume under the elements to the adjacent element.

At the resistance side of Eq. 4.8 side a 'load reduction' term $\phi_{inertia}$ appears. If the acting force has a limited time duration, e.g. 0.1 to 0.5 seconds, the element motion will stop before the element has failed. Failure is defined as uplift of the element over its full height D. If an allowable deformation of $\varepsilon D = 0.1D$ is defined, this can be calculated back to a load reduction term.

$$\phi_{inertia} = 1.8 \frac{\varepsilon\, D^2 (\Delta + 2)}{g t_0^{\,2}} \qquad \text{Eq. 4.10}$$

The load on the block is resisted by the gravity component $G \cos\alpha$, and by friction forces acting on the moving block. It is assumed that the neighbouring blocks have no tendency to move. Initially there is no axial force that creates frictional interlock of the block from two sides. The only axial force is the gravity component of the considered element in motion, being $G \sin\alpha$.

The friction component is limited by slip and by rotation. Columns will slip, blocks rotate before they slip. Equilibrium of a single element that is force to slide upwards between two blocks that are stable on the slope is given below.[121]

$$\Gamma_{friction} = 1 + f_{fr} \tan \alpha\, (1 + f_{fr} \frac{B}{D}) \qquad \text{Eq. 4.11}$$

---

[119] Klein Breteler, *Handboek voor dimensionering van gezette taludbekledingen*
[120] Bakker, "Soil retaining structures - ch. 5: Block Revetments"
[121] This formula is different from the one given in Klein Breteler, 1992.
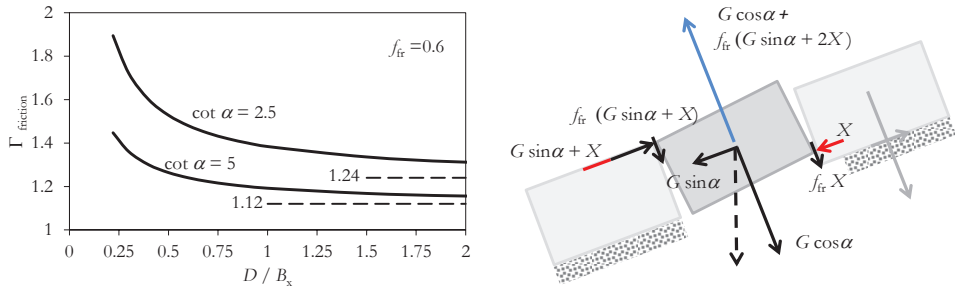
Figure 4-3   Friction forces experienced by element pulled out by perpendicular force

4.1.7   Comprehensive studies by Hussaarts and Stroeve

The MSc-thesis of Hussaarts, 1999[122] intended to give a blueprint of a complete reliability approach. In his thesis Hussaarts focuses on a case in Friesland, because the availability of statistical information on meteorological and hydraulic conditions.[123] The results of 22 storms and the hydraulic conditions caused by these storms, calculated by means of SWAN-models, are evaluated. The parameters flood level h, significant wave height H_s, wave direction β and wave steepness s_{op} are modelled as stochastic parameters, initially assumed as normally distributed, and later in the study refined using other extreme value distributions for h. The found correlation coefficients ρ_{xy} are shown below. The low correlations for β are most probably due to the narrow bandwidth. The directions are between 290 and 330 degrees.

$$\rho_{xy} = \frac{\text{cov}(x, y)}{\sigma_x \sigma_y}$$

Eq. 4.12

Table 4-1   Correlation coefficients wave data sets in (Hussaarts, 1998)

ρ_{xy}	h	H_s	s_{op}	β
h	1	0.92	0.23	0.04
H_s		1	0.48	-0.04
s_{op}			1	0.16
β				1

For the reason of modelling the variable wave steepness on a slope with constant angle, the parameters sop and cotα were separated in the stability formula.

$$\frac{H_s}{\Delta D} = F \sqrt{s_{op}} \cos\alpha \cot\alpha$$

Eq. 4.13

Hussaarts makes the factor F stochastic using curve fitting techniques to the results for irregular waves[124]. It was found that $\mu_F = 4.12$ and $\sigma_F = 0.52$. The scatter in F is largest in the range of smaller values of ξ_{op}, due to breaking waves; an improved formula for σ_M contains ξ_{op} as a variable.

---

[122] M. Hussaarts, "Een probabilistisch ontwerp van een steenzetting" (MSc thesis TU Delft, 1999)
[123] G.B.H. Spaan, G.P. van Vledder, and D.P. Hurdle, *Seventy storms in the Friesche Zeegat* (WL|Delft Hydraulics report H3020, 1996)
[124] As presented in Klein Breteler, *Handboek voor dimensionering van gezette taludbekledingen*

Revetment stability is not the only resistance component. Hussaarts also considers the clay layer failure (after revetment failure) and the resistance of the sand body, or in his case the mine stone body of the dike. The conditional probability of failure of the total system after revetment failure P_f is 0.38, for a clay layer thickness of 0.75 m.

Stroeve[125] discusses a number of available stability formulas and adopts simplified version of the stability formula used in ANAMOS/CUR 155, calibrated to the Delta flume results similar to Hussaarts' approach.

$$\frac{H_s}{\Delta D} = c_f \left(\frac{D}{\Lambda}\right)^{\frac{2}{3}} \xi^{-\frac{2}{3}} \text{ with a maximum of } \frac{H_s}{\Delta D} = 6\xi^{-\frac{2}{3}}$$

<div align="right">Eq. 4.14</div>

with
Λ = the leakage length [m]
c_f = a model factor

To this formula two additional model factors are added, for calibration to measured results (m_Λ) and to compensate for the simplification (m_e).

$$\frac{H_s}{\Delta D} = m_\Lambda m_e c_f \left(\frac{D}{\Lambda}\right)^{\frac{2}{3}} \xi^{-\frac{2}{3}} \text{ with a maximum of } \frac{H_s}{\Delta D} = 6\, m_\Lambda m_e \xi^{-\frac{2}{3}}$$

<div align="right">Eq. 4.15</div>

A common expression of the stability number belonging to these formulas is the factor F.

$$F = \frac{H_s}{\Delta D} \xi^{\frac{2}{3}}$$

<div align="right">Eq. 4.16</div>

The calibration factor $m_\Lambda = F_{measured} / F_{model}$, where $F_{measured}$ = test results in the Delta flume and F_{model} = the stability number calculated with ANAMOS. Since block interaction effects are presumed to be present in the measured results, the calibrated stability formula includes these effects. Stroeve argues that m_Λ should be split in $m_{\Lambda1}$ for measured and calculated single block failure, and $m_{\Lambda2}$ for block interactions effects. Neither the measured results, nor the available stability formulas make this split possible. Also element interaction effects in the Delta flume may differ from effects in real structures. A narrow selection of Delta flume results for open column revetment gives calibration results for m_Λ: $\mu = 1.62$ and $\sigma = 0.16$.

Based on the results of his calculations on clay layer survival Stroeve concludes that studying residual strength after failure of the revetment layer is not interesting because the contribution to resistance against dike failure, under the conditions that lead to revetment failure are far too less.

4.1.8 Models in MSc-theses of Suiker, Gerressen, Van Hoof and Frissen

In the MSc thesis of Suiker, 1995[126] an investigation of the element interaction phenomena is presented using a beam model. Reference is made to the first ideas of H.L. Bakker to consider the equilibrium of an axially restraint row of blocks in geometrically deformed state. In 1993 a wooden test model was made and tested. (Suiker, 1995) presents analytical

---

[125] Stroeve, *Veiligheidsanalyse steenzettingen - voor enkele dijkvakken langs de Westerschelde*
[126] A.S.J. Suiker, "Inklemeffecten bij Steenzettingen op dijken" (MSc thesis TU Delft, 1995) and A.S.J. Suiker, H.L. Bakker, and J.G. Rots, "Niet-lineair mechanisch gedrag van beton-steenzettingen op dijken," *Cement*:4 (1997)

calculations and verifications with finite element calculations. As a practical application a transverse row of Haringman blocks is considered. Axial restraints are provided by the stiffness of the pile row and back fill at the toe and at the top of the revetment. Axial forces are caused by the gravity action on higher blocks and on friction forces between the top-layer and the filter layers. In his calculations Suiker subjects the structure to measured water pressures. The distributed pressure loads, as they appear at successive points in time, are imposed on the structure as static load steps. Suiker finds that the axial forces enhance the resistance against perpendicular loads considerably. This mechanism is presumed to be the most important reason behind what he calls 'hidden safety' in block revetments.

In this mechanism second order forces are generated that increase the existing normal force considerably. Initially almost loosely 'connected' elements can as a group geometrically lock-in and experience a higher frictional interlocking after some upward perpendicular deformation of the beam. Note that the flexural beam model in section 3.1 is different from a bar model as shown in Figure 4-4 with axially stiff or spring-loaded ends that in theory can generate high normal forces as a second-order effect.[127] In his model Suiker did not pay attention to the limited capacity for a reaction force.
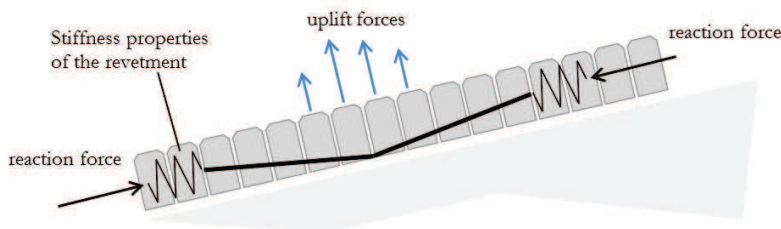
Figure 4-4   **Spring model for lock-in by second order in-plane forces. This model is unsafe.**

Suiker finds a big influence on the block height D on the pull out test results. In the wooden test model, and in FEM calculations simulating these tests, for a double thickness D a 13 times higher pull out force was found, suggesting a relation with the power of 3.7. A close fit of the blocks, and stiff joint properties were important in his simulations. For practical applications the phenomenon of loose blocks is noticed as a weak factor in the structure. Suiker suggests constructing dike slopes with a negative curve, avoiding single blocks to be lifted. The historic and present practice is to construct dike slopes with a slight positive camber. Suiker suggests to further investigate locked-in revetment structures. He requests attention for: 3-dimensional-effects, dynamic calculations, inclusion of more complex (dynamic) hydraulic load effects and improvements in the FEM modelling.

In the MSc thesis of Gerressen[128] the work of Suiker is continued. The focus of Gerressen is on the limitations of the normal force in the revetment. He introduces a model in which the revetment strip is a so-called Winkler beam, a beam on an elastic no-tension foundation. The model enables him to calculate bending moments and shear forces in the beam subjected to

---

[127] In some literature this second-order model is presented as the basic model behind element interaction. This is based on initial investigations with the timber models of RWS-DWW (see section 4.1.7). G.J. Schiereck, *Introduction to bed, bank and shore protection* (Delft: Delft University Press, 2001); H.J. Verhagen, *The stability of pattern placed revetment blocks* (Pianc report WG114, 2011)

[128] B. Gerressen, "Stabiliteit van Steenzettingen - Beschouwing van een dijkbekleding als een verend ondersteunde buigligger" (MSc thesis TU Delft, 1997)

distributed load due to piezometric head differences. His load model is simple and based on the formula for the run-down point: $H_s/\Delta D = 3\,\cos\alpha\,/\xi$. Given this load model, any results higher than 3, are attributed to the favourable effect of the normal force.

Gerressen discusses the effect of the friction between the top-layer and the foundation layer also. Subject to the tendency of the revetment to move up or move down the friction forces will increase or decrease the normal force. Gerressen uses a safe starting point of negative friction where the element rest on the foundation and no friction for the elements when they are lifted.
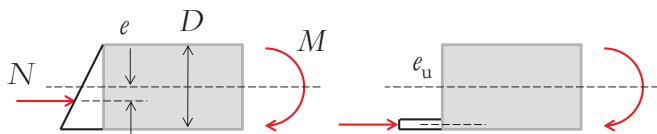
Figure 4–5   **Excentricities in model Gerressen and Vrijling**

As acceptance criterion for the bending moment he uses $M/N = e = D/6$ as a limit value beyond which joint movement and joint material loss may occur. Failure will occur at $e_u = D/2$. Although he uses a load model with very steep gradients he finds that bending failure will be more likely than shear failure. He concludes that when bending moments are exceeded locally in the beam this will result in rotation of an element, which consequently generates other forces that prevents the element from further moving. This suggestion is not quantified or further substantiated.

Another MSc-thesis on pattern-placed revetment resistance is by Frissen, 1996[129]. In this report the focus is on lock-in along longitudinal rows. This is motivated by the results of pull out tests. If the pull out tests show lock-in and lifting of neighbouring elements, these are in longitudinal rows rather than transverse rows. Both Suiker and Frissen refer to rectangular Haringman block structures.

The analytical calculation of snap-through models is discussed and improved by Frissen. As soon as the blocks rotate, the compressive stress concentrates in the edges. There it changes the elastic response of the model and - as a consequence - the results of the snap-through failure. The applied load on the long rows is a distributed load that refers to the wave crest length.[130] Frissen models long rows, where a loaded and lifted part locks in and creates and increases an axial force, which is initially not there. The increased load is balanced with frictional forces in the sub layer under the row left and right of the attacked zone. Frissen only studied blocks of one height: 0.25 m. Stiffness and load length, as well as model length were varied. Attention was paid to modelling of the joints with a discrete crack model for the joint material. The joint opens at a very low tensile stress, virtually zero. The joint has an initial gap of e.g. 2 mm and closes when subjected to a certain compressive stress, e.g. 20 MPa. Frissen used a log-function for this relation. Frissen found that the pull out strengths relate to the square root of the axial stiffness, $\sqrt{E}$, and to the load length as $1/L_y^{\,3}$.

---

[129] C.M. Frissen, "Numerieke modellering van Steenzettingen: effect in langsrichting van de dijk" (MSc-thesis TU Delft, 1996)

[130] Short crested waves, or oblique wave attack on the dike, causes finite, possibly relatively short simultaneous loading of the rows.

Between 1996 and 2000 Frissen produced a couple of TNO reports[131] with finite element modelling of other block and column revetment types. These studies were supervised by H.L. Bakker from DWW. Attempts were made to calibrate the models with pull test results, which lead to promising findings. The studies were not prolonged.

The MSc-thesis work of Van Hoof[132] starts with dissemination of the knowledge of the Winkler beam methods with limited normal force and the snap-through failure approach of H.L. Bakker. Van Hoof continues working with the models and methods described by Gerressen, and calculates more cases. He finds that shear failure will occur earlier than bending failure. He also finds that the stiffness ratio k/EI has significant influence on the results. He therefore recommends closer investigation of the stiffness of both the revetment beam and the foundation.
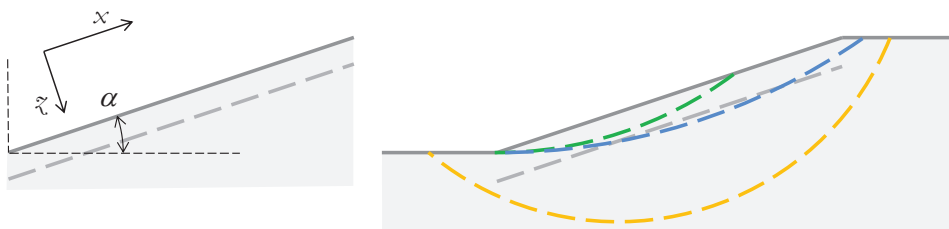
Figure 4–6   Failure modes of slopes

4.1.9   *Geotechnical stability of revetment slopes*

The stability and failure mechanisms of toe structures have been investigated by several researchers.[133] Toe failure is often studied in combination with the mechanism of shear failure or slip failure of the slope and/or of the revetment.

The stability of a submerged infinite slope in Mohr-Coulomb soil is defined by looking into the equilibrium of a soil layer with thickness z. The geotechnical evaluation can be done with drained parameters (c and ϕ) or with undrained parameters (c_u), corrected for the stress level in the clay layer. The safety factor on sliding stability (SF) based on a drained analysis is:

$$\text{SF} = \frac{c}{\gamma_{sat}\, z\, \frac{1}{2}\sin(2\alpha)} + \frac{\gamma'}{\gamma_{sat}}\frac{\tan\phi}{\tan\alpha} \qquad\qquad \textbf{Eq. 4.17}$$

[131] C.M. Frissen and G.M.A. Schreppers, *Inklemming bij steenzettingen op dijken - numerieke analyse en praktijkaanbevelingen*, 1996
C.M. Frissen and G.M.A. Schreppers, *Numerieke modellering van steenzettingen - Zuilenbekledingen met variatiestudies, imperfecties en praktijkaanbevelingen*, 1998
C.M. Frissen, *Numerieke modellering van een blokken- en zuilenbekleding - simulaties van trekproeven en bezwijken door golfbelasting*, 2000
[132] P.J.M. van Hoof, "Inklemeffecten bij steenzettingen, een steenzetting als buigligger" (MSc thesis TU Delft, 2000)
[133] A. Bezuijen, "Geotechnical failure of revetments," *Coast. Zo.*, 1991; P. Meijers, H.J. van der Graaf, and M.B. de Groot, *Taludbekledingen van gezette steen - Grondmechanische stabiliteit in de golfzone en samenvatting van de onderzoeksresultaten* (WL GeoDelft report M1795/M1881 CO 272511, part XXII, section A, 1991); M. Klein Breteler and A. Bezuijen, "Design criteria for placed block revetments," in *Dikes revetments. Des. Maint. Saf. Assess.*, ed. K.W. Pilarczyk (Rotterdam: A.A. Balkema, 1998); P. Meijers, M.B. de Groot, and P. Lubking, *Taludbekledingen van gezette steen - oriënterende berekeningen* (GeoDelft report CO-290730/27, 1990)

with

α = slope angle

c = cohesion

ϕ = soil friction angle

γ_{sat} = saturated soil weight

γ' = effective weight = γ_{sat} - γ_{water}

When the cohesion is zero the critical value of the layer thickness z is undetermined. In cohesive soils a critical depth z_{cr} can be calculated for SF = 1. For infinite slopes there is no contribution of the soil stress in the x-direction of the slope (see Figure 4–6).

If very coarse and permeable top-layers and filter layers are applied on top of an intermediate layer or on a core of granular material this should be relatively course in order to avoid shallow slip failure due to excess pore pressure. The critical depth of the soil z_0 is 0.5 L_{es} $\sqrt{\pi}$, with L_{es} depending on the drainage velocity and the period of the water head difference (the wave period). Bezuijen has published[134] the theoretical background of the influence length L_{es} based on the permeability and the compressibility of the water/air mixture in the voids. In a later publication[135] computed estimates of z_0 as a function of the typical grain size d_{15} of the subsoil show that $z_0 = 0.3$ m for $d_{15} = 10^{-4}$ m and $z_0 = 3$ m for $d_{15} = 10^{-3}$ m. For sandy soils and corresponding large values of z_0 the infinite slope theory is not adequate anymore. For clays ($d_{15} < 10^{-5}$ m) other formulas for the permeability apply and an evaluation including the cohesion, and also an analysis with undrained soil properties applies.

From the mechanism of an assumed slip interface at depth z_0 a minimum revetment weight q' can be calculated to avoid shear failure. In (Meijers, 1994) and in (Pilarczyk, 1995) it is suggested that the top-layer is assumed sliding. See the equations below. The revetment weight only appears in the equations for the normal stress and not in the shear stress in the slip surface, which is beneficial for the outcome and hence not conservative.

$$q' = (\rho_s - \rho)gD + (1 - n_f)(\rho_f - \rho)gd_f$$

$$s_{zz} = q' \cos\alpha + \gamma_{sat} z_0 \cos\alpha - \rho g \Delta\phi \qquad \textbf{Eq. 4.18}$$

$$t_{xz} = \gamma_{sat} z_0 \sin\alpha$$

with

n_f = filter porosity

d_f = filter layer thickness

$\Delta\phi$ = water head difference at depth z_0

A shallow slip failure can be mitigated by a stiff and strong toe.

Cases with a local deep slip circle failure due to wave impacts are analysed also.[136] This is not further studied in this thesis.

For slopes with finite length at the low end of the slope soil stress σ_{xx} can accumulate to the level of K_p σ_{zz}, with K_p being the passive coefficient which can amount 3 to 5 depending on

---

[134] Bezuijen, "Geotechnical failure of revetments"

[135] Klein Breteler and Bezuijen, "Design criteria for placed block revetments"

[136] See: Meijers, Groot, and Lubking, *Taludbekledingen van gezette steen - oriënterende berekeningen*

the soil parameters (see Figure 4–7). This leads to a contribution S_x to the SF in Eq. 4.17, which becomes:

$$\text{SF} = \frac{c}{\gamma_{sat} \, d \, \frac{1}{2}\sin(2\alpha)} + \frac{\gamma'}{\gamma_{sat}} \frac{\tan\phi}{\tan\alpha} + \frac{\gamma'}{\gamma_{sat}} \frac{\frac{1}{2}K_p \, d}{l\cos\alpha} \qquad \textbf{Eq. 4.19}$$

with l = the horizontal slope length

The soil failure mode is developing into a slip circle through the toe of the slope.
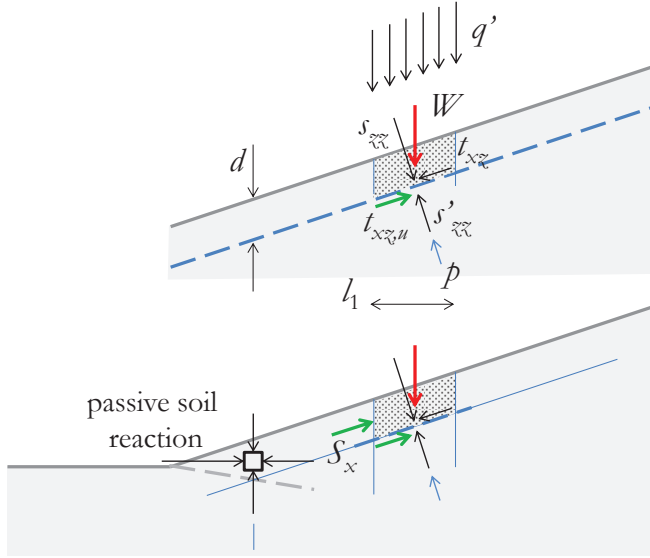
Figure 4–7   Definition diagrams of slope stability

In many cases the soil of the dike body is layered, with the least permeable soil on top. At the interface between this impermeable top-layer (clay) and the soil underneath (sand) there is a tendency to build up a water head difference p. In case of low tide and/or long period waves the water pressure under the clay layer can be higher than above or inside the clay layer, which is a destabilizing factor for the slip stability. In that case the critical depth d_{cr} coincides with the thickness of the clay layer, usually 1 to 1.5 m.
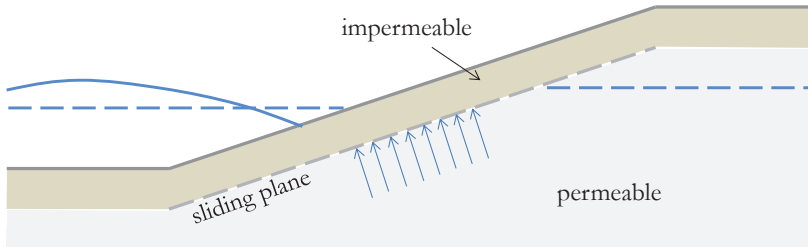
Figure 4–8   Effect of layered soil and different permeability properties

In literature design procedures for loads on the toe structures can be found, although at the start of the research the subject is neglected. In (Glerum and Wolsink, 1984) there is no reporting on the loads of the revetment layer against the toe.

In CUR 155[137] the sliding equilibrium of a layer that includes the revetment and a clay layer is considered. The critical load case is the wave run-down, combined with a static water head under the clay layer. The toe structure itself is considered permeable.

The permeability of the top-layer seems to have no influence because it is assumed that the head difference is present over the thickness of the clay layer.

A slightly different approach that can be found in literature[138] is the sliding equilibrium considered critical when the water head at the toe is minimal, which leads to a lower head difference over the sliding layer and hence a lower toe force.

The sliding of the revetment itself is studied by K. Pylarczyk and also by K.J. Bakker.

4.1.10 Friction model of K.J. Bakker

K.J. Bakker has published about failure mechanisms of block revetments in 1988 and 1989. He included these papers in his PhD-thesis[139], where he presents an analysis of failure mechanisms of the top-layer of a block revetment. Three failure mechanisms are distinguished: uplifting of elements, sliding of the revetment and instability of the sub layers or subsoil (which is beyond the scope of his study).

Uplifting of the elements is resisted by the element weight, by friction to other elements, by inertia when subjected to dynamic loading and restricted inflow of pore-water under the element, which creates suction. Bakker categorises 'friction resistance' under interlocking, but he expresses doubts whether a considerable strength contribution of interlocking should be utilised as the governing parameters are uncertain, and as single element failure would become more important. He also mentions that when structures rely on interlocking, bigger areas of the structure may become potentially unstable and may be lifted, which may cause rearrangement of the sub layer material and affect the integrity of the structure. He more or less recommends to stick to a safe under bound for friction that is based on the friction force of one unstable element on the slope leaning against the neighboring element. He does not include the fact that the neighboring element may be unstable also, potentially leading to stability results less than the mentioned contribution.

Bakker also studies restricted inflow under oblique wave attack conditions. He finds that there is much less load reduction, because a train of element s can move in a wave running along the slope, without volume increase under the system of elements.

Sliding is studied thoroughly. Bakker observes that steep slopes constructed in practice, e.g. 1:3, requires checking against the sliding criterion. When the top-layer is partially lifted, and partially pressed down on the sub layer, several zones can be distinguished that support each other. The equilibrium is analytically calculated, which results in certain length of revetment needed to suffice the sliding criterion. E.g. on a 1:3 slope, subject to $H/\Delta D = 4$ breaking waves, a leakage length Λ of 0.5 m, a friction coefficient μ of 0.47, a revetment length

---

[137] Klein Breteler, *Handboek voor dimensionering van gezette taludbekledingen*

[138] P. Meijers, *Toepassing theorie afschuiven bekledingen, Open taludbekleding* (TAW report, GeoDelft CO-32321O/5, 1994)

[139] Bakker, "Soil retaining structures - ch. 5: Block Revetments"

corresponding to a water depth of 2.5 H is required. If this length is less, than the revetment structure requires support of the toe to avoid sliding. Bakker was able to calibrate his model calculations with a study of the failure of block mattresses on a test site on the Houtrib dike in 1986.

The result of 'sliding instability' and the requirement of a toe support can now be used as a favourable condition for the development of in-plane forces.

4.1.11   Beam model of Vrijling

In 2000 Vrijling published a paper[140] which describes a design approach for a revetment as a beam structure. The load is modelled as a distributed load. The resistance of the revetment to withstand this load relies on the normal force. The normal force is presumed to be built up during the service life. The normal force in the transverse row of elements enables the row to act as a beam that can withstand bending moments and shear forces. This model was compared with the results of pull out tests of Verhagen[141] and was combined with a wave load model. The wave loads were modeled similar to the earlier MSc-studies (see section 4.1.8).

The magnitude the normal force is based on a contribution of the lifted part of the revetment beam only.

The contribution to element stability is given below, assuming failure in shear and in bending respectively.

$$\frac{H_s}{\Delta D} = \frac{3\cos\alpha}{\xi}\left(1 + 2 f_{\mathrm{fr}} \frac{\rho_s}{\Delta \rho_w} \tan\alpha\right) \qquad \text{Eq. 4.20}$$

$$\frac{H_s}{\Delta D} = \frac{3\cos\alpha}{\xi}\left(1 + \sqrt{6 \frac{e}{D} \frac{\rho_s}{\Delta^2 \rho_w} \tan^2\alpha}\right) \qquad \text{Eq. 4.21}$$

When assuming equality, it follows that the eccentricity e/D and the element to element friction coefficient f_{fr} have the following relation:

$$\frac{e}{D} = \frac{2}{3} f_{\mathrm{fr}}^{\;2} \frac{\rho_s}{\rho_w} \qquad \text{Eq. 4.22}$$

The values of $e/D = 0.166$ corresponds to $f_{\mathrm{fr}} = 0.32$ and the limit value of $e/D = 0.5$ corresponds to $f_{\mathrm{fr}} = 0.55$. It can be concluded that shear and bending failure seem of similar importance. The stability number for the limit case $H_s/\Delta D = 4.26 \cos\alpha / \xi$. When introducing a slightly higher normal force and more favourable boundary conditions at both ends of the lifted beam this value raises to 4.80.

Vrijling concludes that

- element interaction results in a 35% increase of stability
- the resistance and stiffness of the bottom end foundation (the toe) is essential for the described mechanism

---

[140] J.K. Vrijling, C. van der Horst, and P.J.M. van Hoof, "The structural analysis of the block revetments on the Dutch dikes," *ICCE* (Sidney, 2000)

[141] Verhagen, *Trekproeven op glooiingsconstructies in de Oosterschelde*

- the loading history of the revetment is important. Newly constructed revetments may have no resistance increase from element interaction.
- The randomness of the pull-out tests is explained by uncertain friction distribution and because of eccentricities in the pull force.

4.2 Comparison with stability of randomly and regularly placed cube revetments

Alternatives for pattern-placed revetments are randomly placed rock, randomly placed cubes or interlocking armour units. Slopes with randomly placed elements can be constructed under water. Disadvantages are higher mobilisation and installation costs due to the larger individual unit weight. Up to waves with $H_s = 2$ to 2.5 m pattern-placed revetments are considered more economic. For higher wave heights this might be subject to a number of variables, amongst them the water depth in front of the structure. Pattern-placed revetments need dry construction above a toe, which is ideally done at low tide. The high waves are always associated with high tides and wind set-up, which has the logical consequence that there is a revetment slope available in the wave attacked zone. When the coastal water is deep, waves can occur at low water levels also and the wave attacked zone reaches below the low tide level, which makes pattern-placing of the revetment impossible, at least for the lower part of the slope. E.g. for the Maasvlakte 2 coastline a regularly placed cube revetment was applied. The water depth is 16 m and $H_s = 6$ m.

4.2.1 Empirical stability or randomly placed armour

In coastal engineering the Hudson formula has been used for many years. It has been derived based on evaluation of tests in the 1950s. In recent publications[142] the formula is written as:

$$\frac{H_s}{\Delta D_{n50}} = \left(K_D \cot \alpha\right)^{\frac{1}{3}}$$

Eq. 4.23

with

Δ = the relative buoyant density
D_{n50} = the nominal average diameter
K_D = empirical stability coefficient
    2.0 to 3.5 for angular Rock armour in breaking waves
    4.0 for angular Rock armour in non-breaking waves
    6.5 for concrete cubes in breaking waves
    7.5 for concrete cubes in non-breaking waves
    higher for interlocking armour units, like X-blocs, tretra-pods and Acropods

The Hudson formula does not count for dependency on wave steepness related to the slope angle, except for the difference in K_D factors for breaking and non-breaker waves which depends on ξ. Later developed formulas by Van der Meer, count for levels of tolerated armour movement and damage. In his PhD thesis[143] Van der Meer derived a series of

---

[142] US Army Corps of Engineers (1984), Shore Protection Manual, CUR-Ciria (2007), The Rock Manual, Van der Meer (1988)

[143] J.W. van der Meer, "Rock slopes and gravel beaches under wave attack" (PhD thesis TU Delft, 1988)

formulas of which the static stability of a double rock layer, on a sub layer, on an impermeable core is the most suitable to compare. Permeable rock cores have a beneficial effect on the stability of the armour layer.

$$\frac{H_s}{\Delta D_{n50}} = 4.1 \left(\frac{S}{\sqrt{N}} \right)^{0.2} \xi_m^{-0.5} \text{ for plunging waves} \qquad \textbf{Eq. 4.24}$$

$$\frac{H_s}{\Delta D_{n50}} = 1.35 \left(\frac{S}{\sqrt{N}} \right)^{0.2} \sqrt{\cot \alpha} \ \xi_m^{0.1} \text{ for surging waves} \qquad \textbf{Eq. 4.25}$$

with
$N =$ the number of waves, which is set to 1000 for comparison to the pitchings
$S =$ the damage factor, see Table 4-2.
The breaker parameter ξ_m refers to the average wave period T_m, which relates to T_p as $T_p = 1.2 \ T_m$.

Table 4-2   Recommended values of S

cot α	Damage factor S = damaged area / D^2	
	Start of damage	Two layer system completely damaged
2.5	2	10
4	3	17

In a publication of 1988 Van der Meer mentions a separate formula for random placed cubes, installed on breakwater slopes in double layers. Those formulas are derived for a slope with $\cot \alpha = 1.5$.

$$\frac{H_s}{\Delta D} = \left(6.7 \frac{N_{od}^{0.4}}{N^{0.3}} + 1.0 \right) s_{m0}^{-0.1} \qquad \textbf{Eq. 4.26}$$

with

$N_{od} =$ the number of displaced cubes in cross section with width $B_y = D$

$$s_{m0} = \frac{2\pi H}{g \ T_{m02}^2}$$

4.2.2   *Comparison with regularly placed cubes*

Several MSc-thesis were published with scale model tests on cube breakwaters. The Thesis of van den Berg, 2004 is interesting since a single layer of regular (underwater) placed cubes is investigated. Van den Berg performs tests on cot α = 1.5 slopes for a range of wave steepness values with empty joints and also with granular joint fill. The latter variant effectively equals a pattern-placed revetment slope. Van den Berg finds that joint fill adds 15% to the stability. The coefficient of 0.1 in his formulas could not be improved on basis of his data and was therefore left unchanged. He found a damage versus wave height dependence with a power of 0.4 (with joint fill) and 0.6 (without joint fill). An acceptable start of damage is normally set at $N_{od} = 0.4$ for $N = 1000$ waves. From this relation the effect of duration on damage propagation tells us that $N_{od} = 1.0$ is reached at $N = 3000$

waves. If we stick to $N_{od} = 0.4$ as a criterion the design wave height for durations over 1000 waves should decrease following $H_s/H_{s1000} = (N/1000)^{-0.1}$.
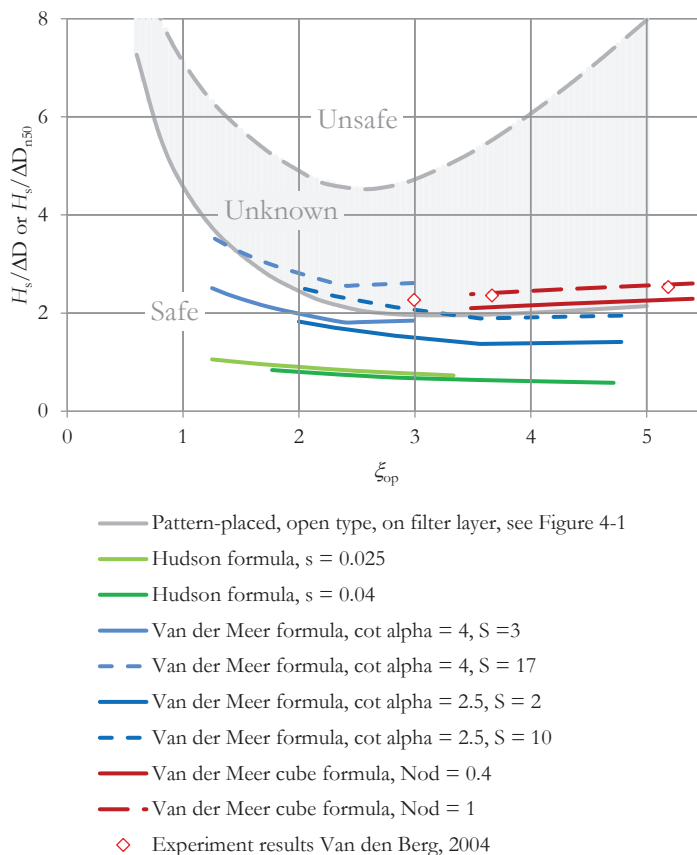
Figure 4-9   **Stability numbers of random placed armour compared to pitched armour**

In Figure 4-9 the Hudson and Van der Meer formulas are compared[144] with stability numbers of pattern-placed revetments, open top-layer on open filter on impermeable layer.[145] It can be noticed that pattern-placing provides significant extra stability and it can also be seen that the doubtful area between safe and unsafe is relatively large. The safe lower bounds for randomly placed rock and pattern-placed revetments differ only slightly. Although the average rock mass of an element with size D_{n50} is larger than a revetment column with height D, it seems obvious that a pattern-placed slope with thickness D is more stable than a rock slope with stones of equal size D_{n50}. The coloured stability curves in Figure 4-9 can therefore be considered as conservative estimates of the under bound between the safe and unknown area of pitched revetment (indicated in grey).

---

[144] Also done in J.W. van der Meer, *Veiligheid in rekentechnieken van steenzettingen*, 2000
[145] Type 3a in *Voorschrift Toetsen Veiligheid*, extracted from *Technisch Rapport Steenzettingen*, 2003

4.3 Failure data of pattern placed revetments

4.3.1 Findings in scale model tests

Scale model tests were undertaken since 1970. Wevers[146] has published an interesting study, where wave loads and pressure loads up and under the revetment are surveyed and failure of the revetment elements is described. The study comprises 1:3 and 1:6 slopes with flat concrete model blocks, 4 × 4 × 2 cm. Top-layer permeability is varied up to 6.5% openings. The test method comprised of a gradual increase of the regular wave height up to damage occurred. The observed damage of the revetment appears in three locations:

- above the point of run-down (due to slowly increasing uplift pressure, dependent on permeability properties),
- above the plunging wave top (due to sudden uplift) and
- in the area of the air pocket at the sea side of the plunging wave top (sudden downward pressure reverting to uplift, just after the air pressure release).

The study also reports the execution of pull-out tests on the model slopes. Quasi static pull-out tests were performed, as well as dynamic tests. Wevers observed that the failure modes during the attack with the plunging wave did not comply with the result of a static load tests. The water pressures in the wave pushed single blocks out and the static tests results showed interaction between the blocks, causing plate bending and uplift of more than one block. Wevers anticipated on this by applying a dynamic load in the pulling tests using a drop weight. The results are discussed in Annex C.

The conclusions of the study are as follows:

- For breaking (regular) waves the damage point is approximately 0.5 H below the still water level.
- A relatively impermeable top-layer on an open foundation layer causes damage cases governed by a quasi-static pressure difference. Dynamic pressure differences cause vibrations that break the interlock and ease failure due to quasi-static overpressure.
- For impermeable foundations the failure mechanism is dominated by dynamical pressure differences. The impulse of the pressure difference lifts the blocks. Increasing the permeability of the foundation and increasing the block weight seems favorable.[147]

4.3.2 Attack zones, failure patterns and failure levels

Glerum and Wolsink (1984) define four load zones: (i) below normal low tide, (ii) normal tidal range, (iii) between normal high tide and design water level and (iv) run-up zone above design water level. The nature of the load differs per load zones: in (iii) the duration of the load is most relevant and in (iv) the extreme magnitudes of the load.

The known failure causes/mechanisms are:

---

[146] A. Wevers, *Stabiliteit taludbekledingen van gezette steen onder golfaanval - verslag modelonderzoek* (WL report M1057, 1970)

[147] This is a very important observation, which has been fully understood and implemented much later, in the late 1990s.

- Forces due to back run of water on a rough slope
- Uplift forces following the run-down of waves due to collected water in the filter layer under the top-layer
- Uplift forces due to filter water fed by the pressure above the slope in the next wave
- Pressure drop above the slope in the water mass of the wave due to turbulence
- Peak pressures due to a plunging wave, first above the slope and slightly later in the filter (duration 0.05 to 0.25 s)
- Uplift forces due to propagated water pressure after and adjacent to the plunging wave
- Pressure drop in the air pocket in the breaking wave above the slope, causing uplift
- In the run-up phase forces may occur on rough slopes, or on elements that are partly lifted

4.3.3 Prototype failure data

In the handbook, Klein Breteler, 1992[148] a number of damage cases are discussed more extensively. Two relevant cases of open column revetment cases are summarised briefly.

Case breakwater Oterdum (1973), slope 1:2.8, concrete blocks $0.5 \times 0.5 \times 0.2$ m, on a 0.6 m mine stone sub layer, oblique wave attack at 45°, water level equals top of revetment stone, damage caused by waves $H_s = 1.1 - 1.5$ m and $T_p = 4.2 - 4.6$ s. Parameters $H_s/\Delta D = 4 - 5.4$, $\xi_{op} = 1.7 - 1.8$. The damage consisted of lifted blocks mostly at $0.4 - 0.7$ H_s below still water level.

Case Philipsdam (1987 and 1988), Basalton columns on the lower part of the 1:4 slope (not on clay), just under a transition at +2.0 m with an upper slope of concrete blocks, damage caused by waves $H_s = 0.85$ m, with estimate wave steepness of 5%. Parameters $H_s/\Delta D = 3.3$, $\xi_{op} = 1.1$, which is lower than predicted with the models in (CUR 155, 1992) based on the model test results.

Hernandez, Johanson & Van der Burg[149] describe the damage case of the Zuidwal Maasvlakte (1988). The slope angle was 1:8. The slope was initially designed as a gravel beach. Due to too much longitudinal transport of material this principle did not persist. Therefore it was decided to apply a cover layer of pitched revetment, consisting of 0.35 m tall Basalton columns, $\rho_s = 2300$, upper edge at NAP +6.25, with up to NAP +8.0 a Basalt rock slope 1:10, 30-300 mm. The damaged section was constructed in 1983. North-North Westerly winds allowed waves to penetrate through the Piers at Hoek van Holland and to directly attack the slope. The section adjacent to the slope has a similar structure but with $D = 0.40-0.42$ m, $\rho_s = 2600$ and 2900 kg/m^3 in middle zone of slope, upper edge at NAP +8.0 m. This section was not damaged at all. The waves at the toe were estimated with help of wave measurements in the Rotterdam approach channel. The estimated figures are $H_s = 3.8$ m and $T_s = 10 - 12$ s (swell). The local depth is −6.0 m. The tidal conditions were such that the low tide coincided with the wind set-up, thus creating during almost 16 hours a constant load with the water level between +1 and +2, which explains the large extent of damage. The load factor $H_s/\Delta D$ has been 8.7, where 4 to 5 is assumed a normal strength. (The

---

[148] Klein Breteler, *Handboek voor dimensionering van gezette taludbekledingen*
[149] Hernandez, Johanson, and Burg, *Zuidwal – analyse schade en ontwerp taludbekleding*

undamaged section had 4.8.) The top-layer permeability was measured also. It was found that the zone below +3.0 m had a lower permeability (k' = 5-10 10^{-5} m/s) than the zone above +3.0 m (k' = 5-10 10^{-6} m/s). Both figures are significantly lower than expected from design formulas (k' = 0.01 m/s). Also the filter permeability was lower than expected. Both effects nevertheless lead to a (theoretical) leakage factor of approx. 10 m instead of 1.2 m, which is also assumed to be an important cause for the damage.

Table 4-3   Data of damage cases column revetments

$H_s/\Delta D$	ξ_{op}	Location	Year	Λ/D	Comment
4 − 5.4	1.7 − 1.8	Oterdum	1973	2–3	
1.2 − 1.4	1.3 − 1.6	Noord-Beveland	between 1972 and 1982 [150]		Basalt 0.2/0.3
1.0 − 1.3	1.3 − 1.6	Terneuzen			Basalt 0.3/0.4
1.1 − 1.3	1.0 − 1.3	Afsluitdijk			Basalt 0.3/0.4
3.3	1.1	Philipsdam	1987/88		Near transition
8.7	0.9	Maasvlakte	1988	>10	
4.8	0.9	Maasvlakte	1988		
5.4 − 6	1.4	Nieuwe Sluis	1990	>3	Piles obstruct in-plane forces

In 1990 Johanson[151] describes a 150 m^2 damage case in a basalt slope. The damage might be caused by on average too small column lengths (0.2 instead of 0.25 m), too permeable filter material, or by old cut piles. The piles were there to limit run up, and as compartment piles. It was reported that these piles indeed limit damage but also initiate damage as they form discontinuities in the layer structure. In this case the piles 'were no longer needed to limit run up because the crest was raised to Delta height', which is a remarkable statement anyway. The piles were not pulled, but were cut above the slope and hammered into the clay. The holes in the slope were filled with new basalt columns. This 1:4 slope appeared not to withstand loads up to H_s of 2.7 - 3.0 m ($H_s/\Delta D$ = 5.4 - 6). The wave steepness may be estimated as 0.03 to 0.04, which gives a ξ of 1.4. Also remarkable is the statement that a noticed damage area of 1 − 2 m^2 on a neighbouring slope with 0.3 m Basalt columns, same load conditions, is accepted as 'normal given the conditions'.

[150] J.J.W. Seyffert, "Praktijkervaringen in het steenzettingen onderzoek," *Informatiedag steenzettingen* (Centrum Onderzoek Waterkeringen, 1982), 47–53

[151] J.C.P. Johanson, *Schade aan taludbekleding te Nieuwe Sluis* (DWW report WBA-N-90054, 1990)
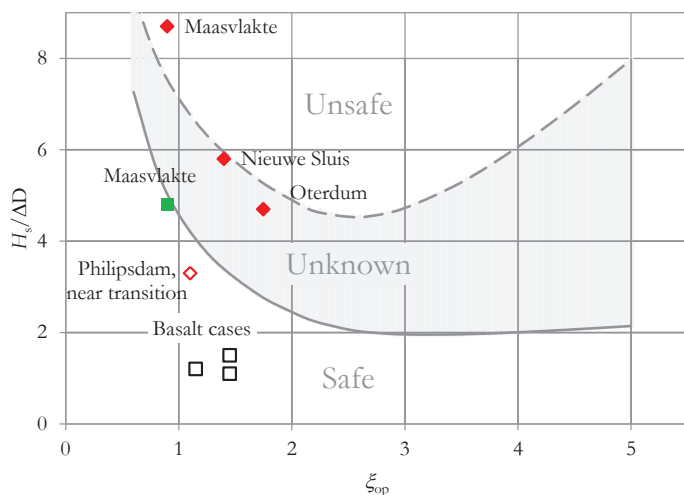
Figure 4-10 **Column revetment failure cases of Table 4-3 plotted in design chart of Figure 4-1**

4.4 Large scale testing

4.4.1 Facilities

A major share of the research on revetments is provided by the large scale testing in the Delta Flume, the large test facility of WL|Delft Hydraulics in De Voorst, Noord-Oostpolder. The test flume measured 220 m long × 5 m wide × 8 m deep and wave fields up to H_s = 1.7 m could be generated.

In 2014/15 the Delta Flume has been dismantled and a new 9.5 m deep Flume is built in Delft. This flume can generate waves up to H_s = 2.2 m.

Flume tests on revetments are also performed by the Forschung Zentrum der Küste in the large flume in Hannover, with a maximum irregular wave field of H_s = 1.3 m.

4.4.2 Reports

Klein Breteler, 1992 provides an summary and evaluation of the tests performed from 1982 to 1991. Most of these tests lead to damage points plotted in $H_s/\Delta D$ graphs, where the wave height that has led to damage is compared to the revetment strength expressed in the effective thickness of the revetment. The results $H_s/\Delta D$ were plotted against the breaker parameter ξ_{op}. With help of the spectral the data can also be plotted against ξ_{m-10} (see Figure 4-11).

Lubbers & Klein Breteler, 2000[152], Klein Breteler, 2000[153] and Smith, Wouters & Klein Breteler, 2000[154] present the results of the tests up to 1999. Many of these tests were

---

[152] C.L. Lubbers and M. Klein Breteler, *Grootschalig modelonderzoek naar stabiliteit van taludbekledingen, Samenvatting van onderzoek in de Deltagoot* (WL|Delft Hydraulics report H3272 rev. 2, 2000)

instrumented, which enabled better evaluation studies. In the reports the research focuses on the details of hydraulic loads and on aspects like the effect of berms, of the drainage factor, of wave breaking, et cetera. After 2004 the tests were continued, with focus on an improved wave load modeling, on the effect of the number of waves, of long waves, on residual strength, and on lock-in effects.

The reports Eysink & Klein Breteler, 2005 and Klein Breteler, Van der Werf & Wenneker, 2007 (revised 2012) focus on basalt slopes, on persistency tests with larger numbers of waves and on long-period waves.[155]

Various types of revetment elements were tested in the previous reports. In a dedicated large test campaign in 2013 and 2014 a number of older and newer types were tested and their performance was purposely compared. The developers, producers and/or contractors of the revetment systems were requested to take part in the financing of the tests and were asked for approval.[156]

German large scale tests[157] on rectangular blocks and on interlocking blocks are included in the data base also.

The inventory only includes irregular wave tests. Older regular wave test are not considered. They might still be interesting for studying phenomena, but not for quantitative analysis.

4.4.3 Results

The available tests are listed in a table in Annex I, including the typical properties. The tests are categorised as concrete blocks CB, concrete columns CC (including Hydroblocks, Basalton and Ronaton etc.), wave run-up absorbing or hollow systems HS (e.g. Hillblocks), natural blocks NB, natural columns NC (e.g. Basalt) and natural stone NS (e.g. Vilvoort).

For many older tests the wave period T_p as a test characteristic was changed for T_{m-10}. Most of the reports provide spectral data, on basis of which T_{m-10} can be found. For the other tests with unknown spectral data a standard relation $T_{m-10} = T_p /1.1$ was used.

Amongst the listed revetments properties the calculated leakage factor Λ/D is included, where possible based on reported data of the top-layer, the joint and the filter. For individual cases a measured leakage factor could be included.

The results are plotted in terms of $H_s/\Delta D$. During the tests the wave height H_s was increased in small steps and after a series of waves the slope was inspected for damage. If damaged the damage was given a category a/b/c/d and the corresponding H_s and the cumulative number of waves N was reported.

---

[153] M. Klein Breteler, *Grootschalig modelonderzoek naar stabiliteit van taludbekledingen - anaylse van resultaten van Deltagootproeven* (WL|Delft Hydraulics report, 2000)

[154] G.M. Smith, J. Wouters, and M. Klein Breteler, *Grootschalig modelonderzoek naar stabiliteit van taludbekledingen - Meetverslag van Deltagootonderzoek* (WL|Delft Hydraulics report H3272-2, 2000)

[155] W.D. Eysink and M. Klein Breteler, *Langeduursterkte van Steenzettingen - Verslag van Deltagoot onderzoek* (WL|Delft Hydraulics report H4475, 2005), and M. Klein Breteler, I. van der Werf, and I. Wenneker, *Kwantificering golfbelasting en invloed lange golven, rev. 2*, 2012

[156] M. Klein Breteler, *Vergelijkend onderzoek zetstenen voor dijken, samenvattend rapport* (Deltares report 1208618-006 for RWS-WVL and revetment element producers, 2015)

[157] F. Gier et al., "Stability of interlocked pattern placed block revetments," *ICCE* (Santander, 2012)

Table 4-4   **Damage categories used in evaluation of Delta Flume tests**

Damage categories[158]			Perpendicular movement of single revetment element relative to neighbour *)	Perpendicular deformation of revetment beam	Settlement due to loss of filter material over transverse length of:
Revetment damage	a	🟩	0.1 D	0.2 D	
	b	🟨	0.1 – 0.2 D	0.2 – 0.3 D	
Revetment failure	c	🟧	0.2 – 0.5 D	0.3 – 0.5 D	8 – 15 D
	d	🟥	>0.5 D	>0.5 D	>15 D
*) If the damage in category c or d was limited to single element failure, a label c1 or d1 is given. Refer to Table 6–2.					

An example of the large flume experiment results is given in Figure 4-11. The results are plotted as $H_s/\Delta D$ at which level the damage of failure occurred, against $\xi_{m\text{-}10}$. As a reference the results are plotted in the design chart earlier presented in Figure 4-1, distinguishing between safe, unknown and unsafe areas.
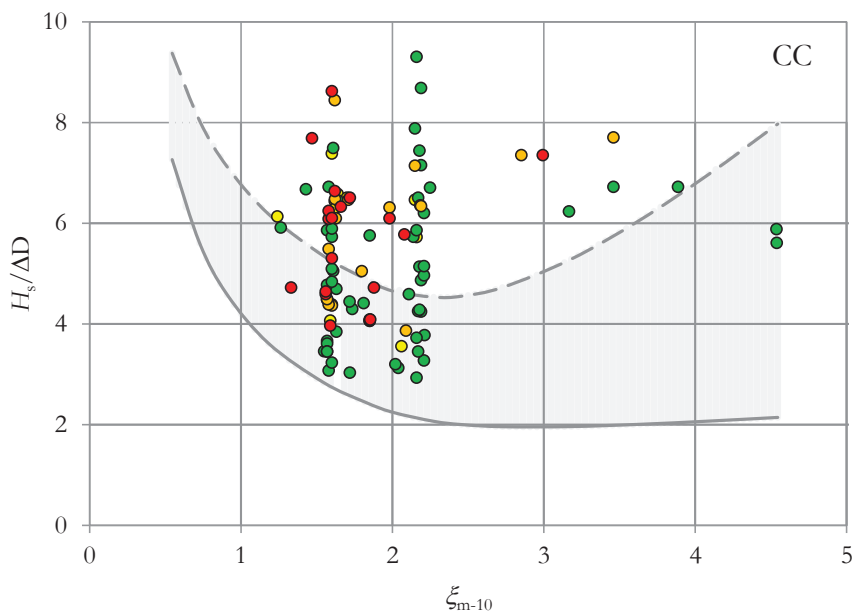
Figure 4-11   **Results for concrete column (CC) revetment plotted in VTV design chart presented in Figure 4-1**

---

[158] Source: Klein Breteler, *Handboek voor dimensionering van gezette taludbekledingen*, and Klein Breteler, *Vergelijkend onderzoek zetstenen voor dijken, samenvattend rapport*

4.4.4   Discussion

The flume experiment results show a lot of scatter. This might be due to a number of reasons of which we mention the most important:

- the tests are on several types of elements, which have different stability performance
- no separate notice of wave steepness and slope angle is made
- the leakage conditions are not constant
- the length of the slopes and in-plane force conditions are not constant
- the revetments are a vulnerable system. The fragility curves are very steep, meaning that complete failure (red markers) may occur at a slightly higher load level than start of damage (green markers).

These issues will be addressed in the remainder of this thesis. Trend analysis on the flume experiment results is presented in Annex J. Calibration of updated model formulas with the experiment results is presented in sections 6.2 and 6.3.4.

The Delta flume tests are virtually all with deep-water conditions. There is no effect of water depth on the wave height. Some tests have short underwater berms with the specific objective of testing the effect of the berm. In real cases the foreland may break the highest waves, which is favourable for the revetment stability since it reduces the significant wave height. Through that it may also decrease the average wave steepness, and hence increase ξ, which in theory corresponds to lower stability numbers.

In early tests the tested revetments may have gained strength from lock-in effects between the walls of the flume, and consequently their stability is overestimated. Later rubber strips were used to avoid development of high normal forces in cross direction of the flume. See also section 3.1.8.

The flume tests are almost all on slopes with $\cot\alpha = 3$ or 3.5. When plotting against ξ, it should be noticed that this is actually plotting against wave steepness. The effects of a steeper or less steep slope on the resistance are not tested realistically.

5 WAVE LOADING

Chapter introduction

The subject of revetment stability has a cross-disciplinary nature, in which aspects of wave theory, wave shoaling and breaking, hydraulics and permeability, soil properties, and aspects of structural mechanics play a role. Therefore the relevant literature and studies covers a wide field. This chapter describes the effects of waves, which form the 'load' of the structure.

For the revetment stability the wave parameters at the toe of the structure are relevant. The deep water wave conditions will have changed while travelling to the revetment slope. Section 5.1 focusses on spectral wave definitions and wave height distributions and on wave versus foreland interaction. These aspects as such will not be further developed in this thesis, but are crucial for the safety philosophy.

Different from earlier research in many flume tests and field tests the wave effects have been measured and analysed. Wave versus slope interaction is the subject of section 5.2. In this section the findings of the Delta flume research are revisited and where possible compared where international literature. This contribution is valuable for gaining insight in what the wave load is for a range of possible values of the slope angle and wave steepness. Also effects of the test scale need attention.

A third subject of wave effects are the water pressures at both sides of the revetment. The insights in the permeability/drainage properties of the revetment system have a profound effect on these pressures, This is described in section 5.3. The combination of the wave load characteristics and the hydraulic response of the system leads to an updated load description in the format of the typical $H_s/\Delta D$ stability curves. The curves supplemented with the spatial distribution of the load form an input for evaluation of the revetment resistance.

5.1 Waves and effects of limited depth

5.1.1 Types of waves

Wind waves and swell are the dominant phenomena that cause instability of revetments. The location of the damage is dependent on the water level. The water level and the associated water depth have a determining effect on the maximum possible wave height. This makes the set of design water level and design wave height the most influential variables for the design of the revetment.

According to their frequency and source waves can be distinguished in:

−   Low frequency water level changes, such as

- Storm surges, with a typical duration of 1 or 2 days
- Astronomical tide, composed of sinusoidal water level fluctuations with twice a day, once a day and fourteen days periods
- Wave set-up, a pseudo-static water level increase caused by the breaking process of wind waves
- Seiches, enclosed basin oscillations, induced by swell of sudden level changes, typical period is 20 minutes

- • Surfbeat, low frequency waves, induced by shoaling and breaking of wind waves near the coast, typical period is 2 minutes

– Wind waves and swell

– Ship induced waves in navigation canals and rivers

For design purposes these phenomena are translated in 'still water levels' and 'waves', characterised with characteristic wave heights and wave periods, for the revetment slope design normally expressed in wave steepness.

The astronomical tide and storm surges are commonly the most dominant components of the design still water levels. Their maximum amplitudes may coincide. Storm surges are caused by low atmospheric pressure and wind set-up and are heavily influenced by the estuary geometry and the water depth. In present times surge level prediction[159] is based on wind statistics and on numerical modelling of the estuary response. In the Netherlands the design levels are laid down in Hydraulic Boundary Conditions, first issued nationally in 2001.

The wind waves can be distinguished in random wind-generated waves, and transformed lower frequency waves (swell) occurring outside wind-field and after the wind has diminished. The waves within the wind field depend on the wind speed[160], the storm duration and the fetch. If the wind speed is increasing and not yet at a constant average, if the storm is not sufficiently long and/or if the fetch is not sufficiently long, we speak about a growing sea state. If these variables are stable and/or beyond certain limit values the sea state is fully developed. Wave parameters are normally defined by deep-water wave characteristics, assuming sufficient water depth, i.e. $d/L_o > 0.5$.
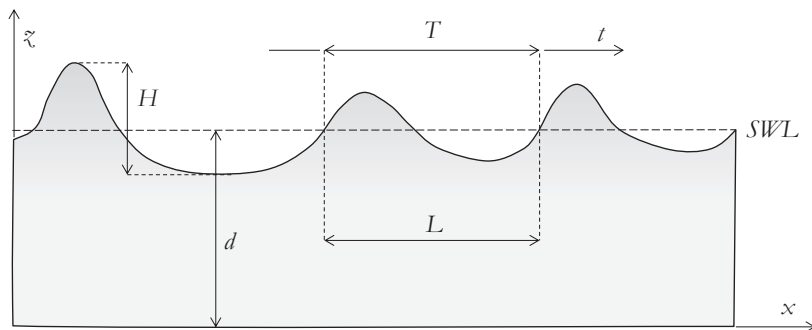
Figure 5-1   Definition diagram wave parameters

Almost all recent wave studies and revetment stability studies use irregular wave series as a representation of reality. Some valuable older studies simplify the random wave field to regular waves.

---

[159] Historically, the surge level was taken or extrapolated form the highest observed level on a certain location. Since the levels depend on so many factors, especially changing local water depth and interference with river discharges, historic surges are unreliable predictors for future surges. In the 1930s and 1940s surge prediction based on analysis and modelling of the physical processes started. E.g. Van Veen (1948) could predict a high flood risk of the Zeeland and Holland delta areas.

[160] Hourly wind speeds for the Dutch coast are 35 to 40 m/s for the 1/4000 yr conditions, depending on the location.

Most common frequency-based descriptions of the sea state are the Pierson-Moskovitz (1964) and the JONSWAP (1973) spectra. The JONSWAP spectrum is for growing seas, fetch-limited in deep water, and the PM spectrum for fully developed seas. Compared to the PM spectrum the JONSWAP spectrum has an enhanced peak.

When a JONSWAP wave field runs into shallow water the energy distribution changes with a reduction of the share of the low-frequency waves. This is described as a TMA spectrum[161].

$$E_{\text{TMA}}(f) = \phi(f, d) \times E_{\text{JONSWAP}}(f),$$

with the transformation function $\phi(f, d) = \dfrac{1}{2n} \tanh^2(\dfrac{2\pi d}{L})$, in which **Eq. 5.1**

$$n = \frac{c_g}{c}$$

$c =$ phase velocity $= \sqrt{\dfrac{gL}{2\pi} \tanh(\dfrac{2\pi d}{L})}$, with limit values $c_o = gT/2\pi$ for

deep water waves and $c = \sqrt{gd}$ for shallow water waves

$c_g =$ group velocity

$n = \dfrac{1}{2}\left(1 + \dfrac{4\pi d / L}{\sinh(4\pi d / L)}\right)$, with limit values ½ for deep water waves

and 1 for shallow water waves

The deep water wave length L_o is defined using T_p, the wave period at the peak of the spectrum.

$$L_o = \frac{gT_p^2}{2\pi}$$

Eq. 5.2

In many practical cases the spectrum does not have one peak and an energy distribution according to the descriptions above but has influences of waves form other directions or influences from swell. In that case it is still possible to use parameter descriptions based on the energy[162] as indicated below.

To derive wave heights from the spectrum the basic energy relation $E = \tfrac{1}{8}\rho_w gH^2$ can be used. The wave that represents the total energy in the spectrum is H_{rms}, and is therefore defined as:

$$H_{rms} = \sqrt{8m_0}$$

Eq. 5.3

with $m_0 = \int S \, df$

the wave variance $S = E/\rho_w g$, integrated over the frequencies

---

[161] By Bouws et al (1985), cited in S.A. Hughes, *The TMA shallow water description and its application* (USACE, CERC report 84-7, 1984). TMA stands for Texel, Marsen and Arsloe, after the data sources used for calibration of the parameters.

[162] J.K. Vrijling, *General wave spectrum model* (TU Delft report for Mast III Proverbs project, 1996)

The 'observed' characteristic wave height is $H_{m0} = \sqrt{2} \, H_{rms}$.

$$H_{m0} = 4\sqrt{m_0}$$
Eq. 5.4

Other characteristic periods can be calculated from the spectrum with functions of the 1st and 2nd etcetera moment of the frequency spectrum.

$$m_n = \int f^n S \, df$$
Eq. 5.5

Characteristic spectral periods are defined with help of the moments of the spectrum.

The mean-frequency period $T_{m01} = m_0 / m_1$ and the mean period[163] $T_{mean} = T_{m02} = \sqrt{m_0 / m_2}$.

The energy period $T_E = T_{m-10} = m_{-1} / m_0$, which period is used to compute the wave power J.

$$J = 0.49 H_{m0} T_{m-10}{}^2$$
Eq. 5.6

Since these period definitions include effects of double-peaked spectra, they are assumed to be better parameters for wave structure interaction and for loads on structures than T_p. The period T_{m-10} is the recommended wave period parameter for wave run-up.[164] The wave steepness is defined as:

$$s_0 = \frac{2\pi H_{m0}}{g T_{m-10}{}^2}$$
Eq. 5.7

5.1.3 Wave heights

The significant wave height H_s is the visually observed wave height and is defined as the average of the highest third part of the waves.[165] Calculation of H_s from a wave height distribution is based on analysis in the time domain. Time domain analysis starts with wave counting from a wave record. All heights H and periods T are ordered, and the average H, the average T and the so-called root mean square can be computed.

$$H_{rms} = \sqrt{\frac{1}{N} \sum_{i=1}^{N} H_i^2}$$
Eq. 5.8

The significant wave height definition is:

$$H_s = H_{1/3} = \frac{1}{\frac{1}{3} N} \sum_{i=\frac{2}{3}N}^{N} H_i$$
Eq. 5.9

H_s is also used to define the deep-water wave steepness: $s_o = H_s / L_o$.

Under certain conditions, as the wave period distribution is Gaussian and the spectrum is narrow banded around one peak, the wave height distribution follows the Rayleigh distribution.

The cumulative distribution function (cdf) of the Rayleigh distribution is given as:

---

[163] Mean of 'zero up-crossing' periods
[164] For JONSWAP spectra: $T_p = 1.1 \, T_{m-10}$, $T_p = 1.19 \, T_{m10}$, $T_p = 1.28 \, T_{m02}$
[165] Now defined as $H_s = 4 \sqrt{(m_0)}$

$$P(\overline{H} < H) = 1 - \exp\left(-(\frac{H}{H_{rms}})^2\right)$$

<div align="right">Eq. 5.10</div>

Exceedance values are calculated with:

$$\frac{H_{p\%}}{H_{rms}} = \sqrt{-\ln(\frac{p}{100})}$$

$$H_{max} \text{ (out of } N \text{ waves)} = \frac{H_{max}}{H_{rms}} = \sqrt{-\ln(\frac{1}{N})}$$

<div align="right">Eq. 5.11</div>

or with extreme value distributions.

Average $1/Q$, e.g. 1/3 or 1/100 values are calculated with:

$$\frac{H_{1/Q}}{H_{rms}} = Q\frac{\sqrt{\pi}}{2}\text{erfc}\sqrt{\ln(Q)} + \sqrt{\ln(Q)} ,$$

where

$$\text{erfc}(x) = \text{the complementary error function} = 1 - \text{erf}(x) = \frac{2}{\sqrt{\pi}}\int_{x}^{\infty} e^{-t^2} dt$$

<div align="right">Eq. 5.12</div>

5.1.4 Shoaling and depth-induced breaking

When waves approach the shoreline a number of phenomena play a role. In coastal water bottom friction dissipates wave energy. Waves tend to rotate towards the coastline and around obstacles. Shoaling is the change in wave height and length when incoming deep water waves run into water with gradually decreasing depth. The wave height first decreases, then increases and the waves finally break on the shallow foreshore or ultimately on the revetment slope. The depth-induced breaking process reduces wave energy. The underwater foreshore geometry is therefore considered as a component of the wave defence system.

Since the larger (or actually the largest) waves of a series of irregular waves actually generate the relevant load conditions for revetments, knowledge of the depth-induced breaking process and a reliable prediction of the highest remaining waves are very important.
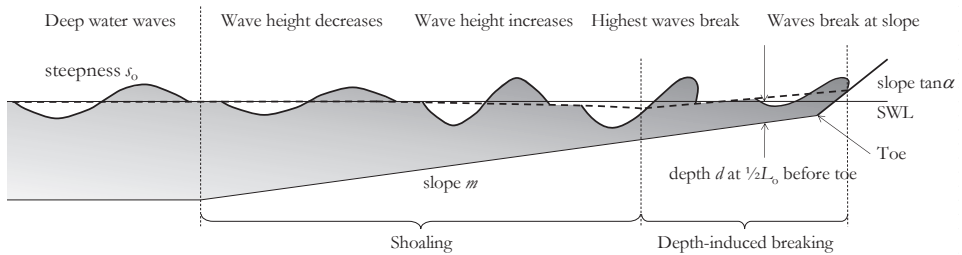
Figure 5-2   **Definition diagram shoaling and depth-induced breaking**

Wave theory describes the transition from deep water waves (indicated with index o) into shallow water waves. The shoaling causes a change of the wave heights. This phenomenon is quantified with help of the shoaling coefficient K_s.

$$K_s = \cfrac{1}{\sqrt{\tanh(2\pi d / L)\left(1 + \cfrac{4\pi d / L}{\sinh(4\pi d / L)}\right)}}$$

The processes of shoaling and depth-induced breaking of waves are often studied in combination.
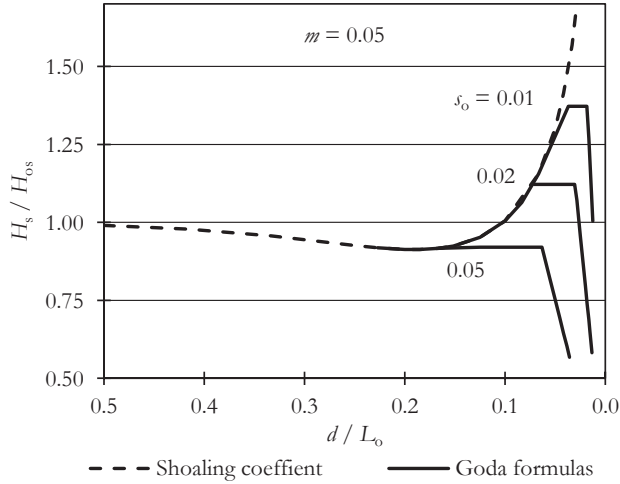
Figure 5-3   Shoaling coefficient as a function of relative depth
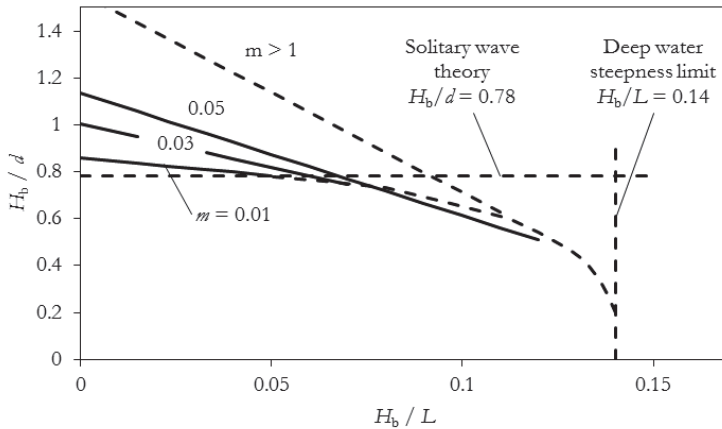
Figure 5-4   Depth- and steepness limited wave breaking

Very steep bed slopes m can result in higher ratios of the height of the breaking wave H_b and the local depth d. This is not relevant for coastal structures with pattern-placed revetments.

5.1.5 Wave breaking

Waves break due to increasing steepness (white-capping), or in case they run into too shallow water. The deep-water breaking limit for a single wave[166] is a steepness of 0.14. In a series of irregular waves a typical measured values of the maximum wave steepness $s_o = H_s/L_o$ is 0.05 (for $H_{m0} > 2.5$ m) to 0.07 (for $H_{m0} < 1.5$ m).[167]

Some authors give depth-induced wave breaking criteria in the form of H/d, others use L/d or d/L as the governing limiting parameter. According to solitary wave theory[168] depth-induced wave breaking for solitary waves happens at

$$H_b = 0.78\,d \qquad\qquad\qquad \text{Eq. 5.14}$$

The breaker index $\gamma\,(= H_b/d)$ for depth-induced breaking is later refined by various authors, resulting in values between 0.5 and 0.9. Several authors[169] present steepness and depth-induced breaking limits in one graph.

Wave breaking on slopes is discussed in section 5.2.
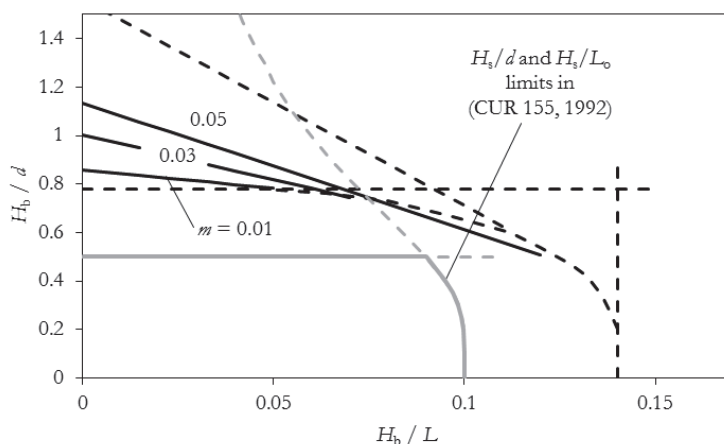
Figure 5-5　　　**Depth- and steepness limited wave breaking with formulas of 1992-Handbook**

5.1.6 Effect of limited depth on H_s

In the process of depth-induced breaking of a series of irregular waves the highest waves start to break first. The wave energy is partly dissipated, and partly transferred to smaller waves. The number of waves may change due to so-called triad interaction. The wave spectrum and the wave height distribution change. What remains is a wave series with a reduced significant wave height.

---

[166] Miche, 1944

[167] Source: (Caires, 2012) assuming $H_s \sim H_{m0}$

[168] First by McCowan (1891), source: J.M. Smith, *Nearshore Wave Breaking and Decay* (USACE, CERC report 93-11, 1993)

[169] J.R. Weggel, "Maximum breaker height for design," *Coast. Eng.* (Vancouver, 1972)
Y. Goda, *Random seas and design of maritime structures* (World Scientific, 2000)

For irregular waves a design formula for the maximum significant wave height of a remaining wave field is given in Glerum & Wolsink[170].

$$H_s < 0.5d$$ **Eq. 5.15**

The 1992-Handbook for revetments[171] is more specific and adds a steepness-limited maximum H_s.

$$H_s < 0.1 L_o \sqrt{\tanh \frac{2\pi d}{L_o}} \text{, which can be rewritten into}$$ **Eq. 5.16**

$$\frac{H_s}{L_o} < 0.1 \sqrt{\tanh 2\pi \frac{d}{H_s} \frac{H_s}{L_o}}$$

It can be noticed that the $H_s < 0.5d$ might be not accurate for smaller values of the wave steepness and also dependency on the bottom steepness m is missing. Depth-induced wave breaking and the effect on the wave spectrum is studied with wave flume tests over many years and a number of authors. Widely used and recommended[172] design graphs are those of Van der Meer (1990)[173], based on one-dimensional ENDEC model calculations and verified with measurements for $s = 0.023 .. 0.047$ and $m = 1/150 .. 1/30$. Also Goda has developed graphs[174]. Various authors have verified and tried to refine these graphs. Here the graphs are presented as H_s/H_{so} against H_{so}/d. In this way they present the transformation of H_{so} as a function of relative depth. In the graphs by Goda the caps shown in the shoaling graph (Figure 5-3) are visible. The Van der Meer graphs were not developed to cover shoaling effects, but nevertheless also show values of H_s/H_{so} above unity. It can be observed that the insights diverge for very gentle bottom slopes. More recent validation by means of a large series of Wallingford tests[175] provides confirmation for lower values of H_s/H_{so}, unfortunately not for $m = 0.01$.

[170] A. Glerum and G.M. Wolsink, *Achtergronden bij de leidraad cementbetonnen dijkbekledingen* (CUR-VB COW-report, 1984)

[171] Klein Breteler, *Handboek voor dimensionering van gezette taludbekledingen*

[172] E.g. in: Pullen et al., *Wave overtopping of sea defence and related structures - Assessment manual*

[173] J.W. van der Meer, *Extreme shallow water wave conditions, Design curves for uniform sloping beaches* (WL-report H0198, 1990)

[174] Goda, *Random seas and design of maritime structures*

[175] N.W.H. Allsop, N Durand, and D.P. Hurdle, "Influence of steep seabed slopes on breaking waves for structure deisgn," *Coast. Eng. Proc.*, 1998
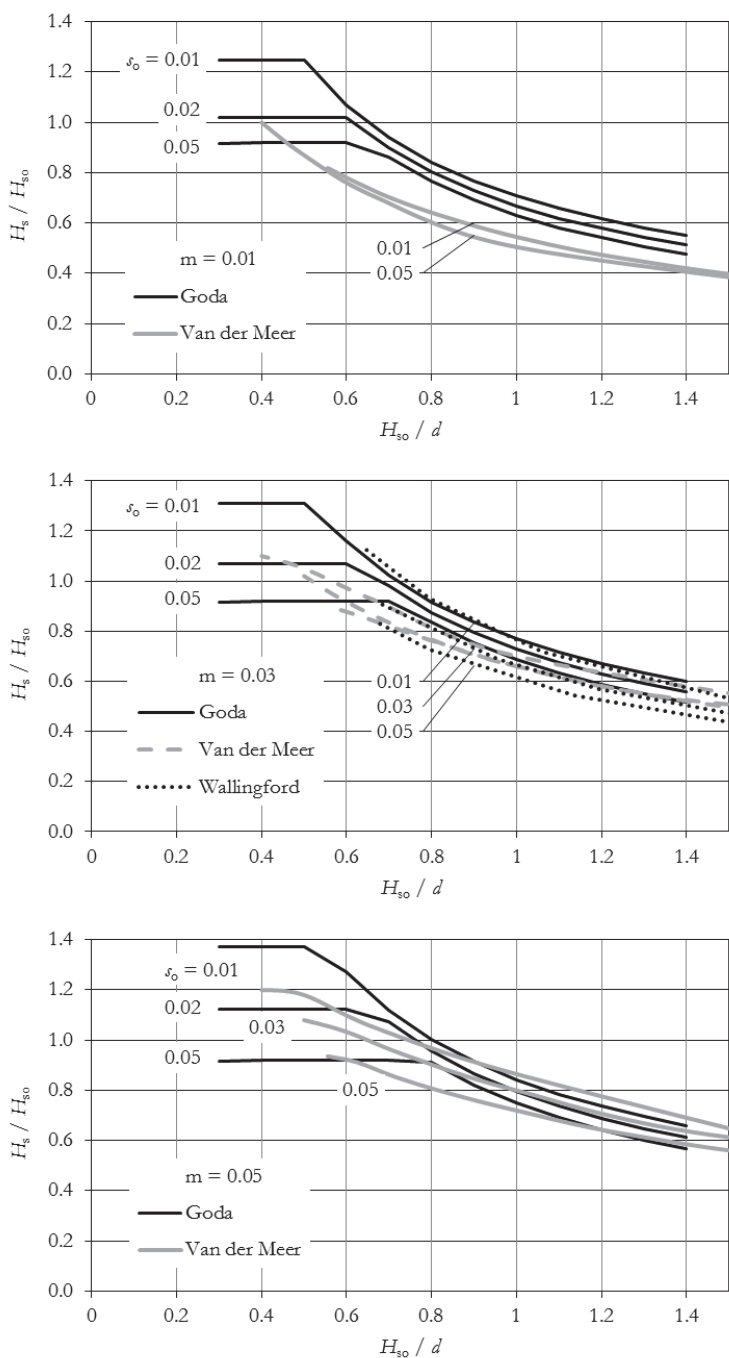
Figure 5-6 Near-shore transformation of H_s given incoming deep water wave H_{so} due to shoaling and depth-induced breaking

5.1.7 Wave set-up

The processes of shoaling and the depth-induced breaking of waves cause a quasi-static water level change. There is a set-down at the point where the breaking starts and a set-up at the coastline. For the wave set-down and set-up several formulas could be derived from linear water wave theory and energy balance equations. For the set down point the surface depression η_{min} following approximation was found.[176]

$$\eta_{min} \approx -\tfrac{1}{16} \frac{H^2}{d}$$ **Eq. 5.17**

Holthuijsen derives a simple formula for the water set-up gradient, after Bowen et al (1962). He assumes a typical breaker index $H_{br} = \gamma\, d_{br}$, with e.g. $\gamma = 0.8$, he assumes waves to remain in a constant ratio to the decreasing water depth, and the waves to be non-dispersive. Then it follows that

$$\frac{d\eta}{dx} = -\tfrac{3}{8}\gamma^2 \frac{d(d+\eta)}{dx}$$ **Eq. 5.18**

Hence the factor between the bottom slope and set-up gradient is $-\tfrac{3}{8}\gamma^2 /(1 + \tfrac{3}{8}\gamma^2)$. For $\gamma = 0.8$, this factor is -0.19.

$$\eta_{max} = \tfrac{5}{16}\gamma\, H_b$$ **Eq. 5.19**

The Rock Manual[177] gives a rough estimation: at the breaker line there is a set-down of typically $0.05 h_{br}$ and at the shallow coastline there is set-up of $0.15 h_{br}$. Using this theory and assuming values of the wave steepness the length of the breaker zone between the set-down and set-up point can be characterised. With $s_b = H_b/L_o$, $H_{br} = \gamma\, d_b$ and $x_b = d_b/m$ it follows that the breaker zone length $x_b = L_o\, s_b/\gamma\, m$, which leads to values between 1 and 6 L_o. Measurements seem to result in significantly higher values of the set-up. Also a large scatter is observed.[178] Goda gives set-up graphs with distinguished relations for various bottom slope angles and wave steepness values.[179] The set-up phenomenon is quasi-static under the assumption of a wave train with more or less constant amplitudes. Since the waves tend to come in groups, the wave set-up will not be constant but will oscillate with the frequency of wave groups. The oscillation is called surf-beat.

5.1.8 Reduced wave height distributions and effect on H_{max}

Depth-induced breaking of irregular waves affects the larger waves first. This process is beneficial for the economy of the revetment. The maximum expected extreme waves are important design input for the revetment. A design approach with a maximum physically possible wave height would create a robust design.

The extreme waves in the depth-transformed wave series are subject of a number of empirical studies. In the 1992-Handbook for revetments[180] formulas of Stive are given.

---

[176] L.H. Holthuijsen, *Waves in Oceanic and Coastal Waters* (Cambridge University Press, 2007)

[177] CIRIA, CUR, and CETMEF, eds., *The Rock Manual - The use of Rock in Hydraulic Engineering (2nd edition)* (London: CIRIA report C683, 2007)

[178] Holthuijsen, *Waves in Oceanic and Coastal Waters*

[179] Goda, *Random seas and design of maritime structures*

[180] Klein Breteler, *Handboek voor dimensionering van gezette taludbekledingen*

Starting from a Rayleigh wave spectrum, the reduced extreme wave height is defined as a reduction to the Rayleigh values.

$$H_{1\%} = 1.517 H_s \frac{1}{(1 + \frac{H_s}{d})^{\frac{1}{3}}}$$

Eq. 5.20

$$H_{0.1\%} = 1.859 H_s \frac{1}{(1 + \frac{H_s}{d})^{\frac{1}{2}}}$$

Eq. 5.21

Goda gives formulas for H_{max} in the same format as for H_s. The formulas include effects of shoaling and depth-induced breaking. Goda defines H_{max} as $H_{1/250}$, which is almost equal to $H_{0.1\%}$.

In 2000 a model for the distribution of extreme wave heights in shallow waters was presented by Battjes and Groenendijk[181]. The model is calibrated on flume test data of WL|Delft between 1988 and 1998. The model uses a combination of a Rayleigh and Weibull distribution and is proven to be more accurate than earlier proposed transformed wave distributions, like the (modified) Glukhovskiy distributions which changed the exponent in the Rayleigh distribution formula from 2 into a depth dependent variable, e.g. $2/(1 - \beta H/d)$. Battjes & Groenendijk proposes to use a Rayleigh distribution for the lower, non-broken waves and a Weibull-distribution for the broken waves. The scale parameters H_1, H_2, the transitional wave height H_{tr} and the Weibull parameter k_2 are calibrated with the available test data. The exponent k_2 appears to give constant value of 3.6.

$$P(\overline{H} < H) = \begin{cases} 1 - \exp\left(-(H/H_1)^2\right) & \text{for } H < H_{tr} \\ 1 - \exp\left(-(H/H_2)^{3.6}\right) & \text{for } H \geq H_{tr} \end{cases}$$

Eq. 5.22

with

Eq. 5.23

$$H_{tr} = (0.35 + 5.8\,m)\,d$$

$d =$ water depth at the toe
$m =$ bottom slope of foreland

Exceedance values of the Weibull wave series can easily be calculated from:

$$\frac{H_{p\%}}{H_{rms}} = \left(-\ln(\frac{p}{100})\right)^{1/3.6}$$

Eq. 5.24

For calculation of the average of the highest 1/3 and 1/100 waves from a Rayleigh distribution an expression with error functions can be used. For a similar calculation from a Weilbull distribution the following formula can be used. Numerical integration gives the results shown in table Table 5-1.

[181] J.A. Battjes and H.W. Groenendijk, "Wave height distributions on shallow foreshores," *Coast. Eng.* 40 (2000): 161–182

H.W. Groenendijk, "Shallow foreshore wave height statistics" (MSc thesis TU Delft, 1998)

$$\frac{H_{1/Q}}{H_{rms}} = \frac{\int\limits_{1-1/Q}^{1}\left(-\ln(-H+1)\right)^{1/3.6} dH}{1/Q}$$

<div align="right">Eq. 5.25</div>

Table 5-1   Average highest wave ratios for Weibull distribution with k = 3.6

Q	3	10	20	50	100	200	500	1000
$\dfrac{H_{1/Q}}{H_{rms}}$	1.2066	1.3831	1.4616	1.5505	1.6097	1.6636	1.7284	1.7735

These values need to be corrected for H_2/H_{rms}. After that they exactly match with the values for $H_{1/3}$ and $H_{1/100}$ given in the paper by Battjes & Groenendijk. H_1 and H_2 are correlated with the continuity constraint in the transition point H_{tr} in the cumulative distribution function (cdf). Battjes & Groenendijk calculate the scale parameters H_1 and H_2 starting from the requirement that the second moment of the probability density function (pdf) of the new, combined distribution equals unity. This requirement is similar to the definition that the root mean square wave height of the new combined distribution is 1. The expressions for H_1 and H_2 cannot be evaluated analytically. Battjes & Groenendijk present the results in tables.
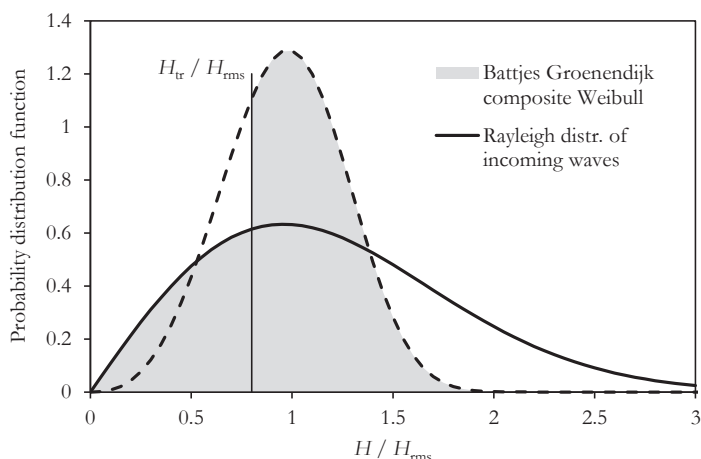
Figure 5-7   Probability density function of composite near-shore wave distribution
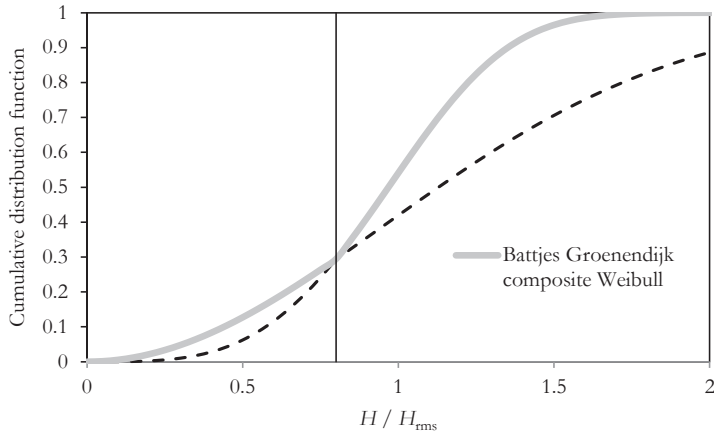
Figure 5-8   Cumulative distribution function of composite near-shore wave distribution
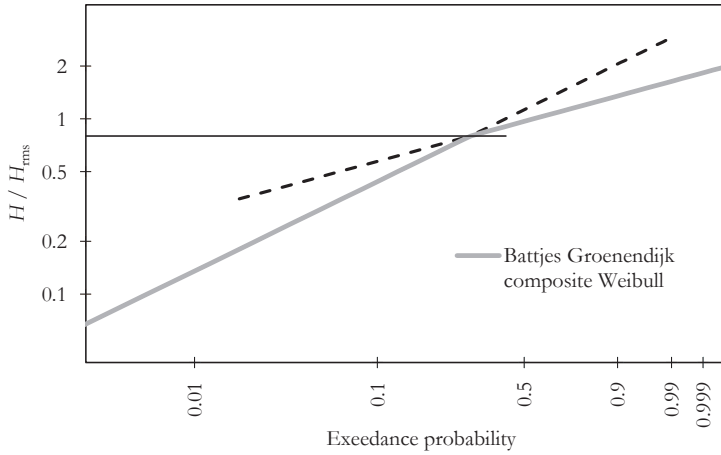
Figure 5-9   Exceedance probability line of composite near-shore wave distribution

The Weibull distribution is in fact a more general case of the Rayleigh distribution. Plotting of the cdf's on a log to double log scale gives straight lines.

$$y = 1 - \exp\left(-(x/\lambda)^k\right) \text{ rewritten as:}$$

$$\ln(x/\lambda) = \frac{1}{k}\ln(-\ln(-y+1))$$

The distribution of Battjes & Groenendijk only gives a best possible descriptive distribution of the waves at a certain point with depth d as an alternative to a Rayleigh distribution of the same field at the same location. It does not relate the distribution to the deep water wave field. This could be done using the formulas of Van der Meer or Goda or using spectral analysis. In case of availability of a depth-transformed spectrum m_0 and H_{m0} will be known.

Given the transformation H_{rms} will not be $H_{m0}/\sqrt{2}$, but is better calculated with:

$$H_{rms} = (0.6725 + 0.2025\frac{H_{m0}}{d})\ H_{m0}$$

<div align="right">Eq. 5.26</div>

Alternatively the share of the non-broken waves ($H < H_{tr}$) might be somehow fitted to the incoming wave height distribution.

Assuming that H_s can be found elsewhere a presentation of what the Battjes & Groenendijk description does to the H_{max} as a function of H_s/d is sufficient. In Figure 5-10 H_{max} is taken as $H_{0.1\%}$. For low Hs/d the waves will not brake and $H_{0.1\%}/H_s = 1.856$, in conformity with the Rayleigh distribution. For the cases that the share with $H > H_s$ is fully above H_{tr}, the value of $H_{0.1\%}/H_s = 1.418$, in conformity with the Weibull distribution.[182] There is a transition zone in between that follow almost straight lines, as indicated below.
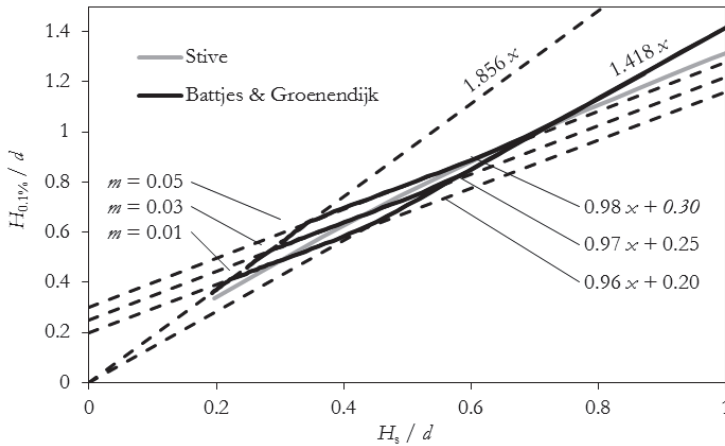
Figure 5-10   **Occurrence of max waves as a function of relative depth within near-shore distribution**

The formula derived by Stive follows the average and continuous to flatten out with high values of H_s/d. This is probably more realistic as it will be very unlikely that when the depth decreases progressively still very high waves can occur in the shallow water. It therefore does not make sense to use the Battjes & Groenendijk Weibull distribution e.g. for waves $H_{0.01\%}$.

More or less constant limit values of $H_{p\%}/d$ have a strong practical meaning. The wave condition at the toe primarily depends on the water depth and not on the incoming wave heights. A shallow foreland is in that case an adequate threshold that dictates the wave conditions for the revetment slope. Insight on what the foreland does to the design wave height is gained by plotting the fit-formulas of the various authors as transformation functions H_s/H_{so} against H_{os}/d (like Figure 5-6) or as H_s/d against H_{os}/d.

---

[182] The ratio $H_{2\%}/H_s$ for the Weibull distribution is 1.21.

DESIGN OF PATTERN-PLACED REVETMENTS

5.1.9   Discussion

A revetment design should be based on a reliable estimation of the wave conditions. The effects of limited depth or foreland on the occurrence of the highest waves and a reliable prediction of the wave steepness are two aspects that are of utmost importance for a good revetment design.

For wave run-up on dikes with shallow foreshores the combination of the Van der Meer formulas to find H_s, and the Battjes & Groenendijk distribution to find extreme waves is considered as state-of-art. This approach is in reasonable equivalence with others, amongst them the empirical formulas of Goda (see Figure 5-11). The Goda formulas seem to give higher, maybe conservative results for bottom slopes $m = 0.01$, which are quite common at the North Sea and Zeeland estuaries coasts. The tests on which the Battjes & Groenendijk model was calibrated were performed with depth ranges H_s/d of 0.10 to 0.83, which covers the complete relevant range for design practise. For revetment design ideally a similar approach with a set of calibrated formulas that produce $H_{0.1\%}$ instantaneously as a function of H_{so}/d, s_o and m would be preferred.
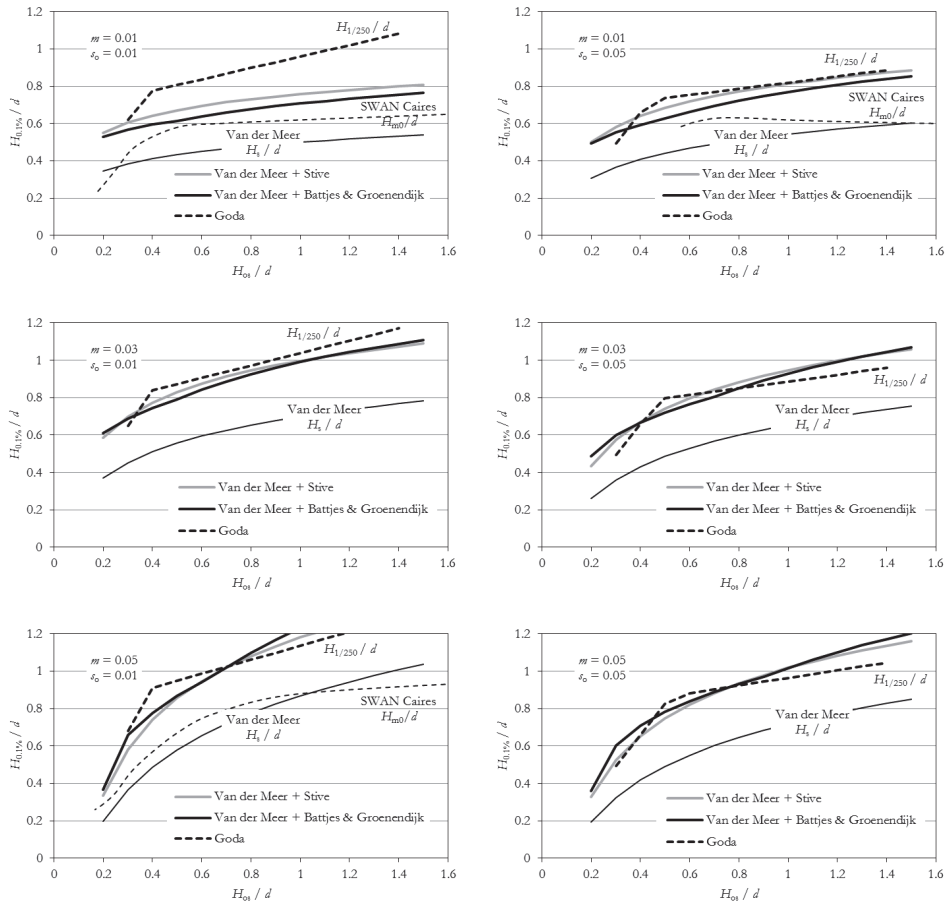
Figure 5-11   **Occurrence of maximum waves as a function of relative depth and original H_{so}**

Battjes & Groenendijk did not find dependency of the wave steepness on the distribution of waves heights. The deep-water steepness has a significant effect on the depth-induced breaking, and determines the remaining H_{rms} or H_s though; it did not seem to affect the wave height distribution too much, although a large scatter is present. In recent verifications of the Battjes & Groenendijk formulas with flume tests and measurements on shallow lakes in the Netherlands[183] an effect of the wave steepness s on the transformed wave height distribution was found. Measurements at the lakes IJsselmeer and Slotermeer covered $0.045 < s < 0.065$. The average value of measured versus calculated $H_{1/N}$ was 0.85, with scatter between 0.7 and 1.0, with no clear dependency on s. The scatter is partly explained by the non-constant number of waves N (most cases < 1000). The flume tests covered the range $0.010 < s < 0.045$. The ratio of measured versus calculated $H_{0.1\%}$ is 0.9, with less scatter and with a clear dependency on s, running from 0.8 at $s = 0.01$ to 1.0 at $s = 0.04$. As a conclusion the potential for refinement of the wave distribution model seems only relevant for the lower values of the wave steepness ($s < 0.025$), where Battjes & Groenendijk might be conservative in the order of 10 to 15%.

The range of potentially occurring values of the deep-water wave steepness s_o forms important input for revetment design. In the hydraulic boundary conditions issued by the Dutch government[184] single values of H_s and T_p are specified. It is not clear whether the combination of the two values gives the only relevant value within a potentially possible range of s_o. Given the dependency of the revetment stability on $\xi_o = 1/(\cot\alpha \sqrt{s_o})$ this would be unlikely.

The specified H_s and T_p are the result of SWAN model calculations. In 2010 it was found that the SWAN model calculations produce unrealistic values of the steepness, mainly caused by underestimation of T_p.[185] Some authors explain this by the effect of triads.[186] A discussion in an earlier verification study[187] mentions various effects, none of which explains the underestimation convincingly. In (Caires, 2012) new calculations are presented with limited local wave growth. The conclusion is in line with (Ris et al, 1999): adding 1 s to the peak wave period calculated by SWAN gives a good comparison with the measurements.[188] Double

---

[183] S. Caires and M.R.A. van Gent, "Wave height distribution in constant and finite depths," *Coast. Eng. Proc.*, 2012

The depth-induced breaking in SWAN is modelled as a change of the total energy dissipated in the breaking process. The maximum wave height is limited by a breaker criterion, γ_d (Holthuijzen). For the SWAN model calculations in this paper the energy loss due to depth-induced breaking was improved using formulas of Van der Westhuysen who distinguishes between depth-induced breaking of deep-water spectra when they run into shallow water and depth-induced breaking of wave-growth in shallow, flat bottom waters. Refer to: AJ van der Westhuysen, "Modeling nearshore wave processes," *ECMWF Work. Ocean Waves*, 2012, 25–27

[184] *Hydraulische randvoorwaarden 2001, voor het toetsen van primaire waterkeringen* (DWW report, 2002)

Hydraulische Randvoorwaarden Primaire Waterkeringen voor de derde toetsronde 2006-2011 (DWW report, 2007)

[185] S. Caires, *Maximale significante golfhoogte bij ondiep water en maximale golfsteilheid*, 2012

S. Vuren, *Validatie methode De Haan - Deel 1: validatie Hydra-K* (WL | Delft Hydraulics report Q4409, 2008)

[186] When waves become steeper triad wave-wave interactions occur, which – according to the theory – basically is the process of two waves to form new higher harmonic waves. Thus, energy is transferred to higher frequencies.

[187] R.C. Ris, L.H. Holthuijsen, and N. Booij, "A third-generation wave model for coastal regions –Verification," *J. Geophys. Res.* 104:C4 (1999)

[188] See also: J. Groeneweg et al., "Wave Propagation into Complex Coastal Systems and the Role of Nonlinear Interactions," *J. Waterw. Port Coast. Ocean Engng* (2015)

peaked spectra occur in quite a number of locations.[189] For revetment design both frequencies are potentially important as they determine the range of the wave steepness. Occurring wave steepness values were investigated using two-dimensional model calculations with realistic bathymetric data and wind directions and subsequent validation with measurements (see Table 5-2). The hindcasting with SWAN yielded quite poor results. The results were only used to support a recommendation for a maximum wave steepness for the design.

Den Heijer presents safety approaches in loads and resistance in a report[190]. He notices that the hydraulic load researchers of the RIKZ and the stability investigators DWW and WL, both have their own safety margins. The so-called hydraulic boundary conditions are calculated wave heights at water levels of +2, +4 and +6 m, based on wind speeds with a 1/4000 yr exceedance frequency. The calculations are performed with a SWAN model that is "known to predict the wave height H_s on average 10% too high and wave period T_p on average 1 second too low". The T_p values are corrected with 1 second. The H_s values are not corrected. Both parameters have a 20% uncertainty.

Table 5-2   Measured wave steepness values (source: Caires, 2012)

	measured average wave steepness s_0 for indicated range of H_{m0}	measured 5-95% CI	for H_{m0} [m]
Northsea (SWB)	0.035	0.03 – 0.04	3 – 4.8
Northsea (SCW)	0.033	0.025 – 0.04	2.5 – 4
Westerschelde (PVT1)	0.055	0.015 – 0.085	0.45 – 0.6
Westerschelde (BAT1)	0.05	0.015 – 0.09	0.4 - 0.55
Oosterschelde (KEET)	0.04	0.025 – 0.057	0.5 – 0.9

In (Caires, 2012) one-dimensional SWAN model calculations of a wide variety of idealised constant sloped bottoms and a range of wave steepness values were calculated also. This resulted in H_{m0}/d graphs, similar to the graphs of Van der Meer. Some of the results are plotted in Figure 5-11 for comparison only.

The SWAN calculations themselves have not been compared with measured data. In general it is recommended to base a design wave height estimate on the Van der Meer formulas combined with a change near-shore wave height distribution according to Battjes & Groenendijk, and not on SWAN calculations. The SWAN calculations compare reasonably well with the Van der Meer formulas for $m = 0.05$. Noticeably, the SWAN-results for $m = 0.01$ show better conformity with the trend of the Goda-formulas.

5.2 Wave loading on slopes

5.2.1   Wave breaking on slopes

Wave loads on slopes are since 1974 described[191] with the breaker parameter ξ, also called surf similarity parameter, or Iribarren number.[192]

---

[189] See also: Vrijling, *General wave spectrum model*
[190] F. den Heijer, *Veiligheid huidige ontwerpmethodiek steenzettingen* (WL|Delft Hydraulics report H3437, 1998)
[191] J.A. Battjes, "Surf similarity," *Coast. Eng. Proc.* (Copenhagen, 1974), 466–480

$$\xi = \frac{\tan\alpha}{\sqrt{H/L}}$$

<div align="right">Eq. 5.27</div>

with

α = slope angle

L = wave length of the incident wave

For irregular waves this expression becomes:

$$\xi_{op} = \frac{\tan\alpha}{\sqrt{H_s/L_o}} \quad \text{with } L_o = \frac{gT_p^{\,2}}{2\pi}$$

<div align="right">Eq. 5.28</div>

or:

$$\xi_{m\text{-}10} = \frac{\tan\alpha}{\sqrt{s_o}} \quad \text{with } s_0 = \frac{2\pi H_{m0}}{gT_{m-10}^{\,2}}$$

The breaker parameter categorises slope angles relative to the wave steepness. On very gentle slopes ($\xi < 1$) the waves break like in gradually more shallow water, the high waves break distant, the smaller waves break close to the coast line. The white-capped breakers travel over a certain distance to the coast line and gradually loose the wave energy.

On less gentle slopes, $1 < \xi < 2.5$, plunging breakers occur. The more sudden depth decrease of the slope, decreases the speed of the wave. The top of the wave travels faster, moves over the wave front, and plunges or slams on the slope. In some cases the down pouring water plunges in a water film of the previous wave. In other cases the water directly hits the revetment slope.

On steeper slopes, $\xi > 2.5$, the wave reflection becomes dominant and surging breakers occur. The waves move up and down along the slope, and (when $\xi < 3.5$) some turbulence occurs when the upper part of the waves collapses and hits the slope. Those breakers are called collapsing breakers.

The slope angle is an important parameter for the wave run-up, and consequently for the crest level and the dike geometry that may include a berm. Wave run-up is extensively investigated and has resulted in the authoritative reports of TAW and EurOtop[193]. Run-up is less relevant for the armour stability.

$$\frac{R_{u2\%}}{H_{m0}} = 1.65\,\xi_{m-10} \not> 4.0 - \frac{1.5}{\sqrt{\xi_{m-10}}}\ ,^{[194]}$$

<div align="right">Eq. 5.29</div>

to be corrected with:

γ_b for the presence of a berm

γ_f for slope roughness

γ_β for oblique waves

---

[192] In American literature for (beach) slopes up to 1:8 a parameter $S_0 = m\,L/d$ is used, with L is the incident wave length of a Boussinesq wave. Transition values of S_0 between the breaker types are: spilling / 0.025 / plunging / 0.30 / surging / 0.37. The parameter S_0 also defines the location of wave breaking.
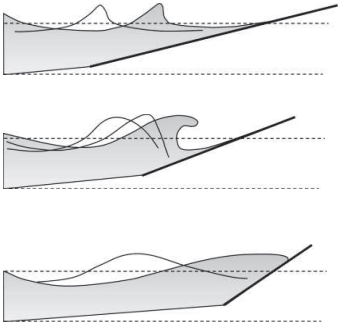
[193] J.W. van der Meer, *Wave run-up and wave overtopping at dikes* (TAW report TR23, 2002) Pullen et al., *Wave overtopping of sea defence and related structures - Assessment manual*

[194] Mind that the slope angle to be incorporated in $\xi_{m\text{-}10}$ in the run-up formula is an average value of the upper and lower part of the slope.

DESIGN OF PATTERN-PLACED REVETMENTS

The permeable top layer of block revetments is destabilised when the pressure in the core and of the filter layers exceed the pressures above the slope. The water pressures in the moving breakers vary within the cycle of a breaking wave. The excess filter pressure decreases over time due to drainage through the top layer. Pressures in the filter therefore follow the wave pressure with some delay. Especially strong gradients in space and time of the water head above the slope are associated with extreme loads of the top layer of the revetment.

Numerous load tests show that at two instants in the wave breaking on the slope these strong gradients occur: (1) the point of maximum wave run-down and (2) the instant of the plunging wave impact. Of these two occurrences the run-down is less dynamic than the impact.

Table 5-3   Breaker types

Breaker type	Transition value of ξ for incident waves	Dominant processes	Range of ξ_o for irregular waves	Crest height	Revetment properties	short wave length, gentle slope ↓ long wave length, steep slope
Spilling		Wave set-up		Low	Long slope, small D	
Plunging	1 ... 2.5	Wave rundown and wave impact	1 – 4		Medium slope length, large D	
Surging		Reflection rundown run-up	2 – 7	High	Optimal element interaction effect	

Collapsing breakers are a transition type of breaker between plunging and surging, with strong rundown and a collapsing, but not overturning wave top.
Revetment slopes and load conditions range from $\xi_o = 1$ to 9. No breaking beyond $\xi = 5.5$ (for incident waves).

5.2.2   Run-down point

The run down point on smooth slopes has been investigated by several researchers. All available formulas are empirical. Before 1985 most tests were executed with regular waves, after that with irregular waves. They mostly refer to H_s and give a wave spectrum. An undisturbed wave height distribution may be assumed. Some tests are meant to measure the effect of an underwater berm. In that case the run-down point of the larger waves will be affected by the berm. In early evaluations of test results authors complain about difficulties in determining the run-down point[195]. Some test series are re-evaluated more than once[196].

---

[195] Glerum and Wolsink, *Achtergronden bij de leidraad cementbetonnen dijkbekledingen*
[196] Klein Breteler, *Taludbekledingen van gezette steen - Waterbeweging en golfbelasting op een glad talud - band 1*

Table 5-4 Dependency parameters for run-down formulas in literature

R_d/H_s dependent on parameter	Exceedance probability	Literature reference	Remark
ξ_o		K. den Boer, *Taludbekledingen van gezette Steen, Stabiliteit van enkele typen bekledingen bij diverse golfomstandigheden, verslag kleinschalig modelonderzoek* (WL|Delft Hydraulics report M1795 deel XIV, 1985)	Suggested formula: $0.5\,\xi_o - 0.2$
$e^{-c/\xi}$	2%	J.P. Ahrens, *Irregular Wave Run-up on Smooth Slopes* (Coastal Engineering Aid No 81-17, 1981)	
$\sqrt{\cot\alpha} \times \xi_o$		J.W. van der Meer, "Rock slopes and gravel beaches under wave attack" (PhD thesis TU Delft, 1988)	For surging waves, for which the run-down point is governing
ξ_o^2 and ξ_o		J.W. van der Meer and M. Klein Breteler, "Measurement and computation of wave induced velocities on a smooth slope," *Coast. Eng.* (Delft, 1990), 191–204	
$(\tan\alpha\,/\,s_o)^{0.8}$		M. Klein Breteler, *Taludbekledingen van gezette steen - Waterbeweging en golfbelasting op een glad talud - band 1* (WL Delft Hydraulics report M1795 part XVII, 1990) M. Klein Breteler, *Handboek voor dimensionering van gezette taludbekledingen* (CUR / TAW report 155, 1992)	Straight wave front, used in computer program Anamos
$\sqrt{\cot\alpha} \times \xi_o$ for the location $(\sqrt{\cot\alpha} \times \xi_o)^{1.25}$ for the wave front depth (to SWL)	2%	J.P. de Waal, M. Klein Breteler, and H den Adel, *Taludbekledingen van gezette steen - Golfdruk op het talud - deel B: verbetering van het analytisch model en STEENZET, verslag bureaustudie* (WL|Delft Hydraulics report H195/H1256/H1770/H2499, 1995)	Curved wave front
$\xi_o\,/\,\tan\alpha = 1/\sqrt{s_o}$ for the location	2%	M. Klein Breteler, I. van der Werf, and I. Wenneker, *Kwantificering golfbelasting en invloed lange golven, rev. 2*, 2012 (revision 1 is from 2006)	Improved complete wave shape description for STEENTOETS, evaluation based on data of slopes with $\cot\alpha$ between 3 and 4
ξ_{m-10}	2%	T. Pullen et al., *Wave overtopping of sea defence and related structures - Assessment manual*, 2007 H. Schüttrumpf et al., "Wave run-up and wave overtopping at armored rubble slopes and mounds," in *Handb. Coast. Ocean Eng.*, ed. Y.C. Kim (World Scientific, 2010), 383–409	Graph presented, no relation given

The empirical formulas are not uniform regarding the dependencies. A simple formula[197] suggest a linear dependency on the breaker parameter ξ.

$$\frac{R_{d2\%}}{H_s} = 0.33\,\xi_o \ngtr 1.5 \qquad\qquad \textbf{Eq. 5.30}$$

In Glerum & Wolsink, a comprehensive literature review, it is already concluded that Eq. 5.30 does not provide a safe upper bound[198]. An additional term $0.33\,\xi_o + 0.15$ is suggested. Many other relations are given also. These relations are functions of the slope angle and the wave steepness in various forms. Later literature continues investigating dependencies.

From Table 5-4 it can be concluded that up to recent years investigations of the run-down point have not produced a clear, established result. This may be partly dependent on the mix of data sources, since slope tests are carried out on asphalt slopes, pattern-placed revetment slopes and rock slopes. For rubble mount or rock-armoured slopes the roughness and the permeability of the core introduce variables that are irrelevant for the smooth revetment slopes.

Recent investigations suggest either ξ_{m-10} or s_o as main independent variable. The formulas in STEENTOETS are based on data points covering a small range of $\cot\alpha$, which may explain a weak dependency on ξ_{m-10} or ξ_{op}. Re-assessing this dataset with a best fit against ξ_{m-10} and against $1/\sqrt{s_o}$ gives variation coefficients of 0.33 and 0.30, respectively. This does not strongly support a preference for s_o. Investigating the dependency on wave steepness s_o and slope angle ($\cot\alpha$) only makes sense in case steep ($\cot\alpha = 2$) and very gentle slopes ($\cot\alpha = 6$) are part of the equation also.

Measurements of the run-down on steep smooth slopes are difficult to find in literature. Ahrens, 1981 indicates upper and lower limits of a range of data, but does not present the data themselves. The verification data points in Figure 5-12 are supplemented with the $\cot\alpha = 2$ data points from Schüttrumpf et al, 2010 (rough slope, impermeable core only) and with the limited number of Delta flume tests[199] that have been carried out on slopes $\cot\alpha = 6$. The measurements of the rough slopes could be corrected for smooth slopes. It is unknown to what extent available correction factors for run-up[200] apply for run-down. Figure 5-12 and Figure 5-13 show the uncorrected data points. The data points for $\cot\alpha = 3$ to 4 were shifted using T_{m-10} instead T_p. The wave spectrum data for all tests could be found[201]. For the data points with $\cot\alpha = 6$ it is uncertain whether the data represent 2% probability. The data points are plotted against ξ_{m-10} (Figure 5-12) and $1/\sqrt{s_o}$ (Figure 5-13). It appears that the

---

[197] The formula appears in the 1992 CUR - Rock Manual and in earlier literature. References to an author are lacking.
[198] Please note that this study is partly about the fact that revetment strength increases with depth on the slope. The deepest run-down point is therefore not by definition the damage point.
[199] Tests carried out in 1984, found in: M. Klein Breteler, *Inventarisatie drukbestanden voor Steenzet* (WL Delft Hydraulics report H3565, 1999)
[200] Meer, *Wave run-up and wave overtopping at dikes*
[201] Sources: Klein Breteler, *Inventarisatie drukbestanden voor Steenzet* and Klein Breteler, Werf, and Wenneker, *Kwantificering golfbelasting en invloed lange golven, rev. 2* In cases the spectrum frequency parameters are not given: $T_p/T_{m-10} = 1.17$ for PM spectra, and 1.10 for JONSWAP.

additional data for steep and less steep slopes support a dependency of the breaker parameter ξ_{m-10}.

Figure 5-12 is represented by a plot with axis "Breaker parameter ξ_{m-10}" on top ranging 0 to 8, and "Rundown $R_{d2\%}/H_s$" on the vertical axis from 0.0 to 3.0. Legend:
○ Schelde flume, slope 1:6
□ Schelde flume, slope 1:3 - 1:4
△ Deltaflume, slope 1:6
◇ Delta flume, slope 1:3 - 1:4
○ (Schüttrumpf et al, 2010), rough slope 1:2
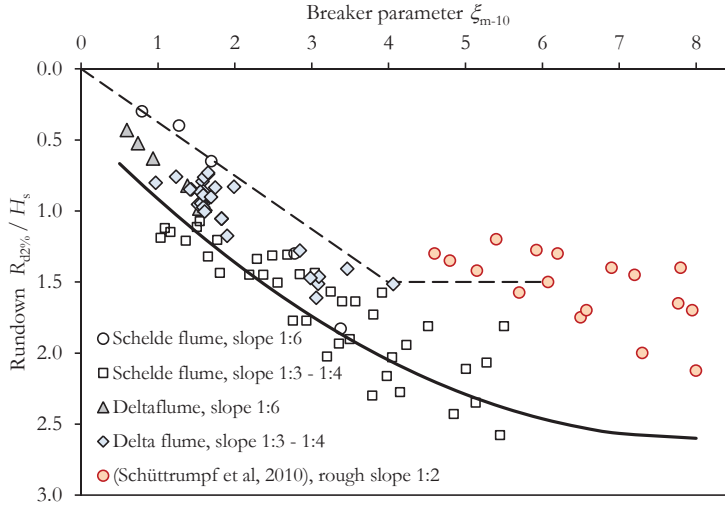
Figure 5-12   **Rundown against breaker parameter, for indicated values of cotα, measured data and run-down formulas Eq. 5.30 and 5.31**

Similar to Van der Meer and Klein Breteler in 1990, a quadratic formula is suggested for the wave rundown on a smooth slope. See Figure 5-12.

$$\frac{R_{d2\%}}{H_s} < a_1\,\xi_{m-10}{}^2 + a_2\,\xi_{m-10} + a_3$$

$$\frac{R_{d2\%}}{H_s} < -0.0344\xi_{m-10}{}^2 + 0.55\,\xi_{m-10} + 0.4 \qquad\qquad \textbf{Eq. 5.31}$$

This formula represents the 5% exceedance value of all large scale tests, and a 20% exceedance value of all tests in Figure 5-12.

The physical background of a limit value for large values of ξ is the reflection of waves. The 'free' wave height of fully reflected waves is $\sqrt{2}\,H$. Reflection against a vertical wall gives $2\,H$ for incident waves, equally divided over run-up R_u and run-down R_d. A value of $R_d = 0.75\,H_i$ for irregular waves can be found in (Goda, 1985), in which H_i the design wave height with the desired exceedance probability. Hence the limit value for a vertical structure it $R_{d2\%}/H_s =$ (0.75 .. 1.0) × 1.4 = 1.05 .. 1.4. The difference of the value of approx 2.5 for a 1:3 slope compared to 1.4 for vertical structures is caused by the wave kinematics that create a concave wave front with a steep angle on the slope and a sloshing wave shape with an almost horizontal water surface at the vertical wall.
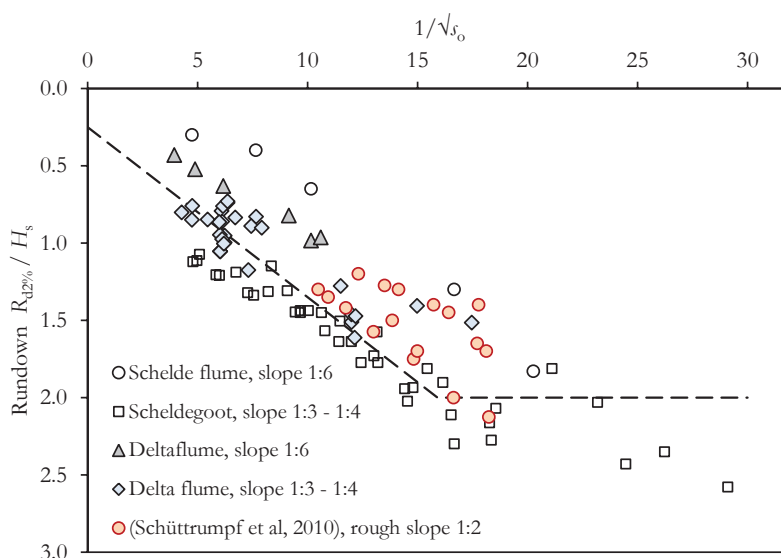
Figure 5-13   **Rundown against breaker parameter, for indicated values of cotα, measured data and plots of Eq. 5.36 used in STEENTOETS 2006**

The damage location data of the investigations by Wevers[202] and Kostense[203] can provide data points for cotα = 3 and 6 also, since it is believed that the deep damage locations are related to the run-down point. Wevers and Kostense collected these data from scale tests with 2 cm thick elements. The data from Wevers are for regular waves. These data points can be transformed to irregular waves using standard relations[204]. Kostense provides a specific (measured) wave spectrum, which enables us to re-assess and plot the data against ξ_{m-10}. It should be noted that Wevers based his statistics on 500 waves and Kostense on 1000 waves, which explains that Kostense gives higher values and which implies that both give values above 2% probability. From comparison of Figure 5-14 and Figure 5-15 it can also be concluded that the breaker parameter is the logic choice as the main variable for the rundown-formula.

Figure 5-14 shows that the measured values tend to exceed the line of Eq 4.31, especially for the 1:3 slope. The damage points that exceed the line are not due to wave impacts. It can be discussed whether a scale effect of slope permeability and porousness of the system plays a role. Also in Figure 5-12 it is clear that the Schelde flume results (average H_s = 0.14 m) are below the Delta flume results (average H_s = 0.94 m). No scaling has been applied for the wave geometry parameters.

---

[202] A. Wevers, *Stabiliteit taludbekledingen van gezette steen onder golfaanval - verslag modelonderzoek* (WL report M1057, 1970)

[203] J.K. Kostense, *Taludbekledingen van gezette steen - invloed van de doorlatendheid van de fundering - modelonderzoek* (WL Delft Hydraulics report M1410 part II, 1981)

[204] D.G. Meijer, J.F. Ruff, and H.J. Verheij, *Waterbeweging op grasdijken door golfaanval* (WL Delft Hydraulics report Q1247, 1993)
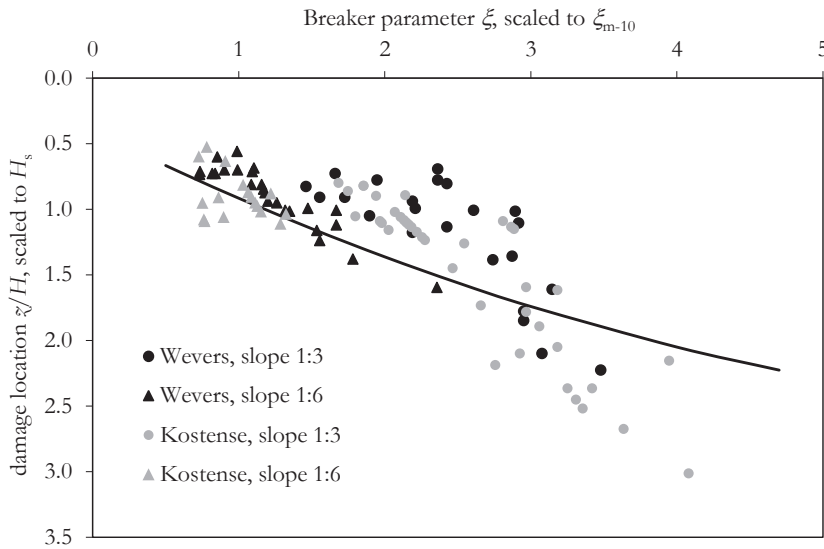
Figure 5-14   **Damage point location of 1970 and 1981 tests, for indicated values of cotα, plotted against breaker parameter, compared with Eq 5.31**
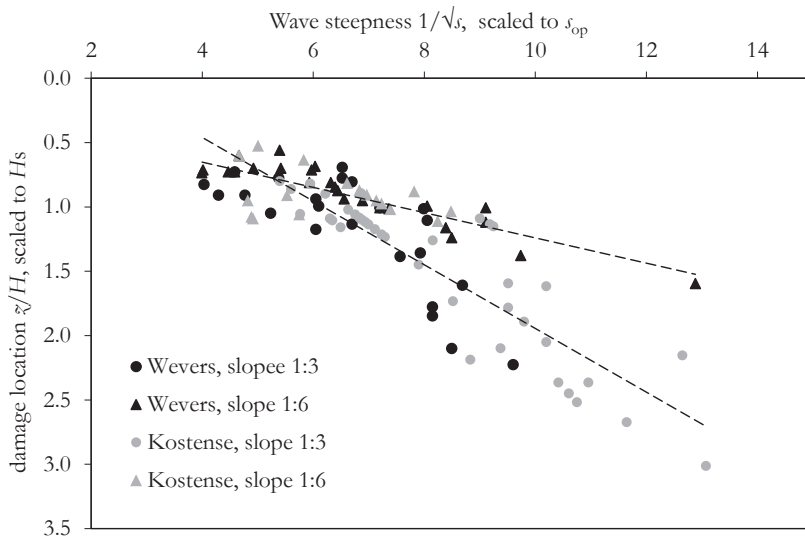
Figure 5-15   **Damage point locations of 1970 and 1981 tests plotted against wave steepness, with trend lines for cotα = 3 and 6.**

5.2.3   *Review of breaker parametrisations in literature*

For the wave load on the revetment slope the distribution of the water pressures along the slope is important. Based on measurements in flume tests attempts have been made in

literature to describe the shape of the wave with characteristic parameters. They include the run-down point and the breaker height, supplemented with the wave front angle and the horizontal position of the wave crest.

Assuming the run-down point as most critical, early parametric descriptions of the shape of the wave front on the slope consisted of a formula for the breaker height and a formula for the angle of the wave front at the run-down point.[205]

$$\frac{\phi_b}{H} = 0.36\sqrt{\frac{\tan\alpha}{H/L_0}} \ngtr 2.2 \qquad\qquad \textbf{Eq. 5.32}$$

$$\tan\theta_f = 5.9\sqrt{H/L_0}$$

with associated run-down point definition as:

$$\frac{R_d}{H} = 0.11\left(\frac{\tan\alpha}{H/L_0}\right)^{0.8} \ngtr 1.5$$

These formulas were derived for regular waves, but in the 1992-Handbook they are used for irregular waves by substituting H_s for H.
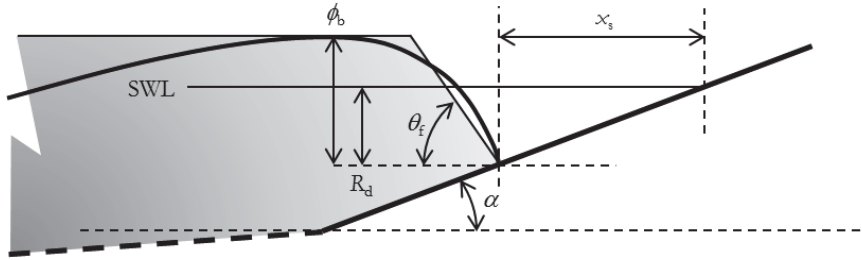
Figure 5-16   **Definition diagram breaker parameters**

After evaluation of irregular wave tests in 1995 the wave description was improved and 2% values were derived from analysed waves of Delta flume tests.[206] This set of formulas is known as the 'curved front' parameterisation. See Figure 5-17. The characteristic parameters are:

$$\frac{\phi_{b,2\%}}{H_s} = 0.27\frac{\xi_\varphi}{(\tan\alpha)^{0.75}} \ngtr 2.5 \qquad\qquad \textbf{Eq. 5.33}$$

$$(\tan\theta_f)_{2\%} = 2.7\frac{1}{\sqrt[3]{\xi_\varphi}}$$

---

[205] M. Klein Breteler, *Taludbekledingen van gezette steen - stabiliteit van de toplaag* (WL Delft Hydraulics report M1795 part XX, vol. B / GeoDelft report CO 285453/7, 1992) Klein Breteler, *Handboek voor dimensionering van gezette taludbekledingen*

[206] Waal, Klein Breteler, and Adel, *Taludbekledingen van gezette steen - Golfdruk op het talud - deel B: verbetering van het analytisch model en STEENZET, verslag bureaustudie*

$$\frac{\phi_{\min,2\%}}{H_s} = -0.16\left(\frac{\xi_\varphi}{\sqrt{\tan\alpha}}\right)^{1.25} \not< \frac{-2.5}{1+0.9/\sqrt{\xi_\varphi}}$$

<div align="right">Eq. 5.34</div>

The horizontal run-down point distance (from the intersection of the SWL and the slope) and the distance to the location of the maximum ϕ_b are:

$$\frac{x_{s,2\%}}{H_s}\tan\alpha = 0.50 + 0.22\frac{\xi_\varphi}{\sqrt{\tan\alpha}} \not> 1.80$$

$$x_m = \frac{3\phi_b + 1.4\phi_{\min}}{\tan\theta_f} + x_s$$
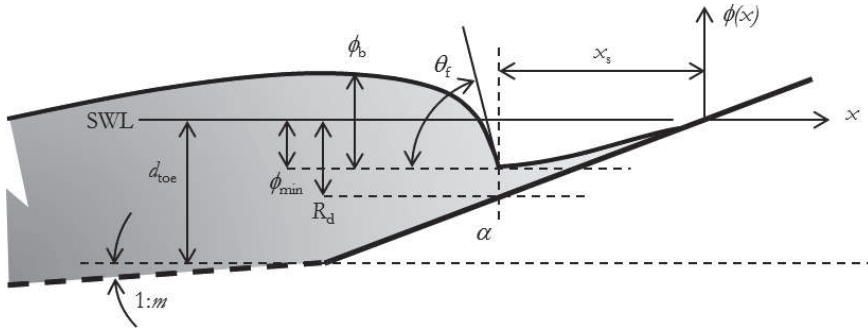
Figure 5-17   **Definition diagram curved breaker front**

The total beaker shape parameterisation as a function of x is:

$$\phi(x) = \left((x_s - x)\tan\theta_f + \phi_{\min}\right) e^{-\frac{(x_s - x)\tan\theta_f}{3\phi_b + 2.4\phi_{\min}}} \qquad \text{for } x < -x_s$$

$$\phi(x) = -x\frac{\phi_{\min}}{x_s} \qquad \text{for } x > -x_s$$

In 2006 a parameterisation of the wave plunging was found and as an additional result changes to the description above were proposed.[207] The formula for $\phi_{\min}$ was not changed.

$$\frac{\phi_{b,2\%}}{H_s} = 0.5 + 0.12\frac{\xi_\varphi}{\tan\alpha} \not> 2.3$$

<div align="right">Eq. 5.35</div>

$$(\tan\theta_f)_{2\%} = 1 \not> 8.8 - 0.41\frac{\xi_\varphi}{\tan\alpha} \not> 5$$

$$\frac{x_{s,2\%}}{H_s}\tan\alpha = 0.25 + 0.11\frac{\xi_\varphi}{\tan\alpha} \not> 2.0$$

<div align="right">Eq. 5.36</div>

In these formulas the front height is a bit lower, and the front angle is steeper. It appears that the 2%-height and 2%-front angle do not need to be combined. A high front and a

---

[207] Klein Breteler, Werf, and Wenneker, *Kwantificering golfbelasting en invloed lange golven, rev. 2*

steep front were defined.[208] The corresponding front angle for the high front is:
$\tan\theta_f = 0.6 \not> 5.5 - 0.3\xi_{op}/\tan\alpha \not> 2.5$

The corresponding parameters for the steep front are:

$\phi_b/H_s = 0.4 + 0.08\xi_{op}/\tan\alpha \not> 1.4$; $\phi_{min}/H_s = -0.05 - 0.14\xi_{op}/\sqrt{\tan\alpha} \not< -0.9$;

$x_s\tan\alpha/H_s = 0.20 + 0.06\xi_{op}/\tan\alpha \not> 0.9$

Taking the sum of ϕ_b and (the negative value of) ϕ_{min} gives a wave crest elevation (see Figure 5-17). In the 1995-parametrisation the crest elevation follows the trend of reflection formulas: the wave height increases with ξ. In the wave parameterisation formulas of 2006 the trend for the crest height is opposite to the reflection coefficient. Moreover the wave descriptions above are based on a limited range of slope angles and the dependencies are hence based on the wave steepness, whilst in literature dependencies are based on ξ. Therefore the wave parameterisations are – in line with the review of the run-down formulas in section 5.2.2 – revisited and compared with measurements that could be found in literature. The process of the review is indicated in the flowchart in Figure and further detailed in the remaining part of section 5.2.
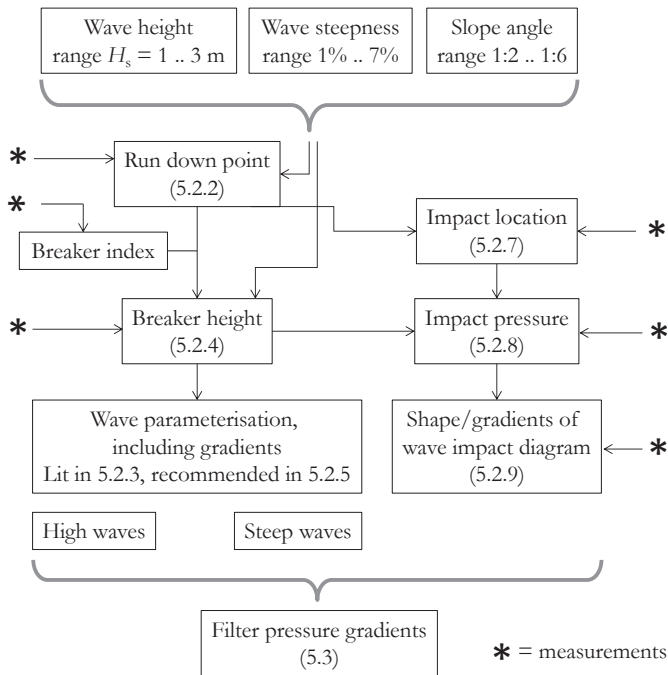
Figure 5-18   Flow chart of review and logic of derivation of wave formulas

---

[208] M. Klein Breteler and I. van der Werf, *Kennisontwikkeling Steentoets 2006* (WL Delft Hydraulics report H4846, 2006)

5.2.4 *Discussion on breaker height on steep slopes*

The 2006-parameterisation of WL|Delft Hydraulics (see 5.2.3, Eq. 5.35) is based on analysis of all waves in 77 fume tests in the Delta flume and the Schelde flume. The water pressures on the slope are measured using sensors on a long transverse line in the breaker attack zone, which have registered pressures at high frequencies. The waves shapes have been analysed and typical parameters have been extracted using a Mathcad programme. Statistics have been performed and maximum values, as well as values exceeded by 2% and 10% of the waves are available of each test. In case we plot the measured ϕ_b/H_s (see Figure 5-17 for definition) against R_d/H_s we can notice a linear relation around a breaker index of 1.1 .. 1.2 (see Figure 5-20). The 10% waves break at a higher point, but with a breaker height with a ratio to the depth at that point that is the same as for the 2% waves. For the registered maximum values that break on a lower point, the same conclusion is valid, but more scatter appears, since the maximum values are single wave records and are not smoothened by any statistical averaging. To avoiding artificial scatter due to combining not correlated singular maximum breaker heights and maximum run-down points, the data of the measured maximum breaker heights have been combined with a calculated run-down point.[209]

The physical process of irregular waves breaking on steep slopes seems to result in a scatter of wave breaking positions, but shows much less spread in the value of the breaker index. Evidently the wave train with irregular wave heights and periods, pushes each individual wave to a certain approximate position on the slope to break. The height to depth ratio induces the actual breaking which is by definition delayed to the moment that this height to depth ratio H_b/R_d is critical for the stability of the front of the individual wave.

The dependency of H_b/R_d on the wave steepness and slope angle needs further investigation. Most studies[210] in literature concentrate on H_b/d_b, where d_b is the depth taken at the top of the wave, and not at the run-down point. The data-points of the Dutch flume tests can also be presented as H_b/d_b by taking the depth at the calculated horizontal position x_m of the wave crest.
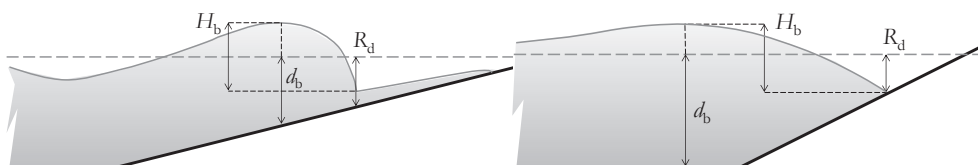
Figure 5-19   **Breaker index definition diagrams**

---

[209] The average 2% run-down relation was found by subtracting 0.25 from Eq. 5.31 From the measurements it was found that that average R_d/H_s was 1.02, 1.34 and 1.68 for 10%, 2% and max respectively. The 'calculated' run-down point to combine with the maximum wave, is: ({Eq. 5.31} - 0.25) × 1.68/1.34. Whilst doing this the average value and standard deviation of γ_b remains the same. Some odd peaks disappeared.

[210] T. Izumiya and M. Isobe, "Breaking criterion on non-uniform sloping beach," *Coast. Eng. Proc.* (Taipei, 1986), 318–327
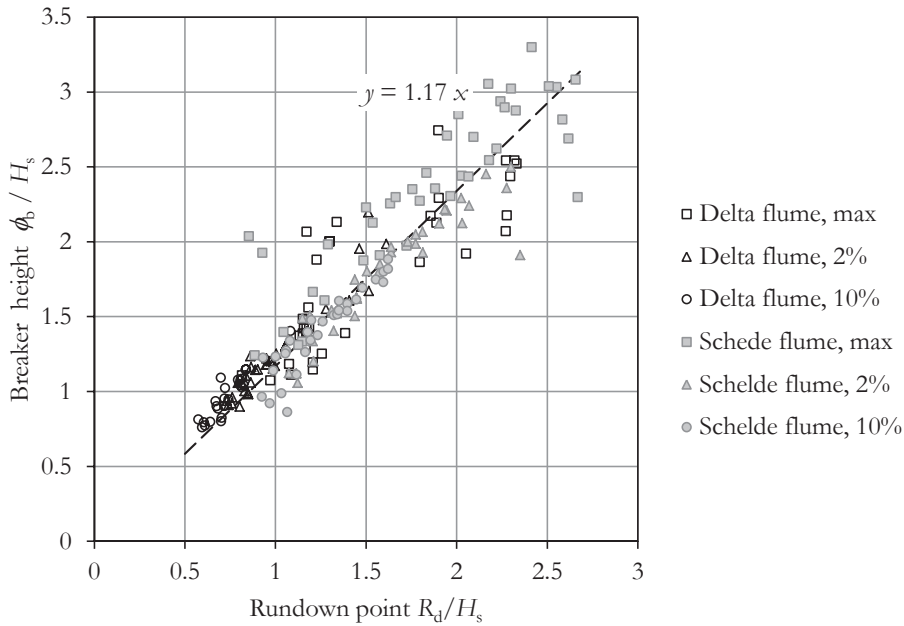
Figure 5-20 **Breaking wave front heights (measured as pressure difference on the slope) against run-down point position**

Wave breaking on beach slopes is often studied using the breaker index H_b/d_b. Based on the limitation $\gamma_b = H_b/d_b = 0.78$ found by Miche, 1944, many variations of this formula have been developed, where deep-water wave steepness, and bottom slope are included as variables. In various literature summaries can be found, including attempts for reliable formulas for steep slopes, like revetment slopes. Very few formulas are developed for irregular waves. Based on the observation of a probably constant critical value of γ_b for each individual wave, the many available results for regular waves may be useful to investigate the relevant dependant parameters.

A constant breaker index would be a reliable predictor for the height of breaking waves on a (relatively) steep slope. Plotting the data points of the measured breaker indexes ϕ_b/R_d against the breaker parameter gives insight in the dependency.[211] This is shown in Figure 5-21. Since these data point are all for slopes with $\cot\alpha$ between 3 and 4, we need to look for other tests data on steeper and milder slopes.

---

[211] Plotting the measured breaker indexes against the breaker parameter with distinguished markers for the Delta and Schelde flumes raises the question of a slight scale effect, see Figure 5-21.
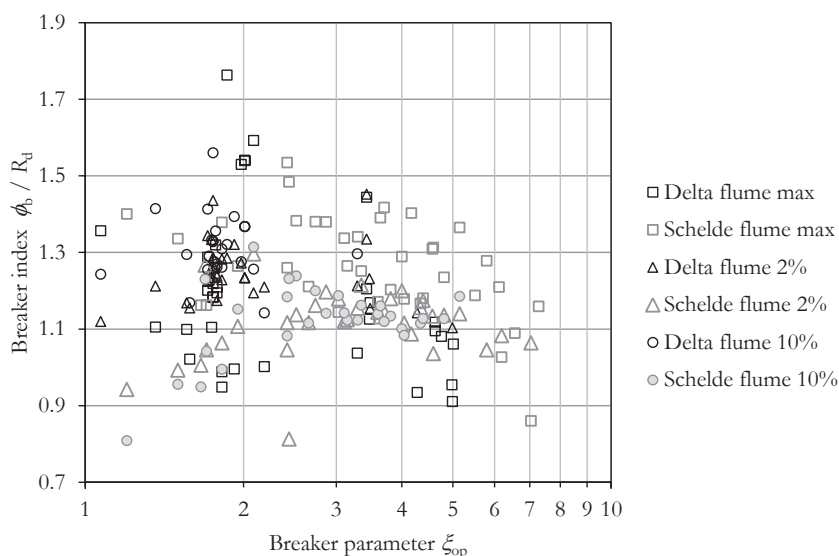
Figure 5-21   **Measured breaker indexes of Delta flume and Schelde flume tests**

Summaries of breaker formulas can be found in the Rock Manual and in papers of Rattanapitikon[212], who also compares the performance of the breaker formulas in the various ranges of ξ_{op}.[213] In the thesis of Jensen, 2002[214] wave breaking on a 1:2 slope is studied extensively with energy dissipation models. In an article of Camenen & Larson[215] existing breaker formulas are re-evaluated in a transparent way, with data points of breaker indexes and breaker type information. These data are plotted in Figure 5-22. The authors observe that the divisions between breaker types not only depend on wave steepness and slope (in ξ), but also on breaker height. This might be a part of the explanation that many authors give other values of the value of ξ, beyond which breakers are no longer spilling, and no longer plunging.

One of the breaker formulas that are evaluated is the relation $\gamma_b = 1.062 + 0.137 \log \xi_{op}$ by Battjes, 1974 as indicated in Figure 5-22. Camenen & Larson suggest a cap of γ_b, which has a maximum in the area of $\xi_{op} = 1 .. 3$ and diminishes for lower and for higher values of ξ_{op}, unlike the formula of Battjes.

---

[212] E.g. W. Rattanapitikon and T. Vivattanasirisak, "Comparison of breaker height formulas using large-scale wave tanks," *Songklanakarin J. Sci. Technol.* 24:4 (2002): 663–674

[213] The formulas that perform best for steep slopes are formulas that relate breaker height H_b to the original wave height in a regular wave series, or formulas with a complicated iterative procedure. Both are not practical in our case.

[214] M.S. Jensen, *Breaking of waves over a steep bottom slope*, 2002

[215] B. Camenen and M. Larson, "Predictive Formulas for Breaker Depth Index and Breaker Type," *J. Coast. Res.* 23:4 (2007): 1028–1041
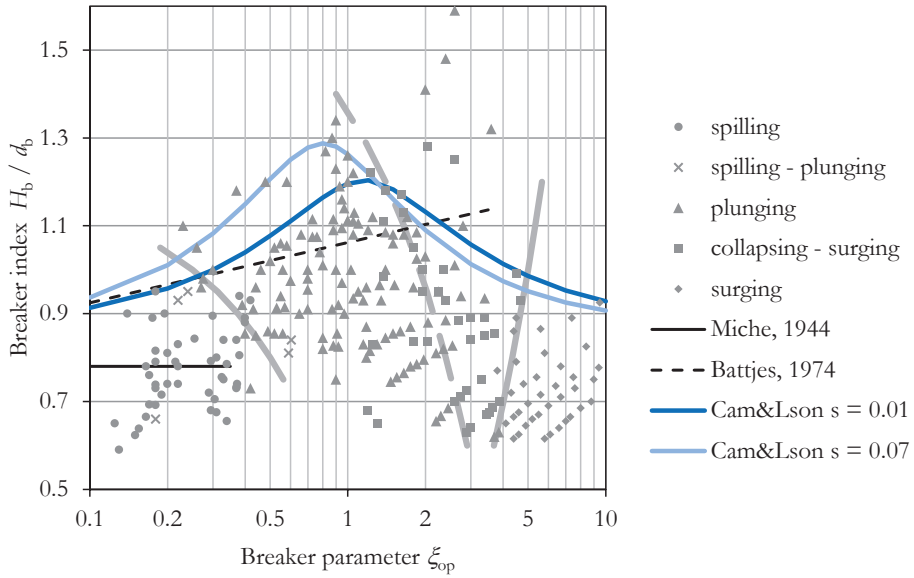
Figure 5-22   Measured breaker indexes from Camenen & Larson, 2007 with indicated transition between the breaker types
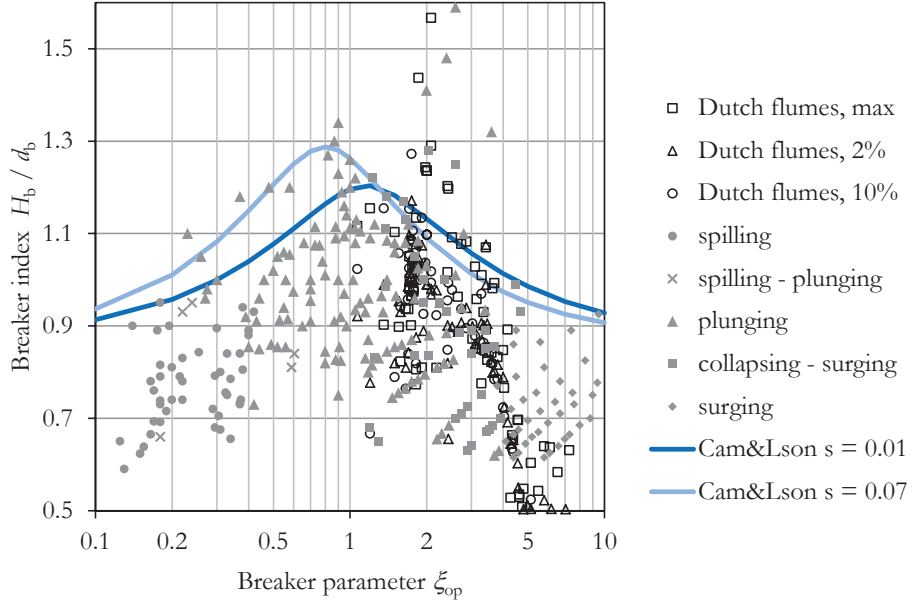
Figure 5-23   Measured breaker indexes from Camenen & Larson, 2007 with additional data points form Dutch flume tests
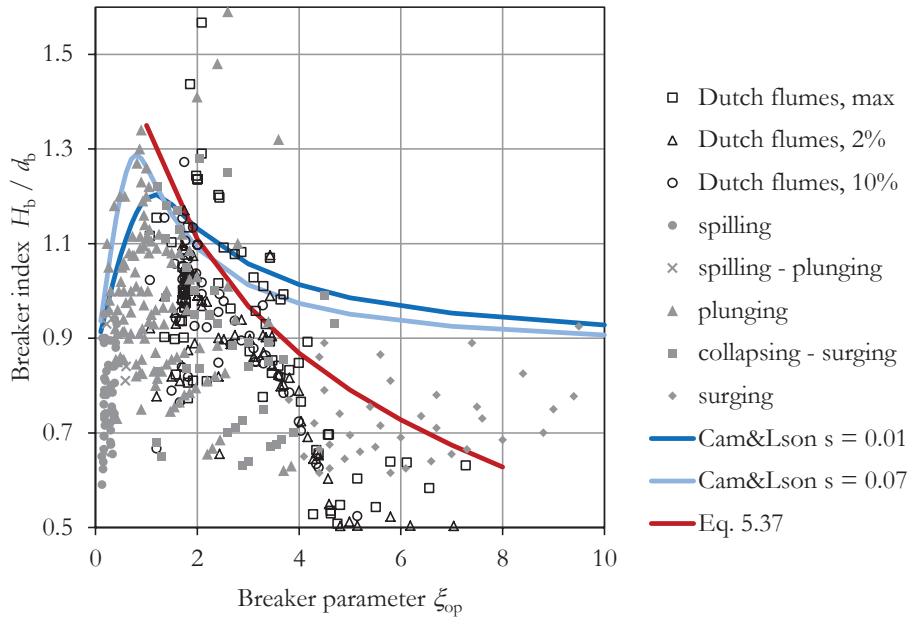
Figure 5-24 Measured breaker index values with suggested relation for design values

By adding the 2% and 10% data of Klein Breteler, Van der Werf & Wenneker of Figure 5-21, a combined picture and a suggested cap can be found in Figure 5-23. For revetment slopes the smaller values of ξ_{op} are less relevant and a plot with a linear scale for ξ_{op} is more common (see Figure 5-24). The data of Camenen & Larson show more scatter to lower values, but they are considered useful to support a definition of a cap of the breaker parameter as a function of ξ_{op}. On basis of the Dutch flume test the relation for a cap can have a much steeper decline in the area of ξ_{op} = 3 .. 8.[216] The surging breaker heights collected by Camenen & Larson are less important for the revetment design. A suggested formula for the cap is given in Eq 5.37.

$$\gamma_b = 1.35 - 0.8 \log \xi_{op} \qquad \qquad \textbf{Eq. 5.37}$$

Like Eq. 5.35 the trend of this formula is opposite to wave heights based on the energy sum of incoming and reflected waves. It appears questionable whether the concept of combination of H_i and H_R has a relation with breaking wave heights on the slope. Even on smooth slopes there seems to be a lot of energy dissipation. Apart from that the concept of combining the wave height might only work one wave length in front of the slope.

---

[216] There could be a little concern of measuring bias, since the pressure sensors on the slope may not reach to the wave crest position for larger values of ξ_{op}, associated with small values of the wave steepness s_o. Linear regression analysis of the measured values of ϕ_b/H_s with dependencies on ξ and H_s resulted obviously in a strong dependency on ξ and a weaker ($p = 0.08$) dependency on H_s with a coefficient of -0.22 for the Delta flume data set with H_s ranging from 0.7 to 1.7 m.

DESIGN OF PATTERN-PLACED REVETMENTS

Wave reflection formulas in literature for smooth slopes do not differ too much. The most recently verified formula was found in Zanuttigh & Van der Meer, 2006, based on tests with a range of $\cot\alpha = 2.5 .. 4$ and $s_o = 0.01 .. 0.06$.[217]

$$C_R = \tanh\left(0.16\xi_{m-10}^{1.43}\right)$$

The height of a reflected wave may be combined with the incoming wave height, using the energy sum: $H = \sqrt{(H_i^2 + H_R^2)} = H_i \sqrt{(1 + C_R^2)}$.[218]

5.2.5 *Recommended breaker height formulas*

Supported by the observed trends the dependency of the 'breaker index' H_b/R_d on the wave steepness and slope angle can be defined as decreasing with increasing breaker parameter ξ_{op}. For the relevant range of $\xi_{op} = 1 .. 8$ the cap can be made linear. Using the better documented data of the Dutch flume tests this linear relation can be best presented with the parameter ξ_{m-10} (see Figure 5-25). The average value was 1.17.

$$\frac{\phi_b}{R_d} = 1.6 - 0.11\xi_{m-10} \qquad\qquad \textbf{Eq. 5.38}$$
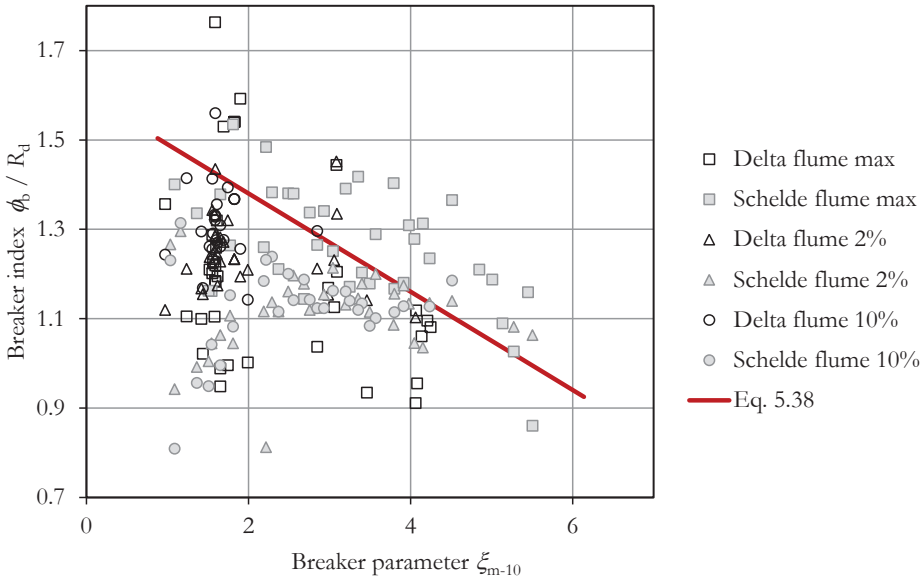
Figure 5-25   **Breaker index data from Klein Breteler, Van der Werf & Wenneker, 2006 against ξ_{m-10}**

For the wave front angle no other data than the data of the Dutch flume tests can be found in literature. The data are derived from tests with slope angles $\cot\alpha$ between 3 and 4 only. Studying the dependencies of the front angle a formula with a dependency on the wave

[217] B. Zanuttigh and J.W. van der Meer, "Wave reflection from coastal structures in design conditions," *Coast. Eng.* 55 (2008): 771–779
[218] Goda, *Random seas and design of maritime structures*

steepness only ($\xi/\tan\alpha$) was preferred (see Eq. 5.40). Although due to lack of variation of $\cot\alpha$ a dependency on ξ is not better, we consider this on better conformity with the other wave shape parameters and propose to omit $\tan\alpha$ form the formulas. This change contributes to a better fit with test results for larger values of ξ.

The trough just before the breaker front might be elevated above the slope. There is a film or layer of water present in front of the breaking wave. This is especially the case at mild slopes. At steep slopes the water of the previous wave has disappeared timely and the lowest point of breaker front touches the dry slope. In order to estimate a conservative, high position of the breaker crest, a lower bound of ϕ_{min} should be considered. Taking a lower bound for ϕ_{min} the difference with R_d becomes approximately 0.5 H_s for the whole relevant range. A linear relation is suggested, $\phi_{min} = -0.40\ \xi_{m-10}$ (see Eq. 5.39) The crest elevation is now found by the sum of the breaker front height $\gamma_b \times R_d$ and ϕ_{min}, all three functions of ξ_{m-10}. As a result, the drop height of a plunging breaker is 1.5 to 2.0 H_s.

The recommended formulas are:

High front:

$$\frac{R_{d2\%}}{H_s} = 0.4 + 0.55\,\xi_{m-10} - 0.0344\xi_{m-10}{}^2 \qquad\qquad \textbf{Eq. 5.31}$$

$$\frac{\phi_{b2\%}}{H_s} = (1.6\ -\ 0.11\xi_{m-10})\frac{R_{d2\%}}{H_s} \qquad\qquad \textbf{Eq. 5.38}$$

$$\frac{\phi_{min2\%}}{H_s} = -\ 0.4\xi_{m-10} \not< -\frac{R_{d2\%}}{H_s} \qquad\qquad \textbf{Eq. 5.39}$$

$$\tan\theta_f = 0.6 \not> 5.5 - 0.92\xi_{m-10} \not> 2.5$$

Steep front:

$$(\tan\theta_f)_{2\%} = 1 \not> 8.8 - 1.25\xi_{m-10} \not> 5 \qquad\qquad \textbf{Eq. 5.40}$$

$$\frac{R_d}{H_s} = 0.5\frac{R_{d2\%}}{H_s}$$

$$\frac{\phi_b}{H_s} = (1.6\ -\ 0.11\xi_{m-10})\frac{R_d}{H_s}$$

$$\frac{\phi_{min}}{H_s} = -\ 0.2\xi_{m-10} \not< -\frac{R_d}{H_s}$$

As can be noticed the 2% values of the parameters are combined as follows.

Table 5-5 **Combination of steep and high front wave parameters**

	R_d	ϕ_b	ϕ_{min}	$\tan\theta_f$
High front	2%	2%	2%	average
Steep front	average	average	average	2%

5.2.6 *Dynamic impact of plunging breakers*

Wave impact of the plunging breaker on the slope is the second instant in the breaking wave cycle that is critical for revetment stability. The deep part of the wave front is slowed down and runs down, while the crest still has forward speed. The top part of the wave moves over an air pocket, curves downward and hits the slope. Descriptions and simulating tests use the equivalent of a water jet, which has speed, turbulence and accompanied air content in the water. The air bubbles in the water play an import role in the compressibility of the water mass, which influences the pressure build up when the jet hits the slope. Slope permeability, and the presence of a water film on the slope also influence the pressure.

Wave impact on asphalt slopes have been investigated since 1950. Together with quasi static run-down the wave impact is the determining load case for the design of asphalt linings. Partly due to the focus on structures determined by an optimum permeability ratio of top layer and sub layers, the effect of wave impact on block revetment slopes was a bit beyond the scope of the research around 1990 and 1995. In Glerum & Wolsink, 1984 wave impact was treated more extensively. In the wave descriptions of 2006 the wave impact has a prominent place.

Making use of earlier summaries the MSc-thesis of Davidse, 2009 provides a comprehensive literature review of wave impact theory and tests on asphalt and smooth open revetment tests.[219]

5.2.7 *Impact location*

Grüne[220] has published run-up and wave impact measurements analysis of field test that have been carried out over a number of storms in 1976 to 1979 at two locations in the German Bight. Detailed wave impact statistical analyses of numbers of impact, impact locations and pressure anatomy have been performed. The presented data are envelopes of normalised data using H_s. The tests have shown that the impact locations follow a normal distribution with the maximum at 0.5 H_s below SWL, ranging from −1 to +0.75 H_s though slightly asymmetric. Details about the wave spectrum during the storms are not given. In a run-up paper[221] analysing the same storms ranges of H_s and mean periods are given, which are used to estimate the breaker parameter ξ_{op}. The results are presented in Figure 5-27.

The indicated range is supported by Delta flume tests with breaker parameters in the range 1 to 2. The tests in the range 3.5 to 4 give impacts at deeper locations. For those tests the wave impacts are less frequent and the magnitude and dynamic nature are less severe. The small-scale test gives a much larger variation of impact locations.[222]

---

[219] M.P. Davidse, *Experiment analysis - The relation between wave loading and resulting strain in an asphaltic concrete revetment* (MSc thesis TU Delft, 2009)

[220] J. Grüne, "Wave-induced shock pressures under real sea state conditions," *Coast. Eng. Proc.* (Malaga, 1988)

[221] J. Grüne, "Wave run-up caused by natural strom surge waves," *Coast. Eng. Proc.* (Capetown, 1982)

[222] See also Figure 5-14. The scale tests of Kostense also showed deviating (deeper) damage points.
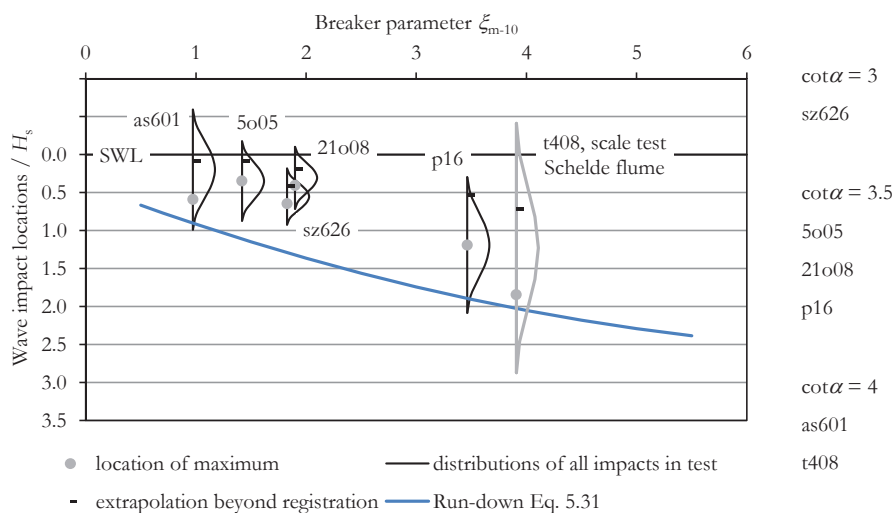
Figure 5-26 **Wave impact location from Dutch flume tests, source: Klein Breteler, Van der Werf & Wenneker, 2006**
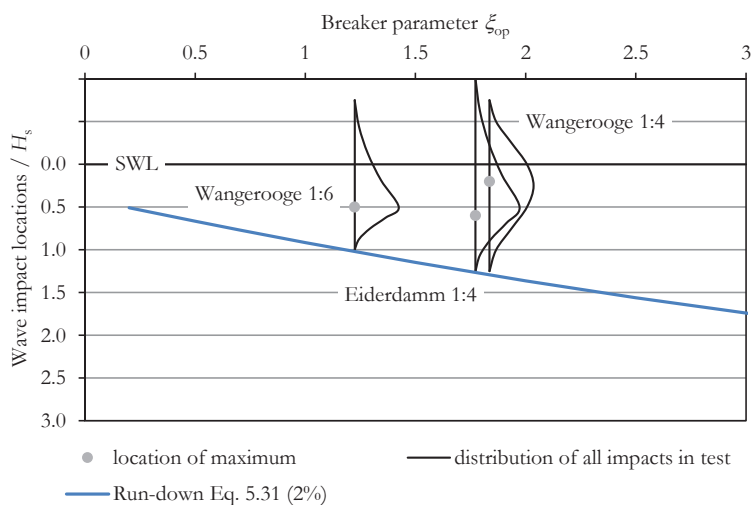
Figure 5-27 **Wave impact location from German field tests, source: Grüne, 1982 and 1988**

The physical pattern behind the impact location is the close relation to the run-down point. It is found that the plunging breaker adheres to a fairly constant breaker index and breaks at a point determined by its original wave height and its 'position' in the wave train. This gives scatter in the run-down point with a defined deepest run-down point that is dependent on the breaker parameter. The impact point is related to the run-down point due to horizontal distance that the plunging water can travel. This distance is limited by the horizontal velocity of the water in the wave crest and by the drop height.

The horizontal velocity can be obtained from the relations of orbital motion of the water particles in shallow water waves.

$$\dot{u}_x = \frac{a}{d}\frac{L}{T} = \tfrac{1}{2}\frac{H}{d}\sqrt{gd}$$

with d is the depth taken at the last position before the breaking at the slope, e.g. half a wave length before the toe.

The crest elevation z_b can be taken from Figure 5-25 as 1.5 or 2 H_s above the deepest run-down point. Assuming values of H/d the horizontal velocity can be calculated. The fall time follows from $z(t) = z_b - \tfrac{1}{2} g\, t^2 = 0$. The fall time is approx. 0.6 to 0.7 sec for $H_s = 1$ m and $z_b = 2$ m, and around 1 sec for the $H_s = 2$ m. The horizontal reach from the run-down point can be calculated using

$$x_{\text{impact}} = \dot{u}_x t = \tfrac{1}{2}\sqrt{2}\,\frac{H}{d}\sqrt{dz}$$
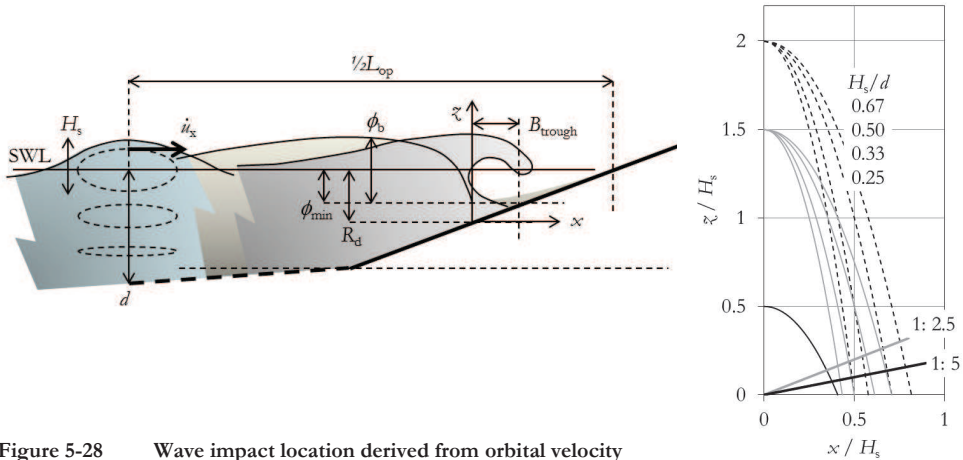
Figure 5-28   **Wave impact location derived from orbital velocity**

The path of the plunging water is calculated and shown in Figure 5-28. The typical outcome for x_{impact} is 0.7 H_s, which leaves a pressure trough of approx. 0.5 H_s. This outcome is in line with observations and measurements. The drop height of 2 H_s corresponds to the mild slope of e.g. 1:4 or 1:5, as the height of 1.5 H_s corresponds to a steeper slope of 1:2.5. It can be seen that the direction of motion is almost exactly perpendicular to the slope. Only in case with a much smaller drop height e.g. $z_b/H_s = 0.5$ and assumed high velocity ($H/d = 0.67$) the plunging jet will hit the slope with an angle of 70 degrees or less. It can now be understood that the large breakers are associated with perpendicular impact and therefore have an increased impact. On steep slopes there seems to be a tendency to a slight 'overshoot' (impact angle > 90°) and a corresponding downward directed component. On milder slopes the jet direction is slightly below 90°.[223]

---

[223] This difference could form the physical background to the observed and described two breaker types in Klein Breteler, Werf, and Wenneker, *Kwantificering golfbelasting en invloed lange golven, rev. 2* Type 1 has a pressure

The horizontal gap between the run-down wave front and the wave impact pressure zone is indicated as B_{trough} and has a typical horizontal distance of 0.5 H_s, with a possible inverse dependency on ξ. The 2006 wave parameterisation gives $B_{trough,2\%} = 0.8\ H_s$ and notes that there is considerable spread. The recommended formulas for range of impact locations include one formula reasoning from the average 2%-rundown point (using Eq. 5.31) and one formula based on the observed locations of the maxima shown in Figure 5-26 and Figure 5-27.

$$\frac{x_{impact}}{H_s} \tan\alpha < 0.4 + 0.55\,\xi_{m-10} - 0.0344\xi_{m-10}{}^2 - 0.7$$

$$\frac{x_{impact}}{H_s} \tan\alpha > 0.45\xi_{m-10} - 0.3$$

5.2.8 Peak pressure

The dynamic pressure measurements are difficult to compare and to rely on since there is a considerable scale effect. The air content plays a prominent role. The dimensions of the pressure gauge and the sample rate during the tests are very important for really measuring the peaks. The extreme values of a group of tests results follow a log-normal distribution.[224] Both magnitude and duration of the peak are important for an assessment of the impact on the structure.

Several researchers have reported peak pressures. In the Table 5-6[225] the results are presented as constants c in the format using Eq. 5.41.

$$p_{max} = c\,\rho_w g\,H_s \qquad\qquad\qquad \textbf{Eq. 5.41}$$

In the Deltares study of 2006 many scale tests in the Schelde flume were analysed also. These tests seem to give severe wave impact at larger values of ξ, compared to the full scale Delta flume tests. The Schelde flume tests are included in the analysis using modified Weber-scaling.

$$\left(\frac{\rho_w g\,H_s{}^2}{c_w}\right)^a$$

with
c_w = the surface tension of the water: 0.073 N/m
a = 0.1 for pressure[226], 0.2 for durations

---

trough between the original wave front and the impact zone and slightly milder slope at the landside. Type 2 has a steep landside slope and the impact zone overlaps with the pressure of the run-down wave. It must be noticed that the authors extracted the two types as idealised shapes from many measured arbitrary shapes.

[224] After: A. Führböter and U. Sparboom, "Full-scale wave attack of uniformly sloping sea dykes," *Coast. Eng. Proc.* (Malaga, 1988), 2174–2188

[225] Partly after: Van Vledder, 1990 in Davidse, *Experiment analysis - The relation between wave loading and resulting strain in an asphaltic concrete revetment*.

[226] Re-analysing the p_{max} / H_s shows that average independency of H_s is achieved using $a = 0.06$. Wrong dominance of the scale test data points in fitting p_{max} / H_s is than increased.

Although lots of attention has been paid to application of the scaling laws the small-scale tests seem to overestimate the wave impacts for larger values of ξ.[227] The small scale tests are further neglected since sufficient large scale tests are available.

Table 5-6   **Measured values of the pressure amplitude of wave impacts**

	Source	Slope	Wave steepness s_{op}	$p_{max}/\rho_w\, g\, H_s$	
				2%	max
Regular waves	Skladnev & Popov, 1969	1:4	0.19	2	
	R. Stive, 1984	1:3	$0.02 - 0.06$	2.7	
		1:4	$0.02 - 0.07$	2.3	
	Führböter & Sparboom, 1988	1:4	$0.01 - 0.24$	4.8	6
		1:6		3.2	4
Irregular waves	Führböter & Sparboom, 1988[228]	1:6	0.027	3.4	3.7
	Grüne, 1988[229] (field tests of natural storms)	Eiderdamm 1:4	$0.015 - 0.031$	4.3[231]	7.4
		Wangerooge[230] 1:4	$0.014 - 0.037$	2.6	4.2
		Wangerooge 1:6	$0.014 - 0.037$	2.7	4.4
	Klein Breteler, Van der Werf & Wenneker, 2006	$1:3 - 1:4$	$0.003 - 0.055$	4.2	7.3

The nomalised peak pressures $p_{max}/\rho\, g\, H_s$ of the available irregular wave tests are plotted in Figure 5-29. The highest values occur for breaker parameter values between 1 and 2, where the plunging breakers appear to be strong and frequent. Above $\xi = 2$ wave impacts occur, but the characteristic peak values are less high. This observation is supported by outcomes of full-scale tests with regular waves also. The indicated 2%-cap is given with the equation below. The pressure $p_{max\ 2\%}$ is a measured special maximum and a peak value in time not exceeded by more than 2% of the waves. It can be noticed in Figure 5-29 than the maximum within the complete wave series can be in the order of 1.6 times higher than $p_{max\ 2\%}$.

$$\frac{p_{max\ 2\%}}{\rho_w g\, H_s} = 8 - 1.6\, \xi_{m-10} - \frac{2}{(\xi_{m-10} - 0.2)^2}$$

                                                            Eq. 5.42

[227] The small scale tests show more wave breaking. The results and parameters of these breaking waves can be scaled down to comply with the parameters of the (fewer) breaking waves in large scale tests. But that does not mean that the small scale tests represent the risk of occurrence of the wave breaking properly.

[228] One narrow-band spectrum irregular wave test is described, for which ξ_{op} is known. In Figure 5-29 ξ_{op} is plotted.

[229] Grüne, "Wave-induced shock pressures under real sea state conditions"

[230] At the Wangerooge location wave breaking before the dyke slope was observed, which prevented higher waves to impact of the slope. The remaining breakers had a bigger share of spilling breakers.

[231] The 2% values are interpolated form reported maximum, upper tenth average, and 50% values and from measured distributions.
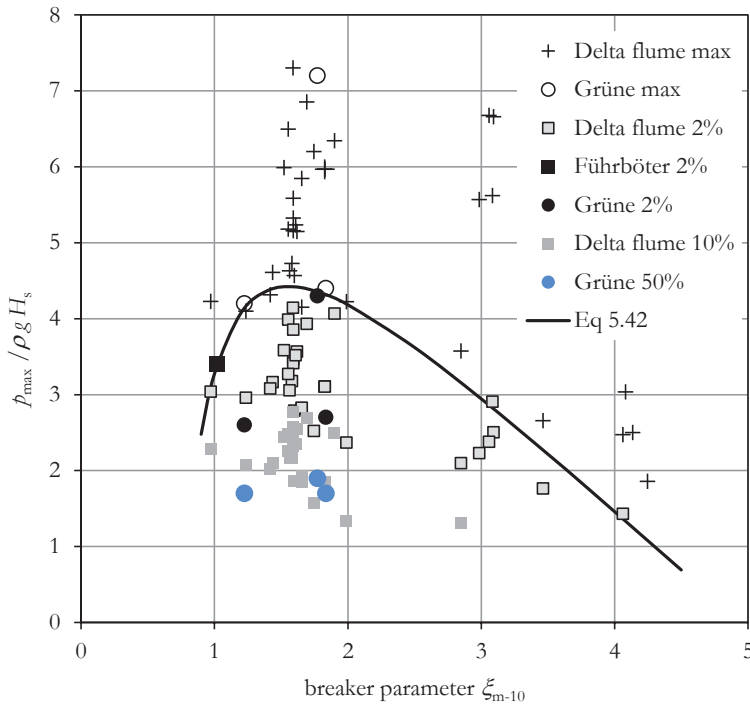
Figure 5-29   **Measured peak pressures during impacts of irregular wave tests**

Authors[232] have analysed full-scale measured normalised values of $p_{max}/\rho_w g H_s$. Entrained air content works as a cushion and does to some extent not further increase impact pressures when the scale of the waves is increased. Although many of the work is focussd on impacts of vertical walls a similarity can be found as the conclusion is that wave impact forces are dependent on $r_p \, \rho \, g \, H^2$, of which one H is equivalent with the foorprint of the load. The values r_p of beyond a certain Bagnold scale number (here estimated as 0.15) tend to become fairly constant, which means for falling peak pressures associated with wave heights above $H_s = 1.6$ m the peak pressure will increase roughly linearly with the wave height H.

Other authors[233] supplement the interpretative work with falling water experiments. From those tests it can also be concluded that the pressure keeps increasing with falling height.

The easured maximum values of p_{max} show consistency to some extend (see Table 5-6 and Figure 5-29), and can therefore be used as reliable design input on the prototype scale.

[232] G. N. Bullock et al., "The influence of air and scale on wave impact pressures," *Coast. Eng.* 42:4 (2001): 291–312; Giovanni Cuomo, William Allsop, and Shigeo Takahashi, "Scaling wave impact pressures on vertical walls," *Coast. Eng.* 57:6 (2010): 604–609; Giovanni Cuomo et al., "Breaking wave loads at vertical seawalls and breakwaters," *Coast. Eng.* 57:4 (2010): 424–439

[233] K. Kamibuko et al., "Experimental Study on Damage to Wave Splash Barrier for a Coastal Road," *Coast. Struct.*, 2011

5.2.9   Impact duration

The peak pressures are highly dynamic. Several researchers report about the time and load-rate parameters. The relevance of the dynamic parameters is partly determined by the structural response. A very short rise time e.g. will enhance the peak structural response. A longer rise time will increase the total impulse of the load. Some literature split the pressure-time signal in a dynamic part, an oscillating part and a quasi-static part. The boundary between the dynamic and quasi-static part is also determined by the structural response. See chapter 6. The rise time of the quasi-static part will – by definition – not generate dynamic amplification of the structural response. The remaining dynamic part will do.

The duration t_d of the wave impact can be estimated by the water velocity and the effective length of the jet, which is typically in the order of the breaker height. Using typical values, the duration time is 0.16 to 0.22 s. Grüne reports duration times from 0.01 to 0.20 s.
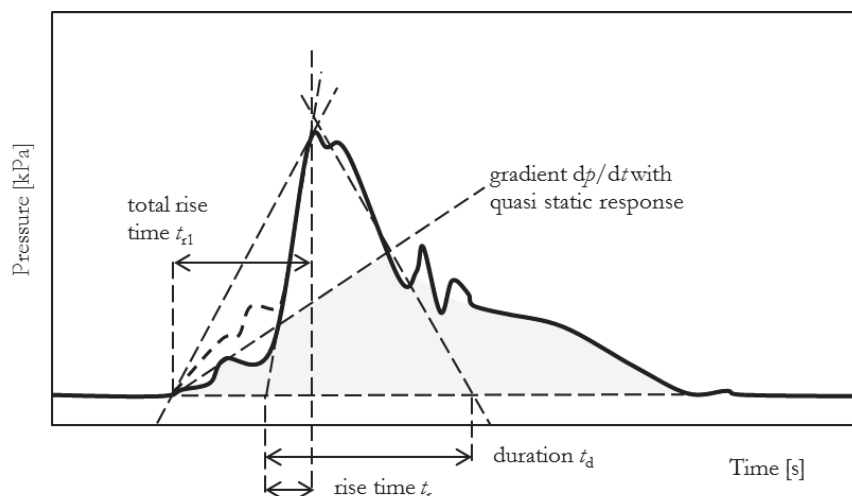
Figure 5-30   Definition diagram of shock pressure-time signal (with exaggerated peak duration)

The rise time as a parameter which seem to lack a consistent definition in literature. Grüne, 1988, gives scatter plots for the rise time which is indicated as t_{r1} in

Figure 5-28. Typical observed values follow a log-normal distribution starting at 0.010 s, a maximum probability at 0.080 s, and a tail up to $0.3 - 0.5$ s. Witte, 1988[234], presented measurements of regular waves and reported rise times t_r of 0.002 to 0.005. Führbötter & Sparboom, 1988, reported 0.010 to 0.060. These rise times were found inversely related to the peak pressure of the same impact.

This inverse relation was also found during analysis of the Delta flume tests. The average relation between measured rise time t_r relative to the peak pressure for the Deltaflume tests is given in Eq. 5.42 This relation is fairly accurate for the maximum impacts, as well as for the 2% and 10% values.

---

[234] From: Davidse, *Experiment analysis - The relation between wave loading and resulting strain in an asphaltic concrete revetment*

$$t_r = 0.10 \left(\frac{p_{max}}{\rho_w g \, H_s} \right)^{-1} \quad [s]$$

<div align="right">Eq. 5.43</div>

upper- and underbound are given with 0.18 and 0.15 instead of 0.10 s.

The nature of the impacts becomes less dynamic with increasing breaker parameter. The peak pressures are lower, and related to that the characteristic impact rate is lower. This is shown in Figure 5-31. It appears that the impact duration time is always about 3 to 4 times longer than the rise time. The ratio t_r/t_d for the Delta flume tests amounts 0.36, 0.29 and 0.25 for the maximum, the 2% and the 10% exceeded values respectively. The variation coefficient is 0.23, 0.27 and 0.23 for the three groups. In Figure 5-31 the ratio between the two indicated trend lines is 0.29. In the region with $\xi = 3$ to 4 the impacts become less and less frequent. However the rare impacts around $\xi = 3$ can still give high maximum values of p_{max} and of t_r, as can be noticed in Figure 5-29 and Figure 5-31.
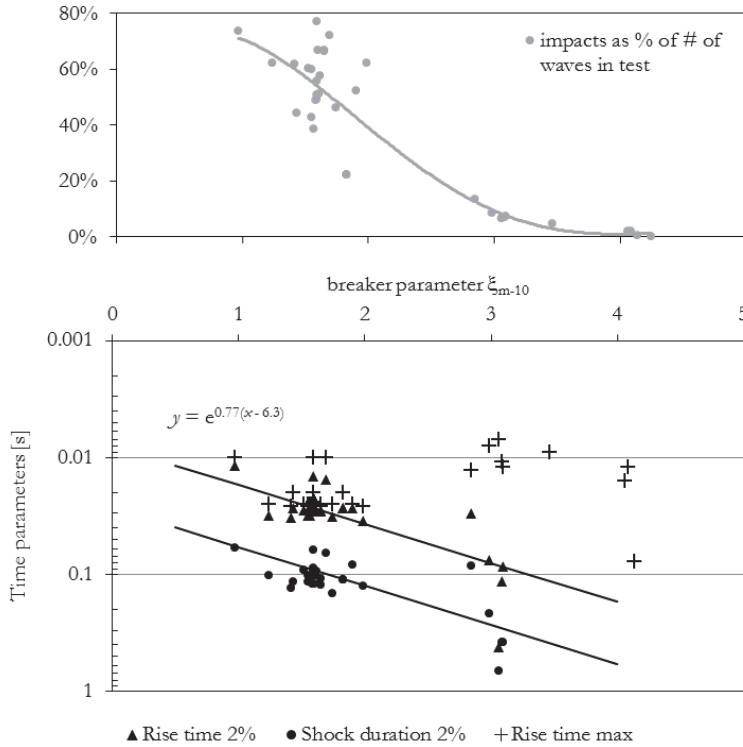
Figure 5-31   **Shock pressure rise time and duration time against the breaker parameter**

The measurements in all studies show a peaked signal in the time domain. In the spatial domain some authors give a distinct peak also, others have observed a wider area with more or less equal pressure. The width of this area, indicated as B_{imp}, follows from the width of the jet. The analysis of the field tests of Grüne, 1988 is concluded with two space graphs for normalised values of $p_{max}/(\rho_w g \, H_s)$ of 7.4 and 4.4. Both have a normalised width B_{imp}/H_s of

0.75 at 50% of p_{max} and $0.5H_s$ at 80% of p_{max}. This suggests that with higher impacts the width remains constant and the gradients of the pressure-space shape increase. In the evaluation of the Delta flume tests $B_{imp\ 2\%}$ also $0.75\ H_s$ was found. At least in the relevant area of $\xi = 1$ to 2. For larger values of the breaker parameter B_{imp} was found to decrease slightly.

The spatial gradient dp/dx of the pressure shape is important because of its effect on the response of the pressure in the filter layers. The wave impact shapes of the Delta flume and Schelde bassin wave tests have been extensively investigated[235]. Following the suggested relation above the gradients of the pressure shape are plotted against the height of the pressure at impact p_{max} (see Figure 5-32). The results are quite scattered but seem to respect an upper bound that has a clear relation with p_{max}. The gradients at the seaside of the wave impact are steeper than at the dike side. The average measured differences for the groups max, 2% and 10% were 0.5, 4 and 10 degrees respectively.

The Delta flume test group consists of a large group with a 1:3.5 slope and very few tests with 1:3 and 1:4 slopes. The 1:4 tests have very steep angles, 86 to 87 degrees, and the 1:3 slopes have angles in the order of 80 to 82 degrees. This difference exists for seaside as well as dike side. The difference is observed in tests with almost identical values of the breaker parameter[236]. The 1:4 slopes experience a more perpendicular impact[236], which can explain steeper gradients.

The earlier discussed Schelde bassin tests are scale tests on 1:3 and 1:4 slopes. In those tests hardly any effect of the slope angle on the gradient is observed. The measured values do not exceed the upperbound of Eq. 5.43.

As an upperbound the following relation is suggested. This relation shows a good agreement with the measured gradients of the Delta flume tests, for the 2% values as well as the maximum values.

$$\tan\theta_i = \frac{d}{dx}\left(\frac{p}{\rho_w g}\right) = 8.5\left(\frac{p_{max}}{\rho_w g\, H_s} - 1.5\right) \text{ at the sea side}$$

Eq. 5.44

$$\tan\theta_i = \frac{d}{dx}\left(\frac{p}{\rho_w g}\right) = 6\left(\frac{p_{max}}{\rho_w g\, H_s} - 1.5\right) \text{ at the dike side}$$

There is too few data to separately investigate a relation of pressure gradient and breaker parameter. It is therefore proposed to use the relation between peak pressure and breaker parameter, and the relation between pressure gradient and peak pressure, that are both quite strong.

---

[235] G.M. Smith, J. Wouters, and M. Klein Breteler, *Grootschalig modelonderzoek naar stabiliteit van taludbekledingen - Meetverslag van Deltagootonderzoek* (WL|Delft Hydraulics report H3272-2, 2000); Klein Breteler, Werf, and Wenneker, *Kwantificering golfbelasting en invloed lange golven, rev. 2*

[236] This is also associated with an observed difference in the values of the peak pressure but the difference in angle is much higher than can be explained by peak pressure difference according to the presented relation.
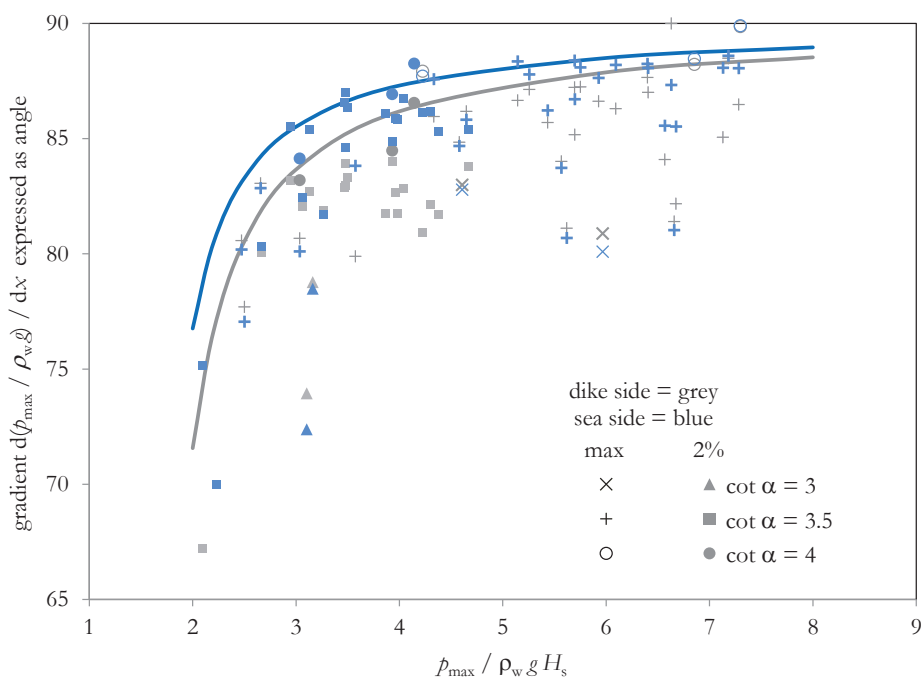
Figure 5-32   Measured gradients of pressure shape
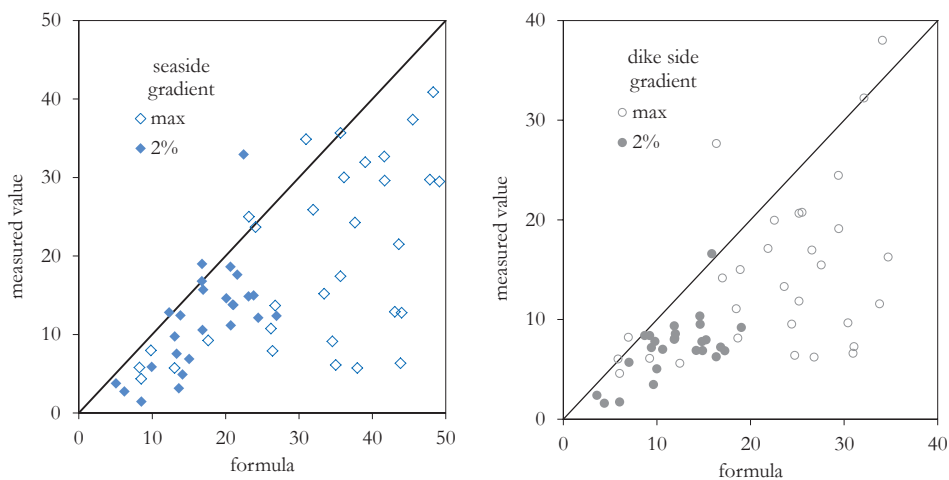
Figure 5-33   Measured gradients of pressure shape compared with formulas
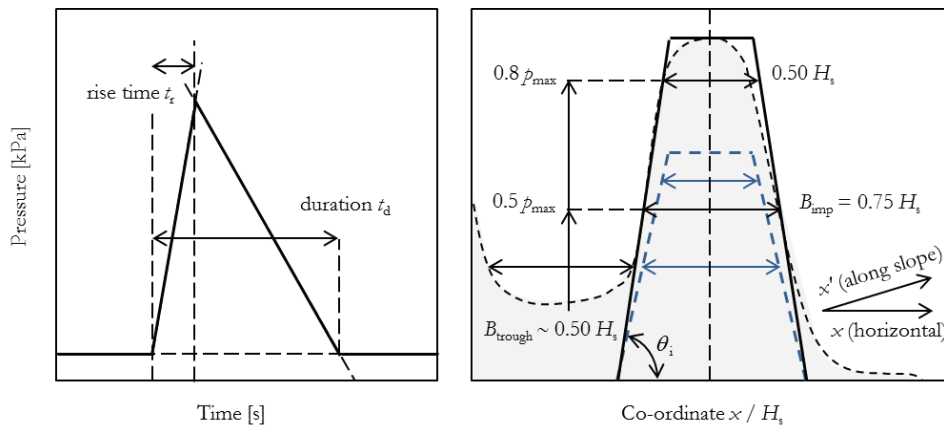
Figure 5-34   Idealised time signal and space diagram

5.2.10   Summary of wave impact parameters

The peak magnitude of the wave impact pressure p_{max} is breaker parameter ξ dependant, with as physical background the falling height. The rise time t_r is inversely correlated with the peak impact. The larger the peak pressure, the shorter the rise time. The normalised width of the pressure diagram B_{imp} is quite constant. The spatial pressure gradients dp/dx or θ_i are not constant and are correlated with the peak value.

Unfortunately no large scale measurements could be found about spatial distribution and pressure shapes in longitudinal direction of the slope. The flume tests are too narrow to give a relevant or reliable result. Disturbance of simultaneous plunging, and as a consequence limitation of the width of the area of attack would be biased by flume wall effects. The field tests of Grüne are measured with only one sensor line.

5.3   Effect of filter drainage

The breaker heights, wave front angles and wave impact pressures cause variations of piezometric head on the interface above the revetment top layer. The top layer is hydraulically open, and as a result the water pressure in the joints and in the filter will respond to the variations in time and space of the water pressure at the outside. For a hydraulically closed top layer a drop of water pressure on the slope below still water level would immediately lead to uplift of the blocks and increased water pressures to compressive forces on the blocks. Leakage enables a stationary flow through the top-layer that equalises the pressure to some extent.

5.3.1   Model calculations with finite leakage factor

In (Klein Breteler & Bezuyen, 1991) a simplified design method is presented. This method is based on the theory of piezometric head differences in the revetment structure. At maximum rundown the water pressure in the wave, and the atmospheric pressure in front of the wave cause a hydraulic flow in the filter, where the piezometric head forms a dampened representation of the head differences above the slope. This theory was first applied to a bi-linear parameterisation of a breaker front and later refined for curved wave fronts and pressure shapes of wave plunging. The exercise is focussed on the difference of the

piezometric head on both sides of the top-layer, here indicated as ϕ_{dip}, the domain where $\phi - \phi'$ is positive and exerts uplift forces on the top layer elements.
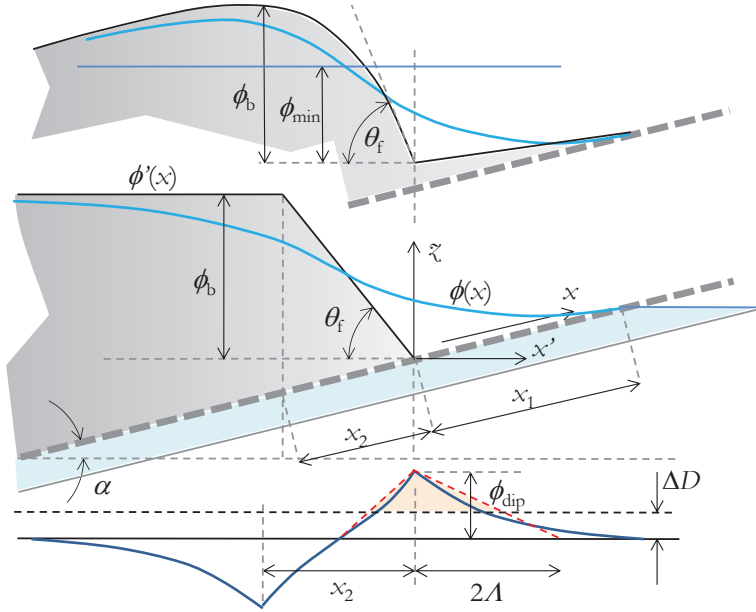
Figure 5-35   Definition diagram of piezometric head calculation in the filter

The piezometric head is calculated with the differential equation Eq. 5.45.

$$\frac{\partial^2 \phi}{\partial x^2} = \frac{1}{\Lambda^2}(\phi - \phi')$$

<div align="right">Eq. 5.45</div>

With

ϕ = piezometric head in the filter layer
ϕ' = piezometric head on the slope
x = coordinate along the slope
Λ = the leakage factor [m], refer to Eq. 3.4

This equation can be solved for any pressure distribution above the revetment slope. In (Burger & Klein Breteler, 1990) the solution is derived for a bi-linear wave pressure diagram, with breaker height ϕ_b and wave front angle θ_f, defined as $\tan\theta_f = d\phi_b/dx$. In the mathematical solution three areas are distinguished.

$$\phi(x) = \phi_b - C_1 e^{x/\Lambda} \qquad\qquad \text{for } x < x_2$$
$$\phi(x) = -x\cos\alpha\tan\theta - C_2 e^{-x/\Lambda} + C_3 e^{x/\Lambda} \qquad \text{for } x_2 < x < 0$$
$$\phi(x) = x\sin\alpha + C_4 e^{-x/\Lambda} + C_5 e^{x/\Lambda} \qquad \text{for } 0 < x < x_1$$

<div align="right">Eq. 5.46</div>

with transition point $x_2 = -\phi_b / \cos\alpha\tan\theta$ and boundary $x_1 = z_1 / \sin\alpha$

The constants C_1 to C_5 are found by demanding continuity for $\phi(x)$ and $d\phi(x)/dx$ and by defining $\phi - \phi' = 0$ at $x = x_1$.

$$C_1 = \tfrac{1}{2}\Lambda\cos\alpha\tan\theta\left(e^{-x_2/\Lambda} - e^{x_2/\Lambda - 2x_1/\Lambda}\right) - \tfrac{1}{2}(\Lambda\sin\alpha + \Lambda\cos\alpha\tan\theta)\left(1 - e^{-2x_1/\Lambda}\right)$$

$$C_2 = \tfrac{1}{2}\Lambda\cos\alpha\tan\theta\, e^{x_2/\Lambda}$$

$$C_3 = \tfrac{1}{2}\Lambda\cos\alpha\tan\theta\, e^{x_2/\Lambda - 2x_1/\Lambda} + \tfrac{1}{2}(\Lambda\sin\alpha + \Lambda\cos\alpha\tan\theta)\left(1 - e^{-2x_1/\Lambda}\right)$$

$$C_4 = -\tfrac{1}{2}\Lambda\cos\alpha\tan\theta\, e^{x_2/\Lambda} + \tfrac{1}{2}(\Lambda\sin\alpha + \Lambda\cos\alpha\tan\theta)$$

$$C_5 = \tfrac{1}{2}\Lambda\cos\alpha\tan\theta\, e^{x_2/\Lambda - 2x_1/\Lambda} - \tfrac{1}{2}(\Lambda\sin\alpha + \Lambda\cos\alpha\tan\theta)e^{-2x_1/\Lambda}$$

The maximum (uplift) value of the piezometric head difference ϕ_{dip} is given as $C_3 - C_2$. This expression can be simplified by ignoring the effect of z_1. For practical values of the leakage factor Λ/D, there is a negligible effect of variation of z_1 on ϕ_{dip}. Therefore the terms with e^{-x1} are assumed zero.

$$\phi_{dip} = \tfrac{1}{2}\Lambda\sin\alpha + \tfrac{1}{2}\Lambda\cos\alpha\tan\theta\left(1 - e^{x_2/\Lambda}\right)$$
$$= \tfrac{1}{2}\Lambda\sin\alpha + \tfrac{1}{2}\Lambda\cos\alpha\tan\theta\left(1 - e^{-\phi_b/(\cos\alpha\tan\theta\,\Lambda)}\right)$$

$$\text{Eq. 5.47}$$

For small leakage factors and mild angles the position of x_2 is not 'felt', and the maximum is dominated by the wave front angle. The limit value of the expression is in that case:

$$\phi_{dip} = \tfrac{1}{2}\Lambda\sin\alpha + \tfrac{1}{2}\Lambda\cos\alpha\tan\theta$$

$$\text{Eq. 5.48}$$

For very steep front angles, the angle is less relevant and the filter response is dominated by the step from 0 to ϕ_b. Using Taylor series for $e^{-x2/\Lambda}$ the expression changes into:

$$\phi_{dip} = \tfrac{1}{2}\phi_b + \tfrac{1}{2}\Lambda\sin\alpha$$

$$\text{Eq. 5.49}$$

For the curved front (see 5.2.3) the expression for ϕ_{dip} is given as:

$$\phi_{dip} = \tfrac{1}{2}\Lambda\left(\sin\alpha + \frac{\cos\alpha\tan\theta}{(1+c\Lambda)^2} - \frac{c\phi_{min}}{1+c\Lambda}\right)$$

$$\text{Eq. 5.50}$$

with $c = \dfrac{\cos\alpha\tan\theta}{3\phi_b + 2.4\phi_{min}}$ [m^{-1}] and $x_2 = \dfrac{3\phi_b + 1.4\phi_{min}}{\cos\alpha\tan\theta}$

In the figures below the effect of parameter variation are shown. The peak value of ϕ_{dip} and the length of the domain where $\phi - \phi'$ is positive is linearly dependant on the leakage factor Λ. Because of this strong dependency unrealistic small values of the leakage factor should be avoided. The length of area that experiences uplift pressure is determined by the leakage factor Λ. At the slope side the pressure difference dampens away. The head difference drops to zero over a distance of 2Λ. At the wave front side this length is the minimum of ½ x_2 or 2Λ (see Figure 5-35).

The dependency on the breaker height assuming constant front angle, and on the front angle assuming constant breaker height are shown in Figure 5-37 and Figure 5-38. The effect of z_1 can be neglected when the distance x_1 is large compared to the leakage length Λ. The effect of z_1 in practise differs per type of wave and is also dependant on the filter volume. At

rundown there will be water volume left on the slope and in the filter. The piezometric head calculation is based on a stationary flow and pressure equilibrium. The water flow through the top layer joints will lower the free water table in the filter. During the concerning part of the wave cycle the filter may also be fed by run-up water of the previous wave.
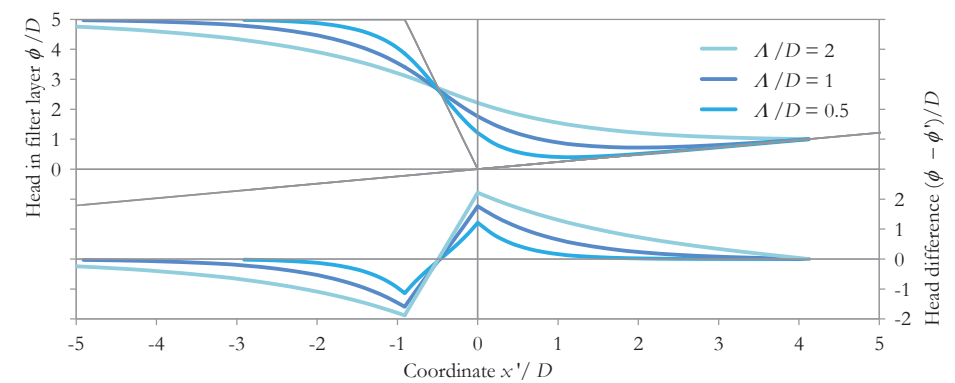
Figure 5-36   Hydraulic response of filter for various values of the leakage factor
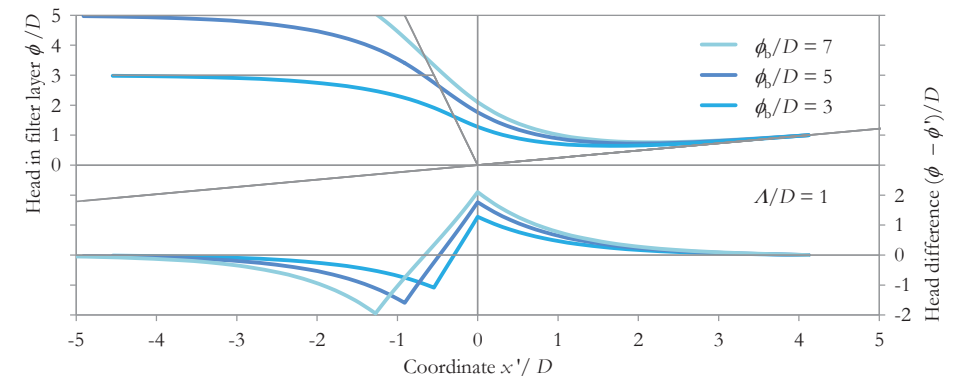
Figure 5-37   Hydraulic response of filter for constant wave front angle (80°) and various values of the breaker height
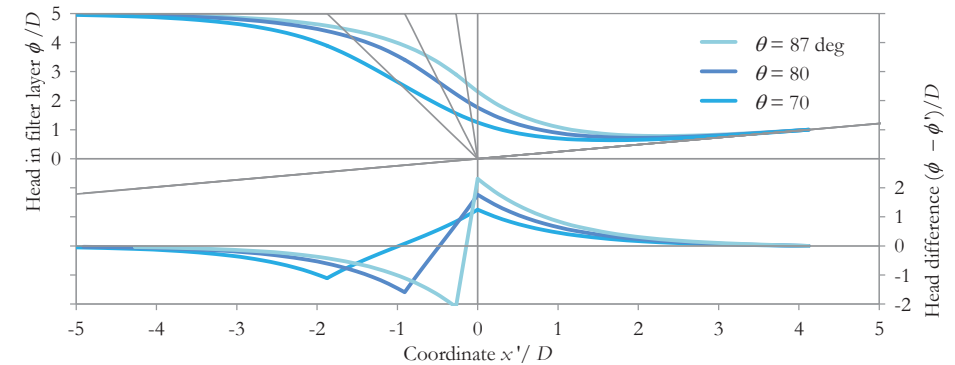
Figure 5-38   Hydraulic response of filter for constant breaker height and various values of the wave front angle

     DESIGN OF PATTERN-PLACED REVETMENTS
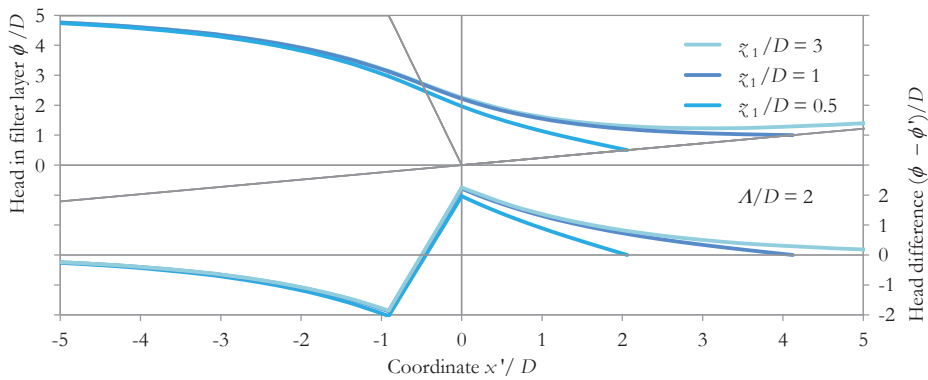
Figure 5-39   Hydraulic response of filter for various values of the water level in the filter z_1

5.3.2   *Hydraulic response to wave shapes on slope*

When this theory is applied to the more advance descriptions of the wave shapes the following results are found. Figure 5-40 shows the distinguished wave descriptions discussed in section 5.2. The high front, the steep front with lower breaker height but steep front angle and the wave impact shapes.
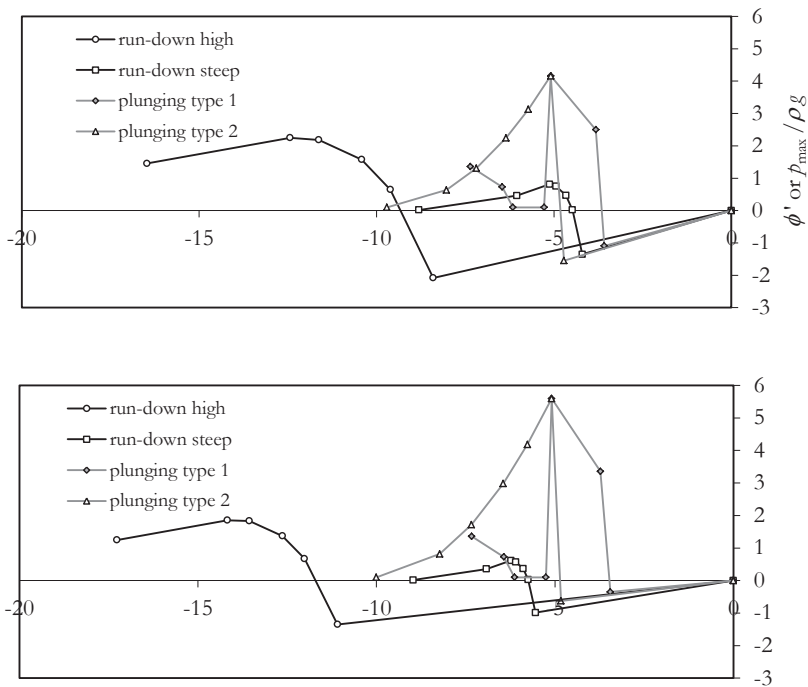
Figure 5-40   Wave pressure diagrams $\phi'(x)$ above the slope for $s_{m\text{-}10} = 0.02$ and cot $\alpha = 2.5$ and 5

Two wave impact types are shown. As a result of observations in the Delta Flume the first shape with a clear almost rectangular shape with sea- and dike-side angles and a trough zone is supplement with a second shape with one clear dike-side angle and a corresponding high peak at the dike side. For this second type the trough is vanished at the moment of the impact.

The four wave types can be seen as four load cases. The hydraulic response of the system in the wave rundown cases is for the larger part determined by the wave front angle θ_f. This effect is also influenced by the leakage factor. If Λ/H_s increases, there will be a larger influence of the breaker height Φ_b. The calculated peak value of ϕ_{dip} is indicated in the figures, as well as the area with positive values of ϕ_{dip}. The slopes of the ϕ_{dip} pressure diagram are based on a linearization with a characteristic length of 2Λ. The zones where ϕ_{dip} exceeds ΔD are potentially instable. The threshold value of ΔD is indicated in Figure 5-42 with the dotted line. The calculations are done for $H_s = 2$ m and $H_s/\Delta D = 4$, hence with $\Delta D = 0.5$ m.

The principle and effect of Λ on the calculation values of ϕ_{dip} has been verified with measurements.[237]
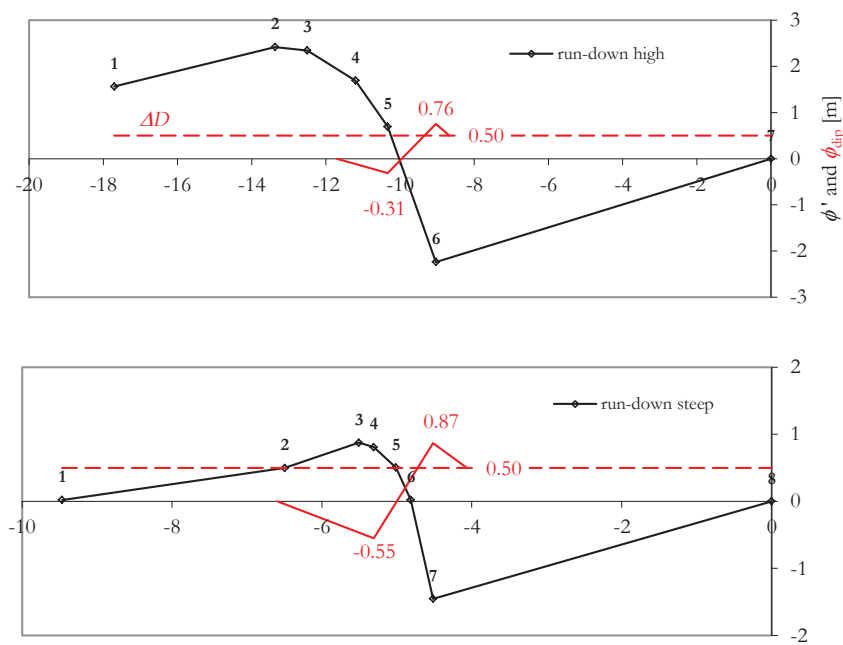
Figure 5-41   **Wave shapes for run down cases with hydraulic response of filter for $H_s/\Delta D = 4$ and $\Lambda/D = 2$**

---

[237] Smith, Wouters, and Klein Breteler, *Grootschalig modelonderzoek naar stabiliteit van taludbekledingen - Meetverslag van Deltagootonderzoek*
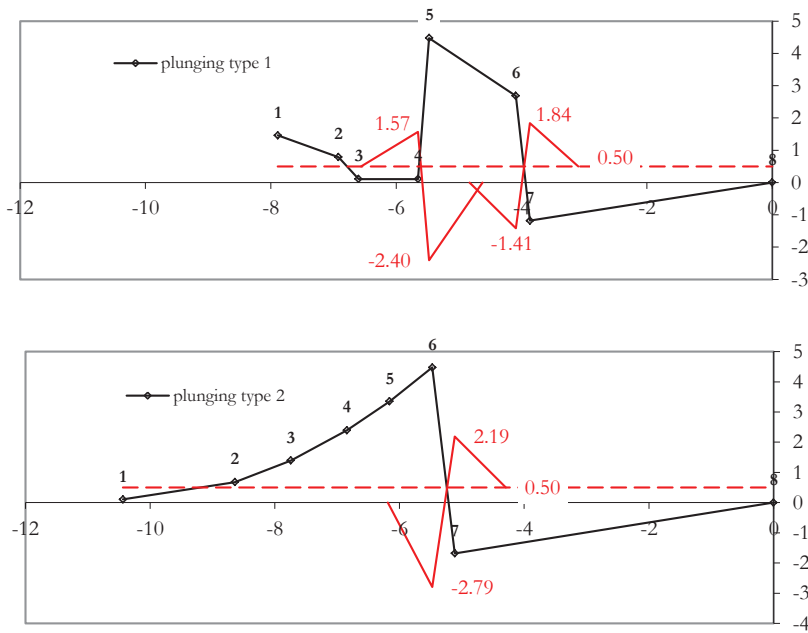
Figure 5-42   Wave shapes for plunging wave cases with hydraulic response of filter for $H_s/\Delta D = 4$ and $\Lambda/D = 2$

5.3.3 *Hydraulic response to shock impact*

The load cases of the plunging waves are a bit more complicated due to dynamic effects. The hydraulic response of the system is due to the very steep gradients determined by the maximum values of the pressure diagrams. The values of ϕ_{dip} should in that case come close to ½ϕ_b. Likely there is some time delay in the filter response to the maximum peak pressure. Since this peak pressure had only a very short duration, it is unsure to what extent the filter pressure really responds to the maximum peak pressure. During a limited number of Delta flume tests the filter response to the wave impacts has been measured and analysed in detail.[238]

The peak value of ϕ_{dip} is measured as well as the integration over the time that $\phi_{dip} > 0.4\,H_s$. The peak values are plotted in Figure 5-43. It can be noticed that the graph shows a remarkable similarity with the p_{max} values in Figure 5-29. A formula expressing the upperbound of the 2% values can be found by taking 25% of the $p_{max}/\rho g\,H_s$ values. On basis of this finding we conclude that the dynamic effect in the filter response can be quantified with a factor 0.6. A ratio between ϕ_b and ϕ_{dip} of 0.35 to 0.5 is caused by averaging due to pressure leakage. A quasi-stationary response of the filter of $\phi_{dip} = 0.25\,p_{max}/\rho g\,H_s$ can hence be found by multiplying the input peak pressure by 0.6 and performing a normal hydraulic response calculation.

---

[238] Klein Breteler, Werf, and Wenneker, *Kwantificering golfbelasting en invloed lange golven, rev. 2*

The measured and analysed durations of the peak uplift load ϕ_{dip} are plotted in Figure 5-44 and Figure 5-45. The values of the duration t_{dip} are calculated from the time-integrated dip-impulse $\int(\phi_{dip}(t)-0.4H_s)dt$ by dividing the integral by the peak value of $\phi_{dip}-0.4H_s$, assuming a block diagram of $\phi_{dip}(t)$.

Typical values of t_{dip} are 0.2 to 0.3 seconds, which is of the same order or slightly longer than the duration of the wave impact duration (see Figure 5-31). Some delay might be explained by the time required for pressure propagation and inertia of water mass flow. It is noticeable that the duration of the filter response looks inversely related to the duration of the impact load (compare Figure 5-45 and Figure 5-31).
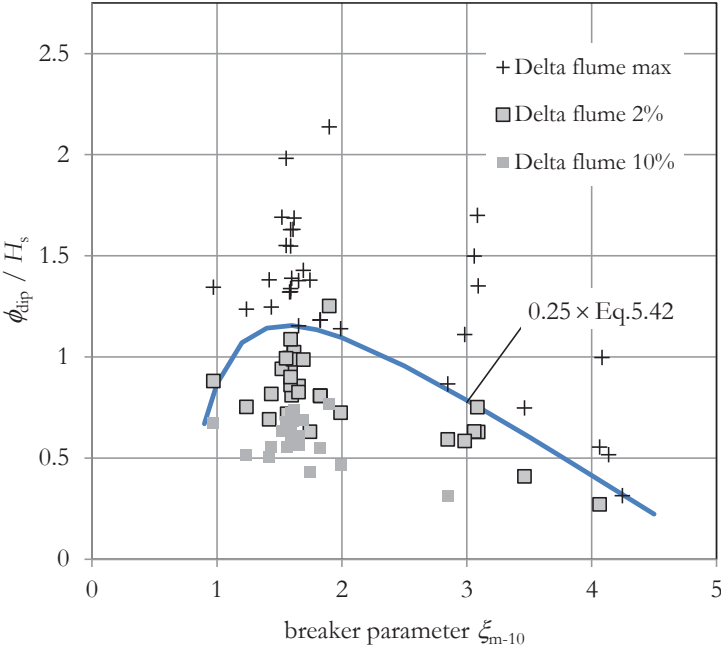
Figure 5-43   **The hydraulic head ϕ_{dip} in the filter as a response to wave impact versus the breaker parameter**
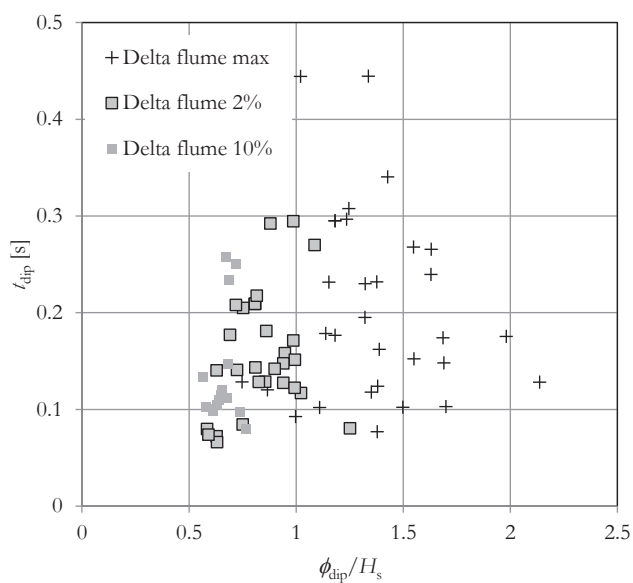
Figure 5-44 Duration t_{dip} for which ϕ_{dip} exceeds a critical value versus the breaker parameter
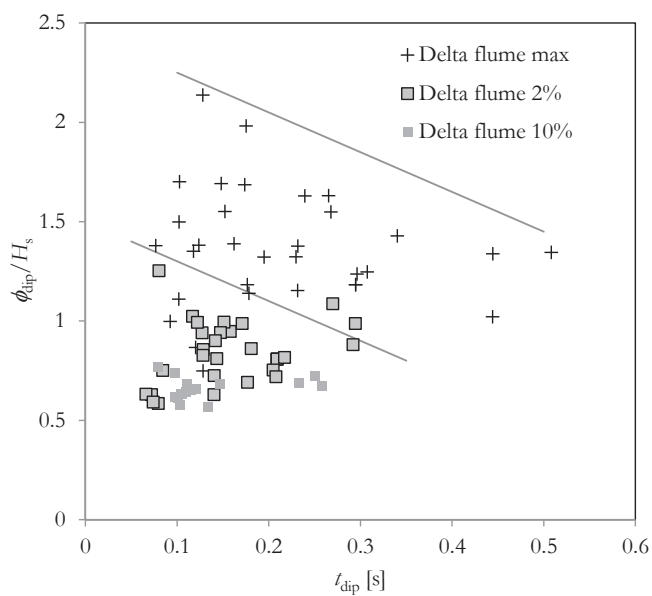
Figure 5-45 Duration t_{dip} for which ϕ_{dip} exceeds a critical value versus ϕ_{dip}

5.3.4 Numerical filter response model ZSteen

Filter water pressure response can also be calculated from detailed data of water pressure variations in space and time. ZSteen is a software tool developed by Deltares that calculates filter response for series of measured wave pressures above the slope. ZSteen calculates the piezometric head of grid points in the filter layer. The input consists of the pressures at the top surface of the revetment, and of the geometric and hydraulic features of the system of the top layer (blocks or columns), the bedding and filter layer, and optionally applied geotextiles. The calculation is performed with the formulas of Darcy and Forchheimer.

The ZSteen model calculation results are calibrated with measured filter pressures in the Deltagoot.[239] Also a 3D version of ZSteen has been developed. This version is suitable for calculation the longitudinal response effects of local dynamic loads, and for studying the effects of oblique wave attack.[240]

Typical results of the peak value of the resultant uplift water head ϕ_{dip} and its distribution in space and time can be extracted from ZSteen model calculations. Although the pressure distributions in time look irregular, a typical pattern with a certain persistent value over a limited duration t_{d1-dip} of 0.025 .. 0.150 seconds can be distinguished, preceded and followed by constant gradients. The total duration t_{dip} is typically 0.075 .. 0.350 seconds which is perfectly in the range of the measured data shown in Figure 5-45. The delay is on average 0.7 t_d, which means that the peak value of p_{dip} is in most cases reached after the peak value p_{max} of the pressure signal above the slope has dropped, as indicated in the definition diagram Figure 5-46.
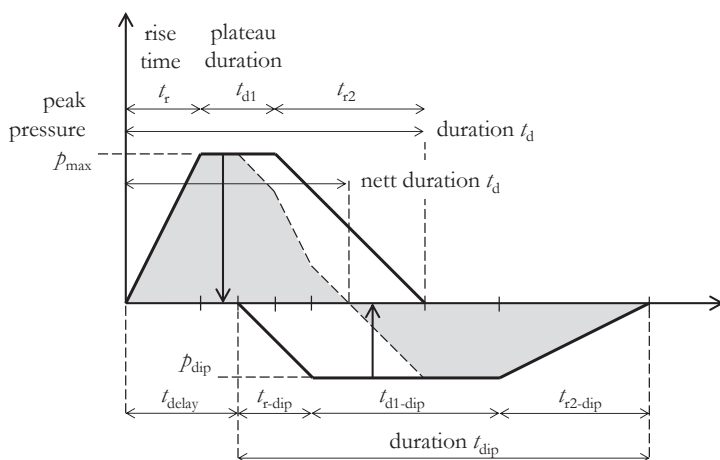
Figure 5-46   Pressure versus time definition diagram of downward and upward water pressures

---

[239] M. Klein Breteler, B. van Vossen, and C. Kuiper, *Testen van ZSteen versie 1.8* (WL Delft|Hydraulics report H4331, 2003) and B. Hofland and M. Klein Breteler, *Nauwkeurigheid van ZSTEEN bij golfklappen* (WL|Delft Hydraulics report H4455, 2005)

[240] M. Klein Breteler, C. Kuiper, and A. Bezuijen, *Invloed scheve golfaanval op stabiliteit van steenzettingen* (WL|Delft Hydraulics report H4420, 2006)

Table 5-7   Data selected ZSteen runs

file	H_s [m]	T_p [s]	s_o	ξ_{op}	cot α	D [m]	Λ [m]	B_{imp} [m]
12co02	1.07	3.9	0.045	1.35	3.5	0.5	0.30	0.6 0.6
12co04	1.05	5.0	0.027	1.74	3.5	0.5	0.27	0.8 0.6

Table 5-8   Pressure duration data of selected wave impacts

file timestep	t_r	t_{d1}	t_{r2}	t_d	side	delay	$t_{r\text{-}dip}$	$t_{d1\text{-}dip}$	$t_{r2\text{-}dip}$	t_{dip}	delay / t_d	t_{dip} / t_d
12co02 1417	0.025	0.025	0.025	0.075	dike	0.030	0.025	0.025	0.025	0.075	0.40	1.00
					sea	0.040	0.025	0.125	0.100	0.250	0.53	3.33
12co02 2276	0.025	0.025	0.025	0.075	dike	0.025	0.040	0.040	0.040	0.120	0.33	1.60
					sea	0.100	0.025	0.125	0.100	0.250	1.33	3.33
12co04 1571	0.040	0.050	0.060	0.150	sea	0.100	0.040	0.150	0.150	0.340	0.67	2.27
12co04 2386	0.015	0.050	0.060	0.125	sea	0.100	0.075	0.075	0.125	0.275	0.80	2.20
typical values											0.68	2.29

5.3.5   Stability curves

The loads cases of rundown and wave impact are expressed in hydraulic head differences ϕ_{dip} over the top-layer. When we assume no resistance against uplift other than the self-weight of the top layer elements, it follows that the required top layer thickness D follows from $\phi_{dip} = \Delta D$. The stability of the revetments is commonly expressed as $H_s/\Delta D$. The findings of the wave parameterizations and the hydraulic responses can now be included in graphs showing $H_s/\Delta D$ versus ξ, for which we choose for $\xi_{m\text{-}10}$.

For the wave rundown cases (presented in Figure 5-47) there is a strong influence of the leakage factor Λ/D. For the smaller, more realistic leakage factors it can be noticed that the stability curve follows a hyperbola but goes up again for larger values of ξ. The physical background is the smaller wave front angle associated with a smaller value of the wave steepness.

The 6 $\cos\alpha/\xi^{2/3}$ −formula is an empirical upper bound of calculation results with less-advanced models and very small leakage factors. The 3 $\cos\alpha/\xi$ −formula has as a background an optimistic run-down formula and neglects effects of leakage and larger breaker heights. The agreement with the present rundown model with a large leakage factor is reasonable. When attempting to update those simple design formulas the leakage should be included. Rationalised formulas are presented in chapter 6.1.

The graphs in Figure 5-47 concentrate on the peak value of ϕ_{dip}, whilst for the resistance of the revetment as a coherent structure, the spatial distribution of the load is important. For the run-down cases the spatial load diagrams can be modelled as triangles or sinus-curves that diminish to zero over a distance of 2Λ [m] in the direction of the dike. For the load dampening length in the direction of the wave the horizontal distance x_2 from the rundown

point to the wave crest is determining. This distance increases with decreasing wave steepness as shown in Figure 5-48.
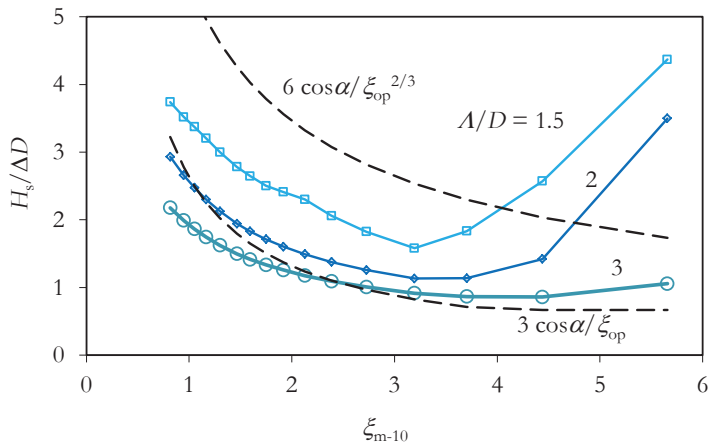
Figure 5-47 Stability curves calculated with constant $H_s = 2$ m and variable wave steepness and variable slope angle
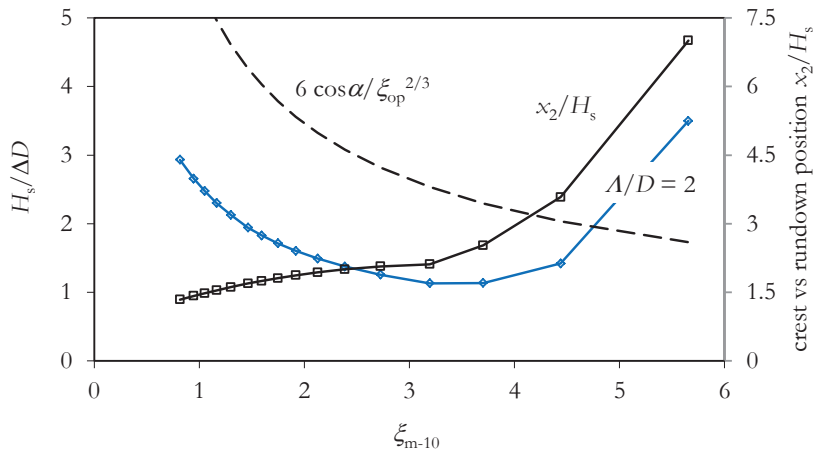
Figure 5-48 Stability curve based on peak value of $\phi/\Delta D$ with parameter x_2/H_s as indication of length of loaded area

The stability curves for the run-down visually reflect to the known stability curves. When we include the calculated effects of the wave impact this image changes and within the range of $\xi_{m-10} = 1 .. 3$ lower values of the stability are found. Since the gradients of the pressure shapes are very steep there is negligible effect of the leakage factor on the peak value ϕ_{dip}. The leakage length Λ still has an effect on the spatial distribution of the uplift pressure $\phi_{dip}(x)$.

In case no additional resistance or dynamic structural response effects would be present the revetment stability numbers will be as indicated in Figure 5-49.
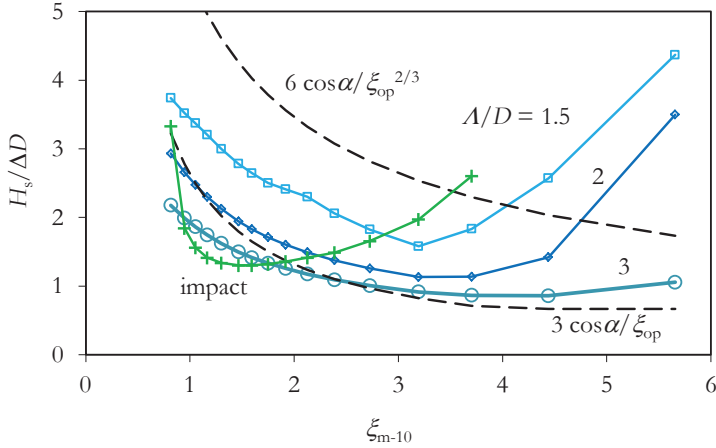
Figure 5-49   Stability curves supplemented with curve based on Eq. 5.42 for wave impact

Following conclusions can be drawn.

- The stability curves with increasing stability above $\xi = 3$ are a reflection of the models for the wave run-down and the breaker shapes, based on detailed study of experiment results. They are more realistic than the hyperbolic $3 \cos\alpha / \xi$ and $6 \cos\alpha / \xi^{2/3}$ rules.
- Steeper slopes contribute to avoidance of high wave impact loading. Combined with longer waves, steep slopes experience a smaller wave front angle which decreases the uplift loads ϕ_{dip} for finite values of the leakage factor Λ/D. And steeper slopes experience less severe wave impacts.
- These considerations are without regard of the obviously better element interaction at steeper slopes.
- For revetment design the peak value of the uplift pressures C considered together with the spatial distribution.
- For the run-down and wave impact a range of possible locations should be considered. For the run-down related load the maximum magnitude is determined by the maximum run-down position. Higher positions give lower loads. The wave impacts are of constant magnitude in a certain range. The distribution of wave impacts on locations on the slope follows a normal distribution.
- For the design value of the breaker parameter ξ_{m-10} a range of possible wave steepness values should be considered, and not a single value of T_p.[241]

---

[241] Which is given in the Hydraulic Boundary Conditions in NL.

6   REVETMENT DESIGN FORMULAS

Chapter introduction

In this chapter the model approach for the load and the resistance of hydraulically open pattern-placed revetments on a thin filter layer is summarised. The model outcomes are compared with large-scale flume test results of revetment stability.

The principle of the in-plane forces in the sloping revetment as the basis for the frictional interlocking can be transferred into a design formula. Section 6.1 summarises the findings with respect to the 'design formula'. An axial beam model predicts the in-plane forces given a certain wave load. A flexural beam model predicts resistance and deformation against uplift pressures. Influences of dynamic loading are modelled with correction factors. Because of uncertainties and variation observed in the in-plane forces the value of the resistance is a stochastic variable. The lower bound of the resistance is the self-weight, which can be considered deterministic.

Under ideal support conditions, such as those that occur in flume tests, the in-plane forces in the revetment are better predictable. The effects of variation of the model parameters are predicted by theory and verified by studying trends within the extensive population of available experiment results. This is summarised in section 6.2. A selection of flume tests provide a valuable set for model calibration (section 6.3). A discussion on the achieved result is presented in section 6.4.

New design formulas based on this study were already included in the STEENTOETS software since 2009.

6.1 Description of a resistance model for pattern-placed revetments

6.1.1   Failure mechanisms considered

The failure mechanisms of the top-layer of pattern-placed revetments (see Figures 3-31 and 3-32) include:

- Uplift of a group of revetment elements during run-down of the waves on the slope
- Dynamic downward load succeeded by uplift of a group of elements caused by plunging breakers
- Single element failure

The risk of failure occurs during two instances in the wave cycle: the run-down of the wave and the impact of a plunging breaker.

The run-down case is dominated by water head differences over the top layer, over an area of which the size is determined by the leakage factor. This load case is considered 2-dimensional. The wave run-down occurs over a large width, and hence no redistribution of forces in longitudinal direction of the revetment is possible.

Plunging breakers cause a peak load with a very short duration. Although the crest of a breaker may overturn over a longer width, the breaking process and the directional spreading cause irregularity, and the peak load will be not exactly simultaneous over larger width. It is

therefore appropriate to consider 3-dimensional-effects in the resistance against the peak load. Refer to Figure 3-22.

It is however disputable whether this 3-dimensional effect can occur in 5 m wide flume tests. The plunging looks like a 2-dimensional process, and the revetment cannot generate resistance from the cross direction of the flume. However there are cases where the revetments actually did develop arching in cross direction (see Figure 6–27). Therefore the model used for calibration with the flume tests only contains longitudinal effects for smaller waves. In reality the effective contribution of the longitudinal direction is estimated at ¼, against ¾ for the transverse direction. For the flume tests hence we applied a load reduction for evaluation of the transverse resistance of a factor of 0.75 for waves below $H_s = 0.8$ m. This factor increases linearly to unity at a value of $H_s = 1.2$ m.

The single element failure has a low probability for many revetment types, although especially for regular block shapes this risk cannot be neglected. In the flume tests only row-oriented block type elements show single element failure. In Figure 4-3 it is shown that prismatic tall elements theoretically have less resistance against single element failure. In practise the columns revetments have better interaction with the neighbouring elements via the joints.

The experiments which showed single element failure whilst the rest of the revetment was not deformed, were labelled with damage category d1, rather than d. Refer to 6.2.1. In the model calculations that test is evaluated with damage category a as well as with damage d1. Single element failure is caused by a lack of normal force, or a non-uniform normal force, which leaves certain elements without contact force, whilst others have a higher-than-average contact force. The resistance against single element failure is equal to the load ϕ_k times a factor for sliding resistance and dynamic effects (see section 3.4). This factor is estimated 1.25 for the cases c1 and 1.4 for the cases d1. Only in the experiments where the single element failure was actually observed this failure mechanism was included in the model calculation.

6.1.2 *Summary of the wave load model*

The wave loads are split between (a) plunging wave loads or wave impacts and (b) wave front loads at run-down position.

(a) *Wave impact*

The wave impact peak load p_{max} [Pa] above the slope is given with the coefficient.

$$\frac{p_{max}}{\rho_w g H_s} = 8 - 1.6\, \xi_{m-10} - \frac{2}{(\xi_{m-10} - 0.2)^2} \qquad\qquad \text{Eq. 5.42}$$

The width of the impact pressure block diagram in transverse direction is $B_{x\ imp} = 0.75\ H_s$ (Figure 5-33). Based on an assessment of the gradients of the impact pressure diagram the length L_a of the upward pressure diagram is estimated as $0.25\ H_s$. The length L_b is set equal to two times the leakage length: 2Λ (see Figure 5-34 and 5-40).

The width of a simultaneous pressure signal of a short-crested plunging wave in longitudinal direction is $0.5\ H_s$. This would in practise lead to a contribution of the longitudinal normal force to the resistance of the revetment. For evaluation of the flume tests this contribution is neglected.

The peak load of the resulting upward pressure diagram p_{dip} is given as 0.25 p_{max}, which consists of a factor 0.35 to 0.5 for the averaging due to leakage in and outside the impact zone, and a factor 0.6 for the effect of hydraulic dampening of the peak value in time.[242]

For the structural response to the sudden downward impact load followed by an upward load a dynamic amplification can be expected. Based on SDOF model calculations a dynamic amplification factor DAF can be 1.2 to 1.4. These values are based on SDOF model calculations with t_{dip} values of 0.5 to 0.7 s, in line with ZSteen model outcomes and in line with the measured uplift-pressure duration t_{dip} belonging to the pressure values beyond the 2% values. The measured 2% values of t_{dip} in the Delta flume are around 0.2 to 0.3 s (see Figure 5.41). For those values the dynamic amplification is around 0.8 to 1.0. For the calibration flume test evaluation an average of 0.9 is assumed. Hence the combined effect of hydraulic dampening and structural amplification can be based on a quasi-static value of p_{dip} = 0.9 × 0.25 = 0.23 p_{max}. For p_{max} Eq. 5.42 is used, which results in the curve plotted in Figure 6–1.

(b)   Wave front at run-down

The peak load caused by the wave front is determined by the position on the slope and the leakage properties of the revetment. The combined effect of the wave description and the leakage properties are given in the simplified formulas below (Eq. 6.1 and Figure 6-1). The formulas are a rational approximation of the outcomes of the Wolsink model (see section 5.3.5). The formulas replace the relation H_s / ϕ_{dip} = 3 $\cos\alpha / \xi_{op}$ (Eq. 4.4 and Eq. 5.30), which safely neglects permeability effects (see sections 4.1.2, 4.1.11 and 5.2.2).

The formulas give the peak value of the upward load ϕ_{dip} in terms of H_s / ϕ_{dip}. Without element interaction there will be not more resistance than ΔD and hence $\phi_{dip} = \Delta D$.

$$\frac{H_s}{\phi_{dip}} = C_1 \left(\xi_{m-10}\right)^{C_2} \qquad\qquad \text{for } \xi_{m-10} < \xi_{transition}$$

$$\frac{H_s}{\phi_{dip}} = C_1 \left(\xi_{transition}\right)^{C_2} + C_3 \left(\xi_{m-10} - \xi_{transition}\right)^{C_4} \qquad \text{for } \xi_{m-10} > \xi_{transition}$$

Eq. 6.1

$$\xi_{transition} = 2.4 \left(\frac{\Lambda}{D}\right)^{0.3}$$

$$C_1 = 1.67 + 0.012 \left(4 - \frac{\Lambda}{D}\right) + 0.008 \left(4 - \frac{\Lambda}{D}\right)^3 \not< 1.67$$

$$C_2 = -0.67 + \left(3 - \frac{\Lambda}{D}\right)^{0.11} \not< -0.67$$

$$C_2 = 0.45 - 0.12 \left(\frac{\Lambda}{D}\right)$$

$$C_4 = 2$$

For a calculation of the resistance $\phi_{dip} > \Delta D$, the model formulas are first evaluated to find the H_{s1} for which $\phi_{dip} = \Delta D$. The peak load $\phi_{dip\ actual} / \Delta D$ is than equal to $H_{s\ actual} / H_{s1}$.

---

[242] Refer to section 5.3.3

The distribution of the load is assumed infinite in longitudinal direction and is characterised by exponential decay in transverse direction. The load diagram in x-direction can be simplified by a linear decay with a length based on two times the leakage length 2Λ to one side (L_b).

To the other side the length (L_a) is determined by the distance between the wave run-down point and the position of the top of the breaker, given by x_2/H_s (see Figures 5-34 and 5-46).

$$\frac{x_2}{H_s} = 1.5 + 0.5 \frac{\xi_{m-10}}{\xi_{\text{transition}}} \qquad \text{for } \xi_{m-10} < \xi_{\text{transition}}$$

$$\frac{x_2}{H_s} = 2 + 0.4\left(\xi_{m-10} - \xi_{\text{transition}}\right) + 0.6\left(\xi_{m-10} - \xi_{\text{transition}}\right)^2 \quad \text{for } \xi_{m-10} > \xi_{\text{transition}}$$

Eq. 6.2

The slope length of the diagram of the distributed upward load L_a is the smallest value of ½ x_2 or 2Λ.
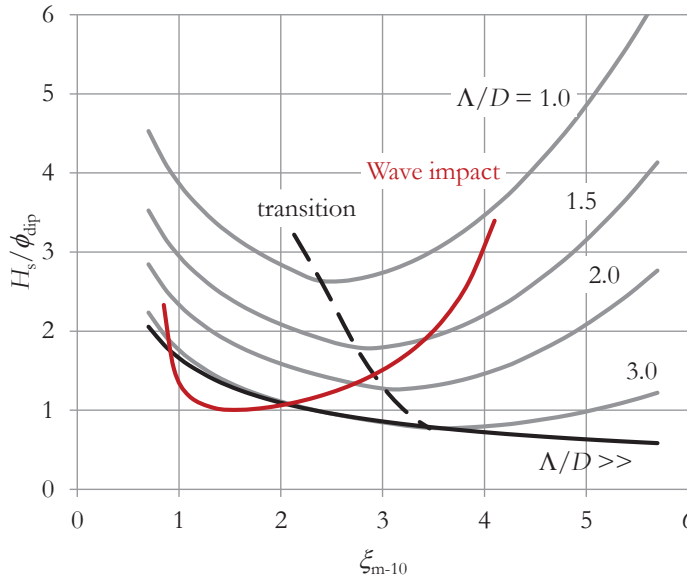
Figure 6–1   Load diagrams of peak head ϕ_{dip} of run-down case, as a function of the leakage factor

6.1.3   Summary of the resistance model in the ultimate limit state

The resistance of the revetment against group uplift relies on the element interaction. For the traditional block and column revetments this interaction is through friction and the presence of normal force, caused by gravity.

Through normal force contact the elements can transfer ´vertical´ forces from one to another. This is associated with the type of force interactions equal to bending moments $M(x)$ and shear forces $V(x)$ in beams. The values of M and V can be determined using models of beams on elastic foundation (see Annex A2.1). For the limit states of instability of a group of elements a simpler model of a small not-supported beam can be used. The beam weight is equal to the load. This equality determines the length. The revetment elements that

form the beam are locked-in and 'connected' through the presence of normal force. The beam model is called a confined beam model. The extreme bending moments and shear forces that occur in the confined beam are based on internal re-distribution (see Figure 3-10). The standard expressions for the coefficients $M_{ext}/q_s L^2$ and $V_{ext}/q_s L^2$ are derived for symmetrical loads. For asymmetrical loads correction factors c_M and c_v are applicable. Negative loads are investigated in Annex A.3.2.
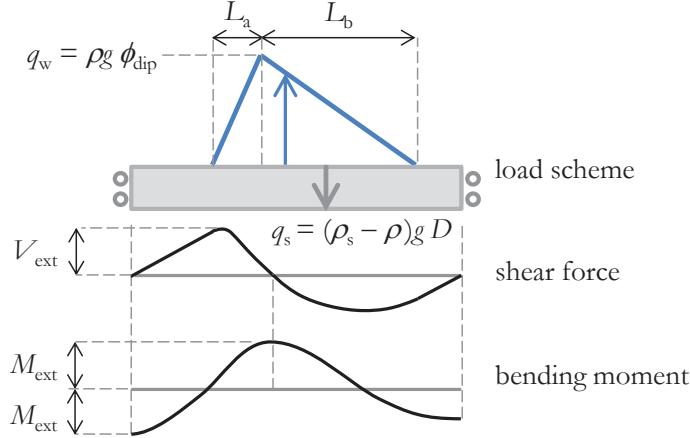
Figure 6–2 **Equilibrium model of confined revetment beam model subject to bi-linear uplift load q_w balanced by the beam weight q_s**

$$\frac{M_{ext}}{q_s L^2} = c_M \left(\frac{1}{48} \frac{q_w}{q_s} + \frac{1}{64} \left(\frac{q_w}{q_s} \right)^2 \right)$$ Eq. A.46

$$\frac{V_{ext}}{q_s L^2} = c_V \left(\frac{1}{4} \frac{q_w}{q_s} + \frac{1}{4} \frac{q_s}{q_w} - \frac{1}{2} \right)$$ Eq. A.47

$$c_M = 1.22 - 0.070 \frac{q_w}{q_s} - 0.039 \frac{L_b}{L_a} \not> 1.0$$

$$c_V = 1.0 + 0.075 \frac{L_b}{L_a} - 0.0045 \left(\frac{L_b}{L_a} \right)^2$$ Eq. A.48

with $\dfrac{L_b}{L_a} \not> 8$ and $\dfrac{q_w}{q_s} \not> 5$

The bending moment resistance and shear force resistance in the revetment beam are dependent of the element aspect ratio B/D, the length of the distributed load along the beam, the overlap in B_x, and the associated damage level.

A small ratio of B_x/D has favourable effects. When the length x_0 of the beam includes a larger number of elements with dimension B_x the probability that a misaligned element and/or sheared joint is in an unfavourable position decreases. A second effect is that when the number of elements with width B_x in a certain length x_0 is large the curvature is followed

easily. If however the number is small the curvature concentrated in one or two joints, which leads to a larger rotation angle per joint. The joint material may in that case become unstable.

Effect of randomness of vertical position on the ability to form arching force lines

Effect of distribution of curvature over many joints (small elements) and over few joints (large elements)
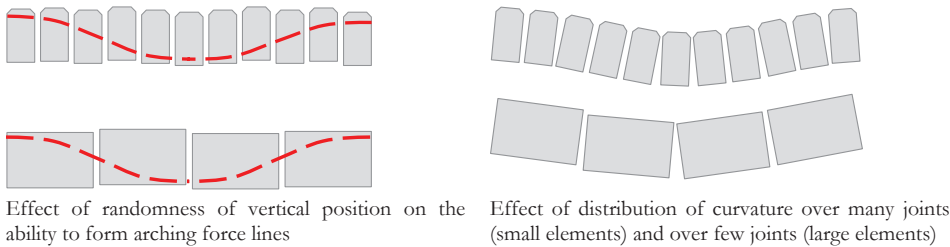
Figure 6–3   Effects of element aspect ratio B/D

Based on trend analysis of the Delta flume experiments in Annex J (see Figure J-2) this effect is estimated and expressed with a factor $r_1 = 0.8$ (see Figure 6–4).
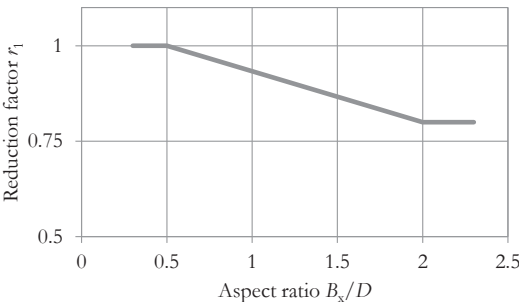
Figure 6–4   Reduction factor r_1 for block width over height ratio
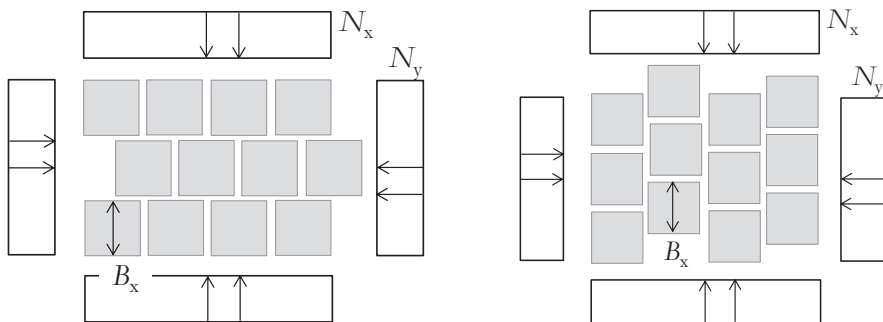
No overlap in B_x. The x-joints are aligned, which causes that a bending moment M_x is controlled by the normal force N_x only. This pattern is typical for Hydroblocks and Haringman blocks.

Overlap in B_x. Rotation in x-joints will be spread over a larger area. Friction in the y-joints can also contribute to the equilibrium. Although their pattern is different this effect plays a role for regular columns C-star, Ronaton, and irregular Basalton and Basalt.

Figure 6–5   Overlap in element position in x-direction

Some revetment types are strictly row-oriented. Other have overlaps, similar to stretcher bond or header bon in brick masonry construction. The principle of overlap in B_x is shown

in Figure 6–5. The transfer of a bending moment M_x in transverse direction relies as a primary mechanism on the occurrence of N_x and on eccentric compressive contact forces in the x-joints. When the elements have overlaps in x-direction and the x-joints are interrupted and have scattered positions, the x-curvature is more smoothly distributed over the joints. Moreover, the y-joints will experience friction when the block will rotate. The friction forces in the y-joints can theoretically transfer the bending moment M_x without N_x.

Quantifying the effect of overlap can be done on a purely theoretical basis. Refer to Annex B.3. The contribution of n_y can be 15 to 30%, depending on the magnitude of n_y. The effect in the flume tests is assessed to be rather limited. With trend analysis of sub-groups a factor r_2 of 0.8 was found for pure row-oriented types, assuming 1.0 for the column types.

The normal force N_x on the slope is an unknown factor. The field experiments show a large scatter and reliable design values are very low. In the large scale flume tests it was observed that – after a gradual increase of the wave height – the normal force develops to the neutral level. For definition see section 3.1.3. A stiff toe structure plays a positive role here. Models for the flume test evaluation can hence be based on a neutral normal force model.

$$N_{\text{neutral}} = \rho_s g D B_y \sin\alpha \, (x_{\text{top}} - x) \text{ [kN]}$$
with x = ordinate in line with the slope

Eq. 3.1

Alternative notations are: $(z_{\text{top}} - z)$ instead of $\sin\alpha \, (x_{\text{top}} - x)$, with z = the vertical ordinate, without B_y, or with $B_y = 1$ m gives [kN/m], ρ_s can be replaced by $\rho \, (1+\Delta)$.

If z_{top} is high above the waterline it might be more realistic to replace z_{top} by z_{SWL}. After assessments of the results, which indicate that there is a contribution of the revetment above the SWL, it was proposed to use a level halfway the SWL and the 2% run-up level.

$$R_{u2\%} = 1.65 \, \xi_{m-10} H_s \not> 4.0 - \frac{1.5}{\sqrt{\xi_{m-10}}} H_s$$

$$N = \rho_s g D B_y (\tfrac{1}{2} R_{u,2\%} + z_{\text{SWL}} - z)$$
with $\tfrac{1}{2} R_{u,2\%} + z_{\text{SWL}} \not> z_{top}$

Eq. 5.29

In the vicinity of the wave action the water pressures in the joints reduce the effective normal force. This occurs for the run-down case as well as for the wave impact more or less in the most severely attacked joint location. Before group failure caused by bending failure can occur the bending resistance must become too low in three cross sections (see Figure 3-10). If the normal force and hence the bending resistance drops in one cross section, redistribution can still lead to sufficient capacity of the revetment beam. Similarly shear failure is not the immediate consequence of drop of axial compression on one side of a revetment element.

An unknown factor in this respect is whether the dynamic load caused by filter pressures is synchronous with the reduction of resistance caused by joint pressures. In reality the pressure waves will come after each other, but will likely have overlap in time, as analysed in section 5.3.4. The joint pressure peak in adjacent cross sections will also not be exactly in the same time. It can therefore be explained that reduction of the normal force by subtracting the peak value of the joint pressure is too conservative. In Figure 5.12 it is shown that the joint pressures in the two relevant cross-sections are approximately 0.8 and 0.2 times p_{max}, e.g. on average 0.5 p_{max}. Through calibration with the experiment results it was found that a

reduction using a value of $r_6\,p_{max}$ with $r_6 = 0.25$ gives a good match with the resistance that was found in the experiments. For the run-down case a value r_7 of 0.10 was found.

In order to avoid that the normal force becomes very low or negative, a minimum value of the revetment weight corresponding to the vertical dimension of 2 to 3 times D is proposed for the 1:3 and 1:4 slopes. This proposal was confirmed by calibration results. Since this minimum value is related to the initial value of the transverse normal force (see section 3.1.7) and is dependent on the ability of the revetment to exceed the friction forces and to slide the following relation is proposed. The vertical dimension z/D corresponding to the minimum normal force can be found at the intersection with the line $y = 5 - x/3$ in Figure 6–6.
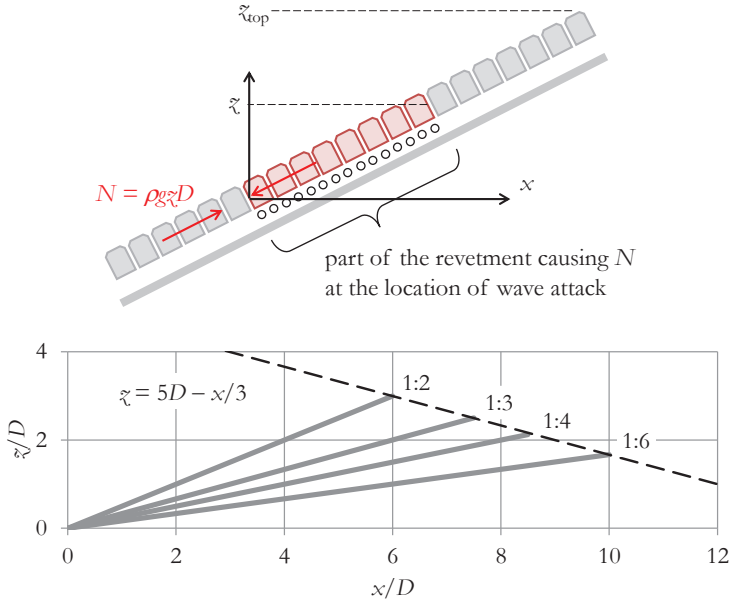
Figure 6–6   **Minimum values of the transverse normal force N_x dependent on slope angle**

This leads to the following expressions for the quasi-static normal force during the moment of wave attack.

For the wave impact case

$$N = \rho_s g D B_y (\tfrac{1}{2} R_{u,2\%} + z_{SWL} - z) - r_6 p_{max} DB_y \not< c_{Nmin}\,\rho_s gD^2 B_y \qquad \textbf{Eq. 6.3}$$

For the run-down case

$$N = \rho_s g D B_y (\tfrac{1}{2} R_{u,2\%} + z_{SWL} - z) - r_7 \rho g \phi_b DB_y \not< c_{Nmin}\,\rho_s gD^2 B_y \qquad \textbf{Eq. 6.4}$$

with $r_6 = 0.25$
$r_7 = 0.10$
$\tfrac{1}{2} R_{u,2\%} + z_{SWL} \not> z_{top}$

$$c_{Nmin} = \frac{5}{1 + \tfrac{1}{3}\cot\alpha}$$

The model characteristics and assumptions are summarised in Table 6–1.

Table 6–1   Summary of model characteristics

	Ultimate limit state damage c/d	Serviceability limit state damage a
Design water level	1/10.000 yr and below	1/100 yr and below
Hydraulic conditions H_s and T_{m-10} based on:	1/100 yr or 1/1000 yr including effects of persistency	1/ 10 yr or 1/50 yr
Indication of number of waves (based on coincidence with peak water level in tidal area's)[243]	1000	1000
Factor on $H_{2\%}$	1.15	1.0
Model for bending moments / shear forces	Confined beam	Beam on elastic foundation
Single element failure	Allowed, if residual resistance is guaranteed	Not allowed
Resistance model	Based on $N_y/N_x = 0.5$ (after full development of N_x)	Based on $N_y/N_x = 1.0$
Effect of ratio B/D	$r_2 = 0.8$ to 1.0, see Figure 6–4.	$r_2 = 0.8$ to 1.0, see Figure 6–4.
Effect of strict alignment in rows	$r_2 = 0.8$ in case of no overlap in B_x 1.0 in case of overlap	$r_2 = 0.8$ in case of no overlap in B_x 1.0 in case of overlap
Contribution of n_y for concentrated wave impact loads	yes $r_3 = 0.75$ (r_3 is the reduction factor on the load effect in x-direction)	yes $r_3 = 0.67$
Additional effect of resistance due to n_y for infinite load	$r_4 = 1.0$ in case of no overlap in B_x 1.1 in case of overlap	$r_4 = 1.0$ in case of no overlap in B_x 1.15 in case of overlap
Bending moment	$e = 0.4\,D$, assuming a flat element-to-element contact or a joint fill with depth d of 0.9 D and a contact zone βz_c of 0.1D, $e = \frac{1}{2} \times 0.8\,D$ (see Figure 3-11 and Figure A-39)	$e = 0.2\,D$
Friction factor	$f_{fr} = 0.6$	$f_{fr} = 0.6$
Normal force	Revetment weight from impact point to halfway run-up point, minus peak joint pressure reduced to $r_6 =0.25$ times the peak pressure above the slope	Same, with $r_7 =0.10$
Minimum normal force	Dependent on slope angle, with 2 to 3 $\rho_s\, g\, D^2$	

---

[243] Based on a 3 hr duration of the combination of the peak of a storm and a surge water level combined with high tide. In cased with constant water level a duration of 6 to 12 hrs might be more realistic.

6.2 Analysis of outcomes of flume test experiments

6.2.1 Available test data

The collection of large scale flume tests includes a total of 340 experiments. Although many different types have been tested the number of tests seems sufficient for an analysis of trends. The majority of the tests have been executed in the Delta flume in Marknesse in the Netherlands. This facility is since 2015 replaced by a new Delta flume located in Delft. A small number of tests are executed in the large wave flume in Hannover, Germany. The tests are reported in literature in numerous reports. Some reports include detailed measurements of filter pressures, permeability properties and even pull tests.

During a number of years (in the 80s and 90s) the study design of the Delta flume investigations included the idea of relating the resistance of the revetment in the flume to the revetment in reality through linking pull tests. The pull tests were unfortunately executed with too small frames[244] and hence generally large pull-out values were found. Those pull test results are not a good basis for comparing tests conditions with the condition in the outside world. During the experiments in Hannover pull tests were performed also. They were executed with assistance of an overhead crane, which is ideal from the perspective of not disturbing the revetment.

Moreover, especially for the row-oriented concrete block type elements arching in cross direction of the flume can be observed on the images in the reports[245]. This does give too favourable results in comparison with the real condition, since there is no reason that arching in cross direction should be limited to a dimension of 5 m, being the cross dimension of the flume. Ideally the revetments in the flume should not gain stability from the flume walls at all.

The damage observed in the flume tests follows a classification system with a to d (see Table 4-4). The damage descriptions of experiments in the various have been re-assessed, which has resulted in some changes of damage categories. The damage category a is reserved for damage according to the criteria in Table 4.4. In many flume tests the wave height was increased in small steps. In case the largest wave height preceding the step which caused damage was chosen, a damage category 0 is deemed more appropriate. Also single element failures are here indicated as c1 or d1, rather than the general categories c and d. The complete list of flume experiments is included in Annex I. The list is supplemented with a calculated value of the leakage length. Where available this calculated length was compared with measured values of the leakage or with measured values of the permeability.

Table 6–2   Legend of Figure 6-7 etcetera

	□	🟩	🟨	🟧	🟥	+	+
Damage category	0	a	b	c	d	c1	d1
Nature of damage (for more detailed definitions, see Table 4-4)	No damage	Start or revetment damage	Revetment damage	Start of revetment failure	Revetment failure	Partial single element failure	Complete single element failure

[244] A.M. Burger, *Sterkte Oosterscheldedijken onder geconcentreerde golfaanval* (WL|Delft Hydraulics report M2036, 1985), G.M. Smith, J. Wouters, and M. Klein Breteler, *Grootschalig modelonderzoek naar stabiliteit van taludbekledingen - Meetverslag van Deltagootonderzoek* (WL|Delft Hydraulics report H3272-2, 2000)
[245] Ibid.

6.2.2 Limitations

The standard presentation of the revetment stability results pictures the stability number $H_s/\Delta D$ against the breaker parameter ξ. As mentioned earlier (see Section 4.4.4) the flume tests have limited variation in slope angle. For the concrete blocks there are tests on 1:3, 1:3½ and 1:4 slopes, for the concrete column tests only 1:3 and 1:3½ slopes. From the theory it is obvious that for steeper slopes the normal force can easier develop itself to larger values and hence has a larger contribution to the stability. It therefore makes sense to split the dependency on ξ into dependencies on the slope angle α and wave steepness s_0. For the concrete blocks we can observe a trend suggesting that steeper slopes have more stable revetments (see Figure J-1). The plots against wave steepness s_0 give the same image as against ξ.

Other important limitations of the Deltaflume experiments are the in-plane stress state in longitudinal direction (cross-direction of the flume) and the always stiff and strong toe structure which is very favourable for the build-up of in-plane force in transverse direction.
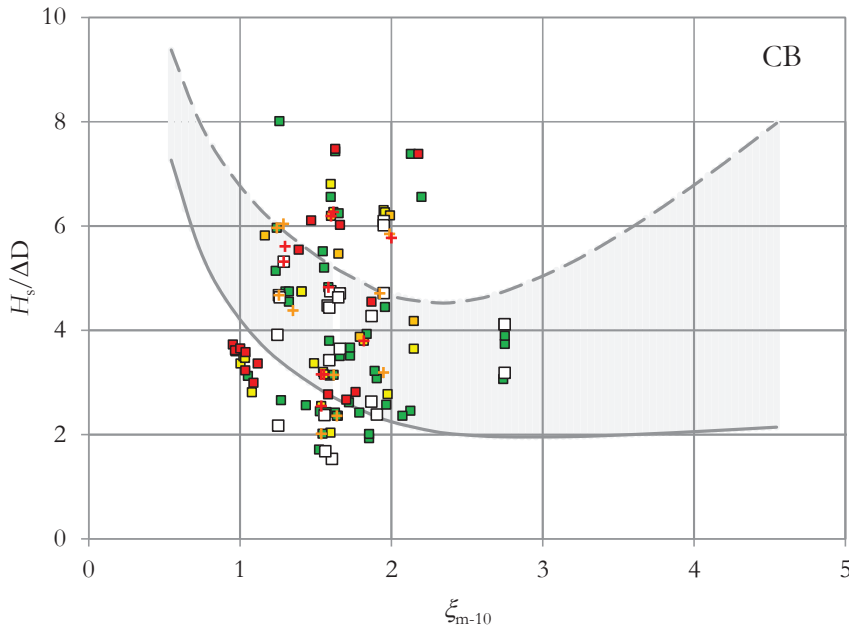
Figure 6–7   **Flume experiment results for concrete blocks CB plotted against breaker parameter, both with VTV design chart of Figure 4-1**
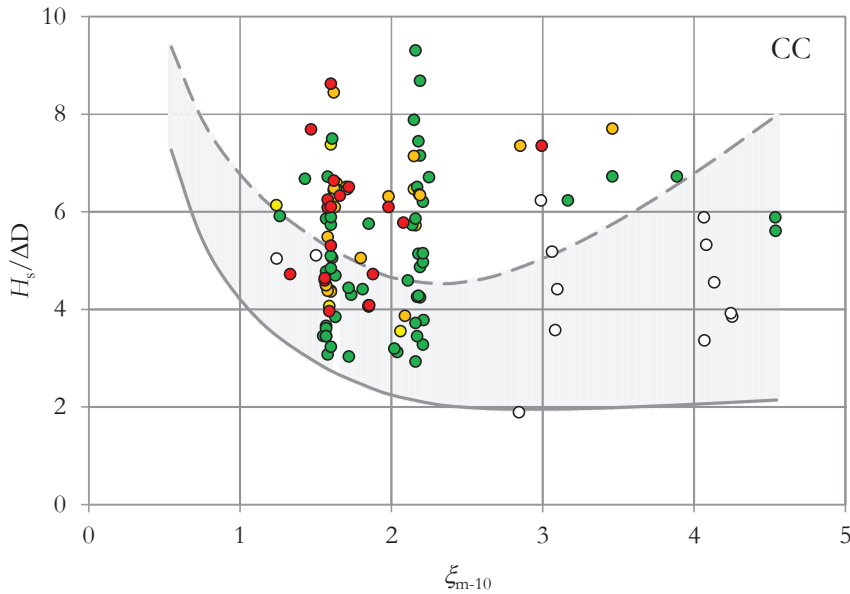
Figure 6–8 Flume experiment results for concrete columns CC plotted against breaker parameter, both with VTV design chart of Figure 4-1

6.2.3 Trends and dependencies

The total population of flume experiments is so large that it might be interesting to analyse the data for trend before we compare the data with model results in section 6.2.3. Trends and dependencies are investigated for the groups concrete blocks (CB) and concrete columns (CC) which represent the majority of the experiments. The results are presented and discussed in Annex J. A summary is given below.

Dependency on slope angle

The group CB includes experiments on 1 : 3, 1 : 3½ and 1 : 4 slopes. The share of 1:4 slopes is small. Nevertheless a clear tendency that larger stability numbers are associated with steeper slopes was found (Figure J−1). In the multiple regression analysis the dependency on the slope angle $\cot \alpha$ is noticeable bit statistically not very strong.

Dependency on aspect ratio D/B, flat or tall element shapes

When plotted against the height/width ratio D/B_x of the elements (see Figure J-2) it is observed that taller blocks and columns are more stable. The difference in stability number for a D/B_x of 0.5 compared to 2 is a factor 0.6 for the blocks (0.8 when we treat the d1 damages as d) and 0.7 for the columns. Mind that the D/B ratio is not the primary properties of distinction between columns and blocks, but the row-orientation and the type of joints. An interesting observation is that single element failures seem to be related with the D/B ratio. This is in line with the beam model theory. Structures with flat elements with small D/B ratios tend to fail as a group. Tall elements can potentially fail as a piston.

The variable D/B keeps statistical significance in the multiple regression analyses in two of the four sub-groups.

Dependency on the leakage length

Plotting the variable $H_s/\Delta D$ against the leakage length gives for the blocks a wide range, and for the columns a smaller range. This is logic due to the hydraulically more open top-layer of the column revetments. For both groups a clear trend to lower stability numbers with increasing leakage length can be noticed. The leakage length remains a statistically significant in the multiple regression.

Dependency on normal force or position on the slope

The dependency of the variable $H_s/\Delta D$ on normal force can be found by looking into the potential for normal force above the wave impact point of the experiments. For the wave impact point we used the formula:

$$z_{\text{imp}} = z_{\text{SLW}} - (0.4 + 0.55\xi - 0.0344\xi^2 - 0.7)\,H_s \qquad \textbf{Eq. 6.5}$$

A dependency was found, for the groups CB and CC, for the damage category a as well as for d. The experiment data had to be re-analysed because it was not always clear what should be assumed as the level of the (unsupported and not axially loaded) top edge of the revetment z_{top}. The two results of an experiment with re-used Hydroblocks and of an experiment on a Basalton slope purposely without joint fill were excluded from the regression.

In the multiple regression analysis the dependency on the position on the slope is strong in only one sub-group and noticeable in one other. We have the impression that the differences in the various types of revetments are large and disturb clear trends in the total group. Also the tested range for the columns revetments is not very large.
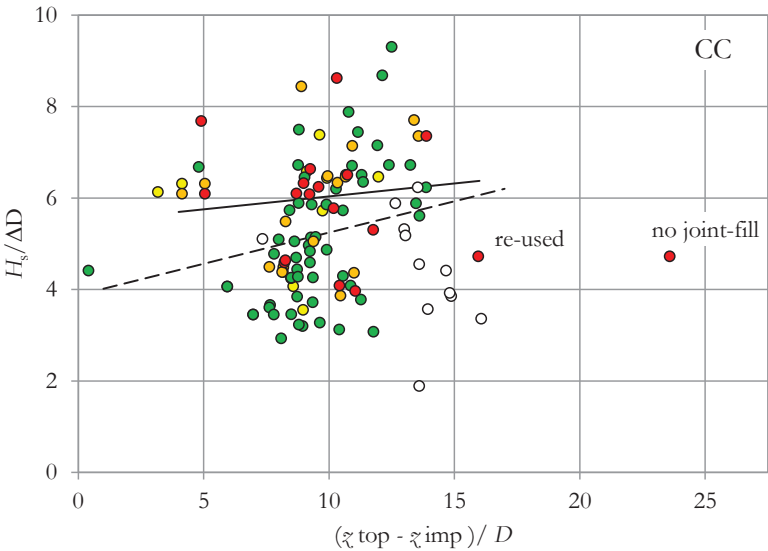
Figure 6–9   Flume experiment results for CC plotted against the position of wave impact relative to the top of the slope, with continuous trend for red and dotted for green markers
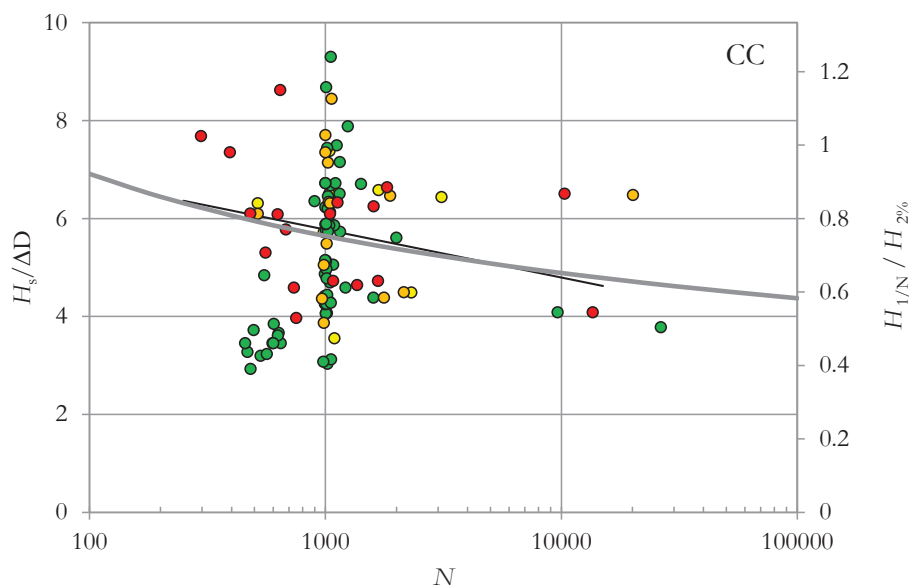
Figure 6–10   Flume experiment results for CC plotted against number of waves **N**

Dependency on the duration of the wave loading

The dependency on the number of waves is plotted in Figure 6–10 for concrete columns. See Figure J-5 for concrete blocks. For both groups experiments have been done with long durations, although the majority of the tests is around $N = 1000$. The objective was to test the performance under repeated wave loading which might be dependent on fatigue or mechanisms of gradually propagating damage. When irregular wave series are extended in time, the probable maximum wave run-down and probable maximum wave impact might be related with the largest wave height via the Rayleigh distribution. In most of the wave effect formulas the value of $H_{2\%}$ is the reference value, e.g. Eq.'s 5.29, 5.30, 5.31 and 5.38. We therefore plotted the ratio $H_{1/N}/H_{2\%}$ as a function of N on the secondary access in Figure 6–10. The intersection of the trend line for the d-damages and $N = 50$ (2%) was found at $H_s/\Delta D = 7.5$ for the concrete columns.

It can be noticed that the falling trends with larger number of waves follow the effect of the highest probable wave quite nicely, which tells that the increased probability of failure during a longer exposure to waves is purely related to the probability of a higher wave in the larger series. This result does hence not indicate strong effects of decay of resistance under long duration loads.

For the evaluation of the experiments for calibration purposes in section 6.2.3 the wave loads are calculated with a wave height H_s corrected with:

$$\frac{\sqrt{-\ln((1/N)^2)}}{\sqrt{-\ln((1/1000)^2)}}$$

Eq. 6.6

Element shape or revetment type

The variety in types of elements is especially large for the columns. An analysis of the average stability number per damage category per element type gives the results shown in Figure 6–11.[246] The error-bars indicate the standard deviation and the indicated number is the number of experiments.

It can be noticed that the curves are quite flat. From the moment that first damage occurs the structure does not have a significantly higher resistance before failure occurs. In other words: the structure is very brittle. Plotted as fragility curves, with damage versus load, the curves would be very steep.
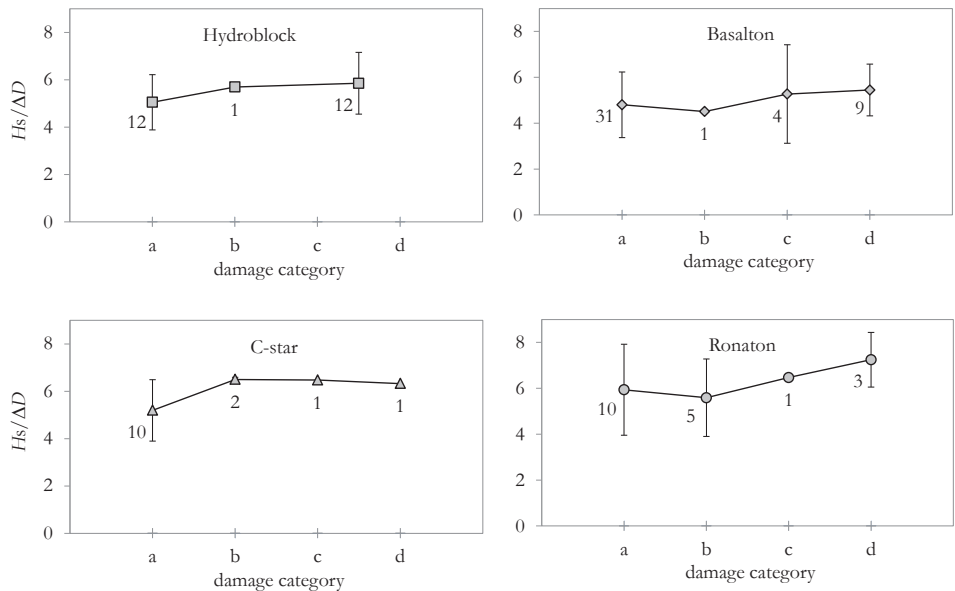
Figure 6–11   **Damage as a function of $H_s/\Delta D$ from flume test results for CC per element type**

It is difficult to compare the types and draw reliable conclusions on stability per type based on these graphs, since the other variables influence the results. Most Basalton tests have been done on 1:3 slopes, and most Hydroblock tests on 1:3½ slopes for instance.

Multiple regression was performed on the CC set including the dependency on the various element types. The types are included in the regression analysis labelling them as a Boolean variable. By doing that the conclusion about significance of the other variables changes a bit. For instance for the category a-damage the slope angle and the number of waves become significant, which they are not in Table J-3 which is based on the sub-group category a-damage for all revetment types.

---

[246] The Hydroblock tests for c and d are merged into one group, because the c damage appeared on average at a higher stability number than the d damage. This might be due to a shift in definition over time.

Amazingly the high *p*-value that was found in the analysis including the type as a variable indicates that the probability of each individual type being an independent variable within the test population is low.

There are calculated average differences in stability numbers amongst the types, though. Based on the results three groups can be distinguished: (i) Hydoblocks and Pit-polygon, (ii) Basalton and C-star and (iii) Ronaton, in order of increasing stability.

<u>Findings</u>

From observations of dependency on individual variables some interesting conclusions could be drawn that were implemented in the model approach in this thesis. Amongst them are the dependency on the leakage length, on the aspect ratio D/B, the position on the slope (explained by the potential for normal force), the slope angle and the revetment type.

The reason that not all of those dependencies remain strong in a multiple regression analysis is that the nature of the structure is so much inherent variability that as soon as all variables are taken into consideration the sub-groups become too small the inherent variability becomes dominant. As can be noticed in the figures, the underbound of stability number above which damage may occur increases with increasing damage category. The scatter is however so large that there is a significant overlap. Many experiments show category a damage above the level the other experiments already show category d damage. This large scatter disturbs a proper statistical trend analysis.

Table 6–3   **Summary of scatter in experiment results**

	$H_s/\Delta D$ for category a 15%-85% CI range	$H_s/\Delta D$ for category d 15%-85% CI range	Factor between 15% values of a and d	Probability of an individual a-result higher than an individual d-result	% of experiments in category a above the 15% value of category d
Basalton	3.4 .. 6.2	4.3 .. 6.6	1.28	35%	63%
Hydroblocks	3.9 .. 6.2	4.6 .. 7.2	1.17	46%	67%
Ronaton	4.0 .. 7.9	6.1 .. 8.4	1.53	57%	48%

Because of the large scatter in the milder damage categories the calibration in section 6.3 is mainly focussed on category c and d damage.

6.3 Calibration of design formulas with flume tests

6.3.1 *Selection of experiments*

For calibration of the model a selection of the experiments is used. Throughout the years many types are tested with variations of revetment type parameters and mechanical boundary conditions. The selection is based on the following criteria:

- Only concrete clocks and concrete columns on permeable filter layers are included. Natural columns (like Basalt) are treated separately.
- Experiments with horizontal transition structures and/or with the top of the revetment z_{top} below or less than one element thickness D above the still water line are excluded from the calibration.[247]

---

[247] Ibid., J. Wouters, *Taludbekledingen van gezette steen - Eindverificatie Deltagoot onderzoek* (WL|Delft Hydraulics report M1795 deel XXIII, 1991)

- Double top layers are excluded.[248]
- The experiments especially designed for testing revetments above the SWL in (Van Steeg & Klein Breteler, 2009) are excluded. Although the top of the revetment is well above SWL, the elements of the top row are fixed to and restrained by the concrete slab that covers the remainder of the slope. This method of fixation is not included in the model.
- Also a selection of tests from the older reports with experiments on thin rectangular blocks are excluded. Those experiments were in many cases executed with two types, each in a 2.5 m wide strip. The results show a large scatter, probably due to effects of cross direction of the flume on the stability.

6.3.2 *Reliability framework*

The reliability of the structure to remain in function is determined by the probability of occurrence of extreme loads and by uncertainty in resistance. The loads are mostly defined in terms of a probability of exceedance per year. Service life and the reference period or return period of the load become part of the equation then. For revetments these periods deviate considerably, being 25/50 yr and 10.000 yr respectively. For regular structures that are evaluated with semi-probabilistic methods those two periods are less different.

Table 6-4   Indicative key reliability parameters of revetment compared to other structures

[yr] or [1/yr]	Service life traditional	Present service life / design life	Design load return frequency	Required failure P_f	Failure P_f given design load
Building or bridge structure	100 to 500	50 or 100	10^{-2}	10^{-4}	10^{-2}
Revetments according to VTV-2007	5 to 25	25 to 50	10^{-4}	10^{-5}	10^{-1}
Revetment recommended		50	water level: 10^{-4} waves: 10^{-2}	10^{-4}	resistance to waves: 10^{-2}

Presumed that required failure probability is 10^{-5}, a design load in terms of water levels with a return frequency of 10^{-4} is a common choice.[249] The conditional failure probability should in that case be 0.1. This is also important because evaluation of overtopping using a lower water level and a lower probability of overtopping violates the physical meaning and the geometrical implications of a higher water level.

For the definition of the design value of the wave height needed for revetment design it is not recommended to extrapolate this estimation to a probability of 10^{-4}. A reliable verification would then be complicated by the high coefficient of variation of the resistance. The application of semi-probabilistic evaluation is bound to a maximum of the difference between the standard deviations of the distributions of the load and the resistance.[250] It is better to accurately estimate for instance a 1/100 yr wave height and prove reliability of a conditional failure probability of 0.01, than to estimate a 1/10.000 yr wave and to prove a 0.1 or e.g. 0.5 failure probability against that higher wave. Given the high coefficient of variation

---

[248] R. 't Hart and G. Wolters, *Oude steenzetting overlagen met zuilen op uitvullaag* (Deltares-report 1205571, 2012)

[249] Joint probability of high water levels and hign waves should be taken into consideration, although there is likely a strong correlation is due to the wind as a primary cause and in case of depth-limitation of the waves.

[250] Eurocode EN 1990 Basis of Design or ISO 2394 General principles on reliability for structures

the 10^{-2} lower bound of the resistance has a more important physical meaning than the average of the resistance. A side issue may be that the effects of very high (10^{-4}) waves fall outside the tested range of waves and revetment thicknesses.
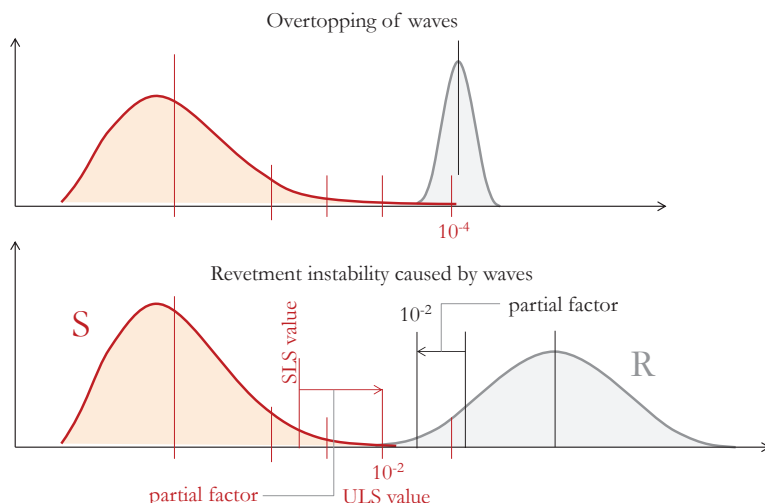
Figure 6–12   **Scheme of uncertainty in load and resistance of revetments and effect of partial factors in case of FORM analysis**

In this thesis we have considered conditional probability of failure given a certain design condition: 1000 irregular waves, characterised by a water level h and wave parameters H_s and T_p or T_{m-10}

Consideration of the length effect on revetment resistance is not in the scope of this study. In order to account for the effect that more cross sections of a dike can fail the target β–factor needs to be increased with 10%.[251] Apart from this practice it should be realised that if the risk-and-cost-based probabilistic design approach is applied in two further identical cases with different dike lengths, without a norm frequency or provided that norm frequencies covering the individual risk and the group risk are met, the length effect could only lead to a lower safety level per cross section. The economically affordable investment must be divided over more dike length, which will lead to a lower amount of money and a lower safety per cross section.

6.3.3   Calibration of parts of the model

In the model we have aimed at an adequate description or methodology for aspects or sub-systems that minimises uncertainty. In a separate study in order to calibrate the software tool STEENTOETS 2009, we have looked into the parameters that are dominant in the scatter and the inherent uncertainty in the model. During some of the flume experiments many parameters have been recorded.

---

[251] *Leidraad Kunstwerken* (TAW report L15, 2003)

DESIGN OF PATTERN-PLACED REVETMENTS

It was found that the variability of permeability properties and the measured wave impact pressures are a dominant cause for the finally observed deviations and between the model outcomes and the experimental results.

The variation in permeabilities and the calibration of the model formulas for the filter and top-layer permeability are discussed in section 3.2. The calculated ratio $\sqrt{(k/k')}$ is on average 25% larger than the measured values, which is safe. A larger leakage length creates higher peak pressures in the filter and a larger area where the filter pressures are present.

The wave impact pressure has been studied by many researchers. This has provided accurately measured data that can be used for calibration of the model formulas. The model formula in STEENTOETS was developed using small scale and large scale testing and therefore it was deemed appropriate to include a scale factor in the formula for the water head.

$$\phi_{k,2\%} = H_s(30 - \xi_{\phi} / \tan\alpha)\left(\frac{\rho_w g H_s^2}{\sigma_w}\right)^{-0.2}$$

with $\left(\dfrac{\rho_w g H_s^2}{\sigma_w}\right)^{-0.2}$ = the Weber scale factor

with σ_w = the surface tension for water [N/m]

Eq. 6.7

This formula was evaluated with measured values of $\phi_{k,2\%}$ in the calibration report and it was found that the match was not perfect, see Figure 6–14. In the summary report on improvements of STEENTOETS[252] a factor for the influence of the berm is given. Although less ideal, it is recommended to correct the measured value with a influence factor of the berm. This factor was found by comparing experiments with and without an underwater berm. The experimental values of experiments with a berm are corrected by dividing them with a factor (larger than unity), thus obtaining 'experimental' values that can be compared with other experiments without a berm and with models without a berm. This approach was also followed in Delta flume analysis report[253] in 2000. By then smaller berm factors were found. If we use $1 + 0.1 \, (h_b/H_s - 2)^2$ with h_b is the height of the berm under water, the larger experimental values are reduced, as can be seen in Figure 6–15.

---

[252] M. Klein Breteler, G.C. Mourik, and M.C.J. Bosters, *Stabiliteit van steenzettingen bij golfaanval, Samenvatting onderzoeksresultaten 2003 – 2013* (Deltares report 1208045-016 for RWS-WVL, 2014)

[253] Smith, Wouters, and Klein Breteler, *Grootschalig modelonderzoek naar stabiliteit van taludbekledingen - Meetverslag van Deltagootonderzoek*
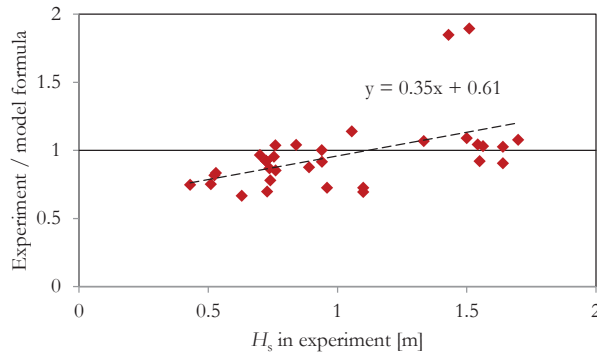
Figure 6–13   Calibration of scaling effect according to Eq. 6.7 as implemented in STEENTOETS

The adequateness of the scaling for the wave height can be tested by plotting the ratio of experiment/model values against the wave height H_s. We conclude that the model formula Eq. 6.7 reduces the calculated values progressively with increasing H_s, resulting in an increase of the ratio experiment/model. The inclination of the trend corresponds to a factor 1.6 between $H_s = 0.4$ and $H_s = 1.65$. The Weber scaling with $(H_s^2)^{-0.2}$ corresponds to a factor 0.6. Without the scaling there will be almost zero dependency on the wave height.
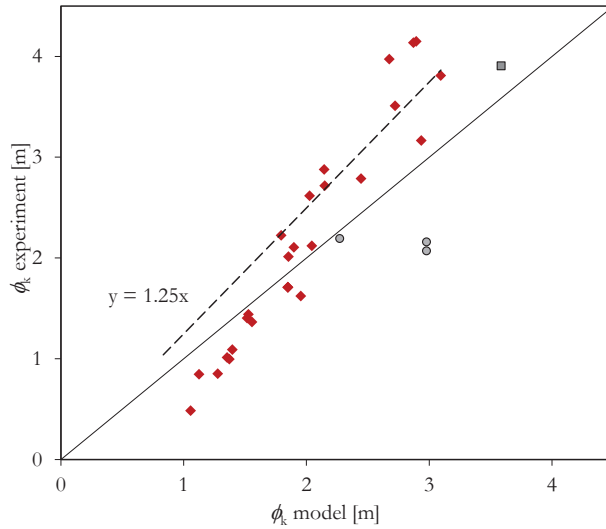
Figure 6–14   Calibration of wave impact formula in STEENTOETS
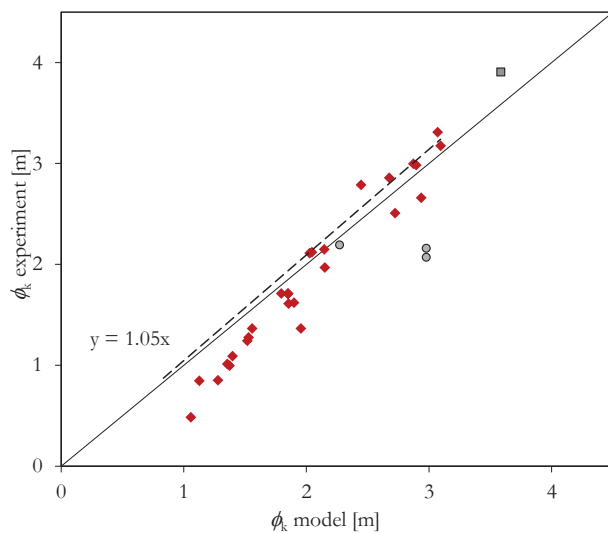
Figure 6–15   Calibration of wave impact formula in STEENTOETS, corrected with berm formula 2014
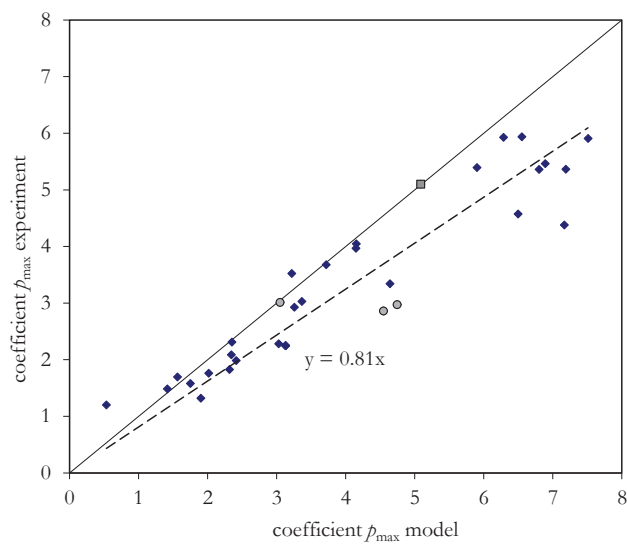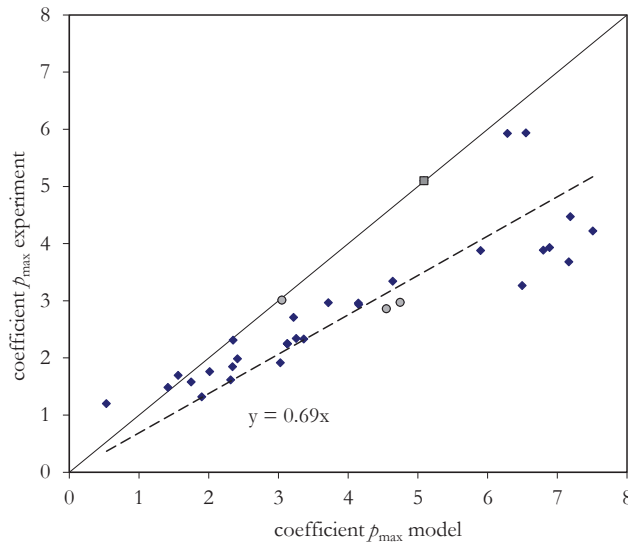
Figure 6–16   Calibration of wave impact formula in this thesis, without and with correction for berm

Similar the design formulas for breakwater armour we have not included a scale factor in the design formula for the wave impact used in this thesis (refer to Eq.'s 4.23 to 4.26). Calibration of this formula is shown in Figure 6–16. It can be noticed that the scatter without a correction for the berm is smaller. The experiments in Delft (blue markers) are also nicely in the range of the German tests (grey markers) as reported by Führbötter and Grüne (see Table 5-5). The match of the formula and the experiments corrected for the berm effect are less nice, but still safe. The calculated variation coefficient is 0.25. The probability of exceedance of the model formula is 0.07.

From Figure 6–17 is can be concluded that there is no reason for scaling in the range of the scale of the Delta flume tests and beyond. The discussion on scaling can be interesting and important for the future where higher flood levels would potentially allow higher waves. Several authors[254] suggest on basis of theory of aeration of the water and on basis on laboratory experiments and field measurements that the pressure reducing effect of aeration levels out to a constant pressure reduction factor. Increasing air content and increasing violence of the impact (in our case increasing breaker height and therewith increasing falling water velocity) does further reduce the peak pressure. Increasing wave height and therewith increasing falling height still increases the pressure, since the reduction factor for aeration becomes constant.

With the larger scale of the new Delta flume scale effects can be studied for a larger range.

---

[254] Bullock et al., "The influence of air and scale on wave impact pressures" and D H Peregrine and L Thais, "The effect of entrained air in violent water wave impacts," *J. Fluid Mech.* 325:1996 (1996): 377–397; Giovanni Cuomo, William Allsop, and Shigeo Takahashi, "Scaling wave impact pressures on vertical walls," *Coast. Eng.* 57:6 (2010): 604–609
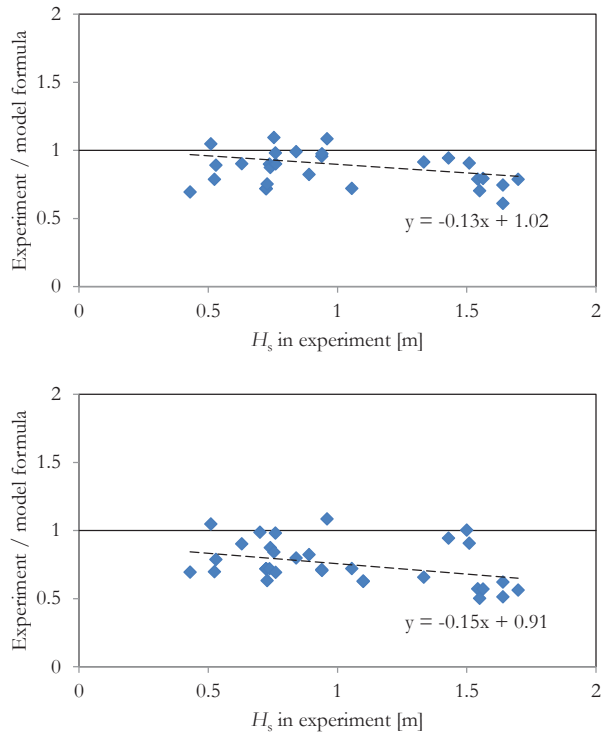
Figure 6–17   **Validation of p_{max} neglecting scale effects, without and with correction for berm**
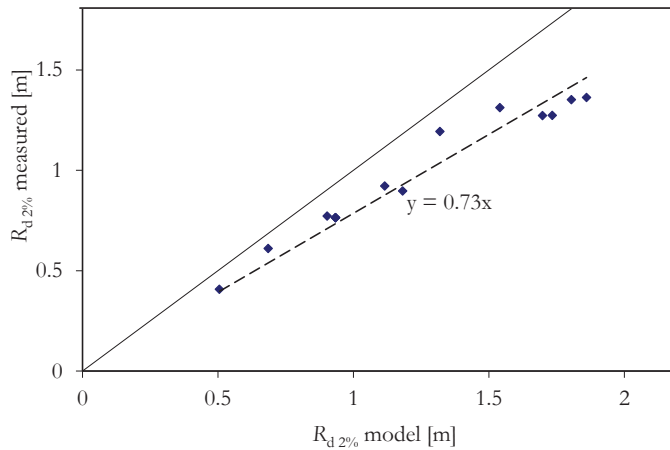
Figure 6–18   **Validation of R_d formula, with Delta flume tests without a berm**

Similar validation of measured parameters can be made for the breaker height h_b or ϕ_b, and the run-down point R_d. Performing this with the dataset used for the calibration study for STEENTOETS, lower measured values were found for larger wave heights. Those appear to be

related with the effect of the berm that was present in a number of tests. Since no berm factor is known, we have excluded the experiments with a berm. The remainder of the data points nicely compares with the model formulas, as can be seen for the run-down point R_d in Figure 6–19. The result is independent of the breaker parameter ξ_{m-10} and has a slight dependency on the wave height H_s.

$$y = -0.11x + 0.90$$
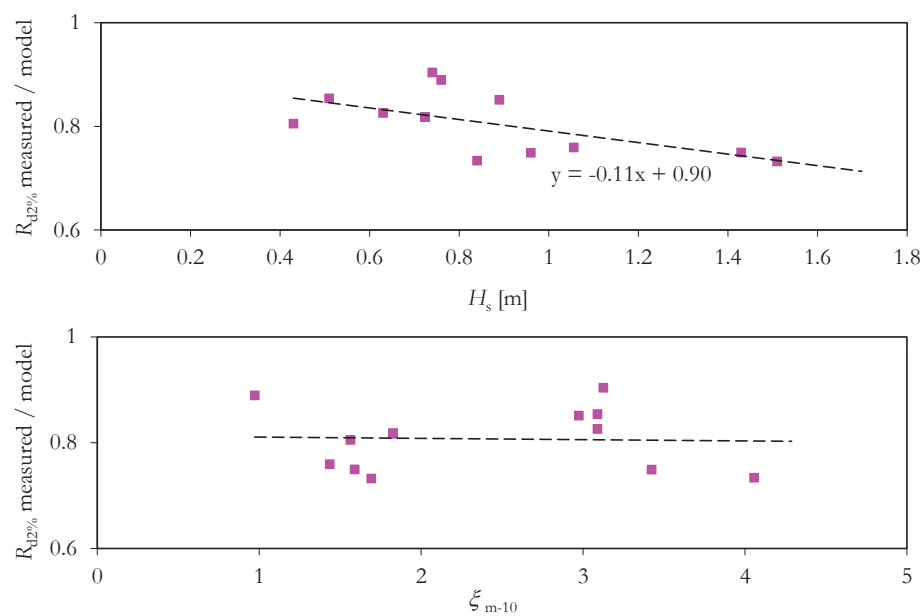
Figure 6–19   **Dependencies of the ratio measured / model for the run-down point $R_{d,\,2\%}$**

The indicative variation of the various parameters is indicted in the table below.

Table 6–5   Indicative coefficient of variation of the various parameters of the model

	Parameter	Type of distribution	Coefficient of variation	Remark / source
P	Top layer thickness D	normal	2%	
P	Specific weight top layer material ρ_s	normal	2%	
P	Open area (column types) A	normal	20%	Refer to section 3.4
	Buoyant distributed weight ΔD	normal	2%	For hydraulic resistance area $(1 - A)$
P	Joint width (block types)	normal	50%	**)
P	Filter grain size D_{f15}	Normal	20%	
P	Filter porosity n	Normal	10%	Refer to NEN 9997-1
P	Filter layer thickness b	Normal	20%	
V	Filter layer permeability k	Normal	20%	Refer to section 3.4
V	Filter layer permeability k'	Lognormal	20%	Real values usually higher than theoretical values, refer to section 3.4
	Leakage factor Λ/D	Lognormal	20%	Real values usually smaller than theoretical values
P	Slope angle $\cot\alpha$	Normal	5%	
P	Water level		5%	Assumed accuracy of prediction/design value
P	Wave height Hs	Normal	5%	Assumed accuracy of prediction/design value
P	Wave period T_{m-10}	Normal	5%	Assumed accuracy of prediction/design value
P	Wave steepness	Normal	5%	Given prediction/ design value
P	Duration, number of waves N	Normal	20%	
P	$H_{2\%}/H_s$	Normal *)	10%	***)
P	$H_{0.01\%}/H_s$	Normal *)	20%	****)
V	$\phi_{b,2\%}/H_s$	Normal *)	10%	Correlated with $R_{d,2\%}/H_s$
V	$p_{max,\ 2\%}/H_s$	Normal	20%	
V	Run-down $R_{d,2\%}/H_s$	Lognormal	10%	Change that R_d is larger is small given the depth limitation, correlated with $\phi_{b,2\%}/H_s$
P	Friction factor f_{fr}	Normal	10%	Annex E
P	Soil properties $c/c_u/\varphi$ for toe resistance		10%	Refer to NEN 9997-1
	Toe resistance	Lognormal	20%	Smaller than soil properties because of uncertainty in overburden mass and depth of piles, and pile resistance
	Toe stiffness	Normal	20%	Refer to Annex H
P	Initial normal force	Lognormal	50%	Lognormal because of cap by zero normal force, refer to Annex F
P	Normal force after movement by wave action	Normal	20%	Based on stiff toe structure and relatively short slope, refer to Annex A.1
		Normal	50%	Based on weak toe structure and relatively long slope, refer to Annex H
V	$H_s/\Delta D$ in flume tests	Normal	25%	Refer to section 6.3
	$H_s/\Delta D$ in reality	Normal	35-40%	

P = primary
V = validated

6.3.4   Model performance

The model described in section 6.1 uses load input (wave impacts and water head differences) based on parameters of incoming waves, and parameters of the slope. Combining this input with the resistance model leads to stability numbers that can be plotted in the design charts in which the flume experiments were presented. Examples for a certain structure are shown in Figure 6–21 and Figure 6–20. In those examples a curve of model results is presented based on a range of incoming wave steepness values. The procedure is that a wave height H_s at which the revetment becomes critical in ULS is calculated. This curve is plotted together with the failure data of all selected failure cases of the concrete blocks and concrete columns respectively, also the ones with a different leakage length, different D/B etc. The figures nevertheless give a good impression of the model performance. The dominance of the inverted wave impact curve, shown in Figure 5-48 and represented by Eq. 5.42 is clearly visible. Especially the narrow range of the breaker parameter where this load case has an effect is important for a good match with the higher stability numbers found in the experiments with $\xi_{m-10} < 1.0$ and $\xi_{m-10} > 2.2$. This is considered an important improvement compared to earlier models.
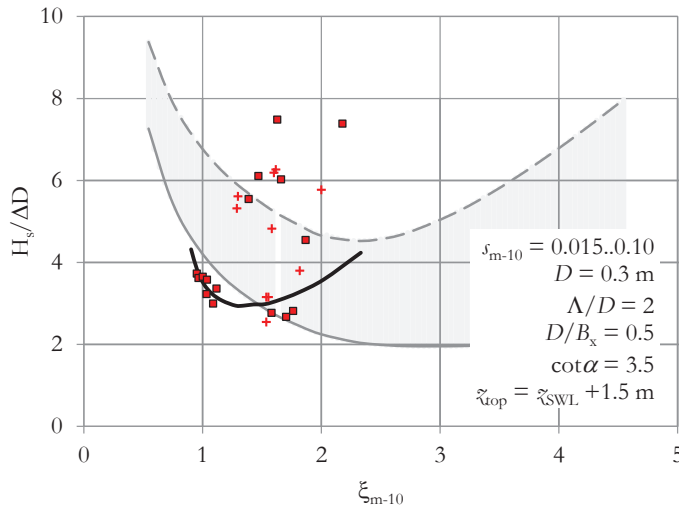
Figure 6–20   **Comparison of experiments on CB and model formula for damage cases d plotted in the VTV design chart of Figure 4-1**
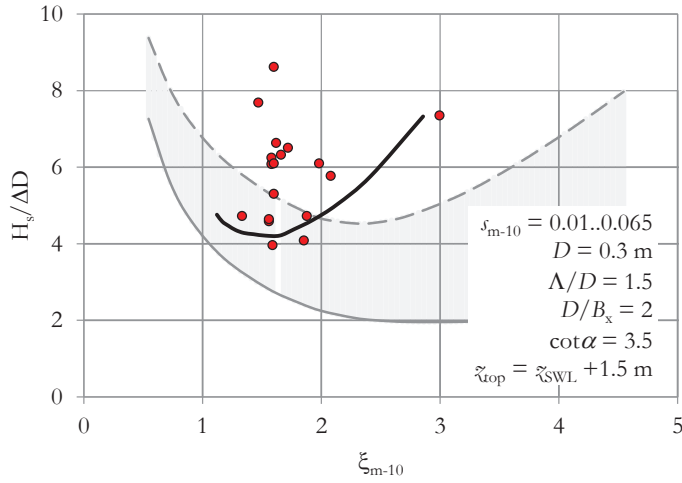
Figure 6–21 Comparison of experiments on CC and model formula for damage cases d plotted in the VTV design chart of Figure 4-1

6.3.5 Model calibration results

In this section the model calculation results are systematically compared with the selected experimental results. The results of the comparison are plotted as markers for the experimental $H_s/\Delta D$ value against model $H_s/\Delta D$ value for each reported and selected experiment. The markers above the line $y = x$ are an indication that the model is safe. In case the markers show a large variation the results are subject to a large variability and/or the model is not very accurate.
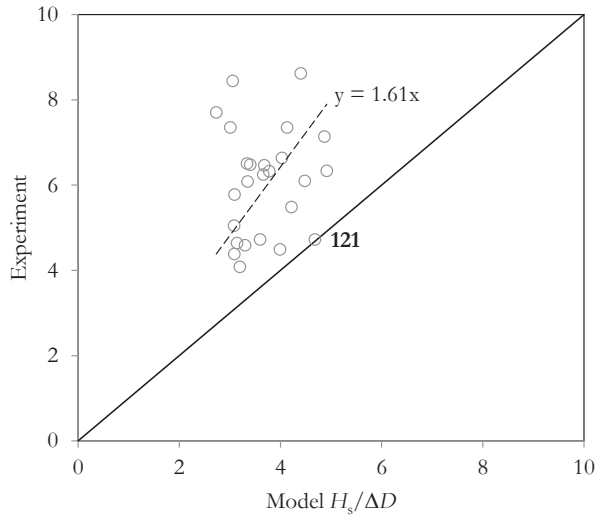
Figure 6–22 Comparison of experiments and model formulas for CC, damage cases c and d

The results for the concrete columns are shown in Figure 6–22. Experiment number 121 is a Basalton revetment without joint fill, which explains its lowest position. The concrete columns include the Hydroblocks for which the model values are corrected as explained in section 11.2. The remaining scatter is partly because the various types that are included. The largest number of available experiments are with Basalton (factor 1.66) and Hydroblock (1.55). Those two sub-groups show the same scatter as in Figure 6–22. The sub-groups C-Star (1.95) and Ronaton (1.97) include a much smaller number of experiments, and less scatter. The reasons that Ronaton and C-star perform better may include: the regular pattern with overlaps in x- and in y-direction, smaller quantities of joint material washed-out, a pattern that generates n_y forces when n_x forces increase.

The concrete block (CB) results for damage category d are shown in Figure 6–23. The model results compare nicely with the experiments, with experiment 238, on Verkalit, as an exception. The reason for this deviation is unknown. Other Verkalit tests give much higher stability numbers. Without this test the average is characterised by a factor 1.63. The CB experiments with damage a+b against model d show a less convincing comparison.
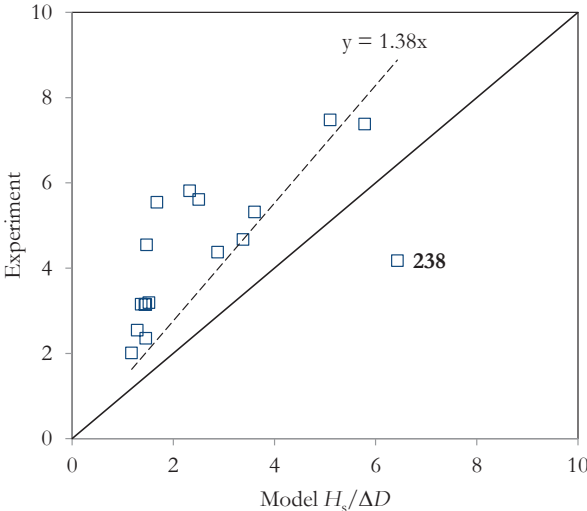
Figure 6–23   **Comparison of experiments and model formulas for CB, damage cases c and d**

The group of concrete blocks has become a bit small due to all exclusions. Some sub-groups can be added without increasing the scatter dramatically. In Figure 6–24 a sub-group of experiments on a Basalton layer on top of an old existing basalt layer is added.[255] The group itself is quite uniform and the results are a bit low compared to the model.

---

[255] 't Hart & Wolters, 2012
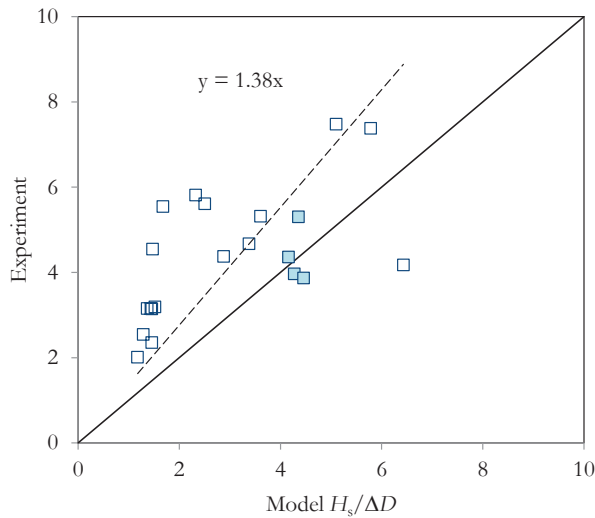
Figure 6–24 Comparison of experiments and model for CB damage d, with additional experiments Basalton as a second layer
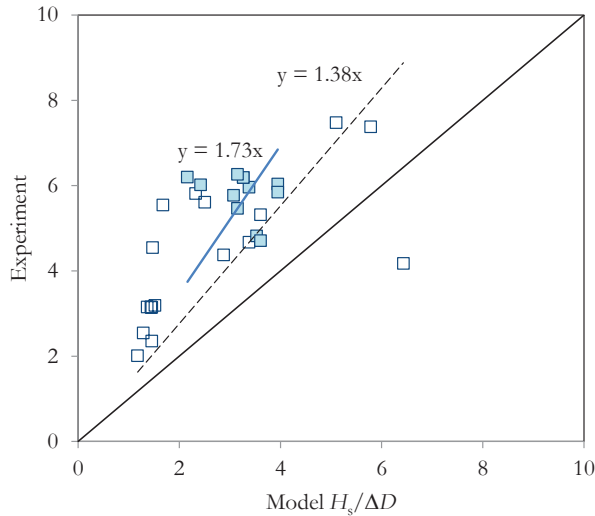
Figure 6–25 Comparison of experiments and model for CB damage d, with additional experiments with small z_{top}/D

A second additional sub-group is a set of experiments on rectangular blocks with $D = 0.2$ m in (Smith et al, 2000) with small values of $(z_{top} - z_{SWL})/D$. This sub-group is quite uniform[256] and has a factor of 1.73 compared to the model (see Figure 6–25). The experiments show a larger stability which might be due to additional friction, to a special support condition of

---

[256] The total group of experiments initially excluded because of a too low z_{top} shows erratic results, partly because very thin blocks and because of other effects.

the top rows or due to effects in cross direction of the flume. Those effects are all not reliable, and therefore purposely not included in a model that also must be suitable to predict the resistance of revetment in reality, not only in the flume.

The model is also suitable for the natural columns. The Basalt columns are sorted in height. Their average weight determines the weight and the ΔD. The bending capacity however should be based on the smallest height. So, for basalt 20/30 the minimum is 80% of the average of 0.25 m. For 30/40 this is 85%. Since the basalt in the flume tests was quite small we assume a percentage minimum/average of 65%. The effective eccentricity for the bending moment capacity is $e = 0.65 \times 0.4\ D = 0.25\ D$. It could be argued that basalt has more difficulties in developing the neutral in-plane force because the top-layer can not slide since it has a strong interlock with the filter layer. A sliding surface would develop underneath the longest columns.
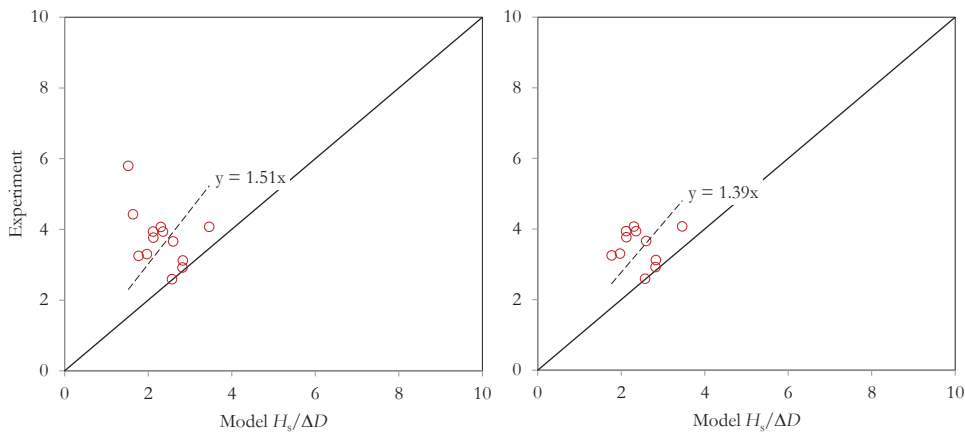
Figure 6–26   **Comparison of experiments and model for natural Basalt columns (NC) damage d, with and without experiments with penetrated joints**

When the experiments are compared with a model calculation based on the same formulas for the in-plane force and a smaller $e = 0.25\ D$, the outcome is shown in Figure 6–26. The left graph shows all basalt experiments with a damage c + d. The two highest values are for penetrated joints. The model accounts for penetrated joints by increasing the leakage length, but not for increased mechanical resistance in the joints. If we exclude the two tests with joints penetrated with asphalt we find a factor of 1.39. The adverse effect of the penetrated joints on the leakage length was already included in the model. Apparently the penetrated joints have a larger resistance.

6.3.6   Scatter and its effect on reliability

The experiments generally show a large scatter, especially in the cases of the beginning of damage (damage category a+b). The model is meant to be applicable for the failure cases c+d. There is still a considerable scatter in the experimental results. The causes are discussed in the next section.

The coefficients of variation of the three groups are calculated using the method in the Eurocode EN 1990, Basis of Design, Annex D. They are in the order of 0.20 to 0.30. Those

values were also found in the calibration for Steentoets 2009. This means that in a design approach with load- and resistance factors those factor need to be in the order of γ = 1.25.

Table 6-6   Calibration results

	CC	CB	NC
Number of experiments *n* for calibration	24	16	11
b in $r_{exp} = b\, r_{model}$	1.72	1.60	1.34
V_δ	0.27	0.24	0.21
Probability *p* that model is unsafe	0.005	0.01	0.05

If the points are too close to the diagonal, or are even under it, the probability that the model predicts unsafe values of $H_s/\Delta D$ might be too high. The target value for this probability is $p = 10^{-2}$. In case p is not in the range 0.005 to 0.02 the model needs to be improved.

The calibration set for the concrete columns CC actually contains too many types of columns which causes too much scatter. Although the Basalton and Hydroblock systems seem to have an inherent scatter of about $V_\delta = 0.25$, the types C-star and Ronaton may have a smaller value. The problem is that for those newer types the number of tests is too low to achieve a better result with the available dataset.

6.3.7   Discussion on typical features of the revetment in the flume tests

The revetment is 5 m wide and has interfaces with the flume walls. In the first test series the wall interface in the Delta flume provided axial support in cross-direction and with that influenced the result.[257] Later the interface was purposely constructed to avoid build-up of normal force in cross-direction of the flume and to avoid too much resistance against uplift.
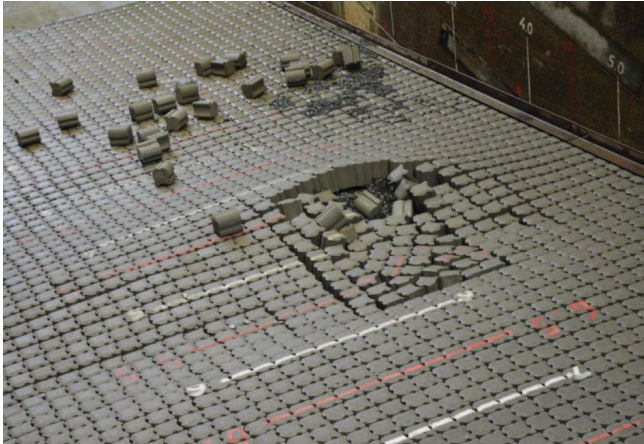
Figure 6–27   Picture of revetment damage in the Delta flume showing arching in cross direction of the flume, after large deformation of the bedding layer

---

[257] A.M. Burger, *Sterkte Oosterschelde dijken onder geconcentreerde golfaanval - Onderzoek naar de stabiliteit van taludverdedigingen onder langdurige golfaanval bij een vaste waterstand - Verslag grootschalig modelonderzoek*, 1985, p14

This worked out well: sometimes steel angles were applied to avoid uplift of the elements along the edge.

In order to be a natural representation of real revetments with infinite longitudinal dimension, there must be some normal force present. For block-type revetment this is difficult to achieve since the 'vertical' and horizontal development are not coupled. Block revetment can have a gap with the flume wall and hence have zero longitudinal in-plane force during the complete test. Contrary they can also have no gap, and in case of no joint flexibility, get jammed, build-up a large in-plane force and act as a beam in cross-direction of the flume. They can even obstruct transfer of in-plane N_x force from rows above downwards. In Figure 6–27 arching in cross direction of the flume can be noticed.

For column-type revetments the development of N_x and N_y is coupled. If there is no support for a certain (relatively low) value of N_y, this can limit the build-up of N_x.

These phenomena are reasons that the developments and distribution of normal force can be different from the model. If the experiment and model results show a match, this can be interpreted that the mechanism of the in-plane forces works based on an estimated average value can be expected.

The toe structure in the flume test is very stiff. This has a positive effect on the normal force in transverse direction. The normal force develops over the years, and also when wave action starts. In reality a deformable, weak toe structure will cause that the revetment slides down and as a result the friction force under the revetment will occur again and will diminish the normal force in the revetments.

In the flume tests there will be hardly any toe deformation and hence the normal force will after it has been developed remain on a high level during the test.

This can also be the reason that flume tests in which slopes are repeatedly loaded to intermediate wave levels give higher results than on maiden slopes. If tests are executed for a certain wave height and steepness, and did not suffer damage, the structure is of course not re-constructed before a new series with e.g. a different steepness value starts. The revetment structure has in the first tests built up its normal force and the outcome of the tests will be higher than for a maiden structure.

Figure 6–28   **Picture of revetment construction in the Delta flume (source: Van Steeg & Klein Breteler, 2009)**

In reality the upper edge of revetments are supported with grass-rooted soil or have a timber pile row, with in many cases a gap above the top row. The upper part of the revetment in the flume is in most cases a concrete slab (see Figure 6–28) that is not supposed to rest against to edge elements of the revetments, but can support the built-up of additional in-plane forces when the revetment is constructed in a compacted fashion and properly washed-in with joint material.

Generally the revetments in flume tests are very young in the sense of wave load history, and also there will be a negligible effect of dike settlement. As a recommendation tested slopes in the flumes might be compacted with vibratory equipment prior to wave loading.

Most of the tests are executed with a constant water level and step-wise increased wave height. With that approach the impact point gradually moves downward, which is favourable for a proper initiation of the in-plane stress-state of the revetment before it will be subjected to more serious waves. It is questionable whether this will also be the case in reality, because the water level and the wave height will increase simultaneously. Ideally the set-up of the wave flume test sequence should reflect reality as good as possible.

The same comment can be made for starting with a low steepness. The wave run-up and run-down are higher which is favourable for build-up of in-plane force over a larger slope length.

6.3.8   Recommendations for analysis of real conditions

The in-plane force N_x is not only a function of the vertical distance between the attack point and a point from which the in-plane force is developed, but also the slope angle and the toe stiffness should be included. Steep slopes are steeper and shorter. Gentle slopes have more difficulty in exceeding the friction force with the bedding, and are longer. The length causes a larger deformation in the revetment beam itself, which reduced the stiffness of support of revetment elements higher on the slope. Hence the generation of in-plane force will be less pronounced. Even longitudinal slits and gaps may occur in the top portion of a long revetment slope.

Finite stiffness of the toe structure causes deformation when the normal force changes which causes relaxation of the in-plane force build up. A finite toe resistance can be the cause of local failure or local large deformation of the toe.

Table 6-7   Estimated recommended values for ratio of forces N_y in longitudinal direction versus N_x in transverse direction

	Initially / after ageing and dike settlement	After first waves
Rectangular blocks	0.2 .. 2	N_y remains the same
Hydroblocks	0.5 .. 2	N_y remains the same
Basalt	0.5 .. 2	0.5
Basalton	0.4 .. 2	0.4
Pit-polygon / Ronaton	0.8	0.8
Circular cylinders	0.6	0.6
Frictionless circular cylinders	1	1
C-star (with legs)	0.6	N_y remains the same

The level of N_y for column revetments should be based on its ability to form arches when the toe support is locally weaker. Similar to arches and cavities in granular soils the revetment can form arches. When the arch is very 'flat' this means that the revetment can form a very high N_y, which is not positive for an equal distribution of N_x. Ideally revetment columns have a quite low friction factor for the in-plane movements, which can mean that they cannot form free spanning arches. The revetment needs every element, but also 'clamps' every element. When the friction is zero the case becomes 'hydrostatic', and $N_y = N_x$.

For the various types recommendations can be made for the ratio between the forces N_y and N_x.

6.4 Updated stability curves

Revetment stability is presented as $H_s/\Delta D$ in Figure 4-1. The effect of the wave loads was presented as a stability curve in section 5.3.5 assuming no contribution of element interaction to the stability. The developed model formulas are now also plotted as $H_s/\Delta D$ curves (see Figure 6–29).

The calibrated model formulas have to be modified for real slopes, with a finite toe stiffness and with effects of friction for the longer slopes. These effects can be incorporated in the model by using the axial beam formulas in section Annex A.1. In order to give a general impression of the effect of implementation of finite toe stiffness and the effect of friction between the top layer and the sublayer on the neutral normal force, we include a reduction factor r_8 on the neutral normal force. The factor is proposed to amount 0.8 for steep slopes ($\cot\alpha = 2.5$), and diminishes to 0.7 for $\cot\alpha = 3.5$ and 0.4 for $\cot\alpha = 5$.

For the wave impact case

$$N_x = r_8\,\rho_s gDB_y(\tfrac{1}{2}R_{u,2\%} + z_{SWL} - z) - r_6 p_{max}DB_y \not< c_{Nmin}\,\rho_s gD^2B_y$$

For the run-down case

$$N_x = r_8\,\rho_s gDB_y(\tfrac{1}{2}R_{u,2\%} + z_{SWL} - z) - r_7 \rho g\phi_b DB_y \not< c_{Nmin}\,\rho_s gD^2B_y$$

with $r_6 = 0.25$
$r_7 = 0.10$
$\tfrac{1}{2}R_{u,2\%} + z_{SWL} \not> z_{top}$

$$c_{Nmin} = \frac{5}{1 + \tfrac{1}{3}\cot\alpha}$$

$$r_8 = 0.8 - 0.1(\cot\alpha - 2.5)^{1.5} \not> 0.8$$

Different from the model setting for back-calculation of the flume tests it is for real slopes assumed that the load effect of wave impact in transverse direction corresponds to ¾ of the total impact load.

When this model is applied stability curves $H_s/\Delta D$ are not only a function of ξ_{m-10} but also of the slope angle α. For the steeper slopes the revetment needs to be constructed to a higher level than for the gentle slope. In the exemplar calculation shown in Figure 6–29 this difference is included quite subtly by setting z_{top} at z_{SWL} +1 m for the 1:5 slope and +2 for the 1:2.5 slope. The stability curves of Figure 6–29 the slope is kept constant and the wave

steepness is made variable. The element thickness is kept constant and the wave height that can be safely resisted is calculated.
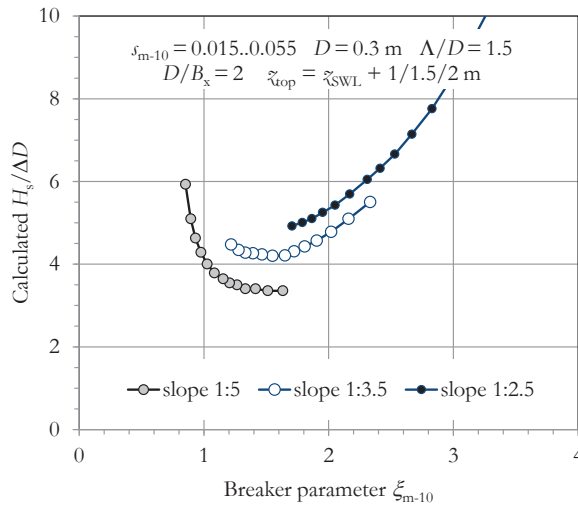
Figure 6–29   Calculated stability curves $H_s/\Delta D$ for concrete columns for various slope angles

Within a practical range of wave steepness s of 1.5 to 5.5% this leads to curves that do not cover the full width of the diagram. It can be noticed that elements with the same thickness D are more stable on the steeper slope due to the build-up of N_x.

A second phenomenon is that the calculated values $H_s/\Delta D$ depend on D. The only difference between the stability curves of Figure 6–30 and Figure 6–29 is that D has been changed from 0.3 m into 0.5 m. As a result of that the stability increases in this case on average with $(0.5/0.3)^p$, with $p = 1.2 .. 1.4$. This is due to the fact that the top layer thickness D plays a role in the bending moment resistance.

In Figure 6–31 the stability curved are plotted and compared with the 'load' curves. The contribution of load reduction through leakage is indicated with arrows as well as the mechanical contribution of element interaction. The share of element interaction increases for the steeper slopes.
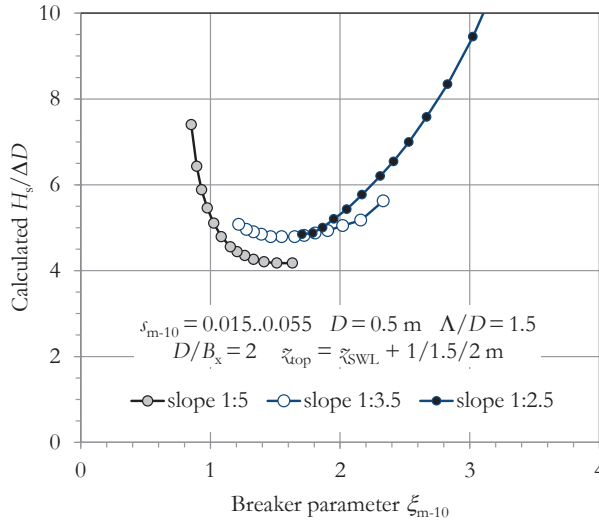
Figure 6–30   Calculated stability curves $H_s/\Delta D$ for various slope angles, with $D = 0.5$ m

There is obviously an effect of the leakage factor Λ/D. Apart from the effect of the leakage length on the upward peak load ϕ_{dip}, this parameter also determines the length of the distributed load along the revetment beam. A larger leakage factor will through that have a more than proportional effect on the bending moment. A smaller leakage factor leads to larger stability numbers, especially in the zones left and right of the zone $1 < \xi_{m-10} < 2$ where the peak and the length of the load depend on Λ/D. An increased leakage factor (see Figure 6–33 with $\Lambda/D = 2.33$) shows that the zones outside the wave impact zone also have higher loads and the stability numbers decrease over the whole range.
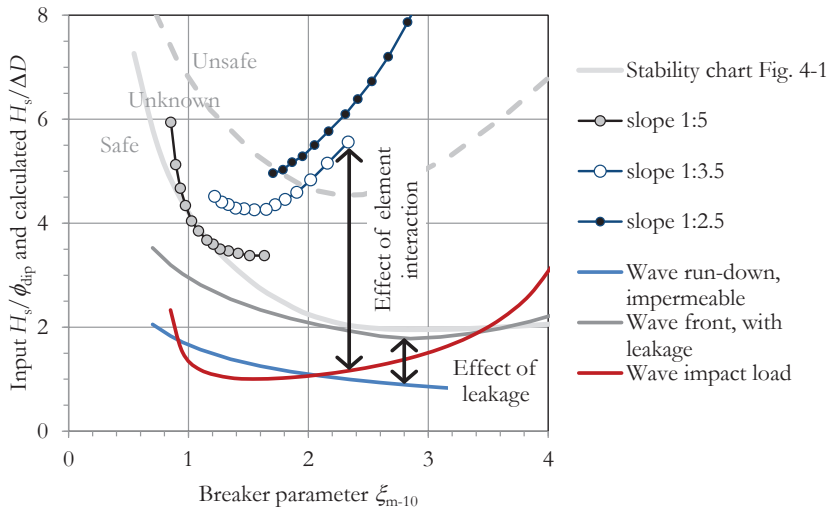
Figure 6–31   Calculated stability curves $H_s/\Delta D$ compared with load input H_s/ϕ_{dip} and $H_s/\rho g p_{max}$
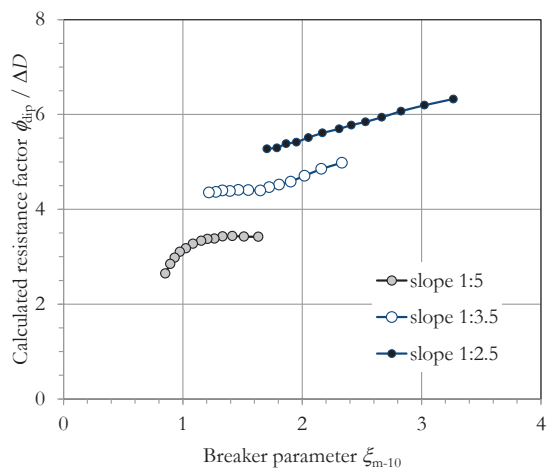
Figure 6–32   Derived results in terms of resistance factor on the peak load

For better understanding we plotted the results of Figure 6–29 with the concrete column case with D = 0.3 m together with the hydraulic input data for this case. The effect of leakage on the peak load in the wave front case can be noticed being roughly a factor 2. The small leakage length also causes a concentrated uplift load which is favourable for the level of resistance that is obtained by element interaction, which is for this roughly a factor 4. As was expected the contribution of element interaction increases for steeper slopes.
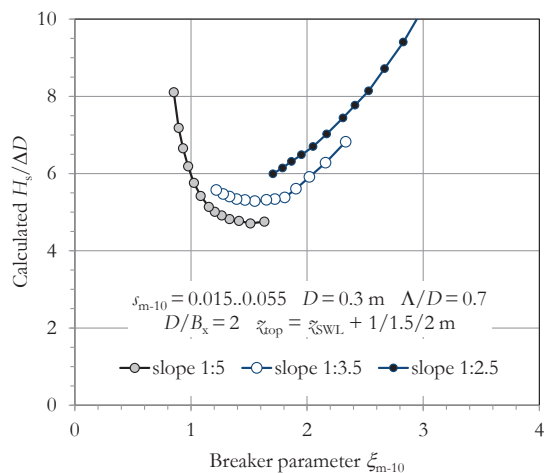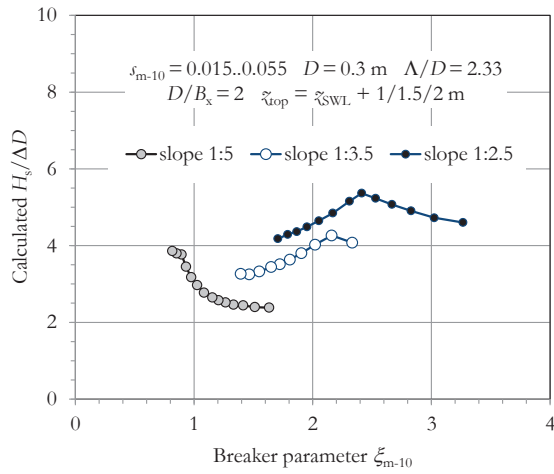
Figure 6–33 Calculated stability curves $H_s/\Delta D$ for various slope angles, with variation of the leakage factor
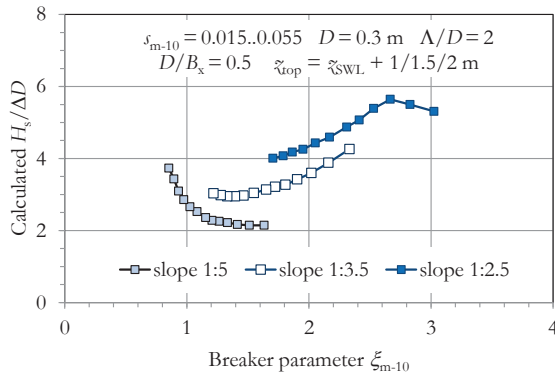
Figure 6–34 Calculated stability curves $H_s/\Delta D$ for concrete blocks, for various slope angles
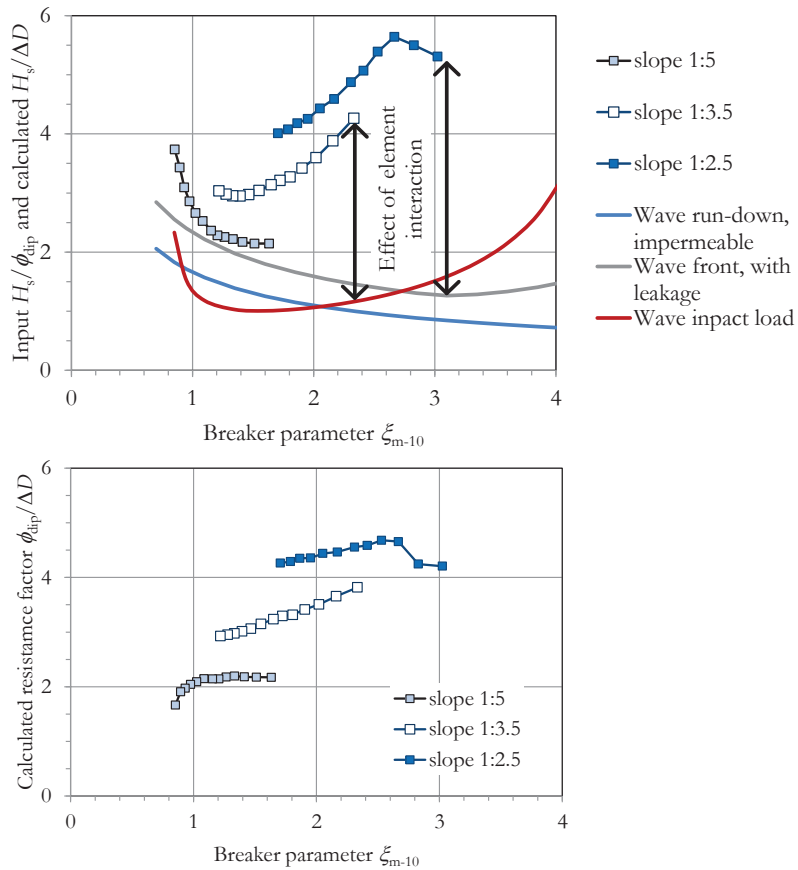
Figure 6–35   Stability curves for CB compared with load input H_s/ϕ_{dip} and $H_s/\rho g p_{max}$

The effects of leakage and element-interaction both have a contribution to the stability of the top-layer. Figure 6–31 includes the stability charts with the black box design formulas[258] discussed in chapter 4 for reference. Although the shape of the curves show similarities, the new load and stability curves make clear where the contributions of drainage or leakage and element interaction are. Element interaction is below $\xi_{m-10} = 1.5$ in the zone that with the knowledge of 2004 was considered 'safe' and above $\xi_{m-10} = 2.0$ in the zone 'unknown'. The results for steeper slopes ($\cot \alpha = 2.5$) are in the 'unsafe' zone. The new model suggests they are safe. It must be realised that the model is not validated for steep slopes.

Cases with column revetments and different leakage lengths give other stability curves. See Figure 6–33. When the leakage length increases the wave-front load case becomes dominant, which decreases the stability progressively. This is due to the increased peak load and due to the load being higher over a larger area.

---

[258] *Veiligheid van de primaire waterkeringen in Nederland, Voorschriften Toetsen op veiligheid voor de tweede toetsronde* (DWW report VTV, 2004)

A case for concrete blocks produces generally lower numbers which is caused by the reduction factors for D/B and for lack of overlap in B_x (see Figure 6–34). For this case a relatively large leakage factor is used, since this is normally associated with concrete blocks with thin joints.

Although the $H_s/\Delta D$ against breaker parameter is a common way of presenting stability numbers, the slope dependency makes it less obvious to stick to this presentation. Figure 6–36 present exactly the same information as the top graph of Figure 6–33, but now plotted against the wave steepness s_{m-10}. It can now be seen that revetments on steep slopes are not for all wave steepness values the most stable.
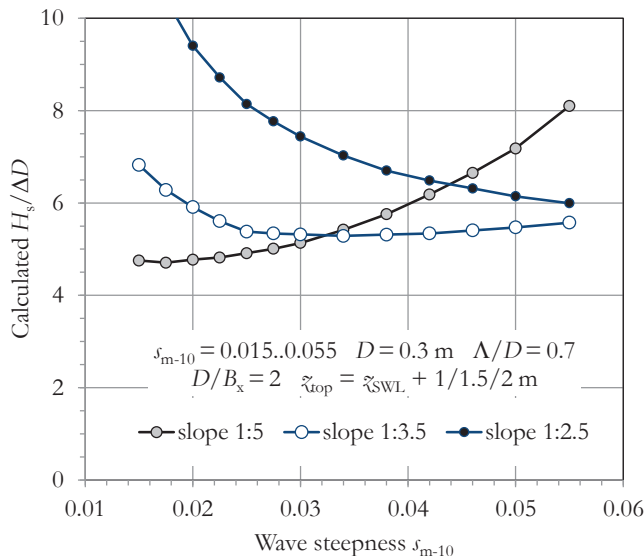
Figure 6–36   Calculated stability curves $H_s/\Delta D$ plotted against wave steepness

7 DISCUSSION ON REVETMENT AND DIKE DESIGN

Chapter introduction

Having derived a new design formula, discussions on what the optimal revetment slope is, and what a dike should look like can be revisited. This chapter contributes to three interesting discussions that engage the flood defence community since many years: (a) the ideal revetment element, (b) the ideal pattern-placed revetment slope and (c) the ideal dike.

The question on the shape of the revetment element itself has attracted many inventors, who created their own block. This study does not come up with a new one, but with conditions for success that apply to all of them. The stone or column shape of the ideal revetment element should avoid lack of flexibility in the pattern in longitudinal direction. A strict row-orientation combined with cyclic temperature loading can cause jamming of the rows and loose elements in colder periods. In traditional pattern-placed revetments the open areas are a bit irregular in position. They allow re-arrangement and enable the top-layer to 'breath' in the two in-plane directions. The open areas function as relief holes as well as joints. Ideally these functions are both fulfilled and do not compromise each other.

Section 7.2 argues that slopes when they are optimised for limitation of overtopping tend to become too gentle from the perspective of an ideal revetment. A dominating drawback of gentle pattern-placed revetment slopes is the inherent variability in resistance due to the uncertainties in the friction forces that restrain the build-up of the normal force N_x. Steeper slopes reduce the chance that the in-plane forces do not develop because of dominant friction forces between the top layer and the sub-layers. Taking full advantage of the in-plane interaction forces asks for relatively steep slopes, with angles of 1:3 or less. Convex and concave slope geometries, and vertically oblique element orientation are discussed.

The effects of ideal revetment designs on optimal dike geometry are discussed in section 7.3. Shallow water could be combined with a gentle slope, and with revetment elements practically resting on self-weight. Deep water requires a steeper slope in the wave attacked zone, followed by a gentle (not armoured?) slope against wave run up.

In areas of significant tidal range, or areas with probability of high surges, distinction should be made between low tide and high tide protection zones, avoiding wave breaking on the gentle slope, which has a strong impact on the required revetment thickness.

Sections 7.4 and 7.5 present the conclusions and recommendations.

7.1 Ideal revetment element design

7.1.1 Summary of history

The history of revetment types is described in chapter 2. As a sublimation of the early types based on natural stone, Basalt columns have during roughly one century been the featured type of revetment on Dutch sea dikes. A structure composed of pattern-placed natural Basalt columns is characterised by:

- tall columns (high D/B ratio),
- good permeability properties of the top layer,
- a granular filter, also facilitates level construction of the columns of unequal length,

- special attention for solid pitching and additional compaction of the pattern during installation, enabling good contact between the elements in order to avoid loose elements and in order
- slightly tapered vertical shapes that kept the joint fill in position and
- a slightly irregular hexagonal shape that enabled a proper build-up of N_y as a consequence of N_x.

All these features are theoretically important factors for stability of the revetment elements and have empirically proven to be so.

To complete the list of criteria of an ideal revetment a stiff toe structure must be added. The importance of the toe structure has not been recognised in the past.

Concrete block revetments (with a less thick top-layer and with smaller D/B-ratios) have been popular during quite a number of years after 1953. They were not always constructed on a granular filter. In recent years the concrete column revetments have made a come-back. They appear susceptible to wave impact as the limiting factor for stability. In other words: if plunging wave impact can be avoided they can – dependent on the drainage/leakage properties (small Λ/D) – be very stable.

This summary indicates the key factors for stability of column revetments: optimised drainage/leakage properties and all mechanical features listed above.

7.1.2 *Ability to generate frictional interlock forces in two directions*

Apart from the D/B-ratio and the top-layer drainage properties an important difference between blocks and columns are the rows-oriented nature of the block revetments.

Revetments on a slope can – subjected to gravity forces – develop in-plane force in transverse direction. The force action is down the slope, and the reaction can either be a friction force on the sub-layers or a support force at the toe. In-plane forces in the other direction (longitudinal or y-direction) seem indifferent and may be unreliable.

In row-oriented systems the two normal force directions are not coupled. Forces in the rows can occur if the rows have a tight packing, or are compressed by temperature expansion of by second order forces due to uplift by waves (or pull tests). If the y-joints in the rows are wide and flexible no longitudinal normal force will occur. A very high N_y may create very strong rows and may create beam-action in the revetment plane, which may cause non-uniform support of the revetment elements underneath. Both extremes (zero N_y and a very high N_y) are undesirable and make the resistance unpredictable. In flume tests and in field pulling test a strong beam action in longitudinal direction may give very high stability/pull-out results, but they are useless for revetment stability under wave action.

Row-oriented revetments are also susceptible to temperature effects will cause cyclic loading and loose elements in colder periods. Those effects were never intended and are undesired.

Non row-oriented systems with a Honey-comb pattern do not have in-line element rows in x- and/or y-direction. This means that when elements experience in-plane force in e.g. the x-direction, the elements are pushed in the force direction, but are also pushed aside, which is associated with force build-up in the other direction. On a macro-scale this effect can be compared with the Poison-effect in homogenous elastic materials. The friction between the elements shifting and rotating in the x-y-plane determines the ratio between the build-up of

N_y force as a consequence of N_x force, which is caused by gravity. This process can also be not instantaneously reversible, meaning that − equivalent to soils − over-consolidation can occur. After vibrations and movements by wave action the stress state will be reset.

If the element shape is e.g. circular, or ideally consisting of smooth, friction-less circular cylinders a transverse normal force would generate equal forces in longitudinal direction ($N_y = N_x$). And in case N_x will change, N_y will change also. In that case support in y-direction will be needed in order to develop forces in x-direction. In case of non-zero friction between the elements N_y will be smaller than N_x, e.g. $N_y = 0.3 .. 0.5 N_x$. If y-support would be completely lacking the elements have no in-plane shearing resistance. On long dikes there will always be y-support caused by the geometrical plane-strain condition, at least on a macro-level. In the flume tests y-support is purposely avoided, and resistance against y-force build-up can be generated by compression of the flexible interface material along the wall, and/or by friction between top-layer and sub-layers in cross-direction of the flume.

The development of an in-plane stress state in two directions is very important for the stability against concentrated wave impact and it is very important for avoiding loose elements.

If there is more than sufficient ability of friction transfer between the elements, in-plane arching can occur, which is e.g. observed in the field tests on Basalton and Hydroblocks. Irregularities and/or non-uniform support by the toe structure create weak spots. The revetment elements do in that case not have the tendency to shift and move into the direction of the weak zone but will bridge this zone, forming strong arches.

The differences in performance of the various column types like Ronaton, Pit-polygon, C-star and Basalton may be due to differences in xy-interaction.[259]

| Pattern with room for re-arrangement and with less xy-friction | Pattern with less room for re-arrangement, high xy-friction and tendency to form arches and loose zones |
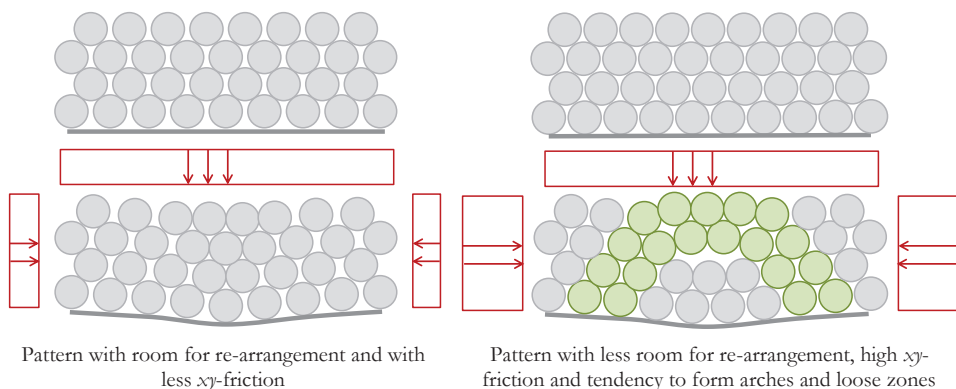
Figure 7–1   Effects of patterns and *xy*-friction

7.1.3   *Overlap of elements*

Revetment patterns with distinct longitudinal rows have long lines with x-joints. Perpendicular wave attack may cause bending moments and shear along longitudinal lines. These load patterns coincides with the weak spot of the revetment-pattern and causes

---

[259] Another cause of different stability performance may be the ability to keep the joint material within the joints.

shearing. This can be observed in flume tests but also in real structures. This shearing is not a cause of immediate shear failure but is weakening the resistance of the structure. Revetment patterns with overlaps in x-direction are much better resistant. Evaluating the flume tests results a difference in the order of 25% was found.
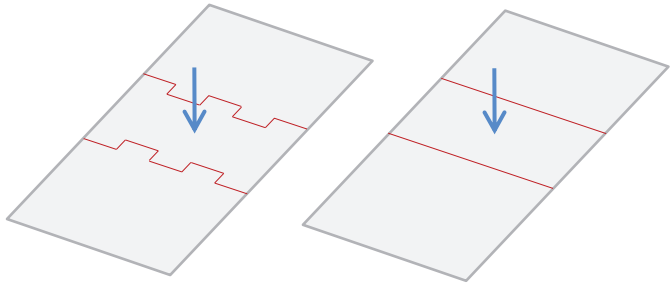
Figure 7–2   Overlap of elements in *x*-direction

7.1.4   *Combined function of the joints*

Joints are now designed to transfer frictional interlocking forces, are providing the revetment flexibility to follow dike settlement and are essential for the permeability of the top layer. These functions interact positively. Element movement disturbs the joint material positions and keeps the joint flexible and avoids that siltation or marine growth degrades the permeability.

Drainage   Frictional interlocking   Flexibility/deformation capacity
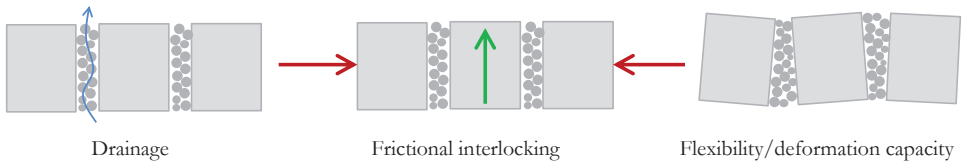
Figure 7–3   Function of joints

A large drawback of the structure with open joints is that the water pressure in the joints reduces the in-plane contact force between the elements and therewith reduces the capacity for frictional interlocking. It would therefore be interesting to optimise the joint functionality and ideally split the drainage function and the mechanical function of the joints.
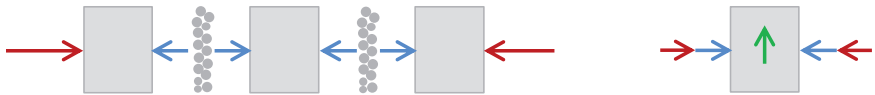
Figure 7–4   Joint pressures reduce capacity for frictional interlocking

7.1.5   *Optimised joint functionality*

In traditional revetments the open areas function as relief holes as well as joints. Ideally these functions should not interfere and compromise each other. Developing a different approach to the joints may go along the lines of making drainage holes in the elements and make flexible and sealed joints.
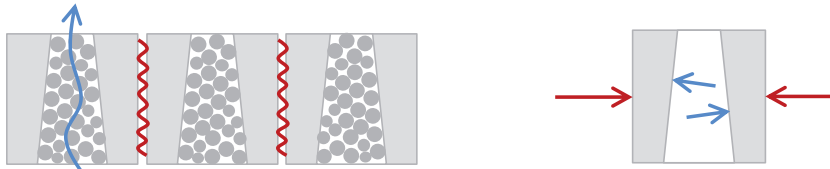
Figure 7–5   **Joint concept with split drainage and mechanical function**

7.1.6   *Drainage holes*

The shape of the drainage holes can be cylindrical. In hydrostatic load cases any geometrical difference in the hole does not change the effect of the forces. In reality the governing load cases are dynamic and the wave pressures do travel through the structure. The pressure reaches its peak value at the surface of the slope first, then in the joints, and finally in the filter. The typical time shift of the peak pressures is 0.2 sec (see section 5.3.4). The joint and element geometry should be optimised to be stable during that moment of the loading cycle (see Figure 7–6).
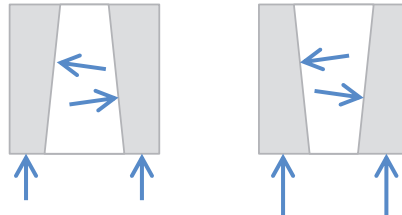
Figure 7–6   **Effect of drainage hole or joint shape on hydraulic during phases of dynamic load sequence**

7.1.7   *Redundancy*

The pattern-placed revetments must include redundancy to avoid progressive collapse after failure of a single element. This means that the structure of frictional interlocking needs to remain if the loss of a single element creates a hole in the top-layer. Also the filter material should be sufficiently coarse to avoid that it is progressively washed-out and the revetment top-layer is undermined. A large D/B ratio is beneficial for avoiding single element failure and is – if an element is missing – also beneficial for filter erosion.

Revetment systems consisting of two layers of pattern placed blocks were investigated in flume test in order to test the effect of the second layer on the stability of the first layer. The idea is that the second layer would limit the consequences of damage of the first layer. The concept of a purposely designed two-layer system to prevent outside slope erosion after failure on the first layer falls outside the scope of this study.

7.2 Revetment slope designs optimised for revetment material quantity

7.2.1 For revetment stability steep slopes are better than gentle slopes

Pattern-placed revetment slopes do exists in many angles of slope steepness. A slope of 1:2 exists on small breakwater type structures[260], and on dikes the slopes range from 1:2.5 to 1:8. The conclusion from this study is that the revetment stability benefits form a relatively steep slope. When a slope has an angle of $\cot\alpha = 3.5$ ($\alpha = 16°$) or steeper the revetment can take advantage of the in-plane interaction forces. In steep slopes the full development of in-plane forces is less hampered by the friction forces between the top layer and the sub-layers. The steep slopes still need to overcome the friction force between element and sub-layer, but measurements learned that moderately severe initial wave loading or intermediate storms can let this happen. For the steeper slopes attention should be paid to the geotechnical stability of the under layers.

For gentle slopes ($\cot\alpha > 3.5$) this contribution to the revetment stability is less reliable. More gentle revetment slopes might need active in-plane pre-loading. Mechanised installation of revetment slabs with packages of concrete elements does not induce in-plane pre-stress. The original installation method with pitching per stone and wedging with stone spalls did. It should be studied whether mechanical vibration leads to overall compaction and increase of in-plane pre-load.
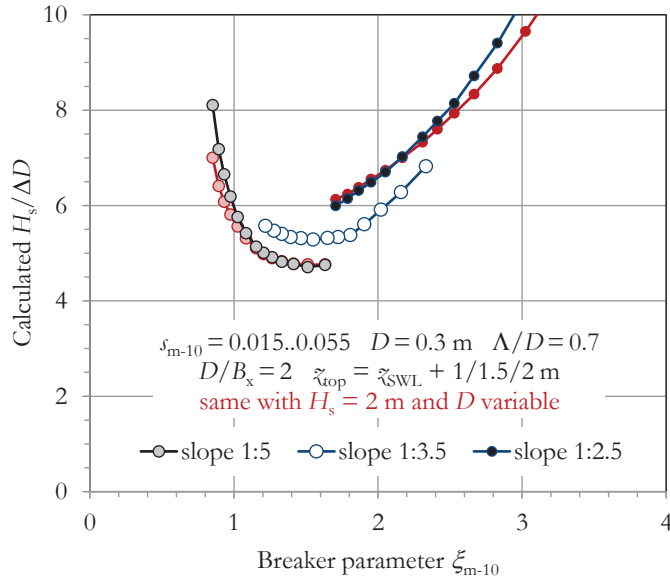
Figure 7–7   **Calculated stability curves $H_s/\Delta D$ with constant D and with constant H_s compared**

---

[260] Steeper BW slopes (e.g. 3:2 or 4:3) are armoured with rock or with interlocking concrete units.

The model outcomes (see Figure 6–29 to Figure 6–33) show that slopes with $\cot\alpha = 2.5$ have a higher stability than with $\cot\alpha = 5$. Since there is a dependency of $H_s/\Delta D$ on the element height D it makes a difference whether H_s or D is taken as a fixed value. The parameter combination $H_s/\Delta D$ suggests that we have looked for a H_s that a revetment with a certain D can resist. In design practice it will be the other way around: the design wave height is known and we need to determine the element height. The outcomes show a numerical difference between the stability numbers (see Figure 7–7).

The $H_s/\Delta D$ plot gives the significant wave height that can be resisted, by a continuous revetment slab with thickness D [m] and specific weight ρ_s [kg/m³], made dimensionless with $\Delta = (\rho_s - \rho)/\rho$. Plotting the stability numbers against the breaker parameter, or Iribarren number, is based on surf-similarity: $\xi = \tan\alpha \,/\, \sqrt{(s)}$.[261] The response of waves in terms of breaking and reflection is such that steeper slopes and less steep waves can compensate each other.

According to the theory of revetment resistance presented in this thesis this similarity is not tenable. Presentation of stability numbers against the breaker parameter is of course still possible and has preference because it refers to known charts, but the information on the slope angle or the wave steepness must be provided.

The search for D given H_s can also be plotted as $\Delta D/H_s$, thus looking for a minimum D instead a maximum H_s. This presentation is shown in Figure 7–8, and looks like the inverse of Figure 6–36.
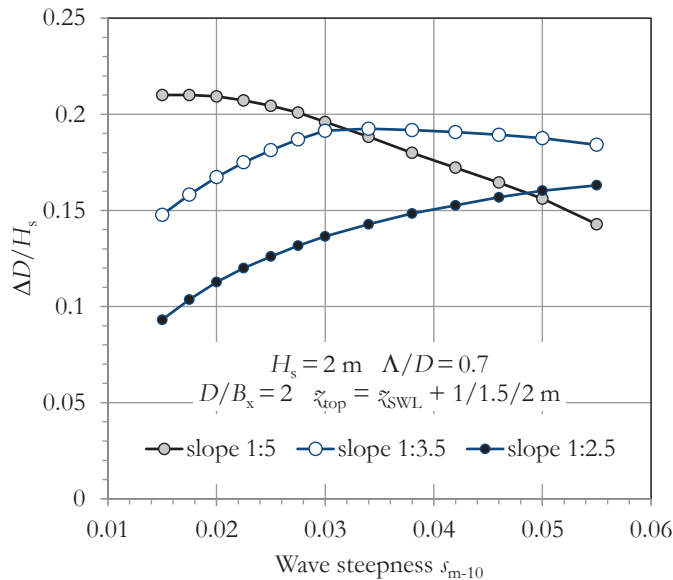
Figure 7–8   Calculated stability curves $\Delta D/H_s$ with constant H_s plotted against wave steepness

---

[261] $\xi_{m\text{-}10}$ stands for the Iribarren number based on spectral wave parameters, in this case: $s = g\,H_{m0} \,/\, (2\pi\,T_{m\text{-}10}^2)$
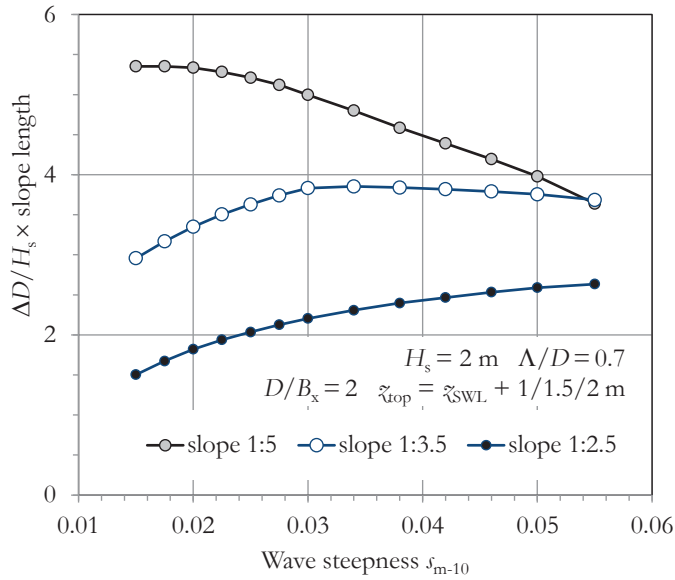
Figure 7–9   Curves of the economy of revetment material: $\Delta D/H_s$ times slope length

The gentle slopes are very long. In order to really compare the material consumption of a revetment armour slope, the height D is multiplied by the revetment length: $(z_{top} - z_{toe}) \times \sqrt{(1 + (\cot \alpha)^2)}$. This is shown in Figure 7–9. It can be noticed that when looking to the isolated question of the economic optimum of a revetment armour top layer, a steep slope is always cheaper. It is true that a steep slope also has disadvantages, such as higher wave run-up, and a lower safety factor on geotechnical stability and shorter piping length.

7.2.2   Discussion on wave growth and load history

Plotting the revetment strength against wave steepness makes the designer aware of the fact that the wave steepness is not a constant value.[262] The wave steepness changes during wave growth. When wind waves are developed and start to grow due to persistent wind speed and not limited by nearby coasts and/or too small depth, the values of the wave height and period both increase.[263] Their ratio expressed as wave steepness tends to start with 8% or higher and comes down to 6 or 5% when the waves are e.g. 2.5 or 3 m. Shoaling and depth-induced breaking reduces the wave steepness further. In order to understand the process of wave growth and the 'development of the load', or – in other words – the load history on the slope before the design load level is reached, the H_s against s_{m-10} plot is changed into H_s against wave period T_{m-10} in Figure 7–10. The three stability curves are the same as in Figure 6–33. Although the development of the parameters during wave growth is just an example, it can be seen that there is a clear difference in 'risk' and robustness.

---

[262] Double-peaked spectra are here neglected for clarity.
[263] A.K. Laing, *Guide to Wave Analysis and Forecasting*, 2nd edition. (Geneva: WMO report 702, 1998)
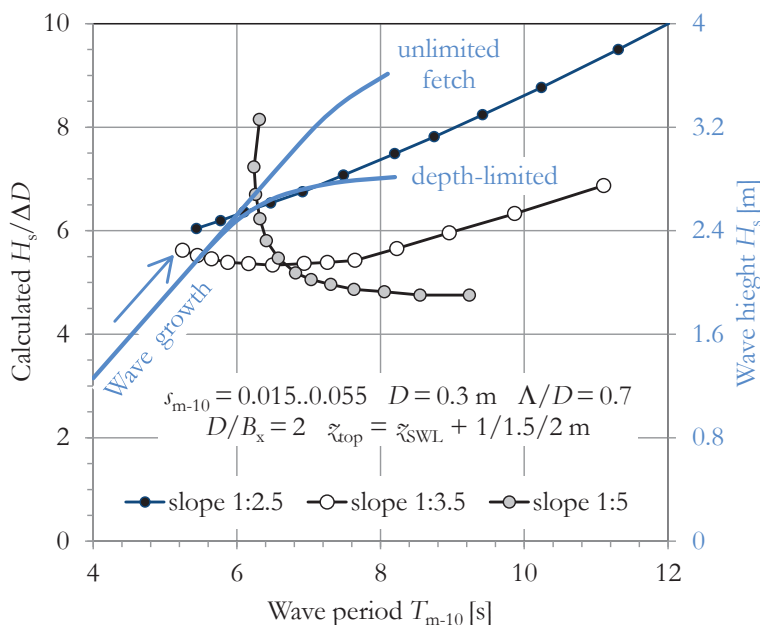
Figure 7–10 Revetment stability $H_s/\Delta D$ plotted against wave period T for given slope steepness, compared with wave parameters H_s and T during wave growth

The gentle slope (1:5) with chosen element thickness $D = 0.3$ m initially has 'infinite' resistance.[264] Up to $T_{m-10} = 6$ s, the breaker parameter ξ is so low that there will be spilling breakers only, with no significant wave attack. After that the slope will be 'hit' by longer wave periods and will require a relatively large revetment thickness to be stable. The steep slope is in this example also not affected be waves with $T_{m-10} < 6$ s, but has a fair chance that the breaker parameter will be higher than the range of ξ_{m-10} between 1 and 2, with high wave impacts. Hence a less thick revetment will be sufficient for stability.

Especially in combination with the inherent load-controlling effect of depth-limitation at design surge level ongoing wave-grow might increase the wave period, whilst the wave height development is limited. In that range the stability curve still rises, which causes that the wave growth does not affect the stability. The combination of a depth limitation and a relatively steep slope would avoid plunging waves on the slope, and would consequently give a high wave resistance, and would provide robustness in case the waves would further intensify.

7.2.3 Toe structure requirement

A steep slope and the associated higher stability is caused by in-plane forces that more easily develop under wave action. This implies that, although it is possible that the revetment

---

[264] This is a fictitious case of course. The stability curve is calculated as the permissible H when $D = 0.3$ m for a given series of values of s. H as an outcome is divided by s to find wave length L and T. Cases with $T < 6$ s are not found. They will be found if D is given a smaller value.

element in axial direction is in stable equilibrium on the slope, it will lean against the lower neighbour, and ultimately requires support by the toe structure. The toe structure of a steep slope will need to be strong and stiff. If the tow is stiff it will be able to resist the force that is built-up by axial pre-loading without relaxation over time. A toe structure consisting of a row of small wooden piles will be not adequate. From a structural point of view the strength and stiffness of the toe is an important pre-condition for the development of the in-plane forces, and via that for the revetment stability against wave attack.

7.2.4   Discussion on variable slopes

In strong tidal areas or areas with storm surge probability, distinction should be made between low-tide and high-tide protection zones, avoiding wave breaking on a gentle slope, which has a strong impact on the required revetment thickness.

The summary of the design approach may be:
- For the low water levels, shallow depth and small waves: make a gentle slope, the revetment elements rest on self-weight.
- For the high water levels, deeper water and higher waves: make a steeper slope in the wave attack zone; followed by gentle (maybe not armoured) slope against wave run up.

In Table 7-1 the effects of some designs of the cross section of the dike on the revetment design are presented. In case of a constant slope angle, the top part of the slope requires heavier revetment.[265] The possible change in revetment thickness (see figure (a)) should be located at the run-down point of the design wave, assumed to occur in combination with a water level that is equal to the depth-limitation for that wave. In figure (b) a change in slope angle is suggested at that location. The lower part of the slope is e.g. 1:5, and will be located in the range of the normal high tides. For this part the frequent waves will keep the slope in good in-plane stress condition, although the angle is small. The upper part angle is e.g. 1:2.5. This part of the slope must withstand the design waves when the water levels are high and the waves will not experience depth limitation. The waves might 'feel' the low part of the slope though, and break slightly earlier. If this happens, it will enhance the potential 'resistance' of the system.

In figure (c) the opposite choice is made, creating a high berm profile, which might be more common than figure (b). High berms are commonly chosen as a cross sectional profile in tidal areas where they at certain flood/surge levels are effective. The high berm solution is beneficial to limit run-up, but is dis-advantageous for the revetment. The higher wave will break on the upper part of the slope, which will have hardly any benefit from normal force and element interaction. The revetment for that part must be designed on bases of its weight only. The stability in the corner point is a concern, since the normal force will push the elements out. When cambered slopes are constructed this effect is also present. The normal force generates an upward distributed radial load.

---

[265] See section 2.3.2 and Figure 3-28.

	Effect on load	Effect on (economy of) Resistance	Execution

Table 7-1   **Effect of variable slope angle on revetment design**

	Effect on load	Effect on (economy of) Resistance	Execution
(a)	O	+	O
(b)	+	+	−
(c)	−	−	−
(d)	+	+	+

Figure (d) is a further development of (c), leaving the berm unprotected[266]. The upper part of the slope can be given a steep slope also.

The trouble with a profile like figure (d) in Table 7-1 is that it will be difficult to make it work for variable water levels. A theoretical ideal slope design will be the S-curve that the waves will create at a gravel beach. For varying water levels different curves will occur, and can occur. Fixing an S-curve and giving it a 'hard' cover layer will therefore only lead to an approximate ideal revetment for one water level.

---
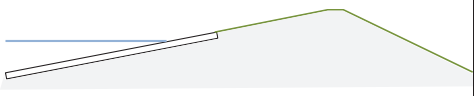
[266] See Pettemer Sea Defence design in Chapter 2.

7.3 The effect of ideal revetment designs on optimal dike geometry

Dike cross sections are designed to limit overtopping in the first place. Other failure mechanisms are less dominant and therefore determine the dike geometry to a lesser extent. A low, wide dike is good for avoidance of overtopping, as well as for the geotechnical stability and piping. For revetment strength a steeper slope may be a better choice (see Figure 7–8 and Figure 7–9). A less wide dike will also require less valuable land. The analysis of what would be an economical and robust dike design has been published by Voortman[267] in 2003. His analysis was based on the simple and conservative revetment formula of Eq. 4.13.[268] It was found that an optimal dike design, neglecting cost of land use, had an outside slope of 1:10.

The analysis can be revisited using the model of this thesis that includes slope-dependency of the in-plane forces. It is expected that the outcome will be much more inclined to the common slope angles of 1:5 and 1:3.

Table 7-2   Comparison of required dike elevation

| Outside 1:3, inside 1:2 | Outside 1:5, inside 1:2 |

A second element in this discussion is the distribution of probabilities over the failure mechanisms. Overtopping is deemed the largest risk. Other failure mechanisms should not contribute too much to the failure risk and are therefore as a first approximation meant be 10 times less probable (combination 1 in Table 7-3).

If you make revetment failure the dominant mechanism the ideal dike geometry will be steeper, and hence the dike needs to be higher against overtopping. The total cost of the dike may be lower if the revetment is designed against the acceptable probability for the dominant mechanism and the overtopping (and all other mechanisms) designed as 10 times less probable (combination 2 in Table 7-3). This will lead to a cheaper revetment and a higher dike.

Table 7-3   Distribution of failure probability over the failure mechanisms

	Overtopping	Revetment failure	Piping	Etcetera
Combination 1	1	0.1	0.1	0.1
Combination 2	0.1	1	0.1	0.1
Combination 3	0.1	0.1	1	0.1
Etcetera	0.1	0.1	0.1	1

---

[267] H.G. Voortman, "Risk-based design of large-scale flood defence systems" (PhD thesis TU Delft, 2003), chapter 7

[268] M. Hussaarts, J.K. Vrijling, and P.H.A.J.M. van Gelder, "The probabilistic optimisation of the revetment on the dikes along the Frisian coast," *Coast. Struct.*, 1999

7.4 Conclusions

Pattern-placed revetments are part of a flood defence system that includes the foreshore and the dike. This – partly engineered – system has to retain flood water levels and has to resist the erosive effects of waves. The system can fail in more than one way, which ultimately may have the consequence of flooding of the protected area.

It is not possible to treat the revetment as an independent sub-system, since the outside slope angle has not only a significant influence on the revetment stability. But also on wave run-up, piping and geotechnical stability. The influence of the slope angle on revetment stability is much bigger than captured earlier in analytical stability studies.

In this thesis the resistance of the revetment is analysed and the revetment stability is calculated based on the laws and practises of applied mechanics for static and dynamic equilibrium of forces. The axial forces, or in-plane forces, play an important role in providing resistance through co-called frictional interlocking. The principle of frictional interlocking was verified with basic experiments that included the properties of gravel filled joints in between the revetment elements.

In order to implement this principle in a realistic and reliable design approach it was tried to investigate the presence of the in-plane forces in reality. This was attempted in the 1990s through numerical modelling and through numerous pull tests on real dike revetments. The pull tests do however not adequately represent the loading of the revetment when it is subjected to wave impacts and when it tends to be lifted during wave run-down. The pull tests can be used as indicators of in-plane strength when interpreted through a dedicated applied mechanics model. In this study the available pull tests were supplemented with larger field experiments especially designed to tests the in-plane stress state in two directions of the slope, transverse and longitudinal. The conclusion of the field testing was that the in-plane stress state in 'dry' conditions was subject to a very large scatter.

- For the row-oriented revetments a temperature dependency was found. The frictional interlocking capacity in longitudinal direction increases when the temperature rises.

- It was found that older slopes have a higher in-plane force than younger slopes. It is believed that the revetment experiences friction forces as a consequence of a history of wave loading and/or of dike settlement. The packing of the pattern gets denser over time.

- Long gentle slopes have a lower in-plane force than short, steep slopes. Although there is no clear transition value, as a boundary between gentle and steep a slope angle $\alpha = \frac{1}{2}\phi$ can apply. With $\tan\phi = f_{\text{fr}} = 0.6$, $\phi = 30°$, $\alpha = 15°$, $\cot\alpha = 3.6$.

- As expected the in-plane force increases with a lower position on the slope. But in the immediate vicinity of the toe at some locations lower in-plane forces were found. This can be expected when an insufficiently stiff toe structure deforms in response to the increasing in-plane force in the revetment.

The development of in-plane forces was measured in the Delta flume and it was found that although initially low, the force increased at the start of larger wave action. This phenomenon was known before as the revetment got to gain strength in the first series of waves. A maiden slope with pattern-placed revetment is soon overloaded when the elements are not first given the opportunity to be lifted and re-arranged, thus overruling and re-setting

the friction forces between the top-layer and the sublayers. It was found that for a 1:3 slope the developed in-plane force after initial wave action in rough lines equals the level of a revetment that slides over a frictionless bedding layer.

Knowing this the revetment resistance can safely be based on a model that is based on the in-plane forces. The model has been developed and detailed. Relevant components of the model description are the wave load magnitudes of wave impacts and wave run-down, the effect of the drainage properties of the revetment sub-systems on the actual differential water head and on the length of the distributed load. All these components are re-visited and then verified by looking for up-to-date model formulas and for validation through measurements. The objective was to have no empirical relations that include phenomena and effects that are not clear. A complicating factor was that some wave load descriptions in literature were based on flume tests with a very limited range of slope angles only.

The results found in this thesis are:

- For the wave impact pressures a new formula was developed that has a more accurate determination of the load magnitude dependent on and within the relevant range of the breaker parameter. The physical background of this description is breaker crest height, the falling height and the angle of impact.

- Within the range of the large scale tests ($H_s > 1.6$ m) no evidence was found for applicability of scaling laws that need to correct for compressibility and/or air content of the water.

- The spatial gradients of the wave impact pressure diagram were found to be related to the peak pressure.

- The effects of hydraulic damping and structural damping and dynamic amplification were investigated separately and as such implemented in model formulas.

- A new wave run-down formula was used and the location of wave impact was related to the run-down point.

The updated wave model descriptions were used as input for a beam model of the revetment. The bending and shear resistance of this beam relies on the in-plane force. The in-plane force is – as said above – first developed and consequently increased under wave loading, but when it comes to heavy wave impacts the water pressure present in the joints reduces the effective in-plane force available for frictional interlocking capacity.

The model with the combined effects of the known load and the unknown components of the resistance was calibrated using the results of the large-scale flume experiments available in literature. This has led to an estimated level of in-plane force that on average must be present in the flume tests. This level nicely corresponds to the neutral level that has been measured in the experiment mentioned earlier, subtracted with joint pressure effects.

As a next step we need to consider to what extent the flume tests represent revetment slopes on real dikes. The real dikes have a wider range of slope angles and the revetment is supported differently in the in-plane directions.

We have based an estimation of the effect of the slope angle (and therewith the slope length) on the occurrence of the in-plane force on model calculations with an axial beam model. This model was calibrated on the dry field tests. The scatter in those tests was too high to

rely on a minimum guaranteed force level, but there was clear evidence for effects of the slope angle.

The effect of toe support was separately studied and verified with experiments.

For the effects of slope angle and weak toe support reduction, factors of the in-plane forces are recommended.

This approach of detailed and verified load and resistance modelling leads to a confirmation of the empirical stability curves. Also, more specifically, it was found that the generally large scatter of flume tests results can be reduced since we can now − based on the model − conclude that:

- The stability curves plotted as $H_s/\Delta D$ against breaker parameter ξ have an extra dependency on the slope angle. The same revetment element with equal ξ is more stable on a steeper slope (see Figure 6–31).

- The stability curves plotted as $H_s/\Delta D$ against breaker parameter ξ have an extra dependency on the revetment thickness D. The stability number $H_s/\Delta D$ increases with larger D, which can be understood by the effect of a larger in-plane force and a larger internal lever arm. This is especially true for the load cases of wave run-down with dominant failure of the revetment beam in bending.

- There is an effect of the element aspect ratio D/B, with larger values of D/B being more stable. The flexural and shear deformation of the revetment can be distributed over more joints in case the elements are taller. The favourable effect of a higher D/B explains the overall better performance of columns over blocks.

- There is a positive effect of types with overlap in element dimension B_x, creating staggered x-joints (see Figure 7–2).

Implementing these conclusions there are still differences in performance of various block and columns types. Especially for the column types these differences are believed to be related to their ability to keep the filter and joint fill material in place and with their pattern characteristics combined with xy-friction properties. Basalton, Ronaton and C-star columns of equal height share the relevant beneficial properties mentioned above but they really have a different shape on plan. The pattern is different which may enhance their resistance against single element failure. Moreover there will be an effect of how these types generate in-plane forces and ability for frictional interlocking in y-direction. Even in the relatively narrow flume, there might be a significant positive effect on stability.

A general conclusion of the study is that the element shape and the pattern-placing of the revetment has a large effect on the stability of the revetment slab.

A second general conclusion is that there is a considerable effect of the slope angle on the stability. This effect will have its impact on the ideal dike design. New positions could be taken in the trade-off between ideal stability and ideal overtopping solutions. This thesis intends to cover everything needed to feed this discussion from the side of the stability.

Pattern-placed revetments are in an increasing number of cases designed for higher design waves than before ($H_s > 3$ m). Making a design of pattern-placed revetment for those design conditions, and in the same time staying within the range of the presently applied thickness ($D < 0.65$ m) would hardly be possible if beneficial effects of a favourable slope angle and adequate toe are not respected and utilised.

7.5   Recommendations

The model of revetment resistance based on in-plane forces has been extensively investigated and proved a reliable basis for understanding and explaining revetment stability under severe wave load conditions. The model offers potential for looking into the effect of slope angle in a different way, which may lead to other views on the revetment strength on existing slopes with very gentle as well as more steeper slopes. The model findings have not been verified for slopes steeper than 1:3 and gentler than 1:4. Slopes with steepness 1:2.5 and 1:5 or 1:6 do exist in reality and are now verified with model formulas based on 1:3 to 1:4 slopes. It is therefore recommendable to execute tests with the objective of experimental verification of the revetment stability for a wider range of slope angles.

The flume tests were always executed with stiff and strong toe structures that led to perfect support conditions of the revetment. The tested revetments were able to build up an in-plane stress state which increases their stability. The typical toe structures applied in real structures are potentially strong enough but are evidently be less stiff than the toe support provided in the flume tests. It is therefore doubtful whether real revetment slopes will be able to build-up and maintain an in-plane stress state similar to the flume tests. This makes a similar stability performance in reality insecure. It is therefore recommended to execute experiments including a simulation of a real toe structure with timber piles and clay, instead of the stiff concrete slabs, and thus test the adverse effect of the presently applied real toe structures on the stability of the revetment.

On the other hand it is recommended to increase the toe stiffness in new designs.

The understanding of the processes of the dynamic hydraulic response with the subsequent and/or partly simultaneous pressure signals above of the slope, in the joints and under the slope, as well as the dynamic structural response may benefit from full numerical modelling. The investigation in this thesis has been limited to combination of output generated with ZSTEEN used as input for finite element analysis with the structural code TNODIANA. The conclusions based on this research method are deemed reliable, but full parameter variation is believed to provide further insight and potential for improving the model formulas.

The in-plane forces have been measured once in the Delta flume which gave a very convincing result. Future flume experiments should include instrumentation to measure and monitor in-plane forces during the course of the experiment. The in-plane forces are developed during the start of serious wave action. The development of the in-plane forces through waves enhances the resistance, which is needed to balance further increased wave load. The sequence of temporal development of resistances and its balance with load is believed to be fragile. If the pre-load-waves are lacking and/or are too short in duration, or their wave height is not properly combined with increase of the water level and/or the wave period, the revetment may be not ready for the higher waves, with sub-standard failure as a consequence. The development of the normal force under various conditions should therefore be measured. For the various types it is recommended to measure the in-plane force in x- as well as in y-direction.

Apart from measuring it should be made possible for in-plane N_y-forces[269] to develop in the flume tests, since for certain revetments types they will occur in reality as well. There shall

---

[269] In longitudinal direction of the dike, in cross direction of the flume.

however be no vertical/shear interaction with the flume walls. In order to achieve that supports with passive elastic pendulum bars could be applied, similar to the ones applied in the laboratory experiments (refer to Annex E).

An interesting question that remains unanswered is the effect of scaling between the 'large' test scale and the reality. There are good reasons for the application of scaling laws in order to match small scale tests with large scale tests. Within the range of large scale tests, which now comprises wave heights H_s between 0.7 and 1.7 to 2.0 m, and between the large test scale and reality the effects of aeration could be captured in a constant factor and there is poor evidence for a need of application of scale laws on the magnitude of the maximum pressure. Further experiments with the new Delta flume will provide an excellent opportunity to validate this statement.

It is recommended to re-visit the risk-based analysis of an optimal dike cross section design using updated model formulas for the various failure mechanisms. The formulas for piping and for revetment stability have been improved, enabling a more accurate analysis. Special attention should be given to robustness of the designs against future high water levels and the associated probability of higher waves.

REFERENCES

[1]   Adel, H den, and A. Bezuijen. *Mechanische sterkte toplaag.*, 1994.

[2]   Agema, J.F., K.W. Pilarczyk, H.J. Verheij, L. de Quelerij, E.H. Ebbens, M.B. de Groot, J. Stuip, et al. *Betonnen bekledingen op dijken en langs kanalen*. Edited by J.F. et. al. Agema. VNC, 1986.

[3]   Ahrens, J.P. *Irregular Wave Run-up on Smooth Slopes*. Coastal Engineering Aid No 81-17, 1981.

[4]   Allsop, N.W.H., N Durand, and D.P. Hurdle. "Influence of steep seabed slopes on breaking waves for structure deisgn." *Coast. Eng. Proc.* 1998.

[5]   Angremond, K. d', and F.C. van Roode. *Breakwaters and closure dams*. Delft: Delft University Press, 2001.

[6]   Baars, S. van, and I.M. van Kempen. "The causes and mechanisms of historical dike failures in the Netherlands." *E-WAter* 2009:6 (2009).

[7]   Bakker, K.J. "Soil retaining structures - ch. 5: Block Revetments." PhD-thesis TU Delft, 1998.

[8]   Bakker, K.J., and P. Meijers. "Stability against sliding of flexible revetments." *Int Symp Model. Soil Water Struct. Interact*. Delft, 1988.

[9]   Barendsen, W. "De Zeedijk van 1730 tot 1900." *OTAR* 47:2 (1962): 34–35.

[10]   _____. "De zeedijk van zijn ontstaan tot het jaar 1730." *OTAR*:45: 9 and 46: 1 (1961).

[11]   Battjes, J.A. "Short crestedness of waves." *Appl. Ocean Res.* 4:3 (1982): 165–172.

[12]   Battjes, J.A., and H.W. Groenendijk. "Wave height distributions on shallow foreshores." *Coast. Eng.* 40 (2000): 161–182.

[13]   Battjes, J.A., and M.J.F. Stive. "Calibration and verification of a Dissipation model for random breaking waves." *J. Geophys. Res.* 90:5 (1985): 9159–9167.

[14]   Bazant, Z.P., and L. Cedolin. *Stability of structures - Elastic, inelestic, fracture and damage theories*. Oxford University Press, 1991.

[15]   Bezuijen, A. "Friction and clamping forces in wave loaded placed block revetments." *Coast. Eng. Proc.* (1994): 932–944.

[16]   _____. "Geotechnical failure of revetments." *Coast. Zo.* 1991.

[17]   Bezuijen, A., and M. Klein Breteler. "Design formulas for block revetments." *J. Waterw. Port, Coastal, Ocean Eng.* 122:6 (1996): 281–287.

[18]   _____. "Oblique wave attack on block revetments." *Coast. Eng. Proc.* (1992): 1030–1043.

[19]   Bezuijen, A., and T.P. Stoutjesdijk. *Meting getij en freatische lijn open taludbekleding - Bundeling van huidige kennis*. Grondmechanica Delft report CO-341960/16, 1993.

[20]   Bezuijen, A., J. Wouters, and H den Adel. "Numerical simulation of the motion of a loose revetment block." *Coast. Eng. …* (1990): 1606–1619.

[21]   Biggs, J.M. *Introduction to Structural Dynamics*. McGraw Hill, 1964.

[22]   Blom, J.A.H. "Veldproeven op steenzettingen in Zeeland - Eindrapport met resultaten en analyse van onderzoek naar de klemming van gezette stenen." MSc thesis TU Delft, 2006.

[23]   Blom, J.A.H., L. van Nieuwenhuijzen, and D.J. Peters. *Test result and analysis report on prototype tests on clamped revetments in Zeeland.*, 2007.

[24]   Blom, J.A.H., D.J. Peters, R. 't Hart, A.J.E.J. van Casteren, and J.K. Vrijling. "Field tests on clamping in block revetments." *Coast. Struct*. Venice, 2007.

[25]   Boer, K. den. *Grootschalig onderzoek ten behoeve van de Oesterdam*. WL|Delft Hydraulics report M1795 deel VI, 1982.

[26]   _____. *Taludbekledingen van gezette Steen, Stabiliteit van enkele typen bekledingen bij diverse golfomstandigheden, verslag kleinschalig modelonderzoek*. WL|Delft Hydraulics report M1795 deel XIV, 1985.

[27]   Bolderman, M.B.N., and A.W.C. Dwars. *Waterbouwkunde*. 2nd ed. Amsterdam: L.J. Veen, 1919.

[28]   Bolier, D. "Zeeuwse dijken op de schop: kosten, tijd en milieu doorslaggevend voor dijkontwerp." *L. en Water* 41:6 (2001): 30–32.

[29]   Bolier, P.L. *Zeeweringen*. Goes: Oosterbaan & Le Cointre, 1916.

[30]   Boon, M.J.J. *Veiligheid Nederland in kaart 2 - Overstromingsrisico dijkringgebied 26: Schouwen-Duiveland.*, 2012.

[31]   Bos, G., E.O.F. Calle, H.L. Jansen, M.T. Van der Meer, and M.T.J.H. Smits. *Technisch rapport kistdammen en diepwanden in waterkeringen*. TAW report TR22, prepared by Furgo and GeoDelft, 2004.

[32]   Bos, G., J.W.R. Heusinkveld, and M.L. Post. *Trekproeven zeedijk Walsoorden*. Fugro report N-0550, 1998.

[33]   Bosters, M.C.J. *Handleiding toetsing en ontwerp, Technische werkwijze projectbureau zeeweringen.*, 2012.

[34]   Bouma, A.L. *Mechanica van constructies, elasto-statica van slanke structuren*. Delft: Delftse Uitgevers Maatschappij, 1989.

[35]   Bowles, J.E. *Foundation analysis and design, 5th ed*. New York: McGraw-Hill, 1996.

[36]   Bright Wilson, E. *An Introduction to Scientific Research*. New York: Mc Graw Hill, 1952.

[37]   Bruin, M.P., and M.H. Wilderom. *Tussen afsluitdammen en deltadijken – deel I – Noord-Beveland*. Middelburg: Littooij & Olthoff, 1961.

[38]   Bullock, G. N., A. R. Crawford, P. J. Hewson, M. J A Walkden, and P. A D Bird. "The influence of air and scale on wave impact pressures." *Coast. Eng.* 42:4 (2001): 291–312.

[39]   Burger, A.M. *Sterkte Oosterschelde dijken onder geconcentreerde golfaanval - Onderzoek naar de stabiliteit van taludverdedigingen onder langdurige golfaanval bij een vaste waterstand - Verslag grootschalig modelonderzoek.*, 1985.

[40]   _____. *Sterkte Oosterscheldedijken onder geconcentreerde golfaanval*. WL|Delft Hydraulics report M2036, 1985.

[41]   _____. *Taludbekledingen van gezette steen, fase 2, Grootschalig gidsonderzoek*. WL|Delft Hydraulics report M1795/M1881 deel IX, 1983.

[42]   Burger, A.M., M. Klein Breteler, L. Banach, and A. Bezuijen. "Analytical design method for block revetments." *21th Int Conf Coast. Eng.* Malaga, 1988.

[43]   Burgt, C. van der. *Literatuurstudie blokken bekledingen.*, 1969.

[44]   Caires, S. *Maximale significante golfhoogte bij ondiep water en maximale golfsteilheid.*, 2012.

[45]   Caires, S., and M.R.A. van Gent. "Wave height distribution in constant and finite depths." *Coast. Eng. Proc.* 2012.

[46]   Calle, E.O.F. *Veiligheidscriterium Steenzettingen, notie voor ZSteen-analyse*. Delft, 2002.

[47]   Calle, E.O.F., and J.G. Knoeff. *Samenvatting dijkdoorbraakprocessen: beschrijving, doorbraakprocessen en reststerkte*. Delft, 2002.

[48]   Camenen, B., and M. Larson. "Predictive Formulas for Breaker Depth Index and Breaker Type." *J. Coast. Res.* 23:4 (2007): 1028–1041.

[49]   CIRIA, CUR, and CETMEF, eds. *The Rock Manual - The use of Rock in Hydraulic Engineering (2nd edition)*. London: CIRIA report C683, 2007.

[50]   Coeveld, E.M. *Invloed van golfklappen op stabiliteit - literatuurstudie*. WL Delft Hydraulics report H4134, 2003.

[51]   Coeveld, E.M., and M. Klein Breteler. *Invloed klemming: statistische analyse trekproeven*. Delft Hydraulics report H4134, 2003.

[52]   Cuomo G., Allsop W., and Takahashi, S., "Scaling wave impact pressures on vertical walls," *Coast. Eng.* 57:6 (2010): 604–609

[53]   Cuomo G. et al., "Breaking wave loads at vertical seawalls and breakwaters," *Coast. Eng.* 57:4 (2010): 424–439

[54]   Davidse, M.P. *Experiment analysis - The relation between wave loading and resulting strain in an asphaltic*

concrete revetment. MSc thesis TU Delft, 2009.

[55]   Davidse, M.P., R. 't Hart, H. de Looff, C.C. Montauban, M.F.C. van de Ven, and B.G.H.M. Wichman. *State of the Art Asfalt dijkbekledingen*. STOWA report W06, 2011.

[56]   Dekker, C. "Tussen twee vloeden. De strijd tegen het water in Zeeland bewesten Schelde tussen 1530 en 1532." *Low Ctries. Hist. Rev. BMGN-LCHR* 103:4 (1988): 607–621.

[57]   Dendermonde, Max, and H.A.M.C. Dibbits. *The Dutch and their Dikes*. Amsterdam: De Bezige Bij, 1956.

[58]   Derkzen, B. *Constructief ontwerp van steenzettingen voor dijkbekleding - Numeriek onderzoek naar de liggerwerking van de toplaag*. MSc thesis TU Delft, 2004.

[59]   Docters van Leeuwen, L. "Toe stability of rubble-mound breakwaters." MSc thesis TU Delft, 1996.

[60]   Doorn, N. *Failure modes for revetments and dunes*. Floodsite report T04-01-2, prepared by WL | Delft Hydraulics, 2007.

[61]   Dorst, C.J. "Blokje eraf en blokje erop voor de veiligheid." *Cement*:7 (2003): 28–31.

[62]   _____. *Handleiding ontwerpen van Steenzettingen - landelijke versie 1*. DWW report, 2001.

[63]   Dutta, S.C., and R. Roy. "A critical review on idealization and modeling for interaction among soil-foundation-structure system." *Comput. Struct.* 80:20–21 (2002): 1579–1594.

[64]   Edelman, T. *Stabiliteit van dijkbelopen*., 1958.

[65]   Exalto, J.A. "Algemene beschouwingen omtrent dijkbouw waartoe de ramp aanleiding heeft gegeven." *Polytech. Tijdschr.* 9:31–34 (1954): 691–694.

[66]   Eysink, W.D., and M. Klein Breteler. *Langeduursterkte van Steenzettingen - Verslag van Deltagoot onderzoek*. WL|Delft Hydraulics report H4475, 2005.

[67]   Flikweert, J.J. *Technisch rapport Steenzettingen*. TR25, TAW report by Royal Haskoning, 2003.

[68]   Flikweert, J.J., and D.J. Peters. *Kennisleemtes versus uitvoering: kosten-baten analyse*., 2002.

[69]   Frissen, C.M. *Modelleren van een blokken- en zuilenbekleding*., 2000.

[70]   _____. *Numerieke modellering van een blokken- en zuilenbekleding - simulaties van trekproeven en bezwijken door golfbelasting*., 2000.

[71]   _____. "Numerieke modellering van Steenzettingen: effect in langsrichting van de dijk." MSc-thesis TU Delft, 1996.

[72]   Frissen, C.M., and G.M.A. Schreppers. *Inklemming bij steenzettingen op dijken - numerieke analyse en praktijkaanbevelingen*., 1996.

[73]   _____. *Numerieke modellering van steenzettingen - Zuilenbekledingen met variatiestudies, imperfecties en praktijkaanbevelingen*., 1998.

[74]   Führböter, A., and U. Sparboom. "Full-scale wave attack of uniformly sloping sea dykes." *Coast. Eng. Proc.*, 2174–2188 Malaga, 1988.

[75]   Gazetas, G. "Formulas and charts for impedances of surface and embedded foundations." *J. Geotech. Eng.* 117:9 (1991): 1363–1381.

[76]   Gelder, P.H.A.J.M. van. *Reliability analysis of flood and sea defence structures and systems*., 2009.

[77]   _____. "Statistical methods for the risk-based design of civil structures." PhD thesis TU Delft, 2000.

[78]   Gelder, P.H.A.J.M. van, J.K. Vrijling, and P.J. Hewson. "Uncertainty analysis of impact waves and scale corrections due to aeration." *Proverbs Proc.* 1998.

[79]   Gent, M.R.A. van. *Wave run-up on dikes with shallow foreshores*. WL|Delft Hydraulics report, 2001.

[80]   Gent, M.R.A. van, S.E. Plate, E. Berendsen, G.B.H. Spaan, J.W. van der Meer, and K. d'Angremond. "Single-layer rubble mount breakwaters." *Coast. Struct.* 1999.

[81]   Gent, M.R.A. van, A.J. Smale, and C. Kuiper. "Stability of rock slopes with shallow foreshores." *Coast. Struct.* 2003.

[82]   Gerding, E. "Toe structure stability of rubble mound breakwaters." MSc thesis TU Delft, 1993.

[83]   Gerressen, B. "Stabiliteit van Steenzettingen - Beschouwing van een dijkbekleding als een verend ondersteunde buigligger." MSc thesis TU Delft, 1997.

[84]   Gier, F., H. Schüttrumpf, J. Mönnich, J.W. van der Meer, M. Kudella, and H. Rubin. "Stability of interlocked pattern placed block revetments." *ICCE* Santander, 2012.

[85]   Glerum, A., and G.M. Wolsink. *Achtergronden bij de leidraad cementbetonnen dijkbekledingen*. CUR-VB COW-report, 1984.

[86]   Goda, Y. *Random seas and design of maritime structures*. World Scientific, 2000.

[87]   Goda, Y., S. Takahashi, Y. Tadahiko, and Y. Shuji. *Technical Standards and Commentaries for Port and Harbour Facilities in Japan.*, 2009.

[88]   Grilli, S.T., I.A. Svendsen, and R. Subramanya. "No Title." *J. Waterw. Port Coast. Ocean Engng* 193:3 (1997).

[89]   Groenendijk, H.W. "Shallow foreshore wave height statistics." MSc thesis TU Delft, 1998.

[90]   Groeneweg, J., M.R.A. van Gent, J Nieuwkoop, and Y. Toledo. "Wave Propagation into Complex Coastal Systems and the Role of Nonlinear Interactions." *J. Waterw. Port Coast. Ocean Engng* (2015).

[91]   Grüne, J. "Wave-induced shock pressures under real sea state conditions." *Coast. Eng. Proc.* Malaga, 1988.

[92]   _____. "Wave run-up caused by natural strom surge waves." *Coast. Eng. Proc.* Capetown, 1982.

[93]   Hart, R. 't. *Afschuiving steenzettingen en stabiliteit teenconstructie in relatie tot klemming toplaag.*

[94]   _____. *Klemming in steenzettingen bepalen met VGD-metingen.*, 2012.

[95]   _____. *Ontwikkeling golfrandvoorvaarden tijdens een storm*. Internal note DWW, 2005.

[96]   _____. *Vaststellen van klemming in dijkbekledingen van gezette steen met valgewichtdeflectie- metingen.*, 2013.

[97]   _____. *Veiligheid in steenzettingen*. Internal note DWW, 2005.

[98]   Hart, R. 't, and G. Wolters. *Oude steenzetting overlagen met zuilen op uitvullaag*. Deltares-report 1205571, 2012.

[99]   Hartog, J.P. *Mechanical Vibrations*. Dover publications, first ed. 1934, 1985.

[100]   Heijer, F. den. *Dimensioneringsmethode "blokken op kant met brede voegen."* WL|Delft Hydraulics report H3272-1, 1999.

[101]   _____. *Veiligheid huidige ontwerpmethodiek steenzettingen*. WL|Delft Hydraulics report H3437, 1998.

[102]   Henderson, A. "Breaking wave loads on offshore wind turbines." *EWEA Spec. Top. Conf. Offshore Wind Energy* Brussels, 2001.

[103]   Hernandez, J.A., J.C.P. Johanson, and J.C. van der Burg. *Zuidwal – analyse schade en ontwerp taludbekleding*. DWW report WBA-N 88.053, 1988.

[104]   Hijum, E. van. *Over schade en ijkpunt.*, 2005.

[105]   Hofland, B. *Stability of stone in the top-layer of a granular filter - Literature survey.*, 2000.

[106]   Hofland, B., and M. Klein Breteler. *Nauwkeurigheid van ZSTEEN bij golfklappen*. WL|Delft Hydraulics report H4455, 2005.

[107]   _____. *Nauwkeurigheid Zsteen bij golfklappen*. WL Delft Hydraulics report H4455, 2005.

[108]   Holthuijsen, L.H. *Waves in Oceanic and Coastal Waters*. Cambridge University Press, 2007.

[109]   Hoof, P.J.M. van. "Inklemeffecten bij steenzettingen, een steenzetting als buigligger." MSc thesis TU Delft, 2000.

[110]   Hughes, S.A. *Combined Wave and Surge Overtopping of Levees: Flow Hydrodynamics and Articulated Concrete Mat Stability.*, 2008.

[111]   _____. *The TMA shallow water description and its application*. USACE, CERC report 84-7, 1984.

[112]   Huitema, T. "De grasmat op waterkerende dijken." *OTAR* 43:10 (1959): 191.

[113] _____. *Dijken*. Antwerpen: Kosmos, 1947.

[114] _____. "Glooiing van zuilenbasalt." *OTAR* 43:4 (1958): 59.

[115] _____. "Golfoploop tegen dijken en de middelen daartegen." *OTAR* 39:7 (1955): 154–156.

[116] _____. "Voorstellen van de Deltacommissie, richtlijnen voor dijkontwerp." *OTAR* (1962).

[117] Hussaarts, M. "Een probabilistisch ontwerp van een steenzetting." MSc thesis TU Delft, 1999.

[118] Hussaarts, M., J.K. Vrijling, and P.H.A.J.M. van Gelder. "The probabilistic optimisation of the revetment on the dikes along the Frisian coast." *Coast. Struct.* 1999.

[119] Huurman, M. "Permanent deformation in concrete block pavements." PhD thesis TU Delft, 1997.

[120] Iversen, H.W. "Waves and breakers in shaoling water." *Coast. Eng.* Cambridge, Massachussets, 1952.

[121] Izumiya, T., and M. Isobe. "Breaking criterion on non-uniform sloping beach." *Coast. Eng. Proc.*, 318–327 Taipei, 1986.

[122] Jansma, K. "Commentary golfoploop." *OTAR* 40:2 (1955): 33–35.

[123] Jensen, M.S. *Breaking of waves over a steep bottom slope.*, 2002.

[124] Jensen, O.J. "Safety of breakwater armour layers with special focus on monolayer armour units." *Coasts, Mar. Struct. Break.* Edinburgh, 2013.

[125] Johanson, J.C.P. *Schade aan taludbekleding te Nieuwe Sluis*. DWW report WBA-N-90054, 1990.

[126] Kanning, W. *Analysis and influence of uncertainties on the reliability of flood defence systems.*, 2007.

[127] Kamibuko, K. et al., "Experimental Study on Damage to Wave Splash Barrier for a Coastal Road," *Coast. Struct.*, 2011

[128] Kaslander, K., and M.C.J. Bosters. *Marges bij ontwerp (als gebruikt in Zeeland)*. Internal note RWS, 2006.

[129] Kleij, W. van der. *From pobability of exceedance to probability of flooding*. TAW report, 2000.

[130] _____. *Grondslagen voor waterkeren*. TAW report L7, 1998.

[131] _____, ed. "Leidraad toetsen op veiligheid." TAW report L5, 1999.

[132] _____, ed. "Leidraad Zee- en Meerdijken." TAW report L3, 1999.

[133] Kleij, W. van der, P. van Maas, and A. Paape. *Het probleem van de stabiliteit van steenzettingen*. Note DWW, attached to letter to RWS Director, 3 maart 1997, 1997.

[134] Klein Breteler, M. *Analyse van doorlatendheidsmetingen van steenzettingen*. WL|Delft Hydraulics report H3911, 2002.

[135] _____. *Effectieve duur van langeduurbelasting met variërende golfhoogte.*, 2012.

[136] _____. *Grootschalig modelonderzoek naar stabiliteit van taludbekledingen - anaylse van resultaten van Deltagootproeven*. WL|Delft Hydraulics report, 2000.

[137] _____. *Handboek voor dimensionering van gezette taludbekledingen*. CUR / TAW report 155, 1992.

[138] _____. *Inventarisatie drukbestanden voor Steenzet*. WL Delft Hydraulics report H3565, 1999.

[139] _____. *Inventarisatie van kennisleemten met betrekking tot steenzettingen*. WL|Delft Hydraulics report, 2000.

[140] _____. *Ontwerp van steenzetting met basalt*. WL|Delft Hydraulics note H4422, 2007.

[141] _____. *Open taludbekledingen - Invloedsfactor minimale klemkracht*. WL|Delft Hydraulics report H2530, 1998.

[142] _____. *Taludbekledingen van gezette steen, Analytische en numerieke berekeningen van de stijghoogte onder de toplaag*. WL|Delft Hydraulics report M 1795/H 195 - part XIX, 1991.

[143] _____. *Taludbekledingen van gezette steen - stabiliteit van de toplaag*. WL Delft Hydraulics report M1795 part XX, vol. B / GeoDelft report CO 285453/7, 1992.

[144] _____. *Taludbekledingen van gezette steen - Waterbeweging en golfbelasting op een glad talud - band 1*. WL

Delft Hydraulics report M1795 part XVII, 1990.

[145]   _____. *Validatie Steentoets2008*. WL|Delft Hydraulics report H4846, 2008.

[146]   _____. *Vergelijkend onderzoek zetstenen voor dijken, samenvattend rapport*. Deltares report 1208618-006 for RWS-WVL and revetment element producers, 2015.

[147]   Klein Breteler, M., and A. Bezuijen. "Design criteria for placed block revetments." In *Dikes revetments. Des. Maint. Saf. Assess.*, edited by K.W. Pilarczyk. Rotterdam: A.A. Balkema, 1998.

[148]   _____. "Simplified design method for block revetments." *Conf. Coast. Struct. Break.* London, 1991.

[149]   Klein Breteler, M., A. Capel, G. Kruse, G.C. Mourik, and D. Kaste. *Erosie van een dijk na bezwijken van de steenzetting door golven.*, 2013.

[150]   Klein Breteler, M., C. Kuiper, and A. Bezuijen. *Invloed scheve golfaanval op stabiliteit van steenzettingen*. WL|Delft Hydraulics report H4420, 2006.

[151]   Klein Breteler, M., G.C. Mourik, and M.C.J. Bosters. *Stabiliteit van steenzettingen bij golfaanval, Samenvatting onderzoeksresultaten 2003 – 2013*. Deltares report 1208045-016 for RWS-WVL, 2014.

[152]   Klein Breteler, M., K.W. Pilarczyk, and R. 't Hart. "Influence of ageing and wide wave spectra on stability of placed block revetments." *ICCE* Sidney, 2000.

[153]   Klein Breteler, M., B. van Vossen, and C. Kuiper. *Testen van ZSteen versie 1.8*. WL Delft|Hydraulics report H4331, 2003.

[154]   Klein Breteler, M., and I. van der Werf. *Kennisontwikkeling Steentoets 2006*. WL Delft Hydraulics report H4846, 2006.

[155]   _____. *Stabiliteit steenzettingen op steile taluds*. WL|Delft Hydraulics report H4699, 2006.

[156]   Klein Breteler, M., I. van der Werf, and I. Wenneker. *Kwantificering golfbelasting en invloed lange golven, rev. 2.*, 2012.

[157]   Knaap, F.C.M. van der, M. Klein Breteler, and M.T. de Groot. *Taludbekledingen van gezette steen - Belasting en sterkte van zetsteenverdedigingsconstructies op oevers en dijken*. WL report M1795/1881 deel XVI, 1985.

[158]   Kolff, P.W., and E.F.M. Nieuwenhuis. *Natuurmetingen op zeedijken bewesten Terneuzen*. Fugro report N-0405, 1997.

[159]   Kool-Blokland, J.L. *De rand van 't land - Waterschapsgeschiedenis van Schouwen en Duiveland.* Middelburg: Koninklijk Zeeuws Genootschap van wetenschappen, 2003.

[160]   Kostense, J.K. *Taludbekleding van gezette steen onder golfaanval - Invloed van de doorlatendheid van de fundering - Verslag modelonderzoek*. WL report M1410 deel II, 1981.

[161]   _____. *Taludbekledingen van gezette steen - invloed van de doorlatendheid van de fundering - modelonderzoek*. WL Delft Hydraulics report M1410 part II, 1981.

[162]   Kremer, R.H.J., M.T. Van der Meer, J. Niemeijer, B.A.N. Koehorst, and E.O.F. Calle. *Technisch rapport waterkerende grondconstructies*. TAW report TR19, prepared by GeoDelft, 2001.

[163]   Kuiper, C. *Verplaatsingsmetingen tijdens trekproeven op ingegoten basalt*. WL|Delft Hydraulics report H3990, 2001.

[164]   Kuiper, J.H. "Commentary Golfoploop tegen zeedijken en middelen daartegen." *OTAR* 39:8 (1955): 199–201.

[165]   Laing, A.K. *Guide to Wave Analysis and Forecasting*. 2nd editio. Geneva: WMO report 702, 1998.

[166]   Linde, Q.M. van der. "De Westkapelse zeewering." *OTAR* (1955).

[167]   Linden, H. van der. "De Nederlandse waterhuishouding en waterstaatsorganisatie tot aan de moderne tijd." *Low Ctries. Hist. Rev. BMGN-LCHR* 103:4 (1988): 543–553.

[168]   Litjens-Van Loon, J., H. de Looff, and M. Klein Breteler. "Design and re-use of placed block revetments." *ICCE* Sidney, 2000.

[169]   Looff, H. de. *User Manual Golfklap*. version 1.3, 2009.

[170]   Lubbers, C.L., and M. Klein Breteler. *Grootschalig modelonderzoek naar stabiliteit van taludbekledingen,*

Samenvatting van onderzoek in de Deltagoot. WL|Delft Hydraulics report H3272 rev. 2, 2000.

[171] Mai, S., J. Wilhelmi, and U. Barjenbruch. "Wave height distributions in shallow water." *Coast. Eng. Proc.* (2010).

[172] McConnell, K., and W. Allsop. *Revetment systems against wave attack – A design manual*. Thomas Telford, 1998.

[173] Meer, J.W. van der. *Extreme shallow water wave conditions, Design curves for uniform sloping beaches*. WL-report H0198, 1990.

[174] _____. "Rock slopes and gravel beaches under wave attack." PhD thesis TU Delft, 1988.

[175] _____. *Technisch rapport golfoploop en golfoverslag bij dijken*. TAW report, 2002.

[176] _____. *Veiligheid in rekentechnieken van steenzettingen.*, 2000.

[177] _____. *Wave run-up and wave overtopping at dikes*. TAW report TR23, 2002.

[178] Meer, J.W. van der, K. d'Angremond, and E. Gerding. "Toe structure stability of rubble mound breakwaters." *ICE Coast. Struct. Break.* London, 1996.

[179] Meer, J.W. van der, and M. Klein Breteler. "Measurement and computation of wave induced velocities on a smooth slope." *Coast. Eng.*, 191–204 Delft, 1990.

[180] Meijer, D.G., J.F. Ruff, and H.J. Verheij. *Waterbeweging op grasdijken door golfaanval*. WL Delft Hydraulics report Q1247, 1993.

[181] Meijers, P. *Toepassing theorie afschuiven bekledingen, Open taludbekleding*. TAW report, GeoDelft CO-32321O/5, 1994.

[182] Meijers, P., H.J. van der Graaf, and M.B. de Groot. *Taludbekledingen van gezette steen - Grondmechanische stabiliteit in de golfzone en samenvatting van de onderzoeksresultaten*. WL GeoDelft report M1795/M1881 CO 272511, part XXII, section A, 1991.

[183] Meijers, P., M.B. de Groot, and P. Lubking. *Taludbekledingen van gezette steen - oriënterende berekeningen*. GeoDelft report CO-290730/27, 1990.

[184] Meijers, T. *Open taludbekledingen - Invloedsfactor minimale klemkracht*. WL|Delft Hydraulics report H1770-4.

[185] Mertens, M. "Stability of rock on slopes under wave attack - Comparion and analysis of datasets of Van der Meer and Van Gent et al." MSc thesis TU Delft, 2007.

[186] Mooijman, O.P.M., and M.L. Post. *Trekproeven en doorlatendheidsmetingen op de meetlocaties Mosselbanken en Kruiningen*. Fugro report N-0703, 1999.

[187] _____. *Trekproeven Oesterdam*. Fugro report N-0689, 1999.

[188] _____. *Trekproeven op meetlocatie Paviljoenpolder*. Fugro report N-0719, 1999.

[189] Mourik, G.C. *Locatie maximale belasting op steenzettingen bij ondiepe voorlanden.*, 2012.

[190] Mourik, G.C., and M. Klein Breteler. *Stabiliteit van steenzettingen boven de stilwaterlijn en invloed van een berm*. Deltares report 1202551-009, 2012.

[191] Mulder, G.S. *Trekken van betontegels uit het talud van een dijk*. RWS Deltadienst ONW report 1.0.29, 1970.

[192] Muttray, M.O. *Hillblock model tests.*, 2011.

[193] Nieuwenhuis, E.F.M. *Natuurmetingen aan Basaltonzuilen aan de Nieuwe waterweg te Maassluis ten behoeve van Steenzetonderzoek*. Fugro report M-0103, 1994.

[194] _____. *Natuurmetingen aan Pit-polygoonzuilen aan de Nieuwe waterweg te Maassluis ten behoeve van Steenzetonderzoek*. Fugro report M-0111, 1993.

[195] Nieuwjaar, M. *Notitie Veiligheid Steenzettingen*. Internal note DWW, 2006.

[196] Oumeraci, H., N.W.H. Allsop, M.B. de Groot, R.S. Crouch, and J.K. Vrijling. *Proverbs: Probabilistic design tools for vertical breakwaters*. MAST contract MAS-CT95-0041 for Commission of the European Union, 1999.

[197] Papachristou, K.S., and D.S. Sophianopoulos. "Buckling of beams on elastic foundation considering discontinuous (unbonded) contact." *Int. J. Mech. Appl.* (2013).

[198] Pehlig, M., and M.T.J.H. Smits. *Natuurmetingen op de afsluitdijk ten behoeve van steenzetonderzoek*. Fugro report M-0073, 1991.

[199] _____. *Natuurmetingen op de zeedijk nabij Breskens ten behoeve van steenzetonderzoek*. Fugro report M-0073, 1992.

[200] Peregrine, D H, and L Thais. "The effect of entrained air in violent water wave impacts." *J. Fluid Mech.* 325:1996 (1996): 377–397.

[201] Peters, D.J. *FEM modelling for block revetment research*. Lecture at DIANA User meeting Brescia, 2010.

[202] _____. *Laboratory testing of clamped placed revetments*. RH report 9P0669 for RWS-DWW, Delft Cluster ref. DC2-710-1, 2004.

[203] _____. *Placed revetments under wave attack - Study of structural mechanics*. Delft Cluster report DC1-325-1, prepared by Royal Haskoning, 2003.

[204] _____. *Recommendations for implementation of clamping strength in SteenToets*. Delft Cluster report DC2-710-4 by RHDHV, 2007.

[205] _____. *Veiligheidsbeschouwing SteenToets 2008 - Bepaling veiligheidsfactoren*. RH report 9S8953 for Deltares, 2008.

[206] _____. *Veldproeven op teenconstructies in Zeeland, meetrapport met verkennende analyse.*, 2008.

[207] Peters, D.J., and A. Pfeiffer. *Investigation implementation clamping strength in ZSteen*. RH-report 9R3640 for Delft Cluster, 2007.

[208] Pilarczyk, K.W. "Design of Revetments." Book section.

[209] Pilarczyk, K.W., M. Klein Breteler, and A. Bezuijen. "Wave forces and structure response of placed block revetments on inclined structures." *Int. conf. Coast. Eng.* 1995.

[210] Piontkowitz, T. "Erograss - large-scale investigations of grass cover faillures at sea dikes." *Hydralab III Jt. user Meet.* Hannover, 2010.

[211] Piontkowitz, T., and K. Christensen. *Erograss - Failure of grass cover layers at seaward and shoreward dike slopes - performance, results and conclusions*. Lemvig, Denmark, 2012.

[212] Plasschaert, L.R. *Oever-, strand-, duin- en dijksverdediging*. Amsterdam: C.A.J. van Dishoeck, 1902.

[213] Plooster, A. *Aanvullende metingen Afsluitdijk*. DWW report A2.94.32, 1994.

[214] _____. *Tussentijdse rapportage eerste meetcampagne natuurmetingen op meetlocatie Noord-Beveland*. DWW report, 1990.

[215] Pohl, W. "Die Bemessung der Kleiabdeckung von Deichausenboschungen. Ein Konzept zum Entwurf gleichermassen sicherer wie wirtschaftlicher Seedeiche." *Tagungsband zum HTG Kongress*, 129–138 Bremen, 2005.

[216] Pullen, T., N.W.H. Allsop, T. Bruce, A. Kortenhaus, H. Schüttrumpf, and J.W. van der Meer. *Wave overtopping of sea defence and related structures - Assessment manual.*, 2007.

[217] Rattanapitikon, W., and T. Vivattanasirisak. "Comparison of breaker height formulas using large-scale wave tanks." *Songklanakarin J. Sci. Technol.* 24:4 (2002): 663–674.

[218] Rigter, B.P. *Inklemming van blokken in een rij*. Internal note DWW, 1995.

[219] Rijke, W.G. de, M. Klein Breteler, T.P. Stoutjesdijk, and L.A. Philipse. *Overgangsconstructies in dijkbekledingen*. WL / GeoDelft report H195.02, 1992.

[220] Rijkswaterstaat, and KNMI, eds. *Verslag over de Stormvloed van 1953.* 's Gravenhage: Staatsdrukkerij- en uitgeverijbedrijf, 1961.

[221] Ris, R.C., L.H. Holthuijsen, and N. Booij. "A third-generation wave model for coastal regions – Verification." *J. Geophys. Res.* 104:C4 (1999).

[222] Schiereck, G.J. *Introduction to bed, bank and shore protection*. Delft: Delft University Press, 2001.

[223] Schijf, J.B. *Golfoploop en golfoverslag*. TAW report, 1972.

[224] Schleicher, F. "Zur theorie der Baugrundes." *Der Bauingenieur* 48/49 (1926).

[225] Schoen, S. "Liggerwerking bij steenzettingen - literatuurstudie." MSc thesis TU Delft,

preperatory report, 2003.

[226]   _____. "Liggerwerkingsonderzoek van steenzetting op een wrijvingsloze bedding - Meetverslag van trekproeven." MSc thesis TU Delft, part II, 2004.

[227]   _____. "Wrijvingsproeven van Steenzetting op filter." MSc thesis TU Delft, part I, 2003.

[228]   Schonian, E. *The Shell bitumen hydraulic engineering handbook*. London: ICE Publishing, 1999.

[229]   Schutter, J. de. *Variabelen voor het mechanisme beschadiging steenbekledingen en erosie van het dijklichaam*., 2002.

[230]   Schüttrumpf, H., J.W. van der Meer, A. Kortenhaus, T. Bruce, and L. Franco. "Wave run-up and wave overtopping at armored rubble slopes and mounds." In *Handb. Coast. Ocean Eng.*, edited by Y.C. Kim, 383–409. World Scientific, 2010.

[231]   Schweiger, H.F, and G.M. Peschl. "Reliability analysis in geotechnics with the random set finite element method." *Comput. Geotech.*:32: 422–435.

[232]   Seyffert, J.J.W. "Praktijkervaringen in het steenzettingen onderzoek." *Informatiedag steenzettingen*, 47–53 Centrum Onderzoek Waterkeringen, 1982.

[233]   Shand, TD, WL Peirson, and RJ Cox. "Engineering design in the presence of wave groups." *Coast. Eng. Proc.*, 1–10 2011.

[234]   Slijkhuis, K., and D. Klaassen. *Inventarisatie onzekerheden steenzettingen*. Bouwdienst RWS report, 1999.

[235]   Smith, G.M., J. Wouters, and M. Klein Breteler. *Grootschalig modelonderzoek naar stabiliteit van taludbekledingen - Meetverslag van Deltagootonderzoek*. WL|Delft Hydraulics report H3272-2, 2000.

[236]   Smith, J.M. *Nearshore Wave Breaking and Decay*. USACE, CERC report 93-11, 1993.

[237]   Spaan, G.B.H., G.P. van Vledder, and D.P. Hurdle. *Seventy storms in the Friesche Zeegat*. WL|Delft Hydraulics report H3020, 1996.

[238]   Staverden, J.E. van. *Wrijving en wrijvingscoëfficiënten*. RWS Deltadienst ONW report R-83068, 1983.

[239]   Steeg, P. van. *Stabiliteit van taludbekleding met Hillblocks bij golfaanval - Grootschalig modelonderzoek in de Deltagoot*., 2012.

[240]   Steeg, P. van, and M. Klein Breteler. *Stabiliteit van steenzettingen onder golfaanval, boven de waterlijn en onder een horizontale overgangsconstructie*. Deltares report 31019678, 2009.

[241]   Stevenson, J.D. "Structural damping values as a function of dynamic response stress and deformation levels." *Nucl. Eng. Des.* 60 (1980): 211–237.

[242]   Stigters, K., and M. Klein Breteler. *Trekproeven op dijkbekledingen van de Alblasserwaard*. WL|Delft Hydraulics report H3009, 1999.

[243]   Stoop, J. *Kapstok probabilisme*. Fugro report, 2005.

[244]   Stoutjesdijk, T.P. *Stabiliteit steenzetting te Breskens*. GeoDelft report, 1995.

[245]   Stoutjesdijk, T.P., and A. Bezuijen. *Modelleren van verouderen van steenzettingen*. GeoDelft report CO-353150/15, 1995.

[246]   Stoutjesdijk, T.P., A. Bezuijen, and P. Lubking. *Taludbekledingen van gezette steen - Verouderen van steenzettingen*. Grondmechanica Delft report CO-316860/3, 1991.

[247]   Stoutjesdijk, T.P., and E.O.F. Calle. *Stabilteitscriterium ZSteen- Ch.3: Van toelaatbare overstromingsbijdrage naar toelaatbare kans op bezwijken bekleding*.

[248]   Stoutjesdijk, T.P., M. Klein Breteler, and J.C.P. Johanson. "Inventory of the stability of existing placed block revetments in the Netherlands." *Coast. Eng.* Copenhagen, 1998.

[249]   Stroeve, J.M. *Veiligheidsanalyse steenzettingen - voor enkele dijkvakken langs de Westerschelde*. Bouwdienst RWS report, 2000.

[250]   Suiker, A.S.J. "Inklemeffecten bij Steenzettingen op dijken." MSc thesis TU Delft, 1995.

[251]   Suiker, A.S.J., H.L. Bakker, and J.G. Rots. "Niet-lineair mechanisch gedrag van beton-steenzettingen op dijken." *Cement*:4 (1997).

[252]   Thijsse, J. Th. *Een halve eeuw zuiderzeewerken 1920 - 1970*. Groningen: Tjeenk Willink, 1972.

[253] Tienstra, H., D.J.F Lagendijk, and H. van Hemert. *Leidraad toetsen op veiligheid regionale waterkeringen*. Stowa report ORK 2007-02, 1999.

[254] Timoshenko, S.P. *Strength of materials - Part II Advanced theory and problems, third edition*. Van Nostrand Reinhold Company Ltd., 1956.

[255] Timoshenko, S.P., and J.M. Gere. *Theory of elastic stability - second edition*. McGraw-Hill, 1961.

[256] Timoshenko, S.P., and S. Woinowsky-Krieger. *Theory of plates and shells - second edition*. McGraw-Hill, 1959.

[257] Veen, J. van. *Dredge Drain Reclaim - The Art of a Nation*. 5th editio. The Hague: Martinus Nijhoff, 1962.

[258] Veen, J. van der. "De schade en de herstelwerkzaamheden in de Provincie Zuid-Holland." *Polytech. Tijdschr.* 9:31–34 (1954): 573–580.

[259] Van de Velde, P.A., E.H. Ebbens, and J.A. Van Herpen. *The use of asphalt in hydraulic engineering*. TAW/COW report TR1, 1985.

[260] Verhagen, H.J. "Geconcentreerde golfaanval, veiligheid Oosterschelde dijken." *PT/Civiele Tech.* 40:12 (1985): 35–42.

[261] _____. *The stability of pattern placed revetment blocks*. Pianc report WG114, 2011.

[262] _____. *Trekproeven op glooiingsconstructies in de Oosterschelde*. RWS report Adviesdienst Vlissingen WWKZ-84.V002, 1984.

[263] Verhagen, H.J., G.P. van Vledder, and S. Eslami Arab. "A practical method for design of coastal structures in shallow water." *Coast. Eng.*, 1–11 Hamburg, 2008.

[264] Verruijt, A. *Grondmechanica*. 4th editio. Delftse Uitgevers Maatschappij, 1993.

[265] _____. *Soil dynamics*. TU Delft, 2008.

[266] Visser, M.M. de. *A clay layer as a revetment for sea dikes – The behaviour of clay under wave loading*. MSc thesis TU Delft, 2007.

[267] Visser, P.J., H. Taat, and H.B. Schoonman. *Taludbekledingen van gezette steen - fase 2 - verslag onderzoek*.

[268] Visser, P.J., and J. van der Weijde. *Basalton - Stability under attack by waves - Report of large scale model investigation in the Delta flume.*, 1983.

[269] Vliet, F. van. "Verouderen van steenzettingen - Doorlatendheid en stabiliteit van een ingezande filterlaag." MSc thesis TU Delft, 1994.

[270] Voortman, H.G. "Risk-based design of large-scale flood defence systems." PhD thesis TU Delft, 2003.

[271] Vrijling, J.K. *General wave spectrum model*. TU Delft report for Mast III Proverbs project, 1996.

[272] Vrijling, J.K., and J. Bruinsma. "Hydraulic Boundary Conditions." *Symp. Hydraul. Asp. Coast. Struct.*, 109–132 Rotterdam, 1980.

[273] Vrijling, J.K., and P.H.A.J.M. van Gelder. "The effect of inherent uncertainty in time and space on the reliability of flood protection." *Eurepean Saf. Reliab. Conf.* Trondheim, 1998.

[274] _____. "Uncertainty analysis of non-breaking waves." *Proverbs Proc.* 1998.

[275] Vrijling, J.K., C. van Horst, and P.J.M. van Hoof. "The structural analysis of the block revetments on the Dutch dikes." *ICCE* Sidney, 2000.

[276] Vrouwenvelder, A.C.W.M., and P. Schiessl. "Durablity aspects of probabilistic ultimate limit state design." *Heron* 44:1 (1999): 19–29.

[277] Vrouwenvelder, A.C.W.M., and J.K. Vrijling. *Probabilistisch ontwerpen*. TU Delft lecture notes b3, 1982.

[278] Vuren, S. *Validatie methode De Haan - Deel 1: validatie Hydra-K*. WL|Delft Hydraulics report Q4409, 2008.

[279] Waal, J.P. de. *Taludbekledingen van gezette steen - Golfdruk op het talud - deel A: analyse van meetgegevens, verslag modelonderzoek*. WL|Delft Hydraulics report H195/H1257, 1992.

[280] Waal, J.P. de, M. Klein Breteler, and H den Adel. *Taludbekledingen van gezette steen - Golfdruk op het talud - deel B: verbetering van het analytisch model en STEENZET, verslag bureaustudie*. WL|Delft Hydraulics report H195/H1256/H1770/H2499, 1995.

[281] Weggel, J.R. "Maximum breaker height for design." *Coast. Eng.* Vancouver, 1972.

[282] Weijers, J.B., and E.P. Haas. *Voorstel inklemming van open steenbekledingen*. Internal note DWW, 1999.

[283] Wemelsfelder, P.J. "Wetmatigheden in het optreden van stormvloeden." *Ing.* 54:9 (1939): 31–35.

[284] Westen, C.J. van. *Veiligheid Nederland in Kaart - Hoofdrapport onderzoek overstromingrisico's*. RWS report VNK 2005, 2005.

[285] Westhuysen, AJ van der. "Modeling nearshore wave processes." *ECMWF Work. Ocean Waves*, 25–27 2012.

[286] Wevers, A. *Stabiliteit taludbekledingen van gezette steen onder golfaanval - verslag modelonderzoek*. WL report M1057, 1970.

[287] Wilderom, M.H. *Tussen afsluitdammen en deltadijken – deel II – Noord-Zeeland*. Middelburg: Littooij & Olthoff, 1964.

[288] _____. *Tussen afsluitdammen en deltadijken – deel III – Midden-Zeeland*. Middelburg: Littooij & Olthoff, 1968.

[289] _____. *Tussen afsluitdammen en deltadijken – deel IV – Zeeuws Vlaanderen*. Middelburg: C.V. Drukkerij G.W. den Boer, 1973.

[290] Wolters, G., and M. Klein Breteler. *Normaalkracht in steenzetting met blokken op hun kant.*, 2007.

[291] Wouters, J. *Taludbekledingen van gezette steen - Eindverificatie Deltagoot onderzoek*. WL|Delft Hydraulics report M1795 deel XXIII, 1991.

[292] Zandwijk, R., and E.F.M. Nieuwenhuis. *Natuurmetingen op meetlocatie Colijnsplaat*. Fugro report N-0099, 1995.

[293] _____. *Natuurmetingen op meetlocatie Oesterdam*. Fugro report N-0300, 1996.

[294] Zanten, E. van, and Y. Provoost. *Effect zandhonger op de steenbekledingen van de dijken van de Oosterschelde*. Internal note RWS RW1809-28/HITM/227, 2013.

[295] Zanuttigh, B., and J.W. van der Meer. "Wave reflection from coastal structures." *ICCE* 2006.

[296] _____. "Wave reflection from coastal structures in design conditions." *Coast. Eng.* 55 (2008): 771–779.

[297] Zhou, H.M. "Towards an operational risk assessment in Flood Alleviation." PhD thesis TU Delft, 1995.

[298] Zhu, Y. "Breach Growth in Clay-Dikes." PhD thesis TU Delft, 2006.

[299] Zwanenburg, S.A.A. "The influence of the wave height distribution on the stability of single layer concrete armour units." MSc thesis TU Delft, 2013.

[300] Zwanenburg, S., W. Uijttewaal, E. ten Oever, and M.O. Muttray. "The influence of the wave height distribution on the stability of interlocking single layer armour units." *Coasts, Mar. Struct. Break.* Edinburgh, 2013.

References without author

[301] "Centrifuge- en wrijvingsproeven voor de Oosterschelde kering." *Deltawerken* 97 (1981): 369–376.

[302] *Damwandconstructies*. CUR report 166, 5th edition, 2012.

[303] *Gedenkboek twee eeuwen waterstaatswerken*. Amstelveen: Kramer, 1959.

[304] *Hydraulische randvoorwaarden 2001, voor het toetsen van primaire waterkeringen*. DWW report, 2002.

[305] *Hydraulische Randvoorwaarden Primaire Waterkeringen voor de derde toetsronde 2006-2011*. DWW report, 2007.

[306] *Leidraad Kunstwerken*. TAW report L15, 2003.

[307] "Ontwikkelingen in het denken over dijken." *Deltawerken*:24 (1978): 175.

[308] *Probabilistic design of flood defences*. CUR/TAW report 141, 1990.

[309] *Schouwsche Voorwaarden – behorende bij de bestekken voor de uitvoering van werken ten laste van het Waterschap Schouwen*. Zierikzee: De Mooij & Mommaas, 1891.

[310] *Trekproeven dijkvak Braakmanhaven Zeeland*. Consulmij report 21.0101.IH, 1999.

[311] *Trekproeven langs diverse dijkvakken Friesland*. Consulmij report 20.0256.MK, 2001.

[312] *Trekproeven langs diverse dijkvakken langs Westerschelde*. Consulmij report V.99.0487.AvG, 1999.

[313] *Veiligheid van bouwconstructies, een probabilistische benadering*. CUR-VB report 109, 1982.

[314] *Veiligheid van de primaire waterkeringen in Nederland, Voorschriften Toetsen op veiligheid voor de tweede toetsronde*. DWW report VTV, 2004.

[315] *Verslag over den Stormvloed van 9 februari 1889*. Algemeene Landsdrukkerij, 1889, 1889.

[316] *Voorschrift Toetsen op Veiligheid Primaire Waterkeringen*. DWW report VTV 2006, 2007.

Acknowledgements

Im normalen Leben wird einem oft gar nicht bewußt,
daß der Mensch überhaupt unendlich mehr viel mehr empfängt, als er gibt,
und daß Dankbarkeit das Leben erst reich macht.

Dietrich Bonhoeffer

Practising engineers devote their professional life to creating new things, at least to things that are new to themselves. Contributing to civil engineering projects that go through the whole cycle of project definition, design, execution and operation is fascinating. The projects are generally beneficial to society, they demand for creativity and enable the engineer to reach out for something new. Over the years I felt the ambition of overarching the project-cycle work by more systematically researching technical problems and subjects and making results available for the engineering community.

Being open for new subjects I met Han Vrijling around 2002 and he suggested that the subject of the design of the pitched revetments might benefit from a research project undertaken from the perspective of a structural engineer.

There was a coincidence with a request for reliable design methods for the numerous projects of revetment replacement initiated after 1997. The Dutch government granted projects for desk studies and experimental work to a number of companies, amongst them my employer Royal Haskoning. I was in the fortunate position to hat I could join a small project team that was given the task to write an analysis report about prioritising the unknowns within the cross-disciplinary field of revetment and dike design. As a research method we started with questionnaires and interviews of revetment-specialists in the country. I am still grateful for the steep learning curve and for the fact that many of the specialists were eager and expectant about the 'unknown factor' of element-interaction (or 'clamping').

I had the feeling that making a contribution here was within my reach. There actually was a perfect synthesis of my knowledge at the time and the clear need of further developing and verifying the insights of the pattern-placed revetments being coherent structures.

Between 2003 and 2009 we have executed a series of reconnaissance studies, experimental verification work, we made analysis reports and we worked on implementation of design and approval methods for the revetments water defences. That work has not been done in isolation. It was a fruitful cooperation between Rijkswaterstaat DWW and the Project Office Zeeweringen as employers, WL|Delft Hydraulics, later Deltares as a partner in the research and Delft Cluster as a funding body. My employer Royal Haskoning has co-funded projects.

During a number of those years the research was coordinated and reviewed by a small steering committee that consisted of Han Vrijling, Robert 't Hart (DWW), Mark Klein Breteler (WL) and Adam Bezuijen (Geodelft). I like to thank them for the inspiring discussions and for the possibilities that were created to extend the chain of investigation tasks with new links.

I have also very much appreciated the support of Yvo Provoost (Projectbureau Zeeweringen) and Henri Opdam and later Frans Rochar (Delft Cluster).

I have enjoyed the support and inspiration of working with the MSc-students Bianca Derkzen, Stijn Schoen and Joris Blom. Especially Stijn and Joris who have set-up and executed the experimental work have gladly spend quite some hours, together with the

personnel of the Stevin II lab of the TU Delft and the colleagues of BAS Research and Development BV.

From the perspective of the content of my contributions I am tributary to many more people that have spent time and efforts in many studies and investigations in the subject of block revetments over the last 30 years roughly.

After 2008 Rijkswaterstaat DWW quitted its central role in identifying and awarding research projects. Most of the research work on 'clamping' was done and results of this study were implemented in the software programme that Deltares has developed for the (dis)approval of the existing pattern-placed revetments and the design of new slopes.

The idea of composing a doctoral thesis in English language out of a pile of Dutch research reports emerged around 2006. Somehow it has taken to 2017 to really complete this task. During a number of the past years the thesis work has been in competition with other professional fascinations. Completion of the thesis partly became a private activity, and it was of course less important than the joy and blessings of family life.

I am very glad though that the work could be completed, and I therefore really express appreciation for the patience, the enduring support and encouragement to complete this work of my promotor Han Vrijling, co-promoter Henk-Jan Verhagen and part-time employer Bas Jonkman.

And last-but-not-least I thank my wife, my daughters and my parents for tolerating my focus on the thesis work now and then, for their love and support and everything else they made possible.

Curriculum Vitae

Dirk Jan Peters was born in Gouda in 1969. He grew up in the small village of Moerkapelle and joined secondary school (Athenuem) in Gouda.

He was trained as a civil engineer at TU Delft and graduated in 1992 on the subject of cable stayed steel bridges. During his military service he joined the laboratory of TNO Defence research, and contributed to research on blast-loaded concrete and steel structures.

Since 1994 he is employed by the consulting engineering firm Haskoning, presently Royal HaskoningDHV, where he worked on numerous civil engineering projects in the building industry and in the field of hydraulic and maritime structures.

He took up research tasks in pattern-placed revetments, and more recently in earthquake engineering, in material fatigue and in local buckling of large steel tubular piles. He participates in national and European research committees on the subjects of quay walls, seismic resistant design, and steel construction.

As a side activity he lectures in structural mechanics and concrete construction for post-BSc degree courses for structural engineers. Since 2014 he is part-time employed by TU Delft, working in the field of hydraulic structures and flood risk.

He is married to Ingrid van Beynum and has three daughters, Cecilia (2006), Eleonore (2008) and Rozemarijn (2011).

DESIGN OF PATTERN-PLACED REVETMENTS

ANNEXES

ANNEX A   RESISTANCE MODELS

The resistance of pattern-placed revetments under wave loading consists of the self-weight of the revetment top-layer elements that are subject to the concentrated wave loading, plus the weight of other revetment elements. In order to mobilise this extra weight the revetment needs to act as a coherent structure.

The model descriptions in this Annex start with introducing and analysing in-plane forces, which are the main cause of coherence. Axial beam models (see section A.1) accurately evaluate the in-plane forces. The principles of the action of gravity on the slope, the function of friction forces and the function of the joints and the toe structure are included in the models. The effect of elastic foundation properties of the sub-layers, staged construction and settlements can be demonstrated. Waves cause uplift forces on the revetment, but also cause pressures in the joints, which decrease the effective in-plane forces in the joints and reduce the resistance.

The water head differences under and above the top-layer elements cause perpendicular loads on the revetments beam. Upward as well as downward loads can generate internal shear forces and bending moments in the revetment beam. This is studied in section A.2 with models of beams on elastic foundations. The wave impact causes dynamic effects in the structure. The uplift loads present themselves a bit more slowly compared to the structures natural frequency and can be treated as static loads. The effects of the elastic foundation are less important for the uplift loads. Hence simple isolated beam models (refer to section A.3) are sufficiently accurate to model the effects of those loads. This results in a simple structural model approach. Simple beam model formulas can be evaluated for single element loads and for wave loads as well. The internal forces provide a basis for comparison of pull test results and resistance to wave loads. Deformation of the revetment beam is governed by deformation in the joints. Therefore the flexibility of the joints is studied in section A.4.

If the revetment beam experiences extreme deformation, it becomes subject to buckling caused by the in-plane forces. This is studied in section A.5 because it occurs in the tests described in annex E. This phenomenon is less relevant in practice since it is not safe to rely on second-order phenomena that might increase stability.

A.1   Axial beam model

A.1.1   Axially loaded beam

In an ideal situation the top-layer can be considered as a row of elements on a sliding foundation. The elements rest against an immoveable toe structure. The component of the gravity force $q_x = -\rho_s gDB_y \sin(\alpha)$ is acting as a distributed axial load. The load is acting in the negative x-direction. Due to this pre-load a coherent beam is formed.
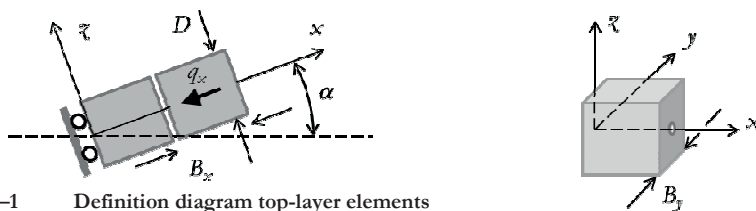
Figure A–1   Definition diagram top-layer elements

Since the foundation is considered as sliding, the element gravity loads are successively transferred to the elements in lower position. The load causes accumulated stresses in the elements and in the joints, which can be expressed as the normal force N.

$$N(x) = -\int q_x dx = -q_x x + c \qquad \text{Eq. A.1}$$
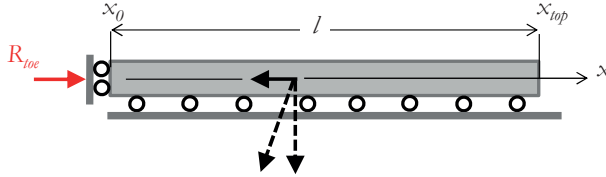
Figure A–2   **Axially loaded beam on sliding foundation**

With boundary condition $N = 0$ at the top edge x_{top} of the revetment, the constant c in the expression becomes $c = q_x x_{top}$.

$$N(x) = -q_x(x - x_{top}) = \rho_s g D B_y (x - x_{top})\sin(\alpha) \qquad \text{Eq. A.2}$$

Counting for the underwater weight, the load function $q_x(x)$ is written as:

$$q_x = \begin{array}{ll} -\rho_s g\, DB_y \sin(\alpha) & x > x_{SWL} \\ -\rho\, g\, \Delta DB_y \sin(\alpha) & x < x_{SWL} \end{array} \qquad \text{Eq. A.3}$$

The outcome of this friction-less model is here – arbitrarily – defined as the neutral normal force N_{neutral}. In reality and as an outcome of more sophisticated models the normal force can become both lower and higher than in this neutral, non-friction case.

$$N_{\text{neutral}} = \rho_s g D B_y (x - x_{top})\sin(\alpha) \quad \text{or} \quad \rho_s g D B_y (z - z_{top}) \qquad \text{Eq. A.2}$$

A.1.2   Axially loaded beam on elastic foundation

The differential equation for the axially loaded elastic beam, axially supported by distributed elastic springs, can be written as:

$$\frac{dN}{dx} + q_x - r_x = 0 \qquad \text{Eq. A.4}$$

with

$$N = E_a DB_y \frac{du}{dx} \quad \text{and} \quad r_x = k_x B_y u \qquad \text{Eq. A.5}$$

$$q_x(x) = -E_a DB_y \frac{d^2 u}{dx^2} + k_x B_y u \qquad \text{Eq. A.6}$$
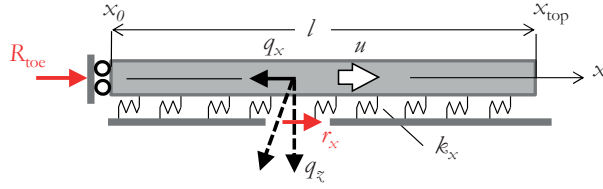
Figure A–3   Axially loaded beam on elastic foundation with unmoveable toe structure

The general form for $q = 0$ is:

$$\frac{d^2 u}{dx^2} - \frac{1}{\lambda_k^{\,2}} u = 0 \ \text{ with } \ \lambda_k = \sqrt{\frac{E_a D}{k_x}} \qquad\qquad \textbf{Eq. A.7}$$

Evaluation of the equation for boundary condition $u = 0$ at x_0, the location of the toe, gives following value of the normal force against the (unmoveable) toe.

$$R_{toe} = q_x \lambda_k \frac{1 - e^{-2l/\lambda_k}}{1 + e^{-2l/\lambda_k}} \qquad\qquad \textbf{Eq. A.8}$$

with

$l = x_{top} - x_0$, being the length of the slope.

The parameter λ_k is a characteristic length, that expresses the relation between the stiffness of the top-layer and the spring supports. Assuming values for $E_a = 3 \times 10^9$ N/m², $D = 0.33$ m and $k_x = 10^7$ N/m³, gives $\lambda_k = 10$ m. For slopes with $l/\lambda_k = 1$, approximately 80% of the in-plane weight component G_x rests against the toe and 20% is balanced with distributed friction forces. For slopes with $l/\lambda_k = 2$, these figures become 50%. Additional slope length above $l/\lambda_k = 2$, hardly contributes to an increase of R_{toe}.
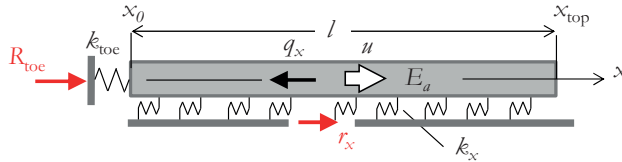
Figure A–4   Elastic axial beam model with elastic toe structure

Evaluation of the equation for boundary condition with a discrete finite stiffness k_{toe} at the toe, gives following formula of the normal force against the toe.

$$R_{toe} = \frac{q_x \lambda_k}{\dfrac{1 + e^{-2l/\lambda_k}}{1 - e^{-2l/\lambda_k}} + \dfrac{k_x \lambda_k}{k_{toe}}} \qquad\qquad \textbf{Eq. A.9}$$

In this equation the ratio $k_x \lambda_k \,/\, k_{toe}$ is important.

A.1.3 Staged construction

The solution presented in the previous paragraph is based on a completed elastic system with a zero initial stress state and a sudden application of the gravity load. In practice it works the other way around: the structure on the slope will be built in stages, whilst the gravity load is present from the beginning. Especially for long slopes, the potential effect of the staged construction on the distribution of normal force in the top-layer seems significant.

A solution for the staged construction can be derived from standard cases of elastic beams with boundary conditions that transfer forces. Consider a beam of finite length $l_n = l/n$ with discrete spring support at the left boundary and a force load at the right boundary. The elastic response at the right boundary is the input spring constant for the next beam element. The load is applied and evaluated per element and the local displacement variable $u(x)$ has a zero value before application of the load.
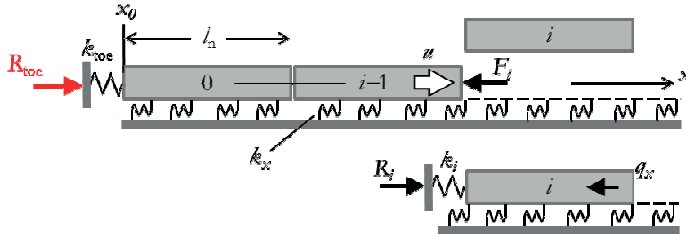
Figure A–5   **Elastic axial beam model of staged construction**

The value of the acting load at the right boundary of the element i–1 is the normal force that exists at the left hand boundary of next element i.

$$F_i = \frac{q_x \lambda_k}{\dfrac{1+e^{-2l_n/\lambda_k}}{1-e^{-2l_n/\lambda_k}} + \dfrac{k_x \lambda_k}{k_i}}$$

Eq. A.10

with

$$k_i = \frac{E_a D B_y}{c_{k,i} \lambda_k} \text{ for } i = 1 .. n$$

$$c_{k,i} = \frac{e^{il_{ni}/\lambda_k}}{e^{il_{ni}/\lambda_k} - (\dfrac{1+k_0/k_x\lambda_k}{1-k_0/k_x\lambda_k})e^{-il_{ni}/\lambda_k}} + \frac{e^{-il_{ni}/\lambda_k}}{(\dfrac{1+k_0/k_x\lambda_k}{1-k_0/k_x\lambda_k})e^{il_{ni}/\lambda_k} - e^{-il_{ni}/\lambda_k}}$$

Eq. A.11

$$k_0 = k_{toe}$$

The applied load F_i is transferred through the system with length $i \times l_n$. The longer the system, the smaller is the fraction of F_i that rests against the toe.

$$N_{0i} = c_{F,i} F_i$$

$$c_{F,i} = \frac{1}{e^{il_{ni}/\lambda_k} - (\dfrac{1+k_0/k_x\lambda_k}{1-k_0/k_x\lambda_k})e^{-il_{ni}/\lambda_k}} - \frac{1}{(\dfrac{1+k_0/k_x\lambda_k}{1-k_0/k_x\lambda_k})e^{il_{ni}/\lambda_k} - e^{-il_{ni}/\lambda_k}}$$

Eq. A.12

The total force against the toe is calculated with:

$$R_{toe} = F_0 + \sum_{i=1}^{n-1} c_{F,i} F_i$$

<div align="right">Eq. A.13</div>

The formulas are evaluated for n = 1, 2, 5, 10 and 20. n = 1 represents the case where the complete structure is loaded in one step. n = 2 represents two construction stages and two load steps. A high value of n represents a more gradual construction process. It was found that in cases where an elastic calculation with one load step results in e.g. approximately 0.5 $N_{neutral}$ at the toe, the solution for a gradually constructed and loaded structure, is roughly 30% higher, e.g. 0.65 $N_{neutral}$. In that case the friction forces in the upper part of the slope are smaller. For cases with short slopes and/or a small value of the foundation stiffness, the difference between the solution for one load step and the gradually loaded slope appears not significant. For very low values of the toe stiffness, the solution for a gradually loaded slope can lead to smaller values of R_{toe}.

A.1.4 Settlement of the foundation

The force distribution in the top-layer is changing over time. Tide and wave action tend to change the position of the elements on the foundation by shaking them and exerting compressive and tensile loads perpendicular to the element. This process changes the force interaction between the top-layer and the foundation. Settlement of the dike body will also create movement and change the axial force distribution.

Settlement of the dike body can be caused by compression of under layers or by compression of core material of the dike. In both cases differential settlement will occur between top and toe of slope. The changed vertical position of the under layer material causes a reduction in length of the slope. Along the slope line, the material of the top-layer elements is less easily compressed than the foundation layers. The under layers and filter layers tend to move down the slope while the top-layer elements tend to keep their position. Shear deformation under the top-layer results in change of relative element position and in friction forces acting on the interface between top-layer and foundation layers.
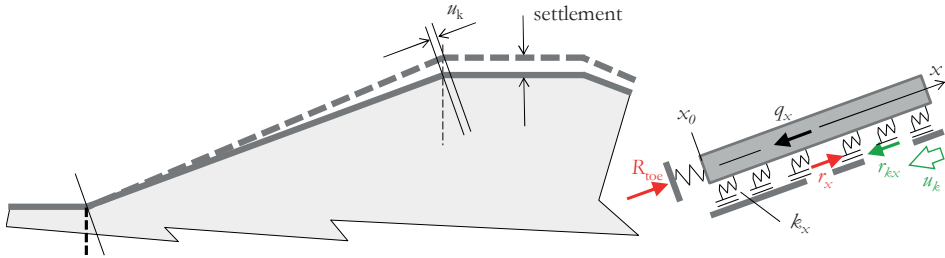
Figure A–6   **Elastic axial beam model on a settling slope**

Presuming the differential displacements being distributed following a linear function, the displacement field is given as:

$$u_k(x) = u_k x / l$$

<div align="right">Eq. A.14</div>

with u_k = the shortening of the line of the foundation of the revetment

This initial imposed displacement function causes a distributed load r_{kx}, which is limited due to the friction capacity on the interface.

$$r_{kx} = -k_x u_k(x)$$

$$r_{kx,max} = f_{fr} q_z$$

with $q_z = \rho_s g D B_y \cos(\alpha)$

This can mean that the function r_{kx} splits in two fields:

$$r_{kx} = k_x u_k x / l \qquad\qquad \text{for } x < a$$

$$r_{kx} = f_{fr} \rho_s g D B_y \cos(\alpha) = q_{2x} \quad \text{for } a < x < l$$

$$a = \frac{q_{2x} l}{k_x u_k}$$

Eq. A.15

Table A–1   Parameters effect of settlement load on normal force

$\cot(\alpha)$	2.5	3	3.5	4	5
α	21.8	18.4	15.9	14.0	11.3
$\sin^2\alpha$	0.1379	0.1000	0.0755	0.0588	0.0385
u_k [m] in case of 0.1 m settlement of 5 m high dike	0.037	0.032	0.027	0.024	0.020
$\cot(\alpha)$	2.5	3	3.5	4	5
α	21.8	18.4	15.9	14.0	11.3
$\sin(\alpha) - f_{fr}\cos(\alpha)$	-0.186	-0.253	-0.302	-0.340	-0.392
$\sin(\alpha)$	0.371	0.316	0.275	0.243	0.196
$\sin(\alpha) + f_{fr}\cos(\alpha)$	0.928	0.885	0.852	0.825	0.784

The equilibrium equation is:

$$\frac{dN}{dx} + q_x - r_x - r_{kx} = 0$$

Eq. A.16

The solution for $R_{toe} = N(x = 0)$ for the elastic case with a linear function u_{kx} is:

$$R_{toe} = \frac{q_x \lambda_k + k_x u_k \dfrac{\lambda_k^2}{l} \dfrac{1 - 2e^{-l/\lambda_k} + e^{-2l/\lambda_k}}{1 - e^{-2l/\lambda_k}}}{\dfrac{1 + e^{-2l/\lambda_k}}{1 - e^{-2l/\lambda_k}} + \dfrac{k_x \lambda_k}{k_{toe}}}$$

Eq. A.17

The solution for the case with maximum negative friction for the part of the slope with $x > a$ is:

$$R_{toe} = \frac{q_x \lambda_k + k_x u_k \dfrac{\lambda_k^2}{l} \dfrac{1 - e^{-a/\lambda_k} - e^{-(2l-a)/\lambda_k} + e^{-2l/\lambda_k}}{1 - e^{-2l/\lambda_k}}}{\dfrac{1 + e^{-2l/\lambda_k}}{1 - e^{-2l/\lambda_k}} + \dfrac{k_x \lambda_k}{k_{toe}}}$$

or

$$R_{toe} = \frac{q_x \lambda_k + q_{2x} \dfrac{\lambda_k^2}{a} \dfrac{1 - e^{-a/\lambda_k} - e^{-(2l-a)/\lambda_k} + e^{-2l/\lambda_k}}{1 - e^{-2l/\lambda_k}}}{\dfrac{1 + e^{-2l/\lambda_k}}{1 - e^{-2l/\lambda_k}} + \dfrac{k_x \lambda_k}{k_{toe}}}$$

<div align="right">Eq. A.18</div>

The analyses outcomes presented in Figure A–7 clearly show the importance of the stiffness of the toe. The difference between the first two graphs is the slope length. For the case with the longer slope and the weak toe is can be noticed that the revetment of the top part of the slope is for almost 100% resting on the shear spring and on friction.

The difference between the second and third graph is the toe stiffness, being in the third graph three times higher than in the second graph. The settlement load case causes extra development of normal force. If the toe stiffness k_{toe} is too low the increased normal force in the upper part of the slope will decrease in the lower part of the slope.

The conclusion of the beam on slope analysis is that small settlement loads and limited toe stiffness have a large influence on the initial normal force distribution.

$f_{\text{fr}} = 0.6$

$\lambda_{\text{k}} = 5.0$

$l\,/\,\lambda_{\text{k}} = 2.0$

$\cot\alpha = 3$

$k_{\text{x}}\lambda_{\text{k}}/\,k_{\text{toe}} = 0.67$

$u_{\text{k}}\,/l = 0.0004$

$l/D = 30$

$\rho_{\text{s}} = 2500 \text{ kg/m}^3$

— neutral, sliding
--- upperbound due to negative friction
--- elastic foundation
— elastic foundation + elastic toe
--o--- elastic foundation + elastic toe + settlement
--o-- elastic foundation + elastic toe + settlement + friction cut off
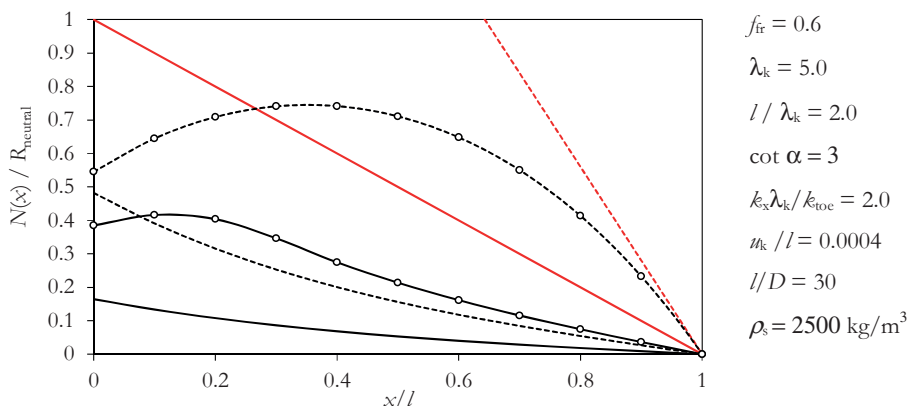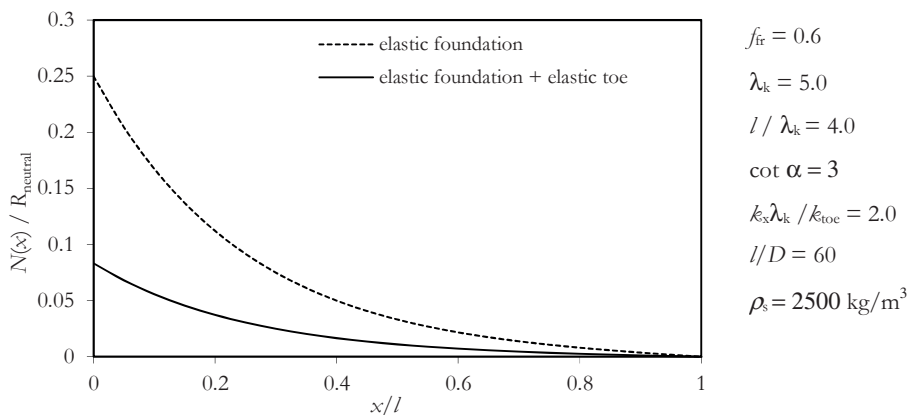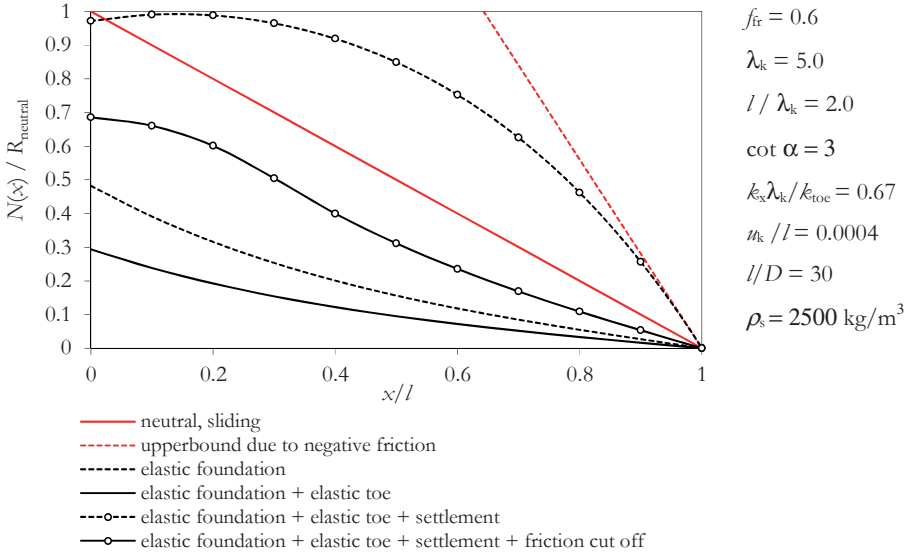
Figure A–7   **Normal force diagrams from model calculations of axially loaded beams on elastic foundation**

A.1.5 *Effects of wave loads*

Wave loads cause water pressure at the topside of the revetment and filter water pressures on the underside and consequently variable perpendicular loads on the revetments. Wave loads also cause water pressures in the joints that – similar to pore pressures in soils – decrease the effective contact pressure in between the elements, and hence the axial force in the revetment beam. Consequently the resistance against bending moments and shear forces is reduced. This effect can be demonstrated using the output of ZSTEEN model calculations.

ZSTEEN is a flow model that computes filter water head values h_{bed} from measured water heads h_{wave} on the slope. Measured data are available from instrumented flume tests. With the ZSTEEN output it is possible to compute forces P on the revetment elements per time step (typically 0.05 sec). The forces P_z are found by integration of the pressures acting on the top and bottom surfaces of the elements. The forces P_x are found by integration of the pressures acting on the sides of the elements, e.g. in the joints. It is assumed that the water head difference above and under the top-layer has a constant gradient over the joint height. For the axial models the forces P_x are of particular interest.

$$
\begin{aligned}
P_{x;i} &= \tfrac{1}{2}\left(p_{wave;i} - p_{wave;i+1} + p_{bed;i} - p_{bed;i+1}\right)DB_y \\
&= \tfrac{1}{2}\rho g\left(h_{wave;i} - h_{wave;i+1} + h_{bed;i} - h_{bed;i+1}\right)DB_y + \rho g DB_x B_y \sin\alpha \\
P_{z;i} &= \tfrac{1}{2}\left(p_{wave;i} + p_{wave;i+1} - p_{bed;i} - p_{bed;i+1}\right)B_x B_y \\
&= \tfrac{1}{2}\rho g\left(h_{wave;i} + h_{wave;i+1} - h_{bed;i} - h_{bed;i+1}\right)B_x B_y - \rho g DB_x B_y \cos\alpha
\end{aligned}
$$

Eq. A.19
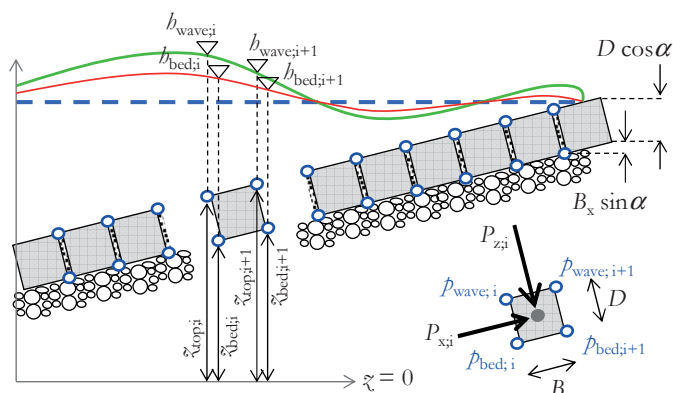
Figure A–8   Definition diagram element forces P_x and P_z extracted from ZSTEEN results

The calculated forces P_x and P_z for a of wave test with H_s = 2.2 m and T_p = 7 sec with a slope angle of 1:5 are plotted in Figure A–11. For the structure a block revetment with D = 0.25 m, ρ_s = 2350 kg/m^3, B_x = 0.5 m and Λ = 1.05 m was chosen[270]. This finally leads to a calculated stability result $H_s/\Delta D$ = 6.5, which would be a rather high load level in practice, but is considered adequate for demonstration of the phenomena. The maximum downward force P_z occurs at the peak of a wave impact. The minimum (upward) P_z occurs 0.2 seconds later. Both time steps are highlighted with blue colours in Figure A–11. It can be seen that the self-weight of the elements is exceeded over a distance of 4 elements and during a number of time steps. The high impact pressures are associated with positive forces P_x at the landside of the wave impact and negative P_x values at the seaside.

The P_x forces are loads on the axial revetment beam and influence the normal force and bedding reaction forces under the elements. When the sliding beam model with an infinitely stiff toe is used (refer to Figure A–2), the normal force as shown in the last picture of Figure A–11 is found. N_x follows from integration of all the forces P_x over the length and the requirement of N = 0 at the top. It can be seen that due to the effect of submergence the normal force at the toe drops with a factor Δ. The peak impact force lowers the effective normal force considerably. Noticeable is that for the time step and the location of maximum uplift (light blue line, element 19/20) the drop of normal force is not very large. It seems that the revetment beam is at the locations of the uplift force adjacent to the wave impact to some extent re-compressed by the force P_x.

The sliding axial beam model is a too simple model with too favourable, not conservative outcomes. To demonstrate this the ZSTEEN results are also applied on a model with axial spring supports with a friction limit of their capacity (see Figure A–9). The perpendicular forces P_z determine the perpendicular load on the interface and hence the friction cut off, and consequently the axial force distribution. Thus an interaction of the perpendicular and axial calculations is introduced. This is mathematically complicating. The problem was first solved[271] finding analytical solutions for the uplift force and associated portions of beam

---

[270] Case #9 in D.J. Peters and A. Pfeiffer, 2007.
[271] D.J. Peters and A. Pfeiffer, *Investigation implementation clamping strength in ZSteen* (RH-report 9R3640 for Delft Cluster, 2007)

lengths that lost contact with the foundation, experienced reduction or increase of contact pressure as a result of sets of forces P_z. This result was used as an input to numerical calculations based on a stiffness matrix, adjusted for each time step, and to be solved iteratively within each time step. Later[272] a model was made with the high-end commercial FEM software TNO-DIANA. In this model axial and lateral spring action was implemented as well as joint interaction. For numerical stability reasons the calculations were carried out with full dynamic time-integration. The perpendicular results were not correct, since it appeared not possible to let elements lift from their no-tension supports, let them 'hover' above the supports and move down back on the supports without generating support forces r_z. The definition of no-tension supports seems to generate a compressive reaction force as soon as the element starts to move down, and not only after is reaches its original vertical position. An implicit integration model will be the solution for this. The axial results however were realistic. An example is shown in Figure A–10, for an identical structure as Figure A–11, but with another selection of time steps. It can be noticed that the initial normal force in the beam is smaller, which causes that the forces P_x lead to 'tension' in the beam. This is not possible and the model seeks equilibrium by increased compressive force left and right of the area in tension. The result is that these areas move up and move down over their friction supports and the central zone of the wave attack becomes more loosely packed, with lower normal force. This model outcome highlights a phenomenon that happens in reality also. The zero-normal force situation remains for a much longer amount of time steps and is than later restored during a successive wave cycle.
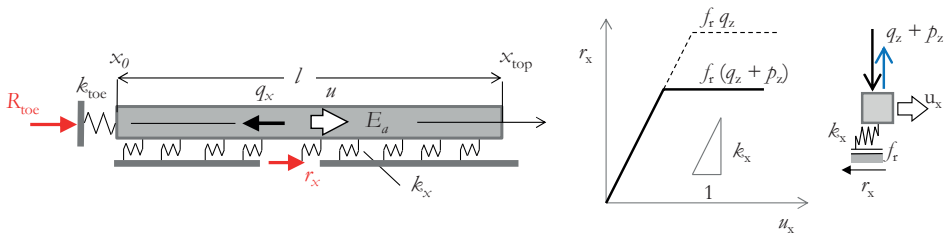
Figure A–9   Axial beam model with axial spring supports and friction cut-off
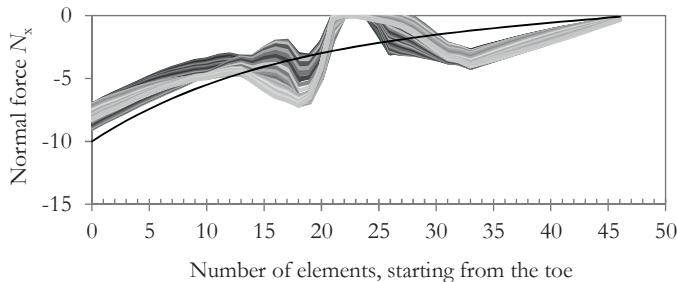
Figure A–10   Normal force results obtained with numerical calculations with an axial beam model with fiction cut-off

---

[272] D.J. Peters, *FEM modelling for block revetment research* (Lecture at DIANA User meeting Brescia, 2010)
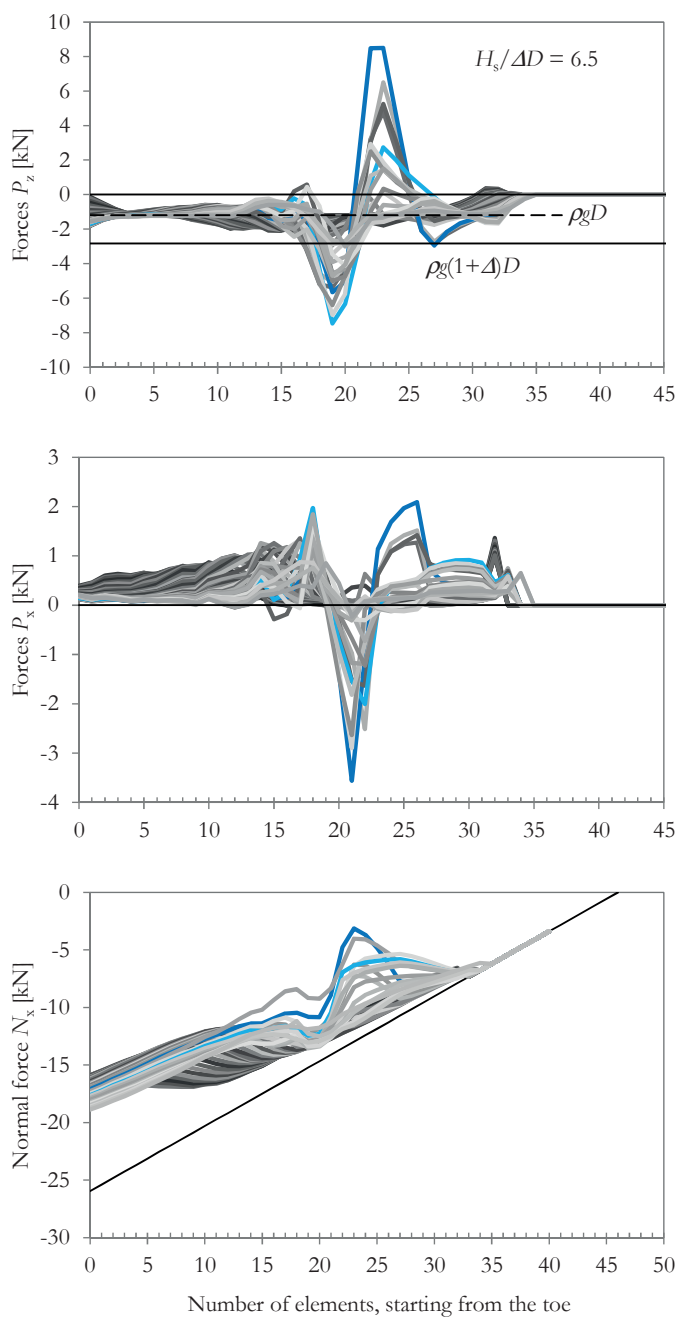
Figure A–11   Sets of perpendicular P_z and axial P_x wave forces (refer to Figure A-8) and calculated normal force in a sliding beam model

In Figure A–12 and Figure A–13 the model results of the development of the reaction force against the toe are shown. These results comply with the development of the force against the toe as measured in the Deltaflume (see Figure 3–7).[273]

The graph shows $k_{toe} = 10$ MN/m^2, $k_x = 10$ kN/m^3, $E_a = 30$ MPa. The y-axis is labelled "Calculated $R_{toe} / N_{neutral}$" ranging from 0.8 to 0.95. The x-axis is labelled "timesteps of Zsteen file" ranging from 0 to 6000.
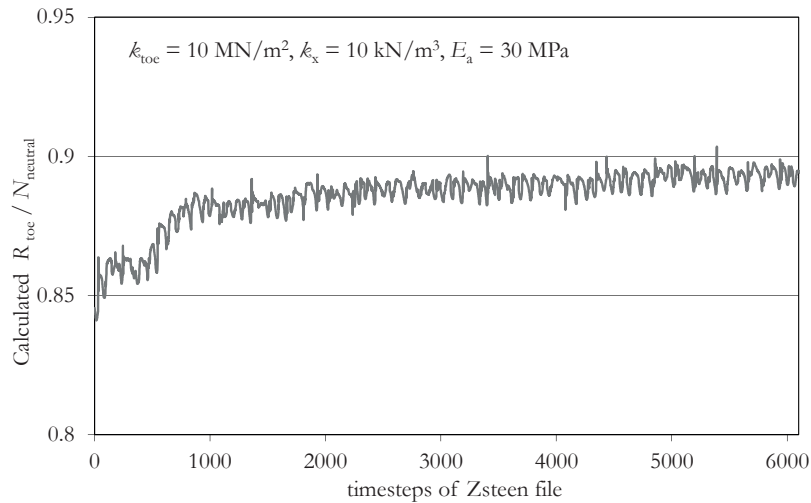
Figure A–12   Development of the in-plane force under repeated irregular wave loading with ZSTEEN and a FEM model, for a relatively stiff toe structure

The graph shows $k_{toe} = 1$ MN/m^2, $k_x = 60$ kN/m^3, $E_a = 30$ MPa. The y-axis is labelled "calculated $R_{toe} / N_{neutral}$" ranging from 0.2 to 0.7. The x-axis is labelled "Timesteps of Zsteen file" ranging from 0 to 6000.
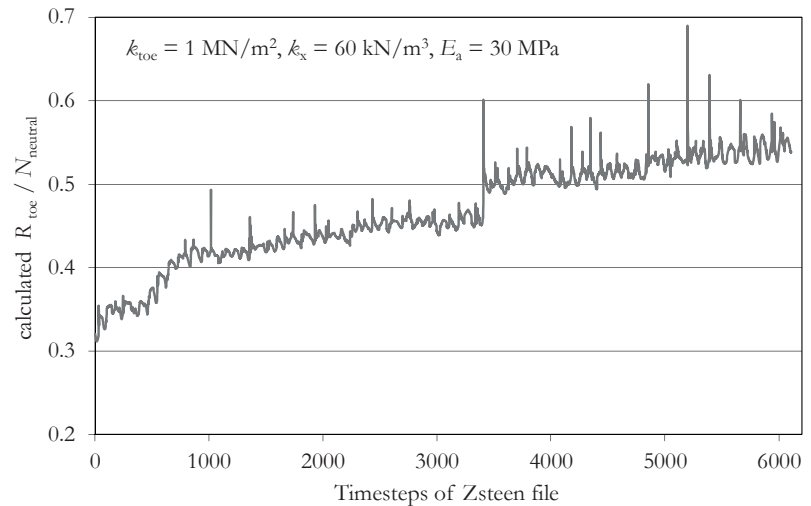
Figure A–13   Development of the in-plane force under repeated irregular wave loading with ZSTEEN and a FEM model, for relatively weak toe structure

---

[273] G. Wolters and M. Klein Breteler, *Normaalkracht in steenzetting met blokken op hun kant*, 2007

A.2 Perpendicularly loaded beam on elastic foundation

A.2.1 Beam on elastic foundation

Flexural beams on elastic foundations are known as Winkler beams. The theory of Winkler (1867) and Hetenyi (1946) has been further developed by various authors[274] and finds applications in railway and pavement construction. A revetment layer on a bedding layer can also be considered as a flexible beam or plate, supported by an elastic continuum. When the beam is long the continuum can be simplified as a series of independent springs.

A uniform downward load on a beam on an elastic foundation creates uniform compression of the springs and does not lead to bending or shear in the beam. A concentrated downward load generates bending moments in the beam and as a result the load is spread over a certain length. The elastic foundation of a revetment cannot be loaded in tension. An imposed uniform upward load can therefore not exceed the weight of the beam. Concentrated uplift loads can be higher than the weight of a beam portion, since bending moments can spread the load and mobilise the weight of a longer part of the beam to balance the upward load. For cases with uplift loads we need to consider a no-tension bedding (see Figure A–14).
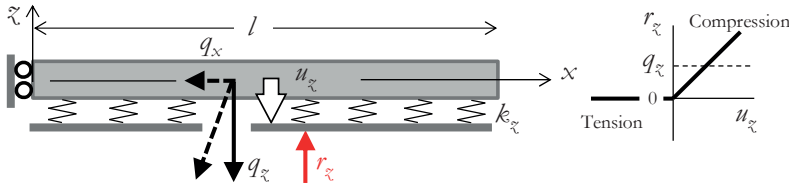
Figure A–14   Perpendicular loaded beam on elastic foundation with no-tension springs

The equilibrium of the flexural beam is given with the 4th-order linear differential equation.

$$EI\frac{\mathrm{d}u_z^{\,4}}{\mathrm{d}x^4} + k_z u_z = q_z(x)$$

$$\text{Or } \frac{\mathrm{d}u_z^{\,4}}{\mathrm{d}x^4} + 4\beta^4 u_z = q_z(x)$$

$$q_z(x) = \rho_s g\, D + \rho\, g\, \phi_w(x)$$

Eq. A.20

The particular solution is generally found as $u_z(x) = q_z(x)/k_z$.

The general solution of the characteristic equation

$$EI\frac{\mathrm{d}u_z^{\,4}}{\mathrm{d}x^4} + k_z u_z = 0 \;\; \text{or} \;\; \frac{\mathrm{d}u_z^{\,4}}{\mathrm{d}x^4} + 4\beta^4 u_z = 0 \;\; \text{with} \;\; \beta = \sqrt[4]{\frac{k_z}{4EI}}$$

Eq. A.21

is found as:

$$u_z = e^{\beta x}(C_1 \sin(\beta x) + C_2 \cos(\beta x)) + e^{-\beta x}(C_3 \sin(\beta x) + C_4 \cos(\beta x))$$

Eq. A.22

---

[274] A.L. Bouma, *Mechanica van constructies, elasto-statica van slanke structuren* (Delft: Delftse Uitgevers Maatschappij, 1989)

The flexural stiffness modulus E of the revetment layer is considered as a Young's modulus of a fictitious homogeneous material. Both the element material and the joints contribute to the flexibility of the beam (see section A.4). Adequate numerical values of E can be extracted from pull tests. See Annex D and G. In the model calculations we adopt $E = 100$ MPa.

As an alternative to the flexural beam a shear beam can be considered. For revetments this might be an adequate choice of the deformation is dominated by shear strain and/or shear failure in the joints. The combination of a shear beam and a continuous elastic support is known as a Pasternak foundation[275]. The equation is:

$$GA \frac{\mathrm{d}^2 u_z}{\mathrm{d}x^2} + k_z u_z = q_z(x)$$

Eq. A.23

With general solution:

$$u_z(x) = C_1 e^{\alpha x} + C_2 e^{-\alpha x} \text{ with } \alpha = \sqrt{\frac{k_z}{GA}}$$

Eq. A.24

A case with a step load p_{max} would give $u_{part} = p_{max} / k_z$ as particular solution, and a dampening shear force $V(x) = \frac{1}{2}(p_{max}/\alpha) e^{-\alpha x}$.
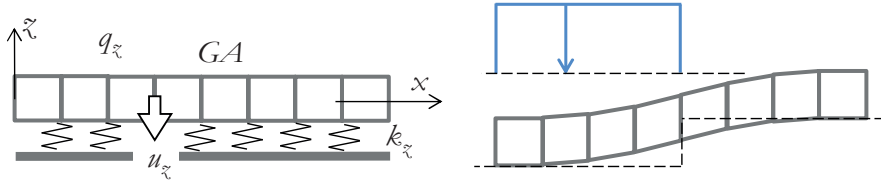
Figure A–15   Perpendicular loaded shear beam on elastic foundation

The modulus of subgrade reaction k_z is difficult to establish. The soil stiffness is increasing with initial soil stress, and therefore with depth. At the surface the soil stress is low, making the subgrade reaction undetermined. Also the model effect of spatial spreading and the corresponding relation between a continuous stiffness E_{bed} and the model parameter of a unidirectional independent reaction k_z introduces uncertainties.

The compressibility of granular soils is described by Terzaghi as:

$$\varepsilon = -\frac{1}{C} \ln\left(\frac{\sigma}{\sigma_1}\right)$$

Eq. A.25

Alternative notations are $\varepsilon = -\frac{1}{C_{10}} \log\left(\frac{\sigma}{\sigma_1}\right)$ or $-\frac{C_c}{1+e} \log\left(\frac{\sigma}{\sigma_1}\right)$

with

σ = vertical effective stress [MPa]
σ_1 = initial value of σ
C or C_{10} = compression constant, $C = 2.3\ C_{10}$
C_c = compression index
e = void ratio

---

[275] (Pasternak, 1954), see S.C. Dutta and R. Roy, "A critical review on idealization and modeling for interaction among soil-foundation-structure system," *Comput. Struct.* 80:20–21 (2002): 1579–1594

The derivative expresses the stiffness and is written as:

$$\frac{\mathrm{d}\varepsilon}{\mathrm{d}\sigma} = \frac{1}{C}\frac{1}{\sigma}$$

Eq. A.26

The stiffness is linearly dependent on the stress level, with a compression constant C. For sands/gravels the recommended[276] values are $C = 50 \; .. \; 500$. A more accurate recommendation is given in NEN 9997, the Dutch national annex to the Eurocode EN 1997-1.

Table A–2   Foundation material parameters

Consistency	Relative density $D_r = \dfrac{e_{max} - e}{e_{max} - e_{min}}$	Compression index $C_c / (1 + e)$		Poisson's ratio[277]
		Sand	Gravel	υ
Loose	$0 - 0.33$	0.0115	0.0046	0.2
Medium	$0.33 - 0.67$	0.0038	0.0023	0.3
Dense	$0.67 - 1$	0.0019	0.0018	0.4

Bedding layers are often characterised with their porosity n, which is ratio between voids and total volume. The void ratio e is defined as void volume divided by grain volume.
Hence $e = n / (1 - n)$.

The Young's modulus for the unidirectional stress-strain relation $\sigma = E_{bed}\,\varepsilon$ is used in the continuum mechanics moduli K and G for omnidirectional compression and shear.

$$K = \frac{E_{bed}}{3(1-2\upsilon)} \;\text{ and }\; G = \frac{E_{bed}}{2(1+\upsilon)}$$

Eq. A.27

In case $\varepsilon_{xx} = \varepsilon_{yy} = 0$, the relation between σ_{zz} and ε_{zz} is given as $\sigma_{zz} = M\,\varepsilon_{zz}$, with M = the constrained modulus.

$$M = K + \tfrac{4}{3}G = \frac{E_{bed}(1-\upsilon)}{(1+\upsilon)(1-2\upsilon)}$$

Eq. A.28

Equality of M and Terzaghi's compression law gives:

$$E_{bed} = \frac{(1+\upsilon)(1-2\upsilon)}{(1-\upsilon)}C\sigma$$

Eq. A.29

The conversion from E_{bed} to subgrade modulus k_z requires the size of the loaded area. The formula of Schleicher[278] is often used for this relation.[279]

$$k_z = \frac{E_{bed}}{B(1-\upsilon)}$$

Eq. A.30

---

[276] A. Verruijt, *Soil dynamics* (TU Delft, 2008)

[277] Source: J.E. Bowles, *Foundation analysis and design, 5th ed.* (New York: McGraw-Hill, 1996)

[278] F Schleicher, "Zur theorie der Baugrundes," *Der Bauingenieur* 48/49 (1926)

[279] In J.D. Stevenson, "Structural damping values as a function of dynamic response stress and deformation levels," *Nucl. Eng. Des.* 60 (1980): 211–237 an alternative formulation is given for a circular footprint: $k_z = 2/\pi \; E/(R\,(1 + \upsilon)(1 - \upsilon))$

A typical value for the footprint B of the concentrated load of revetments caused by plunging waves is 0.75 H_s. Refer to Figure 5–33. When H_s = 2 m, B = 1.5 m. Combining the recommended moduli values and model formulas for a typical bedding layer material of grading 15/50, with d_{15} = 15 mm, n = 0.35 and ρ_{bed} = 2650 kg/m^3 leads to: ρ_{dry} = 1725 kg/m^3, ρ_{eff} = 725 kg/m^3, e = 0.46, loose consistency, $C_c/(1 + e)$ = 0.0046; C_{10} = 220; C = 500; υ = 0.2.

The effective stress at the underside of the bedding layer of 0.5 m thickness with a top-layer thickness of 0.35 m, porosity of 12% and element density of 2500 kg/m^2 is:

σ_{dry} = 9.83 × (0.35 × 0.90 × 2500 + 0.5 × 1725) = 16.2 kPa

σ_{eff} = 9.83 × (0.35 × 0.90 × 1500 + 0.5 × 725) = 8.2 kPa

Based on the initial effective stress the following values are found for the stiffness parameters: E_{bed0} = 3700 kPa, k_{z0} = 3100 kN/m^3. These values would be in the range of the lower bound of literature recommendations[280] of the subgrade reactions for pavements, which are normally laid on artificially compacted granular soils, with an optimal grading. For revetments low values are deemed realistic since the construction on the slope, and the grading complicates compaction during construction. Furthermore the oscillations of the effective stress caused by the tide and peak water pressures and velocities are not contributing to a compact soil matrix.

The subgrade modulus k_z to be used to calculate deformations under wave impact loads of 40 to 60 kPa pressure, could be calculated as a secant modulus based on an effective stress value of 0.5 times the peak load, e.g. 20 to 30 kPa. The bedding stiffness can be based on an effective stress of 25 + 8.2 = 33.2 kPa. This leads to E_{bed} = 15 000 kPa and k_z = 12 500 kN/m^3. Measurements of subgrade reactions of revetment foundation layers are not available. For model calculations of wave impacts a range of 10 to 20 MN/m^3 is recommended for k_z.[281]

The solution of the differential equation consist of complementary dampened sinus-functions with typical wave lengths of $2\pi/\beta$. With the recommended values of beam and bedding elasticity E and k_z the value of β has values in the range of 1.5 .. 2.0 m^{-1}, and the related characteristic half wave length π/β = 5 .. 7D.

A.2.2   *Wave impact load on beam on elastic foundation*

A wave impact load is characterised by high pressures with a block diagram in space and a triangular diagram in time (see section 5.2.9). The magnitude and the width of the load diagram are correlated. The magnitude p_{max} = c ρg H_s, with the constant c dependent on the breaker parameter, here typically chosen as 4. The width of the block diagram B_{imp} is typically 0.75 H_s.

---

[280] Recommendations by (Bowles, 1996) are: loose sand: 4800 to 16 000, medium dense sand: 9600 to 80 000 and sense sand: 64 000 to 128 000 kN/m³

[281] For the subgrade reaction of dense sand under asphalt revetments a value of 100 MN/m³ was recommended as 'safe' (source: H. de Looff, *User Manual Golfklap* (version 1.3, 2009). In M.P. Davidse et al., *State of the Art Asfalt dijkbekledingen* (STOWA report W06, 2011) a recommendation is given of 64 MN/m³ based on field tests with falling weight deflection meters. The bedding layers under hydraulically closed asphalt revetment are not influenced by large variation of pore water pressures and the material will be compacted by external load, rather than disturbed.

The particular solution is a block shape deformation with $u_{part} = p_{max} / k_z$. The boundary condition at point 2 is solved by applying a force P at both sides of the discontinuity at point 2, both compensating $\frac{1}{2} u_{part}$, which gives $P = u_{part} k_z / 4\beta$. Assuming infinite length at both sides the load P causes bending moments and shear forces at point 1 (see Figure A–17).
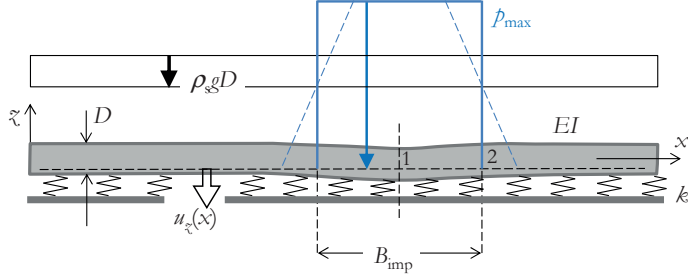
Figure A–16   **Definition diagram of quasi static block-shape impact load on beam on elastic foundation**

Symmetry does not allow a shear force. The internal force D_2 is therefore compensated with a counterforce. The forces P and the counterforce of D_2 both cause rotation of the beam end at point 1. Symmetry requires continuity and therefore a bending moment M_1 is applied to arrive at zero rotation. The bending, shear and deformations caused by M_1 en the counterforce of D_2 are combined with those caused by P. Following this procedure the total internal bending moment at point 1 is $M_1 + M_2$.
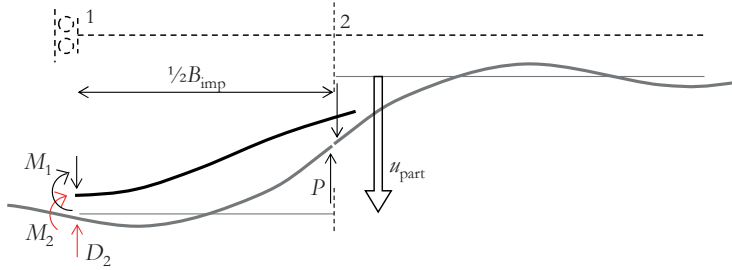
Figure A–17   **Definition diagram of solution**

The outcomes of analytical static calculations for a chosen parameter set are presented in Figure A–18. For small, concentrated loads the negative bending at the center of the impact gives the largest absolute value of the bending moment. For larger block diagrams the discontinuity at point 2 dominates the solution, which causes more equal positive and negative bending moments. The shear force shows a peak at the steep flank of the pressure diagram. When using a trapezoidal load diagram instead of a block diagram (see Figure A–16) the bending moments and displacements results are almost the same, whilst the shear force peak will be reduced to approximately 75%.

An engineering estimate of the shear forces and bending moments can be provided for the discontinuity case.

$$V_{max} = 0.75P = 0.75 \tfrac{1}{2} u_{part} k_z / 2\beta = 0.2 p_{max} / \beta \qquad \textbf{Eq. A.31}$$

$$M_{max} = 0.322 P / \beta = 0.06 p_{max} / \beta^2 \quad \text{at a distance of } \pi/4\beta$$
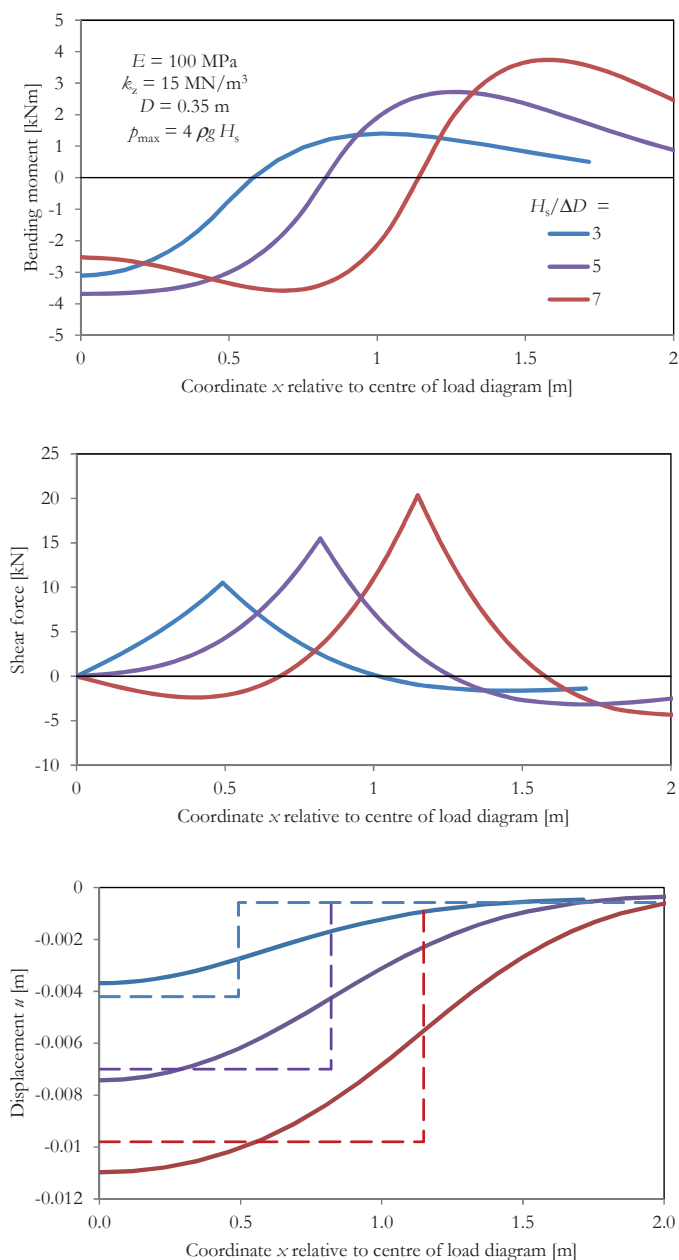
Figure A–18   Bending moment, shear force and displacement of block-shape impact load on beam on elastic foundation

The structural response is determined by the characteristic length parameter, which is constant for the three examples, and thus has a different ratio to the width of the block

diagram. Integrated displacements $\int u(x)\mathrm{d}x \,/\, (u_{\text{part}} \times B_{\text{imp}})$ are 1.53, 1.24 and 1.14 respectively. These factors can be considered as resistance-factors when we use the results for a simple dynamic calculation.

A.2.3 Dynamic amplification of impact load

The impact load has a short duration and a steep rise time. The load might therefore cause response forces that exceed the forces required for a static equilibrium. This effect can be assessed by comparing the duration of the load with the natural period of the system[282], more specifically by looking into a dampened single-degree-of-freedom (SDOF) oscillator, with a mass M [kg], a spring stiffness k [N/m] and a dashpot damper with a linear viscous damping coefficient c [Ns/m]. The dynamic equilibrium with a given excitation force $F(t)$ is given with:

$$M\ddot{u}(t) + c\dot{u}(t) + ku(t) = F(t) \qquad \text{Eq. A.32}$$

The free vibration is described with:

$$M\ddot{u}(t) + c\dot{u}(t) + ku(t) = 0 \qquad \text{Eq. A.33}$$

The system considered is under-dampened with a damping coefficient of $\zeta = c/c_{\text{c}} < 1$. The critical damping c_{c} of the system is:

$$c_c = 2\sqrt{kM} \qquad \text{Eq. A.34}$$

The solution of the ordinary differential equation is:

$$u(t) = Ae^{-\zeta\,\omega_{\text{n}}t}\sin\!\left(\sqrt{1-\zeta^2}\,\omega_{\text{n}}t - \theta\right)$$

with

ω_{n} = the radial natural frequency = $2\pi\,f_n$

A = the initial amplitude

θ = a phase angle

$\qquad \text{Eq. A.35}$

The damping plays an important role in the decay of the response signal of a free vibration. Typical damping coefficients ζ for concrete structures are around 5%. In this case the material damping includes effects of motion of the material of the bedding also. The formulas for the spring and damper values of a mass M with a circular footprint with radius r on an elastic half space are as follows:

$$k\,[\text{N/m}] = \frac{2E_{\text{bed}}r}{(1+v)(1-v)} \qquad \text{Eq. A.36}$$

$$c\,[\text{Ns/m}] = \frac{3.4}{\sqrt{2}}\frac{r^2}{(1-v)}\sqrt{\frac{\rho E_{\text{bed}}}{1+v}}$$

In literature these formulas are mostly expressed using G instead of E_{bed}. The mass ratio of the elastic half space is: $\beta_{\text{p}} = (1-v)\,M\,/(4\,\rho\,r^3)$. When these formulas are combined it is found that $\zeta = 0.425/\sqrt{\beta_{\text{p}}}$. Given the relatively small mass of the revetment layer, the mass

---

[282] J.P. Hartog, *Mechanical Vibrations* (Dover publications, first ed. 1934, 1985)

ratio β_ρ will be small also, and hence the damping coefficients are typically very large, e.g. 50 or 75%.

Formulas[283] to replace the assumed circular footprint by a rectangular shape with width B and length L are:

$$k_z[\text{N/m}^3] = \frac{k}{BL} = \frac{E}{2(1+\upsilon)(1-\upsilon)}\frac{1}{B}\left(0.73\tfrac{B}{L} + 1.54(\tfrac{B}{L})^{1.75}\right) \qquad \text{Eq. A.37}$$

$$c_z[\text{Ns/m}^3] = \frac{c}{BL} = \frac{3.4}{4\sqrt{2\pi}}\frac{1}{(1-\upsilon)}\sqrt{\frac{\rho E}{1+\upsilon}}\left(0.73\sqrt{\tfrac{B}{L}} + 1.54(\tfrac{B}{L})^{1.25}\right)$$

These formulas are rewritten and use B as most important geometrical variable and B/L to express the effect of a non-square shape, with $L > B$. The values compare well with the formulas for the circular shape using $k_z = k/(\pi r^2)$ and $c_z = c/(\pi r^2)$. When we compute k and c for different values of B/L, the effect on the damping coefficient can be found. The high damping values are due to the 3D effect in the elastic half space. When the geometry of the impact load tends towards a strip with infinite length the damping ratio is 6 to 9%, which is a normal value for a strip foundation. In practise the peak impact loads have an aspect ratio of 1:1 of 1:2, and are therefore associated with relatively high damping coefficients.
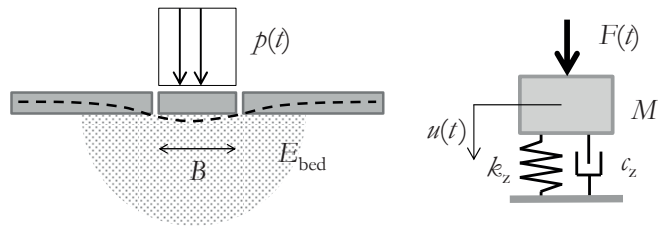
Figure A–19   Schematic view of dynamic structural model

Table A–3   Effect of impact load geometry on the material damping in a SDOF model

L/B	B/L	$f\left(\tfrac{B}{L}\right)$ in k_z	$f\left(\tfrac{B}{L}\right)$ in c_z	k	M	c	c_c	ζ	Effect
1	1	2.27	2.27	2.27	1	2.27	1.51	1.51	$50 - 75\%$
2	0.5	0.82	1.16	2.33	2	1.65	2.16	0.76	$25 - 38\%$
5	0.2	0.24	0.53	2.66	5	1.19	3.65	0.33	$11 - 16\%$
10	0.1	0.10	0.32	3.17	10	1.00	5.63	0.18	$6 - 9\%$

The continuous beam system can be transferred into an equivalent SDOF oscillator according to the theory described by Biggs[284]. A shape function $\Phi(x) = u(x) / u_{\text{peak}}$ for the displacement of the continuous beam is introduced. The equivalent mass M_e and equivalent load F_e are equal to:

---

[283] G. Gazetas, "Formulas and charts for impedances of surface and embedded foundations," *J. Geotech. Eng.* 117:9 (1991): 1363–1381 and Stevenson, "Structural damping values as a function of dynamic response stress and deformation levels"

[284] J.M. Biggs, *Introduction to Structural Dynamics* (McGraw Hill, 1964)

$$M_e = \int m\, \Phi^2(x)\mathrm{d}x \qquad\qquad\qquad \text{Eq. A.38}$$

$$F_e = \int p(x)\, \Phi(x)\mathrm{d}x$$

With load factors $K_M = M_e / M$, and $K_L = F_e / F$. The stiffness $k = R/u$, with in the static case $F = R$. The load factor K_L therefore also applies to the stiffness. The natural period is hence written as:

$$T = 2\pi \sqrt{\frac{K_M M}{K_L k}}$$

For the cases with the block-shaped impact load the beam length is taken as $\tfrac{1}{2}\, B_{\mathrm{imp}} + \pi/\beta$.

Table A–4   **Continuous beam parameters for a SDOF model**

$H_s/\Delta D$	3	5	7
Impact load width $\tfrac{1}{2}B_{\mathrm{imp}}$ [m]	0.49	0.82	1.14
Load factor K_L	0.50	0.47	0.49
Mass factor K_M	0.34	0.34	0.38
Natural frequency f_n [Hz]	14	15	16
Natural period T [s]	0.070	0.066	0.064

The SDOF oscillator can now be subjected to a typical short triangular impact load. The load duration t_d is typically 0.02 .. 0.05 s for wave impacts on slopes with breaker parameter ξ = 1..2 (see Figure 4-30). The response is characterised as a dampened sinus-function in time. The peak of the response can either be amplified (the dynamic amplification factor DAF > 1) or suppressed (DAF < 1) by the inertia forces. Literature values of the DAF are available for a symmetric triangular load. The response with DAF = $u_{\mathrm{dynamic}}/u_{\mathrm{static}}$ = 1 for an non-dampened system is when $t_d/T \sim 0.3$. In the practical cases to be considered here $t_d/T = 0.6$ .. 0.8. The non-dampened response DAF is therefore larger than unity. For $t > t_d$ the system motion follows a free vibration, with rebound values of the same order as the peak response. Note that this rebound occurs without presence of an upward load. A damping coefficient (ζ > 0) would progressively reduce the response. The peak response is lower, and the rebound is dampened much stronger, as can be noticed in Figure A–20. When the damping coefficient is 75% there will be no re-bound at all. With a 50% damping value the revetment reduces its pre-pondered condition but is not lifted from the bedding layer. With 25% damping uplift can be noticed.
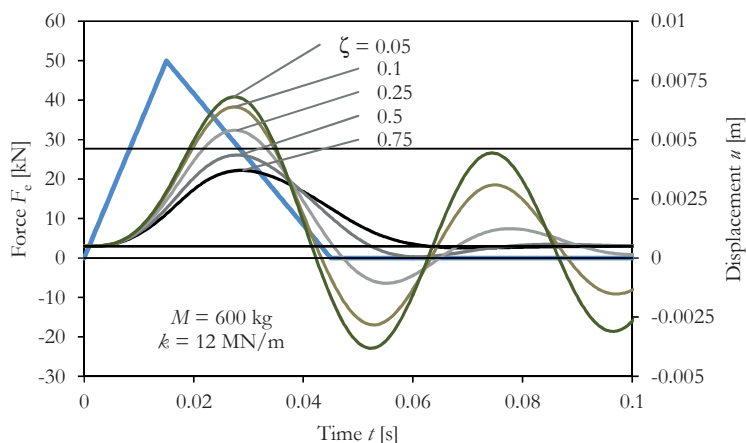
Figure A–20   Dynamic response of revetment an elastic foundation subject to impact loading
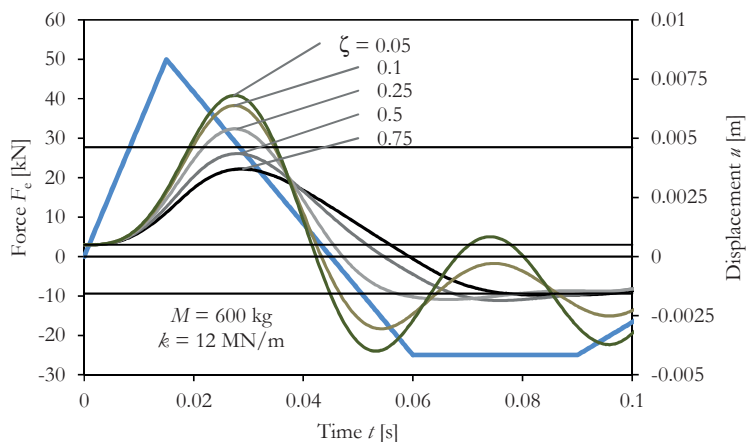
Figure A–21   Dynamic response of revetment an elastic foundation subject to impact loading followed by uplift load

The upward motion as a rebound of the impact load is increased by the upward loading that usually occurs directly after the impact load. Filter pressures are still high during a period of 0.1 to 0.25 seconds, typically long enough for a significant interaction with the upward motion in response to the downward impact load. Figure A–21 shows the same case as Figure A–20, but now with hydraulic filter response after $t = t_{\mathrm{d}}$. The calculated upward displacements are increased.

As will be shown in the following paragraphs uplift of the revetment beam can in reality be associated with a considerable and progressive drop of the stiffness, e.g. with a factor of 10. The equivalent mass increases, since a larger portion of revetment will be lifted. For demonstration purposes the mass is chosen 2 and 3 times the equivalent mass during the impact phase. The material damping will be at a 5 or 10% level, since there is no mass participation of the bedding after uplift. The SDOF model calculation has been carried out

with a sudden change of the properties discussed, at the moment that the mass crosses the zero displacement line. The velocity at that particular moment is corrected for the increased mass, based on equality of kinetic energy. The results are shown in Figure A–22 and Table A–5. It can be noticed that the impact load and more specifically the rebound phase of the uplift load seems to increase the uplift response by 10 to 20% compared to a case where the uplift load is considered as a dynamic load on a SDOF system with no initial velocity (green line in Figure A–22). This effect cannot be neglected. Impact loads and successive uplift loads must therefore be analysed in one dynamic response calculation, or an amplification factor should be applied on stand-alone uplift calculations.
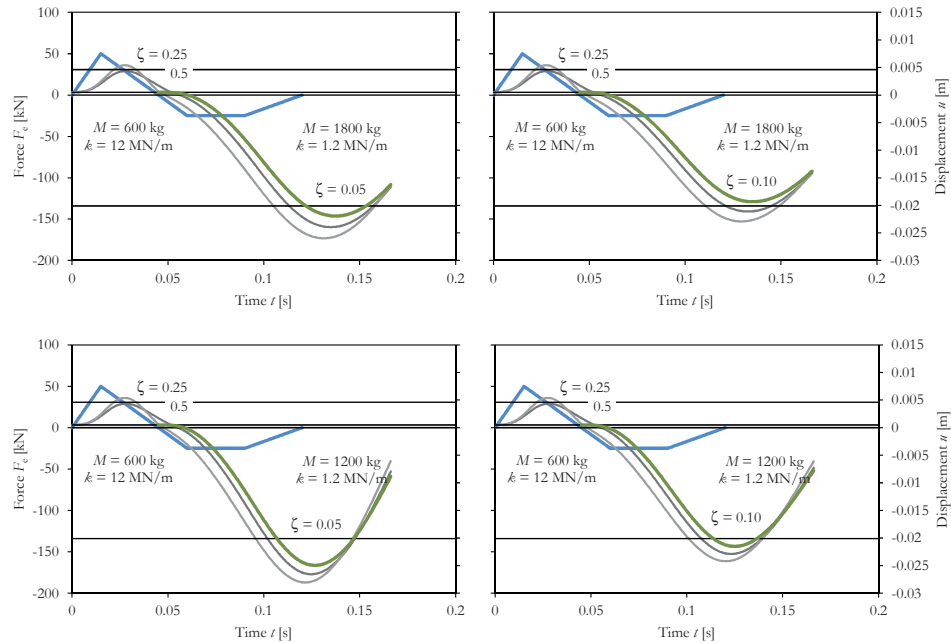
Figure A–22   Dynamic response of revetment subject to uplift load cases preceded by revetment on elastic foundation subject to impact loading

Table A–5   Dynamic amplification factors for uplift load cases preceded by impact loads

Dynamic amplification factors (DAF)	M = 1800 kg k = 1.2 MN/m		M = 1200 kg k = 1.2 MN/m	
Structural damping during uplift	5%	10%	5%	10%
Only uplift (preceding downward impact load neglected, green line in Figure A–22)	1.07	0.94	1.21	1.04
50% structural damping during wave impact	1.16	1.03	1.29	1.11
25% structural damping during wave impact	1.26	1.11	1.36	1.18

A.2.4   Beam on elastic foundation subject to static uplift load

Waves impacts cause concentrated downward loads on the revetment beam, followed by a period of filter layer water over-pressure causing upward loads on the revetment beam. The upward load has a low-dynamic characteristic with longer rise times of the pressure-time signal. The loads are therefore treated as static loads although a remaining dynamic effect of the preceding impact load may be present (see section A.2.3). The spatial distribution diagram of the load is assumed triangular, since it is representing a typical case with leakage lengths to both sides of the peak load (refer to Figures 5–40 and 5–41).

The beam is pre-loaded by its gravity component $q = \rho_s g\, D \cos\alpha$. This pre-load causes a uniform compression of the subgrade and a corresponding elastic settlement, in most cases 0.5 to 1 mm. Small upward loads p that do not fully compensate the pre-load only cause reduction of the compressive subgrade reaction. During real storm conditions the peak of the upward loads will exceed the pre-load. When the upward load is sufficiently localised compared to the characteristic elastic length of the beam-foundation system, load factors p_{max} $/q$ exceeding unity will initially not cause uplift from the no-tension bedding. Limit values of those load factors can be found by super imposing the pre-load q and the upward load p and requiring equality of the deformations caused by the two loads. The deformation caused by a concentrated point load P on one side of a beam − requiring continuity of angular deformation − is $P\beta/k$. This value is equal to q/k, leading to a value of $P = q/\beta$. The case of a concentrated load on a continuous beam just before loss of contact with the subgrade is hence mathematically solved with $P = 2\,\rho_s g\, D\,(\cos\alpha)/\beta$.
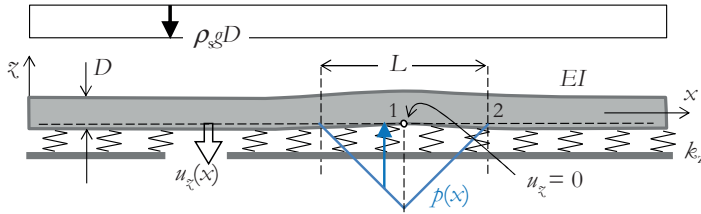
Figure A–23   **Definition diagram of response of revetment on elastic foundation subject to static uplift load, case with maintained compression of the foundation**

Cases with a triangular load with $L/D > 0$ (see Figure A–24) are analyzed in the same manner. The solution of the differential equation uses a triangular displacement field corresponding to the load and transition conditions at the boundaries in point 1 and point 2. The bending moment M_2 is calculated from the imposed angle $\tfrac{1}{2}\,p_{max}/(k_z\,\tfrac{1}{2}L)$. When L is short the moment M_2 requires a vertical reaction force D_2, which cannot exist and need to be balanced with a force. Similar to the case with the block load a bending moment M_1 is introduced to fulfil the requirement of $du/dx = 0$ in point 1. The results of some model calculations and parameter variations are shown in Figure A–26.
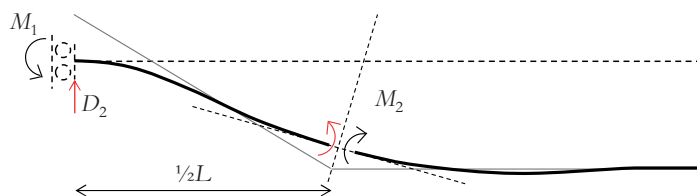
Figure A–24   Definition diagram of the solution

In order to enable a general presentation of the results the length L is made dimensionless by multiplying with β [m^{-1}]. A case with $D = 0.35$ m, $E = 100$ MPa and $k_z = 15$ MN/m^3, $\beta = 1.8$ m^{-1} is considered. For this case $L\beta$ corresponds to 0.4 L/D. Starting with $L\beta = 1$ the load factor p_{max}/q is 4, diminishing via 1.5 when $L\beta = 4$ to 1 for large values of $L\beta$ (see Figure A–25). Combining the load factor with the load length gives a force. The resultant load Q on one side of equals $\frac{1}{2}$ ($p_{max} \times \frac{1}{2}L$). The limit value of the dimensionless parameter $p_{max}/q \times \frac{1}{4}L\beta$ for concentrated loads is 1, which ties-in to the known solution for the concentrated load P shown above.
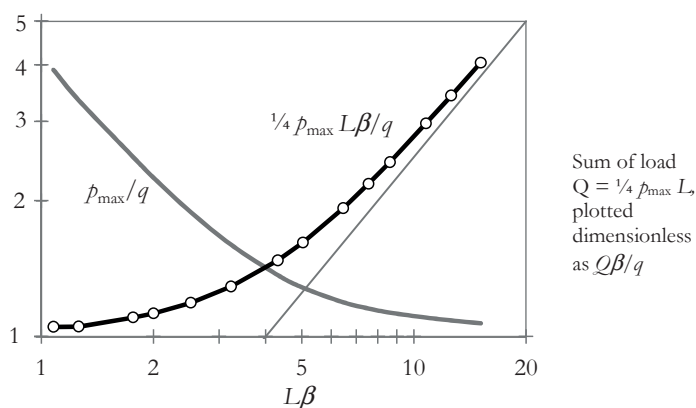
Figure A–25   Load factor results of a revetment beam on elastic foundation, pre-loaded with q subject to triangular upward load p_{max}, with zero uplift
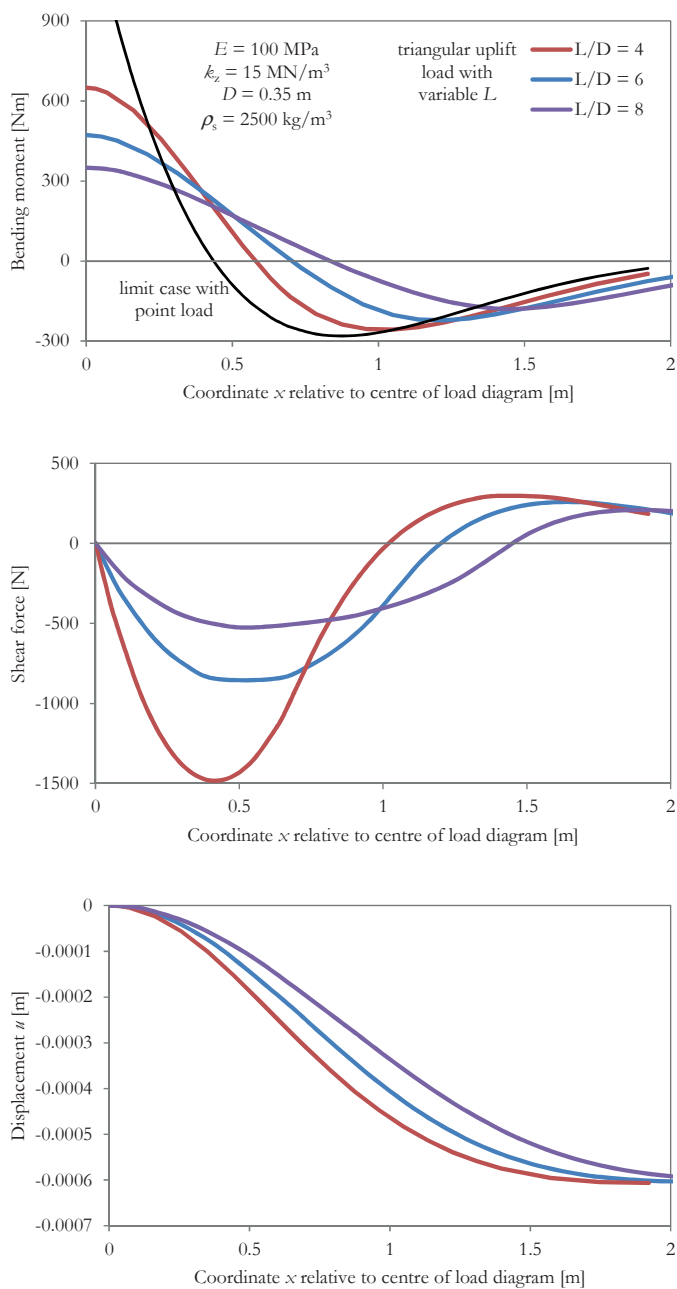
Figure A–26 Bending moment, shear force and displacement of a pre-loaded revetment beam on elastic foundation subject to triangular upward load, case with zero uplift in the centre

When the load-factor exceeds the limit value of the previously discussed case with zero-uplift in the centre, the beam will be lifted from the no-tension foundation and an area with a free span L_0 will occur. The stiffness of the system is then decreased progressively. Two cases can be distinguished (see Figure A–27):

– a case with a relatively 'wide' load diagram, associated with $0 < L_0 < L$, and

– a case with a relatively peaked load diagram, associated with the free span length $L_0 > $ load length L.
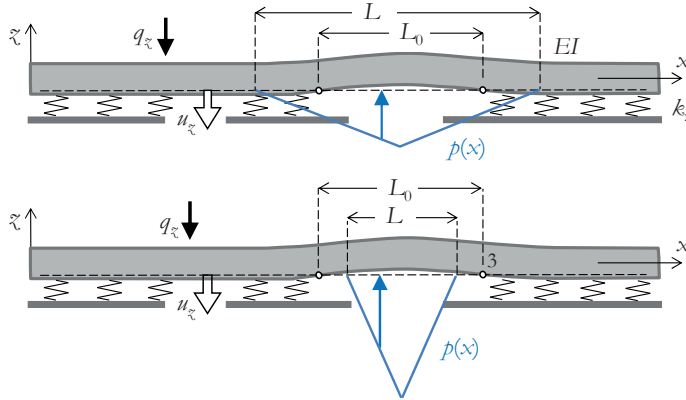
Figure A–27   Beam on elastic no-tension foundation with wide and with concentrated uplift loads causing uplift of the bedding
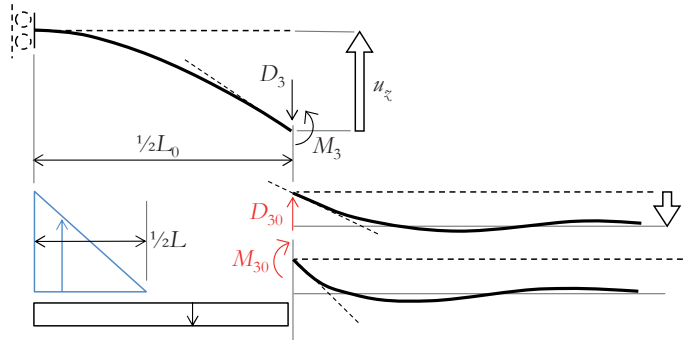
Figure A–28   Definition diagram of the solution

The solution of the case with a free span can be found by combining solutions of the equations

$$EI \frac{\mathrm{d}u_z^{\,4}}{\mathrm{d}x^4} + k_z u_z = q_z(x) \text{ for the elastic supported part}$$

$$EI \frac{\mathrm{d}u_z^{\,4}}{\mathrm{d}x^4} = q_z(x) \text{ for the free-spanning part}$$

Focussing on the case with $L_0 > L$ we can define point 3 as the boundary of a half-infinite beam with the particular solution for compression by the self-weight, $u_q = q\,/\,k_z$. At point 3 the displacement needs to be zero. This can be reached by either a force D_3 or a moment M_3, or a combination of the two. We therefore define a force D_{30} that fully compensates u_q, and

similarly we define M_{30}. $D_{30} = \frac{1}{2}u_q k_z/\beta$ and $M_{30} = \frac{1}{2}u_q k_z/\beta^2$. This means that if $D_3 = f D_{30}$, M_3 equals $(1 - f) M_{30}$. D_{30} and M_{30} both cause a rotation of the elastically supported beam end. The vertical equilibrium of the free spanning beam portion in Figure A–28 is can now be written as:

$$\tfrac{1}{2} p_{max} (\tfrac{1}{2} L) - \tfrac{1}{2} q L_0 - D_3 = 0$$

The self-weight of the revetment beam with length L_0 compensates the uplift force, and the load D_3 also contributes to this. The loads $p(x)$, q and D_3 cause deflections and rotations of the beam. Continuity of the deflections is arranged by the choice of the boundary conditions in point 1 and point 3. Continuity of rotations can be obtained with the introduction of M_3 and variation with the factor f. The rotational equilibrium of the free beam portion is satisfied by the reaction bending moment in point 1. Introduction of a bending moment M_3 is compensated by an equal increase of the bending moment M_1. The solutions for several cases are computed and shown in Figure A–30 to Figure A–32. It appears that in some cases the factor f was negative, meaning that M_3 has a relatively large magnitude, and the force D_3 is a holding down force.

The force distribution of the uplift load cases with the free span is characterised by a maximum hogging bending moment in the centre M_1. The sagging bending moment near the point where the revetment beam is laying on the bed is typically 0.45 to 0.55 times M_1. The position of the maximum sagging bending moment is for the chosen values of E and k_z still within the free span, not on the boundary between the free span and the supported part. Calculations with other values of k_z (see Figure A–32) show that for a very weak bedding stiffness the maximum sagging moment interferes with the boundary point. Moreover, the maximum bending moment, maximum shear and maximum uplift displacement are only marginally influenced by the bedding stiffness k_z. This is the reason that the uplift cases are further investigated with focus on the isolated free spanning part (see sections A.3 and 3.1.4).

The triangular load cases do not cause very high shear forces. Evaluation of the calculated bending moments and shear forces with M / e_{max} and D / f_r learns that the bending moment dominates the requirement for frictional interlocking.

The stiffness of the system progressively decreases when the revetment beam is lifted from the bedding. This is shown in Figure A–29.
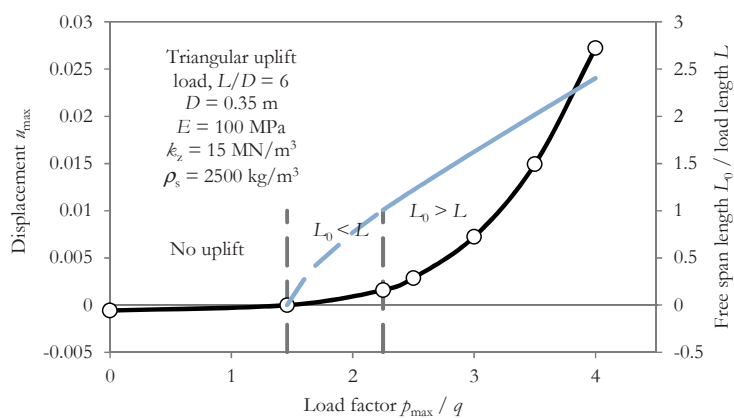
Figure A–29   **Load-displacement curve of beam on elastic no-tension foundation**
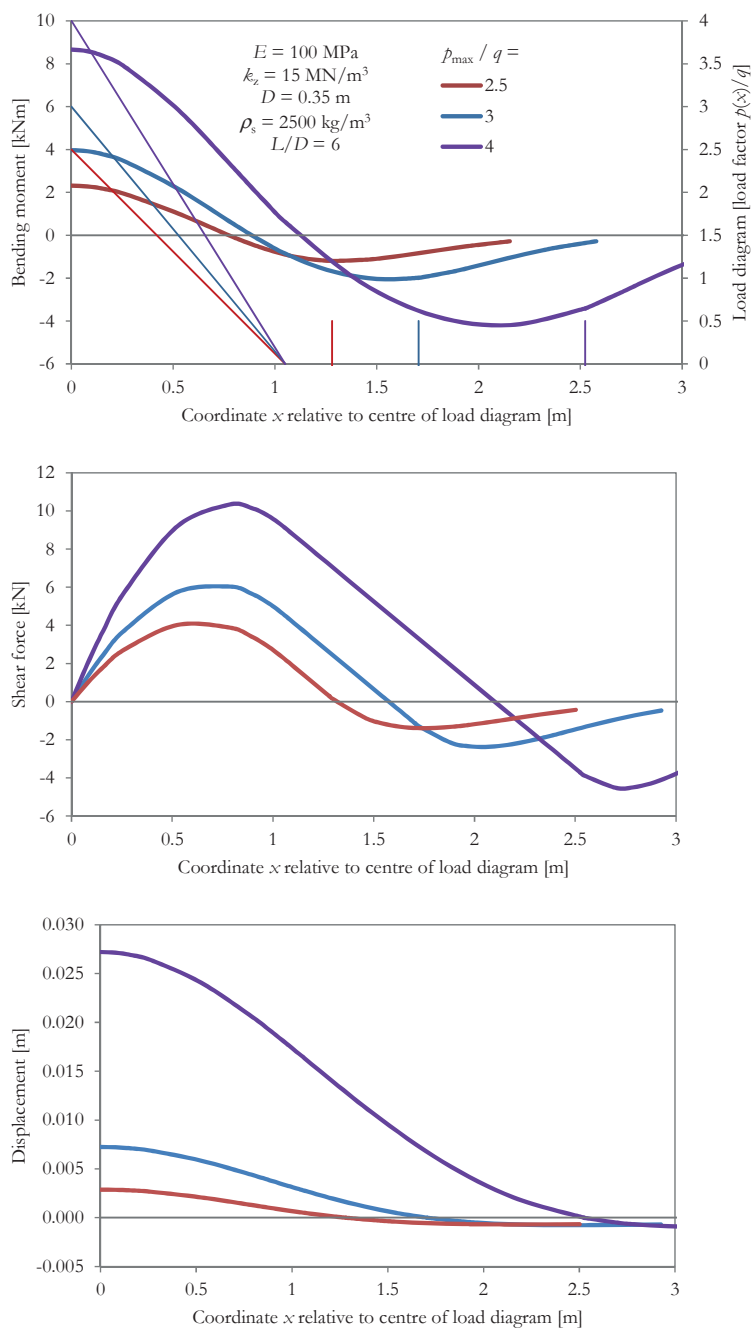
Figure A–30 Bending moment, shear force and displacement of a pre-loaded revetment beam on elastic foundation, a triangular upward load, case with free spanning beam, with p_{max}/q variable
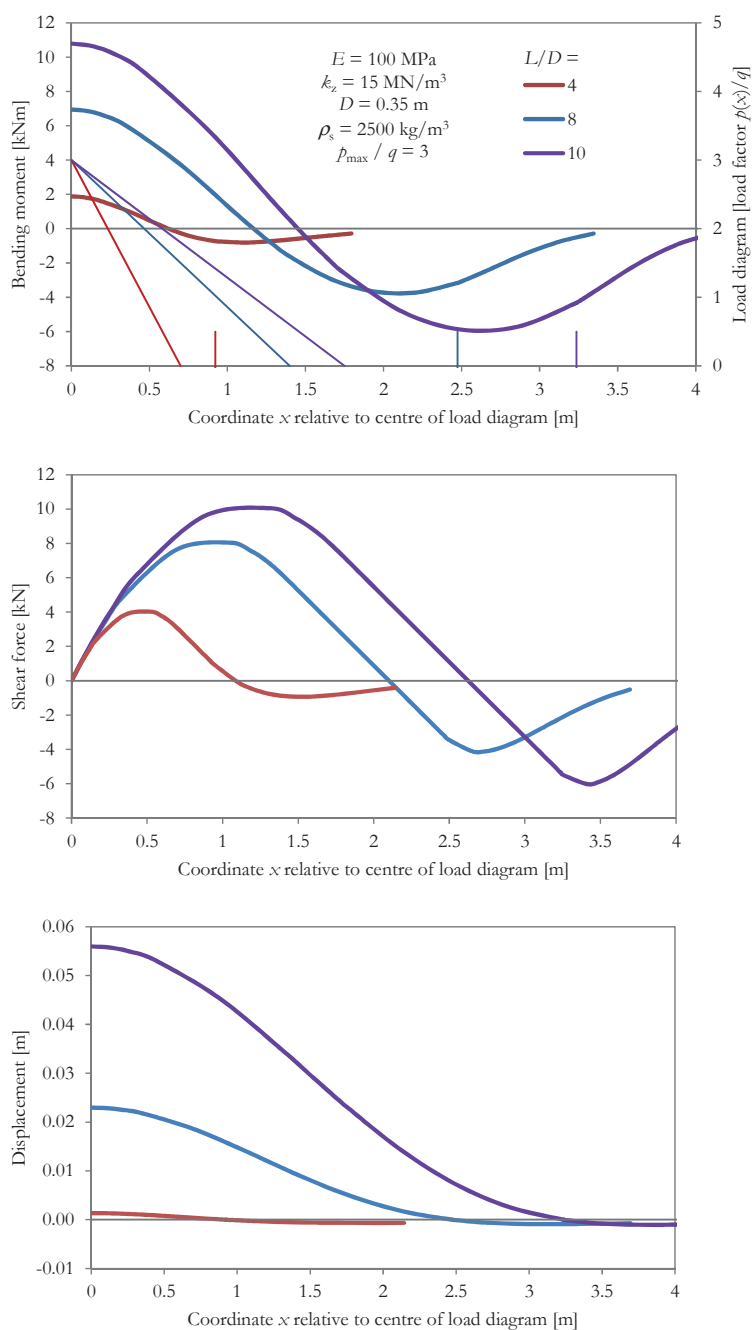
Figure A–31 Bending moment, shear force and displacement of a pre-loaded revetment beam on elastic foundation, a triangular upward load, case with free spanning beam, with *L/D* variable
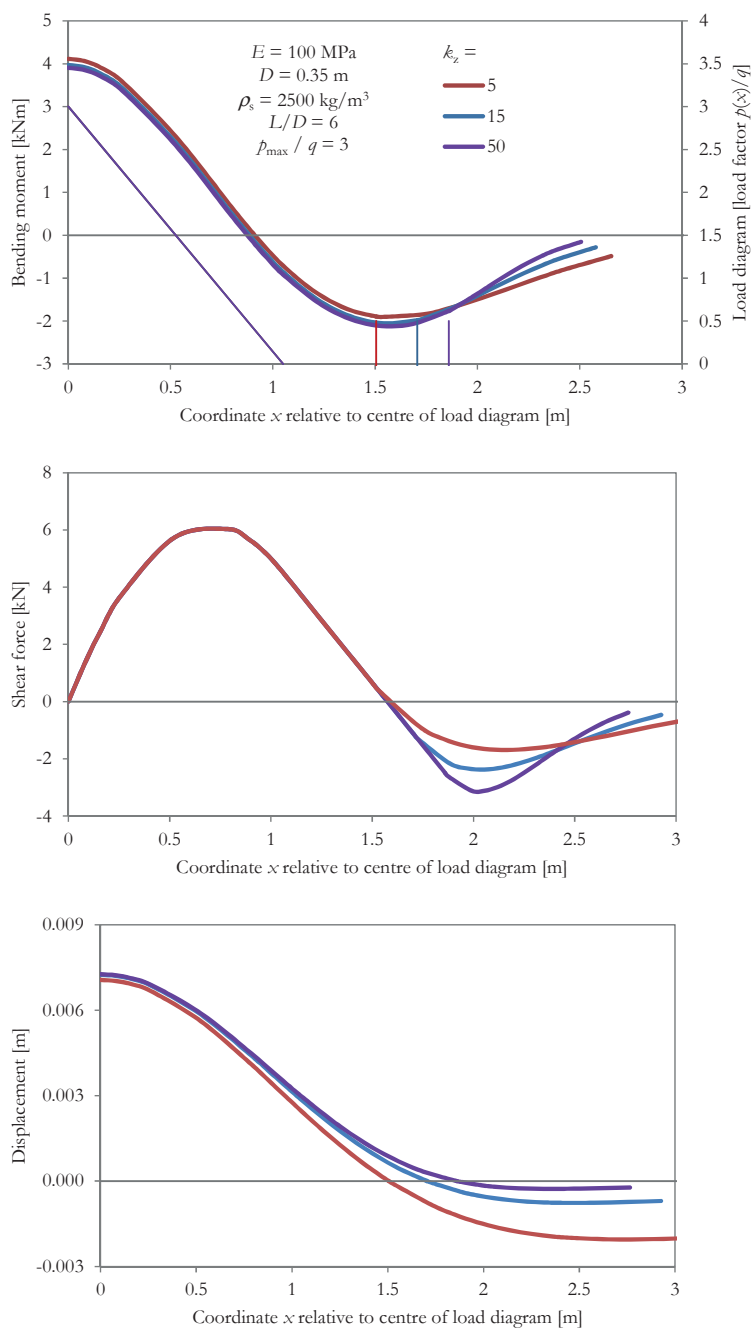
Figure A–32 Bending moment, shear force and displacement of a pre-loaded revetment beam on elastic foundation, a triangular upward load, case with free spanning beam, with k_z variable

A.3 Confined beam model

The revetment top-layer is subjected to perpendicular upward loading due to water head differences. In a more rigorous response analysis (see section A.2) the revetment is modelled as a non-linear elastic beam on an elastic no-tension foundation.
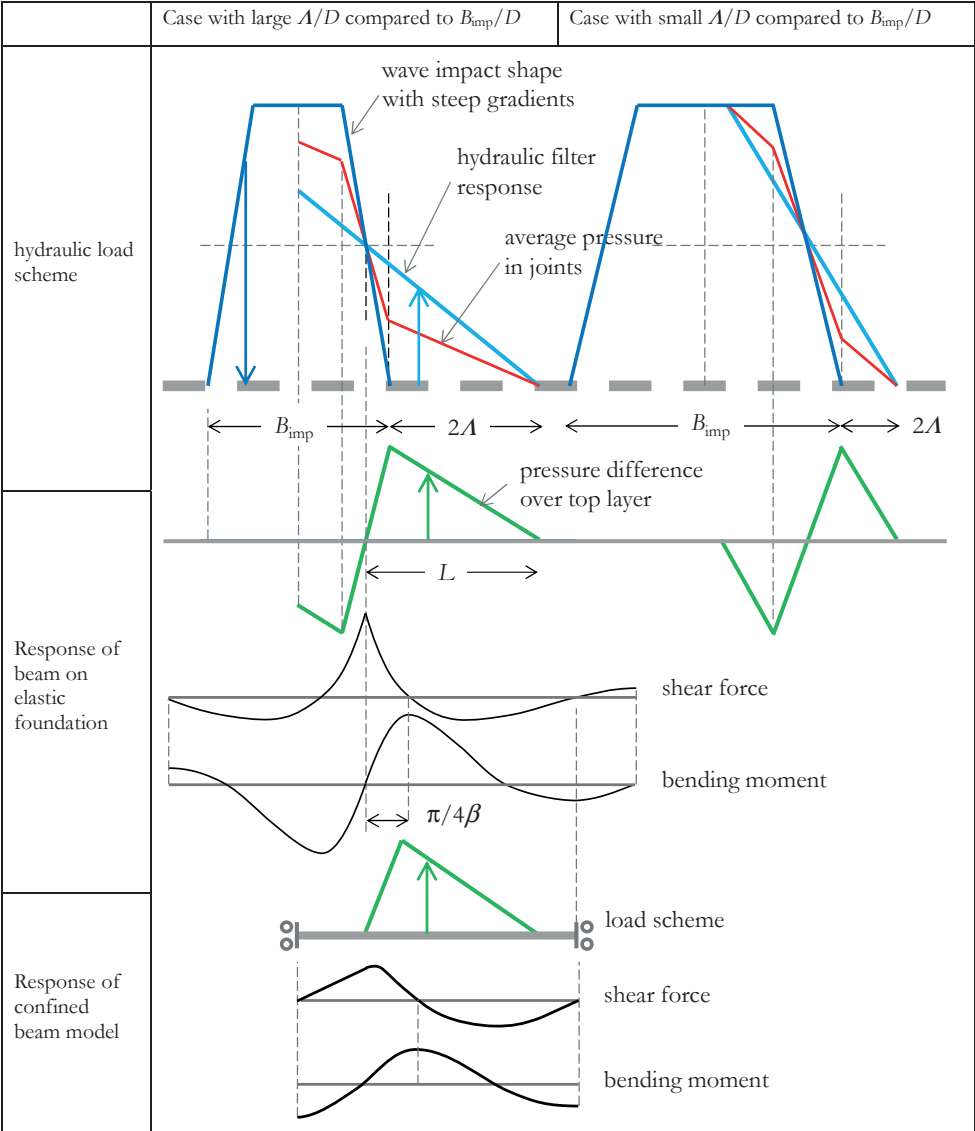
Figure A–33   Summary of load schemes and structural response

The separate elements act jointly as a beam due to the compressive normal force. Occurring bending moments and shear forces in the beam lead to eccentricity of the normal force and by friction between the elements. Upward loading that exceeds the self-weight of the revetment causes upward deformation. At these positions the revetment beam is not supported by the foundation. The 'free spanning' portion of the revetment beam can be isolated from the rest of the beam. A model of a confined beam remains. See Figure A–33. This model is adequate and sufficiently accurate in describing the governing 3-point bending failure mode. Simple equilibrium formulas define the internal forces and the resistance of the top-layer in bending and shear.

A.3.1 Analysis of wave load shape

The load to be applied on a static elasto-plastic confined beam model should represent the real uplift load. The shape of the uplift load is determined by the gradients of the water pressure on the slope and by the leakage characteristics of the revetment structure.

The spatial distribution of the resultant head difference has been measured during Delta-flume tests. ZSTEEN model calculations also provide those data.[285]

Shape factor			
	0.5	$2/\pi = 0.64$	1.0
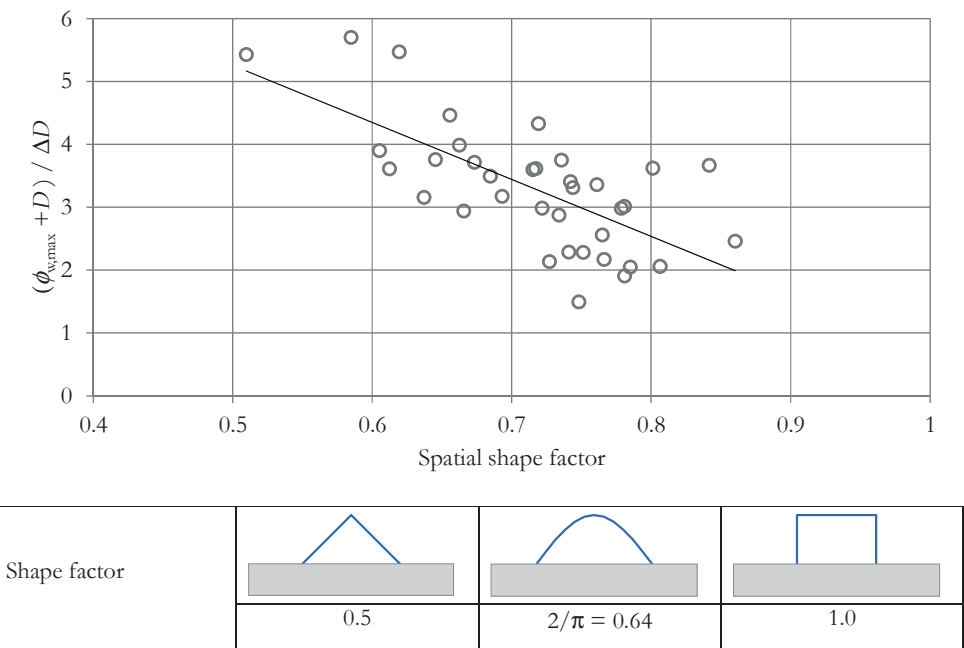
Figure A–34   Shape factor of pressure diagram extracted from ZSTEEN model calculations

The model calculations provide the distribution of hydraulic head difference $\phi_w(x)$ over the length of the revetment beam. Integration over the length $\int(\phi_w(x)+D)\mathrm{d}x$ and dividing by the peak value $\phi_{w,max}+D$ gives a shape factor. Figure A–34 shows calculated shape factors of all time steps within three wave impact incidents. On average the shape tend to a sinus-shape,

---

[285] Peters and Pfeiffer, *Investigation implementation clamping strength in ZSteen*

but looking at the time steps with the largest pressures and the largest integrated force, the shape tend to a triangular shape.

The triangle is in some cases (almost) symmetric, but is in most time steps skew. The gradient of the pressure diagram is at the wave impact side determined by the impact pressure gradient, and the gradient at the other side is determined by the leakage factor (see Figure A–33). For the data points shown in Figure A–34 the average position of the peak is at $0.06\,L$ offset of the centre, with a standard deviation of $0.23\,L$.

A.3.2   Internal forces

In line with the average in Figure A–34 and for the purpose of evaluating the laboratory tests of Annex E the load is defined as a sinus-shaped distributed load (see Figure A–35). The principle of the model is that the length of the model ($2\,x_0$) is derived from the equilibrium calculation. The beam weight equals the water load. The boundaries do not experience shear forces, since the load is fully balanced. The boundaries are clamped and bending moments occur at the clamped boundaries.
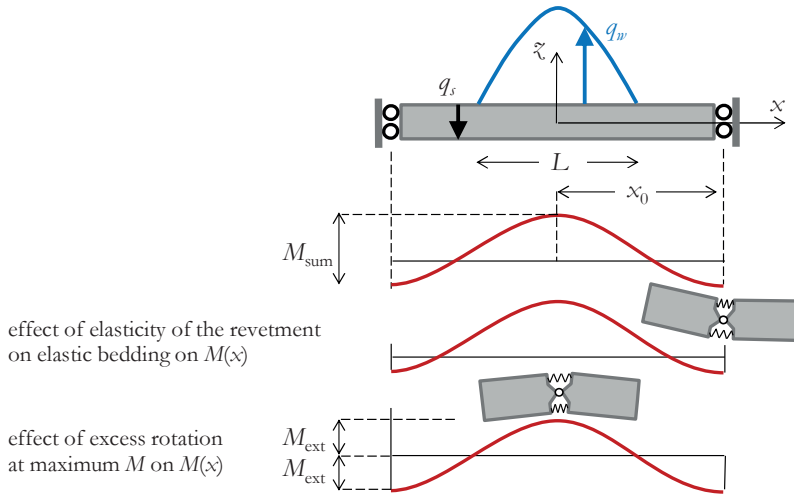
Figure A–35   **Beam portion subject to sinus shape uplift load, beam length balances the load**

The water pressure shape function is as follows:

$$q_w(x) = q_w \cos\frac{\pi x}{L} \text{ for } -\tfrac{1}{2}L < x < \tfrac{1}{2}L$$

with $q_w = \rho_w\,g\,\phi_w$

Integration for x > 0 gives:

$$Q_w = \int_0^{\frac{1}{2}L} q_w \cos\frac{\pi x}{L} = \left[-\frac{q_w L}{\pi}\sin\frac{\pi x}{L}\right]_0^{\frac{1}{2}L} = -\tfrac{1}{\pi}q_w L$$

The length x_0 of the beam model between the boundaries with no shear follows from the definition of load Q_w and weight ($q_s\,x_0$) balance:

$$\frac{x_0}{L} = \frac{1}{\pi}\frac{q_w}{q_s} \quad \text{for } x_0 > \frac{1}{2}L \qquad\qquad \text{Eq. A.39}$$

with q_s = effective top-layer weight: $q_s = (\rho_s - \rho_w)\, g \cos\alpha\, D = \rho_w\, g \cos\alpha\, \Delta D$

In case $x_0 < \frac{1}{2}L$, or $\frac{q_w}{q_s} < \frac{\pi}{2} = 1.57$, the beam length x_0 is calculated with $\int_0^{x_0} q_w \cos\frac{\pi x}{L} = q_s x_0$.

This leads to a solution with complex numbers.[286]

The shear force is calculated with:

$$V(x) = -\int q(x)dx \qquad = \frac{q_w L}{\pi}\sin\frac{\pi x}{L} - q_s x \qquad \text{for x} < \frac{1}{2}L$$

$$= \frac{q_w L}{\pi} - q_s x \qquad\qquad \text{for } x > \frac{1}{2}L$$

Eq. A.40

The extreme shear force occurs at the point where $q_w(x) - q_s = 0$. This point x_1 is defined as:

$$\cos\frac{\pi x_1}{L} = \frac{q_s}{q_w} \qquad\qquad \text{Eq. A.41}$$

The magnitude of the extreme shear force can be written as:

$$\frac{V_{ext}}{q_s L} = \frac{q_w}{q_s}\frac{1}{\pi}\sin(\text{acos}\frac{q_s}{q_w}) - \frac{1}{\pi}\,\text{acos}\frac{q_s}{q_w} \quad \text{for } x_0 > \frac{1}{2}L \qquad\qquad \text{Eq. A.42}$$

The bending moment is calculated with:

$$M(x) = \int V(x)dx$$

The sum M_{sum} of the absolute negative and positive extremes in $M(x)$ at the boundaries and in the middle is found $M(0) - M(x_0)$.

$$M_{sum} = -\frac{2}{\pi}\left(1 - \frac{2}{\pi}\right)q_w(\frac{1}{2}L)^2 + \frac{1}{2}q_s x_0^{\,2} \qquad\qquad \text{Eq. A.43}$$

In the failure stage the bending moment distribution tends to equal the magnitude of the positive and negative extremes, leading to extremes of half of M_{sum}. Evaluation of Eq. A.43 leads to:

$$\frac{M_{ext}}{q_s L^2} = \left(\frac{1}{2\pi^2} - \frac{1}{4\pi}\right)\frac{q_w}{q_s} + \frac{1}{4\pi^2}(\frac{q_w}{q_s})^2 \quad \text{for } x_0 > \frac{1}{2}L \qquad\qquad \text{Eq. A.44}$$

For the domain $1 < \frac{q_w}{q_s} < \frac{\pi}{2}$ the following solution is found: $\frac{M_{ext}}{q_s L^2} = \frac{4-\pi}{4\pi(\pi-2)^2}(\frac{q_w}{q_s} - 1)^2$.

Equations A.42 and A.44 are plotted in Figure A–36.

---

[286] Alternatively a solution for a linear load function is derived and plotted in Figure A–36.

$$\frac{x_0}{L} = (\frac{2}{\pi} - \frac{1}{2}) + \frac{2}{\pi}\sqrt{\frac{\pi}{2} - 1}\sqrt{\frac{q_w}{q_s} - 1} = 0.137 + 0.481\sqrt{\frac{q_w}{q_s} - 1}$$
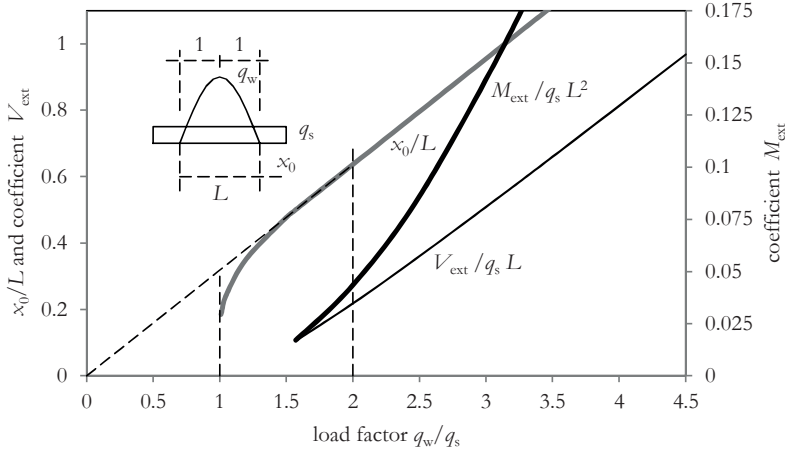
Figure A–36 Dimensionless shear force and bending moment of confined beam model subjected to sinus shaped load

For triangular load shapes the same analysis can be made. The symmetric case can be compared with the sinus shaped load. The total force at a given peak value q_w is smaller, and hence x_0 and the bending moment and shear forces are smaller.

$$\frac{x_0}{L} = \frac{1}{4}\frac{q_w}{q_s} \qquad \text{for } x_0 > \tfrac{1}{2}L$$

$$\frac{x_0}{L} = 1 - \frac{q_s}{q_w} \qquad \text{for } x_0 < \tfrac{1}{2}L \qquad\qquad \textbf{Eq. A.45}$$

$$\frac{M_{ext}}{q_s L^2} = \frac{1}{48}\frac{q_w}{q_s} + \frac{1}{64}\left(\frac{q_w}{q_s}\right)^2 \qquad \text{for } x_0 > \tfrac{1}{2}L$$

$$\frac{M_{ext}}{q_s L^2} = \frac{1}{12}\left(\frac{q_w}{q_s}-1\right)\left(1-\frac{q_s}{q_w}\right)^2 \qquad \text{for } x_0 < \tfrac{1}{2}L \qquad\qquad \textbf{Eq. A.46}$$

$$\frac{V_{ext}}{q_s L^2} = \frac{1}{4}\frac{q_w}{q_s} + \frac{1}{4}\frac{q_s}{q_w} - \frac{1}{2} \qquad \text{for } x_0 > \tfrac{1}{2}L$$

$$\frac{V_{ext}}{q_s L^2} = \frac{1}{4}\left(\frac{q_w}{q_s}-1\right)\left(1-\frac{q_s}{q_w}\right) \qquad \text{for } x_0 < \tfrac{1}{2}L \qquad\qquad \textbf{Eq. A.47}$$

When the confined beam model is evaluated including the reverse (downward) loading at one side of the beam, the required length for equilibrium $2x_0$ becomes smaller. The bending moment reduces, but the maximum shear force increases due to the asymmetry. See the blue lines in Figure A–36.
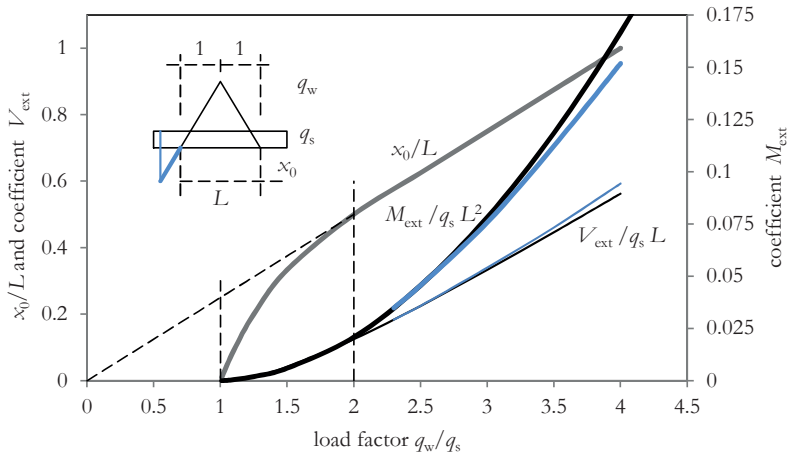
Figure A–37 Dimensionless shear force and bending moment of confined beam model subjected to triangular shaped load

A similar effect occurs when we consider a skewness of the upward load. The effect of local force contributions on the bending moment is largest in the middle of the span. When the peak is shifted to one side, the bending moment reduces and the shear force increases. Analytical formulas for the asymmetric load can be obtained but are quite complicated. The combined effect of the reverse loading and the skewness can be computed with beam software and can be expressed in correction factors on the moment and shear force coefficients $M_{ext}/q_s L^2$ and $V_{ext}/q_s L^2$.

The load diagram length L can be split into L_a and L_b, with $L_a + L_b = L$. The value of L_b/L_a is indicated as a key to the various cases shown in Figure A–38. The correction factors use L_b/L_a as a skewness variable. The factors are valid for the ranges $L_b/L_a = 1 .. 6$ and for $q_w/q_s = 1 .. 5$.

$$c_V = 1.0 + 0.075\frac{L_b}{L_a} - 0.0045\left(\frac{L_b}{L_a}\right)^2$$

$$c_M = 1.22 - 0.070\frac{q_w}{q_s} - 0.039\frac{L_b}{L_a} \not> 1.0$$

Eq. A.48
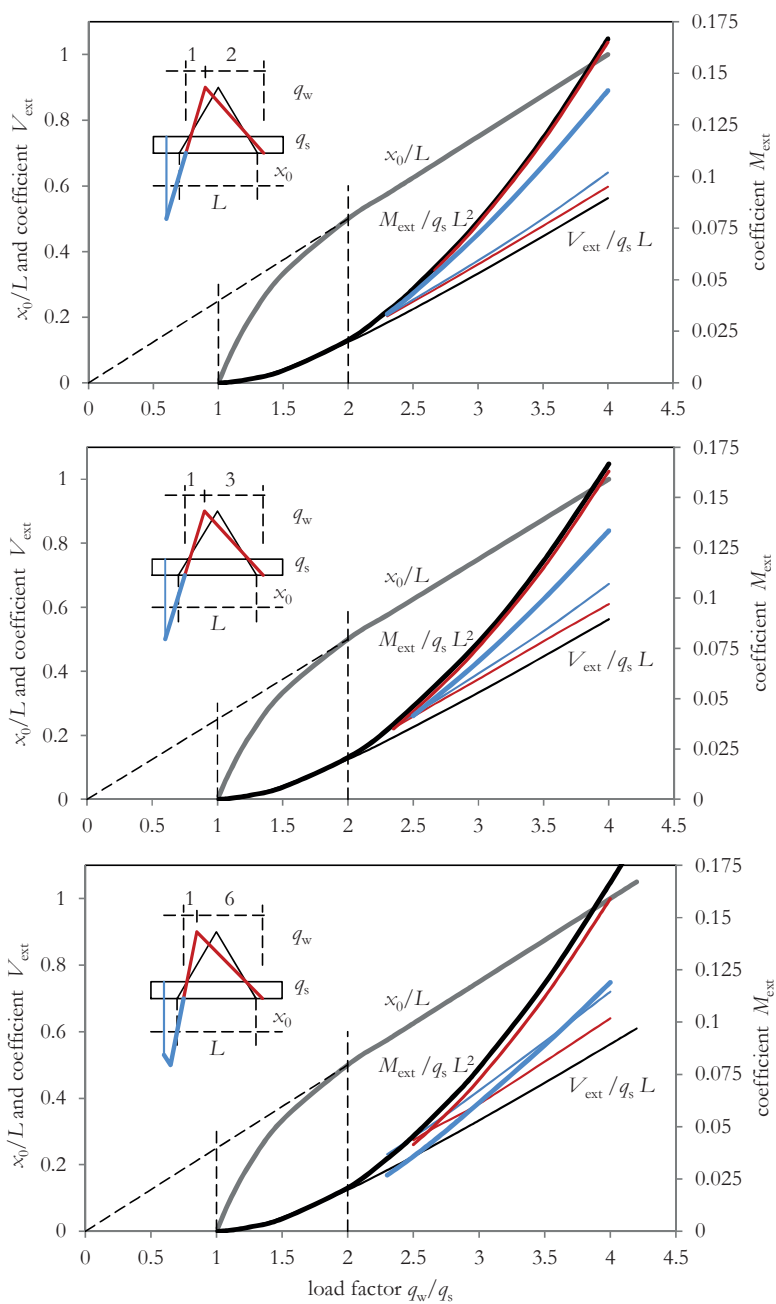
Figure A–38   Dimensionless shear force and bending moment of confined beam model subjected to asymmetrical triangular shaped load

A.3.3   Resistance of a cross section

The resistance of the top-layer is determined by its ability to withstand shear forces and bending moments. The ultimate shear force is:

$$V_u = f_{fr} \times N$$

with N = normal force

f_{fr} = friction coefficient

The bending capacity of the beam is best evaluated by the equilibrium of the half beam, between mid-span and boundary. This equilibrium is defined in a deformed state.

$$M_{sum} = N \times e = N \times (d - 2\beta z_c - \delta) \qquad \text{Eq. A.49}$$

with

e = internal lever arm

d = effective element height, which is D minus chamfered edges

z_c = depth of the stress area

β = factor for stress area

δ = vertical mid span deflection of the beam
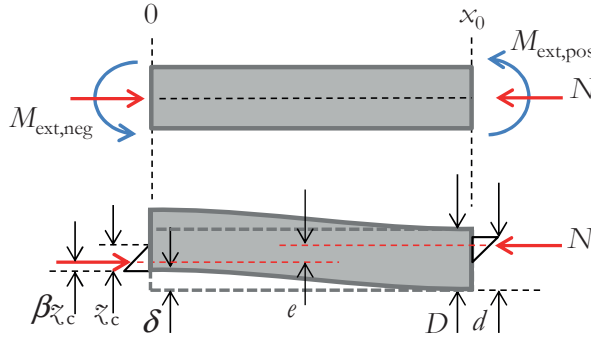
Figure A–39   Equilibrium of beam portion in deformed state

In concrete mechanics and in geotechnics there is a number of assumed shapes of the stress area, and associated values of the factor β. Assuming linear elasticity in the joint material or element material, a triangular stress area will occur. Parabolic or rectangular shapes develop when the strains are higher and plasticity occurs. For a triangular shape the factor β equals 0.33.

The depth z_c of the stress area depends on the force level and the imposed curvature. Assuming linear elasticity and elastic limit of σ_u, and substituting $N = \frac{1}{2}\sigma_u z_c$ Eq. A.49 becomes quadratic in N:

$$M_{sum} = N \times (d - \tfrac{4}{3}N/\sigma_u - \delta) \qquad \text{Eq. A.50}$$

The deflection δ is estimated as 0.01 of the free span. Using Eq. A.39 we can write:

$$M_{sum} = N \times (d - \tfrac{4}{3}\frac{N}{\sigma_u} - \tfrac{0.02}{\pi} L \frac{q_w}{q_s})$$

<div align="right">Eq. A.51</div>

In dimensionless format:

$$\frac{M_{ext}}{q_s L^2} = \tfrac{1}{2}\frac{M_{sum}}{q_s L^2} = \frac{N}{q_s L}\left(\tfrac{1}{2}\frac{d}{L} - \tfrac{2}{3}\frac{q_s}{\sigma_u}\frac{N}{q_s L} - \tfrac{0.01}{\pi}\frac{q_w}{q_s}\right)$$

<div align="right">Eq. A.52</div>

The expressions Eq. A.44 and Eq. A.52 can be set equal, and as a result an unknown parameter can be found, such as the unknown normal force, or the required stone weight given a certain relation between N and q_s.

A.4   Joint model

A.4.1   *Elastic no-tension models*

The flexibility properties of the top-layer are dominated by the joints. A step can be made towards a model in which all deformation capacity and elasticity can be attributed to the joints. Old basalt structures and modern open pattern-placed revetment structures have joints filled with angular gravel and stone split. The hydraulic properties of the joints are described in section 3.4. The mechanical properties of the joints determine strength and stiffness of the system. The strength of the joint material is highly dependent on the fill rate and the number of contact points. The stiffness is determined also by the amount of contact points and by the ability of the material to move, either to slightly changed position or to move/squeeze out. Descriptions of granular joint fill behaviour can hardly be found in literature. In this study tests on the joint behaviour have been done.

The response of the joint material is distinguished in response to axial compression, to shearing and friction and to flexure. In the beam and plate models the joints are compressed, and are subjected to perpendicular loads and to bending moments, that cause eccentricity of the compressive forces.

Compression of the joint material is elastic up to the level that particles move or crush. Also after particle movement, a part of the deformation is elastic. Permanent deformation of the joint material can be considered as to compact the material. The compaction is expressed in strain. In the specially designed tests it was observed that the top-layer structure can experience a permanent volume reduction of 0.5 to 2 10^{-3} under imposed axial compressive load. This compaction process takes place during the first years of the life time of the structure. Dike settlement and wave action provide energy for the compaction process. The compaction process leads to increase of stiffness and increase of joint strength.

The friction properties of the joints have been tested also. The measured friction coefficient was 0.6 on average and 0.8 in incidental cases. There is vast evidence in literature for a friction coefficient of 0.6 between concrete and gravel or crushed stone. Also concrete on concrete shows a friction coefficient of approximately 0.6. New concrete elements have sharp edges that cause interlocking. In that case higher friction coefficients were found, up to 1.0. The sharp edges however will disappear in time, and the friction property will reduce to a normal value.

Positive dilatant behaviour is an important required property of the joints. If shearing is associated with volume decrease there will be a risk of loss of stability of the elements. Dilatant or contraction behaviour is in soils often described by its effect on pore pressure. For the very open granular fill material this is less relevant. The effect of volume increase or decrease should be focussed on the case of a granular fill in a thin void of – in many cases – 3 to 5 times the average grain size.

$$\tan \psi = -\frac{d\varepsilon_{xx}}{d\varepsilon_{zx}}$$

<div align="right">Eq. A.53</div>

The flexural properties of the joints need closer theoretical study. These properties highly affect the subject of the study, and actually determine the strength of the composite top-layer structure. For the flexural properties of the joint a model of concrete mechanics is adopted. The joint material is assumed not to take any tensile stresses. Bending moments can only be taken by eccentric compression. For that reason the bending moment is always less than $N \times \frac{1}{2}D$. When the compressive normal force is concentrated on the edge of the top-layer elements, the joint acts as a hinge and the flexural stiffness is close to zero. On the other hand, when the compressive normal force only slightly moves from its central position, the full height of the joint remains under compression and there is no change in stiffness compared to the pure compression situation. This is the case when the eccentricity e is less than $D/6$. When e > D/6 on one edge of the material the compression is fully released. The contact area decreases, as the flexural stiffness.

The axial stiffness in linear elastic structural mechanics is defined as EA, E for the Young's modulus, and A for the cross sectional area of the material. Elastic strain in Hooke's law is defined as:

$$\varepsilon = \frac{\sigma}{E} = \frac{N}{EA} = \frac{N}{EB_y d}$$

<div align="right">Eq. A.54</div>

For the flexural stiffness the equivalent definition is based on the ratio between the curvature and the bending moment:

$$\kappa = \frac{d\varepsilon}{dz} = \frac{\sigma / E}{\frac{1}{2} d} = \frac{M / W}{E \frac{1}{2} d} = \frac{M}{EI}$$

<div align="right">Eq. A.55</div>

with

W = elastic modulus of the cross section [m^3] = $\frac{1}{6} B_y d^2$

I = quadratic moment of inertia of the cross section [m^4] = $\frac{1}{12} B_y d^3$
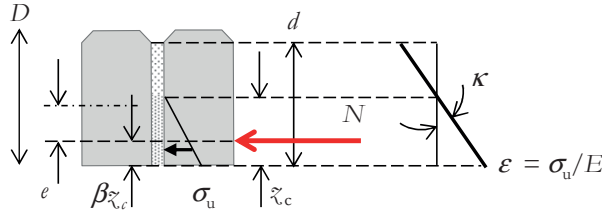
Figure A–40   Definition diagram joint model

Due to the pressure release and opening of the joints the relation between curvature and bending moment is non-linear. Similar to concrete mechanics this can be expressed in a non-constant fictitious value of the Young's modulus E. Here we define this flexural modulus as E_f. This modulus is no longer a material property but a system property.

We define z_c as the height of the contact area in the joints. Working out the definition formula in Eq. A.55 leads to:

$$\frac{E_f}{E_a} = 6\left(\frac{z_c}{d}\right)^2\left(\tfrac{1}{2} - \tfrac{1}{3}\frac{z_c}{d}\right) \text{ for } 0 < z_c/d < 1 \qquad\qquad \textbf{Eq. A.56}$$

The same equation expressed in e/d:

$$\frac{E_f}{E_a} = 54\left(\frac{e}{d}\right)\left(\tfrac{1}{2} - \frac{e}{d}\right)^2 \text{ for } \tfrac{1}{6} < e/d < \tfrac{1}{2} \qquad\qquad \textbf{Eq. A.57}$$

with $e = \dfrac{M}{N}$
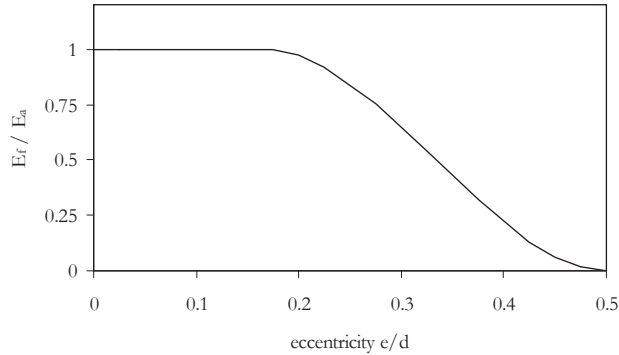
Figure A–41   Relation between eccentricity of force and flexural stiffness

A.4.2   Lumped hinge model

Since the bending moment is not constant over the length of the beam, the relation between curvature and deflection becomes more complex. In structural mechanics these relations are commonly simplified using either averaged Young's moduli over the length of the beam, or lumped spring models where the curvature is concentrated in a hinge. For simple base cases

the properties the elastic restraints in the hinge can be calculated with analytical formulas. The relation between bending moment and curvature can be derived as follows.

z_c = the height of the contact zone with compressive stress

e = the internal lever arm

$$\varepsilon = \frac{\sigma}{E}$$

$$\sigma = \frac{N}{\frac{1}{2} z_c}$$

$$z = \frac{1}{2} d - \frac{1}{3} z_c \text{, or } z_c = 3\left(\frac{1}{2} d - e\right) = 3\left(\frac{1}{2} d - \frac{M}{N}\right)$$

$$\kappa = \frac{\varepsilon}{z_c} = \frac{\sigma}{z_c E} = \frac{N}{\frac{1}{2} z_c^2 E} = \frac{N}{\frac{9}{2}\left(\frac{1}{2} d - \frac{M}{N}\right)^2 E}$$

Define reference values M_0 and κ_0 of bending resistance and curvature:

M_0 = the theoretical maximum bending moment = $N\,\frac{1}{2}\,d$

κ_0 = the corresponding value of the curvature in case the relation was linear-elastic

$$\kappa_0 = \frac{M_0}{\frac{1}{12} d^3 E} = \frac{6N}{d^2 E}$$

The relation κ / κ_0 can now be written and plotted as:

$$\frac{\kappa}{\kappa_0} = \frac{N d^2 E}{\frac{9}{2}\left(\frac{1}{2} d - \frac{M}{N}\right)^2 6NE} = \frac{\frac{1}{6} d^2}{\frac{9}{2}\left(\frac{1}{2} d - \frac{M}{N}\right)^2} = \frac{4}{27} \frac{1}{(1 - \frac{M}{M_0})^2} \text{ for } M > \frac{1}{3} M_0 \qquad \textbf{Eq. A.58}$$
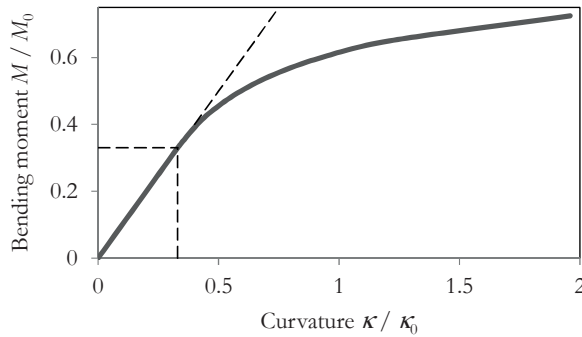
Figure A–42   Relation bending moment vs curvature for linear elastic, no-tension joint

Focussing on a beam portion between two points with zero bending, we can define a bending moment function. A parabolic function would be:

$$M(x) = 4\frac{x}{L}\left(1 - \frac{x}{L}\right)M \qquad \textbf{Eq. A.59}$$
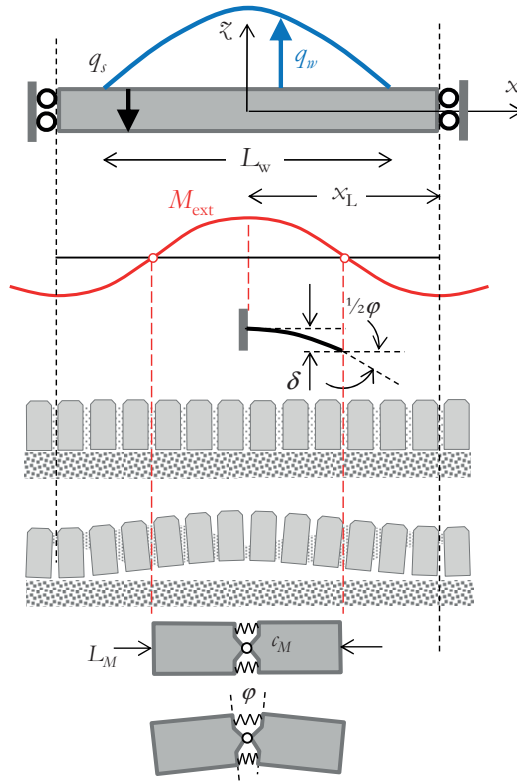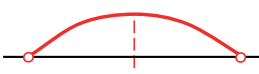
Figure A–43   Relation bending moment vs curvature for linear elastic, no-tension joint
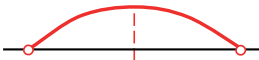
Substituting $M(x)$ for M in Eq. A.58 gives a curvature function $\kappa(x)$. The integrated curvature produces the sum of the rotation in the beam portion. Similarly the deflection of the beam can be found by integrating the curvature times the position.

$$\tfrac{1}{2}\phi = \int\limits_{0}^{L/2} \kappa(x)dx \qquad\qquad \textbf{Eq. A.60}$$

$$\delta = \int\limits_{0}^{L/2} \kappa(x)xdx \qquad\qquad \textbf{Eq. A.61}$$

Evaluating these formulas gives the following results:

	parabola	linear
$M(x)$	$4\dfrac{x}{L}(1-\dfrac{x}{L})M$	$2\dfrac{x}{L}M \qquad$ for $x/L < \tfrac{1}{2}$

	parabola	linear
$\frac{1}{2}\phi$	$\frac{1}{54}\frac{\kappa_0 L}{(1-\frac{M}{M_0})}\left(1+\frac{\frac{M_0}{M}}{\sqrt{\frac{M_0}{M}-1}}\arctan\frac{1}{\sqrt{\frac{M_0}{M}-1}}\right)$ Eq. A.62	$\frac{2}{27}\kappa_0 L\frac{1}{1-\frac{M}{M_0}}$ Eq. A.63
δ	$\frac{1}{54}\frac{\kappa_0 L^2}{(1-\frac{M}{M_0})\frac{M}{M_0}}\frac{1}{\sqrt{\frac{M_0}{M}-1}}\arctan\frac{1}{\sqrt{\frac{M_0}{M}-1}}$ Eq. A.64	$\frac{1}{27}\kappa_0 L^2\left(\frac{M_0}{M}\right)^2\left(\ln(1-\frac{M}{M_0})+\frac{1}{\frac{M_0}{M}-1}\right)$ Eq. A.65

The equations are valid for $M > \frac{1}{3}M_0$

The linear elastic solutions are:

	parabola	linear
$\frac{1}{2}\phi_0$	$\frac{1}{3}\kappa_0 L$	$\frac{1}{2}\kappa_0 L$
δ_0	$\frac{5}{48}\kappa_0 L^2$	$\frac{1}{12}\kappa_0 L^2$

Dividing the solutions for δ and $\frac{1}{2}\phi$, we find values like $0.35L$ for $M/M_0 = 0.7$, which tends to $0.5L$ if M/M_0 gets closer to unity. If we concentrate the cause of the total deflection as rotation in a central hinge, we define the quotient of δ and $\frac{1}{2}\phi$ as $0.5L$ and replace $\frac{1}{2}\phi$ by a fictitious angle. A corresponding rotational spring stiffness c_M can be calculated.

	parabola	Linear
c_M	$\frac{9}{8}\frac{Ed^3}{L}(1-\frac{M}{M_0})(\frac{M}{M_0})^2\frac{1}{f_{M1}}$ with $f_{M1}=\frac{1}{\sqrt{\frac{M_0}{M}-1}}\arctan\frac{1}{\sqrt{\frac{M_0}{M}-1}}$ Eq. A.66	$\frac{9}{16}\frac{Ed^3}{L}(\frac{M}{M_0})^3\frac{1}{f_{M2}}$ with $f_{M2}=\ln(1-\frac{M}{M_0})+\frac{1}{\frac{M_0}{M}-1}$ Eq. A.67

The equations Eq. A.66 and Eq. A.67 are plotted in Figure A–44. The rotational spring stiffness starts at levels of roughly 0.20 and 0.25 Ed^3/L, which are the linear values for the two cases. For $M/M_0 > 0.5$, the values start to deviate from the initial values, and tend to zero for $M/M_0 = 1$. The dimension L is the length of the beam portion that belongs to the lumped hinge.
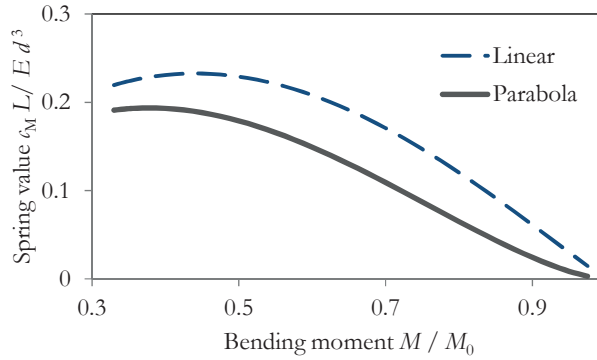
Figure A–44 **Value of rotational non-linear spring resistance as a function of the load level for parabolic and for linear bending diagram**

This result can be adopted in a new model of the revetment beam that lumps all deflections in hinges. A logic choice is a three-point bending scheme, where three hinges occur at the locations of maximum bending. The length L in the formulas above corresponds to the intermediate distance of the hinges. In a progressively deformed stage the bending moments in the beam will redistribute and become more or less equal. Knowing this, the deflection can be calculated fairly easily from an estimate of the load level.

A.4.3   Joint strength and failure envelope

The strength of the joint can be expressed as a maximum permissible strength σ_u. The axial force and the bending moment are a function of the size of the contact area. For the shape of the contact area we again assume a linear stress distribution. At 'failure' the most compressed side has a stress equal to σ_u. The failure envelope is defined by a combination of N and M given in the expressions below and plotted in Figure A–45.

$$N_u = \sigma_u d \qquad\qquad\qquad \textbf{Eq. A.68}$$

$$N = N_u \frac{1}{1 + 6\frac{e}{d}} \qquad \text{for } e / d < \tfrac{1}{6} \qquad\qquad \textbf{Eq. A.69}$$

$$N = N_u\left(\tfrac{3}{4} - \tfrac{3}{2}\frac{e}{d}\right) \qquad \text{for } e / d > \tfrac{1}{6} \qquad\qquad \textbf{Eq. A.70}$$

$$M = N\frac{e}{d} \qquad\qquad\qquad \textbf{Eq. A.71}$$

A.4.4   Finite element joint models

A more sophisticated analysis and parameter variation was performed and reported by Derkzen[287]. The laboratory pull tests of annex E were analysed and hindcasted with help of finite element models. A number of model approaches were used. The finite element programme TNO-DIANA was used.

---

[287] B. Derkzen, *Constructief ontwerp van steenzettingen voor dijkbekleding - Numeriek onderzoek naar de liggerwerking van de toplaag* (MSc thesis TU Delft, 2004)
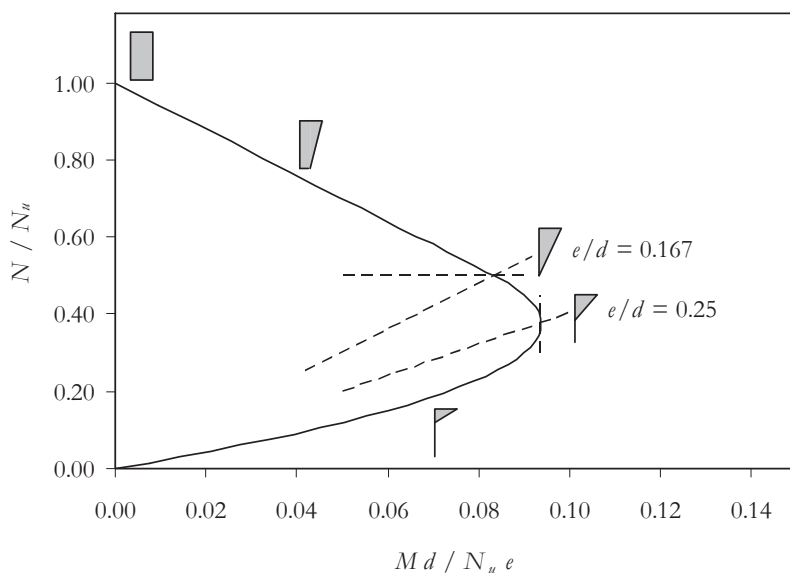
Figure A–45 **Failure envelope of combinations of maximum normal force and maximum bending moment for a given strength**

First a modelling of the single elements and joints was applied. After element mesh dependency verifications, the joints as well as the elastic foundation were modelled with elastic elements with Mohr-Coulomb strength criteria, with zero cohesion. The initially chosen joint properties were a friction coefficient of 0.5, a Young's modulus of the joint material $E = 50$ MPa and joint thickness $s = 3$ mm. The joints were filled with joint material elements over the full height. Consequently a slightly higher bending strength was found compared to the experiments. The Mohr-Coulomb joint model showed a good qualitative similarity with respect to the joint gaps and the shear failures.

Variation of the stiffness of the joints was performed in order to match the experimental results. Stiffness and shape of the deformation could be modelled adequately by adopting a joint stiffness of $1.0 \ 10^9$ N/m^3 for the 2-row tests and $0.5 \ 10^9$ N/m^3 for the 4-row tests and above.

The slope of the falling branch of the force-displacement diagrams of the experiments (see Figure E–5) could only be modelled adequately by softening the joint properties. Loss of joint material was observed as soon as the revetment structure was subjected to an upward deformation of more than the aggregate size. If this material loss is adopted in the model, the model result for the falling branch shows a better correspondence with the measurements.

The FEM joint model provides a better insight in the observed shrinkage and corresponding loss of pre-load just after start of the vertical tension. The mechanism is as follows. As soon as the axial pre-load changes position, the peak stress increases considerably. This is associated with axial compressive strain. Only after some vertical deformation, as a second

order effect an overall axial extension occurs which overrules the initial axial compressive strain.

Besides modeling of the single elements and joints, a homogeneous model with smeared properties was tried also. With help of the available concrete crack models in the TNO DIANA code, a model was made that showed cracks at the locations where the real joints showed gaps. Unfortunately the direction of the cracks cannot be imposed. When the model was used for thicker revetment layers, the cracks tend to rotate and also horizontal cracks occur, splitting the stones in horizontal layers, which is not realistic in the cases at consideration. So, the smeared crack models could not successfully be applied in the case of discrete joints.

A.5 Snap-through model

The resistance of axial beam models relies on the presence of an axial force. In cases when the axial force is very high buckling may play a role. One should be very careful assuming that very high normal forces are beneficial for the design. The practical relevance of buckling issues for the design of the revetment beams is hence doubtful.

Since the buckling hypothesis and buckling theory has been given attention in literature[288], we also cover it in this section on beam models. Use of the snap-through model as a design tool is <u>not</u> recommended.

There might be some practical relevance of this theory when it comes to describing group failure and when it comes to definition of deformation limits in SLS cases.

Deflected compressed bars have a tendency to increase their deflection. This may lead to an unstable equilibrium and to buckling failure. The compressive normal force N in the revetment top-layer may therefore cause instability of the static equilibrium. For investigation of the stability elastic properties were adopted e.i. the foundation stiffness in z-direction k_z and the flexural bending stiffness $E_f I$. The equations for the free part and the embedded part of the beam are:

$$EI \frac{\mathrm{d}^4 u}{\mathrm{d}x^4} + N \frac{\mathrm{d}^2 u}{\mathrm{d}x^2} = 0 \ \text{ with } \ N_{cr} = n^2 \pi^2 \frac{EI}{l^2}$$

Eq. A.72

$$EI \frac{\mathrm{d}^4 u}{\mathrm{d}x^4} + N \frac{\mathrm{d}^2 u}{\mathrm{d}x^2} + ku = 0$$

Eq. A.73

Buckling of partially supported beams is studied by various authors using analytical and numerical solutions.[289] For the revetments beams the stiffness of the elastic bedding is such that the embedded parts can be seen as (rotational) supports at the boundaries of the free length. The risk of buckling of the free span is governing.

The most relevant concern is the interaction of the stiffness and the deflection and the strength limit associated with the loose joint connection of the revetment elements. This is captured under the of snap-through buckling phenomenon. Snap-through buckling is

---

[288] K.W. Pilarczyk, "Design of Revetments" (Book section); C.M. Frissen, *Modelleren van een blokken- en zuilenbekleding*, 2000; A.S.J. Suiker, "Inklemeffecten bij Steenzettingen op dijken" (MSc thesis TU Delft, 1995)
[289] K.S. Papachristou and D.S. Sophianopoulos, "Buckling of beams on elastic foundation considering discontinuous (unbonded) contact," *Int. J. Mech. Appl.* (2013)

described in literature[290] with help of a concentrated load on a two bar truss. The load F has to satisfy the condition:

$$F = 8k\delta(\frac{d}{L})^2\left(\frac{d-\delta}{d+\delta}\right)$$

Eq. A.74

The spring stiffness k can be the representative of the elasticity of the bars themselves. For a small d/L this can be estimated with:

$$k = \frac{EA}{\frac{1}{2}L}$$

Eq. A.75
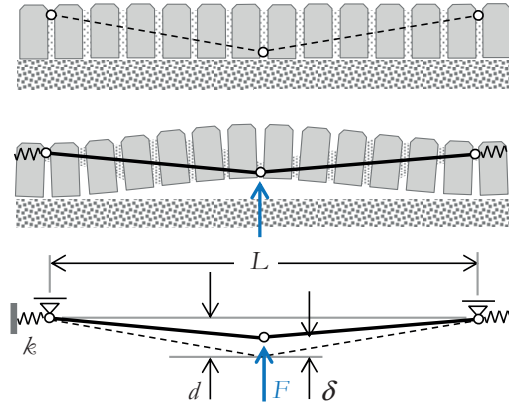
Figure A–46   **Definition diagram snap-through buckling**

The typical load path is that the load F increases to a maximum and then, with further increase of δ, decreases to zero at $\delta = d$, and then flips to tension. In practice only the load path up to the first extreme is relevant. The maximum load F_{max} can be found:

$$F_{max} = 8(3-2\sqrt{2})k\frac{d^3}{L^2} \qquad (= 1.37k\frac{d^3}{L^2})$$

Eq. A.76

$$\text{at } \delta = (-1+\sqrt{2})d \quad (= 0.41d)$$

The snap-trough formulas can be elaborated specific for a confined beam of revetment elements with limited joint strength. In the hinge, the cross sectional area can be replaced by the effectively stressed area $A = N/\sigma$. The maximum external load is set equal to the weight of the two-bar truss, where the length becomes a variable to equal the load. In this model, the structure is loaded with an external pull-out force equal to half of the weight of the structure. In the formula the structures' distributed self-weight is neglected.

$$F = \frac{1}{2}\rho_s g DB_y L$$

Eq. A.77

---

[290] Z.P. Bazant and L. Cedolin, *Stability of structures - Elastic, inelestic, fracture and damage theories* (Oxford University Press, 1991) and S.P. Timoshenko and J.M. Gere, *Theory of elastic stability - second edition* (McGraw-Hill, 1961)

$$N = \tfrac{1}{4} F \frac{L}{z} = \tfrac{1}{8} \rho_s g D B_y L^2 / z$$

A limited joint strength causes the increased normal force to move from the extreme positions closer to the centre of the beam. In the limit state of the geometrical non-linear case the internal lever arm becomes:

$$z = d - \delta - \beta z_c \quad \text{or} \quad z = (2 - \sqrt{2}) d - \beta z_c$$

$$z = (2 - \sqrt{2}) d - \frac{\beta}{\alpha} \frac{N}{\sigma B_y}$$

which gives a quadratic equation in z, solved as

$$z = \tfrac{1}{2}(2 - \sqrt{2}) d \pm \tfrac{1}{2} \sqrt{(6 - 4\sqrt{2}) d^2 - \tfrac{1}{2} \rho_s g DL^2 \beta / \alpha\sigma}$$

with

$\alpha =$ integral factor for the stress diagram: $\int \sigma \, dz / \sigma z_c$ over z_c,

        for the triangle shape: $\alpha = \tfrac{1}{2}$

$\beta =$ factor for position of the centroid of the stress diagram,

        for the triangle shape: $\beta = 0.33$

The formula can be substituted in Eq. A.76, where d is replaced by z.

$$F_{\max} = 8(3 - 2\sqrt{2}) k \frac{z^3}{L^2}$$

For k we use $EA/\tfrac{1}{2}L$.

We obtain an expression for in a snap-trough buckling 'safety factor' when F_{max} is divided by F as defined in Eq. A.77.

$$\gamma_{buc} = 16 (3 - 2\sqrt{2}) \frac{E}{\rho_s g D} \frac{D}{L} \left((2 - \sqrt{2}) \frac{d}{L} + \sqrt{(6 - 4\sqrt{2})(\frac{d}{L})^2 - \frac{\rho_s g D\beta}{\alpha\sigma}} \right)^3 \qquad \textbf{Eq. A.78}$$

Numerical evaluation of this formula, using $d = 0.8\,D$, $D = 0.3$ m, $E = 60$ MPa and $\sigma = 400$ kPa, gives a value of $\gamma_{buc} = 1.0$ for $L/D = 5$. Smaller L/D values have a buckling safety $\gamma_{buc} > 1.0$. This result can be considered as a lower bound, as the effective area taken in the hinges is smaller than in the other joints over the length of the bars. Taking the elasticity as an average of the value in the hinge and a value based on a fully compressed cross section, gives a roughly 25% higher result for L/D. Due to the low Young's modulus and due to the stress concentrations the axial elasticity in the revetment beams is quite low, which results in a fair change that buckling could play a role.

The results of the model calculations show that for values of $L/D >$ say 8, buckling is an issue. In case buckling may not occur in reality, compressive forces close to the buckling value tend to increase the deflection, which can be a problem.

A condition for buckling risks is the occurrence of a corresponding high normal force in the arch. The forces must be balanced in the model boundaries, which is in practical cases mostly not possible. When these normal forces cannot occur, buckling will not be an issue.

ANNEX B   TWO-DIRECTIONAL RESISTANCE MODELS

For single element pull tests on a revetment plate, beam models as described in Annex A are not realistic because of the two-directional distribution of the loads. Therefore the confined beam model of annex A.3 has been developed into continuous elastic plate models that are described in section B.1.

Dis-continuous behaviour occurs when the plate experiences concentrated loading and the plate deforms. This causes changes to the tangential stress state, which influences the elastic plate model.

In section B.2 a simplification of the plate models is presented in the form of a beam model for single element loads. The model consists of two crossing beams, representing the transverse direction and the longitudinal direction.

The plate models developed in annex B provide a basis for evaluation of the pull test results presented in annex C and D.

B.1 Plate model for single element loads

The revetment structure is a slab with element interaction in both the transverse and in the longitudinal direction of the dike. In the transverse direction the gravity action is more obvious, but also in longitudinal direction a normal force can be present (see section 3.1). These forces are measured (see annex G). Lifting single elements is in practise restrained by element interaction in two directions.

B.1.1   Mechanics of centrally loaded circular plates

For the analysis concentrated loads, like in the pull tests, the theory of symmetrical bending of circular plates can be used. The pull force lifts a part of the top-layer, which is assumed to be circular. By definition, the radius of the circle follows from:

$$P = -q_s \pi R^2 \qquad \text{Eq. B.1}$$

with

q_s = the distributed weight: $\rho_s g D$ [N/m^2]

P = pull force

R = radius of circular part of top-layer

The rotation of the edge of the circular plate is restrained.

The model formulas follow from Poisson theory as presented by Timoshenko[291]. The load condition of the model can be considered as a sum of two load cases, a uniformly loaded plate supported at the edges and a similar plate loaded at the centre. Both cases are again a combination of two basic cases, the plate with simply supported edges, and the plate with a uniform edge moment M_2, resulting in an edge with zero rotation.

---

[291] S.P. Timoshenko and S. Woinowsky-Krieger, *Theory of plates and shells - second edition* (McGraw-Hill, 1959)

Figure B–1 Definition diagram circular plate model

For the cases where the circle R is small compared to the element size, the solutions in the centre of the plate must and can be improved. It is proposed to impose the central load P as a uniform load p on a small circular area with radius r, with $r < R$.

$$P = p\pi r^2$$ **Eq. B.2**

where

p = the pull force as a distributed load over the area of the central element [N/m²]

P = pull force

r = radius of pulled element

$$p = -q\frac{R^2}{r^2} \ [\text{N/m}^2]$$

The radial and tangential bending moments for the plate with clamped edges and uniform load q are:

$$M_r = \frac{qR^2}{16}\left((1+\upsilon) - \frac{x^2}{R^2}(3+\upsilon)\right)$$

$$M_t = \frac{qR^2}{16}\left((1+\upsilon) - \frac{x^2}{R^2}(1+3\upsilon)\right)$$ **Eq. B.3**

Figure B–2 Definition diagram parameters of circular plate model

The deflection at the centre of the plate is:

$$u = \frac{q(R^2 - x^2)^2}{64K}$$

$$u_c = \frac{qR^4}{64K} \qquad \text{Eq. B.4}$$

with

$$K = \frac{ED^3}{12(1 - v^2)}$$

The radial and tangential bending moments for a plate with clamped edges loaded with a central load P are:

$$M_r = \frac{P}{4\pi}\left((1+v)\ln\frac{R}{x} - 1\right) = -\frac{qR^2}{4}\left((1+v)\ln\frac{R}{x} - 1\right)$$

$$M_t = \frac{P}{4\pi}\left((1+v)\ln\frac{R}{x} - v\right) \qquad \text{Eq. B.5}$$

The deflection (at the centre) of the plate is:

$$u = \frac{PR^2}{8\pi K}\left((\tfrac{x}{R})^2\ln\frac{x}{R} + \tfrac{1}{2}(1-(\tfrac{x}{R})^2)\right) \text{ or } -\frac{qR^4}{8K}\left((\tfrac{x}{R})^2\ln\frac{x}{R} + \tfrac{1}{2}(1-(\tfrac{x}{R})^2)\right)$$

$$u_c = \frac{PR^2}{16\pi K} \text{ or } -\frac{qR^4}{16K} \qquad \text{Eq. B.6}$$

with

$$K = \frac{ED^3}{12(1 - v^2)}$$

The radial bending moments for the case with the load P replaced by the uniform load p are (expressed in P):

$$M_r = \frac{(1+v)P}{4\pi}\ln\frac{R}{x} + \frac{(1-v)\text{Pr}^2}{16\pi}\left(\frac{1}{x^2} - \frac{1}{R^2}\right) - P\frac{(2R^2 - r^2)}{8\pi R^2} \qquad \text{Eq. B.7}$$

The deflection of the plate in the area $x > r$ is:

$$u = \frac{qR^2}{16K}\left(\frac{3+v}{1+v}(x^2 - R^2) - 2x^2\ln\frac{x}{R} - r^2(\ln\frac{x}{R} - \frac{1-v}{2(1+v)}\frac{R^2 - x^2}{R^2})\right)$$

$$+ \frac{q(2R^2 - r^2)}{8}\frac{(R^2 - x^2)}{2K(1+v)} \qquad \text{Eq. B.8}$$

The sum of expressions Eq. B.3 and Eq. B.7 gives the solution for the model loaded by uniform loads p and q. The moments M_2 and M_1 are at the plate edge and at the radius r, respectively.

$$M_r = -\frac{(1+\nu)qR^2}{4}\ln\frac{R}{x} - \frac{(1-\nu)qr^2}{16}\left(\frac{R^2}{x^2}-1\right)$$

$$+ \frac{q(2R^2-r^2)}{8} + \frac{qR^2}{16}\left((1+\nu)-\frac{x^2}{R^2}(3+\nu)\right) \qquad \text{Eq. B.9}$$

$$M_2 = \frac{q(R^2-r^2)}{8}$$

$$M_1 = -\frac{(1+\nu)qR^2}{4}\ln\frac{R}{r} + \frac{(2+\nu)q(R^2-r^2)}{8}$$

The bending moment in the central area of the plate $(x < r)$ with load $p+q$ is:

$$M_r = \frac{p+q}{16}(3+\nu)(r^2-x^2) + M_1 \qquad \text{Eq. B.10}$$

The shear force V at the model edge is zero (by definition). The maximum shear force occurs at the radius $x = r$.

$$V_1 = \frac{q(R^2-r^2)}{2r} = q\frac{R}{2}\left(\frac{R}{r}-\frac{r}{R}\right) \; [\text{N/m}] \qquad \text{Eq. B.11}$$

Both the bending moment M_1 and the shear force V_1 in the joint around the central element increase with increasing R, or decreasing ratio r/R. The bending moment coefficient M_2/qR^2 at the plate edge tends to be constant.
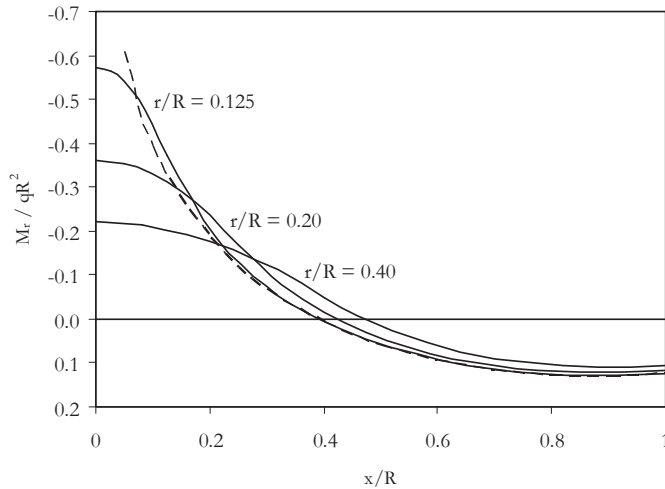
Figure B–3 **Dimensionless bending moment diagrams for pull tests with concentrated load P and with distributed loads p in circle with radius r (for various ratios r/R), scaled to R**
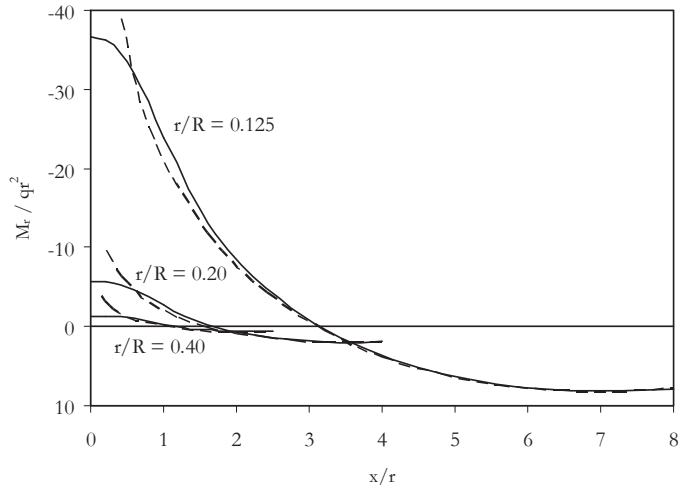
Figure B–4   Dimensionless bending moment diagrams for pull tests with concentrated load *P* and with distributed loads *p* in circle with radius *r* (for various ratios *r/R*), scaled to *r*

The deflection of the plate in the area $x > r$ is:

$$u = \frac{qR^2}{16K}\left(\frac{3+\upsilon}{1+\upsilon}(x^2-R^2)-2x^2\ln\frac{x}{R}-r^2(\ln\frac{x}{R}-\frac{1-\upsilon}{2(1+\upsilon)}\frac{R^2-x^2}{R^2})\right)$$

$$+\frac{q(2R^2-r^2)}{8}\frac{(R^2-x^2)}{2K(1+\upsilon)}+\frac{q}{64K}(R^2-x^2)^2$$

$$u = \frac{qR^4}{16K}\left(2(\frac{x}{R})^2+(\frac{r}{R})^2\right)\ln\frac{R}{x}-\frac{qR^4}{64K}\left(1-(\frac{x}{R})^2\right)\left(3+2(\frac{r}{R})^2+(\frac{x}{R})^2\right) \qquad \textbf{Eq. B.12}$$

The deflection at the circle $x = r$ is:

$$u_1 = \frac{3qR^4}{16K}(\frac{r}{R})^2\ln\frac{R}{r}-\frac{qR^4}{64K}(1-(\frac{r}{R})^2)(3+3(\frac{r}{R})^2) \qquad \textbf{Eq. B.13}$$
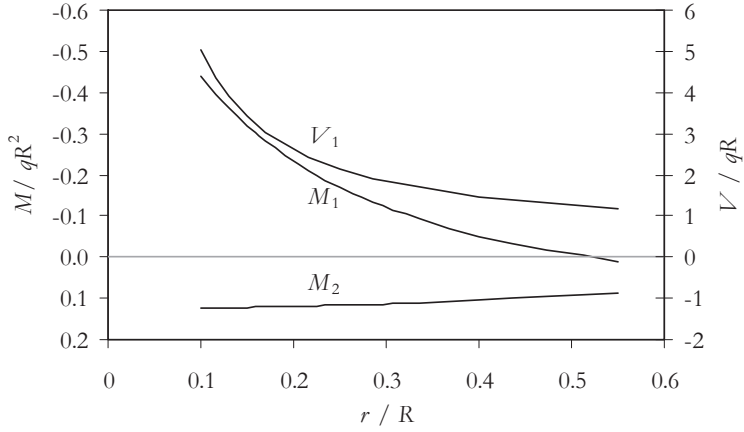
Figure B–5   Dimensionless bending moment at characteristic points as a function of r/R, point 1 for radius r and 2 for radius R, scaled to R
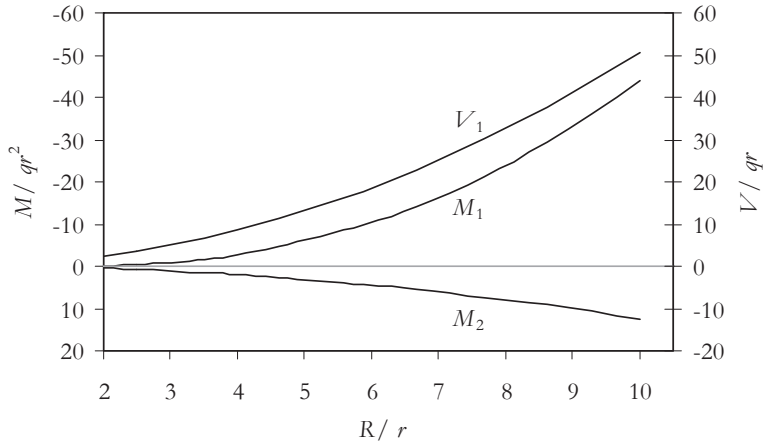
Figure B–6   Dimensionless bending moment at characteristic points as a function of r/R, location 1 for radius r and location 2 for radius R, scaled to r

The deflection of the plate in the central area $(x < r)$ is given as the sum of the solutions of a simply supported plate with radius r, e.g. for a uniform load $p+q$ for a constant edge moment M_1.

$$u = \frac{(p+q)(x^2 - r^2)}{64K}\left(\frac{5+\upsilon}{1+\upsilon}r^2 - x^2\right) + \frac{M_1}{K(1+\upsilon)}\frac{x^2 - r^2}{2} + u_1$$

$$u_c = \frac{qR^4}{16K}\left(\frac{r}{R}\right)^2 \ln\frac{R}{r} - \frac{3qR^4}{64K}\left(1 - \left(\frac{r}{R}\right)^2\right) \qquad \text{Eq. B.14}$$
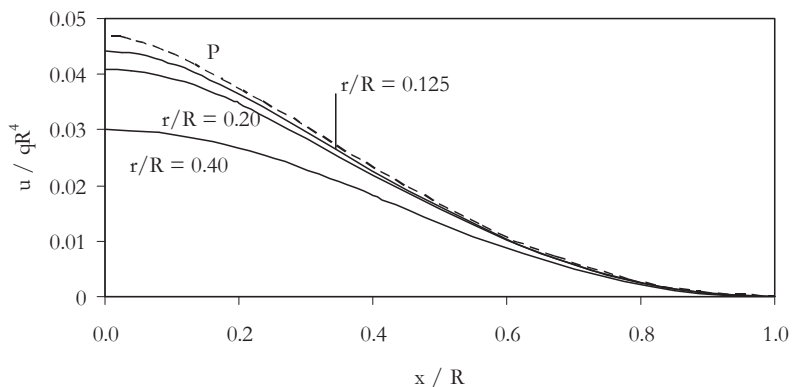
Figure B–7 Dimensionless deflection diagram for pull tests with concentrated load *P* and with distributed loads *p* in circle with radius *r* (for various ratios *r/R*), scaled to *R*
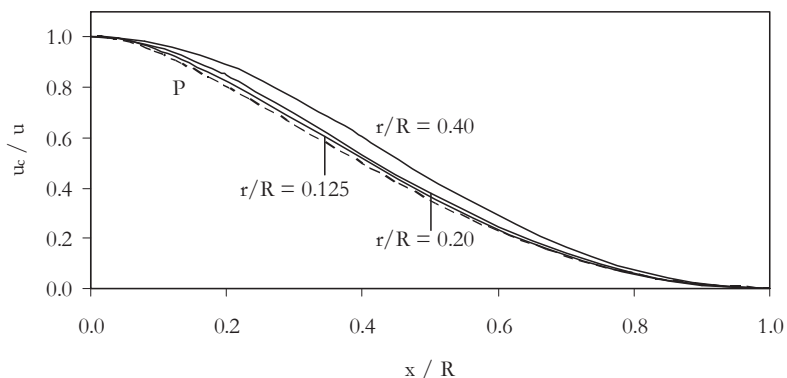
Figure B–8 Shape diagrams of the deflection for pull tests with concentrated load *P* and with distributed loads *p* in circle with radius *r* (for various ratios *r/R*)
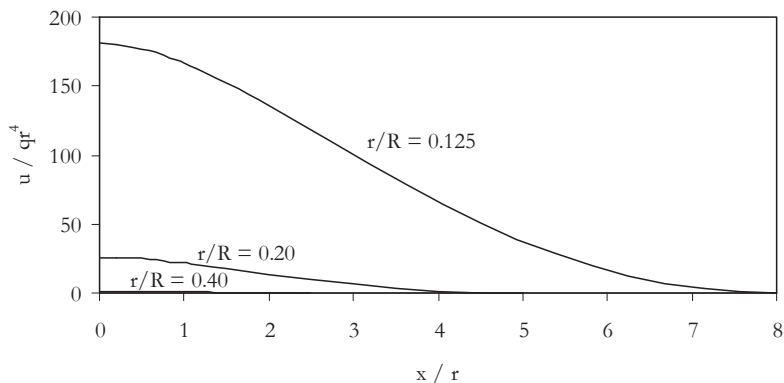
Figure B–9 Dimensionless deflection diagram for pull tests with concentrated load *P* and with distributed loads *p* in circle with radius *r* (for various ratios *r/R*), scaled to *r*

B.1.2 Segmented model application for pattern-placed revetments

The central area $x < r$ is in fact the pulled element. The boundary model of the model, the plate edge is at $x = R$. The model encompasses the total lifted area of πR^2. If we define πr^2 as one element, the number of lifted elements n_{LF} will be:

$$n_{LF} = \left(\frac{R}{r}\right)^2$$

Table B–1 **Load factor versus radius of plate model**

n_{LF}	10	20	50	100	150
r/R	0.32	0.22	0.14	0.10	0.082

During the pull tests the in-plane stress condition is influenced. The test results show remarkably high pull out forces. The corresponding vertical deformations are small, in most of the cases too small to cause horizontal drift of the elements outside the lifted area. Horizontal displacement of the elements outside the area could generate an increase of normal force due to friction between top-layer elements and the sub-layer. The observed high strength in the joint around the pulled stone can be explained by a subtle rearrangement of the elements within the model circle.

If the in-plane stress state of the plate is iso-static, the stress at all boundaries of an eliminated part will be equal. A small expansion of the central element in the model will cause stress relief on the radial boundaries. E.g. the tangential in-plane stresses are released and the radial stress in on the radius $x = r$ can increase with a factor R/r, without affecting the in-plane stress state outside the model.

If the initial in-plane stress state is defined in terms of the distributed normal force $N_0 = \sigma_0 D$ [N/m], than the distributed normal force in the joint at $x = r$ is:

$$N_r = \frac{R}{r} N_0 \qquad\qquad \textbf{Eq. B.15}$$
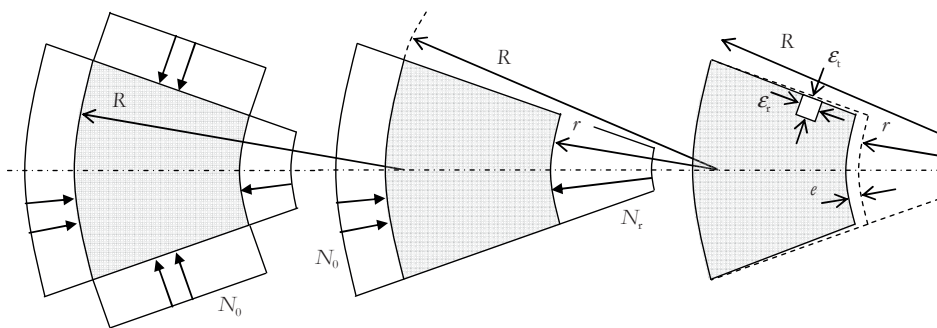
Figure B–10 **Definition diagram for initial and changed stress state of circle segment during pull test**

The elements move to the outer circle. The stress release on the radial boundaries is a consequence of the geometrical phenomenon of the increase of the inner circle radius r with a value e. The initial strain state is assumed constant and equal in all directions.

$$\varepsilon_0 = \frac{N_0}{ED} \ [\text{-}]$$

$$\varepsilon_r(x) = \frac{N_r}{ED} = \frac{R}{x}\varepsilon_0$$

The deviation from the original strain is:

$$\varepsilon_r(x) - \varepsilon_0 = \varepsilon_0\left(\frac{R}{x} - 1\right)$$

The radial shortening e of the circle portion $R - r$ can be calculated by means of integration of the strain over the radius.

$$e = -\varepsilon_0 \int_r^R \left(\frac{R}{x} - 1\right)dx = -\varepsilon_0 R\left(\ln\frac{R}{r} + \frac{r}{R} - 1\right)$$

The corresponding tangential strain is:

$$\varepsilon_t = -\frac{e}{r} = \varepsilon_0 \frac{R}{r}\left(\ln\frac{R}{r} + \frac{r}{R} - 1\right) \qquad \text{Eq. B.16}$$

Apart from that, increase of (negative) radial strain $\varepsilon_r - \varepsilon_0$ generates a positive tangential strain increase ε_t, where $\varepsilon_t = -\nu\,\varepsilon_r$. At the position $x = r$ this strain is:

$$\varepsilon_t = -\nu(\varepsilon_r - \varepsilon_0) = -\nu\varepsilon_0\left(\frac{R}{r} - 1\right) \qquad \text{Eq. B.17}$$

The sum of the geometrical and elastic strain components (Eq. B.16 and Eq. B.17) is:

$$\varepsilon_t = \varepsilon_0\left(\frac{R}{r}\ln\frac{R}{r} - (1+\nu)(\frac{R}{r} - 1)\right)$$

The geometrical effect appears dominant over the elastic Poisson effect. During the pull test this strain is imposed on the initial strain state ε_0.

$$\varepsilon_t - \varepsilon_0 = \varepsilon_0\left(\frac{R}{r}\ln\frac{R}{r} - (1+\nu)(\frac{R}{r} - 1) - 1\right) \qquad \text{Eq. B.18}$$

Evaluation of Eq. B.18 leads to numerical values shown in Table B–2. It can be seen that for load factor below 10 the initial, pressured strain state remains. For load factors above 10 the assumed redistribution of forces leads to 'tension' in the radial joints. Tension in the joints is not possible. Tensile strains will show as gaping in the joints.

If for example the normal force N_0 is equal to $\rho g D z$ [N/m], with z = a given length of revetment structure, that represents the weight component of the revetment that causes the normal force. Than the normal stress $\sigma_0 = N_0/D = \rho g z$ [N/m²]. The strain $\varepsilon_0 = \sigma_0/E_a = \rho g z /E_a$ [-]. Assume $\rho = 2300$ kg/m³, $g = 10$ m/s², $z = 2.0$ m, and $E_a = 100\times10^6$ N/m². Than ε_0

= 2300 × 10 × 2 / 100×10^6 = 450×10^{-6} [-]. In case of a pull test with a capacity of n_{LF} = 44, the tangential strain in the joints is 4.56 ε_0 = 1.9×10^{-3}. For an average concrete column revetment r = 0.13 m. The element perimeter is $2\pi r$ = 0.82 m. In case of six radial joints the gaping of the joints is 1.9×10^{-3} × 0.82 / 6 = 0.28×10^{-3} m = 0.28 mm. This gaping is in the order of magnitude of a crack in reinforced concrete.

Table B–2   **Numerical values of tangential strain in the radial joints around the pulled stone**

$\dfrac{r}{R}$	0.1	0.15	0.20	0.31	0.4
$\dfrac{N_r}{N_0} = \dfrac{R}{r}$	10	6.7	5.0	3.2	2.5
$n_{LF} = (\dfrac{R}{r})^2$	100	44	25	10	6
Tangential strain $\dfrac{\varepsilon_t - \varepsilon_0}{\varepsilon_0}$ *)	10.8	4.56	2.05	0.000	-0.584

*) for υ = 0.25

From this we can conclude that in case the pulled element is initially firmly fixed in position between the neighbours and is embedded in an iso-static state of compression, a mechanism of internal rearrangement of positions and redistribution of compressive forces will develop. The circle will increase, the ratio r/R decreases, and as a consequence a gradually increasing normal force can develop around the pulled element.

As can be seen in Table B–2 the tangential strain is negative below n_{LF} = 10. Below this value the relief strain does not compensate the initial uniform strain ε_0. For the range 1 < n_{LF} < 10 an elastic relation determines the increase of N_r. The joint material may play a role in the initial phase.
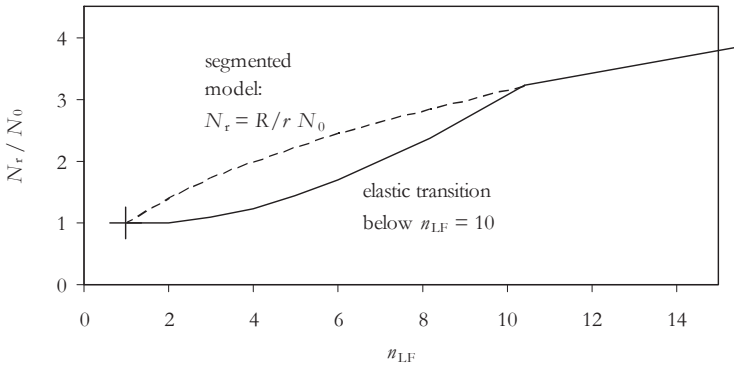
Figure B–11   **Normal force N_r around pulled element as a function of the load factor**

The normal force is the big unknown factor in the analysis of pull tests. Close to the centre of the plate model big normal forces occur that actually make the concentrated pull test physically possible. These concentrated enlarged normal forces are initially not there, and will also not be there in a 2-D load situation in wave attack.

For back-analysis of the normal force from the pull tests using the plate models the friction coefficient is a major unknown factor. In laboratory conditions the concrete-concrete friction coefficient f_r was measured 0.60. For new elements with sharp edges higher values measured. Higher values may be possible in practice also, e.g. when the elements are pulled eccentrically and the element derives grip from single contact points. For the model calculations a combination of the parameters f_r and N_0 as one factor $f_r N_0$ is preferred.
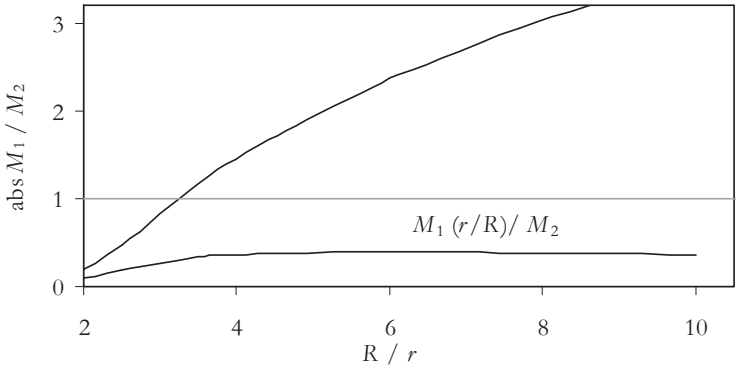
Figure B–12 Ratio of bending moments at location 1 with radius *r* and location 2 with radius *R*, with and without correction with factor *r/R* for increased normal force capacity in 1

From Figure B–12 it can be concluded that, given the redistributed normal force, M_2 is more critical than M_1. In the figures below the conditions whether V_1 or M_2 is the critical parameter are shown. For higher values of the load factor n_{LF} the bending moment M_2 requires a higher normal force than the shear force V_1. Depending on how high the columns are, in the range below 50, or below 25 or 10, V_1 is the determining parameter. In the area below $n_{LF} = 10$ the development of a higher normal force is insecure, where as a result the required 'neutral' normal force is higher (see Figure B–14).
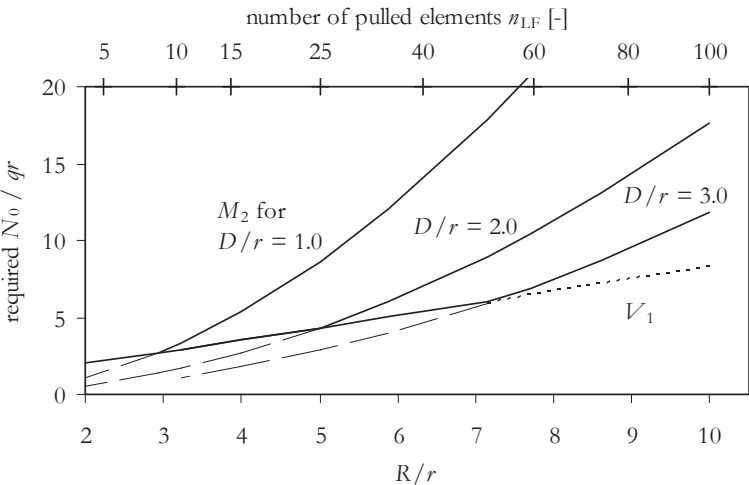
Figure B–13 Dimensionless normal force N_0 required to prevent failure on capacity for internal forces V_1 and M_2 ($f_r = 0.6$)
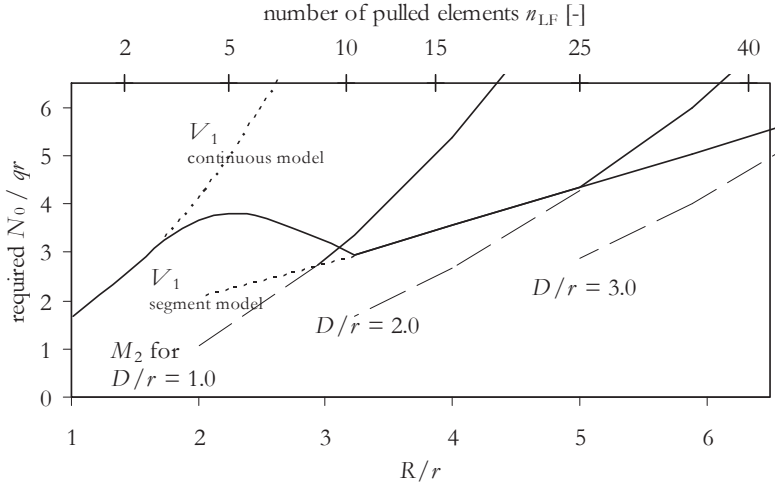
Figure B–14   **Dimensionless normal force N_0 required to prevent failure on capacity for internal forces V_1 and M_2, focus on smaller pull test forces ($f_r = 0.6$)**

Knowing that for loads above $n_{LF} = 10$ the outer part of the model will be physically split into circle segments the plate action in the model need to be revisited. The segmented model behaviour is caused by the axial stress state, and will influence the bending moment distribution. In fact for $r/R > 1/\sqrt{10} = 0.32$ tangential bending moments cannot occur in the area $r < x < R$.

For that reason the circular plate is divided into a number of tapered beam sections with constant depth and variable width. The beam sections transfer forces and moments along the beam axis to the outer boundary $x = R$. Evaluating elastic beam formulas for these tapered sections leads to results for the characteristic sections, which can be compared to the results of the Timoshenko formulas.

Formulas for tapered beam section, where the beam width $B_\theta(x) = x\theta$, with θ is assumed 1.

$$q \ [\text{N/m}^2]$$

$$q(x) = qx \ [\text{N/m}]$$

$$V(x) = -\int q(x)dx = -\tfrac{1}{2}qx^2 + c_1$$

With boundary condition $V = 0$ for $x = R$, it follows that:

$$V(x) = \tfrac{1}{2}q(R^2 - x^2) \ [\text{N}]$$

$$\frac{V(x)}{B_\theta(x)} = \tfrac{1}{2}qR\left(\frac{R}{x} - \frac{x}{R}\right) \ [\text{N/m}]$$

$$M(x) = \int V(x)dx = -\tfrac{1}{6}qx^3 + \tfrac{1}{2}qR^2x + c_2$$

$$EI(x) = EI = E\tfrac{1}{12}B_\theta(x)D^3 = Kx \ [\text{Nm}^2] \text{ with } K = E\tfrac{1}{12}D^3 \ [\text{Nm}]$$

With boundary condition $\int\limits_{r}^{R}\dfrac{M(x)}{EI(x)}dx=0$ it follows that $c_2=\dfrac{q(8R^3+r^3-9R^2r)}{18\ln\dfrac{r}{R}}$.

$$M(x)=-\tfrac{1}{6}q(x^3+3R^2x)+\tfrac{1}{18}q(8R^3+r^3-9R^2r)\dfrac{1}{\ln(r/R)}\quad[\text{Nm}]$$

$$\dfrac{M(x)}{B_\theta(x)}=\tfrac{1}{6}q(3R^2-x^2)+\tfrac{1}{18}qR^2\left(\dfrac{r}{x}\right)\left(8\dfrac{R}{r}+(\dfrac{r}{R})^2-9\right)\dfrac{1}{\ln(r/R)}\quad[\text{N}]$$

$$M_1=\tfrac{1}{6}q(3R^2-r^2)+\tfrac{1}{18}qR^2\left(8\dfrac{R}{r}+(\dfrac{r}{R})^2-9\right)\dfrac{1}{\ln(r/R)}\quad[\text{N}] \qquad \textbf{Eq. B.19}$$

$$M_2=\tfrac{1}{3}qR^2+\tfrac{1}{18}qR^2\left(8+(\dfrac{r}{R})^3-9\dfrac{r}{R}\right)\dfrac{1}{\ln(r/R)}\quad[\text{N}] \qquad \textbf{Eq. B.20}$$

$$\varphi(x)=\int\dfrac{M(x)}{EI(x)}dx$$

$$u(x)=-\int\varphi(x)dx$$

With boundary conditions $\varphi=0$ and $u=0$ for $x=R$ it follows that:

$$u_1=\quad\dfrac{q}{72K}(15R^4-18R^2r^2+3r^4)$$
$$+\dfrac{q}{72K}(32R^4-68R^3r+36R^2r^2+4Rr^3-4r^4)\dfrac{1}{\ln(r/R)}\quad[\text{m}] \qquad \textbf{Eq. B.21}$$

These formulas are for clamped boundaries at $x=r$ and at $x=R$. In reality, the boundary at $x=r$ is not fully clamped. The finite stiffness of the plate portion $x<r$ releases the bending moment M_1.

In the formulas below this extra constant (positive) bending moment M_e is considered as a separate load case on the outer part of the beam segment.

$$M(x)=M_e$$

$$\dfrac{M(x)}{B_\theta(x)}=\dfrac{M_e}{x}$$

$$M_1=\dfrac{M_e}{r}$$

$$M_2=\dfrac{M_e}{R}$$

$$\varphi(x)=\int\dfrac{M(x)}{EI(x)}dx$$

$$\varphi(x)=\int\dfrac{M_e}{Kx}dx=\dfrac{M_e}{K}\int\dfrac{1}{x}dx=\dfrac{M_e}{K}\ln x+c_5$$

with $\varphi = 0$ for $x = R$ follows:

$$\varphi(x) = -\frac{M_e}{K}\ln\frac{R}{x}$$

$$\varphi_1 = -\frac{M_e}{K}\ln\frac{R}{r}$$

$$u(x) = -\int \varphi(x)dx = \frac{M_e}{K}\int \ln\frac{R}{x}dx = \frac{M_e}{K}x(1+\ln\frac{R}{x})+c_6$$

with $u = 0$ for $x = R$ follows:

$$u(x) = \frac{M_e}{K}(x(1+\ln\frac{R}{x})-R)$$

$$u_1 = \frac{M_e}{K}(r-R+r\ln\frac{R}{r})$$

The flexibility of the inner part of the plate $(x < r)$ is characterised with the relation between the edge moment M_1 and the slope of the edge at $x = r$. The simply supported plate with a uniform load $p+q$ has a slope:

$$\varphi_1 = \frac{(p+q)r^3}{8K_v(1+v)} \text{ with } K_v = \frac{E\frac{1}{12}D^3}{(1-v^2)} = \frac{K}{(1-v^2)}$$

Eq. B.22

The defection in the centre of the plate is:

$$u_c = \frac{(p+q)r^4(5+v)}{64K_v(1+v)}$$

Eq. B.23

The simply supported plate with an edge moment M_1 has a slope:

$$\varphi_1 = \frac{M_1r}{K_v(1+v)}$$

Eq. B.24

$$u_c = \frac{M_1r^2}{2K_v(1+v)}$$

Eq. B.25

We define the case of M_1 in fixed position as M_{1f}. Than it follows that $M_1 = M_{1f} + M_{1e}$, with $M_{1e} = M_c/r$. The slopes produces by these moments will be equal. So we can define the equation:

$$\frac{(p+q)r^3}{8K_v(1+v)} + \frac{M_1r}{K_v(1+v)} = -\frac{M_{1e}r}{K}\ln\frac{R}{r}$$

Eq. B.26

We define the following stiffness factors for the inside and outside parts of the plate:

$$c_i = \frac{r}{K_v(1+v)}$$

$$c_o = \frac{r}{K}\ln\frac{R}{r}$$

Eq. B.26 can be rewritten as:

$$(\tfrac{1}{8}(p+q)r^2 + M_{1f} + M_{1e})c_i = -M_{1e}c_o$$

$$M_{1e} = -\left(\tfrac{1}{8}(p+q)r^2 + M_{1f}\right)\frac{c_i}{c_i + c_o}$$

$$M_{1e} = \tfrac{1}{24}q(15R^2 - 7r^2)\frac{c_i}{c_i + c_o} + \tfrac{1}{18}qR^2\left(8\frac{R}{r} + (\frac{r}{R})^2 - 9\right)\frac{1}{\ln(r/R)}\left(\frac{c_i}{c_i + c_o}\right) \quad \textbf{Eq. B.27}$$

or as:

$$(\tfrac{1}{8}(p+q)r^2 + M_1)c_i = (M_{1f} - M_1)c_o$$

$$M_1 = -\tfrac{1}{8}(p+q)r^2\frac{c_i}{c_i + c_o} + M_{1f}\frac{c_o}{c_i + c_o}$$

$$M_1 = \quad \tfrac{1}{8}q(R^2 - r^2)\frac{c_i}{c_i + c_o} + \tfrac{1}{6}q(3R^2 - r^2)\frac{c_o}{c_i + c_o}$$

$$+ \tfrac{1}{18}qR^2\left(8\frac{R}{r} + (\frac{r}{R})^2 - 9\right)\frac{1}{\ln(r/R)}\left(\frac{c_o}{c_i + c_o}\right)$$

Eq. B.28

For the edge moment M_2 it follows:

$$M_2 = M_{2f} + \frac{r}{R}M_{1e}$$

$$M_2 = \quad \tfrac{1}{3}qR^2 - \tfrac{1}{24}q(9R^2 - r^2)\frac{r}{R}\frac{c_i}{c_i + c_o}$$

$$+ \tfrac{1}{18}R^2\left(8 + (\frac{r}{R})^3 - 9\frac{r}{R}\right)\frac{1}{\ln(r/R)}\left(1 - \frac{c_i}{c_i + c_o}\right)$$

Eq. B.29

Both the radial moments M_1 and M_2 increase compared to the results for the continuous model. This is due to the missing contribution of the tangential bending moments.

The deflection u_c in the centre of the plate can be written as the sum of the contribution u_1 and the local deflection of the central part of the plate.

$$u_c = \quad \frac{q}{72K}(15R^4 - 18R^2r^2 + 3r^4)$$

$$+ \frac{q}{72K}(32R^4 - 68R^3r + 36R^2r^2 + 4Rr^3 - 4r^4)\frac{1}{\ln(r/R)}$$

$$+ \frac{q}{24K}(15R^2 - 7r^2)(r^2 - Rr - r^2\ln\frac{r}{R})\frac{c_i}{c_i + c_o}$$

$$+ \frac{q}{18K}R^2(r^2 - Rr - r^2\ln\frac{r}{R})\left(8\frac{R}{r} + (\frac{r}{R})^2 - 9\right)\frac{1}{\ln(r/R)}\left(\frac{c_i}{c_i + c_o}\right)$$

$$+\frac{q(r^2-R^2)r^2(5+\upsilon)(1-\upsilon^2)}{64K(1+\upsilon)}$$

$$+\frac{q(R^2-r^2)r^2(1+\upsilon^2)}{16K(1+\upsilon)}\frac{c_i}{c_i+c_o}+\frac{q(3R^2-r^2)r^2(1+\upsilon^2)}{12K(1+\upsilon)}\frac{c_o}{c_i+c_o}$$

$$+\frac{qR^2r^2(1+\upsilon^2)}{36K(1+\upsilon)}\left(8\frac{R}{r}+(\frac{r}{R})^2-9\right)\frac{1}{\ln(r/R)}\left(\frac{c_o}{c_i+c_o}\right)$$

The exercise leads to an improved model, with significantly bigger edge moments and deflections. The formulas are more complicated. A simplification can be obtained if we consider that M_2 shows more or less constant values when plotted as M_2/qR^2 (see Figure B–15). In the range $r/R = 0.125$ to 0.25 (or $n_{LF} = 16$ to 64) the moment coefficient varies from 0.15 to 0.19. A rough, conservative estimate for M_2 would be $0.20\, qR^2$. A more realistic estimation in the closer range of $n_{LF} = 40$ to 60 is: $0.185\, qR^2$.

An accurate estimate is given as:

$$M_2 = 0.20qR^2(1.13-1.57\frac{r}{R})$$

<div align="right">Eq. B.30</div>

In terms of revetment parameters this expression can be given as:

$$M_2 = 0.20\rho gDr^2\left(\frac{R}{r}\right)^2(1.13-1.57\frac{r}{R}) = 0.20\rho gD\frac{1}{\pi}B_x B_y n_{LF}(1.13-\frac{1.57}{\sqrt{n_{LF}}})$$

$$= 0.064\rho gDB_x B_y n_{LF}(1.13-\frac{1.57}{\sqrt{n_{LF}}})$$

<div align="right">Eq. B.31</div>

For determination of N_0 the value of M_2 can be divided by $0.70\ \frac{1}{2}D$:

$$N_0 = 0.018\rho gB_x B_y n_{LF}(1.13-\frac{1.57}{\sqrt{n_{LF}}})$$

<div align="right">Eq. B.32</div>

For the deflection an acceptable estimation can be obtained with a quadratic function:

$$u_c = \frac{qr^4}{16K}\left(\frac{R}{r}\right)^4$$

<div align="right">Eq. B.33</div>

This expression can be rewritten as:

$$u_c = \frac{1}{16\pi^2}\frac{\rho gD}{E\frac{1}{12}D^3}\left(B_x B_y\right)^2\left(n_{LF}\right)^2$$

$$\frac{u_c}{D} = \frac{3}{4\pi^2}\frac{\rho gD}{E}\frac{\left(B_x B_y\right)^2}{D^4}\left(n_{LF}\right)^2$$

<div align="right">Eq. B.34</div>

The segmented plate model gives increased bending moments and deflections, which was expected since the tangential load path was omitted. The shear force results V_1 are the same. Above $n_{LF} = 10$ the segmented model is considered as a better representation of reality. These model formulas are being used in annex D and G for evaluating the pull test results.
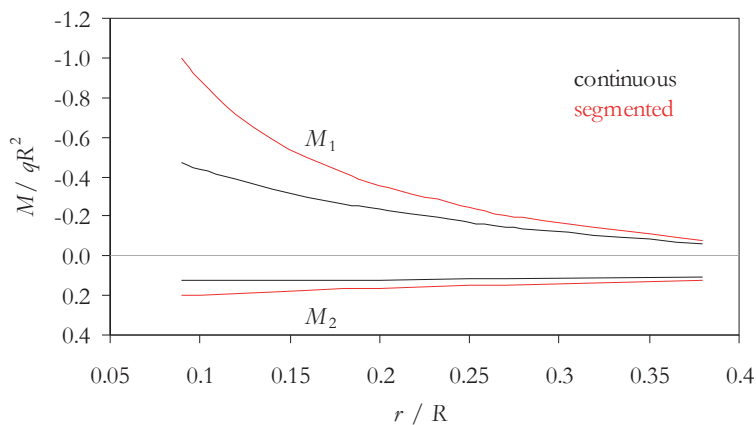
Figure B–15 Bending moment results of segmented plate model
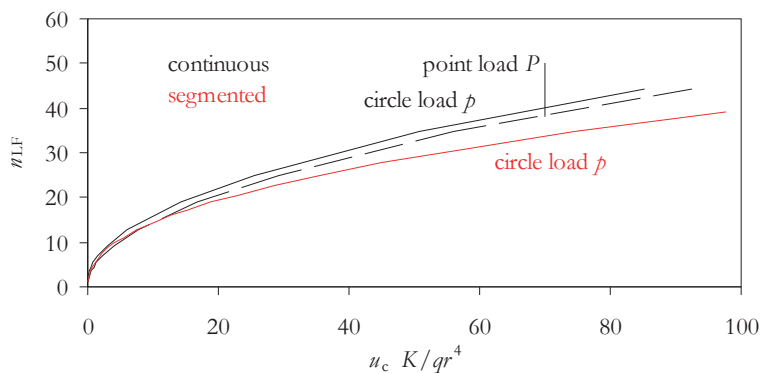
Figure B–16 Elastic displacement results for different plate model calculations
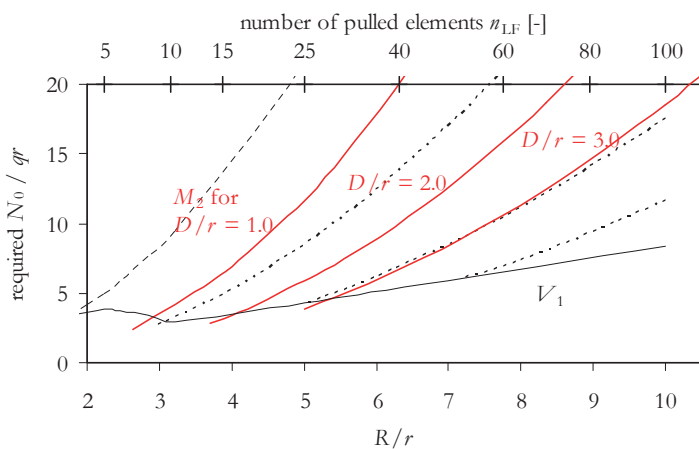
Figure B–17 Dimensionless normal force N_0 required to prevent failure on internal forces V_1 and M_2, with results of segmented plate model ($f_r = 0.6$)

DESIGN OF PATTERN-PLACED REVETMENTS – ANNEXES

B.2 Two-beam model for single element loads

For the reasons of ease of understanding and transfer of the 2-D model to a 1-D loading situation a 2-D beam model with two crossing beams is introduced for the single element tests. The model is assumed symmetric in two axes.
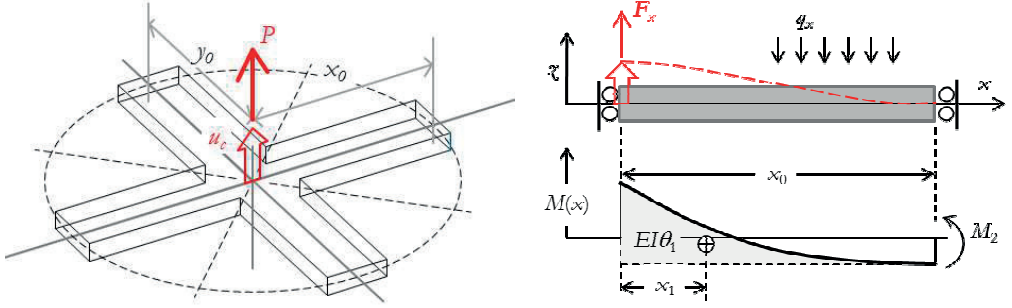
Figure B–18   Two-beam model for single element loads

The beam constraints are rotational constraints. The beam can elongate freely. The definition of the model edge is at the point of zero shear force. So, the complete weight of the model is balanced by the pull force.

In case of a free rotating beam edge, the bending moment $M_0(x)$ can be written as:

$$M_0(x) = \tfrac{1}{2} q_x (x_0 - x)^2 \qquad\qquad \textbf{Eq. B.35}$$

Due to the clamped edge this moment is reduced with a moment M_2.

$$M(x) = M_0(x) - M_2$$

The sum of the rotations θ_1 and θ_2 caused by M_0 and M_2 must be zero. In case of assumed linear elastic behaviour the effects of deformations can be super imposed. It can be found that:

$$\theta_1 = \frac{\tfrac{1}{3} M_0 x_0}{EI}, \; x_1 = \tfrac{1}{4} x_0, \; \theta_2 = -\frac{M_2 x_0}{EI}, \; x_2 = \tfrac{1}{2} x_0$$

$$M_2 = \tfrac{1}{3} M_0 = \tfrac{1}{6} q_x x_0^2$$

For the central moment M_1 follows:

$$M_1 = \tfrac{2}{3} M_0 = \tfrac{1}{3} q_x x_0^2$$

The central displacement u_c is

$$u_c = \theta_1 \left(\tfrac{1}{2} x_0 - \tfrac{1}{4} x_0 \right) = \tfrac{1}{12} \frac{M_0 x_0^2}{EI} = \tfrac{1}{24} \frac{q x_0^4}{EI} = \tfrac{1}{24} \frac{F_x x_0^3}{EI} \qquad\qquad \textbf{Eq. B.36}$$

The beam portion in Figure B–18 represents a quarter of an imaginary circular lifted area. Substitution of the pull test parameters for load and geometry and assuming an effective width of ½ x_0 we achieve a relation for u_c similar to Eq. B.34.

$$F_x = n_{LF\frac{1}{4}}\rho g D B_x B_y, \quad x_0^{\;2} = n_{LF\frac{1}{4}}B_x B_y, \quad I = \tfrac{1}{12}(\tfrac{1}{2}x_0)D^3$$

$$\frac{u_c}{D} = \tfrac{1}{\pi}\frac{\rho g D}{E}\frac{(B_x B_y)^2}{D^4}n_{LF\frac{1}{4}}^{\;2} \qquad\qquad \text{Eq. B.37}$$

$$\frac{u_c}{D} = \tfrac{1}{4\pi}\frac{\rho g D}{E}\frac{(B_x B_y)^2}{D^4}n_{LF}^{\;2} \qquad\qquad \text{Eq. B.38}$$

It appears that assuming an effective width of ½ x_0 for the flexural stiffness of the beam, the expression for the system stiffness u_c/D of the two-beam model perfectly matches with the plate model (Eq. B.34) with coefficients $1/4\pi$ and $3/4\pi^2$ respectively.

Rewriting the expression for the edge moment gives:

$$m_2 = \frac{M_2}{c\,x_0} = -\frac{1}{c}\tfrac{1}{6}q x_0 = -\frac{1}{c}\tfrac{1}{24}\rho g D B_x B_y n_{LF} \;\; \text{[Nm/m]} \qquad\qquad \text{Eq. B.39}$$

with c = factor for definition of effective width for M_2

For the edge moment an effective width value of 0.6–0.7 (of y_0) should be adopted in order to obtain results similar to the circular plate model.

These results provide a double check of the complicated formulas of section Annex B.1, and are also helpful in developing a model for evaluation of the field tests in Annex D.

B.3   Effect of longitudinal normal force N_y in case of element overlap

The effect of overlap in B_x is shown in Figure B–19. The transfer of a bending moment M_x in transverse direction relies as a primary mechanism on the occurrence of N_x and on eccentric compressive contact forces in the x-joints.

No overlap in B_x. The x-joints are aligned, which causes that a bending moment M_x is controlled by the normal force N_x only. This pattern is typical for Hydroblocks and Haringman blocks.

Overlap in B_x. Rotation in x-joints will be spread over a larger area. Friction in the y-joints can also contribute to the equilibrium. Although their pattern is different this effect plays a role for regular columns C-star, Ronaton, and irregular Basalton and Basalt.

Figure B–19   Effect of overlap in element position in *x*-direction

When the elements have overlaps in x-direction and the x-joints are interrupted and have scattered positions, the x-curvature is more smoothly distributed over the joints. Moreover, the y-joints will experience friction when the block will rotate. The friction forces in the y-joints (forces F_{yx} in Figure B–20) can theoretically transfer the bending moment M_x without a normal force N_x present.
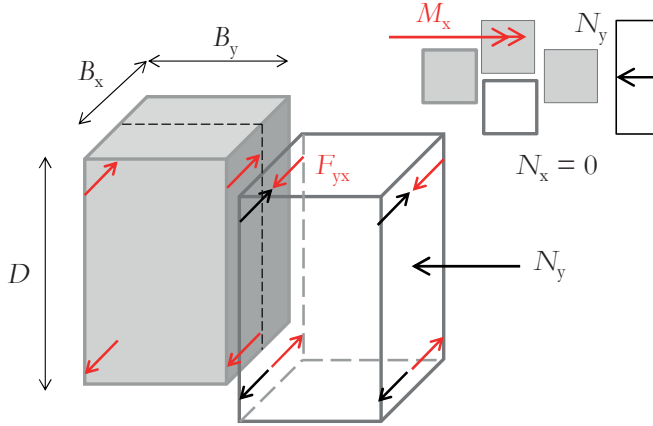
Figure B–20   **Mechanism of friction in the y-joints**

The distributed moment m_x corresponds to a moment $M_x = m_x \, \tfrac{1}{2}B_y$. This moment can be resisted with the forces F_{yx} times the lever arm $0.8\ D$. The normal force N_y on one element corresponds to $n_y B_x$. This force N_y generates four discrete friction forces F_{yx}.

$$f_{fr}N_y = 4F_{yx}$$

$$M_x = F_{yx}\,0.8D$$

Substitution leads to:

$$m_x = 0.1 f_{fr} n_y D$$

The contribution of n_x is typically:

$$m_x = n_x\,0.4D$$

With $f_{fr} = 0.6$, the contribution of n_y is roughly 15% of the contribution of n_x. The ratio of n_y and n_x is subject to large variation. See Annex F. The normal force in y-direction can be larger than the normal force in x-direction, which increases the percentage of 15% to e.g. 20% or 30%. Although n_x will remain the dominant component of the resistance, especially where n_x is low, e.g. at the top edge of the revetment or just below transition structures, the contribution of n_y might become significant.

DESIGN OF PATTERN-PLACED REVETMENTS – ANNEXES

ANNEX C AVAILABLE PULL-OUT TESTS IN LITERATURE

In the past testing of the stability of prototype structures was done with pull tests, exerting concentrated loads on the revetment structure. In some occasions this has been done in conjunction with model testing and simulation of the hydraulic load. The revetment research of the 1990s has resulted in a large amount of field pull-test on prototype structures. Numerous tests were done in order to enhance understanding of the stability and to assess the condition of revetment slopes in reality. However in the beginning those experiments were executed while a model to relate the pull tests to the behaviour under wave attack was lacking.

In this annex the available historical pull tests are collected. The collection that can be found in literature and the typical test results are described in sections C.1 and C.2. The observed failure mechanisms can be distinguished between so-called single element failure and mechanisms where the pulled element mobilises the weight of neighbouring elements. Section C.3 describes how the tests have been evaluated in literature.

A new evaluation method with the aid of a theoretical model is presented in annex D. The new method delivers results that can be linked to the resistance of revetment against its real loads. In section D.4 the findings are summarised.

C.1 Available experimental data

Pull-out tests on pattern-placed revetments have been performed since 1970. The purpose of the tests was to test or prove the resistance of the revetment. Due to observed single element failure during storm conditions, it was assumed that pull tests on single elements are a representative test method for revetment stability. The pull tests showed large scatter in the results. Later test series therefore encompass big numbers of tests.

A limited number of field tests has been carried out before 1990 (see Table C–1). After 1990 an extensive test program has been carried out by the central government organisation Rijkswaterstaat DWW. In the program a standardised method was used. The programme finally included a total of 10,000 pull-out tests (see Table C–2).

Other available reports of field test surveys are a report on testing of new steep riverbank slopes in the Alblasserwaard on Hydroblocks and Basalton by Stigters and Klein Breteler (1999) and a report on testing of asphalt-jointed Basalt at Kruiningen by Kuiper (2001). In 2008 a test series has been performed on the Oesterdam.

Pull tests in laboratory conditions are presented by Wevers (small scale tests), Visser & Van der Weijde (Deltaflume) and more recent by Gier and others (large wave flume, Hannover).

The laboratory and field tests published in the MSc-thesis reports of Schoen (2004) and Blom (2007) are part of the research program of this thesis and are discussed in annex E and F.

Table C–1   Summary of pull test series in literature

	Date of testing	Location	Literature reference
a)	1970	Roggenplaat, Neetje Jans	G.S. Mulder, *Trekken van betontegels uit het talud van een dijk* (RWS Deltadienst ONW report 1.0.29, 1970)
b)	1983	Deltaflume	P.J. Visser and J. van der Weijde, *Basalton - Stability under attack by waves - Report of large scale model investigation in the Delta flume*, 1983
c)	1984	Oosterschelde	H.J. Verhagen, *Trekproeven op glooiingsconstructies in de Oosterschelde* (RWS report Adviesdienst Vlissingen WWKZ-84.V002, 1984)
d)	1999	Alblasserwaard	K. Stigters and M. Klein Breteler, *Trekproeven op dijkbekledingen van de Alblasserwaard* (WL|Delft Hydraulics report H3009, 1999)
e)	2001	Kruiningen	C. Kuiper, *Verplaatsingsmetingen tijdens trekproeven op ingegoten basalt* (WL|Delft Hydraulics report H3990, 2001)
f)	2008	Oesterdam	V.P.C. Schuurmans, *Trekproeven aan koperslakblokken aan de Oesterdam,* Fugro, 2008
g)	2012	Wave flume Hannover	F. Gier et al., "Stability of interlocked pattern placed block revetments," *ICCE* (Santander, 2012)

Table C–2   Summary of pull test campaigns DWW 1990's

Campaign nr. *	Date of testing	Location	Literature reference
01	April – July 1990	Oosterschelde Colijnsplaat	A. Plooster, *Tussentijdse rapportage eerste meetcampagne natuurmetingen op meetlocatie Noord-Beveland* (DWW report, 1990) R. Zandwijk and E.F.M. Nieuwenhuis, *Natuurmetingen op meetlocatie Colijnsplaat* (Fugro report N-0099, 1995)
02	November 1990	Oosterschelde Colijnsplaat	Ibid.
03	April – June 1991	Afsluitdijk	M. Pehlig and M.T.J.H. Smits, *Natuurmetingen op de afsluitdijk ten behoeve van steenzetonderzoek* (Fugro report M-0073, 1991)
04	October 1991 – January 1992	Westerschelde Breskens	M. Pehlig and M.T.J.H. Smits, *Natuurmetingen op de zeedijk nabij Breskens ten behoeve van steenzetonderzoek* (Fugro report M-0073, 1992)
05	December 1992 – November 1993	Nieuwe waterweg Maassluis	E.F.M. Nieuwenhuis, *Natuurmetingen aan Basaltonzuilen aan de Nieuwe waterweg te Maassluis ten behoeve van Steenzetonderzoek* (Fugro report M-0103, 1994)
06	March – April 1993	Nieuwe waterweg Maassluis	E.F.M. Nieuwenhuis, *Natuurmetingen aan Pit-polygoonzuilen aan de Nieuwe waterweg te Maassluis ten behoeve van Steenzetonderzoek* (Fugro report M-0111, 1993)
07	November – december 1994	Oosterschelde Colijnsplaat	Zandwijk and Nieuwenhuis, *Natuurmetingen op meetlocatie Colijnsplaat*
08	April 1996	Oesterdam	R. Zandwijk and E.F.M. Nieuwenhuis, *Natuurmetingen op meetlocatie Oesterdam* (Fugro

Campaign nr. *	Date of testing	Location	Literature reference
			report N-0300, 1996)
09	Spring 1997	Westerschelde West of Terneuzen	P.W. Kolff and E.F.M. Nieuwenhuis, *Natuurmetingen op zeedijken bewesten Terneuzen* (Fugro report N-0405, 1997)
10	Spring 1998	Walsoorden	G. Bos, J.W.R. Heusinkveld, and M.L. Post, *Trekproeven zeedijken Walsoorden* (Fugro report N-0550, 1998)
11	Spring 1999	Oesterdam	O.P.M. Mooijman and M.L. Post, *Trekproeven Oesterdam* (Fugro report N-0689, 1999)
12	Spring 1999	Mosselbanken and Kruiningen	O.P.M. Mooijman and M.L. Post, *Trekproeven en doorlatendheidsmetingen op de meetlocaties Mosselbanken en Kruiningen* (Fugro report N-0703, 1999)
13	Spring 1999	Paviljoenpolder	O.P.M. Mooijman and M.L. Post, *Trekproeven op meetlocatie Paviljoenpolder* (Fugro report N-0719, 1999)
14	June-August 1999 August-Sept 1999 January 2000 Jan-Feb 2000	Slachte Stenen Man Wierum Laauwersoog	(*Trekproeven diverse dijkvakken Friesland*, 2001)
15	Autumn 1999	Zuidoever Westerschelde	*Trekproeven langs diverse dijkvakken langs Westerschelde* (Consulmij report V.99.0487.AvG, 1999)
16	September 1999	Braakmanhaven Westerschelde	*Trekproeven dijkvak Braakmanhaven Zeeland* (Consulmij report 21.0101.IH, 1999)

* Reports of the campaigns 1 to 13 are from Fugro, the campaigns 14 to 16 from Consulmij.

C.1.1   Test method and results of early pull tests

The purpose and methods of the tests were not the same for all test programs. In the report of RWS Deltadienst (Mulder, 1970) the aim of the test is given as finding the pull out force of the elements. A total of 26 tests was performed on 0.3 m thick Haringman blocks (0.5 × 0.5 m, 170 kg per block) on slopes 1:4. The pull tests were carried out with a tripod, with legs at 2 m spacing in longitudinal and 1.2 m in transverse direction. A static force up to 6000 kg could be applied with hydraulic oil jacks.[292] In addition to that a drop weight could be used to induce vibrations. Also pneumatic hammers were used to stimulate movement of the elements under dynamic pull force, though not successful for practical reasons. Many of the tests were interrupted due to failing anchors or spalling concrete. All resisted forces and displacements were reported. Due to various observed early failures only a part of the results represent ultimate revetment resistance.

The tested slopes were on the dikes of the construction polders Roggenplaat and Neeltje Jans for the Eastern Scheldt barrier project. The slopes were newly constructed. The

---

[292] It was later realised that these high force were only possible due to the close distance of the legs of the tripod. Without those legs pushing down the revetment, and preventing axial movement, the pull-out force would be much smaller. The test results were heavily biased by the method. Refer to the work of C. van der Horst.
See also: J.K. Vrijling, C. van der Horst, and P.J.M. van Hoof, "The structural analysis of the block revetments on the Dutch dikes," *ICCE* (Sidney, 2000)

conditions during the test were not reported. Based on the dates in June and July 1970 and the photographs in the report the temperature can be estimated between 15 and 20°C.

(Mulder, 1970) observes that the revetment subjected to high forces tends to be lifted in horizontal rows. Any vertical interaction was not observed, but this was obviously due to the position of the legs of the tripod. The tripod left the horizontal row free to move. In one test a row of 21 elements could be moved. All deflections were reversible. It was concluded that newly constructed slopes were not less stable than slopes that were in place for some time. The most important observation was a dependence on the vertical position on the slope. In the top rows elements could be pulled out. In the middle rows they could only be moved, and in the bottom rows there was no movement at all.

$$n_{LF} = \frac{F_u}{G \cos \alpha}$$

Eq. C.1

with

n_{LF} = load factor, expressed in number of elements
F_u = measured maximum pull force (perpendicular to the slope)
G = single element weight = $\rho_s g V$
α = slope angle
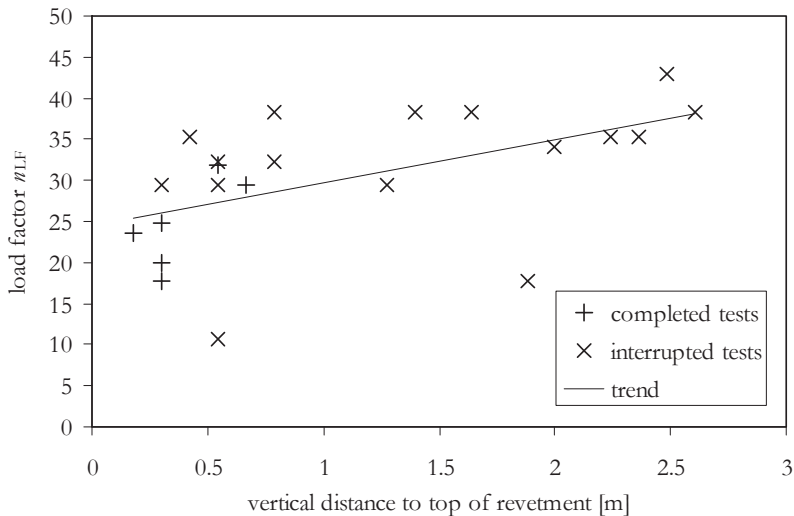
Figure C–1   Applied forces vs. position on the slope ($z_{top} - z$), tests in (Mulder, 1970)

In the report of the regional RWS Adviesdienst Vlissingen (Verhagen, 1984) pull tests are performed on several types of revetments: Lessin stone, Vilvoord stone, Basalt and Haringman blocks ($D = 0.2$ m). The tests were part of an investigation of the strength of Eastern Scheldt revetments when subjected to wave loads. The results were meant to be implemented in the operation philosophy of the flood barrier of the Eastern Scheldt estuary.
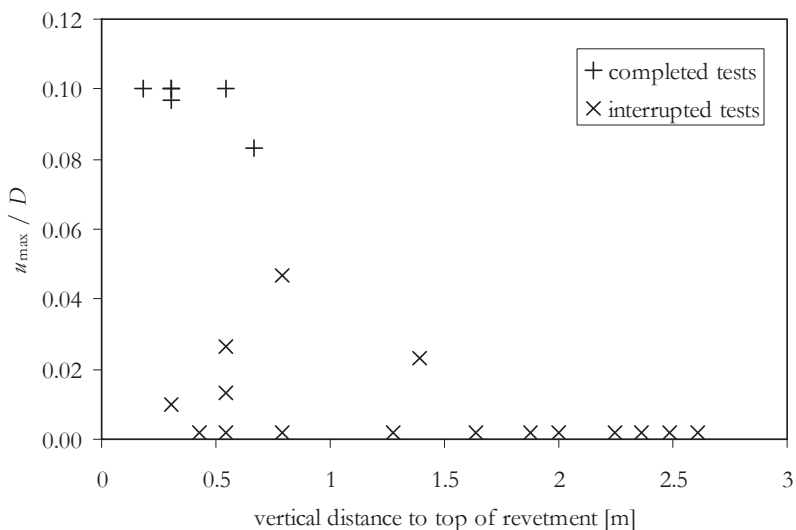
Figure C–2   **Measured displacements vs. position on the slope ($z_{top} - z$), tests in (Mulder, 1970)**
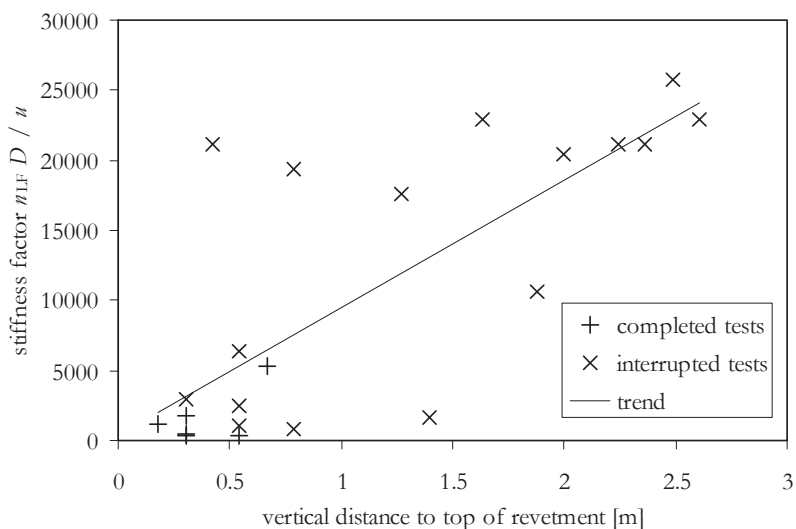
Figure C–3   **Stiffness $n_{LF} / (u/D)$ vs. position on the slope, $z_{top} - z$ (Mulder, 1970), for the completed tests the initial stiffness is plotted**

The in-situ pull force was measured, no deflections were measured. The shape of the load-time diagram was classified. The stone dimensions, weight and joint fill rate were registered. Individual test results were not reported. This is compensated by an extensive statistical analysis of the results.

On some of the locations the tests were repeated after re-placement of the revetment stones. It was concluded that the average strength of the slope after re-placement (and proper joint filling) was only 60% of the original slope. (Verhagen, 1984) concludes that older in-situ slopes are about 1.67 times stronger than new slopes like e.g. the tested slopes in the Delta flume. It is unclear whether this is also true for wave loading.

Many of the statistical analyses require a normal distribution of the parameters, which was not the case. The test results were so erratic, that the t-tests to prove dependant sources on two series on the same revetment type were all negative.

Quite a few tests gave a characteristic stick-slip failure, where the force during slip is about 0.6 times the peak force. On the parameter set a multi parameter regression analysis was performed. The results are not easily understood. The results Vilvoord stone show a very small positive dependency on the distance to the top. For Basalt this is slightly negative. For both, the dependency of the peak force on the element weight is negative, but for the slip force it is positive and almost equal to 1.0, which sounds logic. The correlation between the predicted results on basis of the regression and the measured results is anyway very poor.

Only for the Haringman blocks a stronger relation with the position on the slope was found. The scatter is large, as low is the confidence on the vertical position of the trendline ($p = 0.90$). The confidence for the slope of the trendline is strong ($p = 7.8 \times 10^{-5}$). In Figure C–4 the results (in terms of load factor $n_{LF} = F_u/G$, with $G = 120$ kg) are plotted in the graph together with the results of (Mulder, 1970). The difference in average is remarkable. The slopes are 1:4 and 1:3.5 respectively. The major difference may be the condition of the horizontal stress state, which is likely very high in the slopes tested by Mulder. Also the fact that his tripod allows the horizontal rows to move upward, generates extra horizontal stress. Verhagen uses a tripod for the natural stone slopes and two small tripods left and right of the tested stone on the Haringman slopes. With this test method the initial in-plane stress state is not changed.
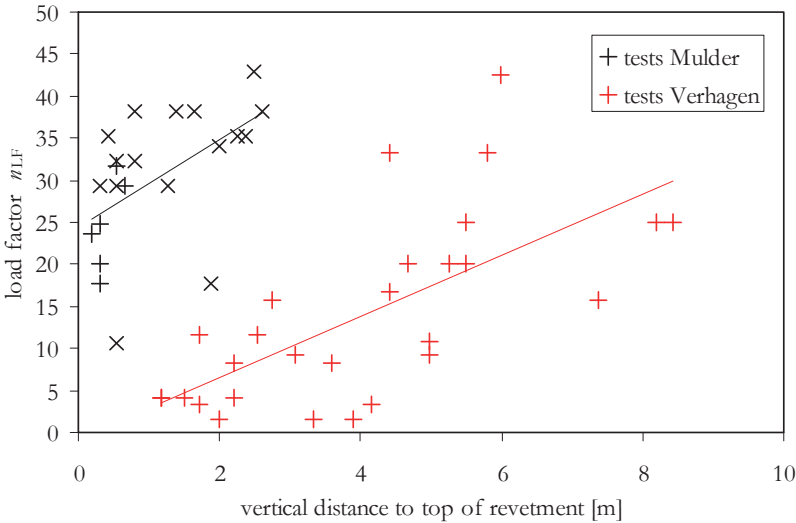
Figure C–4 Applied forces vs. position on the slope ($z_{top} - z$), tests on Haringman slopes in (Verhagen, 1984) and (Mulder, 1970)

The average results for the types of revetments give clear differences, where the basalt is the strongest in terms of load factors. The column shape and the irregular faces give a strong interaction and small change of slipping out. The results on the Lessin and Vilvoord stone are considerably lower, but still give fairly high load factors, taking in mind the round shapes and assumed poor possibilities of the stone to get locked-in by the other stones.
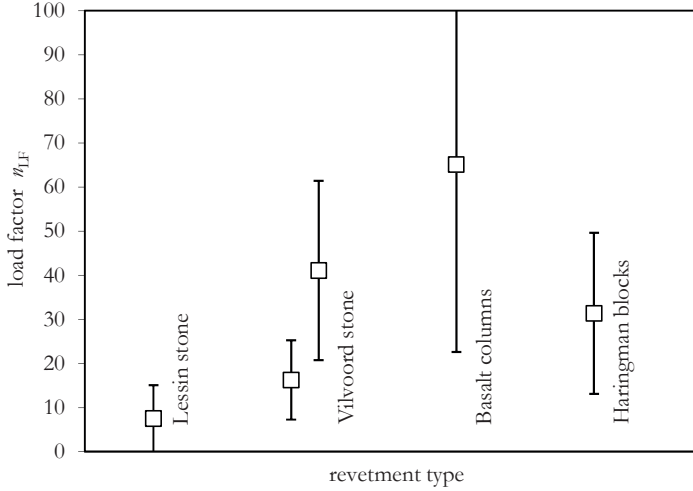
Figure C–5   Average results in (Verhagen, 1984), standard deviation shown as length of error bars

In (Wevers, 1970) pull tests on the laboratory scale model of a revetment were performed as a simulation of the uplift loads during wave attack. The model scale is an approx 1:125 flat block revetment imitation, with blocks $4 \times 4 \times 2$ cm and $\rho = 2100$ kg/m^3. Static pull tests as well as dynamic pull tests were carried out. The dynamic pull tests were meant to create load conditions similar to the wave attacks, where the uplift pressures have a steep rise time and decrease to 0 in roughly 0.1 to 0.2 seconds (wave period $T = 1$ to 1.6 sec). Wevers noticed that his static tests showed other failure mechanisms than his dynamic tests. During the dynamic tests single elements were pulled out, where the static tests did not cause failure at the same load magnitude. And in case of failure, the static tests caused groups and rows of elements to move upward, rather than single elements. The static load factors amount up to 75. In the dynamic pull tests an impulse load is applied with approx 0.04 sec time duration. The load was applied with a drop weight via a steel wire running over a pulley. The impulse was applied 10 times, before stepped up to a larger weight. The pull tests were performed after the wave tests, hence the slope was preloaded.

The results in Figure C–6 are reported peak loads of an impulse load (triangular with $t_d = 0.04$ sec), compared to the element weight. Tests were performed on the submerged part of the slope as well as above water, where for the underwater tests the effective element weight $(\rho_s - \rho)$ was taken. The graph shows the results plotted against the theoretical neutral normal force in het revetment, which is for the submerged part of the slope:

$$N_{\text{neutral}} = \rho_s D \left(z_{\text{top}} - z \right) - \rho D \left(z_{\text{SWL}} - z \right)$$

Eq. C.2

The results show (apart from the usual scatter) a convincing linear trend, independent of the slope angle.

A noticeable detail in this model study is that Wevers tried to omit the built up stresses in the horizontal rows through application of the blocks in diagonals. As can be noticed in the graph a small number of elements in the diagonally constructed top-layer were loose, others performed similar to orthogonal applied elements.
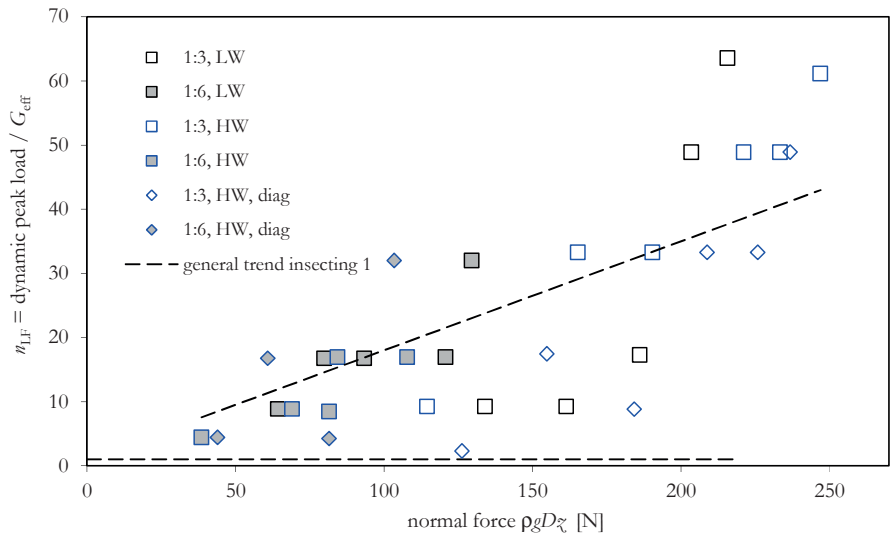
Figure C–6 **Dynamic block test results from (Wevers, 1970)**

All available in-situ pull tests are static. Following (Wevers, 1970), static loads are probably a less adequate simulation of the wave load conditions. The fact that the pull tests are concentrated loads, where the uplift forces during wave attack are distributed and act simultaneously on a group or row of elements. Also the static loads do not account for the effect of inertia of the revetment, which causes delay of motion, dynamic amplification and also a difference in the internal forces. Dynamic loads tend to cause higher shear forces between the elements (see Annex A.2.3).

The static strength tests were meant to gain insight on the stability of the revetment cover layer. Analyzing the results, making comparisons, finding relations etc. is useful, but relating the pull force results as such to an indication of the stability under wave load conditions is not possible.

C.1.2 *Test method in DWW test campaigns*

The DWW (hydraulic department of the Dutch Ministry of Infrastructure) has executed a large pull test campaign in the 1990s. The purpose of the DWW test campaigns was to collect data for examination of element interaction and revetment resistance on the real slopes (see section 6.3). A standardised test method was used. The hydraulic test equipment was mounted on a trailer which supports itself during the tests on four props at the corners of a rectangle of 1.4 m wide and 1.5 m long. The pull force was applied with a suction device

(for the Haringman blocks) or with nails and resin anchors. For a limited part of the tests on Haringman blocks an additional frame was used which distributed the prop forces over the elements directly adjacent to the tested element, thus avoiding movement of the neighbouring elements.

The results of the pull out tests commissioned by DWW were made available in reports as well as in a digital database. The database has been checked and completed as a part of this study.

Table C–3   Details of pull-out test data sets

No	Date	Location	No of tests *	Type	D	slope $\cot\alpha$	construc-tion
01	1990	Colijnsplaat	939	Haringman blocks	0.25	4.0	1980
02	1990	Colijnsplaat	99	Haringman blocks	0.25	4.0	1980
03	1991	Afsluitdijk	928	Basalton	0.35/ 0.40	3.4 – 5.2	1978/ 1988
04	1991/ 1992	Breskens	1202	Basalton	0.35	4.0	1978
05	1992/ 1993	Maassluis	1155	Basalton	0.27	3.9	1992
06	1993	Maassluis	457	Pit-polygoon	0.27	3.8	1982
07	1994	Colijnsplaat	697	Haringman blocks	0.25	4.0	1980
08	1996	Oesterdam	685	Haringman blocks	0.25	4.0	1984/ 1994
09	1997	Terneuzen	745	Concrete blocks	0.20/ 0.25	3.5 – 4.5	1970/ 1975/ 1977
10	1998	Walsoorden	627	Pit poly columns Hydroblocks Granite Concrete blocks on their side	0.35 0.35 0.40 0.50	3.8 3.7 5.0 3.7	1997
11	1999	Oesterdam	914	Haringman blocks Copperslag blocks	0.25	4.0 6.0	1984/ 1994/ 1995
12	1999	Mosselbanken Kruiningen	100	Granite	0.20	Not known	Not known
13	1999	Paviljoen-polder	475	Copperslag blocks	0.25	4.0	Not known
14	1999/ 2000	Friesland	146 (754) (900)	Basalt Copperslag blocks	0.225 0.25	4.3	Not known
15	1999	Zuidoever Westerschelde	257	Copperslag blocks Concrete blocks Granite	Not known	Not known	Not known
16	1999	Braakman-haven	(450)	Granite columns	Not known	Not known	Not known

* (..) results not in database

The database contains revetment slope parameters: the revetment type, the element thickness, the element material density, the slope angle and slope length and year of construction. It also includes the test results and environmental parameters: forces, displacements and temperature.

The test series were performed on horizontal rows, where the tested elements were randomly selected, with intermediate distances of 3 to 5 m. The purpose was to avoid choosing elements that could have interdependencies.

A maximum force of 900 kg (8.9 kN) was applied, built up in a period of 30 seconds, with a preferably constant rate. After that the force was kept constant for another 30 seconds. If the element could not resist this force or moved more than 25 mm, it was considered as loose. In case the force of 8.9 kN was resisted, the element was considered as fixed. At load steps of 1.5 kN the vertical displacement was monitored, thus providing a force displacement diagram.

In many cases the pull tests of the DWW campaign were accompanied by permeability tests on the top-layers using a falling head principle with two open concentric water basin on top of the revetment. These tests are evaluated in (Klein Breteler, 2002)[293].

C.1.3   Test methods in other tests

In (Stigters & Klein Breteler, 1999) 128 pull tests on steep river bank slopes are presented. An interesting element in this study is that it provides a uniform test method, uniform test conditions (11°C), uniform construction age (1 yr), on two types of revetment (Basalton and Hydroblocks) in exactly the same slope design (1:2 slope from +1 to +3 m). The test forces are standardised to 500 kg, individual elements are tested up to failure with a maximum of 1500 kg. For the tests a very small trolley was used with support legs on the elements adjacent to the tested element. For the results compared to other tests see Figure C–9.
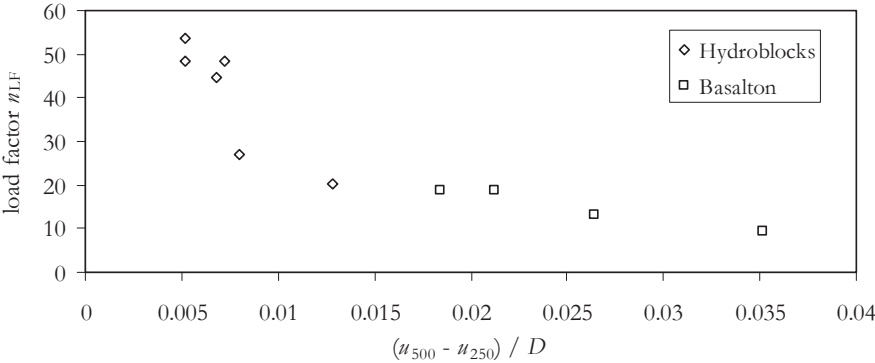
Figure C–7   **Strength vs. stiffness of Hydroblocks and Basalton revetments on river banks in the Alblasserwaard (Stigters & Klein Breteler, 1999)**

[293] M. Klein Breteler, *Analyse van doorlatendheidsmetingen van steenzettingen* (WL|Delft Hydraulics report H3911, 2002)
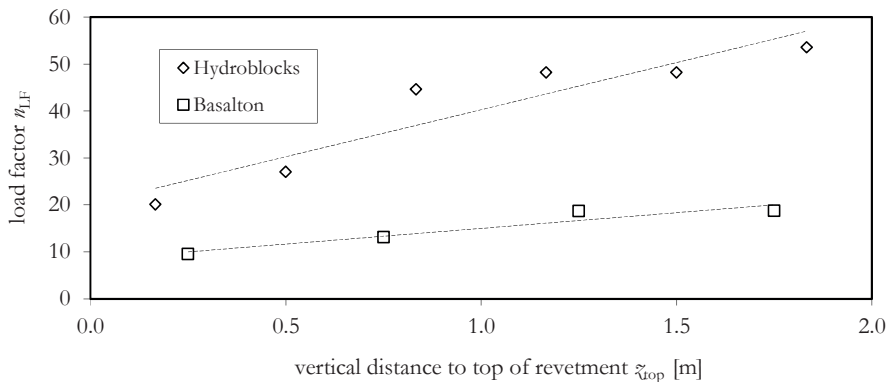
Figure C–8 **Strength vs. position on the slope of Hydroblocks and Basalton revetments on river banks in the Alblasserwaard (Stigters & Klein Breteler, 1999)**

In 2008 a test series on more than 200 Copperslag blocks was performed. The maximum test load was 100 kg, a Copperslag block weighs 42 kg. The used equipment was a light tripod with an electronic load cell. The displacement of the pulled stone was measured relative to the six neighbouring elements, where the measured averages of the movement are 0.03 mm, which is all within the measurement errors. The load level of these tests is too low and the tests are therefore not adequate to support any investigation of element interaction, except from checking the piston mechanism.

Pull out tests with a more extensive instrumentation and deflection measurements were performed by WL (Kuiper, 2001) on an asphalt jointed Basalt slope near Kruiningen. Six tests were attempted, from which four failed due to failure of the resin anchors well below the intended test value. In the two remaining tests forces could be applied of 30 and 40 kN, built up in steps over almost one hour, with displacements of the pulled element of 25 and 10 mm respectively. The load was applied with help of a 4 m long beam, leaving the revetment free to move. The measured displacements of the other elements roughly suggest a bell shaped displacement pattern, with a maximum of 15 mm and radius of 1 m for the first test and 6 mm and 1.2 m for the second test. The displacements were recorded with station keeping logging displacements of 10 elements, recording every 3 minutes. One tested location 6 was 1.6 m lower on the slope (measured vertically), which may provide an explanation for the observed larger stiffness.

Back analysis, assuming ρ_s = 3000 kg/m³, 10% open space and D = 0.25 m, gives 21 kN for the weight of a circle with radius 1.0 m and 30 kN for 1.2 m. This suggests that a ring with a width of roughly one element just outside the measured bell shape was also lifted by the pull force.

C.2 Typical results of the 1990s test campaigns

Typical test results are characterised by a softening load displacement path. In case failure happened, this was mostly a sudden (brittle) slip out of the element. Excessive displacement caused a drop of the applied force, which stopped the movement of the element and stopped the test.

The test results go up to load factors n_{LF} of approx 30 to 40 for the smaller columns and of approx 7 for bigger concrete elements. In both cases, this means that the weight of a significant portion of the area between the legs of the test equipment is activated to withstand the pull force. Given the square area of 1.5 m, the unaffected circular area between the legs can be calculated as $\pi/4 \times (1.5\sqrt{2} - 0.25)^2 = 2.75$ m^2. Divided by 0.25^2 this gives a load factor of 44. For 0.3 and 0.5 m element sizes the maximum load factor becomes 29 and 8 respectively. This suggests that the size of the equipment and the magnitude of the applied load are well balanced.

For various reasons many of the tests failed in the sense that they did not pass the 900 kg force criterion.

Typical results for the column revetments are twofold. In case of failure the pulled element slips out at a certain value of the load. In case of failure at higher load levels or no failure at all the element stays fixed in the revetment layer but can be moved for several millimetres.

For the block revetments (Haringman blocks) a typical result at higher load levels is that neighbouring blocks in the same row also move. The block rows under and above the tested block generally do not move, sometimes restrained by the legs of the equipment. The observed block interaction most of the times appears in the rows rather than in 'vertical' strips.

In the reports a remark is made regards the first 2.5 mm displacement of the Haringman block pull test, because of the deformation of the rubber edge of suction cup. The measured displacement is caused by connection, not by stone movement.

C.3 Evaluation in literature

In (Plooster, 1995) some of the test campaigns on Haringman blocks are evaluated. An effect of the air temperature during testing was noticed, and in 1994 a number of tests of 1990 were redone in order to double-check and validate effects of temperature. For some of the test series on rows-oriented types a clear, almost linear temperature dependency was found. For other types this was not clear.

Plooster also discusses the reasons and effects of application of the additional frame. He is aware that the frame blocks horizontal rows to be lifted. The moving row gives higher displacement, and possibly smaller ultimate forces due to the fact that higher displacements break the friction with the rows higher and lower. There is no explicit reference to the increasing normal force in the moving row. The amount of loose elements is believed to be equal to cases with no frames.

In (Klein Breteler, 1998) and (Coeveld & Klein Breteler, 2003) the DWW test series are evaluated. The focus of the analysis is on single element failure and in translation of the results into a 'clamping factor' as an expression of the stability related to the weight of the single elements. The reasoning behind this is that the revetment is believed to withstand distributed loads with plate and beam action, which generates extra strength above the element weight. For the individual badly fixed element there is a probability to be popped out, either due to a locally higher load or due to a weak spot. The test campaigns were meant to give insight in the single element failure. Also the revetment design methods were based on the single element failure mechanism. The aim of the evaluation studies of Klein Breteler is to compute the probability that a single element fails under a certain load level. The test

results were categorised and statistical analysis is performed mostly based on groups with load test results below and above two times the element weight. Also the effects of air temperature, repeated loading of the same element and the position of the element below, in or above the tidal zone is considered.

The definition of the 'clamping factor' Γ_k is given by the load and resistance balance of a single element, with an assumed resistance against a spatial maximum of the load during wave action.[294]

$$\phi_w = (\Gamma_k + \Gamma_2 + \Gamma_3)\Delta D \cos\alpha \qquad \text{Eq. C.3}$$

where

ϕ_w = the maximum (static) head difference over the element

Γ_k = effect of element interaction (replaces the effect Γ_1 of friction in an older version of the theory)

Γ_2 = effect of inertia of the element subjected to dynamic loads

Γ_3 = effect of hydraulic suction forces under the element, when it should suddenly move upward

The clamping factor is defined for the submerged element weight. Calculating the clamping factor from the pull tests has been done as follows.

$$\phi_w B_x B_y \rho g = (\rho_s - \rho)g D B_x B_y \cos\alpha + F_n \qquad \text{Eq. C.4}$$

with

F_n is the net pull test result: $F_n = F_u - G\cos\alpha$,

F_u is the ultimate pull force

G is the element weight: $G = \rho_s D B_x B_y$

Assuming $\Gamma_2 = \Gamma_3 = 0$ and substituting Eq. C.3 in Eq. C.4, we find:

$$\Gamma_k = 1 + (\frac{\rho_s}{\rho_s - \rho})\frac{F_u - G\cos\alpha}{G\cos\alpha} \qquad \text{Eq. C.5}$$

The value of F_u in this formula should be the minimum measured value, or e.g. the 0.1% felt below value.

If there are no failures in the test series, e.g. no measured ultimate forces, the factor can be computed based on the assumption of a Rayleigh distribution. The known change that $F_t < 3G$ is expressed in the following formula:

$$\Gamma_k = 1 + \sqrt{\frac{0.014N}{-\ln(1-R)}} \qquad \text{Eq. C.6}$$

Where N = the number of tests in the series and R = the reliability (e.g. 0.995 or 0.999)

The disadvantage of this method is that the number of tests influence the results. One has to either accept a lower reliability or a smaller result. In (Coeveld & Klein Breteler, 2003) these

---

[294] This method is in principle incorrect and is not supported of further used in this thesis. The element interaction as a factor on a single element neglects the fact that all neighbouring elements are loaded by the waves also. Refer to beam model theory in Annexes A and B.

formulas are further improved. The DWW test series are evaluated with the formulas above and the results are presented in Figure C–9.
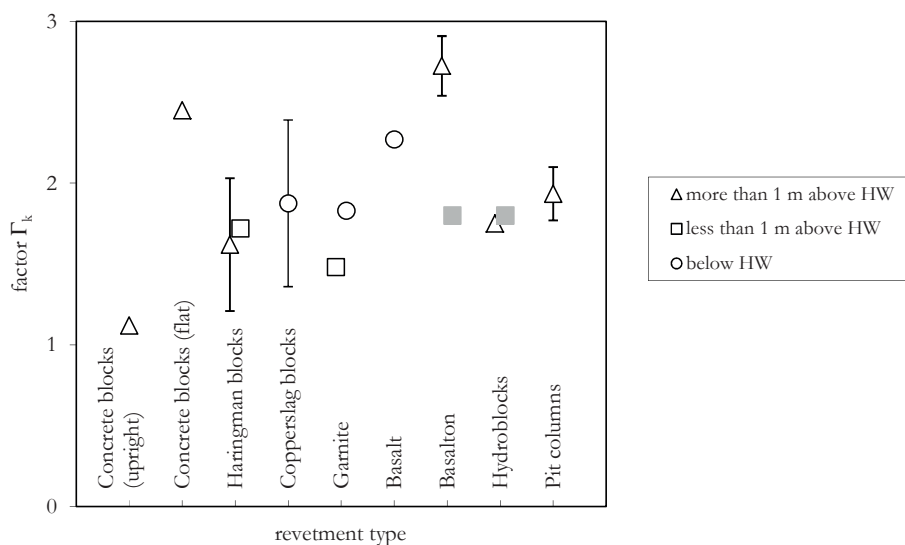
For comment on the factor Γ_k see footnote 294

Figure C–9   Calculated clamping factors in (Coeveld & Klein Breteler, 2003) and (Stigters & Klein Breteler, 1999) in grey

General findings are:

–   The pull force results give a large scatter caused by stochastic parameters, e.g. friction.

–   The columns perform generally better than the flat blocks.

–   The differences between categories below and above high water are not made evident. Other effects of position on the slope are not evaluated in the reports.

–   There is an influence of temperature, which was not modelled but described with an exponential function.

–   For the Alblasserwaard tests it was observed that both strength and stiffness of the hydroblocks were better than the Basalton.

–   For a certain population of Haringman blocks the effect of repeated loading (with time intervals) was investigated. A limited influence could be noticed, but was not convincing due to large scatter and interference with temperature differences.

–   It was not possible to relate the visual reports on loose joints or elements to the measured results.
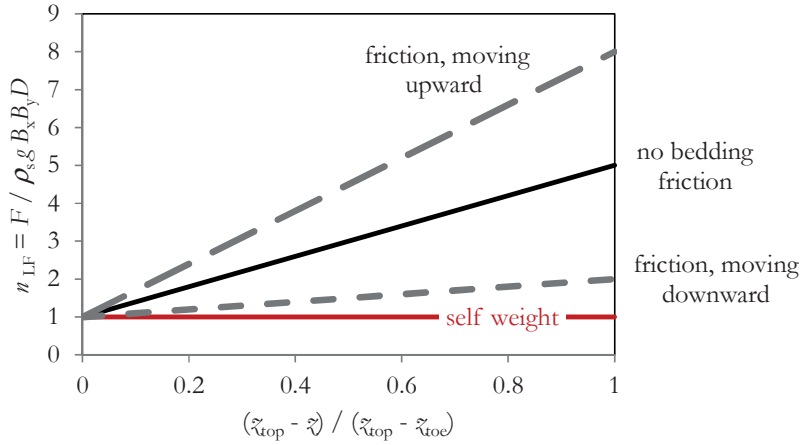
Figure C–10   **Schematic graph of model result for pull out forces based on friction model**

In (Vrijling et al, 2000) is was proposed a model based on the normal force in axial beam. The reliable underbound of the pull out force is the self-weight of the pulled element.

$$F_1 = \rho_s g B_x B_y D \qquad \text{Eq. C.7}$$

On top of this contribution a term based on friction between the top-layer elements can be added.

$$F_2 = 2 f_{fr1} \rho_s g z B_y D \qquad \text{Eq. C.8}$$

with

f_{fr1} = the friction between the top-layer elements

Eq. C.8 is based on a friction less state between top-layer and bedding, i.e. on the neutral state of the transverse normal force (see A.1.1). Friction between the bedding and the top-layer can work in both directions. This changes Eq. C.8 into:

$$F_2 = 2 f_{fr1} \rho_s g z B_y D \left(1 \pm f_{fr2} \tan\alpha\right) \not< 0 \qquad \text{Eq. C.9}$$

with

f_{fr2} = the friction an the interface of the top-layer elements and the bedding

The total pull force $F = F_1 + F_2$. The pull force can theoretically amount between the under bound F_1 and the upper bound of F_2 with positive friction. The test data presented in Figure C–4 and Figure C–6 follow the linear relation according nicely. The scatter in the experimental results can be explained by the model.

Similar as in Figure 3-13 it can be found that the slope angle α has a large influence of the possible scatter of data.

The model neglects bending moments and neglects the elastic effect of an axial beam on a longer slope. Those effects will be included in the analysis in Annex D.

DESIGN OF PATTERN-PLACED REVETMENTS – ANNEXES

ANNEX D ANALYSIS OF 1990S TEST CAMPAIGNS

In this Annex the in-situ pull test series presented in Annex C are analysed. First the mechanisms and potential effects of the various parameters are discussed. The results are systematically analysed in section D.2 and compared with the model formula results in D.3. The findings are summarised in section D.4.

D.1 Influencing parameters and conditions

D.1.1 Element shape and pattern

The capacity of the pulled single element to withstand loads that exceed the element weight comes from shear stress interaction on the faces of the element. This shear stress can be due to mechanical friction on contact points with neighbouring elements or via joint material. Also shear stress can occur due to bond or adhesion of clay, dirt or marine growth. This shear stress may be exceeded at a certain load level, the bond breaks, or the element slips at the contact points. After that two things can happen: the element slides out more or less easy, like a piston, or the element rotates slightly and blocks or jams. In the latter case the test can be continued beyond the single element weight and a group of element is lifted.

Especially when the element has an irregular shape, when the load is not perfectly centric, and/or when angular joint material is applied, the movement of the element is restrained and interrupted. Very slight rotations are sufficient to stop the movement/sliding of the pulled element. Subsequently the pulled element transfers more vertical force to the neighbours, the neighbours also move up and rotate. If the pull test comes in this phase, a mechanism develops which increases the normal force around the pulled stone. In section B.1 it is derived that this mechanism of blocking and gaining strength develops above $n_{LF} = 10$.

Revetment systems with regular, rectangular shapes, the contact points between the elements rely on the (slight) differences in size of the elements. For Haringman blocks these differences have to be accommodated in very narrow joints, which also control the hydraulic properties of the system. There for the presence of joint material is very important.

Table D–1   **Characteristics of tested revetment types**

	regular	rectangular	natural / irregular	blocks D < B	columns D > √A
Concrete blocks (upright)	✕	✕			✕
Concrete blocks (flat)	✕	✕		✕	
Haringman blocks	✕	✕		✕	
Copperslag blocks			✕	✕	
Garnite			✕		✕
Basalt			✕		✕
Basalton	✕				✕
Hydroblocks	✕				✕
PIT columns	✕				✕
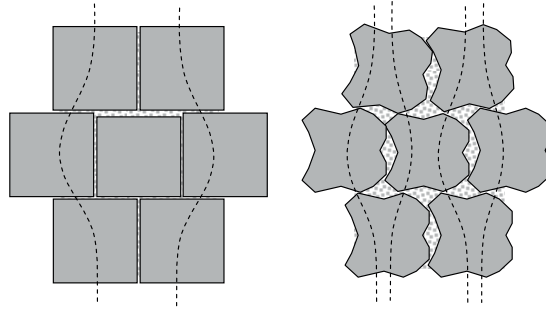
Figure D–1   **Load paths of normal forces in case of one assumed smaller stone in regular, rectangular block revetment and in Hydro block revetment**

D.1.2   *Slope length effect on the normal force*

The correlation with the neutral normal force $N_{\text{neutral}} = \rho g\,(z_{\text{top}} - z)D$ is investigated. There is too less variation in slope angle to find a reliable dependency on the angle. The slope lengths however differ significantly, with the Afsluitdijk and Breskens as the longest slope. The tested row on the slope of Breskens however are below +4 m Ref. Above +4 m ref the slope is covered with an asphalt slab.

For long slopes there will be more friction, and normal force will as a result be smaller, which leads to the tendency that the points of the Afsluitdijk are evaluated against a smaller force. When the normal force is calculated with an elastic spring model (see section 5.3), with $E_a = 50\,000$ kPa, $D = 0.32$ m, $k_x = 20\,000$ N/m^3 and $k_{\text{toe}} = 40\ 10^6$ N/m^2, this leads to a correction which is a function of the slope length and the relative position on the slope. A simplified correction formula can be defined for processing of the results in the database (refer to section A.1).

$$c_{zL} = (1 - 0.10(\frac{z_L}{z_{L\text{ref}}})^2) - 4\,\frac{z}{z_L}(\frac{z_L - z}{z_L})0.10(\frac{z_L}{z_{L\text{ref}}}) \qquad\qquad \textbf{Eq. D.1}$$

with $z_{L\text{ref}} = 4$ m

The choice for the constants in this equation is partly arbitrary. The outcome of the elastic axial beam model formulas can easily be quite different. Refer to Figure A–7.
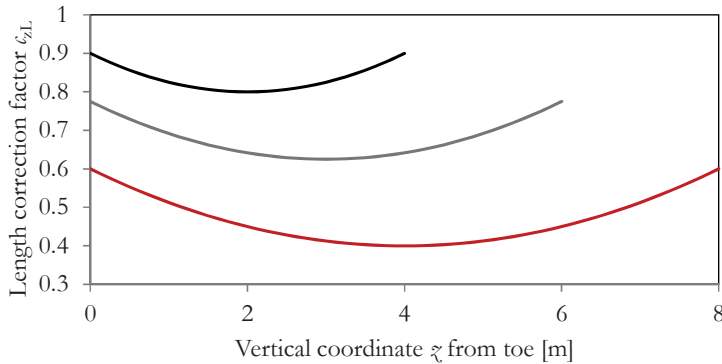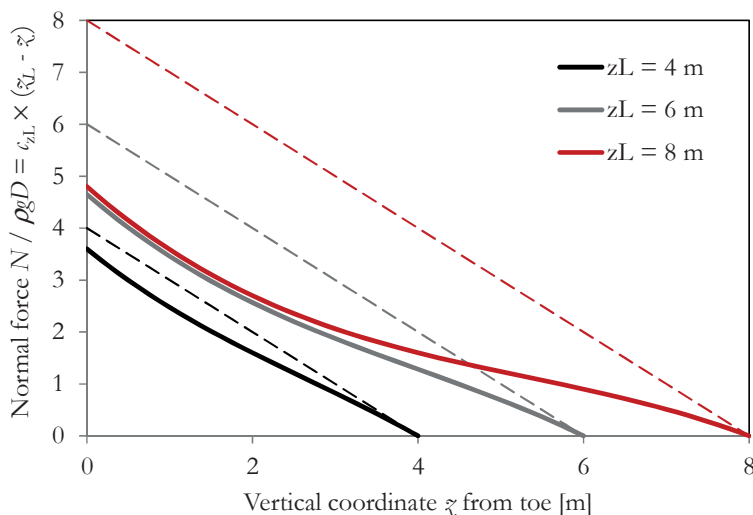
Figure D–2   Correction factors for the normal force on long slopes acc. to Eq. D.1

D.1.3   *Temperature effects on the normal force*

The theory claims that straight blocks are susceptible to temperature influences. The long horizontal rows are constrained. Temperature raise is normally associated with expansion. In the longitudinal direction there is a plain strain condition and the expansion will at last partly be restrained. A 20° temperature rise is accompanied with a strain ε_T of $20 \times 10^{-5} = 0.2 \times 10^{-3}$. Assuming an average Young's modulus for expansion of the system of 1000 MPa, the longitudinal normal stress will increase with $\sigma_T = E\,\varepsilon_T = 200$ kPa. To compare figures: the normal stress due to a neutral gravity force (without friction) is: $\sigma_N = \rho g\, z$, with e.g. $z = 1$ m: $\sigma_N = 2300 \times 9.8 \times 1.0 = 23$ kPa.

The expansion and contraction due to the temperature are cyclic. The strain ε_T of 0.2×10^{-3} is 0.1 mm per block of 500 mm. The average joint thickness, designed at e.g. 5 mm, is in most of the slopes of the field tests measured between 1.5 and 2.5 mm (average per row). For the joints the 0.1 mm movement is between 5 and 10% of the joint thickness. Especially in zones with washed-in joints, and joints filled with sand (and clay) and the temperature stress can actually occur. At very high stresses the joint material will crush, which causes relaxation. At places where the joints stay open, very large temperature stresses are unlikely.

From the comparison between the longitudinal and transverse normal force (section 3.1.8) it can be understood that during the pull tests the beam action in the rows can be dominant. Also the forming of horizontal beams prevents individual elements to move down and rest against their downstairs neighbours, which makes the presence of transverse normal force for individual elements insecure (see Figure D–3).

In case we still find dependency of z_{top} this could be caused by bigger longitudinal normal forces, combined with proper joint filling.
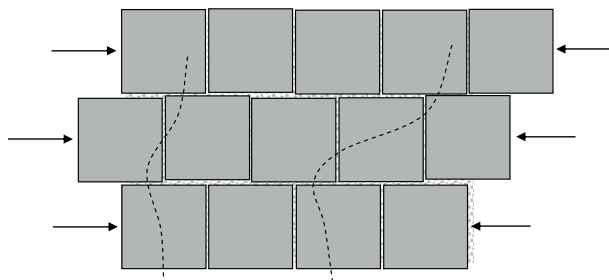
Figure D–3 Load paths of 'vertical' normal forces combined with forming of stiff horizontal beams due to longitudinal normal force

D.1.4 Curved dike sections

In (Plooster, 1990) the Haringman block tests at the location Colijnsplaat are presented and evaluated. At Colijnsplaat they tested straight as well as curved dike streches, with an outside bend. The dike bend is 35°, the radius R of the curvature on plan of the top row is approx 45 m. The dike slope is 1:4. The revetment geometry forms a section of a truncated cone. The radius of vertical curvature of a single row is in this case approx 160 m. The measured pull out results at the curved sections did not differ from the straight sections.
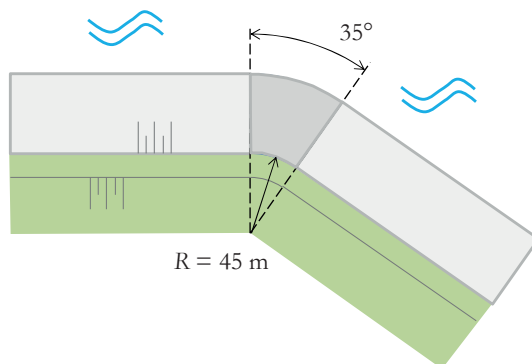
Figure D–4 Top view of curved dike section

The expectation could be that the results should be worse. In the straight sections the horizontal beam action is dominant, and for a curved revetment this beam action is likely weaker. The effect of the curvature can be investigated with help of the snap-through formulas presented in section A.5. Working out Eq. A.76 with substituted D for d, and with k based on $E = 1000$ MPa, gives the solid line in Figure D–6, for a straight beam. Substituting $(D - \delta_0)$ for D, with $\delta_0 = R - \sqrt{(R^2 - (\frac{1}{2}L)^2)}$, produces the dashed lines. The maximum in the graph shifts to the left. For the straight beam the maximum is at $\delta = 0.41D$, for the curved beams we find the maximum at approx $\delta = 0.41D - \frac{1}{2}\delta_0$. The maximum drops, with about 20% for $R/D = 80$. For the Haringman blocks with $D = 0.25$ m, $R/D = 200$ yields $R = 50$ m, which is a quite sharp bend. The curvature of the tested bend was 150 m, thus with $R/D = 600$. Hence it can be explained that there was not much difference observed in the test results.
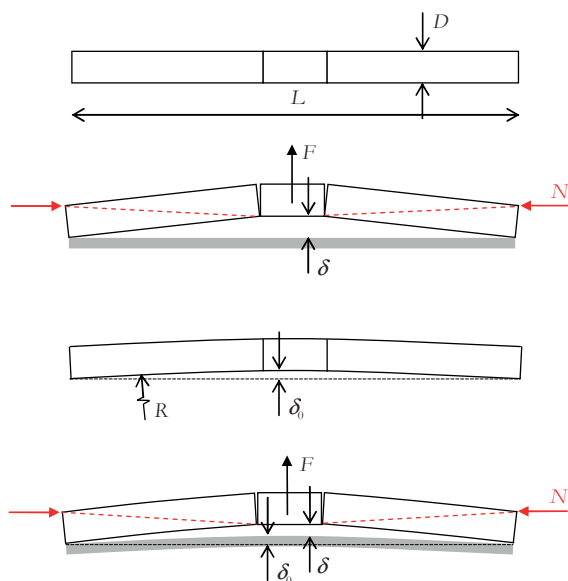
Figure D–5   Beam models with initial curvature
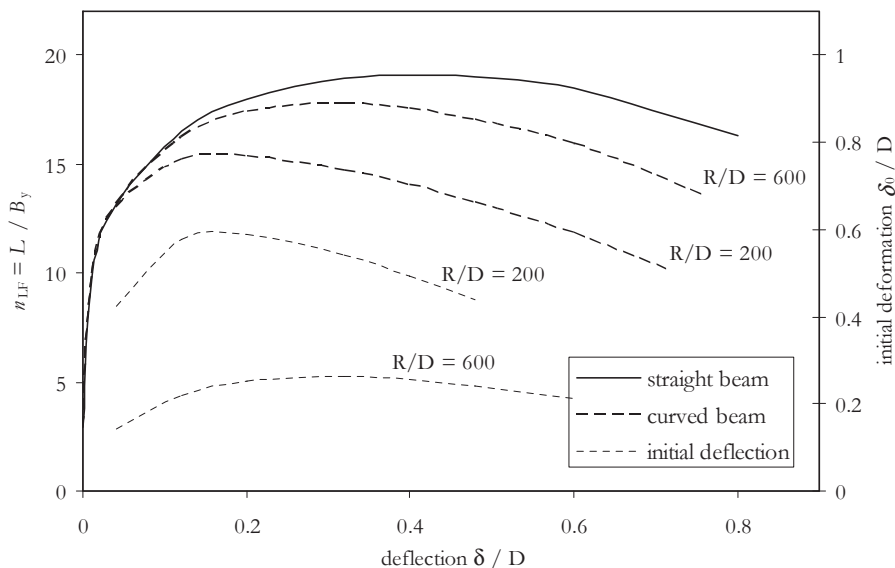
Figure D–6   Theoretical force capacity for lifting a horizontal row, straight and curved as in an outer bend of the dike (numbers are for Haringman blocks $D = 0.25$ and $B_y = 0.5$ m)

The formulas above do not count with an initial horizontal normal force. This brings us to another phenomenon: the effect of curvature on the settlement load on the revetment top-

layer. For a straight dike section the settlement leads to friction under the top-layer which is believed to increase the initial normal force in the cross section.

Due to geometrical constraints, settlement of a curved dike section will cause increase of longitudinal pre-load as well. It could be imagined that a very sharply curved dike section could settle, leaving the revetment as a free-standing dome structure. The curvature creates a load path which diminishes the foundation stress under the top-layer, and increases the radial normal stress in the revetment layer. The extreme limit case is of course only a theoretical idea, but it illustrates that the elements in an outside bend could initially be even more clamped, than in a straight dike section. The potential for development of second-order longitudinal normal force is smaller compared to a straight structure. For an inside bend this works the other way around: less initial normal force and more potential for second order normal force can be expected.

Table D–2   Summary of effects on curved dike sections

	Inside bend	Straight section	Outside bend
Initial transverse normal force	Caused by gravity minus or plus friction forces on the foundation bed		
Initial longitudinal normal force	Tends to decrease	neutral	Tends to increase
Geometry effect on local pull out strength	Positive	neutral	negative

D.1.5 Spatial correlation

The series of similar experiments in rows raises the question whether the variations in results have any spatial correlation. This is investigated by looing in to the stiffness results. For definition of u_{600} and u_{300} see Figure D–24. The variation of the results looks irregular, where the maxima occur as solitary spikes, like in Figure D–7.
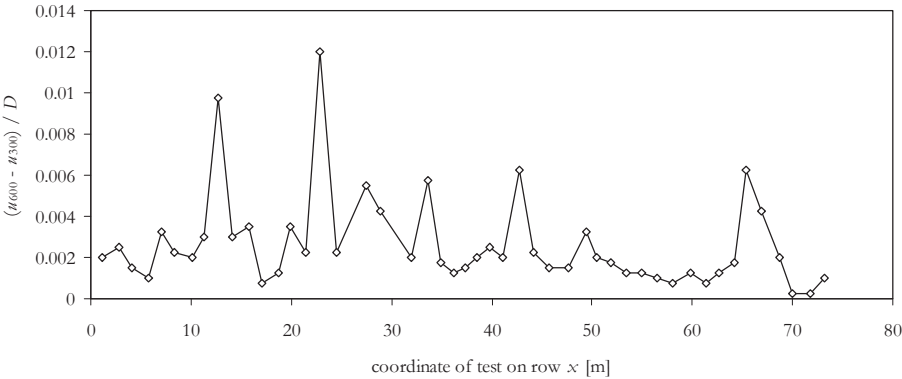
Figure D–7   **Typical test results of displacements of a series of tests on a horizontal row (Basalton, Afsluitdijk, $D = 0.4$ m, at NAP + 4 m, half way of the slope, age of construction 13 yr)**

A physical reason for correlation could be arching, probably caused by weaker parts of the toe structure. The 'vertical' normal force can not rest against on the weaker part and forms an arch in the plane of the revetment. Thus the clamping of the revetment plane could be more or less over several meters. A second physical phenomenon is that the stones interact

with local contact points. Due to its orientation the neighbouring element could be in a better clamped position. Averaged the normal force transfer should be more or less constant. This suggests that local maxima in clamping are compensated / averaged with smaller values at other locations, close or more distant.

Both spatial correlation phenomena are investigated. The arching effect is investigated using autocorrelation procedures.

In a limited number of series a spatial trend can be observed, where it could be the case that there is some correlation of neighbouring test results. This is shown in Figure D–8 and Figure D–9. The autocorrelation was investigated for all series of Basalton tests. In only 9 out of 61 series there was any sign of regularity of positive correlation coefficients decreasing with increasing distance x, as can be observed in Figure D–9. The most appropriate correlation fit function is a quadratic exponential function, not starting at 1.0.

The autocorrelation function:

$$\rho(\delta) = e^{-(\frac{\delta}{\delta_0})^2}$$

Eq. D.2

with

δ = the distance,

δ_0 = the correlation distance

Found average value of the correlation $\rho(\delta = 0)$ is 0.5. This correlation varies with distance and can be compared with a correlation coefficient r^2. The found correlation distance is 5 m. This means that in the series that showed significant results there is a 50% effect of distance and the remaining 50% of is random. In most of the series spatial correlation could not be proved significant. Therefore we conclude that the spatial correlation of the pull-out strength/stiffness of pattern-placed revetments is not convincing.
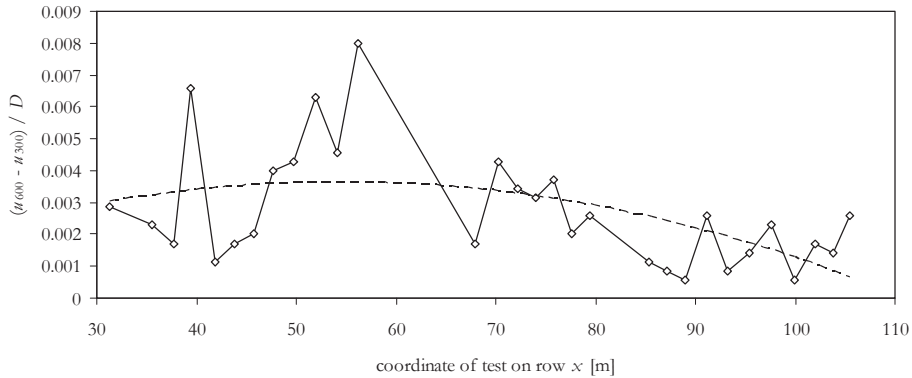
Figure D–8   **Typical test results of displacements of a series of tests on a horizontal row, with suggested spatial trend (Basalton, Breskens, D = 0.35 m, at NAP + 3.8 m, at the top of the slope, age of construction 13 yr)**
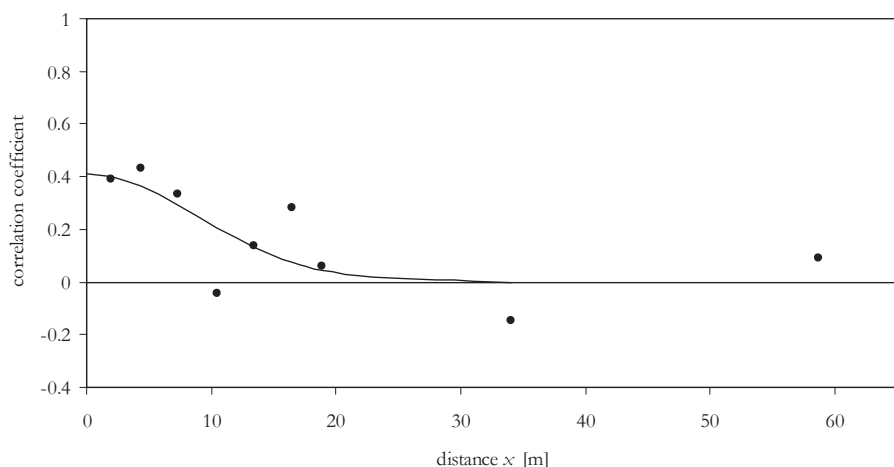
Figure D–9   Typical result of autocorrelation (r^2) in series of Figure D–8, with selected groups of 3 m, one group between 20 en 50 m, and one group for over 50 m.

The physical phenomenon of local contact points would suggest that there may be an opposite correlation. Maxima are expected to be neighboured by local minima. This hypothesis is checked by comparing the two values adjacent to a local peak, with the average distribution of the series. This is done for 60 series of each 40 to 50 test results (u_{600} - u_{300}) /D. Per series the two highest peak values were selected. The values adjacent to the peaks were selected and the probability in the cumulative distribution of the series was computed. The series was assumed normally distributed. For the purpose of determining the position of values in the middle range of the distribution this is deemed adequate. On average all values left and right of the peaks were at 0.48 in the cumulative distribution, so almost at the average. Figure D–10 is an example of these findings. We conclude that maximum values show themselves as spikes surrounded by values of average magnitude.
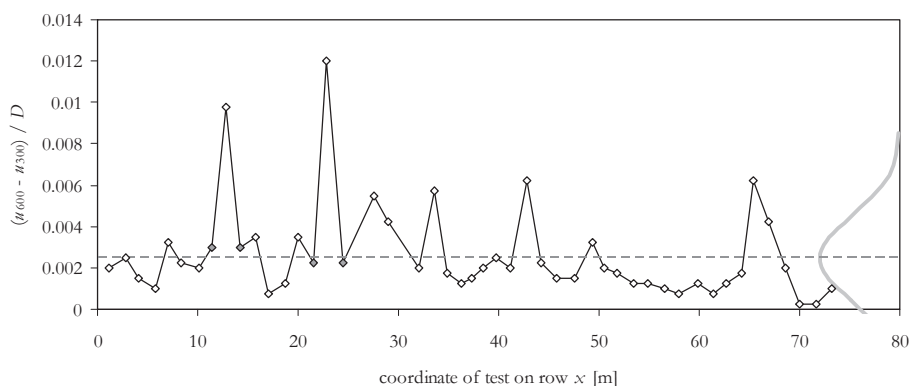
Figure D–10   Values adjacent to peak values compared to average distribution of the series

D.2 Pull out strength results

D.2.1 Typical results and trends

In (Coeveld & Klein Breteler, 2003) it was suggested that the individual results within large series of pull out strengths follow a Rayleigh distribution (Weibull with $k = 2$). A number of typical series are plotted on Weibull scale in Figure D–11. When a scale $(-\ln(p))^{1/k}$ with $k = 4$ is chosen the results of two of the datasets show linear fits. The position of the left most marker indicates the sample size: approx 1000 for each group. The four groups are tested up to 900 kg; only the results below 900 kg are shown. This means that for instance the dataset Basalton Maassluis had 40% of the results below 900 kg and 60% above.
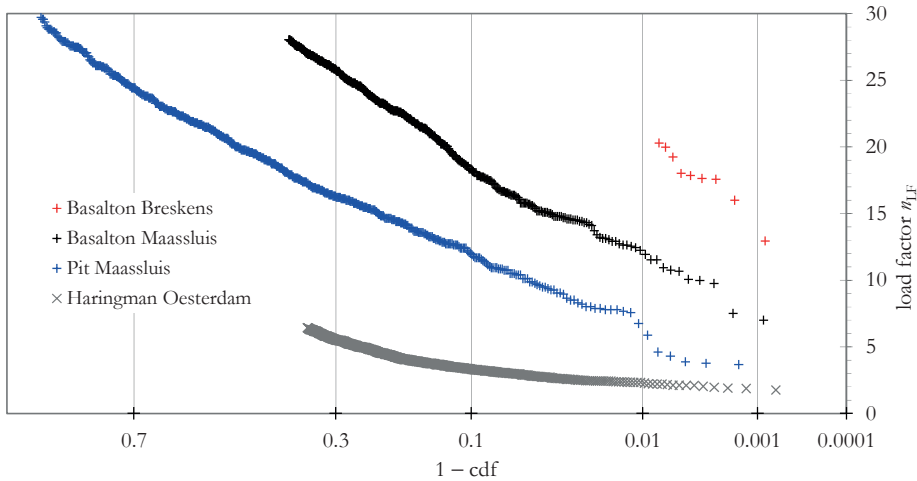
Figure D–11   **Sorted pull out test results of selected groups plotted against Weibull scale with $k = 4$**

Some observations from Figure D–11 are:

- The assorted results follow a regular scheme, which are reasonably well described with a Weibull formula, with cumulative distribution function cdf $= 1 - \exp(n_{LF}/\lambda)^k$, with $k = 4$. At the lower end of the individual series a small number of points drops below the trend. For the Pit data set this drop starts from $n_{LF} = 8$, for the Basalton Maassluis at $n_{LF} = 10$. Our interpretation is that this is due to development of a concentrated normal force in the local circle around the tested stone. The single results that fall below these values are due to an accidental slip out of the element.

- The columns perform better than the Haringman blocks. Not in absolute numbers of pull-out forces, but relative to the element weight. This is due to the larger aspect ratio D/B.

- The Basalton and Pit columns on the slopes near Maassluis show a noticeable parallel behaviour. The stones are of the same thickness and (average) weight, they only differ in shape on plan, where the Basalton is more irregular, and has better possibilities to survive on friction at localised contact points. The force results of the Basalton are processed with the average stone weight. As soon as the force is above $n_{LF} = 10$, it does not matter if a small, middle or larger size column is pulled. In that case the revetment plate is tested, rather than the individual element.

–   The selected datasets of Figure D–11 contain all tests within a series on one location. In case of mixing locations (e.g. two Haringman locations) the results are less regular.

Due to these reasons a statistical analysis of trends with the purpose of finding exceedance probabilities is not effective. Prior to numerical interpretation of the results shown in Figure D–11 a sub-group analysis regarding dependency on parameters is necessary.
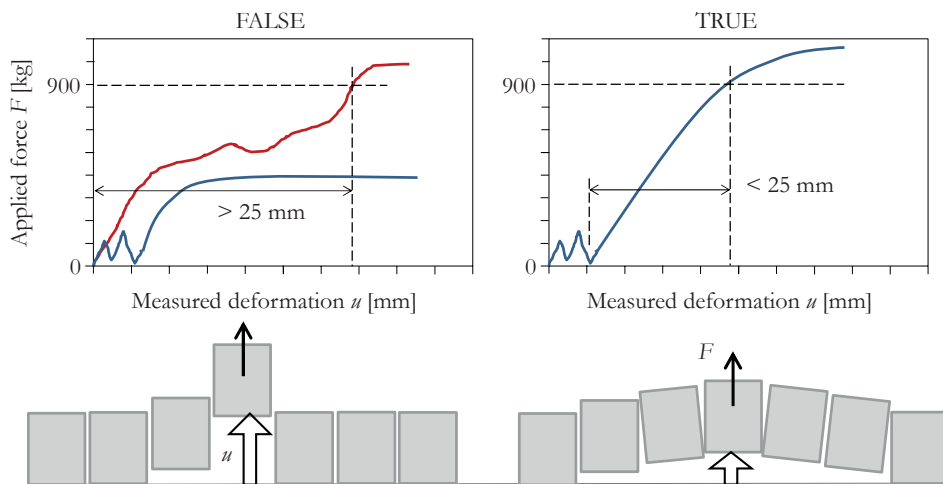
Figure D–12   Definition diagram of tests labelled TRUE and FALSE

D.2.2   *Effect of parameters on pull-out force*

The tests of the 16 in-situ campaigns produce results that split the series in two. The first result is whether the block or column is pulled out or not, loose or fixed, indicated with FALSE or TRUE in the database. The criterion is that the element survives 900 kg, with a displacement smaller than 25 mm. The tests were performed on horizontal rows of 70 to 150 m long, where the spacing of the test varies between 3 to 9 m for the different types of revetments. On most of the slopes the tests were carried out at several vertical positions on the slope. In general the variation in results is large. Due to the large numbers it is possible to perform statistical analysis with acceptable confidence levels.
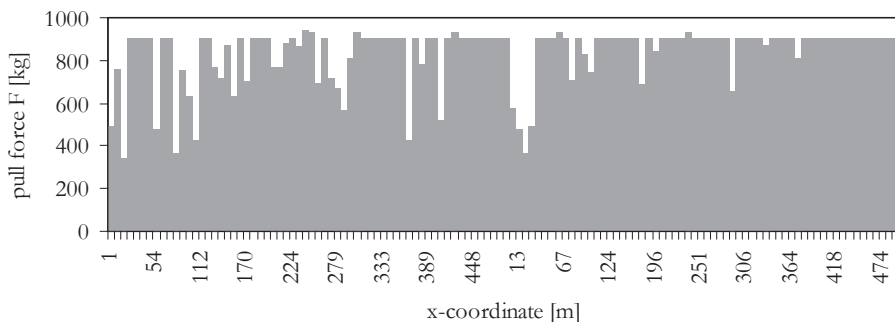
Figure D–13   Typical result of registered pull force of tests on a horizontal row at 1.1 m below top of revetment (Haringman Blocks at the Oesterdam, 1.8 yrs old)

The numbers of loose and fixed elements in groups tell us about the average strength and irregularities in strength and bond or interaction of the elements. Amongst all registered variables the dependencies of element type, location on the slope, age of construction and air temperature play an important role.

The numbers of TRUE and FALSE for 900 respectively less than 900 kg can be presented as fractions of the full number per series. These fractions are presented in the figures below. The results for Haringman blocks are based on 3194 tests, split into 48 groups with equal values of the investigated parameters vertical distance to top, age and temperature. The group sizes vary from 21 to 226 with an average of 67. The numbers TRUE and FALSE in each group are plotted in the figures and are subjected to multiple linear regression. There is a strong dependency on the vertical position, here expressed as distance to the top. There are more loose elements closer to the top. It appears that construction age and temperature also have a significant effect (see Figure D–15 and Figure D–16).

Table D–3   Linear regression on Boolean results Haringman blocks

	Coefficients	Standard Error	P-value	Average of variable in dataset
Intercept	1.01	0.118	5.19×10^{-11}	
Variable z	-0.232	0.0422	1.76×10^{-6}	1.08
Variable temperature	-0.0240	0.00915	0.0118	8.91
Variable age	-0.0224	0.00688	0.00214	8.38
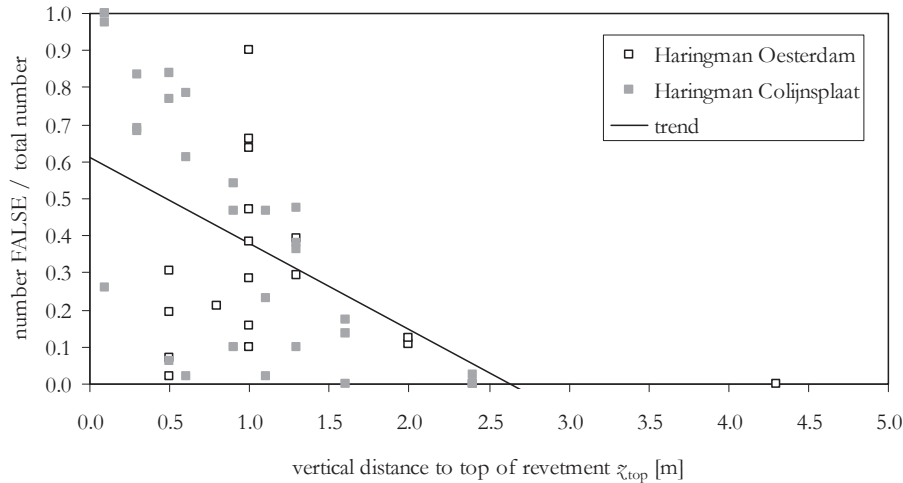
Figure D–14   Boolean results of full population of Haringman tests vs. vertical distance to top with plotted regression results of Table D–3
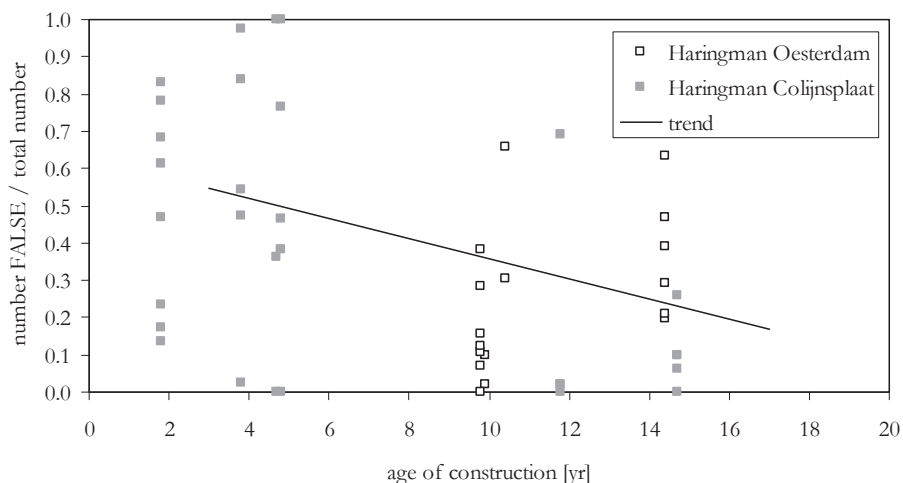
Figure D–15 **Boolean results of full population of Haringman tests vs. age with plotted regression results of Table D–3**
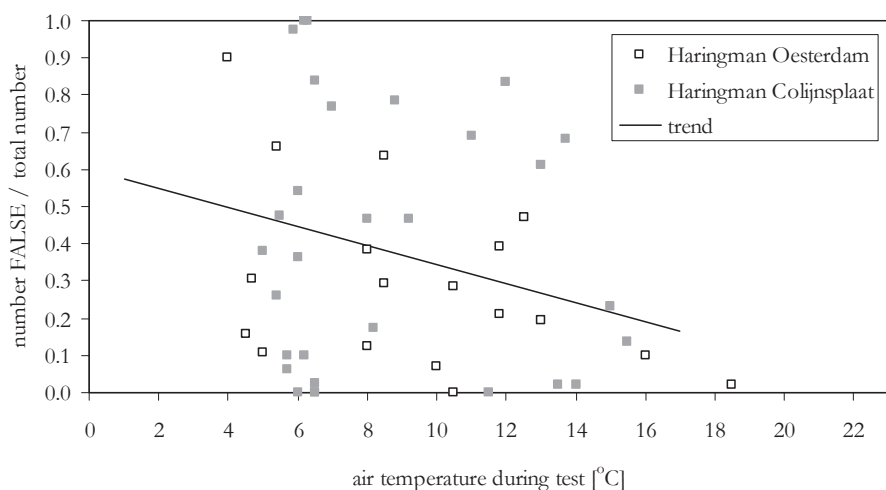
Figure D–16 **Boolean results of full population of Haringman tests vs. temperature with plotted regression results of Table D–3**

A remark must be made regarding the effect of an extra frame which was used in a limited number of test series. The frame supported the neighbouring elements and did effectively only allow the pulled element to slip out. For the test series with the extra frame 68 FALSE test were found against 66 TRUE tests, which gives 0.51. For a group with similar z-position (< 1.3 m) and age (> 11 yr) 245 FALSE and 570 TRUE tests were found, which gives 0.30. The tests where the neighbouring elements are free to move, give stronger results. If the elements rotate they can generate extra normal force, due to the expanded geometry (see Annex A.4.4), which explains the result of less FALSE tests.

Similar results for column type revetments are not easily obtained. All tests are standardised on a 900 kg pull force, which is 6.4 times the element weight for a Haringman block, but is 28 times the weight of a Basalton column of 27 cm, applied in the tested slopes in Maassluis. Although column revetments are expected to have better element interaction, the boolean results for the 900 kg force show a large scatter and are for the smaller columns not better than the Haringman blocks. The column results are split into (a) a group of small columns on Eastern Scheldt dikes and along the Nieuwe Waterweg and (b) a group of heavier columns on Western Scheldt dikes and the Afsluitdijk.

The group of small columns consists of Basalton and Pit columns (a regular hexagonal column) and Hydroblocks, with $D = 0.27$ and 0.35 m. The results are based on 1963 tests, split into 46 groups with equal parameter values. The group sizes vary from 25 to 96, with an average of 43.

Table D–4   Linear regression results small columns

	Coefficients	Standard Error	p-value	Average of variable in dataset
Intercept	0.792	0.0816	2.67×10^{-12}	
Variable z	-0.111	0.0316	0.00112	1.51
Variable temperature	-0.00734	0.00540	0.181	11.8
Variable age	0.0250	0.00543	3.91×10^{-5}	4.08
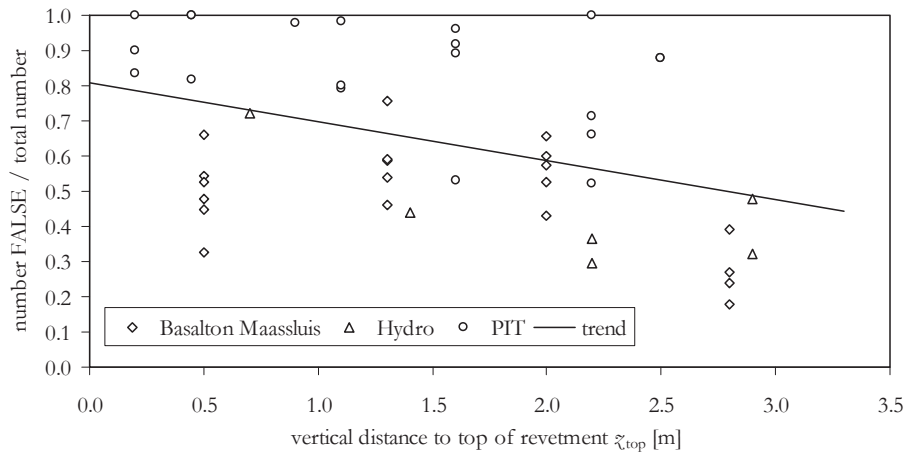
Figure D–17   Boolean results of small columns vs. top of revetment with plotted regression results of Table D–4

The temperate results show a reverse dependency. It is difficult to explain how a higher temperature leads to more loose elements. This result is deemed due to the fact that about 75% of the data in the group of small columns is on slopes with a construction age below 2 years. Only one type of revetment (the PIT columns) is represented in the groups with higher age. It is therefore better to omit these higher age groups and to investigate the dependency with a homogeneous age group. Analysing this dataset, the results of Table D–4 change into: intercept: 0.824, variable z: −0.102, variable temperature: −0.0089, where the

result of the temperature dependency is a little bit insecure, resulting in a positive dependency for the 95% upper bound.
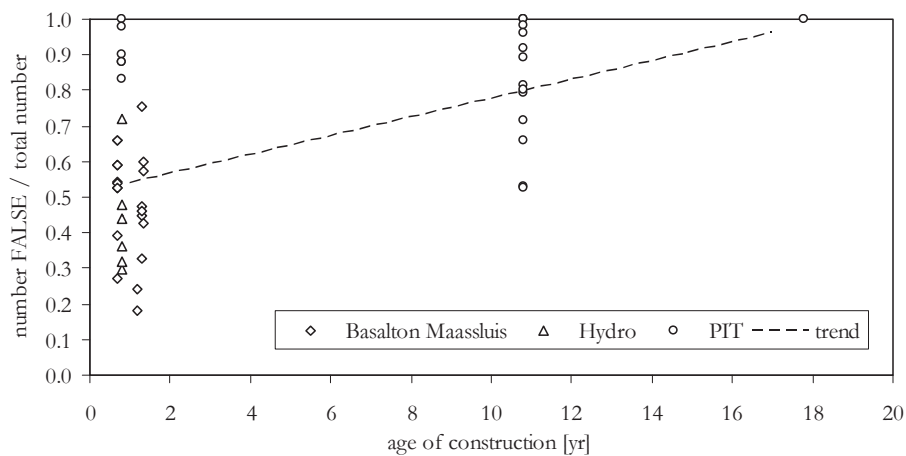
Figure D–18   **Boolean results of small columns vs. age with plotted regression results of Table D–4**
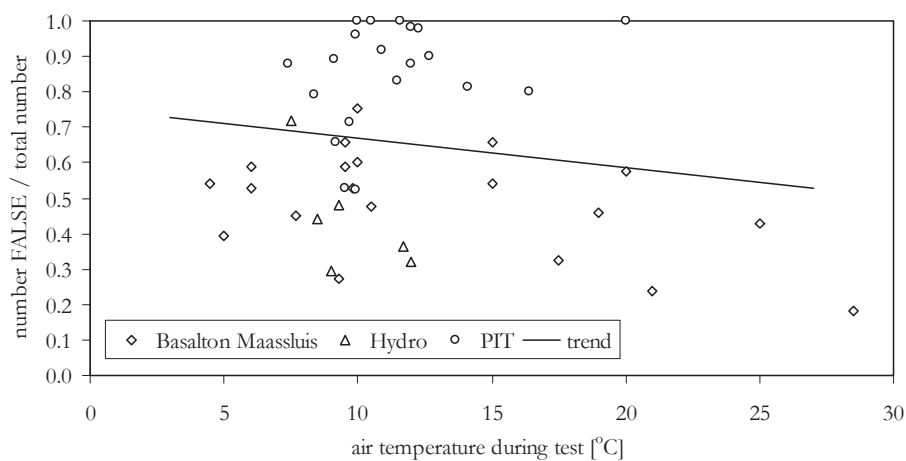
Figure D–19   **Boolean results of small columns vs. temperature with plotted regression results of Table D–4**

In order to get a better picture of what happened to the elements that failed to pass the 900 kg limit, the ultimate forces for all individual tests of the small columns were analysed (Table D–5, Table D–6 and Figure D–20). This dataset has also been analysed, where expected dependencies were found.

	Coefficients	Standard Error	p-value	Average of variable in dataset
Intercept	710	13.0	0	
Variable z	22.9	5.92	0.000115	1.60
Variable temperature	3.49	0.839	3.47×10^{-5}	12.0

Omitting the force results of fixed elements still gives a temperature dependency, but no dependency on z. Since this dataset contains element weights of 30 to 44 kg, the results are better presented as load factors n_{LF}, where n_{LF} is defined as ultimate load F_{ult} / stone weight G. It can be seen that the dependency on the variable z becomes very weak.

Table D–6   Linear regression results small columns: load factors

	Coefficients	Standard Error	p-value	Average of variable in dataset
Intercept	21.3	0.377	0	
Variable z	0.124	0.171	0.469	1.60
Variable temperature	0.186	0.0243	3.38×10^{-14}	12.0
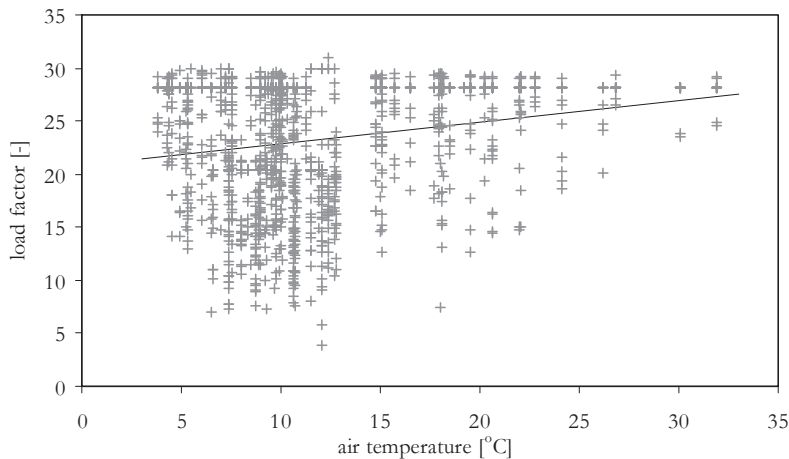
Figure D–20   **Individual test results for FRUE and FALSE tests on selected group of small columns (without age groups above 2 yrs): loadfactor vs. temparature, with plotted regression results of Table D–6**

The results for the selected groups at Western Scheldt dikes (near Breskens) and the Afsluitdijk show a much smaller amount of false test results regarding the 900 kg criterion. The top of the armour slope is higher due to high wave run up at the locations. For the Afsluitdijk z_{top} = 7.75 m +NAP, gradually less steep, for Breskens the top of the element revetment is at +4 NAP. Just above the revetment an asphalt concrete lining starts and goes up to + 7.5 m NAP. The first part of the asphalt concrete slope is 1:5, up to 5.6 m +NAP, followed by a berm section with 1:15 slope. We choose to take z_{top} at +5.6 m.

This dataset contains 2246 tests, split into 14 groups with sizes between 46 and 348, with an average size of 160. The parameters were more uniform over the total population, which

resulted in a smaller amount of bigger groups. This affects the statistical results of the regression analysis. The *p*-values are too high and the 95% boundaries too wide. The dependencies however show logic and comply with the earlier findings.

Table D–7   Linear regression results Boolean results on heavier columns

	Coefficients	Standard Error	*p*-value	Average of variable in dataset
Intercept	0.0853	0.0534	0.14	
Variable z	-0.00763	0.00788	0.36	3.05
Variable temperature	-0.00223	0.00308	0.49	8.77
Variable age	-0.00209	0.00340	0.55	11.7
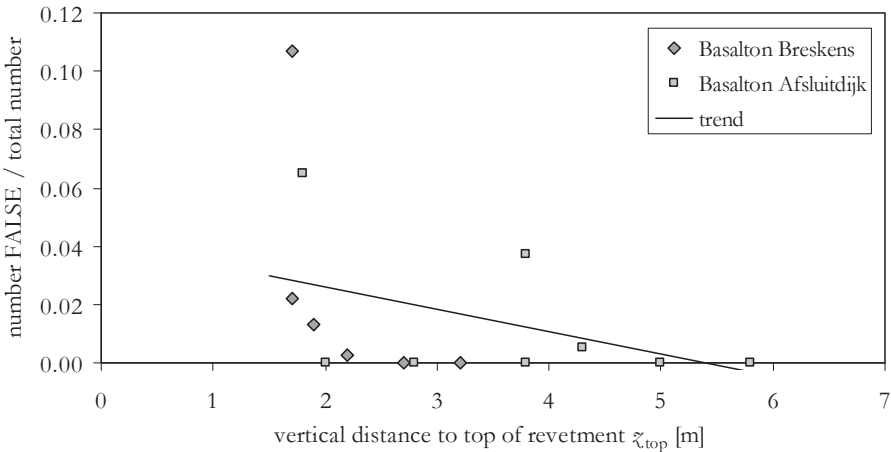
Figure D–21   **Boolean results of Basalton columns at Breskens and Afluitdijk vs. distance z, with plotted regression result of Table D–7**
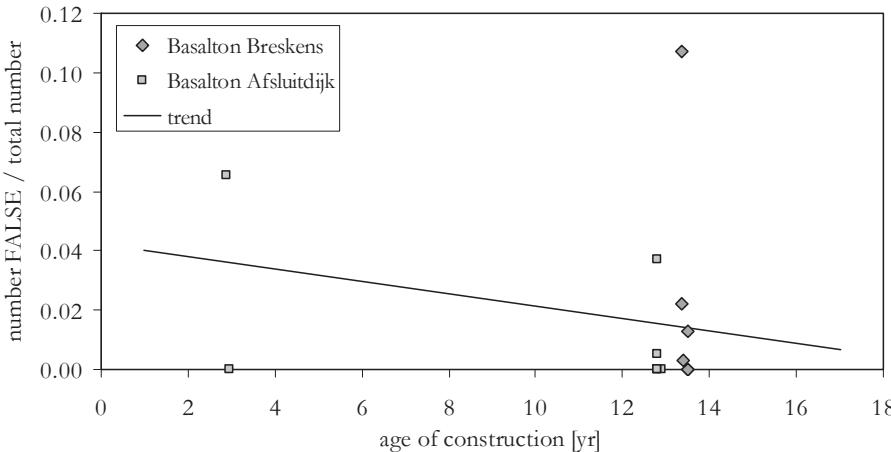
Figure D–22   **Boolean results of Basalton columns at Breskens and Afluitdijk vs. age of construction, with plotted regression result of Table D–7**
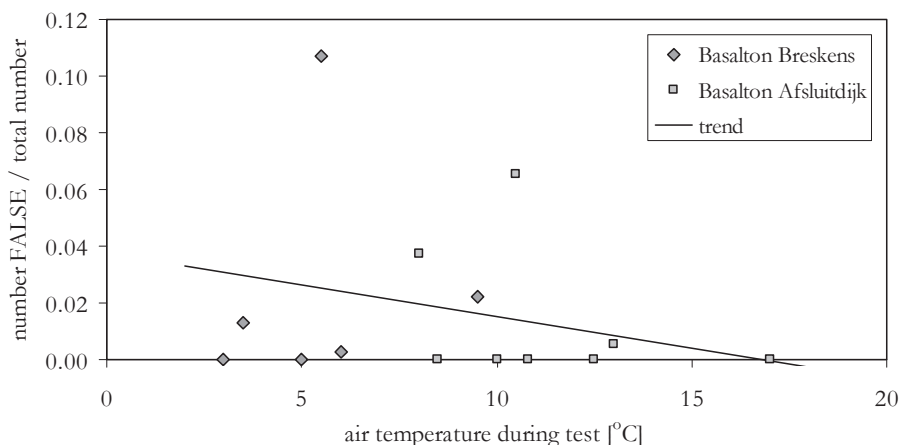
Figure D–23 **Boolean results of Basalton columns at Breskens and Afluitdijk vs. temperature, with plotted regression results of Table D–7**

D.2.3   Comparison of stiffness results

The results on the heavy columns may be further analyzed looking into the displacement data. For the fixed elements there are no actual values of ultimate loads, since the load tests stopped at 900 kg. Based on model calculations (see section 5.8) it is assumed that both the force results and the stiffness results depend on the normal force in the revetment.

As a characteristic parameter of the displacement diagram the differential displacement $u_{600} - u_{300}$ was chosen, representing the difference in displacement normal to the revetment slope at 600 kg and 300 kg pulling force. This parameter was made dimensionless dividing it by the element thickness: $(u_{600} - u_{300})/D$. For the small columns group a choice for $(u_{450} - u_{150})/D$ is more adequate.
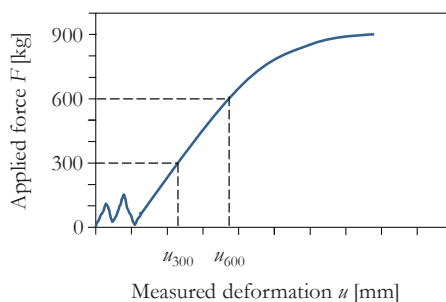
Figure D–24 **Typical force–deformation curve of pull out tests with indication of captured stiffness**

For the group of small columns evidence can be found in plots of strength vs. displacement, where it can be noticed that stronger test are correlated with stiffer tests. The data of the relative displacement $(u_{450} - u_{150})/D$ show a slight dependency on the vertical distance z (also for the FALSE results) to the top of the revetment and a stronger dependency on the temperature. The dataset is filtered omitting displacement values with full slip ($u = 40$ mm),

and for very stiff results which give negative differences $u_{450} - u_{150}$, due to the measurement errors at low values of u (e.g. less than 0.1 mm). Plotting the load factor and the relative displacement in Figure D–25 gives a good correlation. Less strong test results comply with higher displacements. The stiffness parameter $D/(u_{450} - u_{150})$ shows a strong dependency on both the vertical position and the temperature. The stiffness parameter is not a clear actually measured stiffness, but may reflect that in the higher zones more slip occurs.
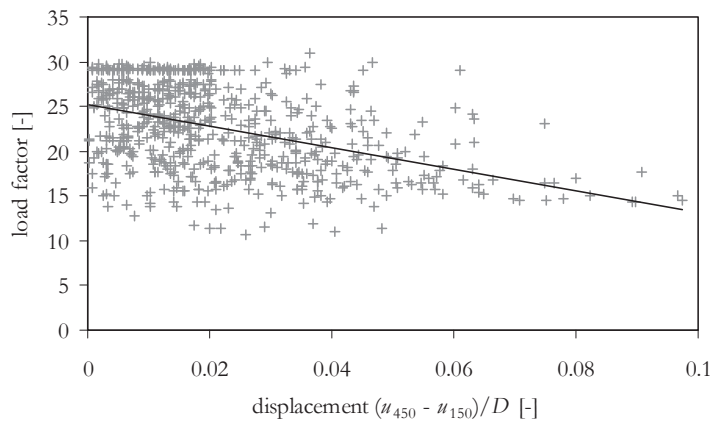
Figure D–25   Small columns: load factor n_{LF} versus flexibility parameter, with linear trend

Table D–8   Linear regression results small columns: stiffness parameter $D / (u_{450} - u_{150})$

	Coefficients	Standard Error	P-value	Average of variable in dataset
Intercept	-54.1	27.7	0.0508	
Variable z	60.9	12.6	1.73×10^{-6}	1.42
Variable temperature	8.015	1.91	3.13×10^{-5}	11.3
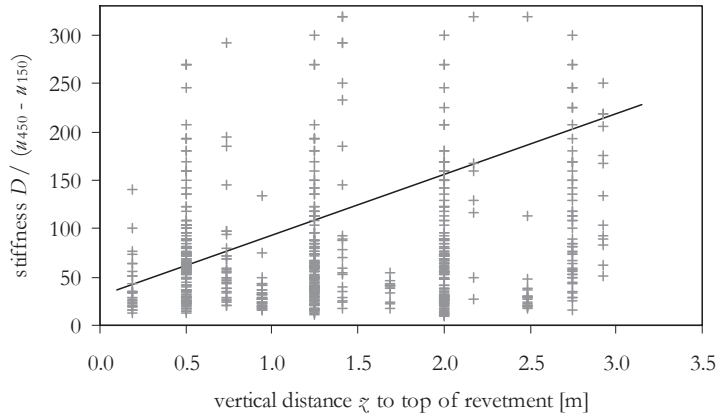
Figure D–26   Small columns: stiffness parameter vs. distance z, with plotted regression results of Table D–8

DESIGN OF PATTERN-PLACED REVETMENTS – ANNEXES

For the Haringman block group a similar approach did not give convincing results.

For the heavier columns group correlation between strength and stiffness cannot be shown, since most of the test results go above the cap of 900 kg. We assume a similar correlation and hence use the stiffness parameter as an indicator of strength as well.
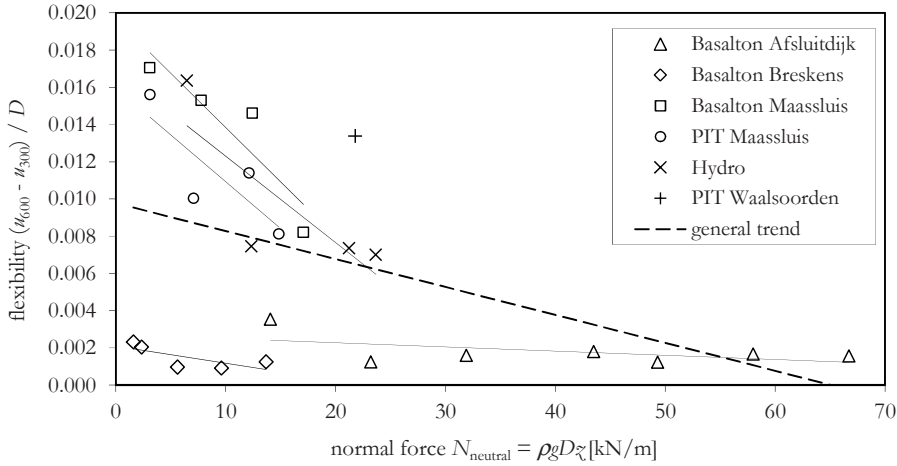
Figure D–27 **Summary of flexibility results for all column revetment slopes vs. theoretical normal force**

In Figure D–27 the stiffness results of all columns datasets are presented (TRUE as well as FALSE tests). On the horizontal axis the normal force $N = \rho g D z$ is indicated instead of z. By doing is differences in ρ en D for the various dataset are expressed also. A correction of the temperature does not decrease the scatter.

D.3   Evaluation with plate model

D.3.1   *Using load displacement relations*

The load displacement relation during the test is investigated by averaging the measured displacements per load step. The result is a softening load displacement curve. The plotted curves are $u/D = c\, n_{LF}^2$, according to Eq. B.34, which perfectly matches with the measurements.

$$\frac{u_c}{D} = \frac{3}{4\pi^2} \frac{\rho g D}{E} \frac{\left(B_x B_y\right)^2}{D^4} \left(n_{LF}\right)^2 \qquad \text{Eq. B.34}$$

Figure D–28 shows the results for three locations, which differ in properties ρ and D. Evaluation of the constants with Eq. B.34, gives the Young's modulus E as outcome. For the locations Afsluitdijk and Maassluis we find $E = 6000$ and 4600 kPa respectively. At both locations there is a limited influence of the location z of the subset of data. Although the load displacement curves of the Afsluitdijk look much stiffer than Maassluis, this is according to the model due to the differences in ρ and D, with the difference of $D = 0.40$ and 0.27 m as most dominant cause.
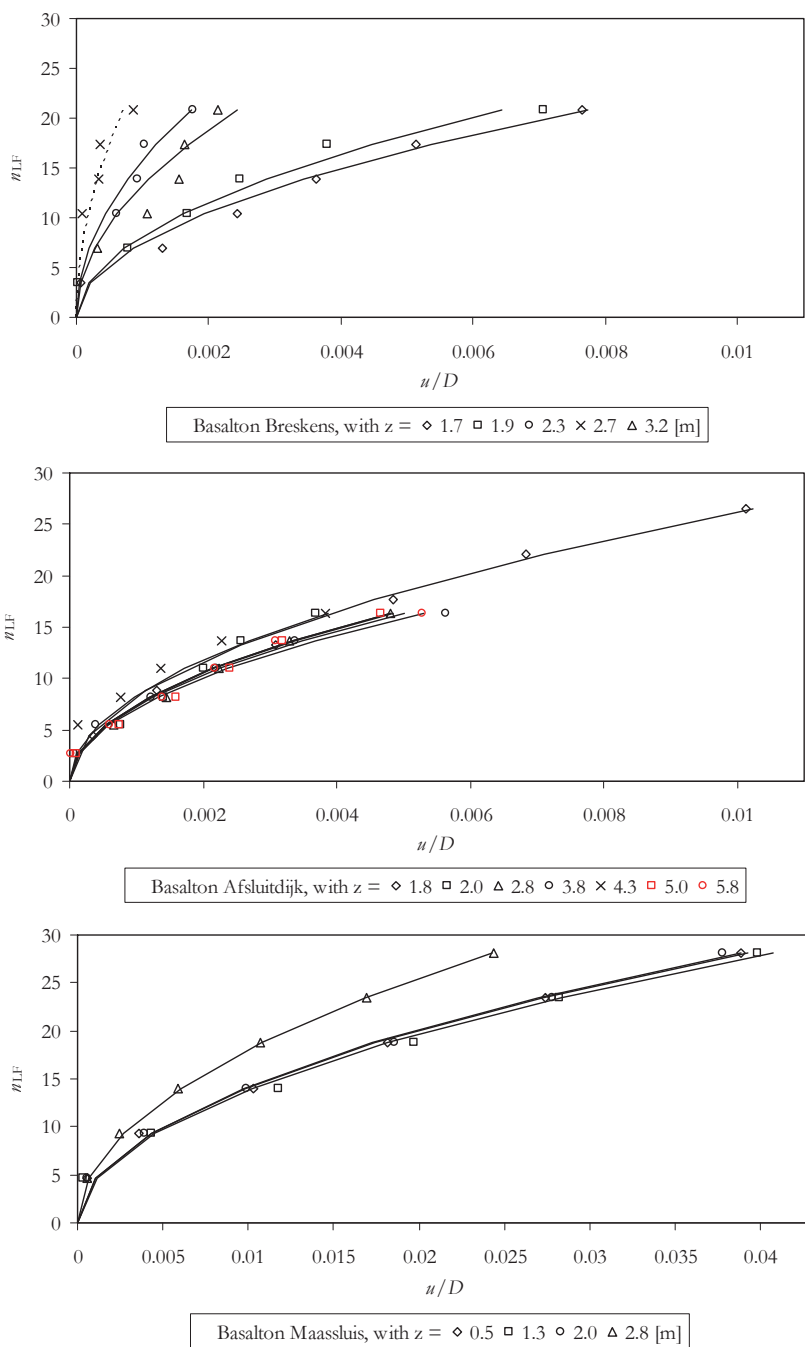
Figure D–28 Load displacement curves with load factor n_{LF} against displacement u/D (Eq. B.34), based on average displacement measurements per load step for the total set of tests

The results for the location Breskens give much more scatter. There is an evident dependency on z, and the results are generally higher. The Young's modulus for the subsets with different z varies between $E = 5500$ and $20,000$ kPa.
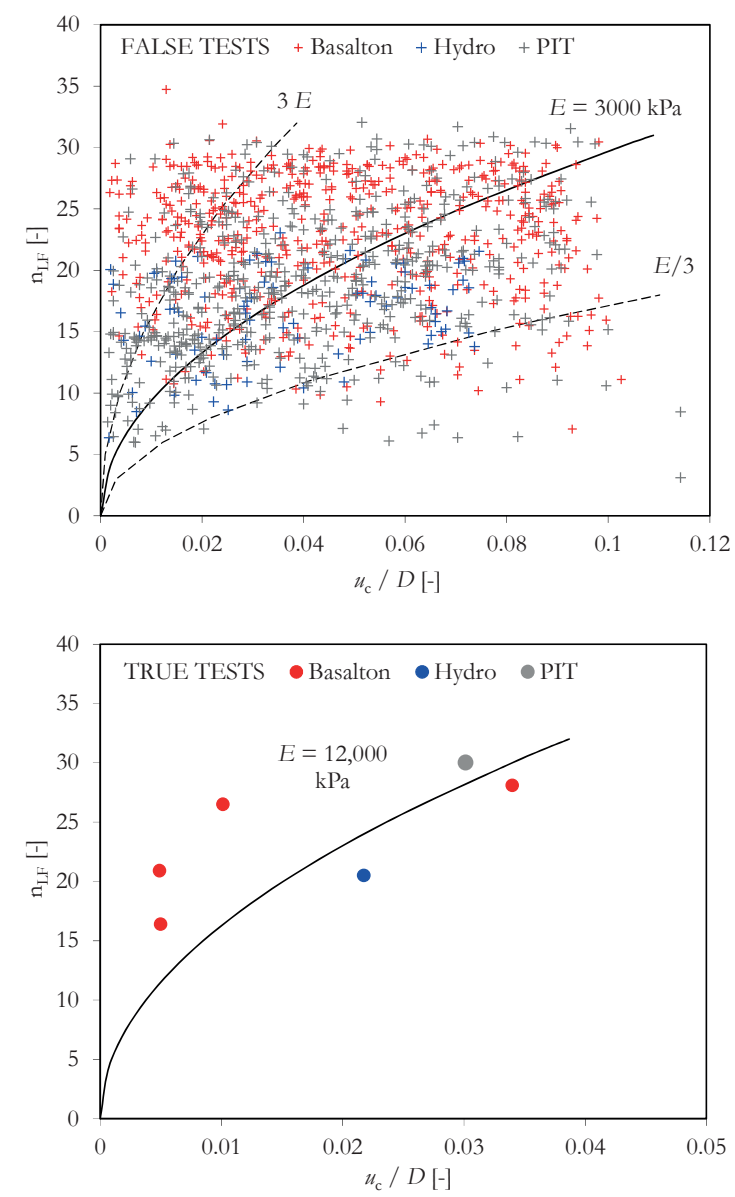
Figure D–29   End points of load displacement curves

In Figure D–29 the end points of the load displacement curves are plotted for all column tests. For the tests with a FALSE outcome the data point before slip failure has been chosen.

FALSE tests show a generally less stiff trend, which is logic as there will be more initial slip deformation in the results. An average value of $E = 3000$ kPa is the outcome of a least-square fit, the scatter is indicated with dotted lines which belong to 0.33 and 3 times this value. For the TRUE tests the average fit curve has a value of $E = 12000$ kPa.

D.3.2   Using model formulas for the normal force

The data sets for the large and the small columns are most suitable for an evaluation with help of the model formulas. The measured load factors can be translated into a minimum present normal force. The sum of the in-plane forces around the pulled element pull-out force P must have a minimum value of $N_p = P / f_{fr}$, with f_{fr} taken as 0.55. Based on the circular model of section B.1 the in-plane force can be re-distributed over the perimeter of the circle with $N = N_p / 2\pi R$ [kNm], with R the radius of the lifted area: $\pi R^2 = n_{LF} B_x B_y \pi/4$. This force is the minimum 'measured' in-plane force N_{test} here, assumed to be present in all directions.
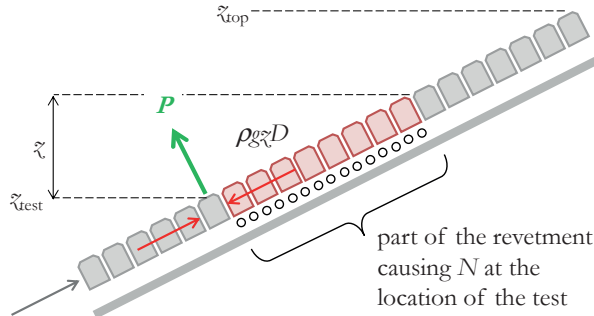
Figure D–30   **Definition diagram of in-plane force**

Further to the omnidirectional presence of the normal force N_{test} we have assumed a neutral longitudinal pressure coefficient of $N_y = 0.5 N_x$. The average of N_x and N_y is $\frac{1}{2}(1+0.5) N_x = 0.75 N_x$. When N_x is caused by a certain length of revetment on a sliding bed, the vertical projection of this length can be calculated from the value N_{test} with the expression $z = N_{test} /0.75 \rho g D$. This length can be made dimensionless by dividing it by the thickness D.
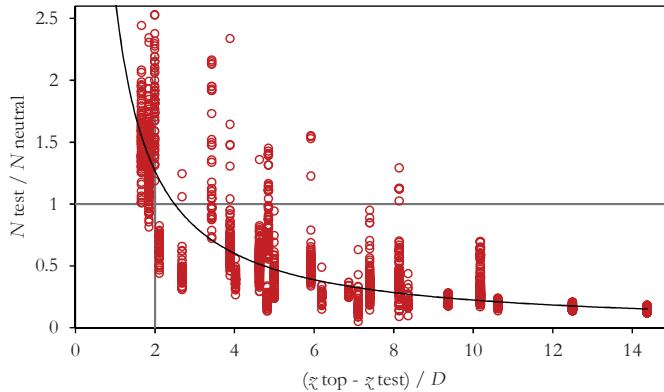
Figure D–31   **Calculated relative normal force versus position on the slope for all column pull tests**
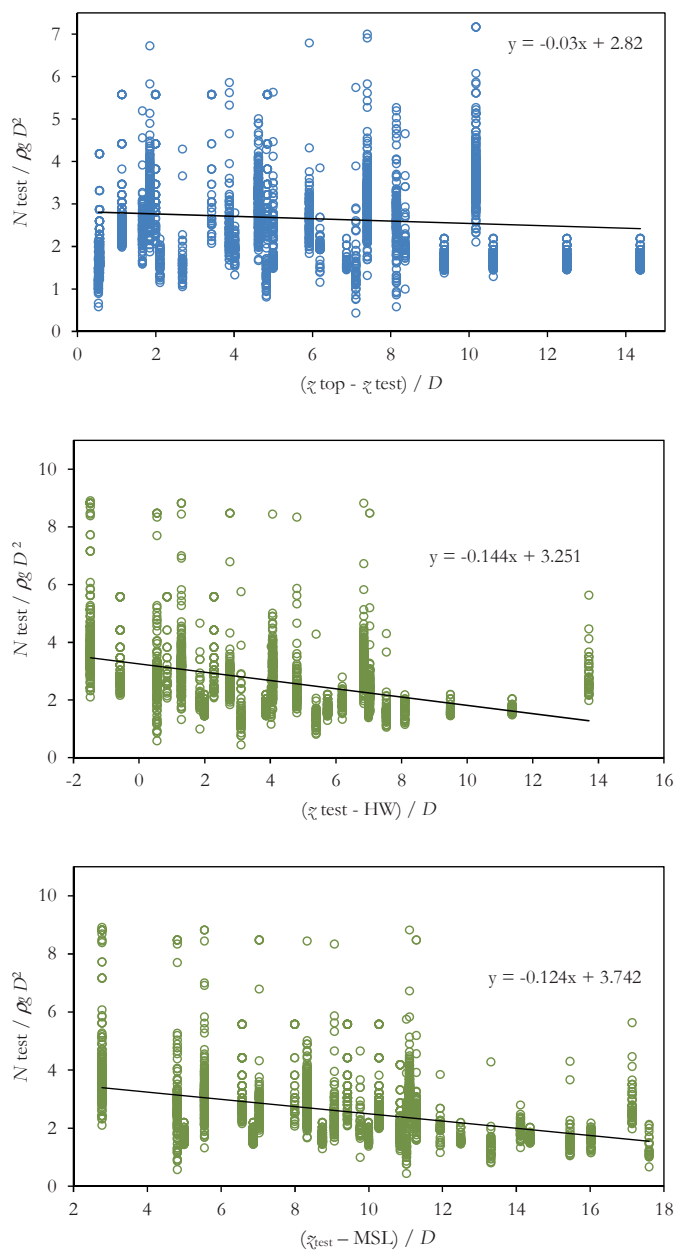
Figure D–32 Calculated normal force levels versus position on the slope for all column pull tests, relative to top of revetment, to high water and to MSL respectively

Analyzing the total population of data points it can be noticed that there is no indication for an increase of in-plane force with position. There seems a rather constant force level, which

can be plotted as the dimensionless $z/D = N_{test} / \rho g D^2$. As explained earlier this is due to the cap of 9 kN, which especially effects the data of the locations Breskens ($D = 0.35$ m) and Afsluitdijk ($D = 0.4$ m). A correlation with position above the MSL level, or above HW spring seems stronger (see Figure D–32).

This image changes when the analysis is limited to the smaller columns at the locations Maassluis and Walsoorden (see Figure D–33, Figure D–35 and Figure D–36). Then a correlation with position on the slope is found, though there seems to be a minimum value independent of the position on the slope. It also appears that the calculated values depend on the parameters temperature and age. The temperature and age dependency are investigated by plotting the variation around the average against the temperature (Figure D–34 and Figure D–37) and the age (Figure D–38). Points $N_{test}/\rho g \, D^2$ are divided by the trend $y = 0.14 \, x + 2.18$, here called 'model', and this quotient is plotted in Figure D–34.

The temperature dependency is assumed to affect the value of the coefficient N_y/N_x. The average temperature in the dataset is 10 °C. The following correction formula is proposed.

$$N_y = \left(1 + \frac{T - 10}{T_0}\right) K_n N_x$$

The sub-group of data points of Maassluis has the widest temperature range. For T_0 a value of 33 degrees was found to equalise the effect of temperature. The Walsoorden points show a positive correlation as well, but have a too small temperature range. The two sub-groups combined give $T_0 = 21$ degrees. The sub-groups of Breskens and the Afsluitdijk show a slight adverse correlation. The dependency of $N_{test}/\rho g \, D^2$ on the age of construction of the slope is weak and not reliable (see Figure D–38).
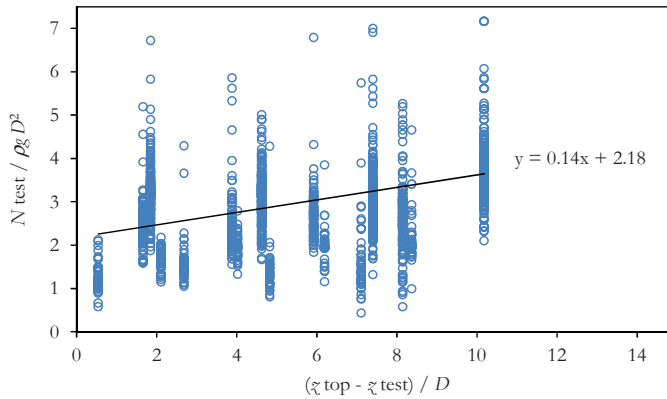
Figure D–33   Calculated normal force levels versus position on the slope for small column tests

The small column dataset consists of the locations Maassluis and Walsoorden of which Walsoorden has the same problem with capacity as the locations Breskens and Afsluitdijk. The data of the location Maassluis are for that reason the best source for estimating the in-situ in-plane force.
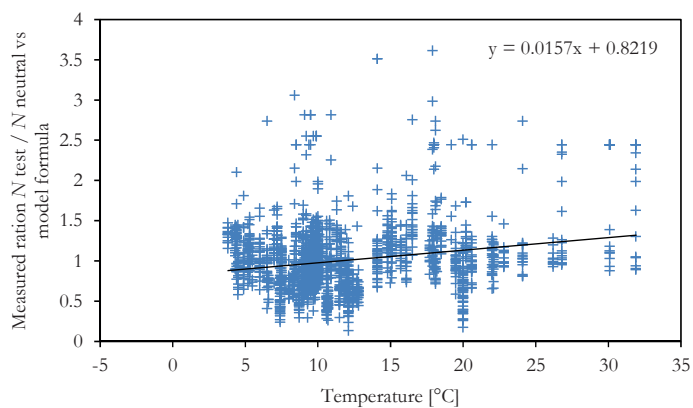
Figure D–34   Calculated normal force levels versus temperature for small column tests
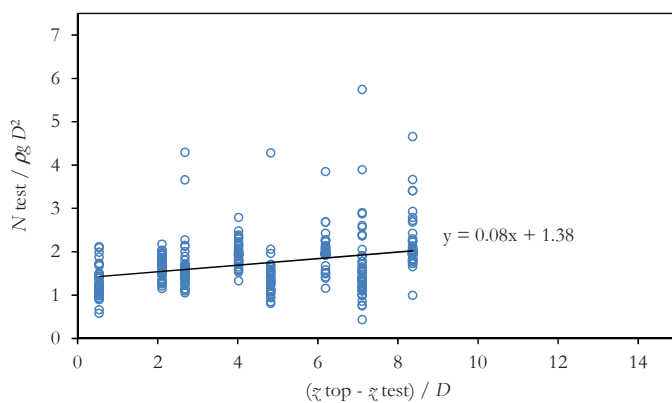
Figure D–35   Calculated normal force levels versus position on slope for location Walsoorden
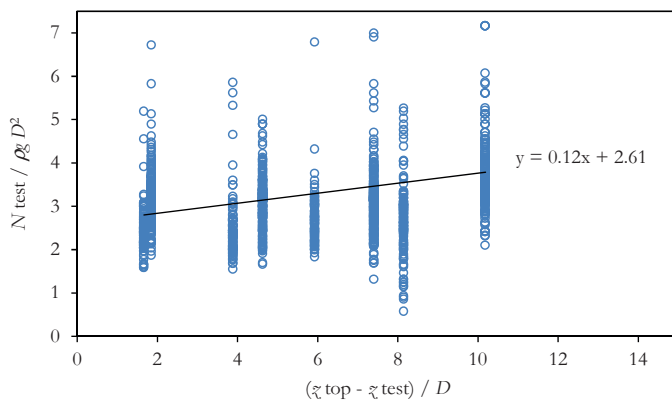
Figure D–36   Calculated normal force levels versus position on slope for location Maassluis
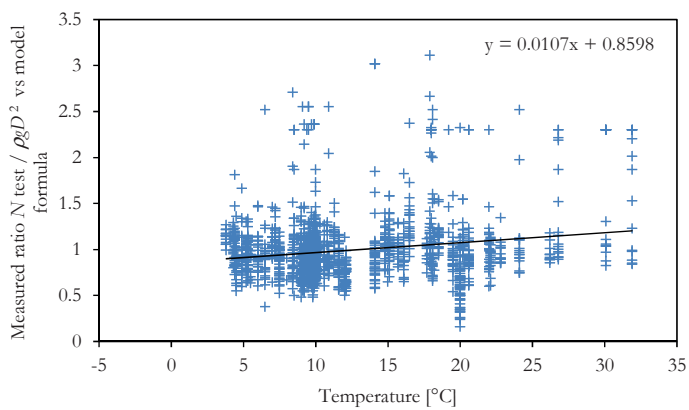
Figure D–37   **Calculated normal force levels versus temperature for location Maassluis**
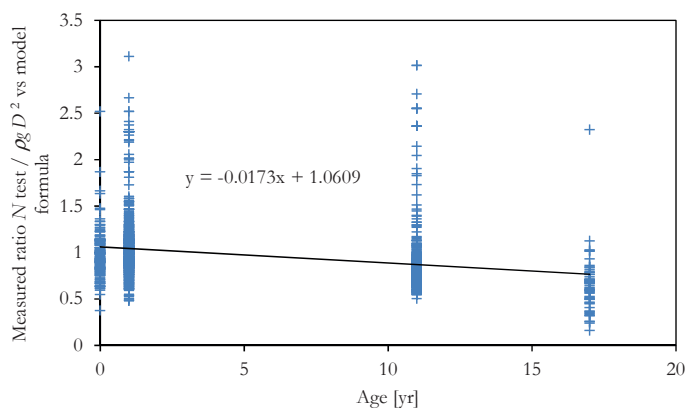
Figure D–38   **Calculated normal force levels versus age of construction for location Maassluis**
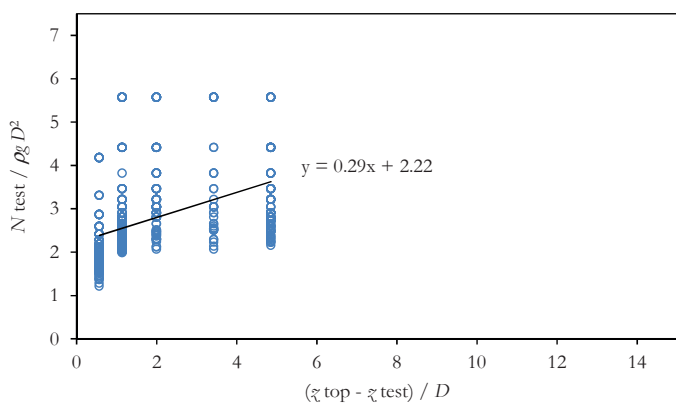
Figure D–39   **Calculated normal force levels versus position for location Breskens**
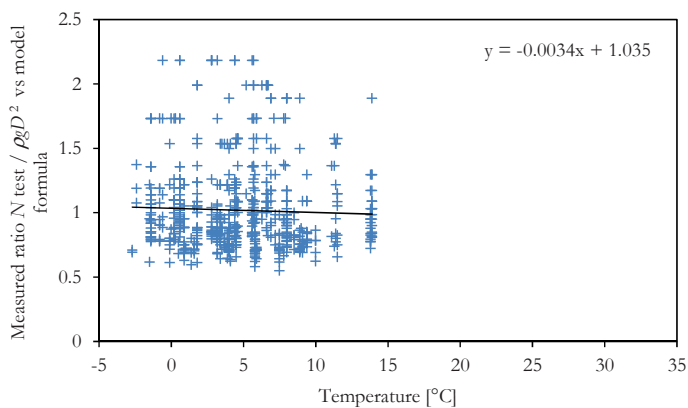
Figure D–40   Calculated normal force levels versus temperature for location Breskens
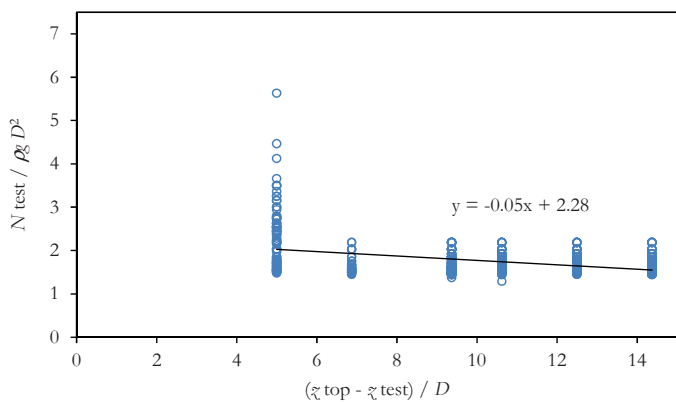
Figure D–41   Calculated normal force levels versus position for location Afsluitdijk
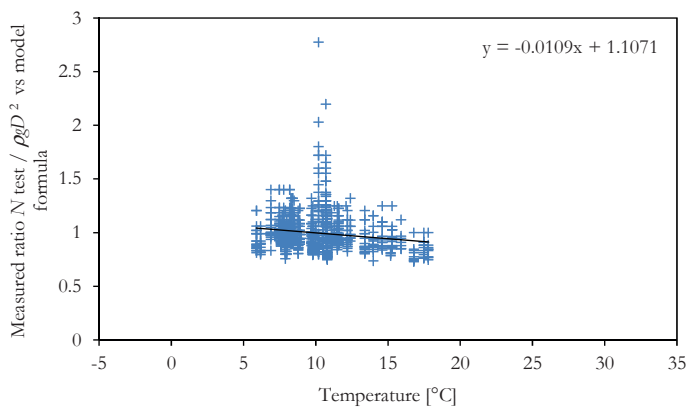
Figure D–42   Calculated normal force levels versus temperature for location Afsluitdijk

In Figure D–43 the data points for the location Maassluis – corrected for temperature – are plotted against position on the slope. The trend suggests an axial force N_x corresponding to a vertical revetment weight of approx $3D$. At a vertical distance of $8D = 8 \times 0.27 = 2.2$ m under the top edge the value is $2.63 + 0.10 \times 8 = 3.43\ D$. The data points follow a log normal distribution with – in this case – a 5% underbound at 0.62 times the average value. $0.62 \times 3.43 = 2.1\ D$.
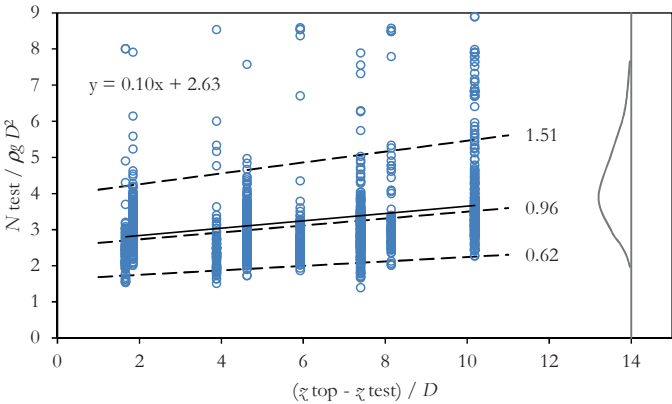
Figure D–43   Calculated normal force levels versus position for location Maassluis

D.4   Findings

As a result of the new analysis of the pull tests a number of findings can be summarized.

Interpreting the pull test results can be summarised as dealing with the big uncertainties and influences of random variables. The scatter in results is very high and remains high after processing and filtering the results.

The distribution of the single results in series of tests follow Weibull extreme value distributions with $1-\exp(x/x_0)^k$, with $k = 4$.

The objective in the interpretation of the pull tests is their relation to the performance of the revetment under real load conditions. The pull test can easily be used for comparisons within the population of tests, between locations or type of revetments. Also in that case it is difficult to judge about what that means for the stability under wave loads, as the types differ strongly in hydraulic properties also. A relation between pull test results and real strength is found in analyzing and relating the pull-test results to the normal force. In Annex A.1 and B.1 the relation between internal and external mechanical loadings is figured out, as well as the stress conditions of the slope. In this Annex D it is attempted to address all dependencies and to connect the pull test results to the stress conditions and other properties (such as the flexural Young's modulus) of the slope.

For the mechanism of a pull out test a uniformly distributed initial packing, bond in the joints, and irregularity of the stone shape and/or the joint material is important to avoid incidental slip out at low load levels. After resistance of forces of approx 10 times the stone weight the friction around the element increases and a circle a elements is activated, where

the ultimate resistance is governed by the initial normal force in the slope. For column revetments the normal force is present, and needs to be present in two directions.

D.4.1 Temperature

In line with conclusions of (Plooster, 1995) and (Coeveld & Klein Breteler, 2003) we find that ambient temperature influences the pull out strength of the tests. The tests have a TRUE or FALSE outcome, whether they pass the 900 kg load or not. For the numbers of FALSE tests in the various series, the temperature influence for the rectangle block revetments is stronger than for the column revetments. Also for the load factors n_{LF} and the measured stiffness of the groups of small columns there is a significant temperature dependency.

A temperature drop from 17.5 to 2.5°C causes a factor of 0.40 less TRUE tests for Haringman blocks, and a factor of 0.30 less TRUE tests for column revetments (which fail at much higher load factors), a factor of 0.15 on the average pull out load factor of the columns revetments and a factor 0.65 loss of stiffness.

Revetment types that are highly susceptible to build up of temperature forces tend to become looser when the temperature drops. Column revetments perform better: due to a larger joint area is the axial stiffness lower, and joint material can move to wider parts of the joints. Column revetments also have the possibility of re-arrangement. Individual elements can move a little bit outside the row, in an upward or downward position. On the scale of the whole structure: temperature expansion in column revetments can lead to re-arrangement and result in transverse expansion, without built up of stresses in longitudinal direction.

D.4.2 Age of construction

Besides temperature dependency, we find dependency on the age of the top-layer as an important variable. It is widely known that revetments need to settle and be subjected to a 'maiden' storm before they are strong enough. It is important that this first wave load is below the design strength. Small damage of young revetments used to be common. The Maasvlakte damage case (refer to section 4.3.3) is an example of a substantial damage as a result of a first wave load (which was also beyond the design load).

Also the pull tests reflect this phenomenon. The influence of the age of construction is for all types of revetment and for all types of results (TRUE/FALSE and the load factors) of the same magnitude as the influence of temperature and vertical position on the slope.

The dependency could be treated as a Boolean for e.g. first year or not, but this does not really cover the effect, since also the settlement is believed to contribute to the increase of strength. Settlement of the dike body is logarithmic in time. In quite a number of the investigated test slopes, the dikes were raised and new stone revetments were placed. In that case a settlement process occurs with significant effects developing over say 5 to 8 years. Given the average lifetime of the structure of 25 years and the change of e.g. 1/10 year that a serious load occurs, modeling the effect of age as a linear process over the lifetime is not unrealistic.

D.4.3 Position on the slope

The position dependency of the pull test results was already observed since the pull tests are carried out. It provides evidence that the pull out strength is related to the normal force in the revetment. For longer slopes a linear relation of the normal force N and the position z was not found. This can be explained because longer slope are generally more gentle, friction between the top-layer and the bedding limits the development of normal force. Moreover long slopes loose effectiveness due to the elastic properties of the joints. The results of the very long slope of the Afsluitdijk (over 30 m) deviate from the results at other locations.

The model in section B.1 gives a formula which produces the required normal force given a certain pull out load factor. The formula is based on 2-dimensional plate action and is therefore only valid for column revetments.

The normal force found to be present in the field during the tests is assumed to be the average normal force in two directions. The magnitude of the normal force in the longitudinal direction is a derivative from the transverse normal force, but effects of element-to-element friction and temperature effects makes this relation inconclusive. For deriving the normal force in the transverse direction we have assumed that $N_y = 0.5\ N_x$. $N_{average}$ is hence $0.75\ N_x$. $N_{x,\ test} = 1.33\ N_{test}$. We compare the normal force N_{test} calculated from the test results with the basic formula is $N_{neutral} = \rho g D z$.

The following conclusions and refinements were found.

- The longitudinal normal force is believed to be susceptible to temperature. We assume a neutral 'pressure' coefficient of 0.5 at 10 °C, which relates the longitudinal normal force as 0.5 times the transverse normal force. This coefficient changes linearly and doubles when the temperature change is 30 degrees. The unidirectional share of the normal force is the average of the transverse and longitudinal normal force.

- The revetment slope becomes stronger over time. This aging effect is not purely due to age, but due to development of a load history of wave loading and survived storms and of dike settlement. The age dependency is difficult to quantify. An age dependency factor following from the formula $0.75 + age/40$ [yr] is proposed, which means that the slope is at full strength after 10 years.

- A factor which corrects the normal force on very long slopes is proposed as well. This factor depends on the length of the slope and the position of the slope and is given with Eq. D.1.

- Evidence was found that for slopes where the test force was sufficiently high an average in-plane force of at least $3\ \rho g\ D^2$ is present, which increases with lower position on the slope. The scatter of the measurements is high, and typically follows a lognormal distribution, with a 5%-underbound of approx $2\ \rho g\ D^2$. With the set-up of the experiments discussed in Annex C and D it was not possible to find evidence of higher normal forces. Reference is made to field pull experiments based on an improved test design as a part of this study (see Annex G). Based on those tests higher normal forces were found.

ANNEX E   TESTING BENDING AND SHEAR IN THE TOP-LAYER

Single element pull tests have been a preferred empirical test method in the 1990s. The evaluation of these tests in annex C and D shows – amongst other findings – that the simulation of the effect of the real wave loads is poor. The single element tests on prototype structures produce results with a large scatter. The resistance of revetment slopes against concentrated pull out loads is highly unpredictable. Wave loads however tend to load groups of elements at the same time.

This Annex describes the design, the execution and results of new pull tests that represent an attempt to simulate wave loading on a group of elements. The tests were carried out in the Stevin II Laboratory in Delft.

The scope and aim of the tests are described in section E.1. The aim of the tests was to study plate bending of the revetment structure. The revetment was loaded with a distributed load, rather than with single element pull forces. A theoretical model (see annex A.3) and a test result prediction derived with that model are presented in section E.2. The test set-up and typical phenomena and results are described in section E.3. The results are quantified and summarised in section E.4 and evaluated and compared with the predictions in section E.5. In section E.6 it is concluded that the tests are a successful demonstration of a plate bending failure with a three-hinge bending mode.

E.1   Scope and aim of testing bending and shear

In the model hypotheses the revetment top-layer is assumed to act as a beam or plate structure. The axial forces in the structure create a coherent structure with joints of certain strength. In 2003 a laboratory test program was designed and executed[295]. The purpose was to verify the principle and determine the parameters of the beam action of a revetment layer. A portion of revetment top-layer with known conditions regarding axial forces and constraints was subjected to pull forces at right angles to the top-layer. The test was meant to imitate the load caused by uplift pressure under a poorly permeable top-layer, occurring shortly after a backwards moving wave front. The uplift pressure was assumed to have a constant value over the width over the revetment strip of the specimen (1.5 m), representing the longitudinal direction of the dike. In the transverse direction of the dike, a half wave length sinus function was assumed, representing distributed uplift forces that have a maximum under a certain row of blocks. In the test program the base length and the magnitude of the uplift load were varied. These variations represent the size of the wave and the value of the permeability relative to the revetment element size.

In the test set-up the in-plane forces act in the transverse dike direction only, and have a constant value. The applied boundary condition with a known force was meant to represent that the revetment beam in the real world can expand itself, and cannot generate much more axial force.

---

[295] S. Schoen, "Liggerwerkingsonderzoek van steenzetting op een wrijvingsloze bedding - Meetverslag van trekproeven" (MSc thesis TU Delft, part II, 2004) and D.J. Peters, *Laboratory testing of clamped placed revetments* (RH report 9P0669 for RWS-DWW, Delft Cluster ref. DC2-710-1, 2004)

Clamped beams with infinite stiff boundary conditions experience a length restraint and will generate an increase of axial force when they try to expand. This model boundary condition was adopted in a small scale timber test model of a beam of blocks, which was pre-stressed and locked with a wedge, and subsequently loaded with a lateral force[296]. The result is a very high resistance, caused by an unlimited increase of the axial force.
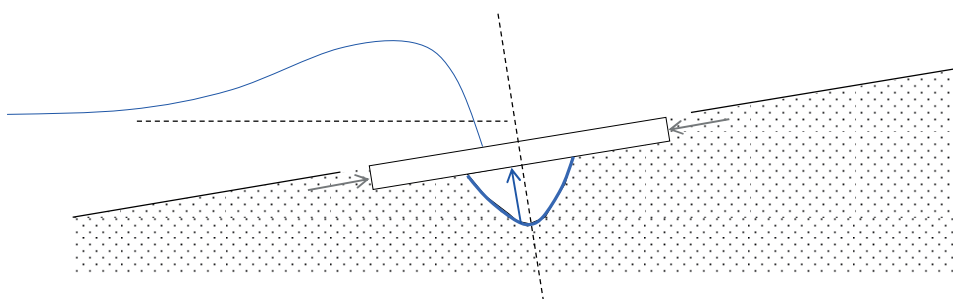
Figure E–1   Position of test specimen with wave front and uplift forces
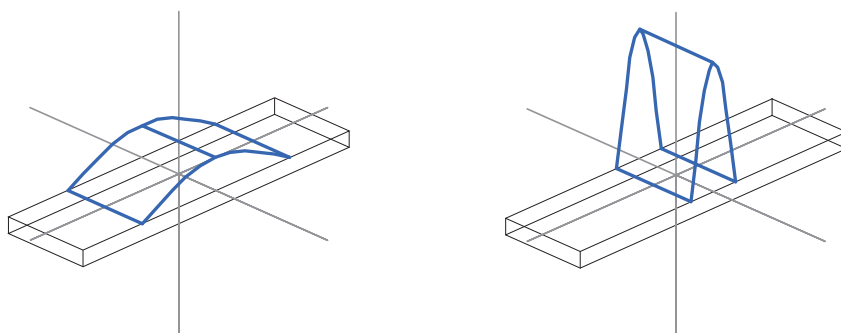
Uplift load of low magnitude distributed over bigger area

Uplift load of high magnitude distributed over smaller area

Figure E–2   Test specimen of 6 × 1.5 × 0.15 m with load geometry

The goal of the test series was to confirm that a revetment top-layer could resist distributed uplift forces while the elements experience an in-plane pre-load. The second goal was to retrieve load level and displacement data for analysis of the mechanical joint properties, as their flexural stiffness, bending capacity and shear strength. The testing of a revetment beam with a distributed load has no precedent. It especially relevant to find possibilities to connect the results with results of single element tests (Annex C and D).

---

[296] B.P. Rigter, *Inklemming van blokken in een rij* (Internal note DWW, 1995)

E.2 Methodology

E.2.1 Model and interpretation method

The test design was based on the confined beam model of section A.3. A revetment top-layer section was tested at full scale, although the smallest available elements were used, 0.15 m thick. A known normal force P was applied on two edges of the model using hydraulics jacks. On the other two edges axial spring constraints were applied. The revetment specimen rests on timber plates on rollers, in order to avoid any loss of axial forces due to friction. Distributed vertical loads were exerted on the rows of stones. The stones in one row were loaded with equal forces using springs. The distribution of the force over the various rows was according to the sinus shape of the model and was applied using balanced beams (see Figure E–3). The number of loaded rows varied from 1, 2, 4, 6 to 8. The magnitude of the total applied vertical force was the unknown parameter. The vertical forces as well as the displacements of all revetment elements were measured. Displacement measurements were executed with optical methods where 3 displacements and 3 rotations were surveyed using stereo photography with two cameras and markers on the stones. This was performed by TNO-TPD in Delft. An accuracy of less than 1 mm was achieved. The axial deformation of the test model was also measured with telescopic electronic transducers.
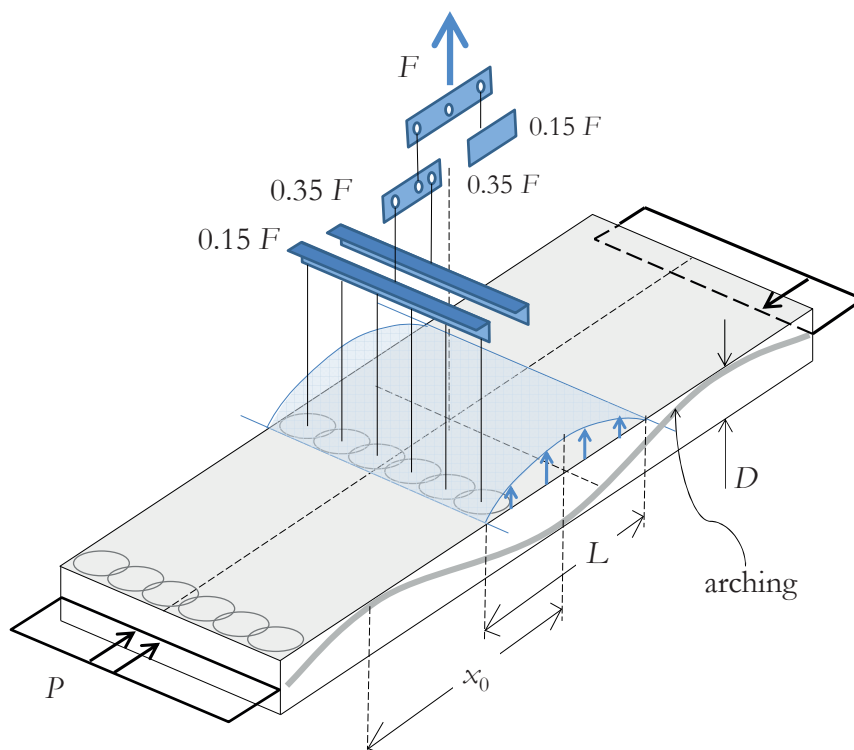
Figure E–3   **Experiment set-up**

E.2.2 Test set-up and execution

The test set-up is shown in the axonometric picture in Figure E–3. The relevant test parameters are listed in the tables.
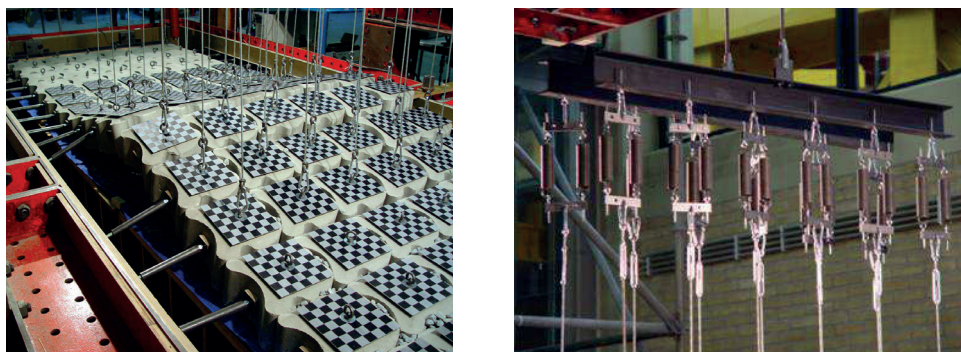
Figure E–4 **Test execution with (left) deformed shape and stereo-metric markers and (right) load distribution beams and springs**

Table E–1

Parameter	Applied variations / remarks	
Element type	Hydroblocks 15 cm, orientation 'fish' in cross direction 2350 kg/m³, test model size 1.5 × 5 m², 16 elements/m²	Design variable
	Basalton 15 cm, type 'Talud' *) 2350 kg/m³, test model size 1.1 × 4.4 m², 30 elements/m²	
Joints	No joint fill	
	Washed in with Noors granite 5-11 mm Also variation of a) first jacking, than washing in and b) first washing in, than jacking	
Sandy joints	Mixing the joint material with sand/bentonite	Conditions variable
Axial force	Low / moderate / high stress level, corresponding to 1, 2 and 4 m²/m top-layer weight	
Load length	L = length 'half' sinus D = element thickness Investigated range of L/D = 1.5 − 13 For the Hydroblocks 15 cm: B/D = 1.67 For the Basalton 15 cm: $B/D \approx 1.15$	Load variable

L/D	1.67	2.3	3.33	6.67	6.9	10.0	13.3
Rows Hydrobl.	1		2	4		6	8
Rows Basalton		2			6		

*) The Basalton type 'Talud' is not the regular type used for dykes, but for protection of steep, dry slopes of abutments.

Table E–2

	Hydroblocks 15 cm	Basalton 15 cm
Shape	fish-shaped	Randomised hexagonal
Element size	0.25×0.25 m	small: 0.15×0.15 m middle: 0.17×0.17 m large: 0.19×0.19 m
Number of elements in test	6×20	4×24
Test specimen size	1.5×5.0 m	1.1×4.4
Element specific mass	2350 kg/m³	2350 kg/m³
Element mass	18.6 kg	7.7, 10.3 and 13.4 kg

Table E–3

	Hydroblocks	Basalton
Pitched stone layer mass [kg/m²]	300	312
% open space	15%	12%
Mass, including joint fill [kg/m²]	325	332

Table E–4

Applied horizontal preloads [kN]	Hydroblocks	Basalton
Middle	10.4	7.6
High	20.7	15.2
Bi-axial preload	2%	5%

The stiffness of the spring supports at the sides was 13.5 kN/m.

The rate of loading was relatively slow. There was no intention of measuring dynamic effects.

The tests were designed to apply repeated loading at different load levels as well as ultimate loading in one load path. The behaviour under small repeated loading as well as failure at large displacements were in the scope of interest.

For the test design model prediction calculations were made using a basic version of the confined beam model of section A.3. The model predictions were used to define the test programme and the scope of variation of parameters to be tested.

The vertical force was applied with a manually operated hydraulic jack. At large displacement rates the jack did not retain the pressure, which – unintentionally – resulted in a displacement controlled load path. This provided measured data of the unloading branch during progressive deformation of the revetment specimen (see Figure E–5).

E.3   Test results

The test results proved that the specimen could be loaded and deformed showing a three point bending failure. There were hardly any loose element failures noticed. In a number of cases the model showed a skew, sideward sloping displacement field. No shear slip failure of stones or complete rows was noticed before the peak load was reached. At excessive deformation distortion of the original model geometry occurred, with as a consequence shear slip failure between the blocks.

The results can be expressed in load deformation diagrams. These diagrams show a nice correspondence with the snap-through buckling theory. The initially steep rising branch of the diagram shows softening, reaches a maximum at a displacement of a few centimetres, and shows a linear slowly descending branch.

The slope of the descent appears to be roughly dictated by the end situation of the test. Between 80 and 100 mm vertical displacement shear slip occurs between the loaded and unloaded rows, which results in a vertical load of roughly the gross weight of the pulled rows. The tests with a small number of pulled rows, therefore have a steeper downward branch. Figure E–10 shows the expected and measured ultimate forces and (in the dotted line) the force level to which the load falls back at the end of the test.
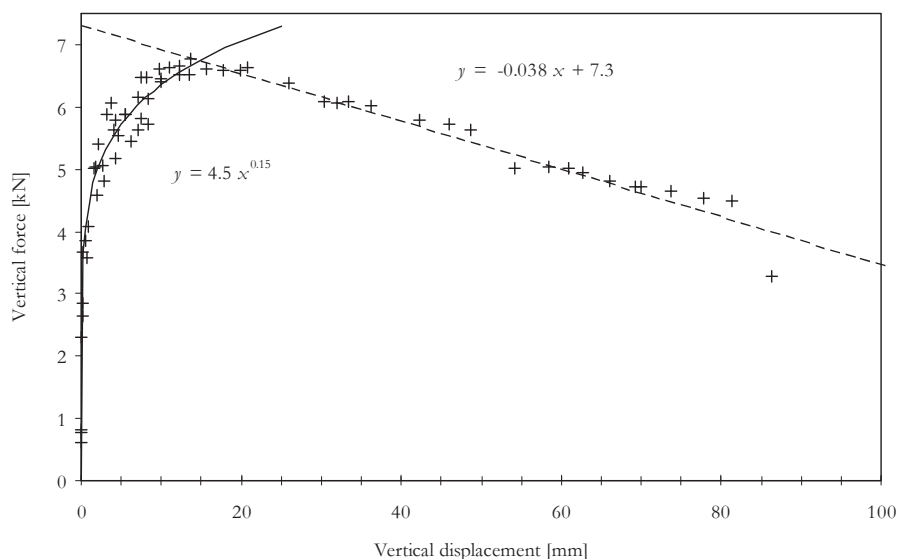
Figure E–5   **Measured forces and displacements of repeated loading and unloading within test no S08, Hydroblocks, 2 rows, middle pre-load. Displacements averaged over the rows.**

The typical power function of the idealised force-displacement diagram can be written as $y = a\,x^b$. The calculated coefficients a and b appear to have a considerable scatter. The variation coefficients of a and b in the different groups of similar tests are 0.23 and 0.37 respectively. Average values can be used as an indication of the measured initial stiffness values. The effect on the test parameter variations on the initial stiffness are shown in Figure E–6. The effect of a distributed load over more rows increases the stiffness. A higher pre-load also produces an increased stiffness. The Basalton tests appear to be significantly less stiff than the Hydroblock tests.
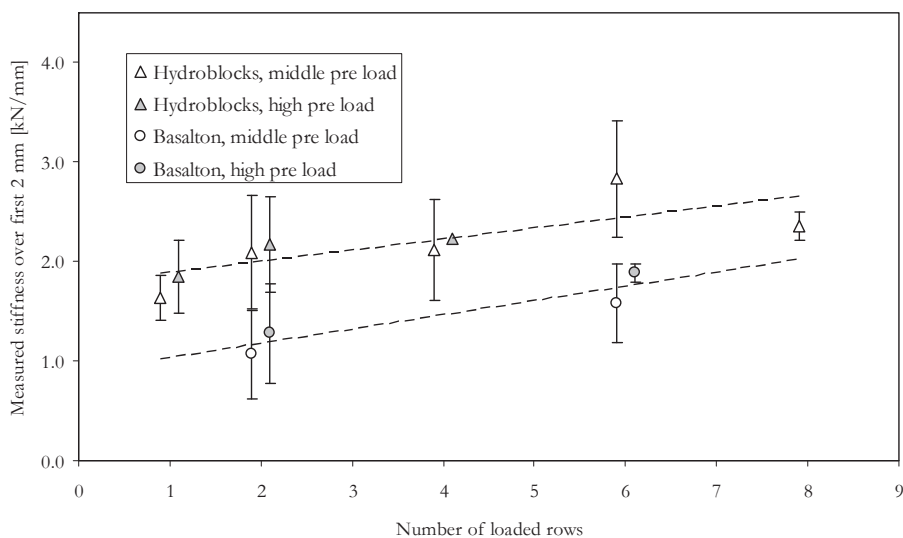
Figure E–6 **Measured stiffness total vertical force / vertical displacement; the error bars show the standard deviation of the displacement measurements within a group of similar tests**
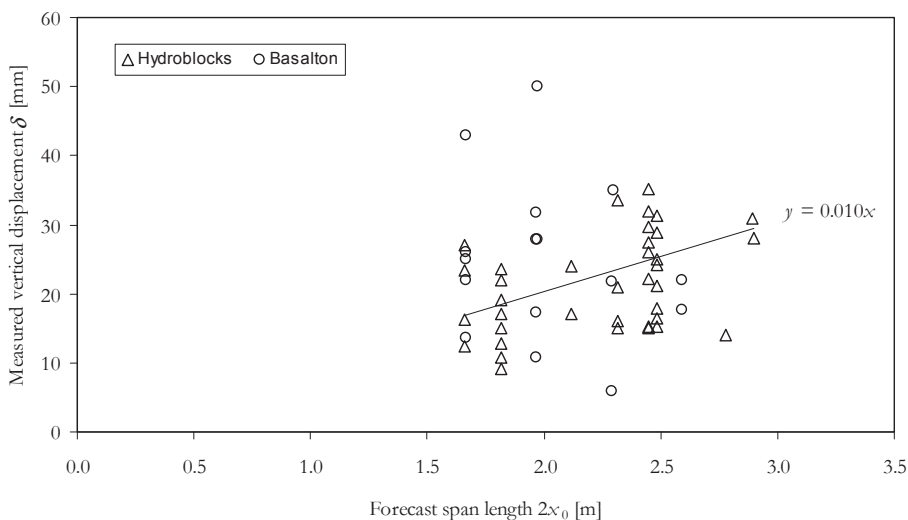
Figure E–7 **Measured vertical displacement at maximum load versus the predicted free span length**

The displacement at the load summit point appears to depend on the length of the free span. See Figure E–7. The snap-through buckling theory with clamped boundaries (see section A.5) predicts a constant value of this displacement of 0.4 D, which is 50 to 60 mm for this case. The measured values are much lower which can be understood, since the failure load in this test depends on the product of the (constant) axial load N and the effective eccentricity

($e = D - \delta$). The theory with infinite stiff edges allows the axial force N to increase, where the maximum of the product $N \times e$ can occur at larger values of the displacement δ. The vertical displacements at the failure point show a wide scatter. The average is found at 0.01 times the span length. This average is implemented in an improved model forecast.

E.4   Feed back to modelling

The model forecasts for the measured forces based on the confined beam model of section A.3 can be improved using the measured displacements and the results of sub groups.

An improvement in modelling is found in implementing the joint model of section A.4 with a dedicated choice for the ultimate stress levels in the joints. The adopted stress levels express the real geometry and stress concentration occurring in the joints. The Basalton and Hydroblocks strongly differ in regularity of the element perimeter and stone orientation. Hydroblocks create contact faces, Basalton creates contact lines. As soon as the elements start to rotate contact faces reduce to lines, and vertical contact lines reduce to concentrated spots. The simple joint model formulas use an upper stress limit. If these stress is lowered for the Basalton, counting for the much smaller contact area on plan (with in reality higher peak stresses), this leads to an increased vertical dimension of the stress area. Also a variation of this stress parameter dependent on the joint fill is implemented, as well as a difference in effective block height d, being 0.12 m for the Basalton and 0.14 m for the Hydroblocks.

Table E–5   **Upper bound for distributed stress in the joints in the model calculations**

σ_u [kPa]	Basalton	Hydroblocks
Washed in granite	225	400
No joint fill	180	320

Adopting the stress limit levels in Table E–5 in the model calculations the average deviation between calcultated and measured ultimate forces equals to approx 0.86. In subgroups for the pre-stress levels, for the element types and for the joint conditions a similar accuracy of the model results is found. See Table E–6. This makes the model adequate for the investigated range of design and load parameters.

Table E–6   **Typical statistical data of test results**

	Hydroblocks		Basalton	
Axial pre-load level	middle	high	middle	high
Number of tests	24	13	7	5
Average factor experiment / model result	0.87	0.86	0.84	0.92
Standard deviation	0.050	0.045	0.089	0.012
Variation coefficient	0.06	0.05	0.11	0.01

The measured ultimate force results show a positive correlation with the axial load level as the confined beam model suggests. A doubled axial pre-load is able to produce a higher vertical force result. If we compare the results of all pairs of tests where the only difference in parameters is the axial pre-load, it can be found that the chance of an unexpected lower instead of a higher force is equal to $p = 10^{-3}$ for the Hydroblocks. For the Basalton this

chance is $p = 0.76$, which means that there is a negative relation as outcome of the measurements. The equilibrium beam model would predict a positive relation, but the improved model with limited joint strength is able to predict the reverse relation. In Figure E–9 the values of axial pre-load N relative to the axial capacity N_u are plotted in the failure envelope of the joint model. It can be understood that for the Basalton tests the high normal force in the tests corresponds with a slightly lower bending moment. Due to the lower ultimate joint stress σ_u the pre-load level of the Basalton tests was closer to the value of N_u.
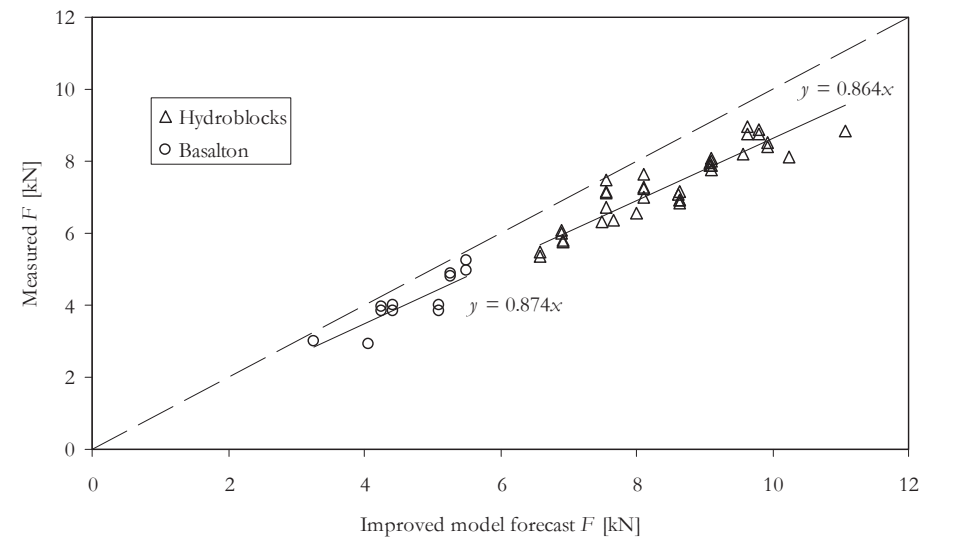
Figure E–8   **Measured versus hindcasted ultimate forces**
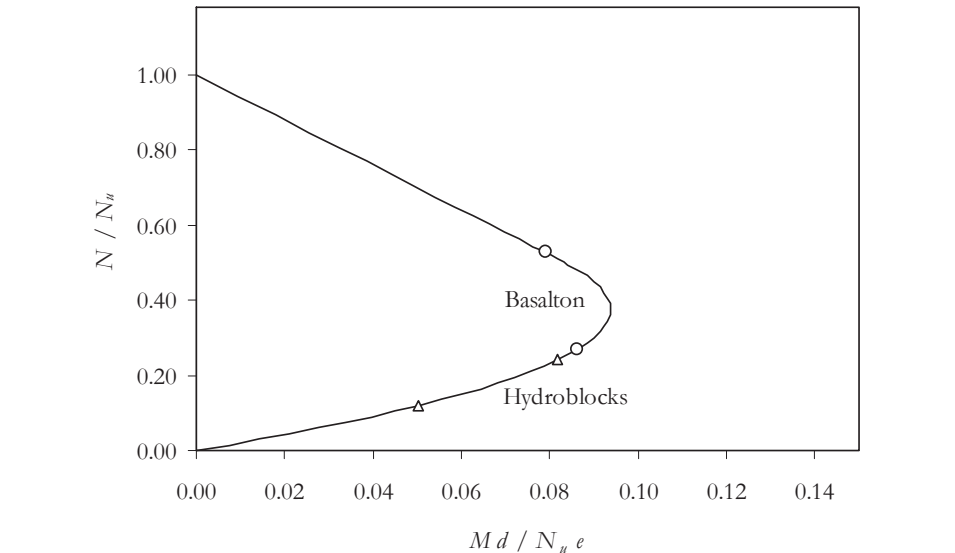
Figure E–9   **Hindcasted values of N/ N_u for medium and low normal forces in failure envelope of joint model with strength values in Table E-5.**
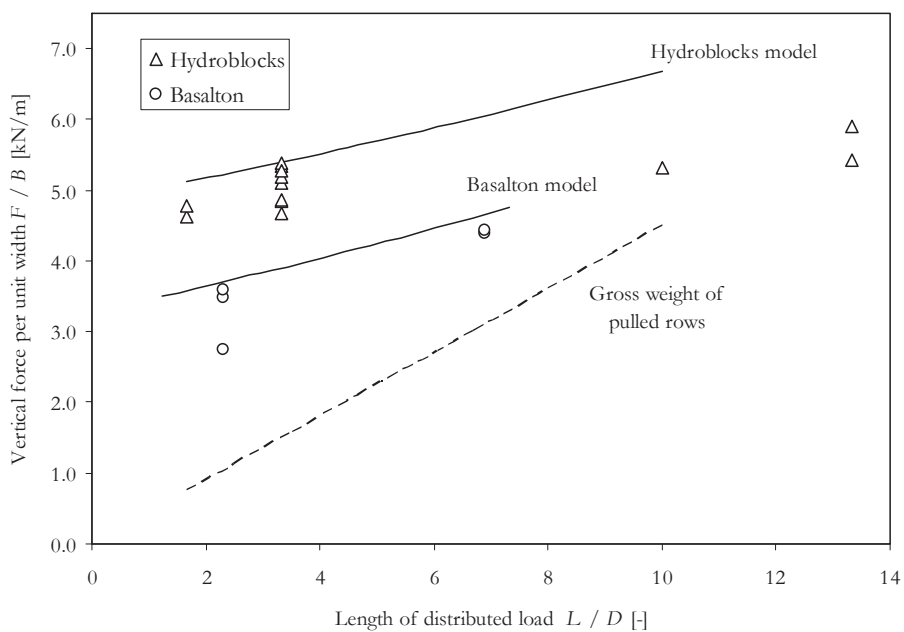
Figure E–10   **Test results compared with model results plotted as forces.**
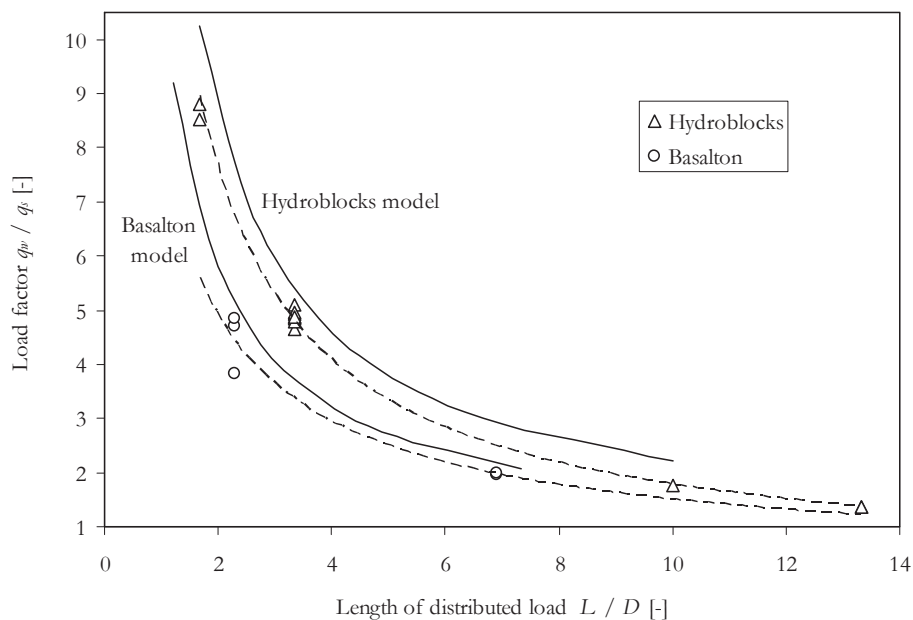
Figure E–11   **Test results with trend lines based on power functions, compared with model results, plotted as load factors**

E.5 Discussion and conclusions

The laboratory test series provides evidence that pull out strength depends on the axial force level. The axial forces enable the revetment elements in the layer to jointly act as a beam. A model based structural mechanics of beam action and a model describing the strength of the joints predict and explain the measured strengths the revetment layer subjected to loading on angle.

When the revetment layer is loaded with forces that exceed the element weights, the initial deformation of the revetment layer follows a bell shape. An increasing load, causes a bigger area of elements to lift from the foundation layers and span freely. The failure mode and final deformed shape is a three-point bending mode, where the rotation concentrates in the hinges. The bell shape is replaced by a saw tooth shape.

The vertical deformation is accompanied by in-plane deformation of the beam. At failure, where the vertical deflection δ typically equals 0.2 D, a horizontal extension of about 10% of the vertical deflection occurs as a second order effect. This phenomena will, if combined with restrained edges, generates a wedge effect which may increase the axial forces in cases where these can be resisted.

In a separate limited series of tests, the pull tests were repeated on a gravel foundation instead of the board-and-roller foundation. Horizontal movement on the gravel foundation would generate friction forces which will contribute to an increase of the axial force. This was actually observed. For all similar tests 5 to 15% extra strength was measured. This extra strength was caused by extra axial force generated by the measured horizontal deformations of 1.5 to 2 mm.

A singular phenomenon is that at the very beginning of the upward vertical deflection of the blocks axial shrinkage is observed. Soon after the vertical deflection increases this flips into axial extension. See also section A4.4 and refer to (Derkzen, 2004)[297].

The tests of the revetment layer on a gravel foundation were also used to determine the axial strength and stiffness parameters. The Young's modulus for axial compression of the system of elements and washed-in joints is measured as 30 MPa. This figure roughly equals the stiffness values of stiff granular soils and is roughly 500 times less stiff than mass concrete. When an axially pre-loaded portion of revetment structure was released, there was hardly any relaxation measured. The level of axial compression could be retained in the middle of the model because of the friction forces generated by the weight of the blocks in the edge zone of the model. Calculated friction coefficients were roughly 0.65. Friction is further studied in annex F.

The normal/axial stress state in revetments on slopes in reality is further studied in annex G.

---

[297] B. Derkzen, *Constructief ontwerp van steenzettingen voor dijkbekleding - Numeriek onderzoek naar de liggerwerking van de toplaag* (MSc thesis TU Delft, 2004)

ANNEX F   TESTING AXIAL PROPERTIES AND BEDDING FRICTION

Friction between top-layer and granular sub-layer plays an important role in the pattern-placed revetment structure. As a part of developing the models and model verification in this study additional testing of friction properties has been performed.[298] Those tests are collected and described in this Annex.

The friction coefficient or friction factor between the revetment elements and the granular sub layer underneath, as well as displacement values were investigated with a test campaign in laboratory conditions. The aim of the testing was to describe friction behaviour and to establish properties relevant for the in-plane stress state of the revetment, as described in section F.1. Some literature on friction coefficients is available and has been explored first.

In section F.2 the laboratory test set up with a 1 m^2-test specimen is described as well as the test method. Results and discussions are presented in section F.3.

The principle that friction can contribute to a higher axial stress state and as a consequence to a higher resistance against pull forces has been verified with pull tests on larger specimen resting on a granular bedding layer. This is presented in section F.4.

In the course of the field experiments presented in Annex G friction tests were performed also. Those are presented in Annex F.5.

The sliding tests are also carried out in-situ. The focus of those tests was on possibilities to actually generate the friction forces and increase of axial force, rather than the theoretical maximum friction factor. In section F.6 the results of those tests are presented. Generally the literature findings on friction properties have been confirmed and are now supplemented with insights in the deformations, in the behaviour during repetitive movements and reverse movements, and in the effects of scale.

F.1   Scope and aim of friction testing

F.1.1   Hypothesis and focus of friction testing for revetment design

The resistance of pattern-placed revetments relies on axial forces in de revetment. This axial force is initially present as a result of the slope angle and an installation procedure that creates an axially pre-stressed condition. It is also possible that the revetment increases its pre-loaded condition over time, due to wave action or dike settlement. On top of this initial axial stress state it is believed that uplift of a group of elements generates axial stress increase. A small upward (z) movement of the elements causes a volume increase that is associated with movement of the elements in x and y directions. This movement generates friction forces on the interface between the top-layer and the granular base layer. These forces change the axial stress state and increase the revetments resistance against uplift.

In 2004 tests have been performed with the aim of verifying this hypothesis. The experiments were split in three groups.

---

[298] S. Schoen, "Wrijvingsproeven van Steenzetting op filter" (MSc thesis TU Delft, part I, 2003) and Peters, *Laboratory testing of clamped placed revetments*

The first group was meant as a verification of the static model and a parameter study of the normal force versus bending resistance relation. Strength and stiffness against uplift were investigated as function of a given subjected normal force. The tests were carried out as pull tests on multiple elements on a friction less support structure, as has been presented and discussed in Annex E.

The second group of tests concerned a verification of the relation of the axial movement and the generated friction forces (refer to Annex F.1 – F.3).

The third group of tests (refer to annex F.4 and Figure F-8) was a repetition of the pull tests of Annex E but on a granular base, thus integrating experiment 1 and 2. The aim of this test was a verification of the hypothesis that pull tests and real wave loads, through geometrical non-linearity, actually have an influence on friction forces on the bedding interface and therewith on the axial stress state.
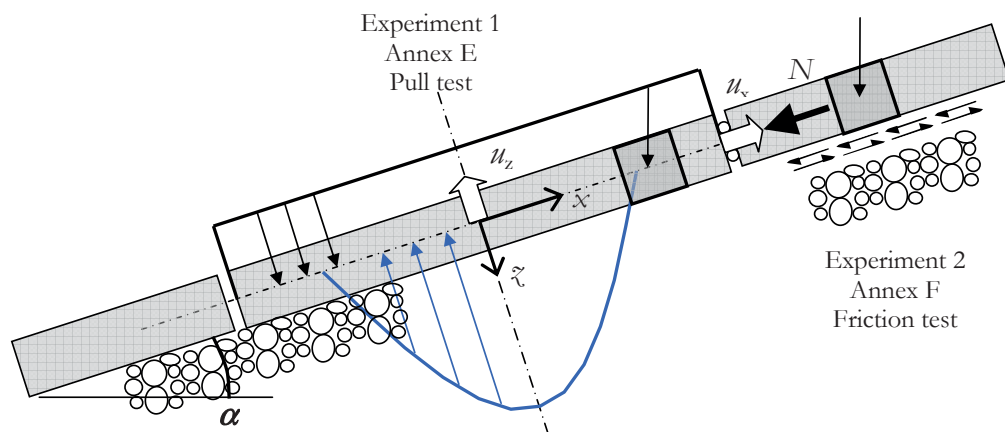
Figure F-1   **Scheme with extracted set-up of experiments**

F.1.2   Literature values

In the test series of experiment 2 the friction on the interface between the top-layer and the granular base is investigated. From literature[299] it is known that the friction coefficient between smooth concrete surfaces and rubble mount is approximately 0.6. In geo-engineering[300] it is common practise to apply a friction factor f_{fr} of $\tan(\frac{2}{3}\varphi)$ for the friction on the interface between a smooth structure and soil with a friction angle φ. The factor f_{fr} is 0.5 when $\varphi = 40°$.

There is not much known about variation of this value and also not much is known about the applicability for small pattern-placed concrete elements. Quantitative effects of specific conditions like the load level or the magnitude of the movement are unknown.

---

[299] Y. Goda et al., *Technical Standards and Commentaries for Port and Harbour Facilities in Japan*, 2009 and
J.E. van Staverden, *Wrijving en wrijvingscoëfficiënten* (RWS Deltadienst ONW report R-83068, 1983)
[300] *Damwandconstructies* (CUR report 166, 5th edition, 2012)

The friction coefficient is defined as the ratio between the horizontal force required to move the element and the vertical force which is equal to the weight of the material located above the sliding surface.

A distinction is made in static friction and dynamic friction. Static friction is the frictional resistance at which movement is about to start. Dynamic friction is the frictional resistance that remains during the sliding movement after the static threshold was exceeded. This behaviour is also know is stick–slip. During sliding over granular material this phenomenon is ongoing. The friction coefficient is increasing up to a maximum after which local unevenness is levelled.

During the construction of the Eastern Scheldt barrier caissons aspects of the behaviour of friction of concrete structures on granular bedding has been investigated.[301] The qualifications of the various effects were helpful to define a test programme.

Table F-1   **Known effects in friction**

Factor	Effect on the friction coefficient
Rate of loading	At a higher loading rate the dynamic friction is lower and is fully developed earlier
Surface roughness	A rough angular surface of the bedding increases the friction coefficient
Pressure load level	The friction coefficient decreases with higher pressure loads
Lubricant	A wet surface decreases the friction coefficient
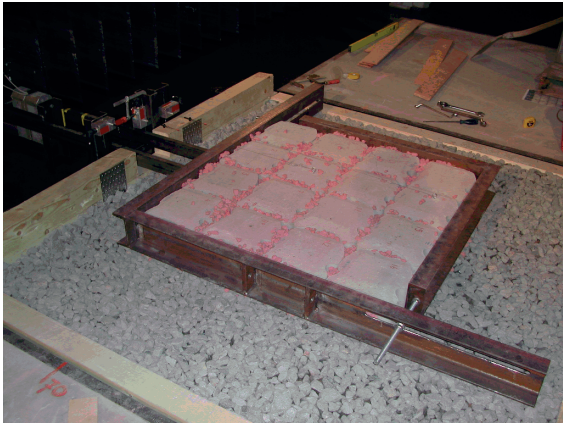
Figure F-2   **Photograph of test specimen of 16 Hydroblocks in a steel frame, with painted joint material on a gravel bed**

Larger roughness, material density and grain size cause an increase of the friction angle. Not uniformly graded granular material has better interlocking and better internal friction. The bedding material of a revetment lacks sand and fine particles since it is selected material to enhance its permeability properties.

---

[301] "Centrifuge- en wrijvingsproeven voor de Oosterschelde kering," *Deltawerken* 97 (1981): 369–376

F.2 Laboratory test design and test set-up

The laboratory test design was a simulation of a portion of revetment top-layer on top of a granular bedding level. The aim was to find friction factors specifically relevant for revetment design. The investigated conditions and variables are presented in Table F-2.

Table F-2   Friction test variables

Variable	Variations / remarks					
Block type	Type	Height [cm]	Density [kg/m³]	Specimen [m²]	No. of blocks	
	Hydroblock	15	2350	1.02×1.03	16	
	Basalton	15	2650	1.18×1.20	38	
	Basalton	25	2350	1.18×1.20	16	
	Basalt	20	2950	1.00×1.03	42	
Filter layer	Material	Particle size [mm]		Remark		Design-variables
	Split	22 − 40		Angular (base case)		
	Split	8 − 11		Smaller		
	Gravel	15 − 40		Round		
	Sand	0.1 − 4		Very small particles		
Joint fill	Course split Fine split No joint fill					
Fixation of the elements	Holding the specimen of loose elements in a frame forcing them to move together, versus doing the same tests without a frame.					
Water	Dry filter material Moist filter material Sliding surface (and filter) under water					
Sand in fill	The bedding layer as well as the joints are filled with an additional sand-bentonite mixture, adding fine material, moist and cohesion.					Conditions
Length of the moving part of the revetment	In order to study the effect of flexibility within the top-layer itself, the specimen length was varied. A limited number of tests was done on a 1×3 m² large specimen, with extra displacement gauges.					
	Basalton	15 cm column height	2650 kg/m³	1.0 × 3.0 m²	80 elements	
Load velocity	Wave attack causes revetment element movements and the rate of movement in time is not exactly known and will vary. An effect is expected because fast movements will not allow granular particles to move and re-arrange. Investigated velocities: 1, 2, 5, 10, 20 en 30 mm/s					
Length of the sliding path	The bedding particle size is assumed to be an influencing parameter. Investigated: 10, 20, 30, 40 en 100 mm.					Load variables
Repetitive movement	Load repletion is investigated since the revetment will be loaded and unloaded constantly. Interrupted and continued movements are investigated, as well as movements repeated from the start position.					
Change of the direction of movement	Are the friction properties in opposite directions equal or is there an orientation caused by a maiden loading direction, or by a preceding movement direction.					
Compressive load level	Is there an effect of a higher compressive stress of the interface? 60 to 100% higher weights were investigated in order to assess the effect of heavier revetment layers.					

The tests were executed on a horizontal bed. The load application was displacement controlled. The test specimen of approximately 1 m^2 was shifted over a granular bed with different sliding paths and velocities. The weight (including the weight of auxiliary parts), the horizontal force and the horizontal displacements were measured.

A series of friction tests is performed with 37 tests providing 368 measurements in total. The test results allow for conclusions on magnitude and dependencies with statistically sufficient confidence.

The typical set-up of movements of the test specimen is indicated in Table F-3.

Table F-3   Typical friction test cycle

code	direction / position	velocity [mm/s]	sliding path [mm]	positive / negative direction	undisturbed bed
001	→	5	10	+	yes
002	←	5	10	−	no
003	——→	10	20	+	yes
004	———→	20	20	+	yes
005	←——	20	20	−	no
006	←——	10	20	−	no
007	——→	2	20	+	no
008	———→	1	20	+	no
009	←———	10	40	−	no
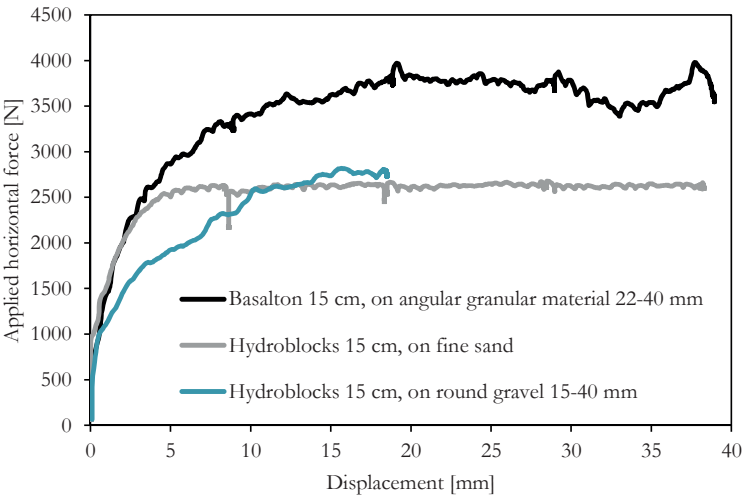
Figure F-3 Typical force displacement diagrams of tests on Basalton and Hydroblocks

F.3   Laboratory slide test results

F.3.1   Typical experiment results

Typical results of the friction experiments can be characterised with force-displacement diagrams (see Figure F-3). The experiment is carried out with a controlled displacement. The achieved resistance level, but also the gradient of the force displacement relation are important.

The maximum friction force divided by the effective weight of the specimen provides the maximum friction coefficient. A total number of 368 coefficients has been measured. The average value is 0.594, the calculated standard deviation is 0.093. The spread in result is shown in Figure F-4. These results are interpreted as normally distributed. The variation coefficient is 0.16. The 5 and 95% confidence bounds are at 0.44 and 0.75.

Various parameters of the test have been varied. In the analyses sub-groups can be formed dependent on those parameters. The difference in average friction factor was analysed statistically sing the Student t-test. The probability p that the difference in fraction factor of the two groups $\mu_{group1} - \mu_{group2}$ is smaller than zero is an indicator of the reliability of the difference. A difference is considered significant if $p < 0.05$.
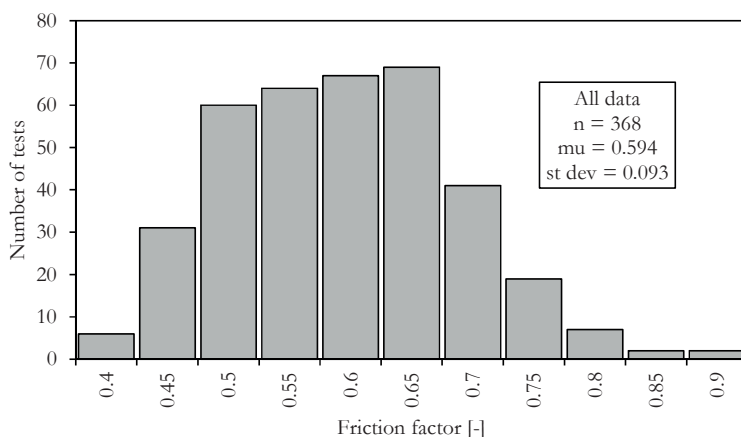
Figure F-4 Summary of all measured friction coefficient results

In the total population of measurements dependencies were investigated of:

   – the element type and size
   – the length of the sliding path
   – the type of granular sub layer, particle size and particle shape
   – the direction and repetition of movement
   – open of filled joints
   – dry versus wet sliding path
   – siltation
   – individually moving or fixed elements
   – the velocity of movement

The parameters element size, the length of the sliding path related to base material particle size and change of direction were found to have significant effects on the friction coefficient.

F.3.2 Effect of element size

The effect of the element size is best expressed in the joint length per square m of top-layer. The joints (with on both sides sharp element edges) form an obstacle when sliding on the bedding layer and are the actual resisting mechanism. The more meters of joint, the higher the friction. An important feature of the basalt is the uneven bottom surface. The underside of the elements is not right-angled and not flat. This causes better grip and the measured friction will become close to the friction of the base material itself.
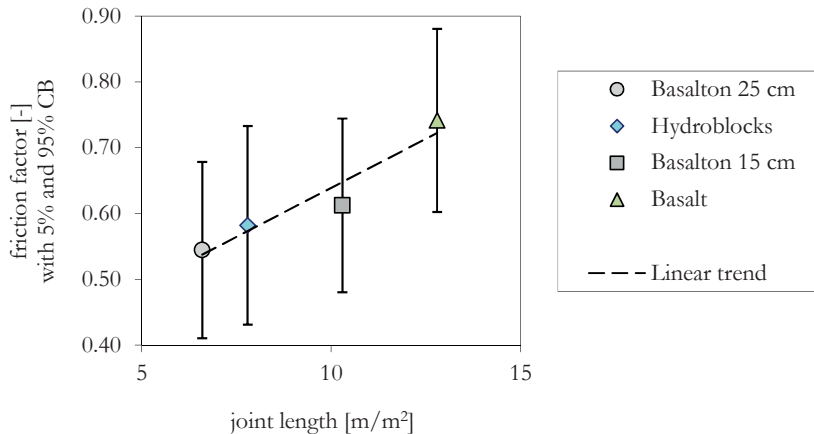
Figure F-5   Results of various element types and sizes

Table F-4   Differences in average friction factor, with statistical reliability

$\Delta\mu = \mu_{group1} - \mu_{group2}$ p-value of $\Delta\mu < 0$	Basalton 25 cm 11 elements / m² n = 19	Hydroblocks 15 elements / m² n = 69	Basalton 15 cm 27 elements / m² n = 19	Basalt (small) 41 elements / m² n = 19
Basalton 25 cm		$\Delta\mu = 0.038$ $p = 0.04$	0.068 0.005	0.197 10^{-13}
Hydroblocks			0.030 0.08	0.159 10^{-12}
Basalton 15 cm				0.129 10^{-6}
Basalt				

The results of the various element types show that there is a similar variation (with $V = 0.15$) amongst all the types. Irrespective of this variation within the groups, the differences between the groups are significant. The two types of Basalton not only differ in height but – more importantly – also in number of elements per m². The size of the Hydroblocks falls in between. The fish shape of the Hydroblocks has convex lines at three sides. The block was moved up and down, in which directions the edge line of the underside of the blocks tends to lock bedding particles in rather than giving them way. This may explain slightly higher

results of the Hydroblocks compared to the Basalton. The high results of the Basalt are likely due to the large number of columns and to the unevenness of the interface, as shown in Figure F-6. This phenomenon causes that the actual sliding surface will be moved below the longest element. The 'real' friction factor will be lower because the contribution of the weight of the portion of the bedding layer above the actual sliding surface. The friction factor is believed to respect an upper bound of 0.77 or 0.84, being tan(37½°) or tan(40°) respectively.
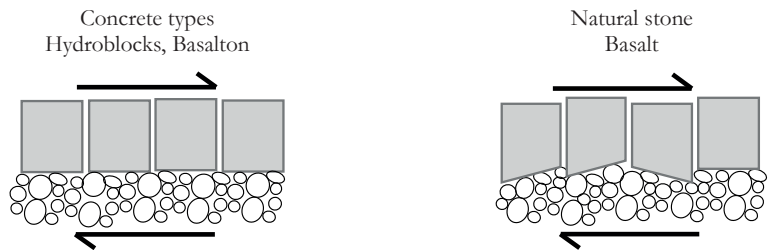
Figure F-6   **Different geometry of interface**

Filling the joints between the elements with joint material not surprisingly appears to increase the friction. The joint material provides extra jamming when sliding the joints over the bedding surface. The friction factor becomes 0.597 (n = 33) instead of 0.548 (n = 44). The difference is statistically reliable (*p* = 0.049).

F.3.3   Effect of sliding path on development of friction force

A second main dependency appears to be the length of the sliding path. As can be seen in Figure F-3 it takes length of movement before the friction is fully developed. Path lengths of 10 up to 40 mm and incidentally 100 mm are investigated. It appears that the friction is earlier developed when the particle size of the base material is smaller. The data were therefore split in groups with sliding paths shorter and longer than the typical D_{50} of the base material. The boundary between these two groups differs per base material type. For the fine sand all movements are larger than the particle size. For the fine split 8 – 11 mm (D_{50} = 8.5 mm) the 10 mm path was treated as smaller and the other distances as larger. For the other two materials the 20 mm path was excluded from both groups.

The results convincingly show that full development of the friction needs a path length of at least the typical D_{50} particle size. Below that path length that friction factor is 0.05 to 0.10 lower.

Table F-5   **Influence of sliding path and base layer particle size on the friction factor**

Base layer material	Sliding path [mm]							difference and *p*-value
	10	15	20	30	40	50	100	
sand D_{50} = 0.5 mm	μ = 0.644 n = 44							
fine split 8.5	0.563 10	0.614 23						$\Delta\mu$ = 0.051 *p* = 0.0048
round gravel 21	0.522 4			0.628 8				0.11 0.011
course split 28	0.573 121			0.618 39				0.045 0.0062

The round gravel has on average a slightly larger friction factor. A relevant selection for the tests give results of μ = 0.608 (n = 20) for the round and 0.576 (n = 112) for the angular material. The difference can be explained by a larger contact surface. It is also possible that the base layer of round gravel 15-40 has a more compact matrix than the angular split 22-40, with less possibilities of re-arrangement of the particles and hence a higher shearing resistance. The difference is statistically not significant (p = 0.07).

The set-up and sequence of testing produces some relevant observations. A reverse movement experiences a significantly lower friction factor than a first movement in a certain direction. $\Delta\mu$ = 0.07, n = 89 and 56, p = 10^{-7}. A slight drop of friction factor ($\Delta\mu$ = 0.02) results can be noticed for the repeated movements on a pre-loaded bedding. Larger friction factors are found when the movements are first reversed and then extended. It seems that the specimen experiences a threshold when the second movement in positive direction is larger than the first, see Table F-3 row 003 versus row 001.

Tests with moist and submerged bedding layers were carried out also, as well as tests with joints and bedding filled up with a mixture of sand, water and bentonite. This was to simulate a condition of the revetment after siltation with sand and clay sediment. In the submerged condition the water level was chosen at the underside of the elements, thus wetting the interface but not changing the effective weight of the revetment.

Water was expected to work as a lubricant.[302] The tests confirmed this. The condition moist or wet bedding material appeared to produce ambivalent results amongst the various types. For the Hydroblock tests there is hardly any difference compared with the dry condition, and for the Basalton tests there is hardly any difference with the submerged condition. For reasons of statistical power the groups moist and submerged were put together. The difference between dry and wet results in: μ = 0.042, p = 0.002.

Table F-6   Friction factors for dry and wet conditions of the interface

μ n σ	dry	moist / under water	moist	under water
Hydroblocks	0.597 33 0.086	0.566 78 0.094	0.604 21 0.096	0.551 57 0.089
Basalton 15 cm	0.612 19 0.081	0.552 38 0.075	0.559 19 0.088	0.546 19 0.062
Hydroblocks + Basalton 15 cm	0.603 52 0.084	0.561 116 0.088		

The tests with siltation of the structure did not show different results.

---

[302] Staverden, *Wrijving en wrijvingscoëfficiënten*

The variation of testing with and without a fixation frame resulted in higher friction results for the loose condition. The specimens were testing with sliding paths of 30 and 40 mm or more. The elements tend to depart from there position and move sideways and appear to experience more resistance compared to the specimen with fixed position of all elements. The difference are on average relatively large (μ = 0.055) but the statistical power is too low (p = 0.11). Moreover, in reality the pattern-placed revetments are believed to behave like the specimen with fixed element positions.

The velocity of the movement was varied but significant trends in the results could were not observed.

F.4 Laboratory pull tests on friction bedding

The tests of Annex E were executed on a friction-less base. They were repeated on a bedding layer of granular material. One of the difficulties with those tests was introducing the axial pre-stress in the top-layer. A pre-load applied on the edge of the model would soon disappear via friction in the bedding layer. Just applying this force on the 4.4 m long specimen without moving the specimen would – according to elasticity theory – lead to an axial force in the middle section of 0.25 times the edge force. In case the load is increased further the specimen is moving and full friction is achieved, this middle section force will amount 0.50 time the edge load. In the test procedure this loading procedure was executed from two sides. As a result the axial pre-stress in the middle section was inflated to a value sufficiently high for successful testing. From these test an axial elasticity modulus could be estimated at E_a = 30 MPa. The friction factor during movement was 0.64.

Principle with distribution of F_{fr}

Elastic distribution of $N(x)$ with finite stiffness E_a of the revetment beam

Plastic distribution of N(x)
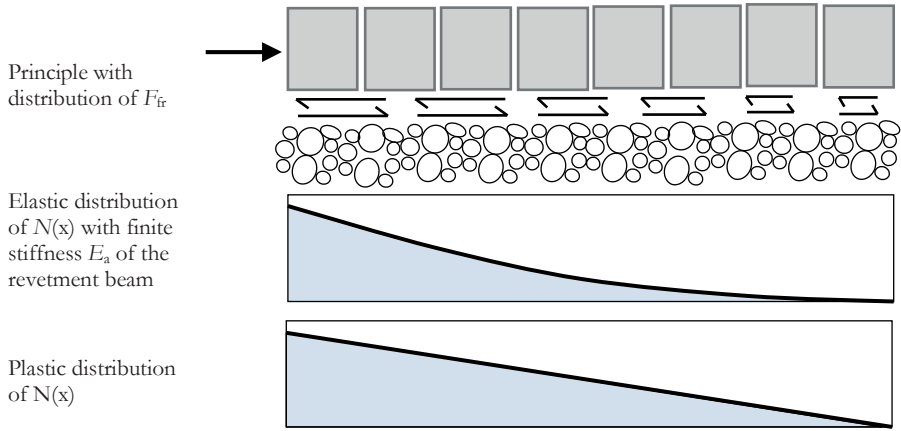
Figure F-7　　**Principle of elastic friction force distribution before movement (a) and plastic during movement (b)**

The pull testing was done and it appeared that the tests all showed higher results than the similar tests on friction-less table structures.

Back-analysis showed that the axial stress state just before the failure point must have taken full advantage of the development of friction forces acting in the interface under the elements still resting on the base layer. The friction factor that could be calculated from the measured force data is 0.40. Keeping in mind that the bedding was pre-loaded in shearing, and given the fact that the horizontally shift was in the order of 3 mm, which is small

compared to the grain size of the bedding material, this result is in line with the solitary friction tests.
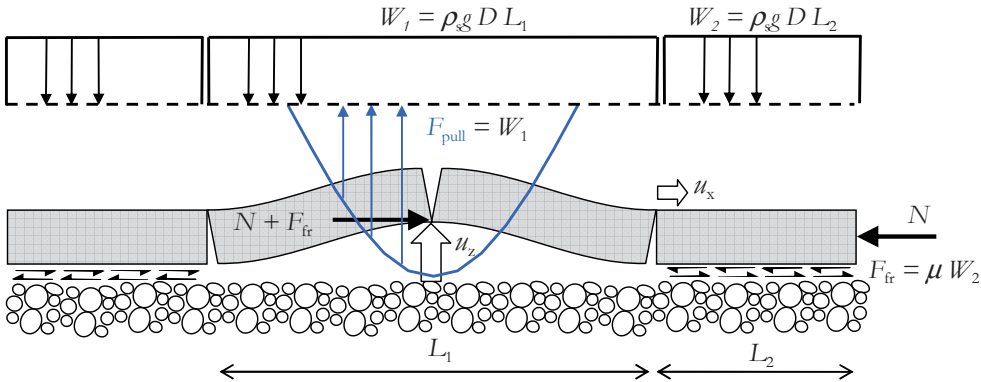
Figure F-8   **Model of laboratory sliding tests on granular bedding (experiment 3)**

The friction is generated by the movement u_x. The relation u_x/u_z can be calculated from geometrical second order effect, plus an effect of elasticity. The relation was also measured. It was found that under the test conditions $u_x = 0.20 .. 0.24\ u_z$. The deviation between calculated and measured values was approx. 10%.[303]

Comparing the pull tests results to the results of Annex E the tests on a friction bedding (W-series) give 4 to 15% higher results than the tests on a friction-less table (S-series). The difference in results are most convincing for the tests with two pulled rows. These test have the smallest lifted length L_1 and leave a larger portion with length L_2 in contact with the bedding.

Table F-7   **Pull test results on friction bedding**

type	# of pulled rows	series	axial prestress level	# of experiments n	maximum force [kN] Average	maximum force [kN] st.dev.	Difference W and S groups [kN]	P-value
Hydro-blocks	6	S[1]	2	6	8.54	0.48	0.34 (+4%)	0.05
		W[2]	2	2	8.88	0.09		
Basalton	2	S[3]	2	3	3.58	0.58	0.55 (+15%)	0.08
			4	3	3.60	0.51		
		W[4]	2	2	4.13	0.26		
	6	S[5]	2	4	4.52	0.68	0.28 (+6%)	0.23
			4	2	4.84	0.03		
		W[6]	2	2	4.79	0.20		
[1] S18-S23, [2] W5, W6, [3] S38-S43, [4] W3, W4, [5] S44-S49 [6] W1, W2								

---

[303] See: Peters, *Laboratory testing of clamped placed revetments*

Table F-8   Pull test results evaluated

Forces [kN]	Prediction F when N = 6.9 kN/m[1]	measured average		Corresponding N with % higher prediction		Theoretical upper limit
		in series S	in series W			
Basalton 2 rows	4.46	3.58	4.13 (+15%)	9.2	2.5 (+35%)	2.5
Basalton 6 rows	5.60	4.52	4.79 (+6%)	8.1	1.3 (+17%)	

F.5   Slide tests in the field

F.5.1   Experiment set-up

In 2006 field tests were designed and executed in order to measure the in-situ axial stiffness, sliding and friction properties of revetment structures. Those tests were a part of one test campaign together with field pull tests (see Annex G). The aim of the axial field tests was to investigate the initial pattern density, the axial stiffness under applied extra load, and the shearing stiffness of the bedding. Friction factors were difficult to extract from the test results.

The test set-up shows similarity to the laboratory slide tests, but was carried out on build-in specimen. The revetment slab was opened up, creating a rectangular gap of 1 m wide and 3 m long. Stiff steel beams and oil jacks were installed to apply axial load at both edges of the opening in the revetment (see Figure F-9). The in-plane displacement of the revetment elements was measured in an area of appropriate size.
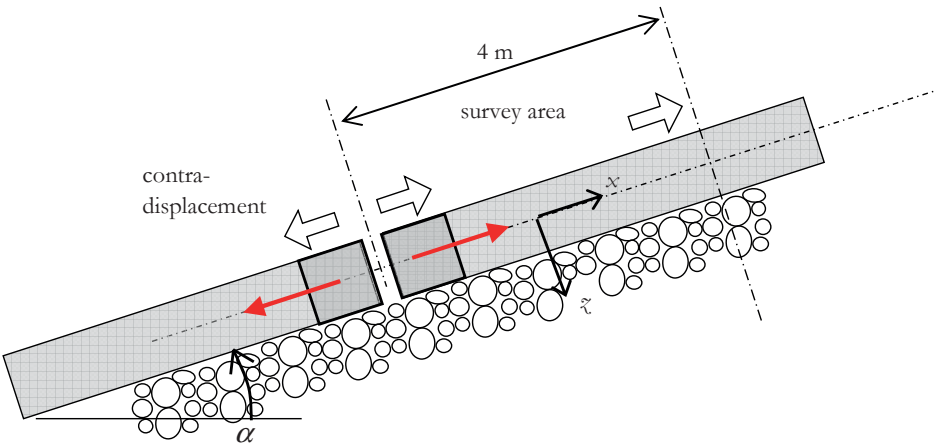
Figure F-9   Cross section of friction field test set-up
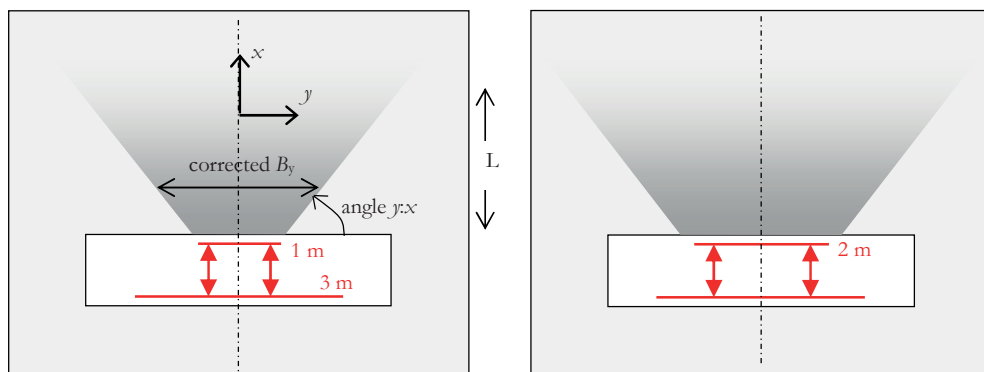
Figure F-10   **Plan view of friction field test set-up**

The tests were varied in location on the slope, in length of the beams creating concentrated loads and more distributed loads.

The tests have been executed on three locations in Zeeland, the Netherlands, at the coastlines of the Western and Eastern Scheldt Estuaries (see Table G–1). All slopes were relatively long slopes due to the large tidal lag. Because of the long slopes the experiments were carried out at lower and at higher positions on the slope.

Table F-9   **Test location on the tested slopes**

Code	Location		Type with specific element weight [kg/m³]	Top-layer thickness	Year of slope construction	Tidal lag normal / spring
A	Bath, Zuid-Beveland	High	Hydroblok 3030	0.385	2002	4.84 / 6.56
		Low		0.345		
B	Poortvliet, Tholen		Basalton 2790	0.24	1980	3.31 / 4.31
C	De Sluis, Sint Philipsland		Basalton 2940	0.245	1997	2.97 / 3.92

Table F-10   **Experiment location on the tested slopes**

Location / position		distance from toe	from top of slope	Reference level NAP *	Position with respect to tide
A	High	10 m	16.5 m	3.4 m *	just above normal HW
	Low	3.8 m	21.7 m	1.9 m	at ¾ of the daily tidal lag
B	High	7.5 m	9.1 m	2 m **	just below normal HW
	Low	3 m	13.6 m	0.76 m	at ¾ of the daily tidal lag
C	****	3 m	6 m	1 m	just below normal HW
*) with berm position at 7.05 m +NAP and slope 1:4.1 **) with berm position at 4.09 m +NAP and slope 1:3.45 ***) with berm position 3.09 m +NAP and slope 1:3.06 ****) average value					

The test set-up differs from the laboratory tests, since the specimen is not free to move and build-up of forces are restrained at three sides of the area of interest. Therefore a model that includes elastic shear spring action must be used, rather than a plastic friction model.
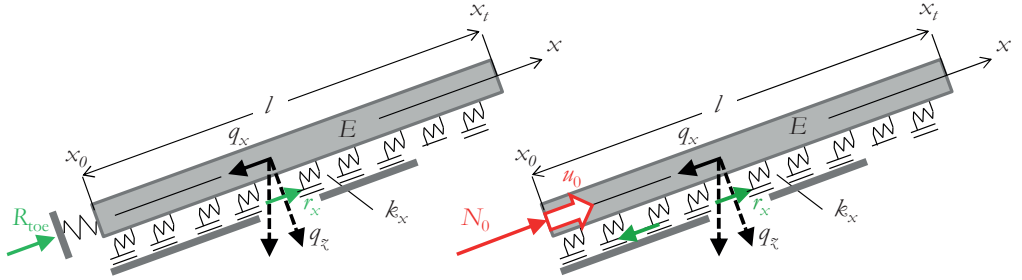
Figure F-11   Model of field slide tests

The top-layer is an elastic slab consisting of elements and joints. The material stiffness of the elements themselves is very high and considered as infinite. Flexibility and finite axial stiffness of the system is caused by joint flexibility. The relative movements of the elements are not always elastic. The elements may initially be placed in a somewhat loose pattern. A response to axial force will in that case first be an increased pattern density with element positions closer to each other. This process can be expressed in (negative) strain. After an optimal close pattern is achieved, the top-layer has a relatively large axial stiffness E_a. The shear stiffness of the bedding k_x is relatively low. This causes that full development of friction and actual sliding and determination of the corresponding friction factor might not be achieved.

Assuming applicability of elastic model properties the relation as force and deformation is given with a differential equation.

$$-EB_y D \frac{d^2 u}{dx^2} + k_x B_y u = q_1 \qquad \text{Eq. F.1}$$

with
$E_a B_y D$ = the axial stiffness of the top-layer [N], E_a in [N/m^2]
$u(x)$ = the in-plane displacement [m]
$k_x B_y$ = the shearing stiffness of the bedding [N/m^2], k_x in [N/m^3]
q_1 = the distributed in-plane force: $\rho_s g\, B_y D \cos\alpha$ [N/m]

The distance over which the applied force will have effect is dependent on the characteristic length λ. The effects will vanish beyond a distance of 2λ. For small values of k_x the characteristic length will be large.

$$\lambda = \sqrt{\frac{EB_y D}{k_x B_y}} \qquad \text{Eq. F.2}$$

A passive and active system can be distinguished, where a passive case is given by a structure resting against a stiff toe structure. The test represents an active system. Actively applied loads experience a threshold value $q_1 \lambda$ as can be noted in the expression for N$_0$. The top-

layer will first start to 'rest' against the load and will move with further increase of the load. The threshold value is significant for cases with large E_a and small k_x.

$$N_0 = \lambda\left(k_x B_y u_0 + q_1\right)\frac{1 - e^{-2L/\lambda}}{1 + e^{-2L/\lambda}} \qquad \text{Eq. F.3}$$

with
N_0 = the normal force at the edge [N]
u_0 = the displacement introduced at the edge [m]
L = the length of the structure [m]

L / λ	0.2	0.5	1	2	5
$\dfrac{1 - e^{-2L/\lambda}}{1 + e^{-2L/\lambda}}$	0.20	0.46	0.76	0.96	1.00

Assuming $q_1 << k_x B_y u_0$ and $L > 3\lambda$ which gives $\dfrac{1 - e^{-2L/\lambda}}{1 + e^{-2L/\lambda}} \to 1$ leads to:

$$N_0 = \lambda\left(k_x B_y u_0 + q_1\right)\frac{1 - e^{-2L/\lambda}}{1 + e^{-2L/\lambda}} \to \lambda k_x B_y \times u_0 = \sqrt{EB_y D \times k_x B_y} \times u_0 \qquad \text{Eq. F.4}$$

In the test set-up the relation between N_0 and u_0 is measured. The characteristic length λ is estimated from the observed gradients in the survey area. As a result E_a and k_x can be determined.

F.5.3   Experiment results

The properties of the material present in the structure were investigated. The element to element friction factor was measured by putting two elements on top of each other. The lower element was upside down fixed in a clamp. The top element was shifted horizontally using a tensile test machine. The friction factors were calculated from the results. The high factors for the Hydroblocks are remarkable. Also the correlation with age is interesting. It seems that new elements have sharp edges and old elements are worn and more smooth.

Table F-11   Friction properties of the elements

Location	Type	Maximum friction factor $f_{fr,max}$	Dynamic friction factor $f_{fr,dyn}$	Year of construction
A	Hydroblock	0.86	0.76	2002
B	Basalton	0.47	0.39	1980
C	Basalton	0.50	0.44	1997
All numbers are averages of two experiments. The variation was 0.1.				

The found bedding and joint material is shown Table F-12. These values can be used to calculate the relative sliding movements. At location C the particle size is relatively large.

The loads were applied with repeated loading and unloading in order to obtain and determine reversible deformations and elastic properties. The typical test process showed rather large differences in initial displacement needed to achieve a more compact pattern. The displacements needed ranged from 0 to 7 mm. It can be noticed that these variation mainly occurred at location B in the lower position. It was found that at lower positions the

pattern density was not constant and might have been affected by the condition and/or flexibility of the toe structure. At locations higher on the slope the initial deformations are much more constant and smaller.

Table F-12   Properties of in-situ bedding and joint material

location	Bedding material			Joint material	
	A	B	C	A	C
D_{15}	13	24	23	4	22
D_{50}	17	32	47	7	27
D_{85}	22		58	10	

The observed elastic deformations were extracted from the data using two methods. In the first method the values were calculated from averaging and extrapolation of a two dimensional field of measured *x*- and *y*-displacement data at certain load levels. In the second method the elastic displacements at 100 kN were read from the force displacement diagram in the central axis of the experiment. The two methods showed minor differences with some exceptions where the second method produced smaller values. The values of the second method were adopted.

Table F-13   Measured maximum displacements at axial load tests

Location	Width B_y [m]	High / Low	Thickness D [m]	Displacement at loaded edge * [mm]	One-off displacement related to increased pattern density [mm]	U el calculated from difference	U el derived from force-displacement diagram	Displacement of contra-sensors [mm]	Distance to zero effect [m]	Observed spread angle [y:x]
A	2.0	L	0.345	** 0.2	0	0.2		0.5		1
	2.0	H	0.385	0.8	0.5	0.3	0.3	0.5	1.3	1
	1.0	L	0.345	1.6	0.9	0.7	0.6	1.0	1.5	1
	1.0	H	0.385	0.7	0.5	0.2	0.6	0.7	1.3	1
B	2.0	L	0.240	0.4	0	0.4	0.35	1.5	1.0	1.5
	2.0	H	0.240	1.7	0.3	1.4	1.2	2.5	1.3	1.5
	1.0	L	0.240	9.0	7.0	2	1.5	0.4	1.5	2
	1.0	H	0.240	0.8	0.55	0.25	0.35	0.7	1.5	1.5
C	2.0	L	0.245	** 1.0	0.3	0.7		1.5		1.5
	2.0	L	0.245	2.8	1.0	1.8	1.2	1.3	2.0	1.5
	1.0	H	0.245	3.3	2.0	1.29	1.3	1.9	3.9	1.5
*)	Automated extrapolated deformation at the loaded edge; at 100 kN load									
**)	No measurements in survey area; readings near edge used									

The observed spreading angle of the movements in *y*-direction (see Figure F-9 and Table F-13) was included in the back-analysis of the results.

Table F-14   Calculated axial and bedding stiffness parameters

Loaction	Width B_y [m]	High / Low	Thickness D [m]	Corrected width at ¼L [m]	Axial stress under 100 kN load at ¼L	Characteristic length λ [m]	Calculated k_x [MN/m³]	Calculated E_a [MPa]	Average E_a per location
A	2.0	L	0.345						
	2.0	H	0.385	3.3	7.9	0.65	155	171	146
	1.0	L	0.345	2.5	11.6	0.75	89	145	
	1.0	H	0.385	2.3	11.3	0.65	111	122	
B	2.0	L	0.240	3.5	11.9	0.5	163	170	
	2.0	H	0.240	3.95	10.5	0.65	32	57	129
	1.0	L	0.240	3.25	12.8	0.75	27	64	
	1.0	H	0.240	4	10.4	0.75	95	223	
C	2.0	L	0.245						
	2.0	L	0.245	5	8.2	1	17	68	79
	1.0	H	0.245	6.85	6.0	1.95	6	89	

Table F-15   Sub-group analysis of axial stiffness

Location	Width B_y [m]	High / Low	Calculated E_a [MPa]	Axial stiffness E_a for subgroups			
				B = 2 m	B = 1 m	Low	High
A	2.0	L					
	2.0	H	171	171			171
	1.0	L	145		145	145	
	1.0	H	122		122		122
B	2.0	L	170	170		170	
	2.0	H	57	57			57
	1.0	L	64		64	64	
	1.0	H	223		223		223
C	2.0	L					
	2.0	L	68	68		68	
	1.0	H	89		89		89
average				116	129	107	143

The calculated stiffness parameters k_x and E_a are presented in Table F-14 and further detailed in Table F-15. Any observed or calculated differences in E_a between the distributed and concentrated load tests could be due to the test-setup or due to poor representation by the model. It is therefore good that the average E_a for the tests with B =1 and B = 2 m are

116 and 129, which is – given the variation – an insignificant difference. There could be a difference between the values of E_a for low and high positions on the slope. This difference between the average results is larger but statistically also not significant. Remarkably the average axial stiffness is higher on the locations higher on the slope. The opposite would have been a more logic result reasoning from the assumed build-up of normal force, which is increasing towards the toe of the slope. The average E_a is about 2 to 5 times higher than measured in the laboratory tests.

F.6 Conclusions on friction tests

Friction forces play an important role in the resistance of pattern-placed revetments. The modern mechanically placed types have a perfectly flat interface between the top-layer and the base layers. The top-layer tends to move down and that movement is restrained by friction. The friction therefore influences the initial axial stress state of the top-layer.

As the revetment will experience tidal water level variations and movements due to water head differences and water pouring through the voids and joint the stress state may change. Head differences can lift the elements and this will clearly change the stress state. Lifted and again lowered elements experience a reset of the shear stress on the interface under the element. Lifting of a group of elements will cause in-plane movements of the surrounding elements. Pattern-placed revetments in good condition will than respond by further development of axial forces. Increase of friction forces plays an important role in this development.

The question is whether this mechanism is reliable. Are those friction forces predictable? In general the statistical variation of the friction properties themselves is on a fairly constant level with f_{fr} = 0.6 and of V = 0.16.

Also the relation between forced sliding path and generated force seems logic and predictable. The forces can be fully developed when the movement exceeds the typical particle size D_{50}.

Known aspects that reduce friction were confirmed: water works as a lubricant, aging and wear will reduce friction also.

Unreliable aspects related to development and utilization of friction are:

- the dependency of prior load direction
- the reducing effect of load repetition
- the amount of axial strain that is needed to close the gaps and compact the pattern

In a laboratory set-up the effect of friction on increase of the axial force was demonstrated. It is therefore believed that this could work in practise also.

Field slide tests confirmed the mechanism that axial forces in the top-layer are transferred to the bedding layer within rather short distances.

ANNEX G TESTING TOP-LAYER RESISTANCE IN THE FIELD

The laboratory test developed in this study (see annex E) was a simulation of the wave pressure distribution on a revetment with a regular pattern, with dry new joint material, and idealised conditions for in-plane forces and friction. It is uncertain to what extend those laboratory conditions represent real revetment structures. This Annex describes experiments that were designed with the purpose of testing plate bending in real revetment structures.

The aim was to test real resistance against uplift loading of a larger surface area. Pull tests were performed with three pulled elements in a row. This was done with the purpose of omitting single element failure. The model of section B.2 is used for interpretation of the results. Assisted with the model measure deformed shapes are translated into stiffness properties and in-plane stress states in two directions (section G.2). The test execution and typical test performance are described in section G.3.

The results (see section G.4) give an indication of the resistance against wave uplift pressures. Like in earlier tests the variability of the results appears large. The results of stiffness and in-plane stress properties show dependency on position, suggesting that gravity induced in-plane forces play a role. The findings (see section G.5) include the observation that the resistance closer to the toe appears to decrease. Elastic axial beam models that count for finite toe structure stiffness therefore become relevant for calculation of the in plane stress state.

The extensive testing and deformation surveying programme contributed to better understanding and to calibration of the models. Better understanding did in this case not lead to 'better' results. Significant uncertainty remained and is believed to be related with the nature of the structure itself.

G.1   Aim and scope of testing

Pull-out resistance of revetment elements larger than the element weight is caused by friction interaction that relies on in-plane stress. The hypothesis is that pattern-placed revetments follow non-linear elastic beam and plate theory. The structural model that explains and predicts this behaviour makes clear that the mechanism is subject to large uncertainties with respect to the effects of bottom friction on the in-plane stress state.

The pull-out tests presented and discussed in Annex C have limitations that make them less suitable for validation of the structural models for the top-layer strength. Shortcomings of these earlier field tests were:

– Lack of displacement data of other stones
– Test load level too low
– Disturbance of the test result by the support forces of the equipment
– No repeated loading
– Loading limited to one element

In order to verify the hypothesis new experiments were defined. In preparation of field experiments a full-scale model was built in a laboratory environment. The subsequent experiments proved that the revetment elements behaved as an interlocked system and could be described by plate theory, as described in Annex E.

The new field experiments were to provide data that can be used as verification of the presence and magnitude of an initial in-plane normal stress. This is the primary parameter needed for frictional interlocking. The experiments were to generate information for joint stiffness, bedding friction, directional differences and pattern density of the top-layer also. Other research questions are: can the deformation be reversed and repeated with similar force? and: will the revetment move back after shifting the top-layer over the bedding layer?

A concentrated load on a friction-interlocked element causes shear forces and bending moments in the interfaces. When the load is increases a number of elements starts to move. As a consequence of the vertical displacement of the elements, adjacent elements rotate and the affected area tends to expand. This phenomenon increases the interlocking resistance and may also increase the normal force on the boundaries.

The new test series was performed in 2004 on three slopes in Zeeland. The test campaign consisted of pull tests and friction tests. The friction tests are discussed in Annex F.5. The tests were carried out on Hydroblock and Basalton slopes. The original scope was to test on slopes of similar age and load history. The slopes were also selected looking for a large tidal range, enabling to test on several vertical positions on the same slope. Not all site selection criteria could be fulfilled.

Table G–1　　Test locations

A. Western Scheldt, near Bath
Tidal range:
4.8 m (average)
6.6 m (spring tide)

B. Eastern Scheldt, island Tholen, near Poortvliet
Tidal range:
3.3 m (average)
Exposed to South-westerly waves, 5 km fetch

C. West side of island St. Philipsland
Tidal range:
2.9 m (average)

Table G–2　　Typical data of test locations and revetment slopes

Location	Top of revetment [m +NAP]	Type	D [m]	Slope angle cot α	Year of construction
A	4.0	Hydroblock	0.385 0.345	4.0	2002
B	4.1	Basalton	0.24	3.8	1980
C	3.1	Basalton	0.245	3.1	1997

G.2 Model and interpretation method

G.2.1 Two-beam model

The pull tests were designed to gain insight in the directional differences in axial stress state and load capacity. The basic idea is that the revetment top-layer has certain axial flexibility characteristics, expressed as a value of the Young's modulus E_a. The axial force may differ in x- and y-directions. As soon as perpendicular loads are applied bending moments will occur. Concentrated perpendicular loads will give bending moments in two directions. In homogeneous omnidirectional revetment types the bending moments in x- and y-direction have no reason to show difference. The moment resistance is determined by the eccentricity of the normal force. With increase of the bending moment, the position of the axial force will move to towards to outer position in the cross section. A smaller normal force will sooner arrive at its extreme position. With movement of the position of the force the effective flexural stiffness E_f will start to deviate from E_a.[304]

This mechanism is introducing differences in in flexural stiffness of the two crossing beams. As a result the load distribution will gradually become direction-dependent. Pre-analysing this phenomenon can be done with the two-beam model of section B.2. The model is assumed to have unequal beam lengths. The load is assumed to divide itself over the x-beam and the y-beam respecting a 45°-intersection, see Figure G–1. This assumption causes that the short beam carries less load than the long beam. This is contradictory to 'normal' load distribution in two way slabs where the short span carries more load than the long span. In the model evaluation the load distribution and the length difference of the beams are associated with the fact that the long beam is stiffer and stronger, both caused by a higher normal force in that direction. Using this model the directional spread of the deformation can tell us the directional differences in axial stress state.

The two-beam model of section B.2 is evaluated with beams of unequal length, $2x_0$ in x-direction and $2y_0$ in y-direction and with variable Young's moduli. The deflection u_c of both beams is set equal.
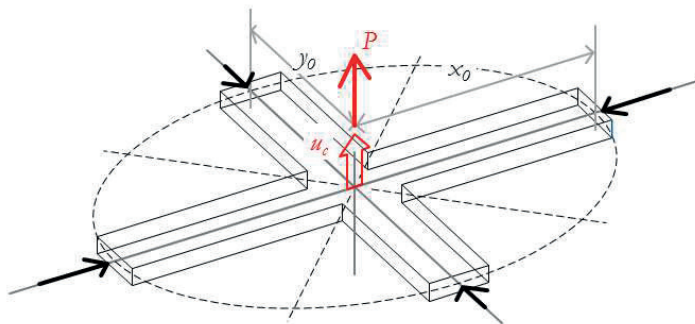
Figure G–1   **Beam model with unequal beam lengths x_0 and y_0**

---

[304] See Annex A.4.1, Eq. A.57 and Figure A-39.

For the edge moment M_2 we find:

$$M_{x2} = \tfrac{1}{6}q_x x_0{}^2 \text{ and } M_{y2} = \tfrac{1}{6}q_y y_0{}^2 \qquad\qquad \textbf{Eq. G.1}$$

For the central moment M_1 we find:

$$M_{x1} = \tfrac{1}{3}q_x x_0{}^2 \text{ and } M_{y1} = \tfrac{1}{3}q_y y_0{}^2 \qquad\qquad \textbf{Eq. G.2}$$

The central displacement u_c is:

$$u_c = \tfrac{1}{24}\frac{F_x x_0{}^3}{EI} \text{ and } u_c = \tfrac{1}{24}\frac{F_y y_0{}^3}{EI} \qquad\qquad \textbf{Eq. G.3}$$

with $2F_x + 2F_y = P$

In the model the effective beam width is kept at $\tfrac{1}{2}y_0$ for both beams, with $x_0 > y_0$.

$$I = \tfrac{1}{12}\tfrac{1}{2}\,y_0 D^3 \qquad\qquad \textbf{Eq. G.4}$$

Substitution of the pull test parameters

$$F_x = n_{LFx\frac{1}{4}}\rho g D B_x B_y \text{ and } F_y = n_{LFy\frac{1}{4}}\rho g D B_x B_y \text{ with}$$

$$n_{LFx\frac{1}{4}}B_x B_y = \tfrac{\pi}{2}(x_0 y_0 - \tfrac{1}{2}y_0{}^2) \text{ and } n_{LFy\frac{1}{4}}B_x B_y = \tfrac{\pi}{4}y_0{}^2$$

leads to:

$$\frac{u_c}{D} = \tfrac{\pi}{4}\frac{\rho g D}{E_x}\frac{(2x_0 - y_0)x_0{}^3}{D^4} \text{ and } \frac{u_c}{D} = \tfrac{\pi}{4}\frac{\rho g D}{E_y}\frac{y_0{}^4}{D^4}$$

Rewriting the equations gives the relation:

$$\frac{E_x}{E_y} = \left(2\tfrac{x_0}{y_0} - 1\right)\left(\tfrac{x_0}{y_0}\right)^3 \qquad\qquad \textbf{Eq. G.5}$$
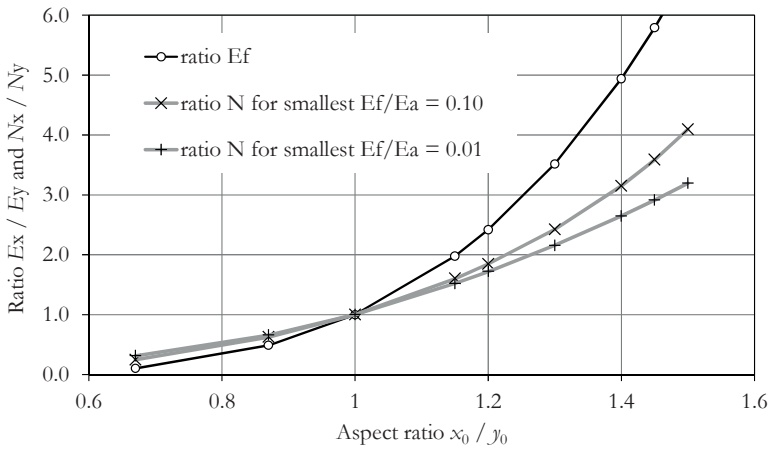
Figure G–2   Model results of directional differences of the flexural stiffness E_f and the normal force N

An aspect ratio x_0/y_0 of the deformed shape of 1.3 is according to Eq. G.5 caused by a $(2 \times 1.3 - 1) 1.3^3 = 3.5$ times higher flexural stiffness in x-direction. When we assume that the highest moment M_{2x} is associated with failure and hence has an eccentricity of for instance $e_y/d = 0.48$ ($E_{fy}/E_a = 0.01$). Since $E_{fx}/E_{fy} = 3.5$, E_{fx}/E_a is 0.035 and the value of e_x/d follows as 0.462 (Figure G–3). For this specific aspect ratio x_0/y_0 the difference in the bending moment M_{2x} and M_{2y} is a factor 2.08. Therefore N_x/N_y is $2.08 \times 0.48/0.462 = 2.15$.
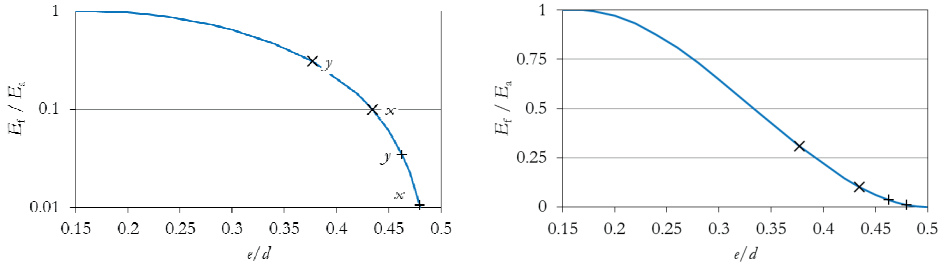
Figure G–3   **Model points for $x_0/y_0 = 1.3$ of e/d in cross sections in x- and y-direction, assuming 0.01 and 0.10 for the smallest E_f/E_a**

G.2.2   Use of the model for test evaluation

The model contains more than sufficient parameters for interpretation of the tests. The measured test data include a force, and perpendicular displacements over an adequate area. At certain load levels the peak displacement value u_c and the sizes x_0 and y_0 of the displacement field are known. The unknown variables are the stiffness moduli E_{fx}, and E_{fy} and the normal forces N_x and N_y. As explained above these values are not independent. Adopting the joint model of section A.4 the independent variables are the modulus E_a and the joint strength σ_1. The number of variables is too large for obtaining one single solution for the parameters.

There are two methods of test evaluating using the model.

1. The load level is necessarily associated with bending moments, which gives – if we assume maximum e/d values respecting a joint strength σ_u – minimum values of the normal forces N at the location of the edge of the deformed area. These normal forces were present in the structure before loading started, since the there is no or hardly any disturbance of the horizontal position of the elements along the perimeter of the deformed area. E_a and σ_1 are assumed equal for the two directions.

2. The second evaluation method focusses on a best match of the stiffness variables. The flexural stiffness values can be calculated from the peak deformation and the size and aspect ratio of the deformed shape. A certain level of the normal force N relates these flexural stiffness values E_f to the original axial stiffness E_a, with the eccentricity of the force. The best match of these variables should also include the right combination of N and e that equals the bending moments.

For some tests various load levels can be evaluated, thus providing more data.

G.2.3 FEM *model for single and triple load tests*

The model evaluation was done with a numerical version of the two-beam model, using the finite element method (FEM). Since there were also tests executed on multiple points the two-directional beam model was extended as indicated in Figure G–4.

The lengths of the beams, the displacements in the free nodes, and the applied forces are known measured data. The bending moments, the flexural stiffness values and the normal forces are derived from the model calculation.
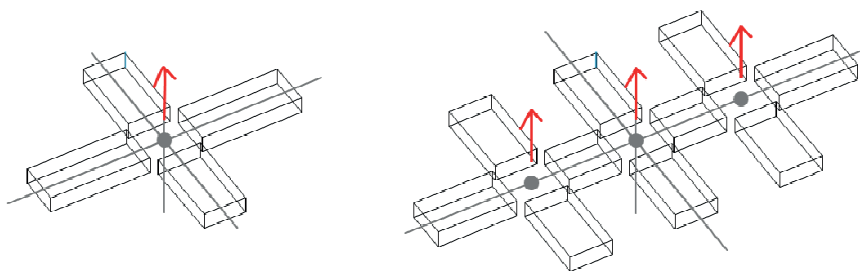
Figure G–4   **Geometry of FEM models for evaluation of single and triple point pull tests**

G.3   Test set-up and execution

On the long slopes of location A and B were executed along two defined lines lower and higher on the slope. On location C only one test line was possible.

A test programme[305] was designed to observe and measure in plane 2-D effects. Therefore vertical displacements were measured in a square of 4 × 4 m. Also in-plane deformations were measured. Separate frames were used for application of the load and for surveying the displacements. The load patterns consist of single pull tests and of three simultaneous pull tests in a row (with 1 m spacing). The 3-in-a-row tests were applied in vertical as well in horizontal rows. These tests were meant to simulate line loads rather than concentrated loads. It was expected that analysing these tests would help to distinguish between x- and y-effects.

The test programme included in most of the cases 5 identical tests per test type (single or 3-in-a-row) on each test line, arriving at a total of 59 tests. The single element tests were executed as simple static load test with stepwise load increase to a deformation criterion of u_c = 0.15 D. Half of the number of single element pull tests were executed with cyclic loading. Prior to loading to the anticipated maximum, the pull force got five cycles of loading and unloading up to 35% of the maximum, and five cycles between 65% and 35% of the maximum.

---

[305] The tests were commissioned by DWW, co-sponsored by Delft Cluster. The tests were executed in January, March and April 2006 by the MSc student Joris Blom and the firms RHDHV and BAS R&T.
J.A.H. Blom, "Veldproeven op steenzettingen in Zeeland - Eindrapport met resultaten en analyse van onderzoek naar de klemming van gezette stenen" (MSc thesis TU Delft, 2006)
J.A.H. Blom, L. van Nieuwenhuijzen, and D.J. Peters, *Test result and analysis report on prototype tests on clamped revetments*, 2007
J.A.H. Blom et al., "Field tests on clamping in block revetments," *Coast. Struct.* (Venice, 2007)
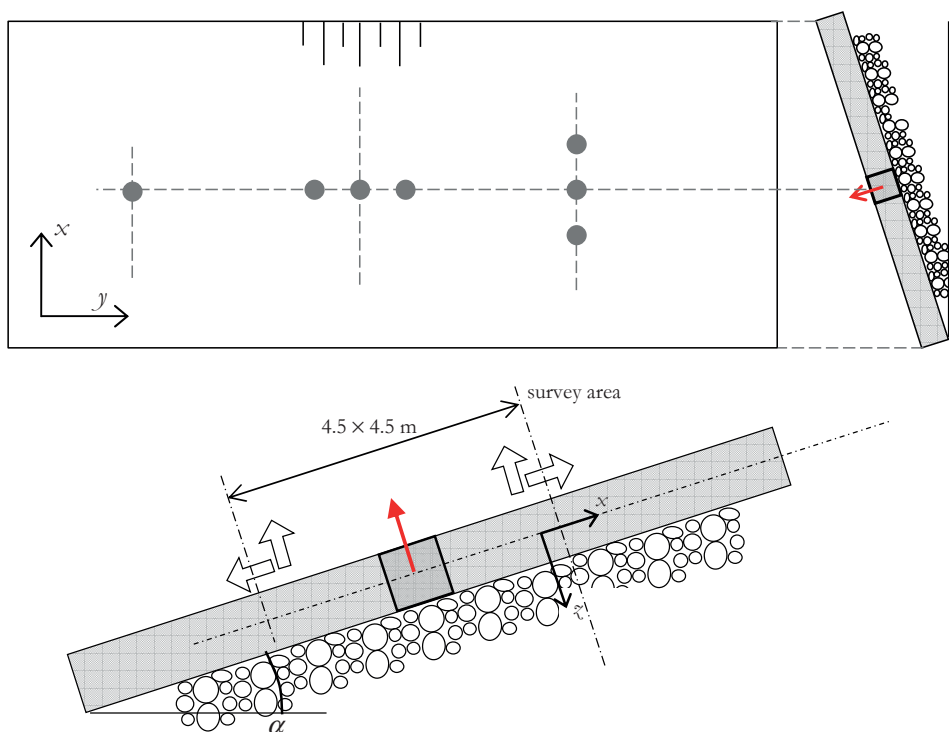
Figure G–5   **Test set-up for one test line**

Table G–3   **Typical laboratory test results of stone parameters**

		measured ρ [kg/m³] *)	measured $f_{r\,max}$ between two stones (stick)	measured $f_{r\,dyn}$ between two stones (slip)	measured E [MPa]
A	Hydroblocks	3032	0.86	0.76	29750
B	Basalton, Tholen	2944 **)	0.47	0.39	29550
C	Basalton, St. Philipsland	2786	0.50	0.44	36100

*) For evaluation of the average weight of the top-layer an open space ratio of 0.10, 0.12 and 0.15 must be adopted for the three locations.

**) All measured values are based on laboratory tests of collected columns of the tested slopes. $n = 2$ for all tests, with less than 10% differences between the two tests results, except for **), where 2571 and 3000 was measured, which suggests a mix of stone with two types of concretes.

The load was applied with oil jacks, a steel beam frame and resin anchors in the concrete element. The deformations were measured with help of 40 rectilinear displacement transducers, with a range of 10 cm.

The parameters of the structure elements were checked with simple laboratory tests. The results of the friction factor show a noticeable trend with the age of the structure. It seems

that loadings, movements and wear and tear of the elements of the revetment top-layer decrease the friction coefficient between the stones.

During the tests the degree of joint fill was registered. 80% of the joints was filled up to a level of 0.94 D at location *A*, up to 0.86 *D* at location B low, 0.65 *D* at B high and 0.76 *D* at location C. The high survey line at location B and location C show the poorest, and also the least constant fill level of the joints.
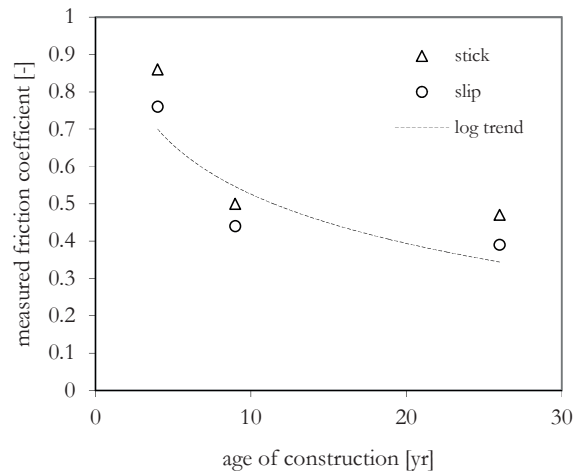
Figure G–6   **Laboratory test results of friction coefficients between two elements against age**

G.4   Experiment results

G.4.1   Typical observations

During the tests large forces were exerted on a single element. In most of the cases the pulled element remained fixed in the revetment plate and, as a result, an area around the loaded element was lifted, creating a bell shaped deformation of the revetment plane. The triple tests were set-up and executed with equal forces among the three points.

The bell shape appeared in many cases not symmetric in *x* and *y*-direction. For the three-in–a-row tests the bell shape was typically irregular.

The single elements were in many cases loaded with slightly eccentric forces. This was done on purpose. The eccentric load incurs rotation and the element clamps itself in a fixed position between the neighboring elements.

During a limited number of tests this mechanism failed and the pulled element could not transfer the forces to the neighbouring stones. The pulled elements tended to move out, either in one smooth move, or in a step by step process of experiencing movement and getting stuck again. The stick-slip mechanism caused short sudden jumps in displacement. As the force relapsed due to the passive jack load system, the movement of the element was not accelerated. In the relevant cases the element got stuck in an approximately 5 mm higher position and could be loaded again, in incidental cases to a higher load level. In most cases this could be repeated three times. After that the element slipped out under further loading.

In cases where the load could not be increased, the element slipped out under a roughly constant load. These tests were stopped after an element displacement of 0.2 times the element height D.

The most important data reading was the deformation of the surrounding revetment field. The size, shape and magnitudes of the deformation were surveyed. For analysis of the shape of the deformed revetment area, the central element was ignored. The displacement of the elements just adjacent to the pulled (and possibly slipped) element was considered as the peak displacement u_c (see Figure G–7).

In natural load conditions the forces on the elements are not extremely concentrated load. The observed slip failure of the single pulled stones is therefore of less practical value. Nevertheless these observations could be used to extract and evaluate properties of the structure.

The displacement data were processed and presented as elevated surfaces, showing the size, the aspect ratio on plan, the gradients and the magnitude of the peak displacement. Also load-displacement curves were made, using u_c as defined in Figure G–7.
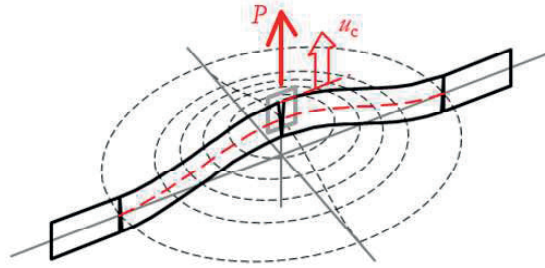
Figure G–7   **Typical idealised bell-shaped deformation on revetment field with slip-failure of the pulled element**

G.4.2 *Load factors*

The test results of the pull forces can be presented as load factors $n_{LF} = F_u/G$, with G as element weight $\rho g D\, B_x B_y$.

For the triple tests a transformation of the results was found in order to compare them with the single pull tests by using the interpretation that the 3 loads lift the stones in between the 1st and 3rd pulled stone anyway. The sum of the three loads complies with an area of the revetment: $A_3 = (F_{u1} + F_{u2} + F_{u3})\, /\, \rho g D$. The three point loads have a spacing of $L_1 = 1$ m each. We assume that the area A_3 has a theoretical shape of two half circles with radius R and a rectangular middle section of $2RL_1$ m. The middle section is omitted when we calculate $n_{LF} = A_1/B_x B_y$ with $A_1 = A_3 - 2RL_1$, where R follows from $\pi R^2 + 2RL_1 = A_3$. The results of the load factors are shown in Figure G–8. The average numbers of the triple tests (n_{LF} 69.1 and 64.7 for horizontal and vertical) based on the transformation described above more or less comply with single pull-out tests ($n_{LF} = 62.1$).

The results for the load factors are summarised in Figure G–8 and Table G–5. All results show a large scatter with a typical variation coefficient of 0.5. The results of location C are lower than A and B. This can be explained by the shorter slope, which is shown in Figure G–9.

Table G–4   Typical test results load factors

Processed results for n_{LF}	All tests		Selected tests not influenced by slip failure	
	Hydroblocks A	Basalton B and C	Hydroblocks A	Basalton B and C
Average	58.3	68.8	66.6	89.4
Number of tests	21	37	14	19
Standard deviation	29.7	38.9	31.8	41.2
Variation coefficient	0.51	0.57	0.48	0.46
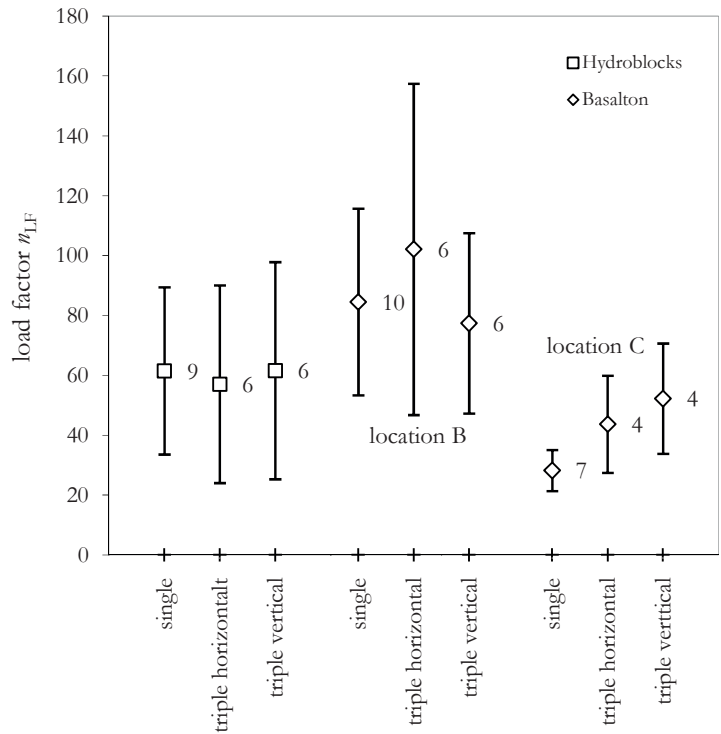
Figure G–8   Measured and derived results of load factors, size of data sets indicated

Table G–5   Summarised test results

Test type	Location	Average maximum total pull force [kN]	Load factor for total of 3 loads	Processed load factor n_{LF}	Number of tests
Single	A high	50		75.7	5
	A low	23.8		40.8	4
	B high	23.8		72.4	5
	B low	30.6		93.1	5
	C	9.4		28.5	7
Triple, horizontal row	A high	98.7	149.4	75.5	3
	A low	53.3	86.5	38.5	3
	B high	60.3	183.6	96.6	3
	B low	65.7	199.9	107.4	3
	C	35.5	108.4	43.6	4

Test type	Location	Average maximum total pull force [kN]	Load factor for total of 3 loads	Processed load factor n_{LF}	Number of tests
Triple, vertical row	A high	89	134.7	67.3	3
	A low	70	120.2	55.7	3
	B high	56	170.5	85.5	3
	B low	47	147.1	69.2	3
	C	41.8	126.7	52.2	4
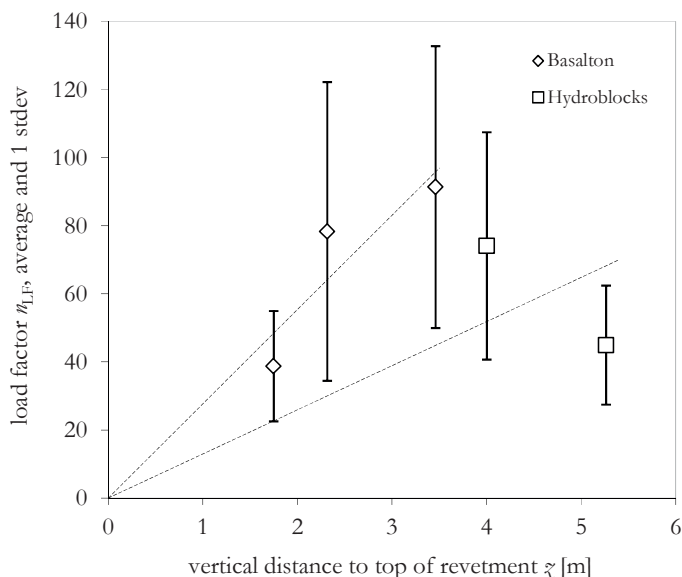
Figure G–9   Load factors results plotted against vertical position on the slope

The trend of the pull-out resistance increasing with a lower position on the slope appears not valid for the tests at location A. The pull-out resistance at the low survey of location A might be affected by the toe structure. The air temperature was also lower during execution of the tests at location A (see Figure G–10). A lower temperature is associated with a lower axial restraining force and with more loose elements.

Like in the 1990s pull tests (see Annex D) a strong temperature dependency can be observed. It can be noticed that the temperature trend of the Hydroblock results is steeper than of the Basalton. Apart from stochastic reasons, this may be caused be the row oriented pattern of the Hydroblocks. The horizontal rows have a tendency to build up more temperature stress than the more random orientated Basalton columns, where the temperature expansion can be transferred in transverse direction also.
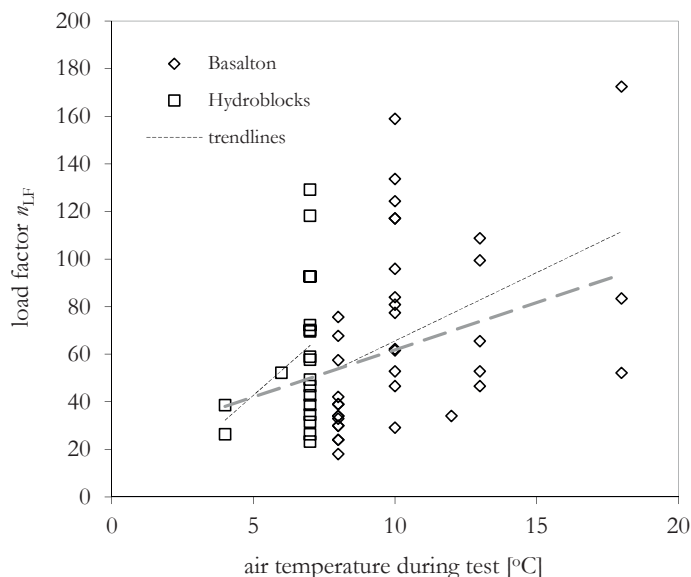
Figure G–10   Load factors results plotted against air temperature

G.4.3   *Regression analysis on load factors*

Linear regression analysis was used to discover what causes show the strongest influence on the differences in the 58 measured values of the load factor n_{LF}. Following variables are investigated: the vertical distance to the top, the vertical distance to the toe (and alternatively a Boolean variable for proximity of the toe), the air temperature, the age of construction, the joint fill grade and the element height-width ratio D/B.

Various combinations of these variables are tested for their effect on the results. The temperature dependency and effect of distance from the top are known positive effects that express themselves here also. The effect of proximity of the toe is very obvious for the location A. A general dependency of proximity to the toe cannot be found. Including a dependent variable z_{toe} as vertical distance to the toe (set 3, 4 and 5) does not improve the picture. Also introduction of a Boolean variable was tried (set 6, 7 and 8) because the models in Annex A.1 prove that at some distance of the toe there will be no effect. A general variable for proximity of the toe does however not produce convincing *p*-values. When the Boolean variable is limited to location A (set 9, 10, 11 and 12), the results are acceptable. The known dependencies (set 1 and 2) are than improved. The condition of the toe at location A has an apparent negative influence on the pull-out strength. The fact that these tests were also carried out at low air temperatures is not the primary cause. The dependency on air temperature is still strong and more reliable after adding a variable for the proximity to the toe. The effects of temperature and age of the revetment seem to level out in this data set. Both show strong dependencies (set 9 and 11) but the dependency is less strong in sets where they are together (set 12).

Dependencies on the aspect ratio height / width [306] and the joint fill level could not be proven.

Table G–6 **Statistical dependencies of test results**

p-values of linear regression *	x_1 temp	x_2 z_{top}	x_3 z_{toe}	x_4 yes/no proximity of toe	x_5 age	x_6 D/B	x_7 z_c/D
Set 1	0.00059	0.043					
Set 2	0.29	0.034			0.044		
Set 3	0.0023	0.11	0.18				
Set 4	0.50	0.027	0.044			0.12 **	
Set 5		0.98	0.042				
Set 6		0.60		0.97			
Set 7	0.00077	0.13		0.96			
Set 8	0.00055	0.98 **		0.99			0.13
Set 9	0.00020	0.0012		0.0011 ***			
Set 10	0.021	0.10		0.0039 ***			0.61
Set 11		0.0011		0.0061 ***	0.0013		
Set 12	0.16	0.00044		0.0042 ***	0.18		

*) low value means a low probability that the sample values of the tests differ from the calculated dependency
**) negative dependency
***) Boolean only for location A

The regression formulas for set 9, 11 and 12 (with chosen zero intercept) are:

$$n_{LF} = 13.6\, z_{z.top} + 3.4\, T - 48.4 \,[\text{yes/no toe location A}]$$ **Eq. G.6**

$$n_{LF} = 16.3\, z_{z.top} + 1.54\, \text{Age} - 46.9 \,[\text{yes/no toe location A}]$$ **Eq. G.7**

$$n_{LF} = 14.3\, z_{z.top} + 1.42\, T + 1.08\, \text{Age} - 43.4 \,[\text{yes/no toe location A}]$$ **Eq. G.8**

Although the first equation gives the best result in terms of statistical reliability, the third (Eq. G.8) is considered most realistic. In earlier pull tests the effects of both age and temperature have been proven. Also a linear dependency of 3.4 point per degree of temperature is believed too strong. The load factor results have been corrected using Eq. G.8 and are shown in Figure G–11. The average of the total population of tests is still at 64.9. The variation coefficient has dropped from 0.55 to 0.45, which means that the value of a lower confidence bound is increased.

The distribution of the total population of load factor results is analysed using Weibull fit curves for the low probability tail. The cumulative Weibull distribution function has the general form of:

$$\text{cdf} = 1 - \exp(-(n_{LF} / a)^b)$$

---

[306] Given the fact that all tests were done on columns with D/B ranging from 1 to 1.5

The measured load factors can be generally described with a Weibull function with $b = 2$, which is a Rayleigh function. This was found by Klein Breteler also. For these tests the low-probability tail, which is most interesting from design perspective, is better described with a distribution with $b = 4$. The corrected load factors are best fitted with $b = 2.5$.

In Figure G–12 the ranked results are plotted together with the distribution functions, on normal scales and log scales. For the measured load factors the results at location C are dominant in the low values. For the corrected load factors location B is dominant.
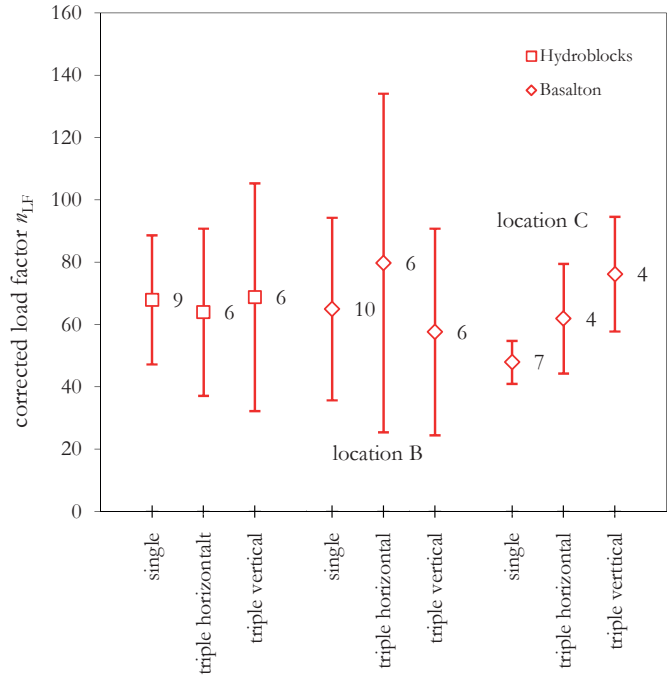
Figure G–11   **Load factors results per test category, corrected for effects of position on the slope, temperature, age and proximity of a weak toe structure**

G.5   Evaluation of directional properties

G.5.1   Methodology of further evaluation of the tests

The tests were carried out with the purpose of learning from directional dependencies. The traditional single element tests were therefore supplemented with three-in-a-row tests in two directions. These tests are evaluated looking into the force results, the displacement magnitude results and the shape of the deformed area. The three-in-a-row tests are expected to show deformed areas stretched into the direction of the three loads. In some cases the three loads were more or less equal in magnitude and the stretched deformed shape was indeed observed. In other cases the loads distribution was asymmetric, or elements slipped

out while the other elements could be loaded further. These situations complicated the FEM analysis with four beams. The respective cases were excluded from earlier published results.

The methodology proposed here is based on converting the load cases back to the two-beam model. First for all cases consistency of the output of forces and size of the deformed shape is checked. The size of the lifted area is corrected if needed, whilst the measured aspect ratio of the deformed shape is unchanged.
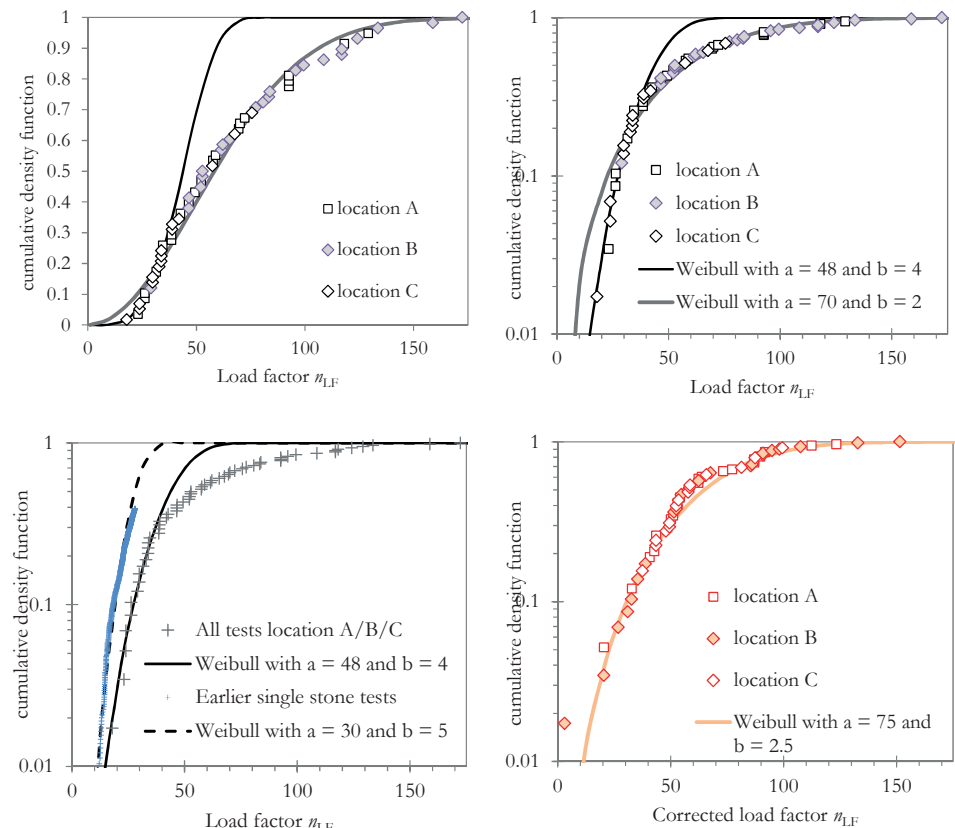
Figure G–12   **Fitted Weibull distributions**

For the cases with asymmetric loads a reduced intermediate distance is calculated which is subtracted from the stretched deformed shape. The corresponding load factor of the remaining part of the shape was determined. For those combinations of load factors and peak deformations compliance with the model formulas is determined. The deformations are compared by calculating a fictitious Young's moduli, first using the circular plate model, and second using the beam model, resulting in Young's moduli per direction x and y and in bending moment in x and y direction. From these bending moments a minimum normal force could be calculated.

The equilibrium of the remaining middle strip could also be checked, also resulting in a value of the normal force. This result was averaged with the result of the two-beam model and presented in Table G–9.

G.5.2 Measured displacements

The measured displacements at the elements adjacent to the pulled element can be presented in force-displacement diagrams. The displacement at the point of the maximum achieved force is plotted in Figure G–13.

The points are compared with curves belonging to the model formulas for the circular plate with central load (Eq. B.34). The measured displacements are in conformity with the model formula results in case fictitious Young's moduli E_f of 70 to 300 MPa are applied. The variation coefficients are mostly in the range of 0.4 to 0.6. In case not only the maximum deformation points, but all intermediate readings were included, the E_f could in many cases not be kept constant during increase of load, which means that the elements were initially loose, and stiffening occurred. Most test that appear strong and stiff, give constant values of E_f during the test.

Table G–7 Model stiffness parameter E_f fit of the measured displacements

E_f [MPa]	D [m]	D/B	Single test	Triple - horizontal	Triple - vertical	All tests	Average per location
Location A – high	0.385	1.54	75	142	85	105	102
Location A – low	0.345	1.38	96	91	109	100	
Location B – high	0.24	1.02	214	265	231	231	248
Location B – high	0.24	1.02	254	314	131	253	
Location C	0.245	1.04	87	71	56	75	75
Per test type			145	176	123		

The results are, given the variation within the group, reasonably constant per location. The Hydroblocks at location A show, together with the Basalton at location C, a 3 to 4 times lower value of the stiffness. The low survey line at location A, that suffered from low pull out strengths does not have lower stiffness values. The results do not seem biased by the test method, which can be noticed in Figure G–13 and Figure G–14 also. The triple tests could be loaded to higher load factors, affecting a larger area of revetment. But the force-displacement points follow the model formulas reasonably well, with similar stiffness as the single element tests.
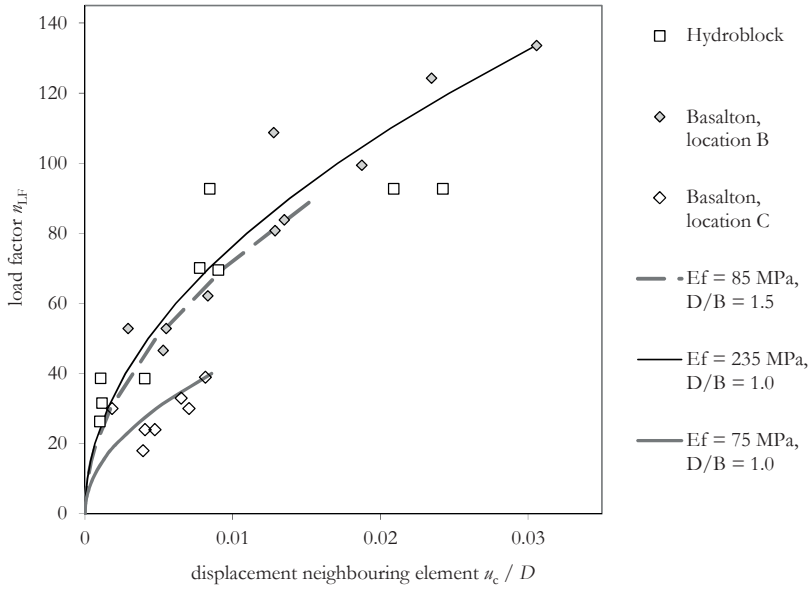
Figure G–13 Measured force-displacement points compared with model graphs, single element tests
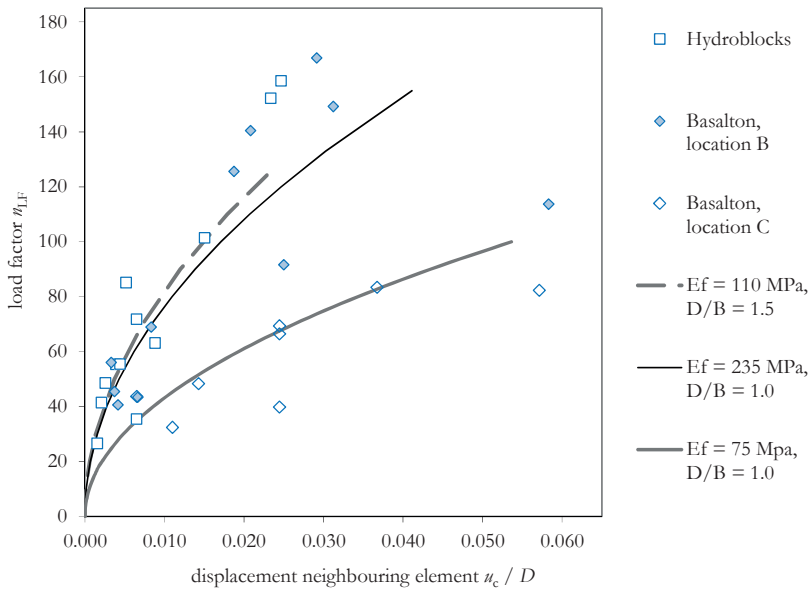
Figure G–14 Measured force-displacement points compared with model graphs, triple element tests

G.5.3 Analysis of deformed shapes

The deformed shapes are characterised by the size and the aspect ratio of the area and the peak deflection. The peak deflection is defined as the deflection of the element adjacent to the pulled element. The Young's moduli and the normal force per direction are calculated with the two-beam model. For the normal force the minimum force that follows from the bending moment and the maximum internal lever arm ½D is adopted.

Table G–8   Directional test and evaluation results of single tests

Test #	Position on slope	m_{LF} of the considered load step	L_y/L_x	L_x [m]	L_y [m]	u_c [mm]	E_x [MPa]	E_y [MPa]	N_x [kN/m]	N_y [kN/m]
TA2	high	92.7	1.58	2.04	3.22	8	10	84	6.4	34.8
TA3		69.5	1.51	1.91	2.89	4	17	116	5.9	27.3
TA4		92.7	1.18	2.39	2.83	3.5	69	157	11.8	22.6
TA13	low	70.1	1.19	2.15	2.55	2.5	79	181	9.5	18.5
TA15		26.3	0.89	1.37	1.22	0.35	112	61	5.2	3.2
TA16		38.6	1.50	1.42	2.14	1.4	18	125	3.3	14.9
TB1	high	108.7	0.99	2.41	2.39	2	348	334	13.2	12.8
TB2		46.6	1.10	1.70	1.86	0.9	177	281	5.9	8.6
TB3		99.4	0.99	2.58	2.55	4.5	205	193	15.2	14.5
TB5		62.1	1.23	1.54	1.89	2	47	126	4.4	9.5
TB12	low	52.8	1.23	1.74	2.14	1.3	118	319	5.5	12.2
TB14		124.2	0.86	2.78	2.40	3	415	193	20.2	10.9
TB15		83.9	1.10	2.20	2.42	3	150	241	10.0	14.5
TB16		133.6	1.01	2.56	2.58	3	293	303	14.7	15.1
TC1		29.9	0.75	1.50	1.12	0.4	246	50	7.2	2.0
TC2		23.9	1.24	1.18	1.47	1	33	93	2.7	6.1
TC3		17.9	0.93	1.05	0.98	0.4	64	45	2.8	2.1
TC4		23.9	1.56	0.99	1.55	0.3	36	294	1.5	7.8
TC5		32.9	1.13	1.45	1.63	1.6	52	94	4.4	7.1
TC6		29.9	1.22	1.24	1.51	1.2	33	88	3.0	6.4
TC7		38.9	1.21	1.33	1.60	2	27	67	3.5	7.1

Table G–9   Directional test and evaluation results of triple tests

Test #	Position and type of test		m_{LF} of the considered load step	L_y/L_x	L_x [m]	L_y [m]	u_c [mm]	E_x [MPa]	E_y [MPa]	N_x [kN/m]	N_y [kN/m]
TA6	high	h	85.1	0.98	2.63	2.57	2	211	187	13.0	11.1
TA7		h	152.2	0.80	3.89	3.12	9	216	67	32.5	12.5
TA8a		h	71.7	0.97	2.43	2.35	2.5	123	103	11.5	9.1
TA8b		h	55.3	1.07	2.03	2.17	1.5	93	131	7.5	8.6
TA9		v	35.5	0.83	1.85	1.53	2.5	68	25	7.1	4.1
TA10		v	63.1	0.80	2.50	2.01	3.4	98	31	13.3	6.4
TA11		v	158.5	0.75	4.10	3.08	9.5	240	51	38.3	13.2

Test #	Position and type of test		m_{LF} of the considered load step	L_y/L_x	L_x [m]	L_y [m]	u_c [mm]	E_x [MPa]	E_y [MPa]	N_x [kN/m]	N_y [kN/m]
TA17	low	h	26.5	0.94	1.50	1.41	0.6	75	54	4.6	3.2
TA18		h	41.4	0.93	1.88	1.75	0.8	140	96	7.1	4.8
TA20		v	55.4	1.30	1.84	2.39	1.7	44	154	4.5	12.3
TA21		v	101.4	0.63	3.59	2.25	5.8	184	11	35.4	5.0
TA22		v	48.6	0.84	2.15	1.80	1	185	74	9.4	5.6
TB6	high	h	43.4	0.61	2.24	1.37	1.6	230	12	11.6	1.1
TB7		h	166.8	1.14	3.22	3.66	7	285	533	15.4	23.7
TB9		v	68.9	1.23	1.99	2.45	2	154	134	5.1	11.6
TB10		v	91.6	0.97	2.58	2.51	6	141	469	10.8	10.7
TB11		v	149.2	1.28	2.87	3.68	7.5	414	307	10.1	26.4
TB17	low	h	125.5	0.94	3.07	2.89	4.5	374	98	16.9	12.4
TB18		h	45.4	0.78	2.03	1.58	0.9	348	357	8.4	2.8
TB19a		h	189.6	1.01	3.65	3.67	10.5	563	248	22.6	21.4
TB19b		h	140.4	0.85	3.41	2.91	5	45	290	22.2	11.1
TB20		v	40.6	1.49	1.39	2.07	1	28	162	2.1	8.8
TB21		v	113.7	1.45	2.35	3.41	14	74	174	6	23.9
TC8		h	43.6	1.19	1.61	1.92	1.6	78	23	4.4	7.1
TC9		h	82.3	0.79	2.71	2.15	14	68	13	15.5	5.6
TC10		h	32.4	0.74	1.76	1.31	2.7	79	60	6.7	1.9
TC11		h	48.3	0.95	1.90	1.80	3.5	95	66	6.8	5.1
TC12		v	83.4	0.93	2.52	2.34	9	16	62	11.3	9.5
TC13		v	84.3	1.34	2.11	2.82	19	10	45	5.5	16.7
TC14		v	39.8	1.37	1.43	1.96	6	146	7	2.5	8.1
TC15		v	69.3	0.62	2.81	1.75	6	211	187	21.4	3.1

Table G–10   Check of dependency of results on test method

Aspect ratio L_y/L_x Average and standard deviation		Type of test		
		single	triple horizontal	triple vertical
Hydroblocks	Location A	0.80 0.19	0.95 0.09	0.86 0.23
Basalton	Location B	0.95 0.12	1.01 0.39	1.28 0.24
	Location C	0.91 0.23	0.92 0.20	1.06 0.36
	Average Basalton	0.93 0.17	0.97 0.31	1.17 0.30
Average total population		0.89 0.18	0.96 0.25	1.01 0.32

In Table G–10 the measured and processed aspect ratios of the deformed revetment areas are compared. Special attention must be paid to the question whether the test methods are a reliable predictor for the investigated directional differences. The triple test might bias the aspect due to their orientation of applied force in a line.

A first observation of the average result is that the horizontal and vertical triple tests show an opposite effect. The vertical tests produce a slightly larger value of L_y/L_x, meaning that the deformed area is larger in longitudinal direction.

A statistical comparison of the three data sets using the t-test for independent samples with unequal variances gives: $p = 0.32$ for set 1 and set 2, $p = 0.10$ for set 2 and set 3 and $p = 0.18$ for set 1 and set 3. There is no reason of rejecting the hypothesis that the individual test results are all from the same set. The test results are therefore deemed reliable and all tests can be used as to increase the power of the findings.

In Figure G–15 the calculated normal forces are presented as N_x against N_y. If a marker is on the line $y = x$, the normal force is equally distributed in x and y direction. If the markers are left or above the line the revetment has a dominant normal force in transverse direction, caused by down slope gravity forces. If the markers are right or below the line, the revetment had a dominant normal force in the longitudinal direction, caused by lack of shear strength in the revetment and possibly be temperature effects. The forces are first made dimensionless by first dividing them by $\rho_s g\, D$, giving a force expressed as the weight of a m^2 of revetment (per running m), and second by dividing them by D.
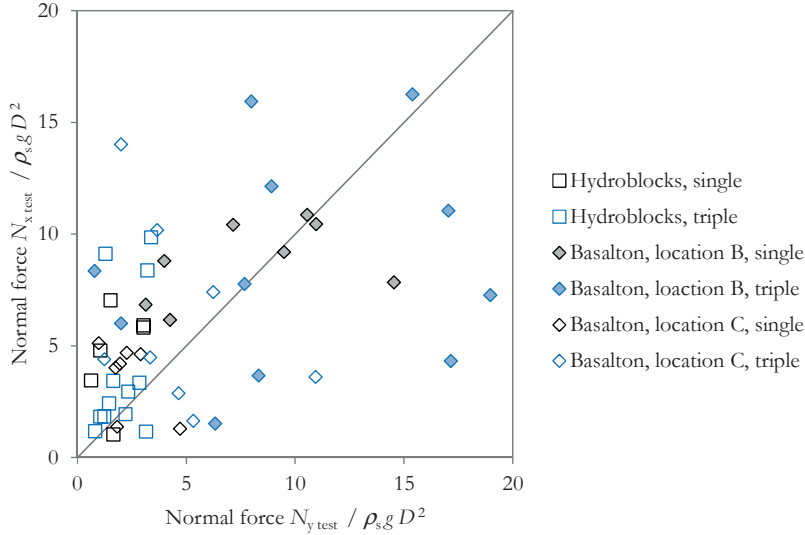
Figure G–15   Calculated normal forces in two directions, expressed as $N/\rho g D^2$

Including the location on the slope in the presentation in the results can be done by dividing the normal force by the theoretical neutral normal force at the test position: $N_{neutral} = \rho_s g$ $(z_{top} - z_{test})$. Figure G–16 makes clear that there is a tendency that N_x is bound a maximum of $N_{neutral}$ and that N_y may exceed the value of $N_{neutral}$, which does not have much physical meaning in the longitudinal direction. Points with $N_x/N_{neutral} = 1$ and $N_y/N_{neutral}$ is 1.5 or 2,

are a sign of a revetment with high developed longitudinal in-plane stress, compare to overconsolidated soils, with $K_h = 1.5$. It might also be possible that a part of the 'measured' normal force was not initially present but is generated by axial movement of the elements caused by sufficiently high vertical deformation of the revetment during the tests.

The two tests in Figure G–16 that are clearly above $N_x/N_{neutral}$ =1 (TC9 and TC15) are on slope C. The top of revetment is not the end of the slope. Above the revetment the slope continues as a grass slope. Soil pressure and axial force acts against the first row of elements and may indeed give a higher neutral force.
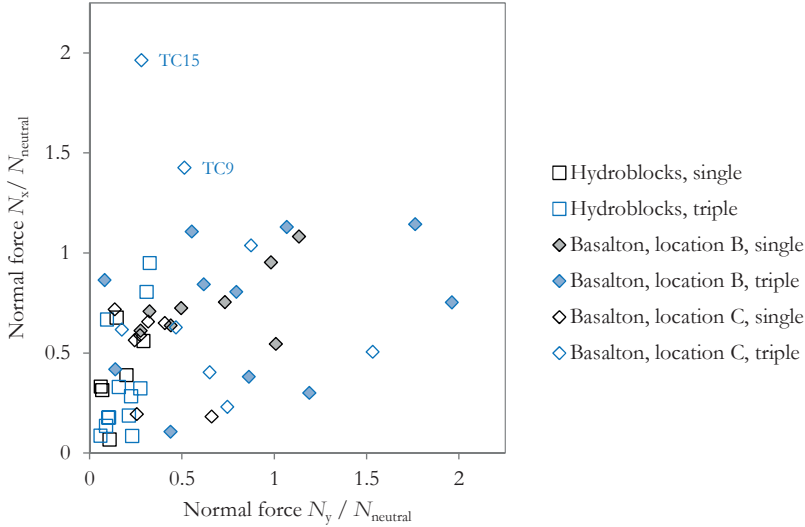
Figure G–16   Calculated normal forces in two directions, expressed as $N/N_{neutral}$

Another observation is that for the majority of the points the normal force in x-direction has the tendency to stay below a value of approximately 1, whilst the normal force in y-direction goes beyond 1. In y-direction the limit value of 1 has no physical meaning. The revetment cannot expand and if the system wants to expand the restraint force will increase. From Figure G–15 is can be concluded that there is no minimum value for both in x- and y-direction.

The strong temperature dependency presented in Figure G–10 is further analyzed by comparing the temperature dependency of N_x and N_y. The results for Basalton are plotted in Figure G–17. The hydroblocks are excluded because of the small range of temperatures during execution of the tests. It appears that $N_y/N_{neutral}$ has a much stronger temperature dependency than $N_x/N_{neutral}$. This is in line with the model. In y-direction the revetment is restrained and in x-direction it can expand.

The dependencies of the test results on the slope angle and position on the slope are investigated by comparing the average (and standard deviation) values of the subgroups. The results $N_{x,test}$ are divided by the model assumption of a neutral normal force. Plotting against z [m] expresses the relation with the length of the revetment beam and the effect of sub-layer friction elasticity. Plotting against z/D moves the points of location C with the relative tall Hydroblocks to the left. See Figure G–18. This way of plotted gives a better indication of
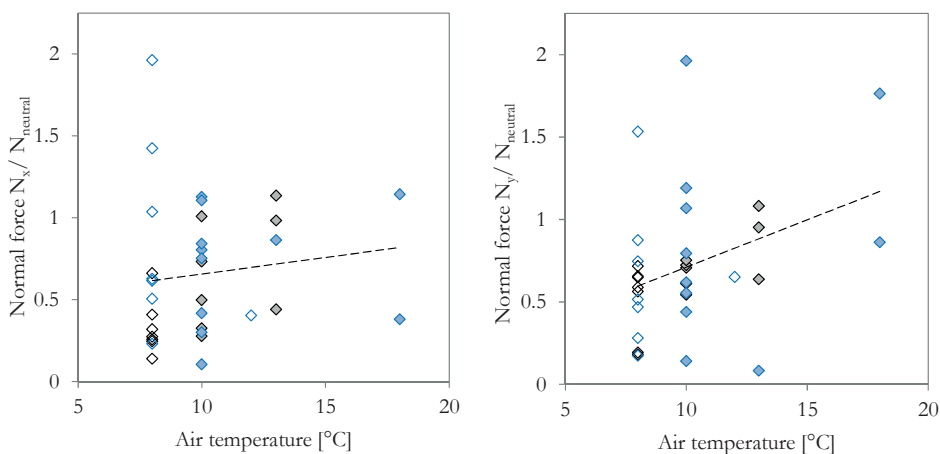
Figure G–17 Calculated normal forces $N_{x;test}$ and $N_{y;test}$ /$N_{neutral}$ plotted against air temperature during test
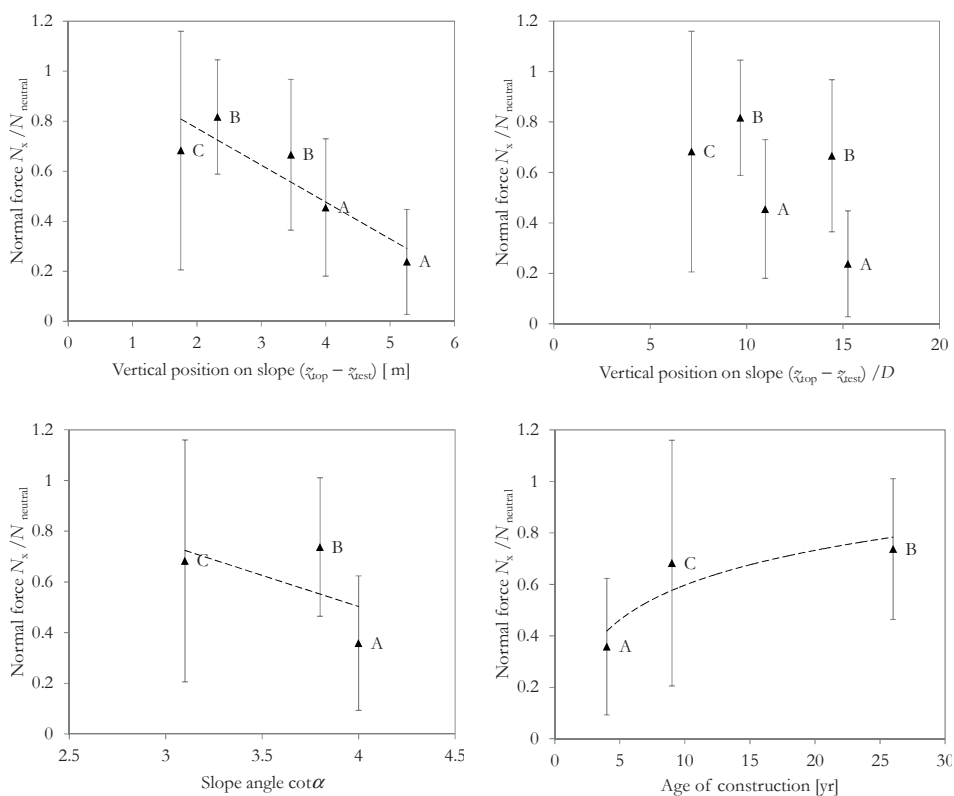
Figure G–18 Calculated transverse normal force expressed as N_x/$N_{neutral}$ against position on the slope, slope angle and age of construction

the revetment beam elasticity itself. It can be noticed that the Basalton revetments on location A and B are closer to 1. Looking at the results for the location A and B there seems on average a constant ratio of 0.7 .. 0.8 with the model of $N_{neutral}$. The conformity with the model and/or the deviaton from the model can have different reasons.

- Location C has a steeper slope, which makes it easier for the revetment to slide.
- Location C has not been exposed to heavy waves, the fetch for local waves in front of the dike is relatively short.
- Location B has experienced a service life of over 25 years, and the location is more exposed to waves. The elements have a smaller D and have hence been lifted and re-arranged in the past.
- Location A is very young. Less settlement of the dike has taken place since the beginning of the service life.

Location A has a lager tidal range, but has no severe wave action. The slope is in a relatively sheltered position at the far end of the Western Scheldt river estuary (see Table G–1). The revetment elements may be moved by the tidal cycle but not lifted from their position.

The number of test locations is too small to accurately differentiate between the mentioned influence factors. The factors interact with each other. Wave action for instance can lead to re-arrangement, a better packing and hence a higher normal force, but at steeper slopes less wave action is required to achieve the same. Age of construction can be interpreted as effect of dike settlement having taken place, but also as an indicator of increased probability that serious wave action has taken place. The proximity of the toe is an issue at location A. The revetment was found to be quite loosely packed with limited effect of frictional interlocking. This is most likely due to a weak toe structure, but also due to the gentle slope.
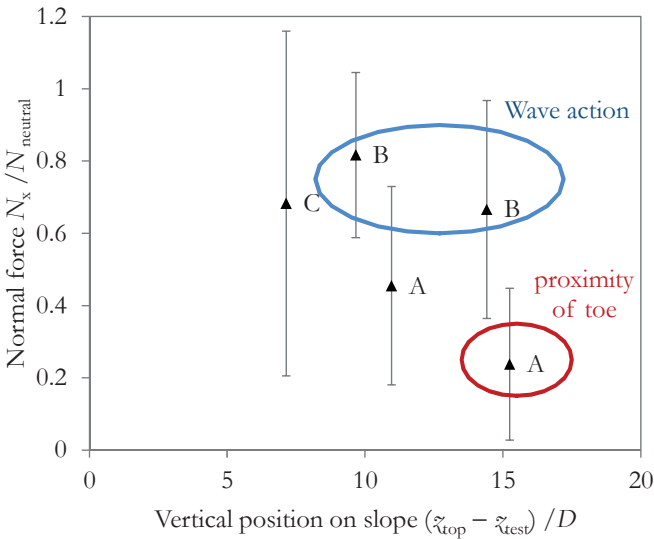
Figure G–19   Calculated transverse normal force expressed as $N_x/N_{neutral}$ against position on the slope

G.6 Discussion and conclusions on field experiments

The experiments with multiple pull tests and measured deformations have proofed very useful and has provided insight in the in-plane stress state of the revetment when it is in rest. It was found that in-plane forces are present in two directions, but in the same time a large scatter was found. The tests were suitable and specific for confirmation of the relation between strength and stiffness and through that relation we could establish the normal force levels.

Other test methods would have been damaging to the revetment. Later an alternative non-destructive test method using dynamic impacts was tried. This method appeared not suitable.[307]

The test method with three pulled elements in a line appeared quite complicated in post-processing. The triple test was designed to transfer a large total force without single element failure and to learn from typical patterns of dominant force action in x- and y-direction, but the measured values showed a large scatter and the triple tests did with hindsight not generate specific insights and different overall conclusions.

The Hydroblocks were expected to show high forces and clamping in the rows, but the slope appeared quite loosely packed. Therefore the conclusions on N_x and N_y and their ratios can only be based on the Basalton slopes. The slope that appeared well pre-loaded is slope B. Specific for that slope there seems to be an issue with the outcomes of the triple tests, as can be seen in Figure G–20. For location B almost all tests with three pulled elements in a vertical row produce $N_y / N_x > 1$ and all tests with three elements in a horizontal row $N_y / N_x < 1$.
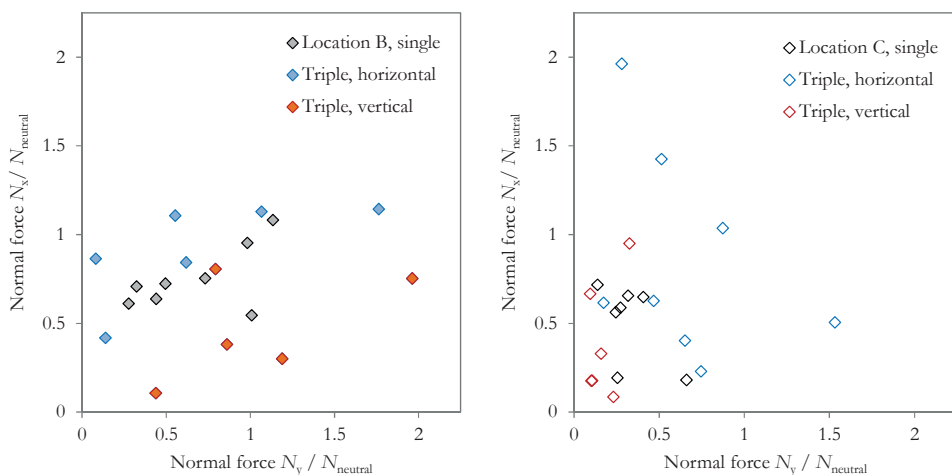
Figure G–20   Calculated normal forces N_x and $N_y / N_{neutral}$ with dependency on test method

The pull tests described in this section make a difference with the earlier small pull tests that were truncated at 9 kN. Contrary to the new tests those tests were not suitable as an

---

[307] See R. 't Hart, *Klemming in steenzettingen bepalen met VGD-metingen*, 2012

indicator of in-plane force. We now have a good insight in the initial normal force in the slope. Based on that we conclude the following.

At older slopes of moderate slope angle ($\cot\alpha = 3.8$ in the tests), with a traditional toe structure, that have experienced wave loading and maybe also have experienced some dike settlement, an average in-plane force in transverse direction of approximately 0.7 $N_{neutral}$ is present.

There is a large scatter in results. If we rely on the slope with the best pre-load condition, we could decrease the scatter by neglecting the triple tests. For the other slopes this is not the case. The conclusion could be that the normal force must be present in significant magnitude before you can produce statistically reliable test results. It we neglect the triple tests the average in-plane force in transverse direction is still approximately 0.7 $N_{neutral}$, but (based on the grey markers in Figure G–20) with a higher 5% underbound. This axial pre-load level is significantly higher than found in Annex D based on the small pull tests performed in the 1990s.

Some other conclusions are:

- A drop of normal force for revetment on a 1:4 slope, close to the toe structure was observed. The deformation of the toe-structure is likely reducing the lateral support of the revetment slab.

- A temperature dependency of the longitudinal normal force was observed. This is in line with the conclusions based on the small pull tests (Annex D).

- The calculated effective axial plate stiffness E_a including the flexibility of the joints is in the order of 300 MPa. The calculated flexural stiffness E_f is in case the normal forces are quite high around 200 MPa (slope B), and in case they are low around 75 to 150 MPa (slope A and C).

Design of pattern-placed Revetments – Annexes

ANNEX H   TESTING TOE STRUCTURES

Irrespective of the weight, the angle and the length of the revetment, toe structures of Dutch dikes in most cases consist of a small timber pile row, supported with randomly placed small rock. Refer to Figure 3–24. The question is whether that is an adequate solution for providing support to the revetment.

Looking at revetments through the model approach of this study toe structures are important. The resistance and stiffness of these toe structures against lateral loads is a pre-condition for developing of in-plane forces in the revetment top-layer.

The in-plane force plays a crucial role in friction interlocked pull-out resistance of the revetment elements, and as a result in withstanding wave attack.

In literature dating from the 1990s desk studies into the geotechnical stability of toe structures can be found. These are discussed in chapter 3 and Annex A.1. The stability and stiffness has as far as we know never been measured. Therefore a small field test series was designed. Toe structures were loaded with a repetitive lateral force. The occurring deformations and the water pressures were measured.

H.1 Aim and scope of testing

H.1.1 Test objective

In 2008 a project[308] was defined in or to test typical toe structures by subjecting them to a lateral load.

The toe structure is to maintain the elements on the slope above in position. The revetment tend to slide over the bedding layer and will be resisted by friction on the bedding layer and by the lateral resistance of the toe. As a result the lateral force on the toe can not be determined in a straightforward manner. Moreover the force may vary in time since settlement and creep of soil occurs. Also variation in water level has influences. Any raise of the water pressure will decrease the effective soil stresses and increase the deformation under a certain load. Deformations may be caused by these effects, causing hysteresis and increasing permanent deformations.

Therefore the tests were executed with repeated loads and also with loads that remained constant during a longer period, including several astronomical tide cycles. Forces and displacements were to be measured all the time. Initially the load application was meant to be force-controlled as well as deformation-controlled, but the latter appeared not practically possible.

In practise the development of normal force over time has different time scales:

- Within a wave period (of maximum 5 to 10 seconds) the water pressure above and under the top-layer and the effective in-plane force vary, and as a result the in-plane force against the toe.
- Within a tidal cycle the revetment weight changes from gross into buoyant weight, and back.

---

[308] D.J. Peters, *Veldproeven op teenconstructies in Zeeland, meetrapport met verkennende analyse*, 2008

- During heavy storms the revetment elements are subject to dynamic variations of joint pressures and lift forces. As a result friction forces decrease and the in-plane force increases. This process was observed and measured in Delta flume experiments.[309] The time scale of this process is minutes to several hours.
- During the process of settlement of the dike body the in-plane force can increase. The time scale of this process is months to several years.

The aim of the test described in this Annex was to investigate the resistance and spring stiffness of the toe response for moderate and high loading rates. The chosen loading rates during the tests were several minutes to 6 hours. Also a 24-hour measurement embracing two tidal cycles was carried out.

The required output is:

- The resistance / lateral failure load of the toe of the toe structure
- The spring stiffness of the toe structure
- The pre-load that was present before test loading of the toe structure

H.1.2 Experiment set-up

Lateral load tests on toe structures while they support an armoured slope were not carried out before and are - given the set-up - potentially destructive. Therefore the available locations were limited to the slopes that were scheduled for a large overhaul in the next year. The tests were done in limited numbers in order to learn lessons and repeat the tests at a later date. The test evaluation is as a result focussed on the observed phenomena and order of magnitude of the forces and displacements, and not on statistical analysis and/or the reliability of the results.
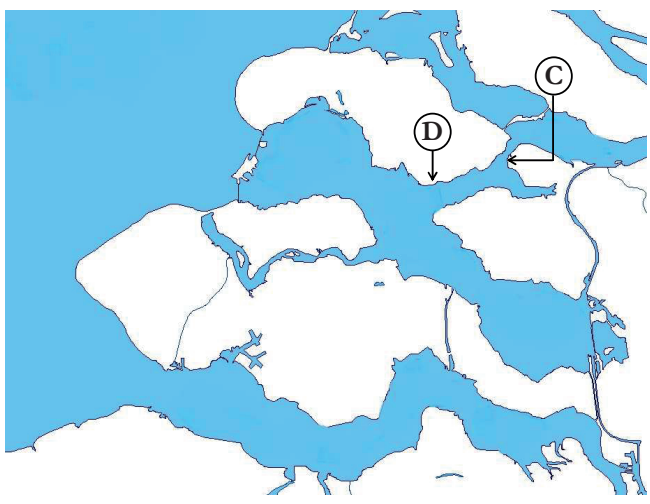
Figure H–1   **Locations of tests on toe structures**

---

[309] G. Wolters and M. Klein Breteler, *Normaalkracht in steenzetting met blokken op hun kant*, 2007. See Figure 3–7.

Available locations were the Willemspolder, near Sluis at St. Philipsland (location C) and the Vierbannen polder near Ouwerkerk at the South side of Schouwen-Duiveland (location D).

Table H–1   Typical data of tested structures

	Location C	Location D
Type of revetment	Hydroblocks	Basalt
Thickness D	0.40 m	0.25 m at the test location 0.35 m above +1.50
Type of toe structure	Timber piles (estimated 1.2 m long) with spacing	Timber sheet pile wall, 1.8 m long, $d = 0.08$ m
Slope	1 : 3.07	1 : 3.41
Toe level	+0.46	−0.50
Top of revetment	+3.19 Plus concreted strip up to +4.11	+3.07
Foreland	Sloping down to -0.50 m at 1:4 After that relatively flat Rock present	Sloping at 1:10 Rock present
Year of construction (estimated)	1992	1954
Remarks	Neighbouring sections have 0.25 m high columns	Slope looks in perfect condition with convex section just above the toe and slight concave slope

In the tests an in-plane load was applied in the revetment relatively close to the toe. The weight of the revetment above the test location provided the counter force.

The application of the force and measurement of the displacement were independent in the test set-up. The force was applied with a hydraulic (oil) jack and small beams for spreading of the load over a length of 1 m of revetment. The jack was connected to a computer-controlled compressor.

Loading up to failure would possibly imply (permanent) deformations of 50 to 100 mm. Damages of this magnitude were not permitted on the selected slopes, since they had to serve one more winter season. Only tests with predicted deformations up to 20 to 30 mm were included in the test design. 3D-effects were purposely avoided as much as possible. Deformations were measured in the centre line of the tests and also on a line just adjacent to the test line. In case any deformations were measured there, 3D effects were to be included in the back-analysis and hindcasting.

The deformations were measured with linear electric transducers (LVDTs). Deformations were measured in a transverse strip in and above the load application zone and in a transverse strip adjacent to the test area in order to compare displacement effects due to e.g. tide and waves (see Figure H–3). The outputs are: deformation measurements at the top of the toe sheet pile, just under and just above the load application, half-way the slope and at the top edge of the slope. The oil pressure and the elongation of the jack are measured as well.

The load is applied over 1 m length, at location C at a distance of three blocks from the toe, which is 0.75 m. The Hydroblocks have in this case an orthogonal pattern without longitudinal bond. Assuming a 1:2 spreading angle the load can be distributed over 1.75 m. From the deformed shape of the toe sheet piles (see Figure H–4) it can be derived that the

deformation along the length adopts a sinus shape with a full wave length of 13 blocks, which is 3.25 m. This is equivalent with a block distribution of 1.625 m width. For location D these values are similar. The applied loads of 25, 45, 65 and 80 kN are hence equivalent to 15.4, 27.7, 40 and 49.2 kN/m respectively.
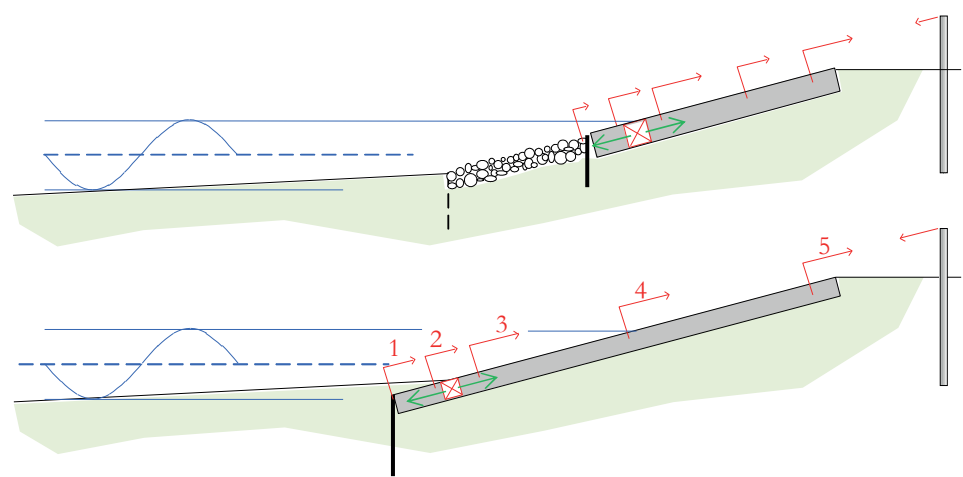
Figure H–2   **Schematic view of test set-up with applied loads and measured deformations**

Figure H–3   **Test set-up at location C**

Table H–2   **Test programme**

Test ID	Load level	Loading rate
1	Short test at 25 kN	Three cycles of 1, 5 and 30 minutes
2	Short test at 45 kN	Three cycles of 1, 5 and 30 minutes
3	Short test at 65 kN	Three cycles of 1, 5 and 30 minutes
4	Test at 80 kN, force-controlled	Force to increase during 6 hours starting at low water, after that 18 hours constant force

Figure H–4   Observed toe permanent deformation on location C

The toe-force that the revetment can develop is in the same range as the maximum test load, with a neutral value of 14 respectively 20 kN/m for location C and D and with 40 and 52 kN/m as theoretical maxima.

$$N_{neutral} = \rho_s g D \frac{z_{top} - z_{toe}}{\sin \alpha} \sin \alpha, \text{ or with } (\rho_s - \rho) \text{ in case under water}$$

Eq. H.1

$$N_{max/min} = \rho_s g D \frac{z_{top} - z_{toe}}{\sin \alpha} (\sin \alpha \pm \mu \cos \alpha)$$

Table H–3   In-plane force levels at test locations

	Location C Hydroblocks	Location D Basalt	
slope 1:	3.07	3.41	
sinus	0.32	0.34	
cosinus	0.95	0.94	
assumed friction coefficient [-]	0.60	0.60	
top of revetment relative to the toe, $z_{top} - z_{toe}$ [m]	2.71	2.0	1.57
revetment thickness [m]	0.40	0.25	0.35
specific density ρ_s [kg/m³]	2300	2600	
lateral toe force [kN/m]			
minimum	0	0	
neutral LW	25	27	
neutral HW (+1.5)	21	22	
maximum	70	72	

H.2 Experiment results

H.2.1 Typical observations

The application of the load as an in-plane force in the revetment leads to a resultant load on the toe (sheet) piles initially acting at ½*D* and, after some rotation, at *D* below the top of the revetment. Normally and logically, when a load is applied in point 2 the measured deformation at point 1 is smaller than in point 2 (see Figure H–5, left). The revetment between point 1 and 2 is compressed. As a consequence of the rotation of the toe piles the load is transferred at the contact point at the underside of the revetment (see Figure H–5, right), which causes that the deformation at the top of the toe piles (1) can be larger than the displacement of the revetment beam portion (2, neglecting axial compression). This effect is, due to the difference in pile length at location C more dominant than at location D. In Table H–4 the difference between the deformation in point 1 and 2 is indicated. In the displacement–time and force–displacement graphs (Figure H–7) the results of point 2 are shown.
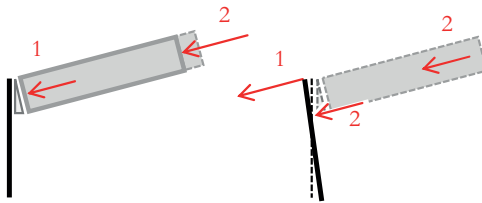
Figure H–5   Interpretation of measured deformations of the revetment and the toe

The typical test result (as shown in Figure H–7) shows that the structure deforms up to 8 mm, which is less than 0.01 of the pile length. There were no signs of failure of the structure. The majority of the deformation is permanent. Deformation only starts after application of 20 kN of load. The re-bound of the structure responding to unloading is very stiff, though this might be due to the sudden unloading. The hysteresis loops of the second and the third loading step look similar, irrespective of the different cycle times.
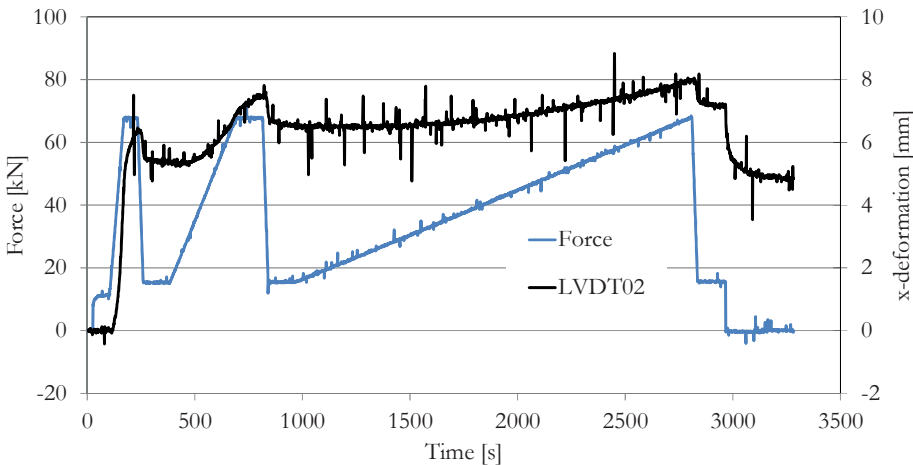
Figure H–6   Measured forces and deformations of 65 kN test on location C against time
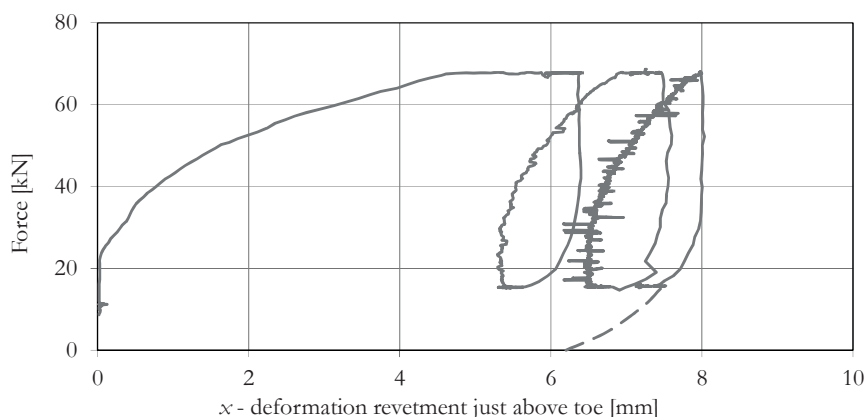
Figure H–7   **Measured force-deformation diagram of 65 kN test on location C**

Results of the long-duration 80 kN tests at Sluis also include observed effects of the load on the revetment slab above. At 25 kN load level the displacements are: -1.35 / -0.3 / 0 and at 80 kN level: -3.85 / -0.65 / -0.5 for just above the load, in the middle and at the top of the revetment.

Table H–4   **Typical test results**

Load level	Treshold value of force causing deformation	Initial deformation LVDT2 at first maximum	Including plastic deformation	First re-bound	Initial defromation second cycle	Including plastic deformation	Second re-bound	Initial defromation third cycle	Including plastic deformation	Third re-bound	Deformation of revetment above (LVDT3)	Difference at toe and just above (LVDT 1 – LVDT2)
					Location C							
25	10	0.6	0.8	0	0.2	0.3	0	0.2	0.3	-0.2	0.6	0.5
45	28	3.4	4.8	-0.2	0.5	1	0	0.7	0.2	-0.1	1.1	-0.9
65	25	4.2	6.4	-1.5	2.2	3.2	-1.4	2	3	-1.8	2.5	4
80	15	9	12								3	8.5
					Location D							
25	10	4.2	4.8	-0.2	0.3	0.6	-0.3	0.4	0.4	-0.2	10	-1
45	19	3.8	4.8	-1.7	1.6	2.5	-1.5	2	2	-3.3	5	-1.8
65	30	9.2	10	-1.7	2.5	3.2	-2.0	2.5	2.5	-4.8	5	-2.5
80	10	13.5	17.5								4	4

The load-displacement curves of the various tests are compared and plotted in Figure H–8. The difference in threshold levels can be explained from the sequence of the tests. At location C the tests were carried out in order of ascending load, at location D the series was started with the 45 kN tests. It can be observed that for both locations the 25 kN test the soil does not respond to the unloading, and the subsequent test can be seen as a

continuation of the 25 kN test. If we take the average of the remaining three threshold load levels we find 10.3 kN/m for location C and 8 kN/m for location D.

It can also be noticed that the first test experiences the stiffest response.
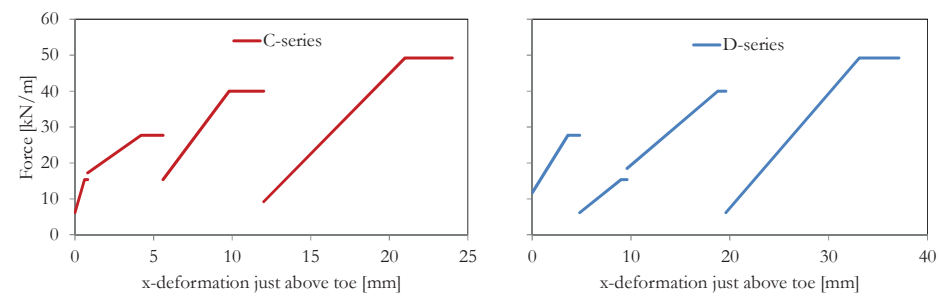
Figure H–8   **Force-displacement diagrams in sequence of test execution**
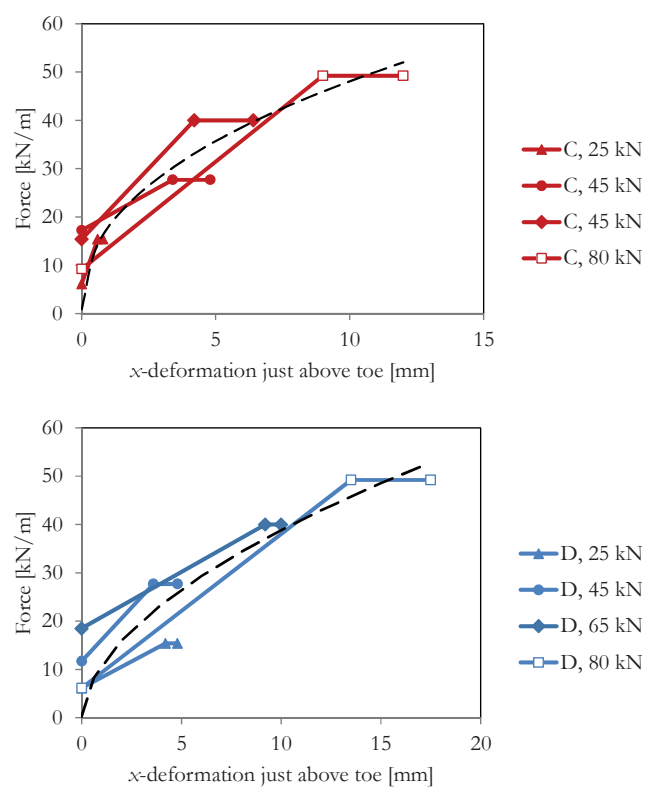
Figure H–9   **Collected force-displacement diagrams**

The comparison of the force displacement diagrams in Figure H–9 shows that the suddenly applied loads (closed markers) do not show much difference with the load applied over 6 hours (open markers). The structure of location C has a higher stiffness with a characteristic

deformation of 12 mm, and at location D of 17.5 mm. Also the initial stiffness of location C is higher. A fit with a power function $y = a \, (x/x_{max})^b$ gives $b = 0.43$ for location C and $b = 0.55$ for location D. The measured linearized toe stiffness against additional lateral load up to the neutral load level is 9 MN/m^2 for location C and 6 MN/m^2 for location D. Caused by further sliding revetment the stiffness reduces to 4.5 MN/m^2 for location C and 3 MN/m^2 for location D.[310]

H.2.2   Back analysis

The test result of location D has been simulated with a Finite Element Model using the Plaxis software. Mohr-Coulomb models as well as the Hardening soil models were used. It appeared that the measured results could be perfectly reproduced with a model using normal average soil parameters.[311] The model included the dike body and clay layers, the filter and top-layer, the toe sheetpile and the foreland soil body. The rock on the foreland was modelled as surcharge load. The calculated displacements were in the same order of magnitude. Also the hysteresis effect with more-or-less elastic behaviour up to level of the neutral load and with non-linear behaviour above that level was confirmed.
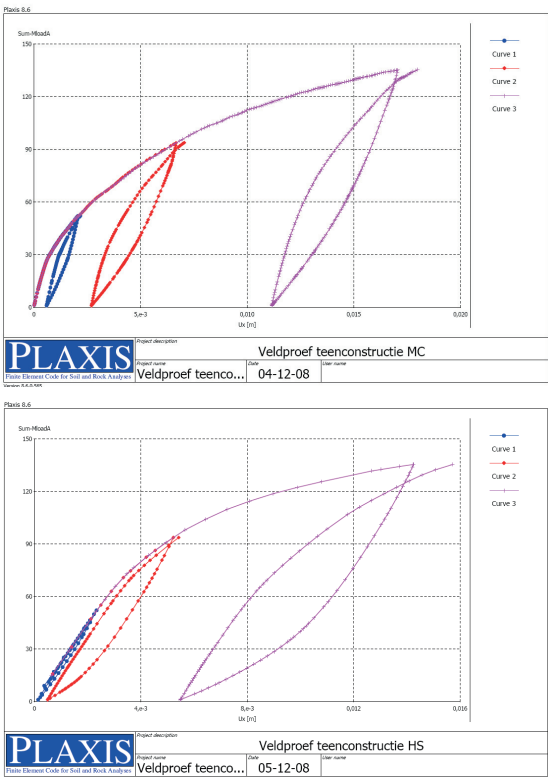
Figure H–10   **Calculated force-displacement diagrams at three load levels with two soil models**

---

[310] Refer to Annex F for further discussion and interpretation of the ratio between toe stiffness and stiffness of sliding revetment.

[311] Back-analysis with sheet-pile design software also provides reasonably compliant results.

The initial in-plane force in the revetment at the position of the toe found in the Plaxis analysis was 30 kN, which is higher than the neutral force. This result shows that if the revetment is not installed on a settlement-free dike, but is an integral part of a soil mass that is subjected to deformations caused by gravity, the load-path of the in-plane forces is relatively stiff and the soil has the tendency to subside and move down the slope, causing reverse shear stresses on the interface between the top-layer and the bedding layers. The soils can cause drag-down forces on the revetment beam, similar to soil causing 'negative skin friction' to piles.

Since it was not possible to test the failure level of the toe structure the Plaxis calculation was used to calculate the failure loads. With an automate c-phi-reduction calculation it was found that for the 65 kN (40 kN/m[1]) case a partial safety factor on the soil of 1.15 applies. The failure load on the toe in reality is larger because we have removed some of the overburden load on the foreland during the test and in the back analysis. With introduction of the overburden load to the real level the partial safety factor is 1.5.

H.2.3   Summary of findings of the back-analysis

The typical toe structures that were tested are in fact transition structures with a soil mass carrying an overburden of rock in front. The stiffness of the transition structure against additional in-plane load from the revetment slab determines whether the structure is suitable as a support to the revetment. The load level at which the structure remains in the elastic range, or is starting to show plastic deformation under repeated load is important as a criterion for suitability as well.

Table H–5   Typical test results

	Value of the load	Factor
Neutral load $N_{neutral}$	22 kN/m	1
Maximum 'passive' load	72	3.3
Elastic load in Plaxis	30	1.4
Test range	15.4 – 49.2 kN/m	0.7 – 2.2
Calculated ultimate resistance	60 kN/m	2.7
Level with linear elastic hysteresis	15.4	0.7
Levels with non-linear hysteresis	27.7	1.25
Stiffness at neutral load point	9000 kN/m², corresponding to 2 mm	
Stiffness up to maximum test level	4500 kN/m², corresponding to 11 mm	
Indicative deformation first load up to neutral level	5 mm	

Design criteria for a toe structure can be formulated as:

- Elastic response under repeated variation between 0 and $N_{neutral}$
- Failure with SF = 1.15 for the case with $N_{passive}$

H.3 Conclusion and discussion on loading of the toe

The test was meant to find the actual in-plane force level when the revetment is not loaded with waves. If we use the threshold value in the force-displacement diagram as a level of pre-load we find 10.3 kN/m and 8 kN/m, which corresponds to 0.44 and 0.33 times the neutral normal force for the two slopes at location C and D respectively.

For location C elastic properties were derived from the 80 kN load test. Those properties can be used to calculate the portion of revetment weight that is resting on friction and the portion that is leaning against the toe force. Estimated and calculated values are: the characteristic length λ_k = 3.6 m (½ slope length L), k_x = 5.8 MN/m^3, E_a = 187 MPa and k_{toe} = 9 MN/m^2.

With those values the force N_o against the toe will become $0.48 \times N_{neutral}$ when we consider the revetment as an elastic beam on a friction bedding and a stiff toe (model of Figure A−3). The force N_o against the toe will become $0.29 \times N_{neutral}$ when we account for the actually measured toe stiffness (model of Figure A−4).

The values are more or less in line with the found threshold force levels, although the measurements of revetment stiffness may not be very accurate. In a number of other experiments (see Annex F) smaller values of λ_k were found. Smaller values of the characteristic length would however lead to small toe forces, which gives a less good match of the observed threshold values and the values found with the elastic calculation.

Design of pattern-placed Revetments – Annexes

ANNEX I   FLUME EXPERIMENT DATA

ID	Selection	Type	Toplayer	Permeability remarks	Geometry remarks	D	D/B_x	Λ/D	cot α	ξ_{m-10}	SWL	z_{top}	H_s	T_{m-10}	N	$H_s/\Delta D$	Damage	Updated damage	Reference
122		CB	Armorflex elements	Geotextile under blocks		0.108	0.4	2.2	3	1.55	5	8.75	0.84	3.4	552	5.5		a	Lindenberg (1983), 45
124		CB	Armorflex elements	Geotextile under blocks		0.108	0.4	4.3	3	1.26	5	8.75	1.22	3.3	750	8.0		a	Lindenberg (1983), 58
123		CB	Armorflex elements	Geotextile under blocks		0.108	0.4	2.2	3	1.47	5	8.75	0.93	3.4	552	6.1		d	Lindenberg (1983), 46
49		CB	Haringman blocks	Wide y-joints	On their side	0.2	2.0	2.5	3.5	1.65	4.98	5	1.56	5.8	1045	6.2		a	Smith et al (2000), 21o14
115		CB	Haringman blocks			0.2	0.4	3.0	3.5	1.24	5	8.5	1.33	4.0	27349	5.1		a	Burger (1985), 10
196		CB	Haringman blocks			0.2	0.4	2.9	4	1.90	4.8	8.5	0.8	5.5	100	3.1		a	Sparboom (1989)
50		CB	Haringman blocks	Wide y-joints	On their side	0.2	2.0	2.5	3.5	1.60	5.01	5	1.7	5.8	1045	6.8		b	Smith et al (2000), 21o15
51	*	CB	Haringman blocks	Wide y-joints	On their side	0.2	2.0	2.5	3.5	1.99	5	5	1.55	6.9	1045	6.2		c	Smith et al (2000), 21o16
116	*	CB	Haringman blocks			0.2	0.4	2.9	3.5	1.17	5	8.5	1.5	4.0	941	5.8		c	Burger (1985), 15
114	*	CB	Haringman blocks			0.2	0.4	3.0	3.5	1.39	5	8.5	1.43	4.7	13746	5.5		d	Burger (1985), 6
190		CB	Rectangular blocks			0.18	0.6	0.6	3	1.53	4.5	7	0.58	2.8	998	2.4		a	Gier (2011), 5
191		CB	Rectangular blocks			0.18	0.6	0.6	3	1.49	4.5	7	0.8	3.2	1013	3.4		b	Gier (2011), 7
192	*	CB	Rectangular blocks			0.18	0.6	0.6	3	1.87	4.5	7	1.08	4.7	843	4.5		d	Gier (2011), 12
7		CB	Rectangular blocks	Siltated, measured Λ		0.2	0.4	1.3	3.5	1.89	3.77	5	0.86	4.9	1045	3.2		a	Smith et al (2000), 4bo06
8		CB	Rectangular blocks	Siltated, measured Λ		0.2	0.4	2.8	3.5	1.27	3.77	5	0.71	3.0	1045	2.7		a	Smith et al (2000), 4co01
9		CB	Rectangular blocks	Siltated, measured Λ		0.2	0.4	2.8	3.5	1.84	3.78	5	1.05	5.3	1045	3.9		a	Smith et al (2000), 4co07
13		CB	Rectangular blocks	Mine stone		0.25	0.5	2.5	3.5	1.30	4.02	5	1.64	4.7	1045	4.7		a	Smith et al (2000), 5o05
13		CB	Rectangular blocks	Mine stone		0.25	0.5	2.5	3.5	1.41	4.02	5	1.64	5.1	1045	4.7		b	Smith et al (2000), 5o06
15		CB	Rectangular blocks			0.25	0.5	2.5	3.5	1.87	2.23	5	0.91	5.0	1045	2.6		0	Smith et al (2000), 6o21
16		CB	Rectangular blocks	Small joints	On their side	0.2	2.0	2.3	3.5	1.26	4.65	5	1.23	3.9	1045	4.7		0	Smith et al (2000), 12ao4
18		CB	Rectangular blocks	Small joints	On their side	0.2	2.0	1.7	3.5	1.59	4.71	5	1	4.5	1045	3.8		a	Smith et al (2000), 12ao8

ID	Selection	Type	Toplayer	Permeability remarks	Geometry remarks	D	D/B_x	Λ/D	cot α	$\xi_{m\text{-}10}$	SWL	z_{top}	H_s	$T_{m\text{-}10}$	N	$H_s/\Delta D$	Damage	Updated damage	Reference
23		CB	Rectangular blocks	Wide x-joints	On their side	0.2	2.0	1.9	3.5	1.25	4.67	5	1.03	3.5	1045	3.9		0	Smith et al (2000), 12bo06
25		CB	Rectangular blocks	Wide x-joints	On their side	0.2	2.0	1.9	3.5	1.26	4.79	5	1.22	3.9	1045	4.6		0	Smith et al (2000), 12co3
29		CB	Rectangular blocks	Wide x-joints	On their side	0.2	2.0	2.0	3.5	1.60	4.93	5	1.25	5.0	1045	4.7		0	Smith et al (2000), 12cco5
32		CB	Rectangular blocks	Wide y-joints	On their side	0.2	2.0	1.4	3.5	1.29	4.9	5	1.4	4.3	1045	5.3	a	0	Smith et al (2000), 12do6
37		CB	Rectangular blocks			0.2	0.4	1.9	3.5	1.61	4.15	5	0.41	2.9	1045	1.5	a	0	Smith et al (2000), 20ao3
39		CB	Rectangular blocks			0.2	0.4	3.1	3.5	1.25	4	5	0.58	2.7	1045	2.2	a	0	Smith et al (2000), 20ao5
43		CB	Rectangular blocks			0.1	0.4	3.0	3.5	1.91	4.58	5	0.32	3.0	1045	2.4	a	0	Smith et al (2000), 20b03
46		CB	Rectangular blocks			0.1	0.4	3.0	3.5	1.56	3.62	5	0.32	2.5	1045	2.4	a	0	Smith et al (2000), 20b07
52		CB	Rectangular blocks	Wide y-joints	On their side	0.2	2.0	0.9	3.5	1.56	4.55	5	0.43	2.9	1045	1.7	a	0	Smith et al (2000), 23o1
54		CB	Rectangular blocks	Wide y-joints	On their side	0.2	2.0	2.5	3.5	1.56	4.97	5	1.33	5.0	1045	5.2		a	Smith et al (2000), 23o10
56		CB	Rectangular blocks		On their side	0.5	2.0	0.9	3	1.63	4.69	5.45	1.55	4.9	20715	2.4		a	Klein Breteler et al (2005), T13-17
57		CB	Rectangular blocks		On their side	0.5	2.0	0.9	3	2.13	4.91	5.45	1.57	6.4	15384	2.5		a	Klein Breteler et al (2005), T22-26
75		CB	Rectangular blocks		On their side	0.2	2.0	4.1	3.5	1.57	4.9	6	0.64	3.5	1067	2.4		a	Klein Breteler et al (2005), 4931
78		CB	Rectangular blocks		On their side	0.2	2.0	4.1	3.5	1.52	4	6	0.45	2.9	1314	1.7		a	Klein Breteler et al (2005), 4040
101		CB	Rectangular blocks			0.151	0.6	3.0	3	1.73	4.99	8.5	0.73	3.5	1179	3.5		a	Wouters (1991), 128
102		CB	Rectangular blocks			0.151	0.6	3.0	3	1.32	4.73	8.5	0.94	3.1	1000	4.5		a	Wouters (1991), 154
103		CB	Rectangular blocks			0.151	0.6	3.0	3	2.75	4.74	8.5	0.78	5.8	1000	3.7		a	Wouters (1991), 155
104		CB	Rectangular blocks			0.147	0.6	3.2	3	1.73	4.99	8.5	0.73	3.5	1179	3.7		a	Wouters (1991), 128
105		CB	Rectangular blocks			0.147	0.6	3.2	3	1.32	4.73	8.5	0.94	3.1	1000	4.7		a	Wouters (1991), 154
106		CB	Rectangular blocks			0.147	0.6	3.2	3	2.75	4.74	8.5	0.78	5.8	1000	3.9		a	Wouters (1991), 155
107		CB	Rectangular blocks	Geotextile under blocks		0.15	0.3	6.0	3	1.86	4.77	8.5	0.40	2.8	1113	1.9		a	Wouters (1991), 248
108		CB	Rectangular blocks	Geotextile under blocks		0.147	0.6	5.4	3	1.86	4.77	8.5	0.40	2.8	1113	2.0		a	Wouters (1991), 248

ID	Selection	Type	Toplayer	Permeability remarks	Geometry remarks	D	D/B_x	Λ/D	cot α	$\xi_{m\text{-}10}$	SWL	z_{top}	H_s	$T_{m\text{-}10}$	N	$H_s/\Delta D$	Damage	Updated damage	Reference
109		CB	Rectangular blocks			0.3	0.6	3.5	3	1.44	4.94	8.5	1.06	3.5	1123	2.6		a	Wouters (1991), 627
125		CB	Rectangular blocks			0.15	0.6	6.6	3	1.97	4.5	4.4	0.52	3.4	1111	2.6		a	Burger (1983), 30
127		CB	Rectangular blocks			0.15	0.6	6.6	3	1.79	4.5	4.4	0.49	3.0	1111	2.4		a	Burger (1983), 34
129		CB	Rectangular blocks			0.15	0.6	6.6	3	1.72	4.5	4.4	0.53	3.0	1111	2.6		a	Burger (1983), 38
138		CB	Rectangular blocks		Restrained x-movement	0.1	0.4	2.8	4	1.05	4.01	4.5	0.44	2.2	1000	3.1		a	Den Boer (1982), c.3.1-57
150		CB	Rectangular blocks		Above SWL.	0.1	0.5	1.6	3	1.76	4.54	5.49	1.1	4.4	1030	8.1		a	Van Steeg et al (2009), L4
151		CB	Rectangular blocks		Above SWL.	0.1	0.5	1.6	3	1.72	4.84	5.49	0.94	4.0	997	6.9		a	Van Steeg et al (2009), N3
14		CB	Rectangular blocks	Mine stone		0.25	0.5	2.5	3.5	1.41	4	5	1.64	5.1	1045	4.7		b	Smith et al (2000), 5o06
20		CB	Rectangular blocks	Small joints	On their side	0.2	2.0	1.7	3.5	1.98	4.7	5	0.73	4.7	1045	2.8		b	Smith et al (2000), 12ao10
26		CB	Rectangular blocks	Wide x-joints	On their side	0.2	2.0	1.9	3.5	1.29	4.9	5	1.4	4.3	1045	5.3		b	Smith et al (2000), 12co4
35		CB	Rectangular blocks	Wide x-joints	On their side	0.2	2.0	2.1	3.5	1.60	4.92	5	1.25	5.0	1045	4.7		b	Smith et al (2000), 12cdo5
40		CB	Rectangular blocks			0.2	0.4	3.1	3.5	2.07	4.23	5	0.63	4.6	1045	2.4	b	a	Smith et al (2000), 20a06
41		CB	Rectangular blocks			0.2	0.4	3.1	3.5	1.65	4.17	5	0.63	3.7	1045	2.4		b	Smith et al (2000), 20a07
44		CB	Rectangular blocks			0.1	0.4	3.0	3.5	1.59	4.58	5	0.42	2.9	1045	3.1		b	Smith et al (2000), 20b04
47		CB	Rectangular blocks			0.1	0.4	3.0	3.5	1.55	3.77	5	0.43	2.8	1045	3.2		b	Smith et al (2000), 20b09
53		CB	Rectangular blocks	Wide y-joints	On their side	0.2	2.0	0.9	3.5	1.60	4.55	5	0.52	3.2	1045	2.0		b	Smith et al (2000), 23o2
131		CB	Rectangular blocks		Restrained x-movement	0.15	0.6	4.7	4	1.00	3.99	4.5	0.69	2.7	1000	3.4		b	Den Boer (1982), c.1.1-6
133		CB	Rectangular blocks		Restrained x-movement	0.15	0.6	4.7	4	0.97	4.23	4.5	0.73	2.7	1000	3.6		b	Den Boer (1982), c.1.2-17
135		CB	Rectangular blocks		Restrained x-movement	0.1	0.4	6.2	4	1.08	3.99	4.5	0.39	2.1	1000	2.8		b	Den Boer (1982), c.2.4-46
140		CB	Rectangular blocks	Blocks with holes	Restrained x-movement	0.1	0.4	3.5	4	1.02	4	4.5	0.47	2.2	1000	3.5		b	Den Boer (1982), c.3.2-60
142		CB	Rectangular blocks			0.1	0.4	6.2	4	1.03	4.02	4.5	0.48	2.3	1000	3.5		b	Den Boer (1982), c.4-64

ID	Selection	Type	Toplayer	Permeability remarks	Geometry remarks	D	D/B$_x$	Λ/D	cot α	ξ$_{m-10}$	SWL	z$_{top}$	H$_s$	T$_{m-10}$	N	H$_s$/ΔD	Damage	Updated damage	Reference
10	*	CB	Rectangular blocks	Siltated, measured Λ		0.2	0.4	2.8	3.5	1.35	3.77	5	1.17	4.1	1045	4.4	c	c1	Smith et al (2000), 4co08
21	*	CB	Rectangular blocks	Small joints	On their side	0.2	2.0	1.7	3.5	1.95	4.81	5	0.84	5.0	1045	3.2	c	c1	Smith et al (2000), 12ao11
27	*	CB	Rectangular blocks	Wide x-joints	On their side	0.2	2.0	1.9	3.5	1.24	5.03	5	1.57	4.4	1045	6.0	c	c1	Smith et al (2000), 12co5
27	*	CB	Rectangular blocks	Wide x-joints	On their side	0.2	2.0	1.9	3.5	1.24	5.03	5	1.57	4.4	1045	6.0	c	a	Smith et al (2000), 12co5
30	*	CB	Rectangular blocks	Wide x-joints	On their side	0.2	2.0	2.0	3.5	1.65	4.94	5	1.44	5.5	1045	5.5	c	c	Smith et al (2000), 12cco6
33	*	CB	Rectangular blocks	Wide y-joints	On their side	0.2	2.0	1.4	3.5	1.29	5	5	1.59	4.5	1045	6.0	c	c1	Smith et al (2000), 12do7
34	*	CB	Rectangular blocks	Wide y-joints	On their side	0.2	2.0	1.4	3.5	1.99	5	5	1.54	6.9	1045	5.8	c	c1	Smith et al (2000), 12do10
38	*	CB	Rectangular blocks			0.2	0.4	1.9	3.5	1.64	4.2	5	0.63	3.6	1045	2.4	c	c1	Smith et al (2000), 20ao4
38	*	CB	Rectangular blocks			0.2	0.4	1.9	3.5	1.64	4.2	5	0.63	3.6	1045	2.4	c	a	Smith et al (2000), 20ao4
42	*	CB	Rectangular blocks			0.2	0.4	3.1	3.5	1.62	4.28	5	0.84	4.2	1045	3.1	c	c1	Smith et al (2000), 20a08
42	*	CB	Rectangular blocks			0.2	0.4	3.1	3.5	1.62	4.28	5	0.84	4.2	1045	3.1	c	a	Smith et al (2000), 20a08
45	*	CB	Rectangular blocks			0.1	0.4	3.0	3.5	1.79	4.61	5	0.52	3.6	1045	3.9	c	c	Smith et al (2000), 20b05
73	*	CB	Rectangular blocks		On their side	0.2	2.0	4.1	3.5	1.54	4.1	6	0.83	3.9	958	3.2	c	d1	Klein Breteler et al (2005), 4120
79		CB	Rectangular blocks		On their side	0.2	2.0	4.1	3.5	1.55	4.11	6	0.53	3.2	4176	2.0	c	a	Klein Breteler et al (2005), 4140+4141
80	*	CB	Rectangular blocks		On their side	0.2	2.0	4.1	3.5	1.54	4.38	6	0.53	3.1	48000	2.0	c	c1	Klein Breteler et al (2005), 4540+4541
11	*	CB	Rectangular blocks	Siltated, measured Λ		0.2	0.4	2.8	3.5	1.30	4.04	5	1.5	4.5	1045	5.6	d	d1	Smith et al (2000), 4co13
17	*	CB	Rectangular blocks	Small joints	On their side	0.2	2.0	1.7	3.5	1.29	4.8	5	1.4	4.3	1045	5.3	d	d1	Smith et al (2000), 12ao5
19	*	CB	Rectangular blocks	Small joints	On their side	0.2	2.0	1.7	3.5	1.58	4.91	5	1.27	5.0	1045	4.8	d	d1	Smith et al (2000), 12ao9
19	*	CB	Rectangular blocks	Small joints	On their side	0.2	2.0	1.7	3.5	1.58	4.91	5	1.27	5.0	1045	4.8	d	a	Smith et al (2000), 12ao9
22	*	CB	Rectangular blocks	Small joints	On their side	0.2	2.0	1.7	3.5	1.92	5	5	1.24	6.0	1045	4.7	d	c1	Smith et al (2000), 12ao13
24	*	CB	Rectangular blocks	Wide x-joints	On their side	0.2	2.0	1.9	3.5	1.26	4.77	5	1.23	3.9	1045	4.7	d	c1	Smith et al (2000), 12bo07
28	*	CB	Rectangular blocks	Wide x-joints	On their side	0.2	2.0	1.9	3.5	1.60	5	5	1.63	5.7	1045	6.2	d	d1	Smith et al (2000), 12co7

ID	Selection	Type	Toplayer	Permeability remarks	Geometry remarks	D	D/B_x	Λ/D	$\cot\alpha$	ξ_{m-10}	SWL	z_{top}	H_s	T_{m-10}	N	$H_s/\Delta D$	Damage	Updated damage	Reference
28	*	CB	Rectangular blocks	Wide x-joints	On their side	0.2	2.0	1.9	3.5	1.60	5	5	1.63	5.7	1045	6.2	d	c	Smith et al (2000), 12co7
31	*	CB	Rectangular blocks	Wide x-joints	On their side	0.2	2.0	2.0	3.5	1.62	4.95	5	1.65	5.8	1045	6.3	d	d1	Smith et al (2000), 12cco7
31	*	CB	Rectangular blocks	Wide x-joints	On their side	0.2	2.0	2.0	3.5	1.62	4.95	5	1.65	5.8	1045	6.3	d	b	Smith et al (2000), 12co7
36	*	CB	Rectangular blocks	Wide x-joints	On their side	0.2	2.0	2.1	3.5	2.00	4.96	5	1.52	6.9	1045	5.8	d	d1	Smith et al (2000), 12cdo8
48	*	CB	Rectangular blocks			0.1	0.4	3.0	3.5	1.82	3.76	5	0.51	3.6	1045	3.8	d	d1	Smith et al (2000), 20b10
48	*	CB	Rectangular blocks			0.1	0.4	3.0	3.5	1.82	3.76	5	0.51	3.6	1045	3.8	d	b	Smith et al (2000), 20b10
55	*	CB	Rectangular blocks	Wide y-joints	On their side	0.2	2.0	2.5	3.5	1.66	4.94	5	1.54	5.8	1045	6.0		d	Smith et al (2000), 23o11
74	*	CB	Rectangular blocks		On their side	0.2	2.0	4.1	3.5	1.56	4.1	6	0.83	4.0	3429	3.2	d	d1	Klein Breteler et al (2005), 4120-4122
74	*	CB	Rectangular blocks		On their side	0.2	2.0	4.1	3.5	1.56	4.1	6	0.83	4.0	3429	3.2	d	b	Klein Breteler et al (2005), 4120-4122
77	*	CB	Rectangular blocks		On their side	0.2	2.0	4.1	3.5	1.54	4.9	6	0.67	3.5	6797	2.5	d	d1	Klein Breteler et al (2005), 4931-4934
77	*	CB	Rectangular blocks		On their side	0.2	2.0	4.1	3.5	1.54	4.9	6	0.67	3.5	6797	2.5	d	b	Klein Breteler et al (2005), 4931-4934
126	*	CB	Rectangular blocks			0.15	0.6	6.6	3	1.70	4.5	4.4	0.54	3.0	1111	2.7		d	Burger (1983), 31
128	*	CB	Rectangular blocks			0.15	0.6	6.6	3	1.58	4.5	4.4	0.56	2.8	1111	2.8		d	Burger (1983), 35
130	*	CB	Rectangular blocks			0.15	0.6	6.6	3	1.76	4.5	4.4	0.57	3.2	1111	2.8		d	Burger (1983), 37
132	*	CB	Rectangular blocks		Restrained x-movement	0.15	0.6	4.7	4	0.95	4.01	4.5	0.76	2.7	1000	3.7	d	d	Den Boer (1982), c.1.1-7
134	*	CB	Rectangular blocks		Restrained x-movement	0.15	0.6	4.7	4	0.97	4.26	4.5	0.74	2.7	1000	3.6	d	d	Den Boer (1982), c.1.2-18
136	*	CB	Rectangular blocks		Restrained x-movement	0.1	0.4	6.2	4	1.09	3.98	4.5	0.41	2.2	1000	3.0	d	d	Den Boer (1982), c.2.4-47
137	*	CB	Rectangular blocks		Restrained x-movement	0.1	0.4	6.2	4	1.12	4.26	4.5	0.46	2.4	1000	3.4	d	d	Den Boer (1982), c.2.3-51
139	*	CB	Rectangular blocks		Restrained x-movement	0.1	0.4	2.8	4	1.04	4	4.5	0.46	2.2	1000	3.2	d	d	Den Boer (1982), c.3.1-58
141	*	CB	Rectangular blocks	Blocks with holes	Restrained x-movement	0.1	0.4	3.5	4	1.00	4.00	4.5	0.49	2.2	1000	3.6	d	d	Den Boer (1982), c.3.2-61
143	*	CB	Rectangular blocks		Restrained x-movement	0.1	0.4	6.2	4	1.04	4.01	4.5	0.49	2.3	1000	3.6	d	d	Den Boer (1982), c.4-65

ID	Selection	Type	Toplayer	Permeability remarks	Geometry remarks	D	D/B_x	Λ/D	cot α	ξ_{m-10}	SWL	z_{top}	H_s	T_{m-10}	N	$H_s/\Delta D$	Damage	Updated damage	Reference
152	✳	CB	Rectangular blocks		Above SWL; top edge fixed in cement	0.1	0.5	1.6	3	1.73	4.84	5.49	1.1	4.4	306	8.1	d	d1	Van Steeg et al (2009), N4+N4a
244		CB	Verkalit mgv			0.152	1.0	0.3	3	1.60	4.7	5.5	1.35	4.5	1028	6.6	a	a	Klein Breteler (2015), V08
245		CB	Verkalit mgv			0.152	1.0	0.3	3	1.63	4.7	5.5	1.53	4.9	989	7.4	a	a	Klein Breteler (2015), V09
249		CB	Verkalit mgv			0.152	1.0	0.3	3	2.20	4.7	5.5	1.35	6.1	1030	6.6	a	a	Klein Breteler (2015), V21
250		CB	Verkalit mgv			0.152	1.0	0.3	3	2.13	4.7	5.5	1.52	6.3	1055	7.4	a	a	Klein Breteler (2015), V22
237		CB	Verkalit mgv			0.152	1.0	0.3	3	2.15	4.55	5.5	0.75	4.5	455	3.6	a	b	Klein Breteler (2015), V01
238	✳	CB	Verkalit mgv			0.152	1.0	0.3	3	2.15	4.7	5.5	0.86	4.8	825	4.2	b	c	Klein Breteler (2015), V02
246	✳	CB	Verkalit mgv			0.152	1.0	0.3	3	1.63	4.7	5.5	1.54	4.9	1386	7.5	c	d	Klein Breteler (2015), V10
251	✳	CB	Verkalit mgv			0.152	1.0	0.3	3	2.18	4.7	5.5	1.52	6.5	1782	7.4	d	d	Klein Breteler (2015), V23
193		CB	Verkalit modified			0.25	0.8	1.2	3	2.74	4.5	7	1.04	6.7	1028	3.1		a	Gier (2011), 16
194		CB	Verkalit modified			0.25	0.8	1.2	3	1.96	4.5	7	1.51	5.8	677	4.4		a	Gier (2011), 17+19+22
195		CB	Verkalit modified			0.25	0.8	1.2	3	1.66	4.5	7	1.19	4.4	4814	3.5		a	Gier (2011), 14+18+20+21+25
181		CB	Verkalit porous			0.18	0.6	0.6	3	1.59	4.5	7	1.12	4.0	1051	3.4	a	0	Gier (2011), 14
182		CB	Verkalit porous			0.18	0.6	0.6	3	2.75	4.5	7	1.04	6.7	1020	3.2	a	0	Gier (2011), 25
183		CB	Verkalit porous			0.18	0.6	0.6	3	1.95	4.5	7	1.54	5.8	383	4.7	a	0	Gier (2011), 26+31
184		CB	Verkalit porous			0.18	0.6	0.6	3	1.66	4.5	7	1.19	4.4	5210	3.6	a	0	Gier (2011), 23+27+28+29+30
175		CB	Verkalit standard			0.18	0.6	0.6	3	1.58	4.5	7	1.13	4.0	1016	4.5	a	0	Gier (2011), 11
176		CB	Verkalit standard			0.18	0.6	0.6	3	1.87	4.5	7	1.08	4.7	843	4.3	a	0	Gier (2011), 12
177		CB	Verkalit standard			0.18	0.6	0.6	3	1.59	4.5	7	1.12	4.0	1051	4.4	a	0	Gier (2011), 14
178		CB	Verkalit standard			0.18	0.6	0.6	3	2.75	4.5	7	1.04	6.7	1020	4.1	a	0	Gier (2011), 25
179		CB	Verkalit standard			0.18	0.6	0.6	3	1.95	4.5	7	1.54	5.8	383	6.1	a	0	Gier (2011), 26-31

ID	Selection	Type	Toplayer	Permeability remarks	Geometry remarks	D	D/B_x	Λ/D	cot α	ξ_{m-10}	SWL	z_{top}	H_s	T_{m-10}	N	$H_s/\Delta D$	Damage	Updated damage	Reference
180		CB	Verkalit standard			0.18	0.6	0.6	3	1.66	4.5	7	1.19	4.4	5210	4.7	a	0	Gier (2011), 23+27+28+29+30
185		CB	Verkalit standard			0.18	0.6	0.6	3	2.75	4.5	7	1.04	6.7	1026	4.1	a	0	Gier (2011), 13
186		CB	Verkalit standard			0.18	0.6	0.6	3	1.95	4.5	7	1.52	5.8	720	6.0	a	0	Gier (2011), 8+2-+21+22
187		CB	Verkalit standard			0.18	0.6	0.6	3	1.65	4.5	7	1.17	4.3	5258	4.6	a	0	Gier (2011), 9+16+17+18+19
188		CB	Verkalit standard			0.18	0.6	1.4	3	1.95	4.5	7	1.52	5.8	720	6.3		b	Gier (2011), 8+20+21+22
189		CB	Verkalit standard			0.18	0.6	1.5	3	1.96	4.5	7	1.51	5.8	677	6.3		b	Gier (2011), 17+19+22
1		CC	Basalton		Low berm	0.15	0.5	2.6	3.5	1.24	4.95	4	1.04	3.5	1045	5.0	a	0	Smith et al (2000), 1o02
2		CC	Basalton		Low berm	0.15	0.5	2.6	3.5	1.26	4.94	4	1.22	3.9	1045	5.9		a	Smith et al (2000), 1o03
67		CC	Basalton			0.2	1.0	2.5	3.5	2.21	4.7	6	1.38	7.3	26385	3.8		a	Klein Breteler et al (2005), nov03-4805
95		CC	Basalton			0.2	1.0	2.5	3.5	1.73	4.74	6	1.57	6.1	1042	4.3		a	Eysink et al (2003), 26
153		CC	Basalton	Under transition		0.198	0.7	2.8	3	1.81	4.67	4.1	1.15	4.7	993	4.4		a	Van Steeg et al (2009), C2
154		CC	Basalton	Under transition		0.198	0.7	2.8	3	1.85	5.15	4.1	1.5	5.4	1006	5.8		a	Van Steeg et al (2009), E1
155		CC	Basalton	Under transition		0.198	0.7	2.8	3	1.72	4.8	4.1	0.79	3.7	1020	3.0		a	Van Steeg et al (2009), A3
156		CC	Basalton	Above transition		0.198	0.7	2.8	3	1.85	5.15	5.46	1.5	5.4	1006	4.1		a	Van Steeg et al (2009), E1
157		CC	Basalton			0.198	0.7	2.8	3	1.85	5.15	5.46	1.5	5.4	1006	4.1		a	Van Steeg et al (2009), E1
161		CC	Basalton			0.15	1.0	2.1	3.5	1.43	4.6	4.7	1.39	4.7	1051	6.7		a	Wolters et al (2011), P03
169		CC	Basalton	Double top-layer system		0.15	0.6	2.0	3	2.04	4.3	5.46	0.63	3.9	1057	3.1		a	t Hart et al (2012), T5
171		CC	Basalton	Double top-layer system		0.15	0.6	2.0	3	1.58	4	5.46	0.62	3.0	980	3.1		a	t Hart et al (2012), T4
197		CC	Basalton			0.15	1.0	2.5	3	2.02	4.55	5.5	0.62	3.8	532	3.2		a	Klein Breteler (2015), P01
198		CC	Basalton			0.15	1.0	2.5	3	2.11	4.7	5.5	0.89	4.8	1217	4.6		a	Klein Breteler (2015), P02
200		CC	Basalton			0.15	1.0	2.5	3	1.55	4.55	5.5	0.67	3.0	647	3.5		a	Klein Breteler (2015), P04

ID	Selection	Type	Toplayer	Permeability remarks	Geometry remarks	D	D/Bₓ	Λ/D	cot α	ξm-10	SWL	z top	Hs	Tm-10	N	Hs/ΔD	Damage	Updated damage	Reference
201		CC	Basalton			0.15	1.0	2.5	3	1.57	4.7	5.5	0.71	3.2	634	3.7		a	Klein Breteler (2015), P05
202		CC	Basalton			0.15	1.0	2.5	3	1.61	4.7	5.5	0.98	3.8	1080	5.1		a	Klein Breteler (2015), P06
204		CC	Basalton			0.15	1.0	2.5	3	1.57	4.7	5.5	0.7	3.2	629	3.6		a	Klein Breteler (2015), P08
205		CC	Basalton			0.15	1.0	2.5	3	1.60	4.7	5.5	0.85	3.5	1598	4.4		a	Klein Breteler (2015), P09
210		CC	Basalton			0.179	1.0	2.2	3	2.21	5.4	6.6	0.76	4.6	468	3.3		a	Klein Breteler (2015), B01
211		CC	Basalton			0.179	1.0	2.2	3	2.18	5.6	6.6	0.99	5.2	994	4.3		a	Klein Breteler (2015), B02
212		CC	Basalton			0.179	1.0	2.2	3	2.19	5.6	6.6	1.13	5.6	996	4.9		a	Klein Breteler (2015), B03
213		CC	Basalton			0.179	1.0	2.2	3	2.14	5.6	6.6	1.33	5.9	1155	5.7		a	Klein Breteler (2015), B04
214		CC	Basalton			0.179	1.0	2.2	3	2.17	5.6	6.6	1.51	6.4	1148	6.5		a	Klein Breteler (2015), B05
215		CC	Basalton			0.179	1.0	2.2	3	2.19	5.6	6.6	1.66	6.8	1153	7.2		a	Klein Breteler (2015), B06
216		CC	Basalton			0.179	1.0	2.2	3	2.15	5.9	6.6	1.83	7.0	1244	7.9		a	Klein Breteler (2015), B07
217		CC	Basalton			0.179	1.0	2.2	3	1.63	5.6	6.6	1.09	4.1	1046	4.7		a	Klein Breteler (2015), B08
218		CC	Basalton			0.179	1.0	2.2	3	1.57	5.6	6.6	1.36	4.4	1089	5.9		a	Klein Breteler (2015), B09
219		CC	Basalton			0.179	1.0	2.2	3	1.58	5.8	6.6	1.56	4.8	1103	6.7		a	Klein Breteler (2015), B10
220		CC	Basalton			0.179	1.0	2.2	3	1.61	5.9	6.6	1.74	5.1	1117	7.5		a	Klein Breteler (2015), B11
222		CC	Basalton			0.179	1.0	2.2	3	1.60	5.4	6.6	0.75	3.3	565	3.2		a	Klein Breteler (2015), B13
208		CC	Basalton			0.15	1.0	2.5	3	1.57	4.7	5.5	0.87	3.5	2315	4.5		b	Klein Breteler (2015), P12
170	*	CC	Basalton	Double top-layer system		0.15	0.6	2.0	3	2.09	4.4	5.46	0.78	4.4	984	3.9		c	t Hart et al (2012), T6
172	*	CC	Basalton	Double top-layer system		0.15	0.6	2.0	3	1.60	4.25	5.46	0.88	3.6	969	4.4		c	t Hart et al (2012), T8
206	*	CC	Basalton			0.15	1.0	2.5	3	1.58	4.7	5.5	0.85	3.5	1772	4.4		c	Klein Breteler (2015), P10
221	*	CC	Basalton			0.179	1.0	2.2	3	1.62	6	6.6	1.96	5.4	1062	8.4		c	Klein Breteler (2015), B12
121	*	CC	Basalton	No joint fill		0.18	0.7	1.6	3	1.33	5	8.75	1.19	3.5	1078	4.7		d	Lindenberg (1983), 4

ID	Selection	Type	Toplayer	Permeability remarks	Geometry remarks	D	D/B_x	Λ/D	cot α	ξ_{m-10}	SWL	z_{top}	H_s	T_{m-10}	N	$H_s/\Delta D$	Damage	Updated damage	Reference
162	*	CC	Basalton			0.15	1.0	2.1	3.5	1.47	4.7	4.7	1.6	5.2	297	7.7		d	Wolters et al (2011), P04
173	*	CC	Basalton	Double top-layer system		0.15	0.6	2.0	3	1.60	4.23	5.46	1.07	4.0	557	5.3		d	t Hart et al (2012), T9
174	*	CC	Basalton	Double top-layer system		0.15	0.6	2.0	3	1.59	4.2	5.46	0.8	3.4	752	4.0		d	t Hart et al (2012), T1
199	*	CC	Basalton			0.15	1.0	2.5	3	2.08	4.7	5.5	1.12	5.3	681	5.8		d	Klein Breteler (2015), P03
203	*	CC	Basalton			0.15	1.0	2.5	3	1.58	4.7	5.5	1.18	4.1	627	6.1		d	Klein Breteler (2015), P07
207	*	CC	Basalton			0.15	1.0	2.5	3	1.56	4.7	5.5	0.89	3.5	735	4.6		d	Klein Breteler (2015), P11
209	*	CC	Basalton			0.15	1.0	2.5	3	1.56	4.7	5.5	0.9	3.6	1365	4.6		d	Klein Breteler (2015), P13
223	*	CC	Basalton			0.179	1.0	2.2	3	1.58	5.6	6.6	1.45	4.6	1603	6.2		d	Klein Breteler (2015), B14
58		CC	C-Star			0.18	1.5	1.9	3	2.18	4.5	5.5	1.53	6.5	899	6.4		a	Van der Werf et al (2007), T15
252		CC	C-star			0.175	1.8	1.9	3	2.16	4.55	5.5	0.69	4.3	482	2.9		a	Klein Breteler (2015), C01
253		CC	C-star			0.175	1.8	1.9	3	2.19	4.7	5.5	1	5.3	1001	4.2		a	Klein Breteler (2015), C02
254		CC	C-star			0.175	1.8	1.9	3	2.18	4.7	5.5	1.21	5.8	1006	5.1		a	Klein Breteler (2015), C03
255		CC	C-star			0.175	1.8	1.9	3	2.16	4.7	5.5	1.38	6.1	1039	5.9		a	Klein Breteler (2015), C04
256		CC	C-star			0.175	1.8	1.9	3	2.25	4.7	5.5	1.58	6.8	1416	6.7		a	Klein Breteler (2015), C05
257		CC	C-star			0.175	1.8	1.9	3	1.60	4.7	5.5	1.2	4.2	1003	5.1		a	Klein Breteler (2015), C06
258		CC	C-star			0.175	1.8	1.9	3	1.60	4.7	5.5	1.35	4.5	1026	5.7		a	Klein Breteler (2015), C07
259		CC	C-star			0.175	1.8	1.9	3	1.64	4.7	5.5	1.52	4.9	1026	6.5		a	Klein Breteler (2015), C08
262		CC	C-star			0.166	1.3	1.4	3	2.17	4.7	5.5	0.73	4.5	457	3.5		a	Wolters (2015), H01
59		CC	C-Star			0.18	1.5	1.9	3	1.62	4.5	5.5	1.55	4.8	3107	6.4		b	Van der Werf et al (2007), T24-32
260		CC	C-star			0.175	1.8	1.9	3	1.64	4.7	5.5	1.55	4.9	1679	6.6		b	Klein Breteler (2015), C09
60	*	CC	C-Star			0.18	1.5	1.9	3	1.62	4.5	5.5	1.56	4.9	20120	6.5		c	Van der Werf et al (2007), T24-34
261	*	CC	C-star			0.175	1.8	1.9	3	1.66	4.7	5.5	1.49	4.9	1125	6.3		d	Klein Breteler (2015), C10

ID	Selection	Type	Toplayer	Permeability remarks	Geometry remarks	D	D/B_x	Λ/D	cot α	ξ_{m-10}	SWL	z_{top}	H_s	T_{m-10}	N	$H_s/\Delta D$	Damage	Updated damage	Reference
144		CC	Cylindrical columns		Above SWL	0.08	0.8	2.7	3	1.87	4.54	5.49	1.46	5.4	102	13.6		a	Van Steeg et al (2009), L6
145		CC	Cylindrical columns		Above SWL	0.08	0.8	2.7	3	1.74	4.84	5.49	1.1	4.4	1020	10.3		a	Van Steeg et al (2009), N4+N4a
147		CC	Cylindrical columns		Above SWL	0.08	0.8	2.7	3	1.72	5.34	5.49	0.4	2.6	966	3.7		a	Van Steeg et al (2009), H1
148	*	CC	Cylindrical columns		Above SWL	0.08	0.8	2.7	3	1.69	5.34	5.49	0.51	2.9	1006	4.8		c	Van Steeg et al (2009), H2
146	*	CC	Cylindrical columns		Above SWL	0.08	0.8	2.7	3	1.78	4.84	5.49	1.32	4.9	433	12.3		d	Van Steeg et al (2009), N5
149	*	CC	Cylindrical columns		Above SWL	0.08	0.8	2.7	3	1.70	5.34	5.49	0.61	3.2	330	5.7		d	Van Steeg et al (2009), H3
275		CC	Hydroblock			0.15	0.6	2.3	3.5	2.84	4.2	6	0.27	4.1	1000	1.9		0	Klein Breteler, Van der Werf, Weneker (2012), P10
276		CC	Hydroblock			0.15	0.6	2.3	3.5	4.07	4.2	6	0.48	7.9	1000	3.4		0	Klein Breteler, Van der Werf, Weneker (2012), P11
277		CC	Hydroblock			0.15	0.6	2.3	3.5	4.25	4.5	6	0.55	8.8	1000	3.9		0	Klein Breteler, Van der Werf, Weneker (2012), P12A
278		CC	Hydroblock			0.15	0.6	2.3	3.5	4.24	4.52	6	0.56	8.9	1000	3.9		0	Klein Breteler, Van der Werf, Weneker (2012), P12B
279		CC	Hydroblock			0.15	0.6	2.3	3.5	4.13	4.8	6	0.65	9.3	1000	4.6		0	Klein Breteler, Van der Werf, Weneker (2012), P13
280		CC	Hydroblock			0.15	0.6	2.3	3.5	4.08	5.02	6	0.76	10.0	1000	5.3		0	Klein Breteler, Van der Werf, Weneker (2012), P14
281		CC	Hydroblock			0.15	0.6	2.3	3.5	4.06	5.17	6	0.84	10.4	1000	5.9		0	Klein Breteler, Van der Werf, Weneker (2012), P15
284		CC	Hydroblock			0.15	0.6	2.3	3.5	3.08	4.4	6	0.51	6.2	1000	3.6		0	Klein Breteler, Van der Werf, Weneker (2012), P22
285		CC	Hydroblock			0.15	0.6	2.3	3.5	3.10	4.41	6	0.63	6.9	1000	4.4		0	Klein Breteler, Van der Werf, Weneker (2012), P23
286		CC	Hydroblock			0.15	0.6	2.3	3.5	3.06	4.75	6	0.74	7.4	1000	5.2		0	Klein Breteler, Van der Werf, Weneker (2012), P24
287		CC	Hydroblock			0.15	0.6	2.3	3.5	2.99	4.8	6	0.89	7.9	1000	6.2		0	Klein Breteler, Van der Werf, Weneker (2012), P25
96		CC	Hydroblock			0.15	0.6	2.0	3.5	4.54	5.17	6	0.84	11.7	1000	5.9		a	Klein Breteler et al (2006), 15
97		CC	Hydroblock			0.15	0.6	2.0	3.5	4.54	5.10	6	0.80	11.4	2000	5.6		a	Klein Breteler et al (2006), 14+15
98		CC	Hydroblock			0.15	0.6	2.0	3.5	3.89	5.18	6	0.96	10.7	1000	6.7		a	Klein Breteler et al (2006), 16

ID	Selection	Type	Toplayer	Permeability remarks	Geometry remarks	D	D/B_x	Λ/D	cot α	ξ_{m-10}	SWL	z_{top}	H_s	T_{m-10}	N	$H_s/\Delta D$	Damage	Updated damage	Reference
99		CC	Hydroblock			0.15	0.6	2.0	3.5	3.17	4.8	6	0.89	8.4	1000	6.2		a	Klein Breteler et al (2006), 25
263		CC	Hydroblock			0.166	1.3	1.4	3	2.17	4.7	5.5	0.9	4.9	1007	4.3		a	Wolters (2015), H02
264		CC	Hydroblock			0.166	1.3	1.4	3	2.21	4.7	5.5	1.05	5.4	1010	5.0		a	Wolters (2015), H03
268		CC	Hydroblock			0.166	1.3	1.4	3	1.57	4.7	5.5	0.73	3.2	597	3.5		a	Wolters (2015), H07
269		CC	Hydroblock			0.166	1.3	1.4	3	1.57	4.7	5.5	1.01	3.8	1013	4.8		a	Wolters (2015), H08
272		CC	Hydroblock			0.166	1.3	1.4	3	1.57	4.7	5.5	0.73	3.2	602	3.5		a	Wolters (2015), H11
282		CC	Hydroblock			0.15	0.6	2.3	3.5	3.46	5.18	6	0.96	9.5	1000	6.7		a	Klein Breteler, Van der Werf, Weneker (2012), P16
265		CC	Hydroblock			0.166	1.3	1.4	3	2.16	4.7	5.5	1.21	5.7	984	5.7		b	Wolters (2015), H04
266	*	CC	Hydroblock			0.166	1.3	1.4	3	2.19	4.7	5.5	1.34	6.1	1034	6.3		c	Wolters (2015), H05
267	*	CC	Hydroblock			0.166	1.3	1.4	3	2.15	4.7	5.5	1.51	6.4	1025	7.1		c	Wolters (2015), H06
270	*	CC	Hydroblock			0.166	1.3	1.4	3	1.58	4.7	5.5	1.16	4.1	1012	5.5		c	Wolters (2015), H09
273	*	CC	Hydroblock			0.166	1.3	1.4	3	1.57	4.7	5.5	0.95	3.7	2150	4.5		c	Wolters (2015), H12
283	*	CC	Hydroblock			0.15	0.6	2.3	3.5	3.46	5.18	6	1.1	9.5	1000	7.7		c	Klein Breteler, Van der Werf, Weneker (2012), P16S
288	*	CC	Hydroblock			0.15	0.6	2.3	3.5	2.85	4.9	6	1.05	8.2	1000	7.4		c	Klein Breteler, Van der Werf, Weneker (2012), P26
100	*	CC	Hydroblock			0.15	0.6	2.0	3.5	3.00	4.9	6	1.05	8.6	394	7.4		d	Klein Breteler et al (2006), 26
271	*	CC	Hydroblock			0.166	1.3	1.4	3	1.60	4.7	5.5	1.29	4.4	481	6.1		d	Wolters (2015), H10
81		CC	Hydroblock			0.15	0.6	2.2	3.5	1.72	5.2	6	0.95	4.7	1019	4.4		a	Klein Breteler et al (2005), 5250
84		CC	Hydroblock			0.2	0.8	2.3	3.5	1.85	4.47	6	1.11	5.5	9658	4.1		a	Klein Breteler et al (2005), 4260-4660
82	*	CC	Hydroblock			0.15	0.6	2.2	3.5	1.80	5.2	6	1.08	5.2	985	5.0	d	c	Klein Breteler et al (2005), 5251, damage d at Hs=1.98
85	*	CC	Hydroblock			0.2	0.8	2.3	3.5	1.85	4.56	6	1.11	5.5	13582	4.1		d	Klein Breteler et al (2005), 4260-4860
83	*	CC	Hydroblock		Re-used	0.15	0.6	2.2	3.5	1.88	4.2	6	1.01	5.3	1672	4.7		d	Klein Breteler et al (2005), 4250+4251
86		CC	Pit-polygon			0.2	1.0	2.2	3.5	1.24	5	5	1.64	4.5	1045	6.1		b	Wouters (1998), 4

ID	Selection	Type	Toplayer	Permeability remarks	Geometry remarks	D	D/B_x	Λ/D	cot α	ξ_{m-10}	SWL	z_{top}	H_s	T_{m-10}	N	$H_s/\Delta D$	Damage	Updated damage	Reference
89		CC	Pit-polygon			0.2	0.8	2.2	3.5	1.63	5	5	1.63	5.8	518	6.3		b	Wouters (1998), 5
87	*	CC	Pit-polygon			0.2	1.0	2.2	3.5	1.63	5	5	1.63	5.8	518	6.1		c	Wouters (1998), 5
90	*	CC	Pit-polygon			0.2	0.8	2.2	3.5	1.98	5	5	1.63	7.1	1045	6.3		c	Wouters (1998), 6
88	*	CC	Pit-polygon			0.2	1.0	2.2	3.5	1.98	5	5	1.63	7.1	1045	6.1		d	Wouters (1998), 6
224		CC	Ronaton			0.145	1.1	2.0	3	2.16	4.55	5.5	0.6	4.0	497	3.7		a	Klein Breteler (2015), P01
225		CC	Ronaton			0.145	1.1	2.0	3	2.18	4.7	5.5	0.69	4.4	1054	4.3		a	Klein Breteler (2015), P02
226		CC	Ronaton			0.145	1.1	2.0	3	2.21	4.7	5.5	0.83	4.8	998	5.1		a	Klein Breteler (2015), P03
227		CC	Ronaton			0.145	1.1	2.0	3	2.21	4.7	5.5	1	5.3	1022	6.2		a	Klein Breteler (2015), P04
228		CC	Ronaton			0.145	1.1	2.0	3	2.18	4.7	5.5	1.2	5.7	1019	7.4		a	Klein Breteler (2015), P05
229		CC	Ronaton			0.145	1.1	2.0	3	2.19	4.7	5.5	1.4	6.2	1007	8.7		a	Klein Breteler (2015), P06
230		CC	Ronaton			0.145	1.1	2.0	3	2.16	4.7	5.5	1.5	6.4	1055	9.3		a	Klein Breteler (2015), P07
231		CC	Ronaton			0.145	1.1	2.0	3	1.60	4.7	5.5	0.95	3.8	1007	5.9		a	Klein Breteler (2015), P08
234		CC	Ronaton			0.145	1.1	2.0	3	1.63	4.55	5.5	0.62	3.1	604	3.8		a	Klein Breteler (2015), P11
235		CC	Ronaton			0.145	1.1	2.0	3	1.60	4.55	5.5	0.78	3.4	550	4.8		a	Klein Breteler (2015), P12
163		CC	Ronaton			0.16	1.2	1.9	3	2.06	4.5	5.4	0.83	4.5	1092	3.6		b	Wolters (2010), T1
164		CC	Ronaton			0.16	1.2	1.9	3	2.15	4.5	5.4	1.51	6.3	1036	6.5		b	Wolters (2010), T5
165		CC	Ronaton			0.16	1.2	1.9	3	1.59	4.5	5.4	0.95	3.7	1016	4.1		b	Wolters (2010), T6
166		CC	Ronaton			0.16	1.2	1.9	3	1.70	4.5	5.4	1.52	5.0	1039	6.5		b	Wolters (2010), T9
232		CC	Ronaton			0.145	1.1	2.0	3	1.60	4.7	5.5	1.19	4.2	1042	7.4		b	Klein Breteler (2015), P09
167	*	CC	Ronaton			0.16	1.2	1.9	3	1.71	4.5	5.4	1.51	5.1	1880	6.5		c	Wolters (2010), T9-T10
168	*	CC	Ronaton			0.16	1.2	1.9	3	1.72	4.5	5.4	1.52	5.1	10322	6.5		d	Wolters (2010), T9-T11B
233	*	CC	Ronaton			0.145	1.1	2.0	3	1.60	4.7	5.5	1.39	4.5	643	8.6		d	Klein Breteler (2015), P10

ID	Selection	Type	Toplayer	Permeability remarks	Geometry remarks	D	D/B_x	Λ/D	$\cot \alpha$	ξ_{m-10}	SWL	z_{top}	H_s	T_{m-10}	N	$H_s/\Delta D$	Damage	Updated damage	Reference
236	*	CC	Ronaton			0.145	1.1	2.0	3	1.62	4.7	5.5	1.07	4.0	1826	6.6		d	Klein Breteler (2015), P13
314		HS	Hillh testblock			0.15	1.1	2.8	3.5	1.84	4.55	0	0.6	4.0	491	2.9		a	Klein Breteler (2015), S01
316		HS	Hillh testblock			0.15	1.1	2.8	3.5	1.34	4.55	0	0.54	2.8	672	2.6		a	Klein Breteler (2015), S03
317		HS	Hillh testblock			0.15	1.1	2.8	3.5	1.36	4.7	0	0.67	3.1	131	3.2		a	Klein Breteler (2015), S04
318		HS	Hillh testblock			0.15	1.1	2.8	3.5	1.35	4.7	0	0.79	3.4	1034	3.8		a	Klein Breteler (2015), S05
320		HS	Hillh testblock			0.15	1.1	2.8	3.5	1.34	4.55	0	0.53	2.8	440	2.5		a	Klein Breteler (2015), S07
321		HS	Hillh testblock			0.15	1.1	2.8	3.5	1.35	4.55	0	0.53	2.8	441	2.5		a	Klein Breteler (2015), S08
322		HS	Hillh testblock			0.15	1.1	2.8	3.5	1.38	4.7	0	0.67	3.2	2490	3.2		a	Klein Breteler (2015), S09-a
315		HS	Hillh testblock			0.15	1.1	2.8	3.5	1.85	4.7	0	0.93	5.0	391	4.5		d	Klein Breteler (2015), S02
319		HS	Hillh testblock			0.15	1.1	2.8	3.5	1.35	4.7	0	0.99	3.7	463	4.7		d	Klein Breteler (2015), S06
323		HS	Hillh testblock			0.15	1.1	2.8	3.5	1.36	4.7	0	0.66	3.1	589	3.2		d	Klein Breteler (2015), S09-b
324		HS	Hillh testblock			0.15	1.1	2.8	3.5	1.35	4.7	0	0.68	3.1	1807	3.3		d	Klein Breteler (2015), S09-c
325		HS	Hillh testblock			0.15	1.1	2.8	3.5	1.32	4.7	0	0.72	3.2	1187	3.5		d	Klein Breteler (2015), S09-d
158		HS	Hillblock			0.2	1.5	2.3	3	2.11	4.5	5.5	1.49	6.2	1077	5.4		a	Van Steeg (2012), T005
159		HS	Hillblock			0.2	1.5	2.3	3	1.77	4.5	5.5	1.5	5.2	986	5.5		a	Van Steeg (2012), T014
160		HS	Hillblock			0.2	1.5	2.3	3	1.68	4.5	5.5	1.43	4.8	25062	5.2		a	Van Steeg (2012), T008-T015
326		HS	Hillblock			0.2	1.5	2.3	3.5	1.80	4.5	0	0.8	4.5	1102	2.9		a	Klein Breteler (2015), T001
327		HS	Hillblock			0.2	1.5	2.3	3.5	1.82	4.5	0	1.01	5.1	1117	3.7		a	Klein Breteler (2015), T002
328		HS	Hillblock			0.2	1.5	2.3	3.5	1.78	4.5	0	1.21	5.6	1086	4.4		a	Klein Breteler (2015), T003
329		HS	Hillblock			0.2	1.5	2.3	3.5	1.80	4.5	0	1.38	6.0	1129	5.0		a	Klein Breteler (2015), T004
330		HS	Hillblock			0.2	1.5	2.3	3.5	1.82	4.5	0	1.49	6.2	1077	5.4		a	Klein Breteler (2015), T005
331		HS	Hillblock			0.2	1.5	2.3	3.5	1.44	4.5	0	0.98	3.9	949	3.6		a	Klein Breteler (2015), T006

ID	Selection	Type	Toplayer	Permeability remarks	Geometry remarks	D	D/B_x	Λ/D	cot α	$\xi_{m\text{-}10}$	SWL	z_{top}	H_s	$T_{m\text{-}10}$	N	$H_s/\Delta D$	Damage	Updated damage	Reference
332		HS	Hillblock			0.2	1.5	2.3	3.5	1.39	4.5	0	1.23	4.3	1049	4.5		a	Klein Breteler (2015), T007
333		HS	Hillblock			0.2	1.5	2.3	3.5	1.46	4.5	0	1.46	4.9	1007	5.3		a	Klein Breteler (2015), T008
334		HS	Hillblock			0.2	1.5	2.3	3.5	1.43	4.5	0	1.43	4.8	4201	5.2		a	Klein Breteler (2015), T009
335		HS	Hillblock			0.2	1.5	2.3	3.5	1.44	4.5	0	1.42	4.8	719	5.2		a	Klein Breteler (2015), T010
336		HS	Hillblock			0.2	1.5	2.3	3.5	1.43	4.5	0	1.42	4.8	10702	5.2		a	Klein Breteler (2015), T011
337		HS	Hillblock			0.2	1.5	2.3	3.5	1.49	4.5	0	1.5	5.2	986	5.5		a	Klein Breteler (2015), T014
338		HS	Hillblock			0.2	1.5	2.3	3.5	1.44	4.5	0	1.45	4.9	1017	5.3		a	Klein Breteler (2015), T015
339		HS	Hillblock			0.2	1.5	2.3	3.5	1.30	3.1	0	0.74	3.2	953	2.7		a	Klein Breteler (2015), T016
340		HS	Hillblock			0.2	1.5	2.3	3.5	1.67	3.1	0	0.81	4.2	1038	3.0		a	Klein Breteler (2015), T017
341		HS	Hillblock			0.2	1.5	2.3	3.5	1.75	3.1	0	0.94	4.8	1061	3.4		a	Klein Breteler (2015), T018
342		HS	Hillblock			0.2	1.5	2.3	3.5	1.40	3.1	0	0.91	3.8	960	3.3		a	Klein Breteler (2015), T019
289		HS	Ronaton Taille			0.151	1.2	2.3	3.5	1.85	4.55	0	0.71	4.3	478	3.8		a	Klein Breteler (2015), R01
291		HS	Ronaton Taille			0.151	1.2	2.3	3.5	1.84	4.55	0	0.7	4.3	473	3.7		a	Klein Breteler (2015), R03
294		HS	Ronaton Taille			0.151	1.2	2.3	3.5	1.35	4.7	0	0.73	3.2	2428	3.9		a	Klein Breteler (2015), R12
292		HS	Ronaton Taille			0.151	1.2	2.3	3.5	1.34	4.7	0	0.84	3.5	994	4.5		b	Klein Breteler (2015), R04
295		HS	Ronaton Taille			0.151	1.2	2.3	3.5	1.35	4.7	0	0.75	3.3	4780	4.0		b	Klein Breteler (2015), R13
290		HS	Ronaton Taille			0.151	1.2	2.3	3.5	1.87	4.7	0	0.84	4.8	224	4.5		d	Klein Breteler (2015), R02
293		HS	Ronaton Taille			0.151	1.2	2.3	3.5	1.36	4.7	0	0.99	3.8	934	5.3		d	Klein Breteler (2015), R05
296		HS	Ronaton Taille			0.151	1.2	2.3	3.5	1.37	4.7	0	0.73	3.3	2182	3.9		d	Klein Breteler (2015), R14
297		HS	Verkalit GOR			0.151	1.0	0.8	3.5	1.87	4.55	0	0.68	4.3	475	3.4		a	Klein Breteler (2015), V24
298		HS	Verkalit GOR			0.151	1.0	0.8	3.5	1.82	4.7	0	0.86	4.8	1012	4.2		a	Klein Breteler (2015), V25
299		HS	Verkalit GOR			0.151	1.0	0.8	3.5	1.89	4.7	0	0.99	5.3	999	4.9		a	Klein Breteler (2015), V26

ID	Type	Toplayer	Permeability remarks	Geometry remarks	D	D/B_x	Λ/D	cot α	ξ_{m-10}	SWL	z_{top}	H_s	T_{m-10}	N	$H_s/\Delta D$	Damage	Updated damage	Reference
300	HS	Verkalit GOR			0.151	1.0	0.8	3.5	1.90	4.7	0	1.14	5.7	983	5.6		a	Klein Breteler (2015), V27
301	HS	Verkalit GOR			0.151	1.0	0.8	3.5	1.91	4.7	0	1.32	6.1	1013	6.5		a	Klein Breteler (2015), V28
302	HS	Verkalit GOR			0.151	1.0	0.8	3.5	1.84	4.7	0	1.56	6.4	1036	7.7		a	Klein Breteler (2015), V29
303	HS	Verkalit GOR			0.151	1.0	0.8	3.5	1.36	4.55	0	0.84	3.5	567	4.1		a	Klein Breteler (2015), V30
304	HS	Verkalit GOR			0.151	1.0	0.8	3.5	1.34	4.7	0	0.85	3.5	1033	4.2		a	Klein Breteler (2015), V31
305	HS	Verkalit GOR			0.151	1.0	0.8	3.5	1.34	4.7	0	1.01	3.8	1013	5.0		a	Klein Breteler (2015), V32
306	HS	Verkalit GOR			0.151	1.0	0.8	3.5	1.37	4.7	0	1.15	4.1	124	5.7		a	Klein Breteler (2015), V33
309	HS	Verkalit GOR			0.151	1.0	0.8	3.5	1.36	4.55	0	0.67	3.1	627	3.3		a	Klein Breteler (2015), V36
310	HS	Verkalit GOR			0.151	1.0	0.8	3.5	1.36	4.7	0	1.1	4.0	2008	5.4		a	Klein Breteler (2015), V37
311	HS	Verkalit GOR			0.151	1.0	0.8	3.5	1.33	4.7	0	1.12	4.0	3900	5.5		a	Klein Breteler (2015), V38
312	HS	Verkalit GOR			0.151	1.0	0.8	3.5	1.35	4.7	0	1.11	4.0	8065	5.5		b	Klein Breteler (2015), V39
307	HS	Verkalit GOR			0.151	1.0	0.8	3.5	1.38	4.7	0	1.36	4.5	980	6.7		c	Klein Breteler (2015), V34
313	HS	Verkalit GOR			0.151	1.0	0.8	3.5	1.36	4.7	0	1.11	4.0	12013	5.5		c	Klein Breteler (2015), V40
308	HS	Verkalit GOR			0.151	1.0	0.8	3.5	1.43	4.7	0	1.45	4.8	176	7.2		d	Klein Breteler (2015), V35
5	NB	Granite blocks	Siltated		0.21	0.8	0.9	3.5	1.42	4.04	5	1.52	4.9	1045	4.6		a	Smith et al (2000), 4ao06
12	NB	Granite blocks	Siltated, measured Λ		0.21	0.8	1.6	3.5	1.50	4.26	5	1.68	5.5	1045	5.1	a	0	Smith et al (2000), 4do10
6	NB	Granite blocks			0.208	0.8	0.8	3.5	1.39	4.03	5	1.6	4.9	1045	4.9		b	Smith et al (2000), 4ao07
3	NC	Bazalt	Penetrated joints / sand in filter		0.196	0.7	0.7	3.5	1.36	4	5	1.26	4.3	1045	3.3		a	Smith et al (2000), 3o10
61	NC	Bazalt	Half penetrated joints		0.129	0.6	1.4	3.5	1.66	3.9	6	0.68	3.8	4894	2.6		a	Hofland et al (2006), P01-02
91	NC	Bazalt			0.2	1.0	2.6	3.5	1.65	4.58	6	1.4	5.5	1038	3.6		a	Eysink et al (2003), 5
117	NC	Bazalt			0.3	1.2	1.7	3.5	1.33	5	6.5	1.55	4.7	404	2.6		a	Burger (1985), 21
119	NC	Bazalt			0.3	1.2	1.7	3.5	1.46	5	6.5	1.85	5.6	337	3.1		a	Burger (1985), 23

ID	Selection	Type	Toplayer	Permeability remarks	Geometry remarks	D	D/B_x	Λ/D	cot α	ξ_{m-10}	SWL	z_{top}	H_s	T_{m-10}	N	$H_s/\Delta D$	Damage	Updated damage	Reference
63		NC	Bazalt	Penetrated joints		0.129	0.6	3.3	3.5	1.83	3.07	6	1.07	5.3	2403	4.1		b	Hofland et al (2006), LW 17-19
65		NC	Bazalt	Penetrated joints		0.129	0.6	3.3	3.5	1.73	4.16	6	1.02	4.9	2655	3.9		b	Hofland et al (2006), HW 12+13+14
70		NC	Bazalt			0.2	1.0	2.5	3.5	1.78	4.5	6	1.43	6.0	8835	3.7		b	Klein Breteler et al (2005), 4215-4616
68	*	NC	Bazalt			0.2	1.0	2.5	3.5	1.71	4.5	6	1.29	5.4	6577	3.3		c	Klein Breteler et al (2005), 4411+4610
71	*	NC	Bazalt			0.2	1.0	2.5	3.5	1.76	4.42	6	1.59	6.2	2115	4.1		c	Klein Breteler et al (2005), 4418
92	*	NC	Bazalt			0.2	1.0	2.6	3.5	1.70	4.78	6	1.54	5.9	1030	3.9		c	Eysink et al (2003), 6
93	*	NC	Bazalt			0.2	1.0	2.6	3.5	1.68	4.68	6	1.47	5.7	2068	3.8		c	Eysink et al (2003), 5 en 6
4	*	NC	Bazalt	Penetrated joints / sand in filter		0.196	0.7	0.7	3.5	1.38	4.39	5	1.56	4.8	1045	4.1		d	Smith et al (2000), 3o11
62	*	NC	Bazalt	Half penetrated joints		0.129	0.6	1.4	3.5	1.65	3.9	6	0.96	4.5	4323	3.7		d	Hofland et al (2006), P03-05
64	*	NC	Bazalt	Penetrated joints		0.129	0.6	3.3	3.5	1.85	3.23	6	1.16	5.6	3742	4.4		d	Hofland et al (2006), LW 17-21
66	*	NC	Bazalt	Penetrated joints		0.129	0.6	3.3	3.5	1.52	4.7	6	1.52	5.2	2580	5.8		d	Hofland et al (2006), HW 22-23A
69	*	NC	Bazalt			0.2	1.0	2.5	3.5	1.72	4.7	6	1.27	5.4	16296	3.2		d	Klein Breteler et al (2005), 4411-4812
72	*	NC	Bazalt			0.2	1.0	2.5	3.5	1.76	4.5	6	1.54	6.1	4516	3.9		d	Klein Breteler et al (2005), 4418+4618
94	*	NC	Bazalt			0.2	1.0	2.6	3.5	2.24	4.85	6	1.22	6.9	1118	3.1		d	Eysink et al (2003), 8
118	*	NC	Bazalt			0.3	1.2	1.7	3.5	1.42	5	6.5	1.75	5.3	6088	2.9		d	Burger (1985), 22
120	*	NC	Bazalt			0.3	1.2	1.7	3.5	1.33	5	6.5	1.55	4.7	23651	2.6		d	Burger (1985), 24
110		NS	Vilvoord flat			0.22	1.5	1.2	3.5	1.22	2.87	3.5	0.67	2.8	20228	2.0		a	Burger (1985), 26
113		NS	Vilvoord flat			0.22	1.5	1.2	3.5	1.42	5	3.25	1.75	5.3	10744	5.2		d	Burger (1985), page 57
111		NS	Vilvoord round			0.22	1.5	1.2	3.5	1.28	2.87	3.5	0.74	3.1	1012	2.2		d	Burger (1985), 1
112		NS	Vilvoord round			0.22	1.5	1.2	3.5	1.92	2.87	3.5	0.75	4.7	809	2.2		d	Burger (1985), 3

DESIGN OF PATTERN-PLACED REVETMENTS – ANNEXES

ANNEX J   TREND ANALYSIS OF FLUME EXPERIMENT RESULTS

J.1   Dependencies on single parameters

The flume experiment results of Annex I can be compared and dependencies can be investigated without comparing them with a theoretical model. This is done in this section.

Table J–1   Legend of Figure J-1 etcetera

	☐	🟩	🟨	🟧	🟥	+	+
Damage category	0	a	b	c	d	c1	d1
Nature of damage (for more detailed definitions, see Table 4-4)	No damage	Start or revetment damage	Revetment damage	Start of revetment failure	Revetment failure	Partial single element failure	Complete single element failure

The concrete block experiment results can be plotted against results the slope angle. For concrete column experiments this makes less sense because of the small range of slope angles (only 1 : 3 and 1 : 3½). The trend lines for both the red and the green makers indicate a convincing decrease of stability for gentle slopes.
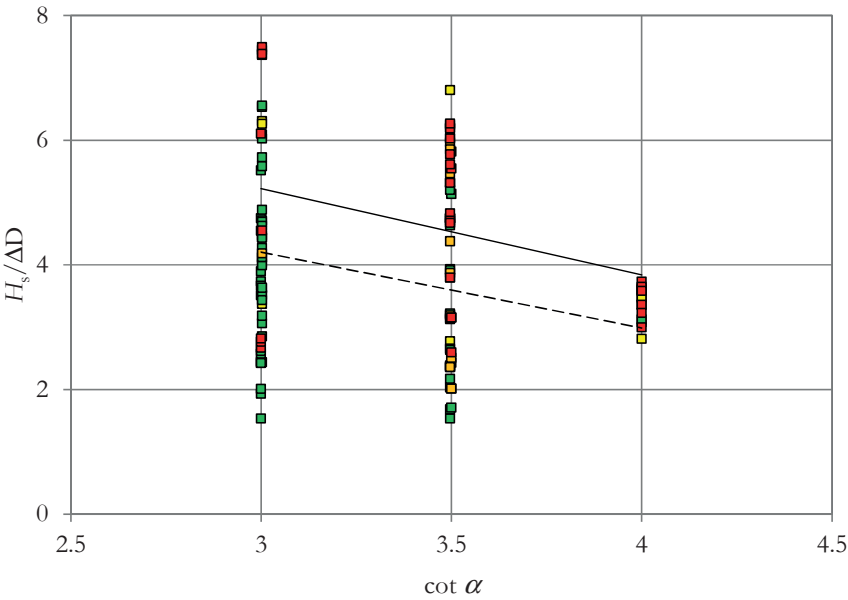

Figure J–1   Flume experiment results for CB plotted against slope angle cot α

When plotted against the height/width ratio D/B_x of the elements (see Figure J–2) it is observed that taller blocks and columns are more stable. The difference in stability number for a D/B_x of 0.5 compared to 2 is a factor 0.6 for the blocks (0.8 when we treat the d1

damages as d) and 0.7 for the columns. Mind that the D/B ratio is not the only reason of distinction between columns and blocks. The row-orientation and the type of joints are also different. An interesting observation is that single element failures seem to be related with the D/B ratio. This is in line with the beam model theory. Structures with flat elements with small D/B ratios tend to fail as a group. Tall elements can potentially fail as a piston.
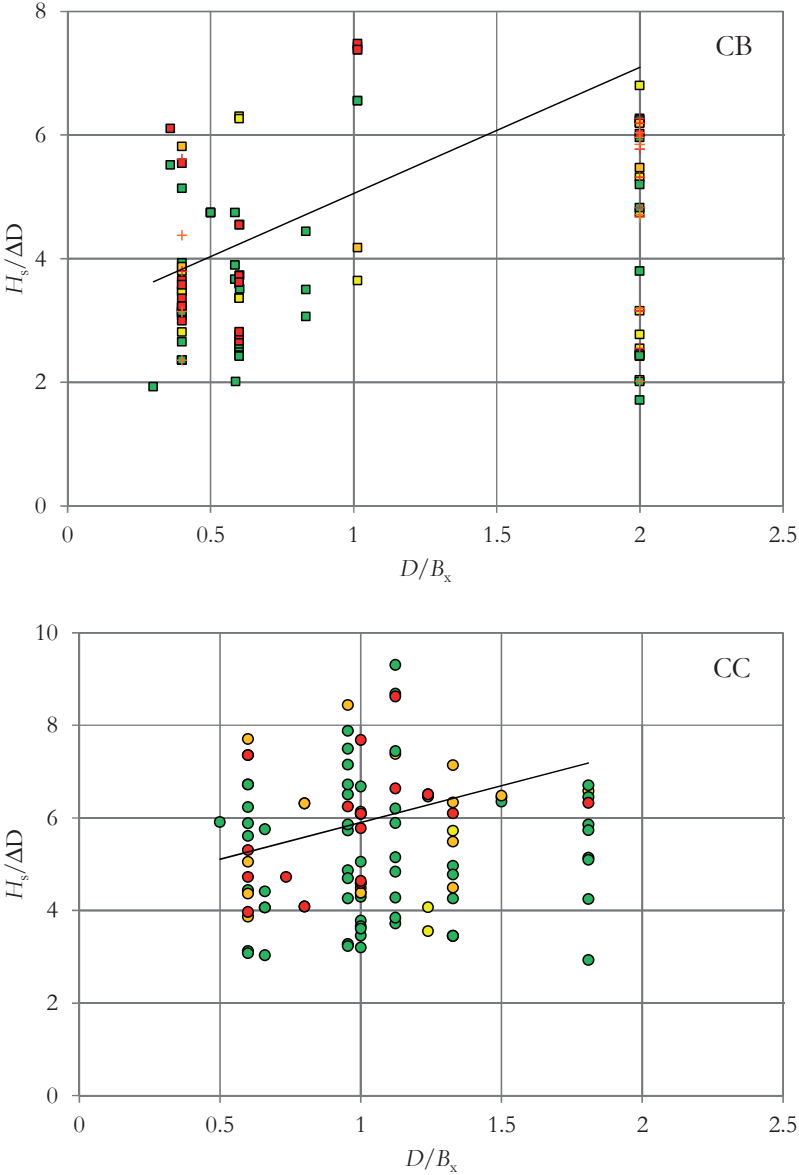

Figure J–2   Flume experiment results for CB and CC plotted against the height/width ratio of the individual revetment elements

Plotting against the leakage length covers a wide range for the blocks, and a smaller range for the columns. This is logic due to the hydraulically more open top-layer of the column revetments. For both groups a clear trend to lower stability numbers with increasing leakage length can be noticed. The dotted trend line is for the green markers, the continuous line for the red markers
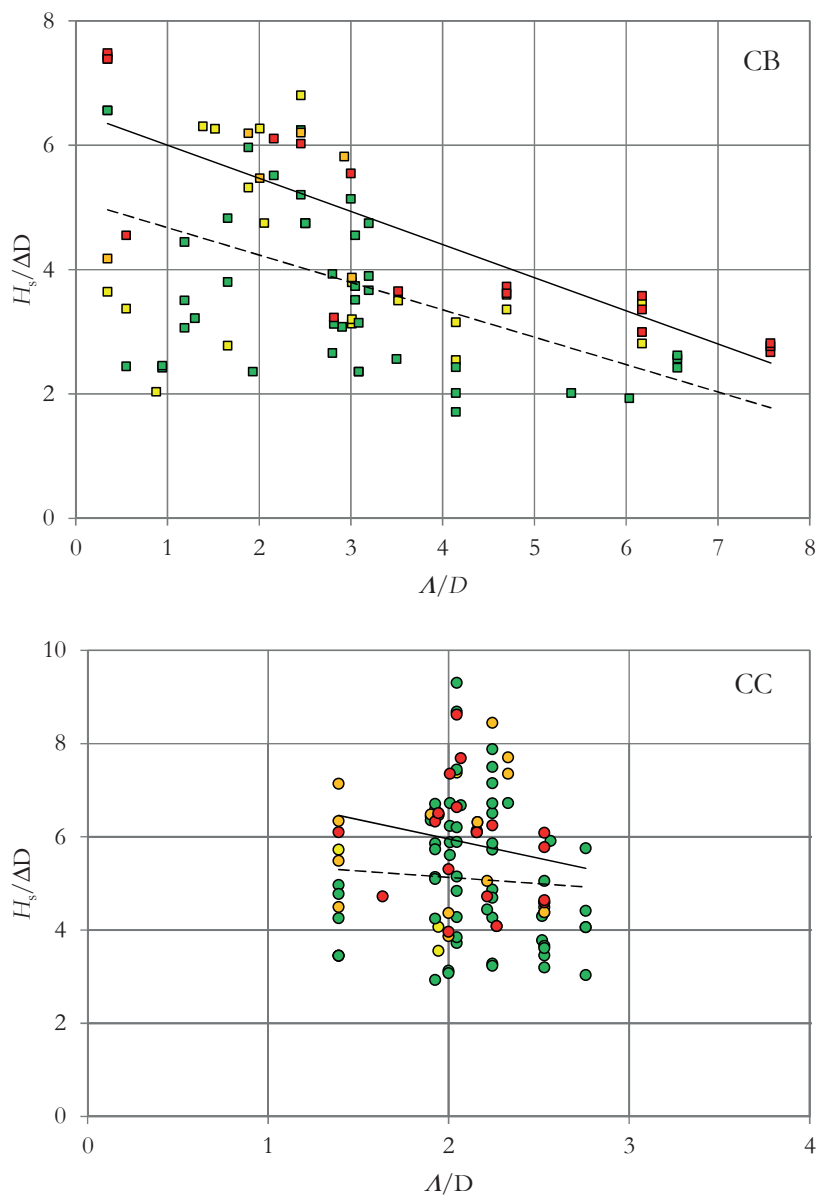

Figure J–3   **Flume experiment results for CB and CC plotted against the leakage factor**

The dependency on axial force can be found by looking into the potential for axial force above the wave impact point of the experiments. For the wave impact point we used the formula:

$$z_{imp} = z_{SLW} - (0.4 + 0.55\xi - 0.0344\xi^2 - 0.7)\,H_s \qquad \textbf{Eq. J.1}$$

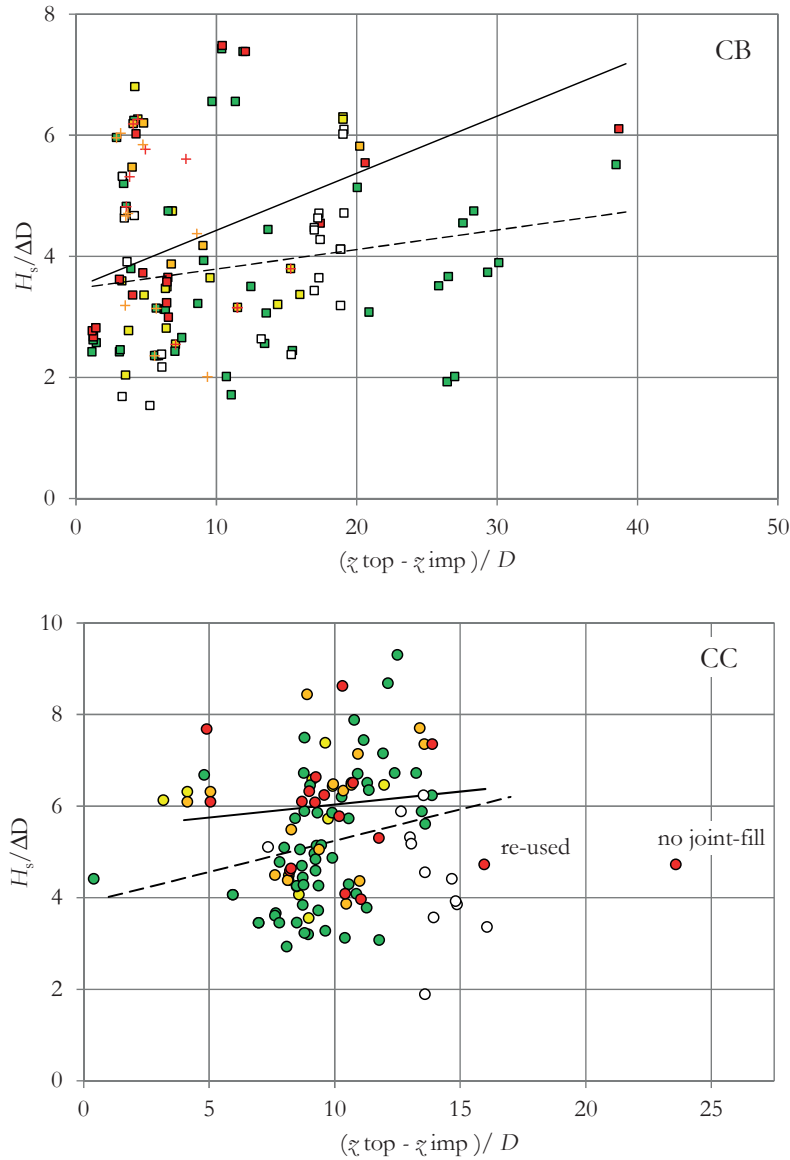In Figure J–4 positive dependency can be observed.

Figure J–4   **Flume experiment results for CB and CC plotted against the position of wave impact relative to the top of the slope**
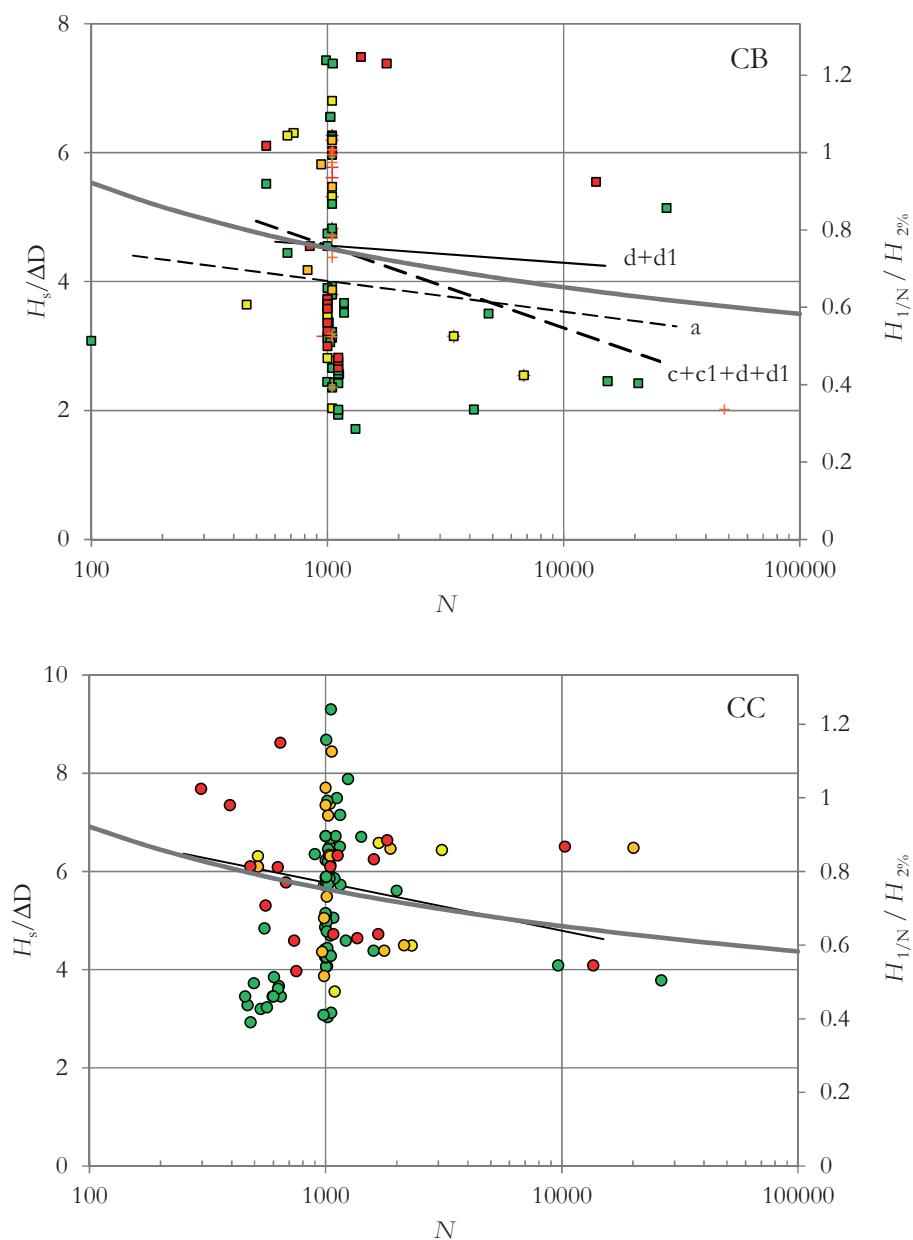
Figure J–5   Flume experiment results for CB and CC plotted against number of waves *N*

The dependency on the number of waves is plotted in Figure J–5 for concrete blocks and concrete columns. For both groups tests have been done with long durations, although the majority of the tests is around $N = 1000$. The objective was to test the performance under

repeated wave loading which might be dependent on fatigue or mechanisms of gradually propagating damage. When irregular wave series are extended in time, the probable maximum wave run-down and probable maximum wave impact might be related with the largest wave height from the Rayleigh distribution. In most of the wave effect formulas the value of $H_{2\%}$ is the reference value, e.g. Eq.'s 5.29, 5.30, 5.31 and 5.38. We therefore plotted the ratio $H_{1/N}/H_{2\%}$ as a function of N on the secondary axis. The intersection of the trend line for the d-damages and $N = 50$ (2%) was found at $H_s/\Delta D = 6$ for the concrete blocks and 7.5 for the concrete columns.

It can be noticed that the falling trends with a larger number of waves follow the effect of the highest probable wave quite nicely, which does not give room for strong conclusions on decay of resistance under long duration loads.

For the evaluation of the experiments for calibration purposes the wave loads are calculated with a wave height H_s corrected with:

$$\frac{\sqrt{-\ln((1/N)^2)}}{\sqrt{-\ln((1/1000)^2)}}$$

When the total population of experiments is plotted against H_s quite a strong positive dependency can be observed. The parameter $H_s/\Delta D$ should be independent of H_s. However when various subgroups perform better, they have a higher H_s and a higher $H_s/\Delta D$. It is therefore not possible to draw conclusions on a dependency on H_s on basis of the total population of tests.
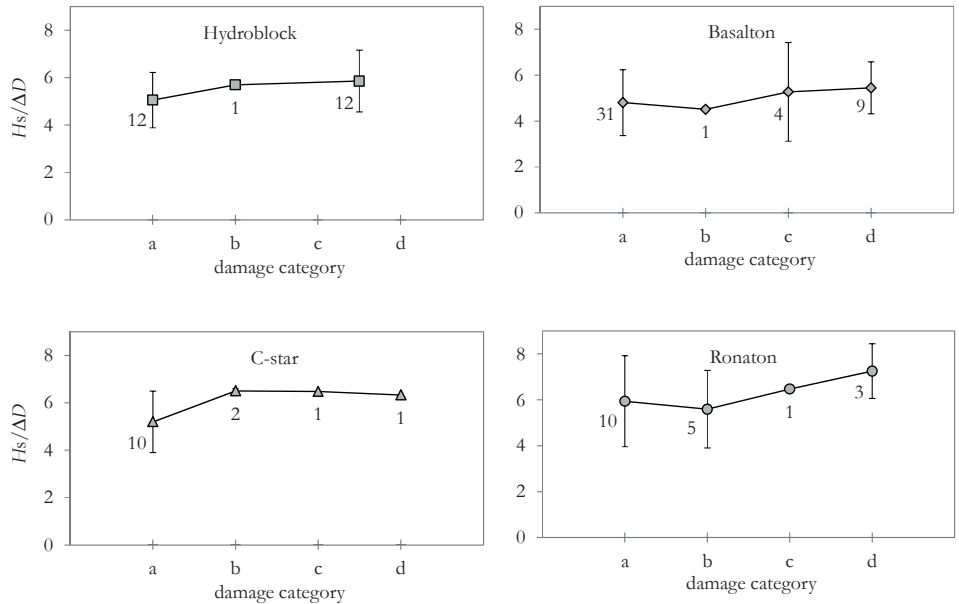

Figure J–6   Flume experiment results for CC per element type

The type of element seems a relevant parameter especially for the columns. An analysis of the average and variation coefficient per damage category gives the result shown in Figure J–6.[312] The error-bars indicate the standard deviation and the number is the number of tests. No conclusions on stability per type can be based on these graphs since the other variables influence the results. Most Basalton tests have been done on 1:3 slopes, and most Hydroblock tests on 1:3½ slopes for instance.

J.2   Multi-parameter linear regression

In order to test the statistical value of the observed trends amongst the total of variables in the total population multiple regression analysis has been performed. The results are presented in Table J–2 and Table J–3. It can be noticed that only a limited number of parameters maintains a significant effect throughout the total population. The number of variations of other test-conditions is too large, and also the inherent variability of the results is too high to generate useful results using a regression analysis, even in the case the non-linearity would be included.

Table J–2   Regression analysis results flume experiments on concrete blocks CB

CB with a-damage	coefficient	p-value	y-effect (coefficient × x-range)	significance
intercept	8.80	0.0004		no
D/B	0.69	0.058	0.61	yes
Λ/D	-0.21	0.003	0.74	yes
$\cot\alpha$	-0.94	0.15	0.65	doubtful
$1/\sqrt{(s_0)}$	-0.11	0.39	0.91	no
N	0.0001	0.16	1.19	doubtful
$(z_{top} - z_{imp})/D$	0.03	0.24	0.87	no
D	-9.79	0.008	1.11	yes

CB with d-damage	coefficient	p-value	y-effect (coefficient × x-range)	significance
intercept	12.7	0.027		no
D/B	-0.37	0.50	0.88	no
Λ/D	-0.40	0.0013	1.17	yes
$\cot\alpha$	-1.59	0.079	0.85	doubtful
$1/\sqrt{(s_0)}$	-0.084	0.79	0.98	no
N	0.0001	0.39	1.52	no
$(z_{top} - z_{imp})/D$	-0.028	0.54	1.69	no
D	-0.28	0.98	1.07	no

---

[312] The Hydroblock tests for c and d are merged into one group, because the c damage appeared on average at a higher stability number than the d damage. This might be due to a shift in definition over time.

Table J–3   Regression analysis results flume experiments on concrete columns CC

CC with a-damage	coefficient	p-value	y-effect (coefficient × x-range)	significance
intercept	-3.47	0.52		no
D/B	0.67	0.35	0.94	no
Λ/D	0.54	0.44	0.94	no
$\cot\alpha$	1.71	0.23	0.70	no
$1/\surd(s_0)$	0.036	0.77	1.37	no
N	-0.0001	0.12	1.70	yes
$(z_{top} - z_{imp})/D$	0.12	0.08	1.22	yes
D	1.58	0.87	1.13	no

CC with c and d-damage	coefficient	p-value	y-effect (coefficient × x-range)	significance
intercept	-8.44	0.23		no
D/B	3.00	0.010	1.30	yes
Λ/D	0.73	0.30	0.93	no
$\cot\alpha$	2.63	0.23	1.06	no
$1/\surd(s_0)$	0.11	0.66	2.02	no
N	-7.8E-05	0.18	0.76	no
$(z_{top} - z_{imp})/D$	0.19	0.20	2.79	doubtful
D	-3.63	0.74	1.32	no

The CC sets were also investigated for their dependency on the various element types. When the types are included in the regression analysis with labelling them as a Boolean variable, the conclusion about significance of the other variables changes a bit. For the a-damage the slope angle and the number of waves become significant. Remarkably the high p-value indicates that the probability of each individual type being an independent variable within the test population is low. There are calculated average differences in stability numbers amongst the types, though. Based on the results three groups can be distinguished: (i) Hydroblocks and Pit-polygon, (ii) Basalton and C-star and (iii) Ronaton, in order of increasing stability.